

DEPARTMENT OF THE INTERIOR

U.S. GEOLOGICAL SURVEY

---

NATIONAL EARTHQUAKE HAZARDS REDUCTION PROGRAM,  
SUMMARIES OF TECHNICAL REPORTS VOLUME XXXIII

VOLUME I

Prepared by Participants in  
NATIONAL EARTHQUAKE HAZARDS REDUCTION PROGRAM

October 1991

---

OPEN-FILE REPORT 92-258

This report is preliminary and has not been reviewed for conformity with U.S. Geological Survey editorial standards or with the North American Stratigraphics Code. Parts of it were prepared under contract to the U.S. Geological Survey and the opinions and conclusions expressed herein do not necessarily represent those of the USGS. Any use of trade, product, or firm names is for descriptive purposes only and does not imply endorsement by the U.S. Government.

Menlo Park, California

1992

## DIRECTIONS FOR PREPARATION OF REPORTS

1. Use 8 1/2 x 11" paper for both text and figures.
2. Leave at least 1" margins at top, sides and bottom.
3. Type all text single-spaced.
4. Type only on one side of the paper.
5. Draft figures in black ink (color, weak or grey lines will not photo-reproduce) and make them simple and legibly lettered.
6. Type figure captions on the same page as the figure.
7. Please do not use staples.
8. Do not number pages.
9. Send original copies of text and figures. Do not send xerox copies as they do not photo-reproduce clearly. Do not send oversize photos. They should be able to be placed on regular sized paper and the caption must fit under it.
10. Do not type headings such as "Technical Report" or "Summary".
11. Do not use scotch tape. Use paste.
12. If you use photographs please send a glossy print of each.

UNITED STATES  
DEPARTMENT OF THE INTERIOR  
GEOLOGICAL SURVEY

---

NATIONAL EARTHQUAKE HAZARDS REDUCTION PROGRAM,  
SUMMARIES OF TECHNICAL REPORTS VOLUME XXXIII

Prepared by Participants in  
NATIONAL EARTHQUAKE HAZARDS REDUCTION PROGRAM

---

Compiled by

Muriel L. Jacobson

The research results described in the following summaries were submitted by the investigators in September 1991 and cover the period from April 1991 through October 1, 1991. These reports include both work performed under contracts administered by the Geological Survey and work by members of the Geological Survey. The report summaries are grouped into the four major goals of the National Earthquake Hazards Reduction Program.

Open File Report No. 92-258

This report has not been reviewed for conformity with U.S. Geological Survey editorial standards or with the North American Stratigraphic Code. Parts of it were prepared under contract to the U.S. Geological Survey and the opinions and conclusions expressed herein do not necessarily represent those of the USGS. Any use of trade, product, or firm names is for descriptive purposes only and does not imply endorsement by the U.S. Government.

The data and interpretations in these progress reports may be reevaluated by the investigators upon completion of the research. Readers who wish to cite findings described herein should confirm their accuracy with the author.



# EARTHQUAKE HAZARDS REDUCTION PROGRAM

## CONTENTS - VOLUME I

### Goal I - Understanding what happens at the earthquake source

Why and how does a segment of a geologic fault suddenly slip and produce an earthquake? What physical conditions within the Earth control where and when an earthquake occurs?

Abers.....	1
Aydin.....	6
Biegel.....	8
Boatwright.....	9
Boyd.....	11
Crosson.....	16
Dmowska.....	18
Doser.....	22
Evans.....	25
Fletcher.....	28
Hall.....	32
Hamburger.....	34
Hauksson.....	39
Helmberger.....	43
Hickman.....	46
Jackson.....	48
Kanamori.....	52
Kanamori.....	55
Kisslinger.....	58
McEvelly.....	76
Moses.....	85
Nicholson.....	86
Okol.....	89
Peppin.....	92
Scholz.....	95
Shearer.....	97
Smith.....	99
Stuart.....	104
Talwani.....	106
Unruh.....	112
Vernon.....	115

### Goal II - Evaluating the potential of future earthquakes

Where are future earthquakes likely? How large will they be? How often will they occur? When will they occur? Where are future earthquakes unlikely?

Abers.....	121
Agnew.....	126
Allen.....	131
Anderson.....	133

Arabasz.....	135
Atwater.....	137
Beavan.....	139
Beavan.....	145
Bierman.....	151
Bilham.....	153
Bilham.....	157
Bird.....	159
Bock.....	166
Bonilla.....	172
Borchardt.....	174
Borcherdt.....	177
Brown.....	186
Bucknam.....	188
Butler.....	191
Carver.....	192
Catchings.....	195
Celebi.....	199
Clark.....	202
Clarke.....	205
Clayton.....	213
Combellick.....	219
Crone.....	221
Crosson.....	231
Davis.....	234
Dewey.....	236
Ellsworth.....	240
Engdahl.....	245
Espinosa.....	248
Evans.....	250
Fischer.....	254
Fletcher.....	255
Galehouse.....	256
Gilbert.....	269
Gladwin.....	273
Guccione.....	276
Habermann.....	279
Hall.....	288
Hall.....	290
Herrmann.....	294
Herrmann.....	296
Hill.....	299
Holcomb.....	303
Hunt.....	304
Irwin.....	306
Jachens.....	308
Jacoby.....	315
Jensen.....	318
Jin.....	319
Johnson, H.....	325
Johnson, S.....	329
Johnston, A.....	334
Johnston, A.....	341
Johnston, M.....	344

Jones.....	350
Jones.....	354
Julian.....	356
Keller.....	359
Kelson.....	360
King.....	363
Kisslinger.....	369
Lahr.....	373
Lajoie.....	381
Langbein.....	385
Langbein.....	400
Langston.....	409
Larson.....	413
Lee.....	414
Lester.....	415
Lettis.....	420
Lettis.....	422
Levine.....	424
Lienkaemper.....	426
Linde.....	427
Linde.....	436
Lindvall.....	437
Lisowski.....	440
Luetgert.....	449
Machette.....	453
Malin.....	457
Mason.....	464
McCarthy.....	466
McCrory.....	473
McEvelly.....	475
McEvelly.....	486
Michael.....	489

## EARTHQUAKE HAZARDS REDUCTION PROGRAM

### CONTENTS - VOLUME II

#### Goal II - Evaluating the potential of future earthquakes

Where are future earthquakes likely? How large will they be?  
How often will they occur? When will they occur? Where are  
future earthquakes unlikely?

Minster.....	491
Mooney.....	493
Mori.....	498
Mortensen.....	505
Morton.....	507
Munson.....	510
Nelson.....	512
Noller.....	519
Obermeier.....	521

Oppenheimer.....	525
Park, R.....	528
Park, S.....	529
Peppin.....	538
Plafker.....	542
Ponti.....	549
Potter.....	554
Prentice.....	560
Reasenbergs.....	563
Reilinger.....	570
Repetski.....	573
Rockwell.....	578
Roeloffs.....	579
Salyards.....	587
Sarna-Wojcicki.....	590
Sato.....	593
Schultz.....	599
Schwartz.....	604
Segall.....	607
Sharp.....	611
Shaw.....	619
Sieh.....	623
Silvernman.....	628
Sims.....	630
Sipkin.....	633
Smith.....	637
Snavely.....	643
Stein.....	648
Stewart.....	652
Swanson, D.....	655
Swanson, M.....	660
Sykes.....	662
Sylvester.....	665
Sylvester.....	669
Teng.....	673
Tinsley.....	681
Trehu.....	685
Tullis.....	686
Valentine.....	694
VanArsdale.....	695
Vaughn.....	698
Vernon.....	703
Vidale.....	705
Weaver.....	712
Wells.....	716
Wentworth.....	718
Williams.....	721
Wyatt.....	723
Wyss.....	728
Yeats.....	741
Yeats.....	744
Yeats.....	748
Zoback.....	749

### Goal III - Predicting the effects of earthquakes

During an earthquake of a certain magnitude, how severely and for how long will the ground shake? Where will hillsides slide, and flatlands fissure and crack? On what types of ground will earthquake damage be concentrated? Which faults will offset the Earth's surface? By how much? Which coastlines will be elevated or submerged? Where will destructive sea waves be generated? What losses to structures are expected?

Algermissen.....	755
Andrews.....	763
Arabasz.....	765
Bernknopf.....	766
Boore.....	768
Borcherdt.....	769
Borcherdt.....	771
Borcherdt.....	773
Brady.....	774
Brady.....	776
Breckenridge.....	777
Bundock.....	787
Celebi.....	789
Chang.....	790
Chang.....	796
Dieterich.....	802
Etheredge.....	805
Frankel.....	808
Gibbs.....	810
Goldhaber.....	811
Graves.....	819
Harp.....	824
Harty.....	825
Hartzell.....	830
Herrmann.....	841
Hutt.....	843
Liu.....	845
Lockner.....	847
Madin.....	854
McGarr.....	855
Mueller.....	858
Olshansky.....	862
O'Rourke.....	866
Palmer.....	873
Person.....	877
Peterson.....	881
Safak.....	882
Saikia.....	884
Sass.....	892
Schwartz.....	977
Shaw.....	614
Simpson.....	903



Sowers.....	905
Spudich.....	907
Spudich.....	910
Spudich.....	912
Taylor.....	914
Verkes.....	916

#### Goal IV - Using research results

What new hazard reduction strategies become possible as understanding of earthquake phenomena advances? What scientific information is needed and can be furnished to practitioners in the engineering, land-use planning and emergency managements communities? How can such information be most effectively communicated to these practitioners?

Bolton.....	917
Campbell.....	919
Choy.....	923
Day.....	926
Durkin.....	931
Dusseau.....	934
Goter.....	940
Herrmann.....	942
Holmes.....	948
Jacoby.....	951
Kulm.....	954
Marks.....	964
May.....	966
Mueller.....	967
Nishenko.....	968
Qamar.....	973
Rymer.....	975
Schwartz.....	977
Stark.....	979
Stokoe.....	985
Stover.....	989
Taggart.....	991
Tarr.....	992
Tinsley.....	995
Tuttle.....	998
Tyler.....	1000
Yamaguchi.....	1004
Yamaguchi.....	1006

Index 1: Alphabetized by Principal Investigator...1008

Index 2: Alphabetized by Institution.....1014

## Analysis of Seismic Data from the Shumagin Seismic Gap, Alaska

# 14-08-0001-G1981

Geoffrey A. Abers, Klaus H. Jacob  
Lamont-Doherty Geological Observatory of Columbia University  
Palisades, New York 10964  
(914) 359-2900

### Investigations

The mechanics of rupture on plate boundary faults remain poorly understood, but play a critical role in the nucleation and extent of major earthquakes. This is particularly true of subduction zones, where little local seismic data exist. The Shumagin network has recorded 10 years of digital seismic data within 0-100 km of the main Aleutian interplate thrust, with a variety of types of instruments. We analyze here the spatial distribution, mechanisms, and rupture processes of small-to-moderate ( $M < 5$ ) earthquakes, by using the local network seismic data. A primary task is to use empirical Green's function techniques to remove path effects in waveforms of moderate-sized earthquakes, by deconvolving from these seismograms the waveforms of small earthquakes from the same location and with the same mechanism. The resulting wavelets reflect the source behavior of the larger earthquakes, and can be quantified using a variety of standard measures (e.g., seismic moment, radiated seismic energy, duration, directivity, stress drop). We explore these measures and their variation between different parts of the main thrust zone, in order to document variations in the mechanical behavior of the interplate thrust. We are testing the possibility that variations exist between shallow and deep parts of the thrust zone, following the suggestion from teleseismic analyses that deeper earthquakes (40-50 km depth) have much higher stress drops than shallower events (25-35 km) closer to the trench. As a parallel part of this study, we analyze the spatial variability of seismicity and earthquake properties in regions near the main interplate thrust zone, in order to gain insight into the stress field at a subduction zone and of mechanical differences between the interplate thrust and the surrounding region.

### Results

1. A compilation of instrument response characteristics and polarities over time has been completed. This information is a necessary first step to quantitative analysis of earthquake size and signal frequency content. Previously unknown instrument characteristics were measured during the 1991 Shumagin field season, estimated from particle-motion studies, or determined from laboratory calibrations following the network removal (see report in this volume for cooperative agreement #14-08-0001-A0616, Seismic Monitoring of the Shumagin Seismic Gap, Alaska). Some strong differences existed from previously-used, nominal values. Several discrepancies were documented in horizontal-component orientation (checked with particle motion analysis), non-standard telemetry component gains (checked in laboratory tests, only a problem for two stations), and seismometer free periods (nominal 1 Hz instruments exhibited free periods varying from 0.9 Hz to 1.6 Hz). A data-base is nearly completed for the period of digital recording, 1982-1991.

2. Redetermined ray parameters, together with new picks, have been used to determine single-event fault plane solutions from Shumagin data. Ray parameters have been redetermined for the larger earthquakes using rays traced through a recently-determined laterally-varying velocity model, using the exact ray-tracing scheme used in the velocity inversion. Preliminary work has been done on shallow upper plate events, which provide evidence on the state of stress in the subduction zone and its mode of deformation. Results for upper-plate events (Figure 1) show both strike-slip and thrust mechanisms, in all cases with  $P$ -axes roughly perpendicular to the direction of plate convergence (one  $M=1.5$  normal-faulting event occurred as an aftershock 33 minutes after a  $M=4.6$  mainshock, and is not thought to represent long-term tectonic deformation). These earthquakes are all less than 20 km deep, and overlie both the interplate thrust zone and the deeper part of the descending seismic zone (Figure 1C). These mechanisms suggest that the maximum horizontal stress is perpendicular, rather than parallel to the arc in the forearc.

3. Two new methods have been developed for determining source pulses and rupture durations from empirical Green's function (EGF) data. The first method is direct inversion of the seismogram pairs for source duration. We assume a simple source model, such as a boxcar, ramp, or a "Brune" ( $k\tau e^{-t/D}$ ) source pulse parameterization (Figure 2A), and directly invert seismograms for the duration and amplitude of the pulse. Although the inversion is nonlinear the number of parameters being sought is small (one, usually), so fully nonlinear inversions are feasible. These inversions directly incorporate estimates of the uncertainties due to the model and due to the simplified parameterization, and calculate *a posteriori* probabilities for all values of source duration. The result is a complete nonlinear probability density function for source duration, which is used to investigate confidence limits (e.g., Figure 2B,C). Because the number of parameters are very small the method is usually robust, and provides a direct estimate of desired measures of the earthquake source. The method is being extended to incorporate multiple stations for the same event pair, and to determine rupture directivity as well average duration (a three parameter problem). The example shown in Figure 2 shows ~50% variations in duration between stations for a given rupture model, although the variation does not depend on a simple way with either distance or azimuth.

The second method is a time-domain deconvolution of EGF events from seismograms for larger earthquakes (Figures 3,4). In this approach the convolution of an EGF with a source pulse is directly inverted for the source pulse time series, similar to least-squares deconvolution methods used in seismic reflection processing. An inverse operator is constructed from the EGF seismogram, incorporating *a priori* estimates of uncertainties in the large event seismogram, the Green's function, and in the source pulse. The time-domain formalism allows *a priori* uncertainty estimates to be introduced in a natural way, and the strictly linear nature of the problem allows reasonable uncertainties and resolution estimates to be made. We find that small amounts of stabilization are considerably more effective using this procedure than using frequency-domain methods, allowing us to determine source pulses more reliably and for more events.

This approach has been found to be considerably more robust with respect to nonstationary errors in the Green's function (i.e., decreasing reliability of the Green's function with time into the record). In the synthetic-seismogram example shown on Figure 3, the phase of late arrivals seismograms is changed by increasing the depth 0.2 km. Increasing phase incoherence with time in the seismogram is often observed, and usually dealt with by careful windowing or selection of seismogram pairs by ad hoc visual comparisons of coherence. The time-domain inversions are able to correctly reproduce the early part of the seismogram that are not affected by EGF phase errors, because inversion for the early part of the seismogram is to first order independent of the later, incoherent part. By contrast, the frequency-domain inversion result is contaminated at all times. Similarly, deconvolution "errors" due to seismogram truncation produce relatively larger errors in the source pulse for frequency-domain deconvolutions than time-domain deconvolutions, even when the otherwise correct Green's function is used.

An example using Shumagin network data is shown in Figure 4. This data is recorded digitally at 100 samples per second with 12-bit samples, the sensors have a flat velocity response between ~1 Hz and 30 Hz. The same pair of events is used as in Figure 2, both aftershocks of a  $M=4.6$  upper-plate event in May, 1988. Resolution effects are shown by plotting rows of the resolution matrix corresponding to three representative times in the source pulse (Figure 4C, E). For the single-seismogram inversion the width of the resolution peak is 0.04-0.05 s and the peak becomes broader with increasing lag. These peak-widths are a significant fraction of the 0.15 s observed pulse duration, and suggest that finite resolution width may provide a minimum bound on observable source durations. A frequency-domain approach would not improve matters, as low-pass filtering and other stabilizers will also limit resolution of the source duration. One way around this problem is to invert several seismograms simultaneously for the same event-EGF pair (Figures 4D,E); the redundancy introduced here makes the resolution rows much more peak-like, at least for small lags. The primary difficulty with this approach is that duration is assumed constant at all stations, and directivity effects are ignored. For metrics such as stress drop that require a single source duration, the joint inversion probably provides a reasonable estimate.

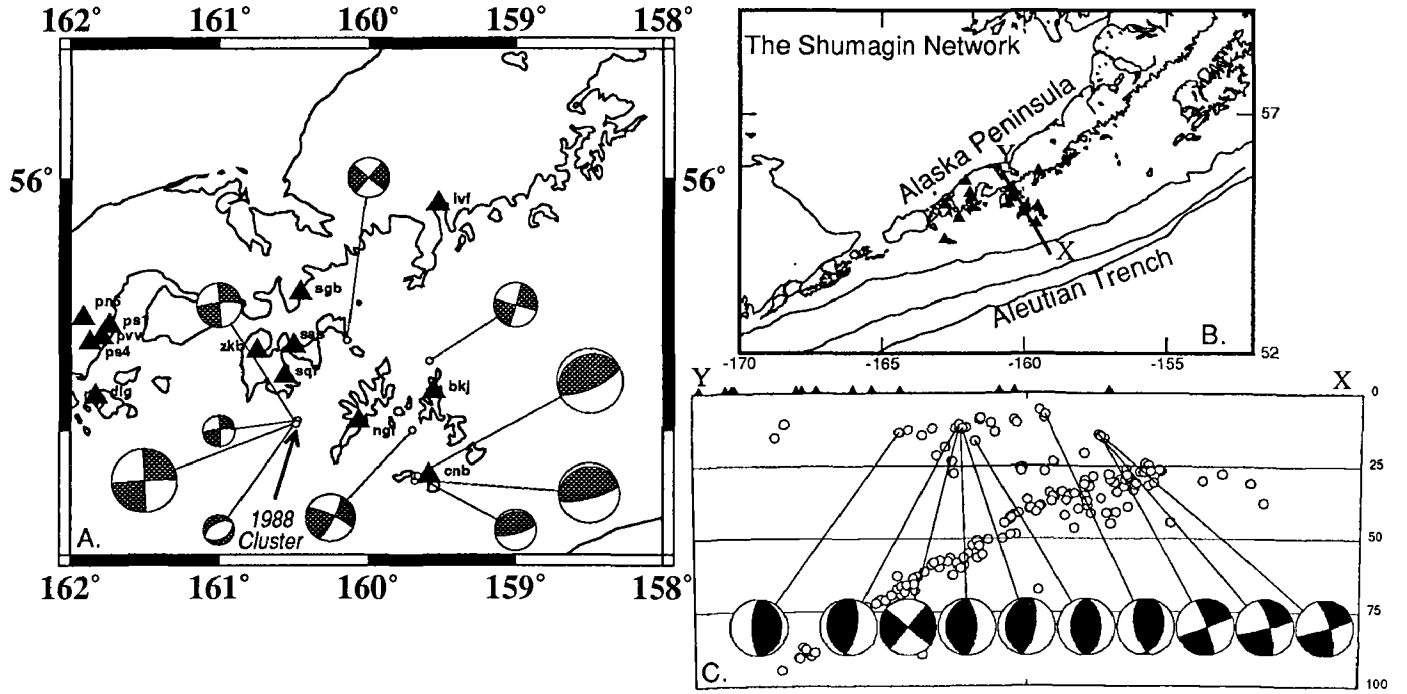


Figure 1. Fault-plane solutions for shallow, upper-plate earthquakes in the Shumagin Islands region determined from first motions. Fault plane solutions are determined for individual events, using ray parameters determined from exact ray-tracing through 3D velocity model. A. Map showing mechanisms and station locations. Fault-plane solutions are plotted as lower-hemisphere projections, and radii are scaled to magnitude (magnitudes range from 1.5 to 4.7). B. Location map, Y-X is cross-section location. C. Cross-section of seismicity. Depths in km at right. Earthquakes are relocated in 3D model; only stable locations are plotted. Fault-plane solutions are plotted in a back-hemisphere projection. Triangles show station locations, projected onto section.

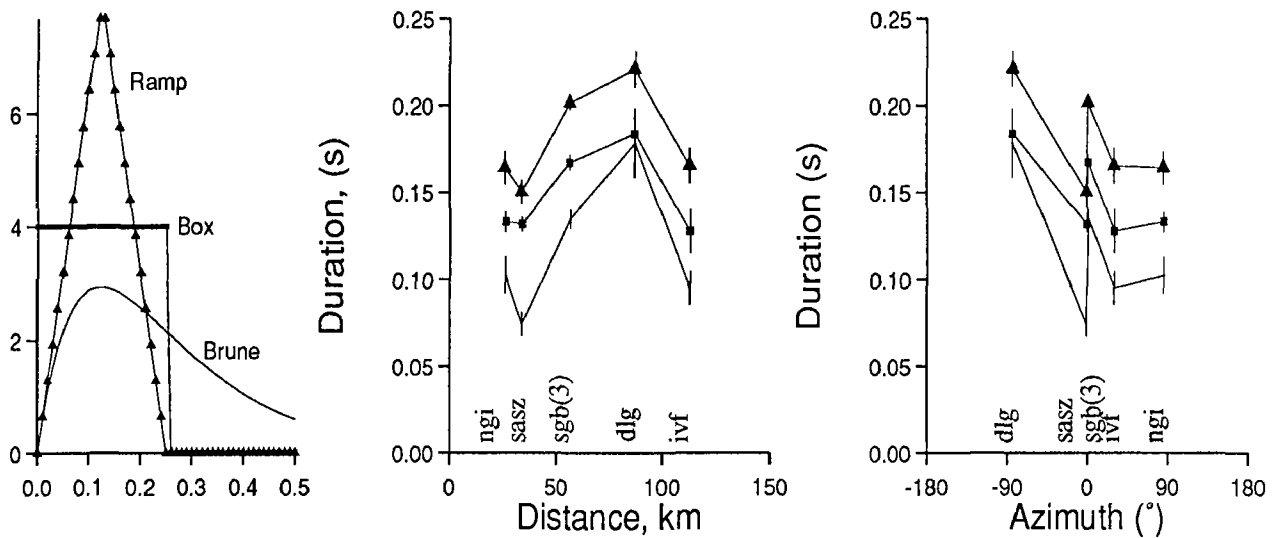


Figure 2. Single-parameter inversions for source duration. A. Shape of characteristic pulses used; all have 0.25s duration or 0.125s rise-time. B. Results for deconvolution of EGF for event in 1988 Cluster (Fig. 1A, Fig. 4) vs. distance of station; same stations as Fig. 4. Symbols are for different source models: triangle, ramp; square, box; none, "Brune". C. Same as B, plotted vs. azimuth to station. Calculation described in text. Errors are one-sigma, calculated from second moment of a posteriori probability density functions for pulse duration.

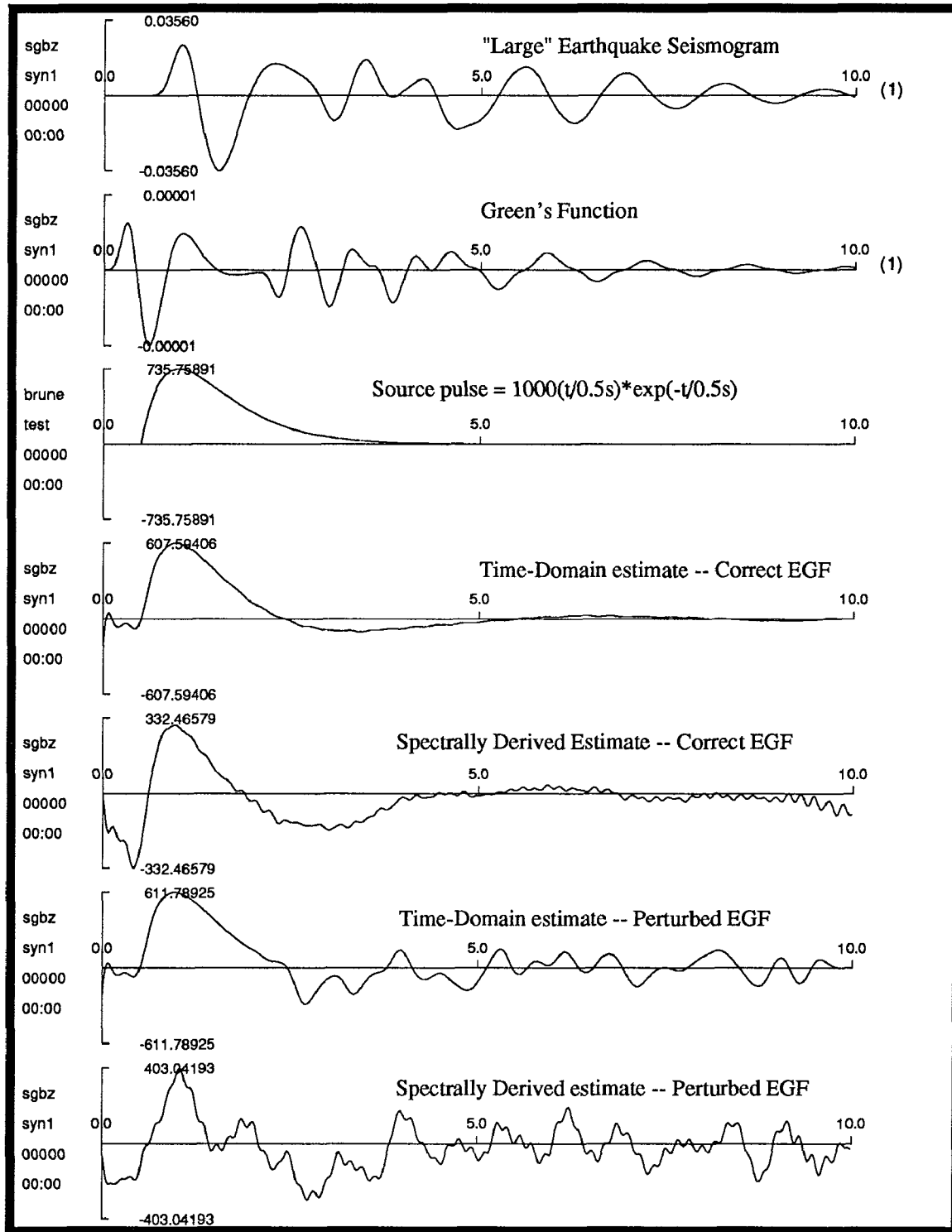


Figure 3. Tests of empirical Green's function (EGF) deconvolution using synthetic seismograms. The true Green's function TGF (second record) was calculated as a teleseismic event recorded by Shumagin network short-period sensors (flat response to velocity, 1-30 Hz). The receiver-structure was half-space, assumed source-region structure was 0.5 km thick water-layer over half space. Other parameters for TGF: source depth 2.5 km, ray parameter 0.08 s/km (for 30° distance), attenuation parameter  $t^*=0.6$  s; source duration of 0.01 s; thrust mechanism with 45°-dipping planes striking parallel to ray azimuth. The top seismogram was generated by convolving the TGF with the source pulse shown third from top. Fourth record is result of time-domain deconvolution of the top record from TGF, assuming a priori uncertainties typical of real data. The fifth record is the result of doing the same deconvolution by taking the ratio of complex spectra, low-pass filtering the result at 6.25 Hz, 1/4 the Nyquist frequency, with a 6-pole Butterworth filter. The bottom two source pulse estimates were made in the same way as the fourth and fifth records, except that a perturbed EGF was used. The perturbed EGF was calculated identically to the TGF, except the source depth was increased by 200 meters, resulting in phase errors at lag times greater than 2.0 s.



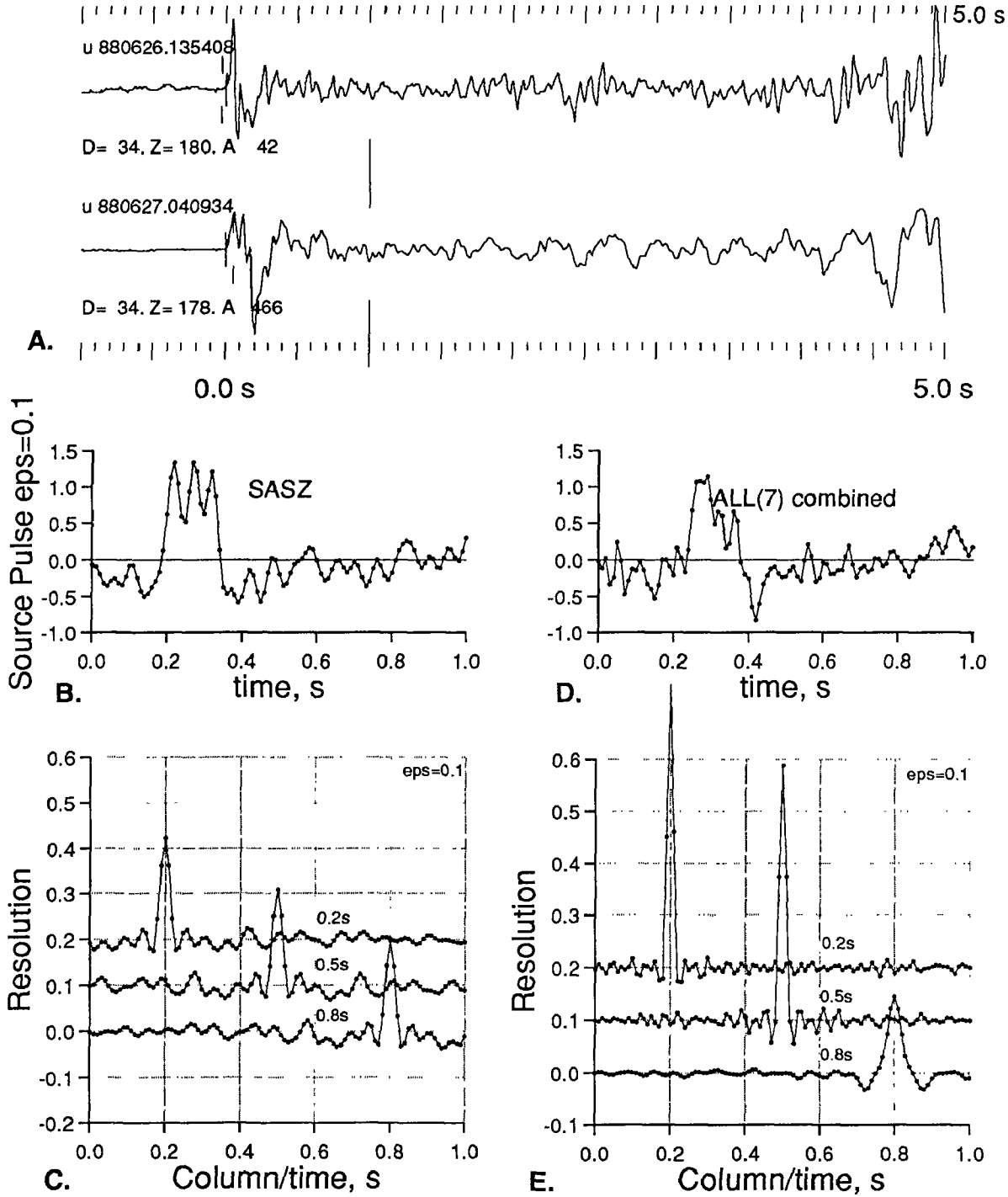


Figure 4. A. Example of a pair of seismograms from a colocated small (top) and large (bottom) event, recorded at station SAS (Sand Point) 34 km from the epicenter. Shumagin magnitudes are 1.9 and 2.7 for the top and bottom event. B. Resulting source pulse derived by time-domain deconvolution of the seismograms in A; only first second of P is used and signal-generated noise is assumed to be 10% of power in signal. C. Three selected rows in the resolution matrix for the inversion in B, corresponding to lags of 0.2, 0.5, and 0.8 s. A delta-function row with unit amplitude indicates that source pulse points are perfectly resolved; the width of the resolution rows indicate length of time over which true source pulse is being averaged to generate estimate in B. D. Same as B, except that 7 seismogram pairs are jointly inverted for a single source pulse (DLG, IVF, NGI, SASZ, and 3 components at SGB). The joint inversion averages over directivity effects; results of parameterized inversions show no systematic variation in rupture duration with azimuth or with distance. E. Same as C, for combined inversion.

Patterns of Slip Distribution at Depth and Stress Transfer Associated with  
Three Sequential Earthquakes Along the Calaveras Fault, California

Agreement No. 14-08-0001-G2063

Atila Aydin  
Department of Applied Earth Sciences  
Stanford University  
Stanford, CA 94305-2225

Phone (415) 725-8708  
Fax (415) 725-0979  
E-mail address: aydin@pangea.stanford.edu

The progression of slip and the associated stress field from one fault segment to the adjacent segment poses an interesting problem, with wide-ranging implications ranging from earthquake prediction to the nature of loading system in the upper crust. Three sequential moderate earthquakes, the 1979 Coyote Lake, the 1984 Morgan Hill and the 1988 Alum Rock, along the central Calaveras fault in the eastern San Francisco Bay Area (Figure 1) provide a unique opportunity to decipher the coseismic evolution of slip distribution and the perturbed stress field from one earthquake to the other.

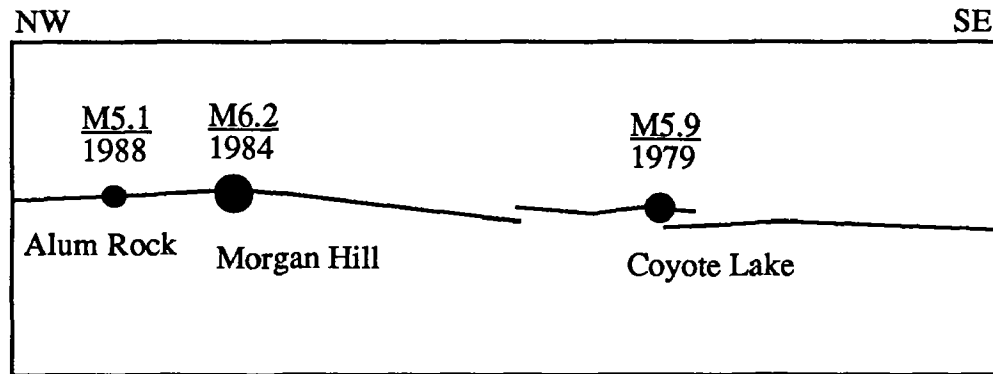


Figure 1. Three sequential earthquakes on the central Calaveras fault

We inverted coseismic geodetic data, recorded by the U.S. Geological Survey Network, for slip at depth for the Coyote Lake and Morgan Hill earthquakes using a 3-D elastic dislocation model in half space. We calculated the stress field corresponding to each displacement field, thus describing quantitatively the mechanical process of slip and stress transfer from one segment to the next during a given earthquake. The results, summarized in Table 1, are: (1) The average stress drops for the Coyote Lake, Morgan Hill and Alum Rock earthquakes are estimated to be 30, 25 and 15 bars, respectively. (2) The coseismic stresses at the hypocenters of the sequential main shocks are 0.1 bar for the Morgan Hill, and 0.5 bar for the Alum Rock induced by the Coyote Lake and the Morgan Hill earthquakes, respectively. These coseismic stress contributions from preceding earthquakes on the adjacent segments only account for a few percent of the whole stress drops, and are equivalent to the stress accumulation due to the remote tectonic loading (0.1 bar/yr based on previous investigations [Li and Rice, 1983; Tse et al., 1985]) in 1 to 5 years. Therefore, coseismic stress transfer does not contribute significantly to the whole stress accumulation. It, however, can trigger the adjacent earthquakes, in the sense that adjacent earthquakes would have occurred at a later time if there was no coseismic stress transfer. (3) The reported recurrence intervals for moderate earthquakes along the Coyote Lake, the Morgan Hill and the Alum Rock segments are 82, 73 and 45 years, respectively [Oppenheimer et al., 1990]. The corresponding

remote tectonic loading contributions, which are simply the product of the recurrence interval and the remote tectonic loading rate, are 8.2, 7.3 and 4.5 bars, and account for 27, 29 and 30% of the total stress drops, respectively. (4) These results imply that the most significant process of the stressing is due to the viscoelastic relaxation of the lithosphere and asthenosphere. Relaxation takes place vertically and laterally in such a way that earthquake-generated stress is transferred downward and upward as lower lithosphere and asthenosphere relax, and laterally to the adjacent segments. A large amount of stress accumulation due to relaxation also implies that the low viscosity layer or aseismic slip zone may extend up into shallow levels of the crust. (5) The average stressing rate, given by the average stress drop over the recurrence interval, is nearly constant (0.37 bar/yr for Coyote Lake, 0.34 bar/yr for Morgan Hill, and 0.33 bar/yr for Alum Rock). This suggests that the recurrence interval is determined by the stress drop, which is the characteristics of the so-called "time predictable model" of Shimazaki and Nakata [1980]. Interestingly enough, similar behavior was found for the small earthquakes with magnitudes ranging 3 to 4 along a 9-km-long segment of the central Calaveras fault zone [Bufe et al., 1977]. A manuscript including these results has been recently submitted to the Journal of Geophysical Research.

#### References

- Bufe, C. G., P. W. Harsh, and R. O. Burford, Steady-state seismic slip - a precise recurrence model, *Geophys. Res. Lett.*, 4, 91-94, 1977.
- Li V. C., and J. R. Rice, Precursory surface deformation in great plate boundary earthquake sequences, *Bull. Seism. Soc. Am.*, 73, 1415-1434, 1983.
- Oppenheimer, D. H., W. H. Bakun, and A. G. Lindh, Slip partitioning of the Calaveras fault, California and prospects for future earthquakes, *J. Geophys. Res.*, 95, 8483-8498, 1990.
- Shimazaki, K., and T. Nakata, Time-predictable recurrence model for large earthquakes, *Geophys. Res. Lett.*, 4, 279-282, 1980.
- Tse, S. T., R. Dmowska, and J. R. Rice, Stressing of locked patches along a creeping fault, *Bull. Seism. Soc. Am.*, 75, 709-736, 1985.

Table 1. Stress Decomposition for the 1979 Coyote Lake, 1984 Morgan Hill and 1988 Alum Rock Earthquakes

	<u>Coyote Lake</u> (1979)	<u>Morgan Hill</u> (1984)	<u>Alum Rock</u> (1988)
recurrence interval (T-yr)	82	73	45
remote tectonic loading rate (bar/yr)	0.1	0.1	0.1
average stress drop ( $\Delta\sigma$ , bar)	30	25	15
remote stress contribution (bar)	8.2	7.3	4.5
coseismic stress transfer (bar)	-	0.1	0.5
average stressing rate ( $\Delta\sigma/T$ , bar/yr)	0.37	0.34	0.33

**Investigation of Slip Localization in Large-Displacement Faults  
for Application to Laboratory Fault Modelling**  
USGS 14-08-0001-G19466

Ronald. L. Biegel<sup>1</sup> and Frederick Chester<sup>2</sup>

<sup>1</sup>*Lamont-Doherty Geological Observatory of Columbia University  
Palisades, New York 10964*

<sup>2</sup>*Department of Earth and Atmospheric Sciences  
St. Louis University  
3507 Laclede Ave.  
St. Louis University 63103*

A set of thin sections have been made from samples of fault rock collected across the width of the San Andreas and San Gabriel faults. Results show that the fault zone is internally zoned. Fault cores consist of an ultracataclasite layer bounded by zones of damaged and brecciated rock. The grain size distribution away from the center of the fault is fractal suggesting gouge deformation at that distance is described by a constrained comminution model (Sammis et al., 1987). Closer to the core the fractal distribution breaks down due to the action of other mechanisms. In the cores, cataclastic and fluid assisted processes were significant as shown by pervasive syntectonic alteration of the host rock minerals zeolites and clays, and by folded and sheared cross-cutting veins. Total volume of veins and neocrystallized material reaches 50% in the fault core, implying episodic fracture and healing with time.

These results were presented to the Spring '91 AGU conference in Baltimore (Biegel et al, 1991). A fault model incorporating these features was presented at the Fall '91, GSA conference in San Diego (Chester et al., 1991) and a manuscript is now in preparation.

### References

Biegel, R.L., F.M. Chester, and J.P. Evans, Cataclasis and slip localization in the San Gabriel Fault, southern California, *Trans. Am. Geophys. Union*, 72, 264, 1991.

Chester, F.M., J.P. Evans, and R.L. Biegel, Internal structure and weakening mechanisms of large-displacement faults of the San Andreas system, *Geol. Soc. Am., Abstracts*, 23, 103, 1991.

Sammis, C.G., G. King, and R.L. Biegel, The kinematics of gouge deformation, *Pure Appl. Geophys.*, 125, 777-812, 1987.

# SEISMIC SOURCE ANALYSIS USING EMPIRICAL GREEN'S FUNCTIONS

**9910-02676**

John Boatwright and Leif Wennerberg  
Branch of Engineering Seismology and Geology  
U.S. Geological Survey  
345 Middlefield Road, MS 977  
Menlo Park, California 94025  
415/329-5609, 5659 or FTS/459-5609, 5659

## Investigations

Our research has focused on extending the Green's function technique to separate source and site spectral characteristics from multiple recordings of moderate-sized earthquakes. We have devised and applied a series of inversions to recordings of the aftershocks of the 1989 Loma Prieta earthquake.

## Results

- 1) The relative site response has been determined as a function of frequency for a set of eleven stations in and around the Marina District in San Francisco. The seismic amplification of six stations within the Marina District appears remarkably consistent relative to a nearby station at Fort Mason, sited on Franciscan Sandstone. The Marina stations exhibit a peak at 1 Hz amplified by a factor of 6-10 and a broad sidelobe at 2-3 Hz amplified by a factor of 3-4. Two stations sited just outside the Marina on dune sands do not exhibit the strong low-frequency peak in amplification.
- 2) We have devised a new method of empirically determining site response and source spectra by fitting Brune models conditioned by a frequency independent  $Q$  to the recordings, and projecting the residuals on the sites. This analysis has been applied to four San Francisco stations using epicentral distances of about 100 km, and four accelerograph sites which recorded the Loma Prieta main shock at epicentral distances from 2-25 km, by Boatwright, *et al.* (1991). The absolute site amplifications are fixed through frequency-specific geotechnical constraints. The epicentral studies determined  $Q = 380$  and  $414$  for S and P waves, respectively. The stress drops of the 28 aftershocks did not vary as a function of seismic moment for earthquakes with  $M_0 < 10^{21}$  dyne-cm.



- 3) We have extended this spectral inversion technique to analyze the geometrical and anelastic attenuation using a line of stations sited along the axis of the San Francisco Peninsula from the Santa Cruz Mountains up to San Francisco. After fitting the sources and attenuation, the residuals are projected onto the set of stations and to a set of distances, resulting in a map of residual attenuation as a function of distance and frequency. The residual attenuation for the P and S waves is surprisingly similar. There are a series of troughs and peaks which are reasonably constant over frequencies  $> 5$  Hz in the distance range from 30 to 60 km, which are assumed to represent arrivals which have been critically refracted from a series of velocity discontinuities from 10 to 20 km in depth. Then a broad region of relatively little variation extends from 60 to 90 km at high frequencies; there are some weak peaks and holes for frequencies  $< 3$  Hz. Finally, there is a strong peak at low frequency ( $\approx 1$  Hz) at 100 km which is at a slightly further distance than a broad amplification at frequencies  $> 15$  Hz, but it is unclear whether this high-frequency amplification corresponds to a critically refracted arrival or to a frequency dependence of the attenuation.

### Reports

Boatwright, J., Seekins, L.C., and Mueller, C.S., Seismic amplification in the Marina District: *Bulletin of the Seismological Society of America*, in press.

Boatwright, J., Fletcher, J.B., and Fumal, T.E., A general inversion scheme for source, site, and propagation characteristics using multiply recorded sets of moderate-sized earthquakes: *Bulletin of the Seismological Society of America*, in press.

Fletcher, J.B., and Boatwright, J., Geometric and anelastic attenuation along the San Francisco Peninsula inferred from a joint inversion of digital seismograms: submitted to *Bulletin of the Seismological Society of America*.

## **Analysis of the 1957 Andreanof Islands Earthquake**

Award number 14-08-0001-G1766

Thomas M. Boyd  
Colorado School of Mines  
Department of Geophysics  
Golden, Colorado 80401

### **Project Summary and Goals**

Recent studies have indicated that the spatial distribution of moment release can be quite heterogeneous along any particular rupture zone. The most common explanation for this heterogeneity has been the rupture of strong patches, or asperities, along the fault plane [e.g., Ruff and Kanamori, 1983]. These strong patches could arise from spatial variations of the frictional characteristics along the fault or from geometrical barriers inherent to the fault's shape. Alternatively, the spatial distribution of moment release could have little to do with the physical characteristics of the fault's surface and may be related to the dynamics of slip and how regions of the fault interact with neighboring regions [e.g., Rundle and Kanamori, 1987; Horowitz and Ruina, 1989].

Distinctions between these two models can not be made from the analysis of single events [e.g., Thatcher, 1990]. Conclusive observations can only be drawn from a study of the moment-release distribution generated by several great earthquakes, all of which rupture the same fault segment. In this context, an excellent region of study is the central Aleutian Arc. In 1986, a magnitude 8.0 ( $M_w$ ) earthquake occurred near the Andreanof Islands. Its slip distribution, aftershock, and preshock sequence have been described in detail in a number of recent studies. Prior to 1986, the central Aleutian Arc was ruptured by another great earthquake in 1957 ( $M_w > 8.5$ ). The 1957 Andreanof Islands earthquake, however, remains poorly understood. Its seismic moment, slip distribution, and rupture area have not been well constrained.

The short time span between the 1957 and 1986 earthquakes provides us with a unique opportunity to study a complete seismic cycle bounded by two instrumentally recorded great earthquakes. In fact, it represents the only complete seismic cycle instrumentally observed along the Aleutian Arc. As briefly described in this annual report, we have assembled and begun interpreting observations pertinent to the 1957 earthquake and the interseismic period between the 1957 and 1986 events. During the current reporting period, we have scanned and relocated all of the seismicity listed in the *BCIS* and *ISS* for the years 1957 thru 1963, and listed in the *ISC* for the years 1964 through 1989.

### **Seismicity Relocations and Magnitudes**

Using the slab geometry described by Boyd and Creager [1991] and Creager and Boyd [1991] we have calculated *P-wave* travel-time perturbations to 686 stations as a function of epicentral position. The calculated residuals are used directly as epicentrally varying

station corrections to generate relocated epicenters without additional ray tracing. We use this procedure to relocate all of the shallow seismicity, listed in the *BCIS*, *ISS*, and *ISC* bulletins that occurred between 160°W and 175°E longitude between the years 1957 and 1989.

Travel-time observations for the period between 1957 and 1963 do not exist in computer readable format. These observations have been optically scanned and reformatted for our analysis. Also magnitudes for many of the events listed in the *ISS* and *BCIS* bulletins are not known. In order to determine the distribution of earthquake sizes, we have determined magnitudes for as many of these events as possible using microfilms of the Pasadena seismograms stored at the USGS microfilm archives in Denver. Using the standard relationships for magnitude determination, we determined  $M_S$  using the maximum amplitude on the vertical component of the long-period Benioff instrument, for the period range 18 - 22 seconds, and  $m_b$  using the maximum amplitude of the P-wave train (usually within the initial 20 seconds) on the vertical component of the short-period Benioff instrument. Discussions on the appropriateness of this approach are given by Abe [1981] and Geller [1976].

Our relocated earthquakes form a catalog of 7359 events. Of these 7359 events, 4845 are well located (i.e., their locational standard errors are less than 25 km). Of the 4845 well located earthquakes, 4471 have magnitudes. Figure 1 shows a cumulative magnitude plot for the entire data set.

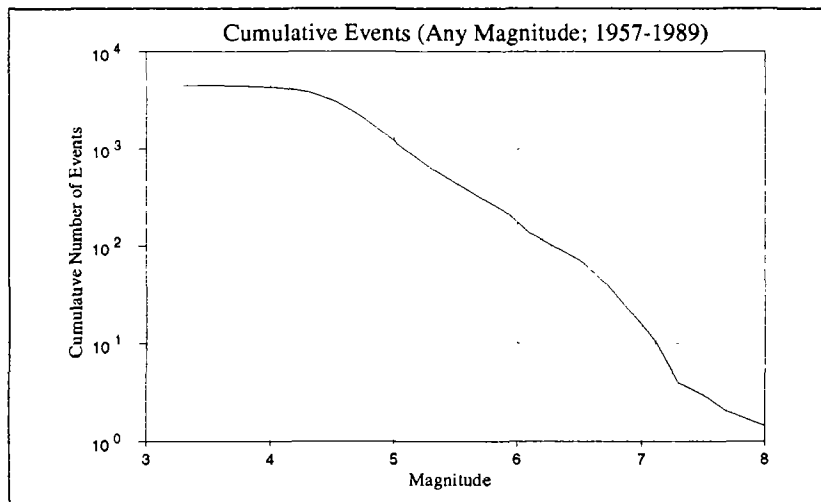


Figure 1: Cumulative number of events for the entire catalog. All, well located, events occurring from 1957 through 1989 have been included. Any reported magnitude is used. Preference is given first, however, to reported  $M_S$ . If  $M_S$  is not reported,  $m_b$  is used.

Based on this figure, it appears as though our catalog is homogeneous down to magnitude 4.5. As shown in Figure 2, however, before the advent of the WWSSN, a

higher level of homogeneity is apparent in the data.

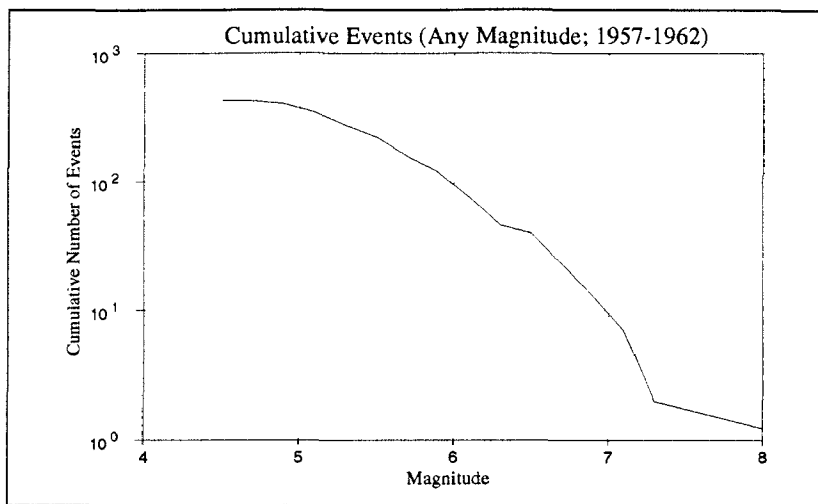


Figure 2: Cumulative number of events for all, well located, events occurring from 1957 through 1962. Any reported magnitude is used. Preference is given first, however, to reported  $M_S$ . If  $M_S$  is not reported,  $m_b$  is used. Most magnitudes have been determined in this study using records from Pasadena.

For this earlier time period, the level of homogeneity appears to be about 5.5.

Figure 3 shows our relocations of the earthquake activity recorded between the 1957 and 1986 events. All events whose magnitudes are greater than 5.4 and whose depths are less than 70 km are plotted. Figure 4 shows our relocations of the seismic activity immediately proceeding the 1986 event.

Note that there is an apparent gap in seismicity between the 1957 and 1986 events just south of Amilia Island ( $174.5^\circ\text{W}$ ). After the 1986 event this gap is filled with seismicity and activity commences north of Amilia Island. We tentatively interpret these observations as indicating the region south of Amilia Island, which ruptured during the 1986 event, did not have a significant amount of slip during the 1957 event. This speculation may be confirmed from the analysis of tsunami observations being undertaken by Johnson and Satake [1991].

A preliminary description of the earthquake catalog we have created will be presented at the Fall, 1991 AGU meeting in San Francisco [Boyd et al., 1991].

1957 Event through 1986 Event:  $M > 5.4$   $z < 70$  km

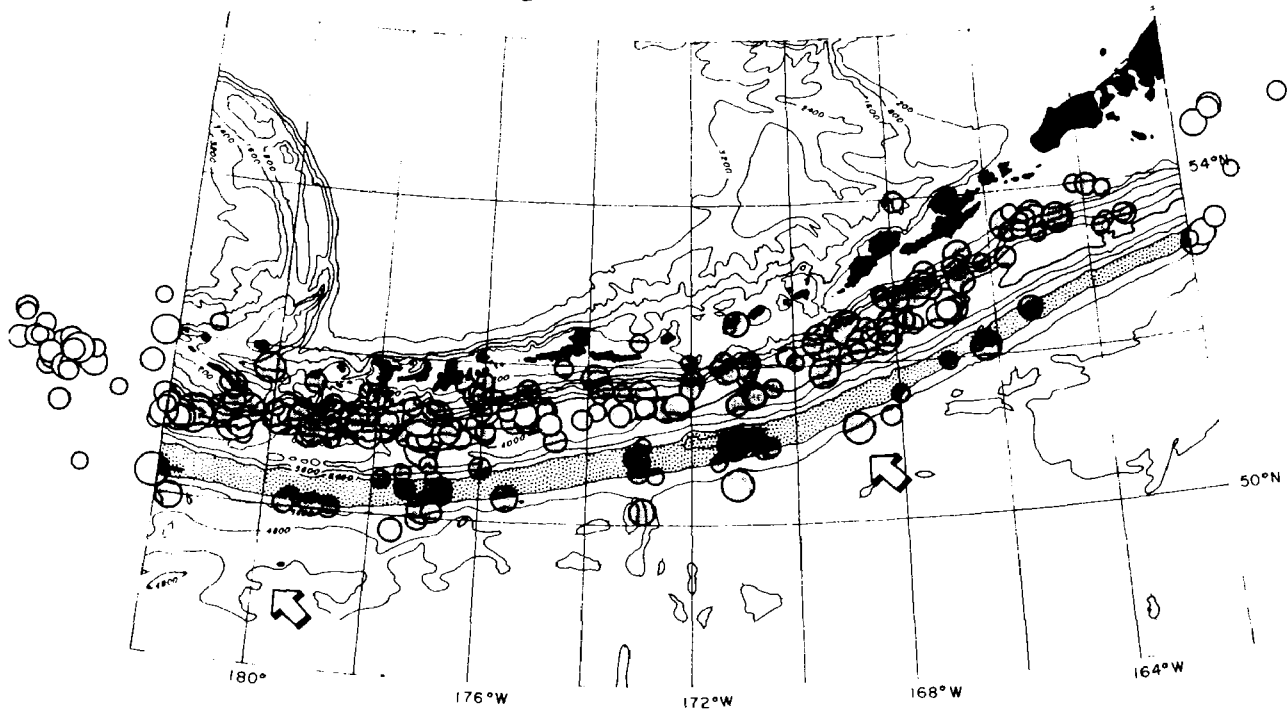


Figure 2: Seismicity occurring between the 1957 and 1986 events.

Post 1986 Event:  $M > 5.4$   $z < 70$  km

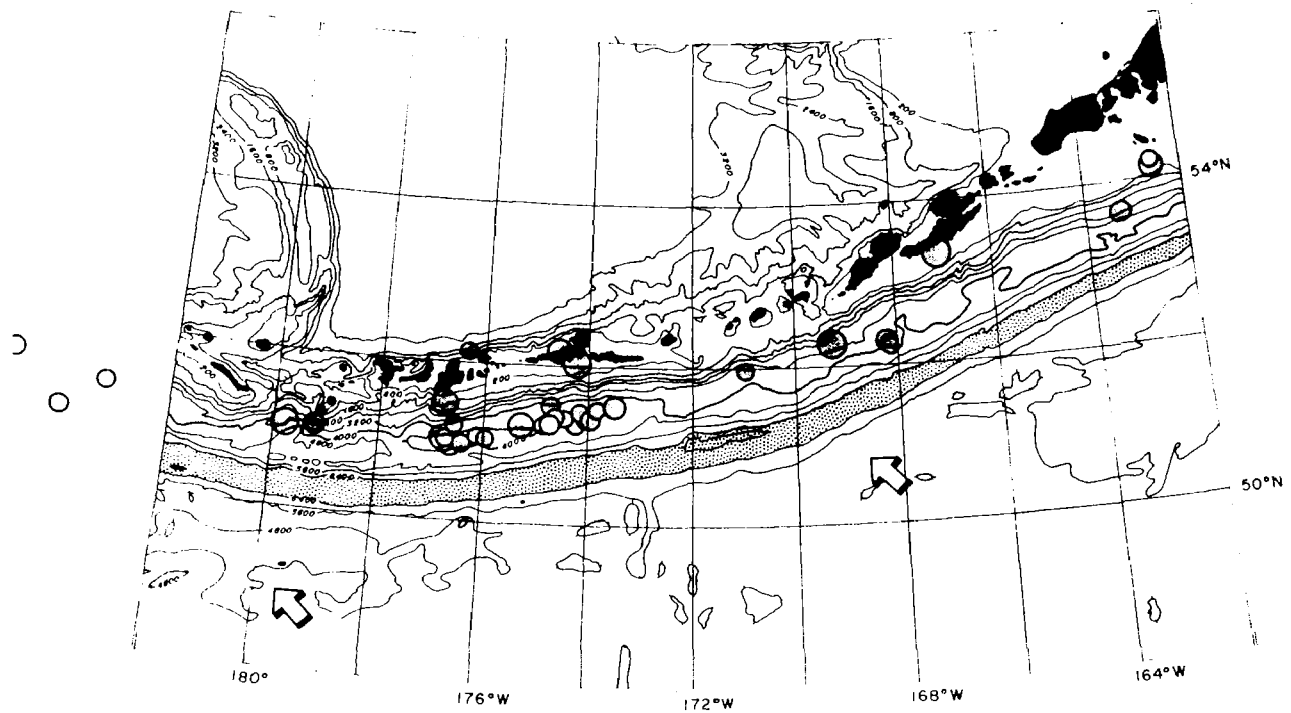


Figure 3: Seismicity occurring after the 1986 event.



## References

- Abe, K., Magnitudes of large and shallow earthquakes from 1904 to 1980, *Phys. Earth Planet. Int.*, 27, 72-92, 1981.
- Boyd, T. M., and K. C. Creager, The geometry of Aleutian subduction: Three-dimensional seismic imaging, *J. Geophys. Res.*, 96, 2267-2291, 1991.
- Boyd, T. M., E. R. Endgahl, and W. Spence, Aleutian earthquake catalog: 1957 through 1989, *EOS*, 72, 348, 1991.
- Creager, K. C., and T. M. Boyd, The geometry of Aleutian subduction: Three-dimensional kinematic flow model, *J. Geophys. Res.*, 96, 2293-2307, 1991.
- Geller, R. J., Scaling relations for earthquake source parameters and magnitudes, *Bull. Seism. Soc. Amer.*, 66, 1501-1523, 1976.
- Horowitz, F. G., and A. Ruina, Slip patterns in a spatially homogeneous fault model, *J. Geophys. Res.*, 94, 10,279-10,298, 1989.
- Johnson, J. M., and K. Satake, Use of tsunami waveform data to determine the source area of the 1957 Aleutian earthquake, *EOS*, 72, 384, 1991.
- Ruff, L., and H. Kanamori, The rupture process and asperity distribution of three great earthquakes from long-period diffracted P-waves, *Phys. Earth and Planet. Inter.*, 31, 202-230, 1983.
- Rundle, J. B., and H. Kanamori, Application of an inhomogeneous stress (patch) model to complex subduction zone earthquakes: A discrete interaction matrix approach, *J. Geophys. Res.*, 92, 2606-2616, 1987.
- Thatcher, W., Order and diversity in the modes of Circum-Pacific earthquake recurrence, *J. Geophys. Res.*, 95, 2609-2624, 1990.

## Earthquake Hazard Investigations in the Pacific Northwest

14-08-0001-G1803

R.S. Crosson and K.C. Creager  
Geophysics Program  
University of Washington  
Seattle, WA 98195  
(206) 543-8020

April 1, 1991 - September 30, 1991

### Investigations

This research focuses on earthquake hazards in the Pacific Northwest, including large scale plate interactions, through the study of regional structure and tectonics. Current investigations by our research group include determining the configuration of the subducting Juan de Fuca plate, kinematic modeling of the minimum strain-rate configuration of the plate, and determining source moments of local earthquakes.

#### *Deep three-dimensional velocity structure of the Cascadia Subduction zone:*

A recently completed doctoral dissertation investigated the large scale velocity structure of the upper mantle (VanDecar, 1991). The findings of this study include the identification of a seismically "fast" (3-4% velocity perturbation) planar feature that dips steeply to the east (at approximately 60°) with a thickness of 100 km or less. This is inferred to be the seismic manifestation of the thermal and compositional anomaly associated with the subducting Juan de Fuca oceanic plate. At shallow depths (less than about 80 km) this feature is consistent with the projections of models of shallow slab structure. The high velocity zone is located at a depth of 100-120 km beneath the Cascade volcanos, consistent with other subduction zones. Under central and northern Washington the high velocity feature extends to depths of 400 km or more, while beneath southern Washington and Oregon, it dies out at much shallower depths. This apparent lack of deep slab material in Oregon and southern Washington, when considered with the tectonic history of the region and other geophysical observations, is consistent with a deep slab that has torn away from the shallow portion of the slab.

#### *Kinematic Modeling:*

A recently completed doctoral dissertation on the geometrical configuration of the subducting slab flow-field that produces the minimum total strain-rate (Chaio, 1991), found that for Cascadia, the proposed arch structure revealed by seismic observations is a natural consequence of the subducted slab responding to the concave-oceanward bend of the trench. The arch also provides a plausible explanation for the origin of the Olympic Mountains accretionary prism in the context of the "critical taper" theory. The concentration of seismicity beneath the Puget Sound area may be the result of bending the already arched slab. The computed deformation rate is dominated by N-S compression in the Puget Sound area and the peak compressional strain-rate is around  $2 \times 10^{-16} \text{ sec}^{-1}$ , which is comparable to the value estimated from the seismic moment release rate of the last century. In both the Alaska-Aleutian and NW-Pacific subduction zones, preliminary experiments performed also indicate that the predicted arch structures are the natural results of slabs subducting in a concave-oceanward trench geometry.

#### *Source moment estimation and magnitude determination through use of S-coda amplitude:*

Magnitude determinations using regional and local (mainly vertical component) short-period data remain problematical. The most common approach, using S-wave coda duration, is subject to noise level variations that compound the inherent difficulty of assigning duration times. Signal frequency variations also add considerable problems. We have found the machine algorithms to automatically assign coda durations are far from satisfactory.

To alleviate the limitations of the coda duration magnitude, we are developing a method to base magnitudes on coda amplitude rather than duration. Using standard coda amplitude models based on scattering theory (e.g. Aki and Chouet, 1975), we can relate the amplitudes back to the source spectrum and hence directly to moment. Magnitudes can then be derived directly from the moment estimates.

We are currently using a single scattering model to source-equalize the coda amplitude measurements from a number of stations for each event. We have found that using a large number of stations in a least squares estimation results in stable estimates of relative station gains and relative source factors. Source factors estimated in this way are linearly related to magnitudes estimated from coda durations. While we could empirically estimate magnitudes at this point, we are seeking an improved understanding of the source scaling that will allow us to make valid moment measurements using coda amplitudes.

### Articles

- Lees, J.M. and R.S. Crosson, (in press), Bayesian ART versus conjugate gradient methods in tomographic seismic imaging: An application at Mount St. Helens, Washington, AMS-SIAM: Conference on spatial statistics and imaging - June, 1988.
- Ma, Li, R.S. Crosson, and R.S. Ludwin, (submitted), Preliminary Report on Focal Mechanisms and stress in western Washington, in: USGS Professional Paper "Assessing and Reducing Earthquake Hazards in the Pacific Northwest")
- Mundal, I., M. Ukawa, and R.S. Crosson, 1991 (in press), Normal and anomalous P phases from local earthquakes, and slab structure of the Cascadia Subduction zone, BSSA

### Abstracts

- Chiao, L.Y., and K.C. Creager, 1991, Geometry and membrane deformation rate of the subducted Cascadia slab, EOS, V. 72, # 44, p. 314.
- VanDecar, J.C., R.S. Crosson, and K.C. Creager, 1990 (in press), Teleseismic travel-time inversion for Cascadia subduction zone structure employing three-dimensional ray tracing (extended abstract), presented at the XXII General Assembly, European Seismological Commission, Barcelona, Spain, Fall, 1990.
- VanDecar, J.C., R.S. Crosson, and K.C. Creager, 1991, Inferences on the tectonic evolution of deep Cascadia subduction zone structure, Vienna 1991 IUGG meeting, IUGG IASPEI Programs and Abstracts, p. 163.
- VanDecar, J.C., R.S. Crosson, and K.C. Creager, 1991, Tectonic inferences from the three-dimensional upper mantle velocity structure of the Cascadia Subduction Zone, EOS, V. 72, # 44, p. 326.

### Theses

- Chiao, L.Y., 1991, Membrane deformation rate and geometry of subducting slabs, Doctoral dissertation, University of Washington Geophysics Program, Seattle WA
- VanDecar, J.C., 1991, Upper-mantle structure of the Cascadia Subduction Zone from non-linear teleseismic travel-time inversion, Doctoral dissertation, University of Washington Geophysics Program, Seattle WA

## Stressing, Seismicity and Rupture of Slip-Deficient Fault Zones

14-08-0001-G1788

R. Dmowska and J. R. Rice (PI)

Division of Applied Sciences and Department of Earth and Planetary Sciences,  
Harvard University, Cambridge, MA 02138  
(617) 495-3452 and 3445

### Investigations:

- 1.1 Influence of asperities along subduction interfaces on the stressing and seismicity of adjacent areas.
- 1.2 The effective viscosity of the San Andreas fault beneath the seismogenic zone: Constraints from the response to the 1989 Loma Prieta earthquake
- 1.3 Configurational stability of the uniform upward growth of a shear crack along a strike-slip fault zone, and sources of spatio-temporally complex slip
- 1.4 First order perturbation solution for a dynamic planar crack with a non-uniformly moving front

### Results:

2.1 We have investigated the influence of large-scale fault inhomogeneities, in large subduction earthquakes, on the style of deformation and seismic behaviour of the incoming oceanic plate and of the slab at intermediate depths during the earthquake cycle (Dmowska and Lovison, 1991).

The zones of the large subduction events of Rat Islands 1965, Alaska 1964 and Valparaiso 1985 were searched for earthquakes with  $m_b \geq 5.0$ , if available, and for as long time periods as possible. It was found that in general the seismicity in the incoming oceanic plate clusters in front of asperities (=areas of highest seismic moment release and strongest locking) and is positioned relative to them in the direction of plate motion. Our studies had previously shown that the outer-rise areas where seismicity clustered, while located near to the asperities, often had small trench-parallel offsets from them. However, by considering the direction of plate convergence, we found in all cases studied that the trench-parallel offsets were in the same sense as the angle between a line perpendicular to the trench and the direction of ocean floor convergence. That is, the active areas were located by proceeding oceanward from the asperities approximately along a line aligned with the direction of convergence.

Seismicity is usually lacking in areas adjacent to non-asperities, that is to zones that slip during the main event but with appreciably smaller seismic moment release, and possibly slip seismically/aseismically during the whole cycle. Similar behaviour occurs in the downgoing slab at intermediate depths, where seismicity during the cycle clusters (but less strongly than in the oceanic crust) next to asperities and down dip from them, at locations oriented approximately along the convergence direction. We infer that the locking of asperities causes higher stresses associated with the earthquake cycle itself to occur in areas adjacent to asperities, both updip and down dip from them along the direction of plate motion, and that such stressing is much less pronounced in the areas adjacent to non-asperities; this is to be a subject of future numerical modeling. The work opens the possibility of identifying the areas of highest seismic moment release in future subduction earthquakes, and carries implications for where the highest deformation and, possibly, precursory phenomena and/or nucleation of a future event might occur.

2.2 Recent geodetic observations (Lisowski et al. abstract, *AGU Fall Meeting*, 1991) indicate that the velocity field at the earth's surface has been perturbed by the Loma Prieta earthquake. We (Linker and Rice, 1991) interpret this change in terms of a model in which transient postseismic slip occurs deep in the crust along the San Andreas fault beneath the locked, or slipped and re-locked, seismogenic portion of the fault zone. In the first 1.3 years since the

earthquake, as much as 30 mm of fault-trace-parallel postseismic displacement had been observed beyond that expected by extrapolation of the previously established secular rate. The majority has occurred to the SW of the surface trace of the San Andreas fault, consistent with our model of buried postseismic slip on a SW dipping fault.

In our 3D finite element calculations, using ABAQUS, the crust and upper mantle are represented by an elastic region. The San Andreas fault is represented by a thin layer in which the shallow region is either locked or is slipped coseismically and then re-locked, and the deep aseismic region is treated as linear Maxwell viscoelastic. Coseismic slip produces stress throughout the body. Given time, the viscoelastic lower portion of the fault shears in response to those stresses, producing displacements at the free surface that can be compared to the geodetic observations. Comparison of our model prediction to the observed postseismic displacements provides a constraint on the ratio of Maxwell relaxation time for material in the deep aseismic region of the fault zone and the fault-normal thickness,  $t_m/h$ , but neither quantity can be constrained independently.

We obtain  $0.07 \leq t_m/h \leq 0.26$  yrs/km, which is consistent with the value determined by Fares and Rice (abstract T32B-07, *AGU Fall Meeting*, 1988) for their asymmetric model of postseismic deformation in Northern California in response to the 1906 earthquake. In their model,  $h$  was taken to be the vertical thickness of a lower crustal asthenosphere, but our estimate here indicates that their crustal asthenosphere might equally well be represented by a horizontal detachment fault. If we assume that postseismic slip has occurred in a 1 km thick fault zone, then using  $G = 3 \times 10^{10}$  Pa and our estimate for  $t_m/h$ , we obtain  $6 \times 10^{16} \leq \eta_{\text{eff}} \leq 3 \times 10^{17}$  Pa-sec for the effective viscosity of material in the deep aseismic region of the fault zone. Previous estimates made for the material of the lower crust exceed this range by at least a factor of ten. However, if we accept levels of elevated pore pressure compatible with the Lachenbruch and Sass heat flow constraint, then our estimate of  $t_m/h$  is in the range that could plausibly be met by Stesky's (Ph.D., MIT, 1975) and Blanpied et al.'s (GRL, 1991) lab derived parameters for frictional sliding at elevated temperature.

**2.3(a)** Plate boundaries and major intraplate fault zones usually do not rupture along their entire length in a single great earthquake, but rather fail as quasi-independent fault segments. A fundamental question which we are trying to address here, and also in a different way in the study described in (b) below, is whether this segmentation is due entirely to nonuniformities along strike in fault zone geometry (jogs, offsets), lithology or loading, or whether such tendency for segmentation is inherent to the earthquake process and would result even if geometry, material properties and loading were uniform along strike. This issue can be addressed for a given class of fault models by assuming that there is uniformity in the along-strike direction, devising the solution in which the stress and slip distributions along the fault zone vary with depth but not along strike, and then examining the configurational stability of that solution. The stability analysis is necessarily 3D in character.

Gao, Rice and Lee (1991a,b) have carried it out as summarized here for a highly simplified fault model, consisting of an upwardly growing mode III shear crack along a strike-slip fault zone. That is, we modeled the deeper, more stably sliding, portions of the fault zone as a slipping shear crack which penetrates upward from depth and is blocked in the lower portions of the seismogenic layer. Using a first order perturbation scheme aided by 3D finite element calculations, we analyzed whether a perfectly straight crack front, parallel to the Earth's surface, is configurationally stable against small perturbations from uniformity in the along-strike direction, i.e., if the crack front will tend to remain straight as the crack penetrates upward from depth. It was found that for infinitesimal periodic crack-front perturbations with wavelength beyond a critical value, on the order of the elastic lithospheric thickness, the stress intensity factor is higher at the most advanced portions of the crack front than at the least advanced. The opposite is true at shorter wavelengths. This means that the straight crack front is configurationally unstable at long wavelengths when resistance to crack growth (fracture toughness) is essentially uniform over the fault plane, i. e., uniform with respect to depth as well as along strike. The analysis also shows, however, that an

upward gradient in fracture toughness will stabilize the straight crack front configuration to longer wavelengths, and that a sufficiently strong gradient may completely stabilize it. Such an upward gradient might be reasonably assumed within the model for a crack that is penetrating under increasing load into the base of the seismogenic zone.

**2.3(b)** The goal in this phase of the work is also to understand what kinds of fault models do or do not allow the development of spatio-temporally complex slip histories. Work accomplished so far (Rice, 1991 a,b) has been on computational analysis of slip on a long vertical strike-slip fault between elastically deformable crustal blocks. These are driven such that each point on the fault moves, in long-term average, at an imposed "plate" velocity. The analysis is done by rigorously incorporating 3D elastic interactions between the slip and stress distributions, through boundary integral equation methods based on the Chinnery solution. Rate- and state-dependent friction applies on the fault surface, and  $A-B [= Vd\tau_{ss}(V)/dV]$  varies with depth, in a way specifically constrained by data on granite under hydrothermal conditions (Blanpied et al., GRL, 1991), being negative in the cool/shallow crust and positive in hot/deeper regions ( $V$  = slip speed;  $\tau_{ss}$  = steady state frictional strength). At each depth, constitutive properties in the models are either uniform in the along-strike direction or are perturbed, sometimes only slightly, from uniformity. Results thus far, from simulations with sufficiently refined grids to approach the continuum limit (which, unfortunately, means large and rather slow computations, and which constrains the range of characteristic slip distances  $L$  for state transitions which can be studied;  $L = 40$  mm was used in the studies discussed here), suggest that uniform fault models are remarkably resistant to breakup into spatially complex slip patterns along strike.

This is in interesting contrast to the conclusions which other investigators have drawn based on inherently discrete models such as cellular automata models, or spring-block arrays with simplified classical friction laws. Those inherently discrete models do not realistically incorporate continuum elastic interactions of slip and stress distributions and neglect key constitutive features such as slip-dependent strength transitions. They have no well defined continuum limit upon reduction of cell or grid size, in the sense that the stress or other measure of state in adjacent cells can remain finitely different as cell size is reduced arbitrarily. Indeed, our 3D simulations, for runs with computational cell sizes that are too large to meet limits for acceptable simulation of a continuum, do show complex slip histories suggestive of a self organized critical state, with a spectrum of earthquake sizes, aperiodic recurrence, variable rupture area, and with highly variable moment release along strike in some large events. For these unacceptably large cell sizes, one cell can slip independently of its neighbors, thus mimicking the properties of the inherently discrete models.

However, in all cases studied, the spatial complexity in slip history diminishes with cell refinement. It disappears entirely, in the sense that the same slip variation with depth and time occurs at all locations along strike, for cases in which it is feasible to do calculations with cell sizes that meet criteria for achieving something close to the continuum limit (i. e., with cell dimension small enough that the spring stiffness associated with slip of a single cell in the grid is, say, two or more times larger than the critical stiffness  $(B-A)/L$  from the rate and state dependent friction law). Thus, in these studies, the self organized criticality appears to be a simple numerical artifact of strongly oversized cells in the computational model. Some simplified model involving quasi-independent fault segments may ultimately emerge as a physically justified response to the geometric irregularity of fault zones, but the physics of justifying any such simplification seems not yet to have been addressed.

**2.4** Studies here represent a first attempt (Rice, Ben-Zion and Kim, 1991) to extend to elastodynamics some of the static elastic crack front perturbation techniques discussed in item 2.3(a) above. A half-plane crack propagates nominally in the  $x$  direction along the plane  $y = 0$  in an unbounded solid. The crack front at time  $t$  lies along the arc  $x = a(z,t)$  where  $a(z,t)$  differs only slightly from being independent of  $z$  and where  $v(z,t) \equiv \partial a/\partial t$  differs only slightly from being constant in time, allowing analysis in the framework of a first order perturbation. We have successfully addressed the problem so far only within a model 3D elastodynamic theory involving

a single displacement variable  $u$ , representing tensile opening or shear slippage, and associated tensile or shear stress  $\sigma = M \partial u / \partial y$  across planes parallel to the crack ( $M$  = elastic modulus). The problem is then one of finding a solution to the scalar wave equation  $c^2 \nabla^2 u = \partial^2 u / \partial t^2$ , satisfying the boundary conditions  $u = 0$  on  $y = 0$  ahead of the growing rupture and  $\sigma = 0$  on  $y = 0$  within the rupture. When  $a(z, t) = a(t)$ , independent of  $z$ , the solutions for  $u$ ,  $\sigma$  and  $K$  (stress intensity factor) are familiar 2D results.

We have developed the 3D solution only within the small perturbation theory, but we write the result in a way which precisely duplicates the exact 2D result even for large perturbations. The result thereby obtained for the stress intensity factor  $K(z, t)$  at position  $z$  along the moving crack front is

$$K(z, t) = \sqrt{1 - v(z, t)/c} K^* [1 + I(z, t)], \quad \text{where}$$

$$I(z, t) = \frac{1}{2\pi} PV \int_{-\infty}^{+\infty} \int_{-\infty}^{t - |z - z'|/\alpha c} \frac{c(t - t') [v(z', t') - v(z, t')]}{(z - z')^2 \sqrt{\alpha^2 c^2 (t - t')^2 - (z - z')^2}} dt' dz'$$

where  $\alpha^2 = 1 - v^2(z, t)/c^2$  and  $K^*$  is the  $K$  attained when the velocity of a strictly 2D crack is suddenly reduced to zero. This solution is being used in continuing studies to address how a crack front moves unsteadily through regions of locally variable fracture resistance.

### Reports:

- R. Dmowska, L. C. Lovison and J. J. Durek, "Partial breaking of a mature seismic gap: The 1987 earthquakes in New Britain", *Pure and Applied Geophysics*, vol. 137, no. 1 - 2, 1991, in press
- R. Dmowska and L. C. Lovison, "Influence of asperities along subduction interfaces on the stressing and seismicity of adjacent areas", in review for *Tectonophysics* (special issue on *Earthquake Source Physics and Earthquake Precursors*), 1991
- H. Gao, J. R. Rice and J. Lee, "Penetration of a quasistatically slipping crack into a seismogenic zone of heterogeneous fracture resistance", *Journal of Geophysical Research*, in press, 1991
- H. Gao, J. R. Rice and J. Lee, "Configurational stability of the uniform upward growth of a shear crack along a strike-slip fault zone" (abstract), AGU 1991 Fall Meeting Program and Abstracts (supplement to 29 Oct. 1991 EOS), S31C-6, p. 325, 1991
- M. F. Linker and J. R. Rice, "The effective viscosity of the San Andreas fault beneath the seismogenic zone: Constraints from the response to the 1989 Loma Prieta earthquake" (abstract), *ibid*, S21C-9, pp. 310-311, 1991
- J. R. Rice, "Spatio-temporally complex fault slip: 3D simulations with rate- and state-dependent friction on a fault surface between elastically deformable continua" (abstract), AGU-MSA 1991 Spring Meeting Program and Abstracts (supplement to 23 April 1991 EOS), T42A-08, p. 278, 1991a
- J. R. Rice, "Spatio-temporal complexity of slip on a fault" (abstract), XX General Assembly IUGG, Vienna, Union Program and Abstracts, Jeffreys Symposium U1 on Interrelation Between Geophysical Structures and Processes, p. 7, 1991b
- J. R. Rice, "Crustal fluids and the weakness of major faults" (abstract), *ibid*, Symposium U8 on Water and Ice as Geophysical Agents, p. 83, 1991c
- J. R. Rice, "Fault stress states, pore pressure distributions, and the weakness of the San Andreas fault" in *Fault Mechanics and Transport Properties of Rocks*, ed. B. Evans and T.-F. Wong, Academic Press, in press, 1991d
- J. R. Rice, Y. Ben-Zion and K.-S. Kim, "A first order perturbation solution for a dynamic planar crack with a non-uniformly moving front" (abstract), AGU 1991 Fall Meeting Program and Abstracts (supplement to 29 Oct. 1991 EOS), S31C-7, p. 325, 1991

## Source Characteristics of Earthquakes Along the Northern San Jacinto Fault Zone and Faults Within Northern Baja California, Mexico

Agreement No. 14-08-0001-G1954

Diane I. Doser  
Department of Geological Sciences  
University of Texas at El Paso  
El Paso, TX 79968

(915)-747-5501

### Investigations Undertaken

Seismograms have been collected for the 1918 San Jacinto and 1923 San Bernardino earthquakes along the northern San Jacinto fault zone and for large ( $M > 6.0$ ) earthquakes occurring within northern Baja California between 1915 and 1956. Body waveforms obtained from the seismograms are modeled to determine the source parameters (focal mechanism, focal depth, seismic moment) of the earthquakes. The earthquakes and associated foreshocks and aftershocks are also relocated to better determine the rupture history of the earthquake sequences. The source parameter information is used to determine fault slip rates and the portions of the faults that have been active in historic time. The slip rate information will be used to estimate how plate motion is being transferred across Baja California to the San Andreas, Imperial, and San Jacinto fault systems and how it may affect the recurrence rates of earthquakes within southern California.

### Results Obtained

Research has been completed on two phases of the project. The sources processes of three large earthquakes (magnitude 6.8, 6.4, and 6.3) occurring between February 9 and 15, 1956 along the San Miguel fault in northern Baja California have been determined through body waveform inversions (Table 1). Results of the study suggest that the mainshock on February 9 was responsible for the 20 km of surface faulting observed during the sequence. Although previous researchers had suggested a complex rupture history for the mainshock, uncertainty estimates of source-time function shape indicate a single or double source model fit the observed waveforms equally well. The February 15 aftershock, however, appears to have consisted of two events. Locations and focal mechanisms obtained for the three events suggest that the rupture process may have been controlled by cross faults to the main trace of the San Miguel fault.

Determination of the source parameters for the 1918 and 1923 earthquakes along the northern San Jacinto fault has also been completed (Table 1). The 1918 earthquake source parameters are consistent with a  $> 22$  km rupture along the Claremont fault at a depth of  $7 \pm 5$  km. Limited data for the 1923 earthquake are more consistent with rupture along the San Jacinto fault than rupture along the San Andreas fault or a buried cross fault. An analysis of the results of this study and previous studies of historic earthquakes along the southern San Jacinto fault shows that rupture lengths along the San Jacinto fault system are shorter for an equivalent moment-magnitude than those along the Imperial Valley-Mexicali system. The higher heat flow of the Imperial Valley may be responsible for this observed difference. Correspondence between event rupture length and the length of fault segments seen at the surface along the San Jacinto fault suggests that the rupture length, and hence the magnitude-frequency distribution for larger earthquakes of the San Jacinto system is controlled by fault geometry.

Seismograms of the 1954 El Alamo, Baja California sequence have been digitized and are currently being analyzed. The collecting of seismograms for the 1915 Cerro Prieto and 1934 Calexico sequences is also complete and the seismograms are currently being digitized.



**Reports Published**

Results of studies of the 1956 San Miguel sequence were presented at a special session on historic earthquakes at the spring meeting of the American Geophysical Union. A manuscript summarizing the results was also submitted to Pure and Applied Geophysics in September, 1991 for a special volume on historic earthquake studies. A manuscript on the results of the study of the northern San Jacinto earthquakes and a comparative study of source processes along the entire San Jacinto fault zone was submitted to the Bulletin of the Seismological Society of America on November 4, 1991.

We are planning to submit an abstract on the preliminary studies of the El Alamo and Calexico earthquakes for the spring meeting of the Seismological Society of America.

Table 1

## Source Parameters From Waveform Inversions or Waveform Modeling

Event	Mechanism (str, dip, rake)	Focal Depth (km)	Moment ( $\times 10^{25}$ dyne-cm)	M*	Rupture Length (km)
San Jacinto 4/21/18					
a priori	140 $\pm$ 40 85 $\pm$ 30 -170 $\pm$ 40	8 $\pm$ 10	9 $\pm$ 5	---	----
final	150 $\pm$ 15 87 $\pm$ 6 -176 $\pm$ 9	7 $\pm$ 5	14 $\pm$ 5	6.8	>22
San Bernardino 7/23/23					
final	320 $\pm$ 10 85 $\pm$ 10 180 $\pm$ 10	7 $\pm$ 5	2.6 $\pm$ 0.5	6.3	14 $\pm$ 4
San Miguel 2/9/56					
a priori	110 $\pm$ 30 85 $\pm$ 30 -177 $\pm$ 40	12 $\pm$ 5	12 $\pm$ 6	---	----
final	108 $\pm$ 8 88 $\pm$ 3 -176 $\pm$ 3	12 $\pm$ 2	10 $\pm$ 2	6.7	20-25
San Miguel 2/14/56					
a priori	110 $\pm$ 30 85 $\pm$ 30 -177 $\pm$ 40	12 $\pm$ 5	2 $\pm$ 2	---	----
final	115 $\pm$ 19 86 $\pm$ 10 -178 $\pm$ 11	12 $\pm$ 5	2.9 $\pm$ 0.9	6.3	15-20
San Miguel 2/15/56					
a priori	130 $\pm$ 30 85 $\pm$ 15 -170 $\pm$ 30	10 $\pm$ 5	2 $\pm$ 2	---	----
final	129 $\pm$ 22 84 $\pm$ 13 -170 $\pm$ 16	9 $\pm$ 4	1.8 $\pm$ 1.6	6.2	3-5 <sup>#</sup>

\*moment-magnitude

<sup>#</sup>average rupture length for each subevent

## Strength Recovery in Rocks and Minerals: Collaborative Research

Brian Evans and Teng-fong Wong, Co-Principal Investigators

*USGS Grant # 14-08-0001-G1806*  
*Dept. of Earth, Atmospheric, & Planetary Sciences*  
*Massachusetts Institute of Technology*  
*Cambridge MA 02139*

*USGS Grant # 14-08-0001-G1807*  
*Dept. of Earth & Space Sciences*  
*State University of New York, Stony Brook*  
*Stony Brook NY*

### Objectives:

Along geologic faults, repeated earthquake instabilities generate wear materials, which result in a thickening gouge zone as seismic slip accumulates. Seismologic observations suggest that faults may recover in strength during the aseismic period of the earthquake cycle. Field observations of fault zones indicate that minerals in the gouge, breccia, and wall rocks can participate in complex petrologic reactions which probably affect the mechanical properties of the fault as well. The coupled effect of wear processes which occur during slip, and healing processes which operate in the interseismic period, may result in variation of seismic stress drop and productivity with recurrence time, tectonic environment, and cumulative slip. It is important to have a fundamental understanding of the wear and healing mechanisms and their relation to fault instability.

### Long Term Evolutionary Effects

Evans and Fredrich at M.I.T. have investigated the effect of solution transfer processes on strength recovery of granular aggregates. In these tests, a 0.6 mm thick layer of simulated quartz gouge with a mean grain size of 3  $\mu\text{m}$  was sheared between forcing blocks of Sioux Quartzite in an internally-heated, gas-medium, servo-controlled deformation apparatus. The sample assembly was saturated with water and sheared at temperatures,  $T_1 = 230 \pm 5^\circ\text{C}$ , confining pressures,  $P_c = 250 \text{ MPa}$ , and pore pressures  $P_{\text{H}_2\text{O}} = 75 \text{ MPa}$ . In some runs, temperature was elevated to a new value, for varying periods of time prior to loading at a reduced temperature  $T_1$ . Thus, the experiments are equivalent to *slip-hold-slip* experiments, except that the *hold* period occurs at a higher temperature than the *slip* portion.

The diameter and length of the forcing blocks were 15.9 mm. Pore fluids had access to the sample through a hole drilled in the upper forcing block to within 2 mm of the sawcut. Load and displacement were measured externally. The axial displacement rate was  $28 \times 10^{-5} \text{ mm per second}$ .

Samples loaded at confining pressures of 250 MPa and pore pressures of 75 MPa at 235° without prior healing, slide stably with a shear strength of roughly 180 MPa. Samples slid at identical conditions after being held at an elevated temperature are stronger (i.e. higher initial coefficient of friction). These samples exhibit instability with stress drops of 35-100 MPa. The peak frictional strength of three samples held for 60 minutes at 636° prior to loading is about 50 MPa greater than that of the unhealed samples. Two samples healed for 60 minutes at  $817 \pm 8^\circ\text{C}$  prior to loading were strengthened by 50 and 130 MPa. Whereas a steady-state frictional strength is eventually established after the initial stick-slip event in samples healed at 636°C, samples healed at 817°C stick-slip repeatedly. Experiments in which the time of loading is held constant for healed and unhealed samples indicate that the strength recovery is not due to increases in the time of stationary contact alone, but that the time of healing is important. Experiments in which the healing time is varied indicate that much of the strength recovery occurs during the first 60 minutes of healing, as might be predicted on the basis of hot isostatic pressing results (e.g., *Brantley, PhD. dissertation, Princeton University, 1987; Evans and Lockner, 1989*).

Scanning electron microscopy (SEM) indicates that sliding in the unhealed samples is accompanied by the development of shear zones within the gouge layer. Abundant evidence for the activity of solution-transfer processes is observed in the healed samples. Current efforts are focused on the quantitative characterization of neck growth and contiguity in the healed samples. Additional experiments to determine the effect of fluid pressure, temperature, and particle size on the healing behavior are also underway.

In a previous semi-annual report, we discussed strength recovery in a series of triaxial mechanical tests at temperatures ranging between 700-950°C in faulted samples of Maryland diabase. Generation of the melt apparently causes large variations in the effective pressure which promote fracturing and rapid migration of the melt [*Fredrich and Evans, 1990*]. During the remainder of the grant period, we plan to prepare two papers discussing both the quartz experiments and the diabase results.

### **Wear Processes and Short Term Evolutionary Effects**

Using the conventional triaxial configuration, Wong and coworkers at SUNY, Stony Brook are investigating the stabilization of slip by wear processes. In these experiments the frictional sliding behavior was monitored as a function of cumulative slip when a simulated gouge layer of ultrafine quartz was sheared. In a typical experiment, the sliding behavior evolved from dynamic instability to stable sliding through several sequential stages. Supercritical oscillations marked the onset of dynamic instability. Tens and sometimes hundreds of stick-slip events occurred, while the stress drop amplitude decreased monotonically with accumulated slip. The results could be interpreted with a simple wear model and allow the estimation of the friction constitutive parameters through the observation of the oscillation period as a function of load point velocity. Preliminary results have been written and will appear in Wong et al. [1991]. Similar results have also been observed in Tennessee sandstone with or without halite gauge. The nonlinear dynamical behavior in the transition from stable sliding to cyclic stick-slip in response to load point velocity perturbation was also systematically observed. These new results will be presented at the fall AGU meeting

[Gu and Wong, 1991]. In parallel with the experimental work, we have conducted numerical simulation on the dynamics of a single degree of freedom spring-slider system. The effects of loading velocity, frictional parameters and inertia on the dynamics and recurrence time of cyclic stick-slip were investigated. The result were summarized by Gu and Wong [1992]. New simulations on the effects of frictional behavior complexity (specifically additional state variables and velocity cutoff were also performed. The simulation show good agreement with our experimental data on two country rocks (Westerly granite and Tennessee sandstone) and two simulated gauges (ultrafine quartz and halite) These results will also be presented in the upcoming AGU meeting.

## References

- Evans, B., and D. Lockner, Densification and Electrical Properties of Hot Pressed Quartz Aggregates, *EOS*, 70, 1323, 1989.
- Evans, B., and J. Fredrich, Strength recovery along a fault by solution transfer processes, presented at "Mechanical Instabilities in Rocks and Tectonics", *TERRA Nova*, 3, *TERRA Abstracts Supplement* 5, 13, 1991.
- Fredrich, J. T. and B. Evans, Effect of solution transfer processes on the frictional properties of simulated fault gouge, *EOS*, 71, 440, 1991.
- Gu, Y. and T.-f. Wong, The effects of loading velocity, stiffness, and inertia on the dynamics of a single degree of freedom spring-slider system, *J. Geophys. Res.*, in press, 1992.
- Gu, Y. and T.-f. Wong, Nonlinear dynamics of a spring-slider system with high speed cutoff of velocity dependance, *EOS, AGU*, 325, 1991.
- Wong, T.-f., Stabilization of faulting by wear processes, *International Symposium on Earthquake Source Physics and Earthquake Precursors*, Tokyo, 1990.
- Wong, T.-f., Y. Gu, and T. Yanagidani, and Y. Zhao, Stabilization of faulting by cumulative slip, in *Fault Mechanics and Transport Properties of Rocks, A Festschrift in Honor of W. F. Brace*, B. Evans and T.-f. Wong, editors, in press, Academic Press, London, UK., 1991.

## **The USGS Parkfield Dense Seismograph Array (UPSAR)**

Project No. 9910-03974

Jon B. Fletcher, Paul Spudich, Lawrence M. Baker, Margaret Hellweg

Branch of Engineering Seismology and Geology

U.S. Geological Survey

345 Middlefield Rd.

Menlo Park, CA 94025

(415) 329-5628, 5654, 5608, 5647

### Investigations

- 1.) Operate the 14-station array at Work Ranch near Parkfield, CA.
- 2.) Organize and maintain data base of waveforms.
- 3.) Investigate shear wave polarizations.
- 4.) Array calibration for beamed coda

### Results

- 1.) UPSAR is a short-baseline array (maximum aperture of  $\sim 1$  km) operating on the Work Ranch nearly due West of Gold Hill. Each station has a three-component accelerometer and velocity transducer to insure that ground motion from microearthquakes as well as damaging temblors can be recorded on scale. New software was installed in the data acquisition systems to transmit differences between the internal and external clocks from field stations each second to the central computer. This improvement provides a means of monitoring the phase-lock system that synchronizes the internal clocks to time from the GOES satellite.
- 2.) Parameters describing each waveform file and its associated event are stored in a new database organized in 21 tables using the SyBase relational database. As of Nov. 1991 the data base contained information on more than 3000 events, more than 893 of which could be correlated with events recorded by one of the microearthquake networks in California. The magnitudes range from 0.8 to 7.1 (Loma Prieta) over a distance range of 8 km to 100°. Teleseismic body waves, such as a Peruvian deep earthquake (Nov., 1990), have also been recorded.
- 3.) Shear-wave splitting is being investigated with the UPSAR data. Waveform data is analyzed using the method of Bowman and Ando (1987) which rotates the seismogram along the fast and slow polarization directions, and cross correlates the fast shear wave against the slow to compute the delay of the slow shear wave. The effectiveness of the procedure is judged by the linearity of the resulting shear pulse after removing the delay and rotating back to the original component directions. Figure 1 shows a magnitude 2.3 event from Middle Mtn. which is nearly due north of UPSAR. It is apparent that the polarization of the synthetic (calculated from the focal mechanism) is close to the polarization of the initial S-wave from this event. Consequently, either the anisotropy along this path is weak or the fast or slow direction coincides with the polarization of the initial shear wave arrival. Events of magnitude around 2.0 from different azimuths will be investigated, although attenuation appears to be so severe that only events within about 20 km of the array have impulsive S-waves at the array.
- 4.) To use UPSAR array data for beamed coda measurements, it is necessary to calibrate the array by measuring station delays. In the ideal case, the earth is homogeneous and isotropic and seismic waves cross the array as a plane. The set of arrival delays measured at all stations can be used to precisely determine the azimuth and slowness of the wave. Realistically, the arrival delays can only be used to approximate a plane wave, which may have an azimuth and slowness different from those given by the local velocity model. In Figure 2, events with various azimuths, depths and distances from the array are plotted. The vectors show systematic differences between theoretical and measured wave propagation

directions. The small tangential vectors indicate that there is little lateral refraction. For the beamed coda measurements, this information can be used to correlate the coda sources with a location.

#### References

- 1.) Bowman, J.R., and M. Ando (1985). Shear-wave splitting in the upper-mantle wedge above the Tonga subduction zone, *Geophys. J. R. astr. Soc.*, 88, 25-41.
- 2.) Spudich, P. and L.N. Frazer (1984). Use of ray theory to calculate high-frequency radiation from earthquake sources having spatially variable rupture velocity and stress drop, *Bull. Seism. Soc. Amer.*, 74, 2061-2082.

#### Reports

- 1.) Fletcher, J.B., L.M. Baker, P. Spudich, P. Goldstein, J.D. Sims and M. Hellweg (1991). The USGS Parkfield, California, dense seismograph array-UPSAR, accepted for publication by the *Bull. Seis. Soc. Amer.*
- 2.) Hellweg, M., P. Spudich, J. Fletcher and L.M. Baker (1991). Increasing the resolution of beamforming: An example from the USGS Parkfield seismograph array (UPSAR): submitted to XX General Assembly of the International Union of Geodesy and Geophysics, April 11-24, Vienna, Austria.
- 3.) Hellweg, M., J. Fletcher and P. Spudich (1991). Coda coherence and Q from UPSAR, Parkfield, California: submitted to 1991 Fall Meeting of the AGU, December 9-13, 1991, San Francisco, California

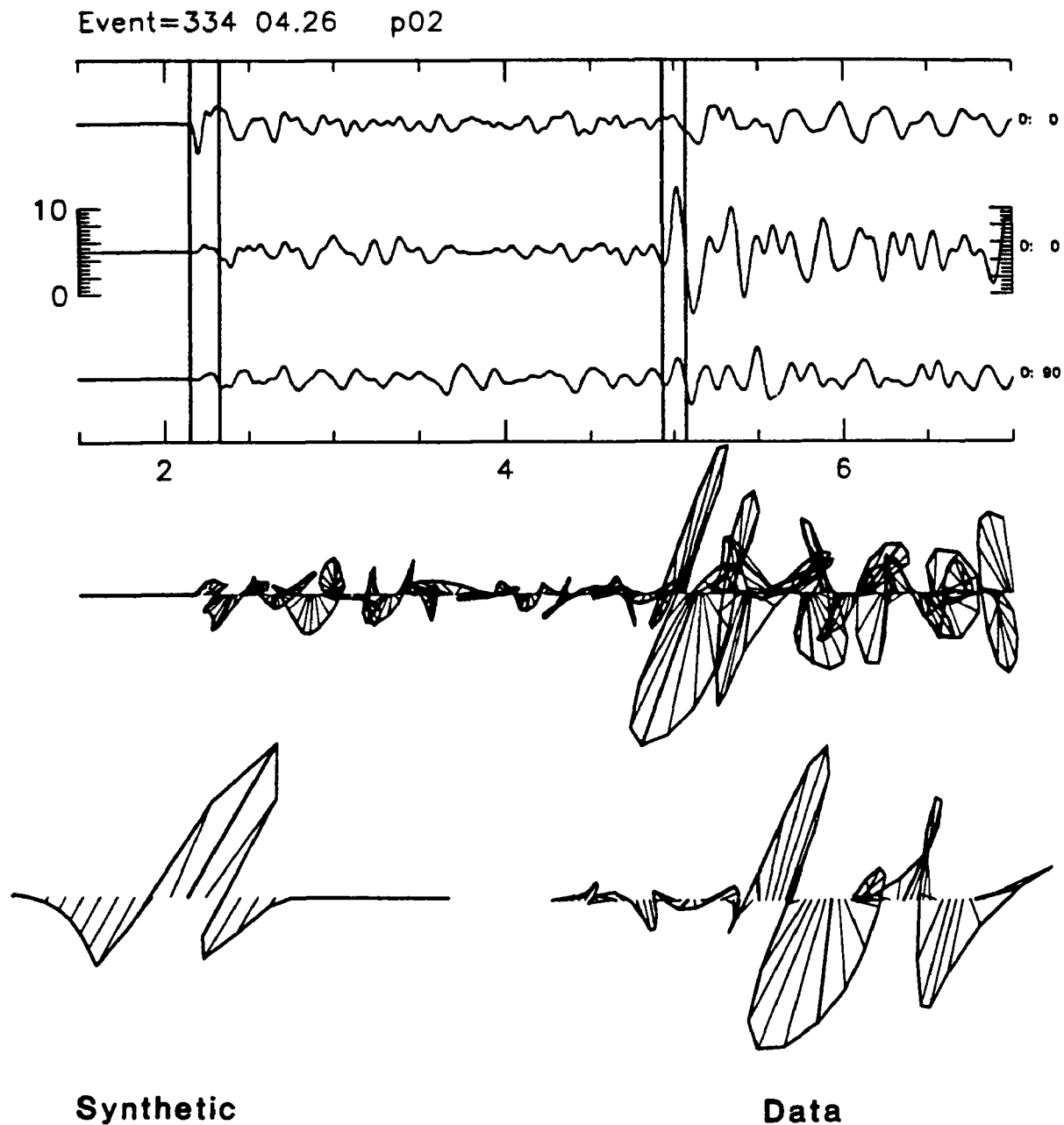
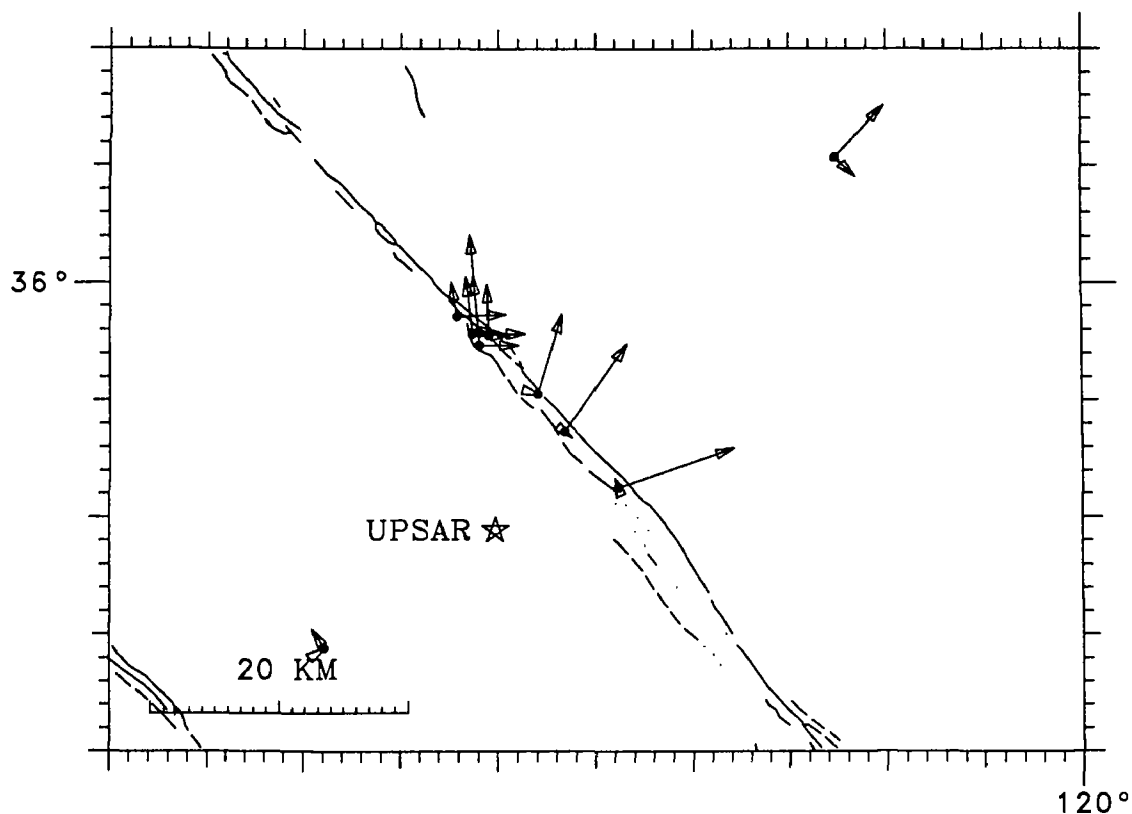


Figure 1. Displacement traces for a magnitude 2.3 at a distance of 12.9 km. Seismograms are plotted to the same scale. Time is noted in seconds. Component orientations are given on the right with the degrees from upward vertical first and the compass orientation second. The horizontal projection of the ground displacement at each time step (decimated by three) is given in the middle plot with its envelope. A slightly expanded segment, which surrounds the S-wave is in the bottom plot to the right and a synthetic computed using the isochron technique (Spudich and Frazer, 1984) is on the left. The focal mechanism determined from CALNET data was specified for the synthetic. Note the similarity in polarization directions between the synthetic and the initial polarization of the real data.



## Events for Calibration



**Figure 2.** Locations of events with various azimuths, depths and distances from the array. The radial vectors are proportional to the difference between the theoretical horizontal slowness and the horizontal slowness calculated from a least-squares best-fit plane wave fit to the wave front. The tangential vectors denote the misfit between the calculated azimuth and the azimuth measured from the plane wave.

# Central California Network Operations

9930-01891

Wes Hall  
Branch of Seismology  
U.S Geological Survey  
275 Middlefield Road-Mail Stop 977  
Menlo Park, California 94025  
(415)329-4730

## Investigations

Maintenance and recording of 397 seismograph stations (512 components) located in Northern California, Central California and Yellowstone National Park. Also recording 68 components from other agencies. The area covered is from the Oregon border south to Santa Maria and Yellowstone National Park.

## Results

1. Site maintenance visits	639
2. Bench Maintenance Repair	
A. seismic VCO units	232
B. summing amplifiers	36
C. seismic test units	04
D. VO2H/VO2L VCO units	59
E. dc-dc converters	09
3. Production/Fabrication	
A. J512A VCO units	120
B. J512B VCO units	10
C. summing amplifier units	28
D. dc converter/regulators (J601)	36
E. lithium battery packs	117
F. seismometer housing/cable	72
4. Rehabilitation:	
VCO enclosures	52
5. Discriminator repair and tuning (J120)	64
6. Equipment Shipped:	
A. J512A VCO's for Cal Tech	50
B. J512A VCO's for HVO	10
B. J601 DC-DC converters for Cal Tech	75
C. Iceland project (B. Julian)	
a. dc-dc converters	14
b. solar panels	17
D. J110 discriminators to Mount St. Helens Visitor Center	8
E. J110 discriminators for College of Siskiyou's	2
D. Seismometer enclosures for (D. Harlow)	6
E. J512A VCO's for University of Idaho	15
F. Mt. Pinatobo	
a. J512A VCO's	10
b. J110 discriminators	4
c. radio cables	18
d. miscellaneous supplies to install 8 station network.	
G. J512A VCO'S for U.S. Bureau of Mines, Spokane, WA	5

7. Completed RFP for "Repair, Modify, Calibrate, and Perform Quality Control Checks on Seismic Instruments." Contract was awarded to Don Ritchey & Company.
8. Completed RFP for "Seismic Instrumentation Maintenance" (maintenance of field sites). Contract was awarded to Bendix Field Engineering Corporation. A 30 day training period was completed by the two seismic field technicians from Bendix.
9. Completed draft on "Tuning Procedures for J120 Discriminators".
10. Ordered and load components for 100 additional J512 VCO's
11. New seismic stations:  
JJR (Joaquin Road); LPK (Park); LRB (Red Bank); GRO (Round Mountain); LPG (Panther Gulch); LVR (Valentine Ridge); CVPE, CVPN, CVPV (Vollmer Peak); KMHE, KHMN, KHMV (Horse Mountain); CSLE, CSLN, CSLV (San Leandro); JCHE, JCHN, JCHV (Cahill Ridge); NHFE, NHFN, NHFV (Hamilton Field); KJJ (Johnny Jack Ridge); CPM (Point Molate); NMI (Mare Island)
12. Stations Deleted:  
HPR (Peckam Road); HFH (Flint Hills); HKR (Kinkaid Ranch); BSCE, BSCN, BSCV, BSCZ (Stone Canyon).
13. Fabricate 256 channel interface for Tustin Digitizer to Cusp.
14. Fabricate 256 channel interface for PC computer system.

## **Seismicity and Crustal Structure in an Active Collisional Orogen, Soviet Central Asia**

14-08-0001-G1802

Michael W. Hamburger, Gary L. Pavlis,  
Haydar J. Al-Shukri, Bingjun Zheng, John M. Holbrook  
Department of Geological Sciences, Indiana University  
Bloomington, Indiana 47405  
(812) 855-2934

Terry L. Pavlis, Rodrick D. Myers  
Department of Geology and Geophysics  
University of New Orleans  
New Orleans, Louisiana 70148  
(504) 286-6797

### **Investigations**

This program focuses on the highly active seismic zone between the Pamir and Tien Shan mountain belts in Soviet Central Asia. The Garm region is located directly atop the collisional boundary between the Indian and Eurasian plates, and is associated with a dense concentration of both shallow and intermediate-depth earthquakes. The fundamental aims of this collaborative research project with the USSR Academy of Sciences are: (1) to elucidate the structures and processes involved in active deformation of a complex collisional plate boundary, and (2) to examine the temporal variations in seismicity near Garm, in the form of changing spatial, depth, and stress distribution of microearthquakes that precede larger events. The seismological data base for this study includes the combined resources of the global, regional, and local seismic networks. Geological structures in the Garm region have been studied using compilation of published geological information, analysis of satellite imagery, and geological field work in the Peter the First, Gissar, and Darvaz mountain ranges near Garm.

### **Results**

*Velocity Structure.* We have expanded our previous work on crustal velocity structure of the Garm region [Hamburger *et al.*, 1991a], with a study of three-dimensional velocity variations in the region [Hamburger *et al.*, 1991b]. This expanded study makes use of data from the Soviet Complex Seismological Expedition (CSE) network, as well as the USGS/CSE telemetered network nested within the CSE network. Our analysis of seismic velocities was limited to a rectangular area, 100 km by 80 km, which includes the most active zones of earthquake activity. The ray path coverage of the study area limited our analysis to a depth of about 30 km. One- and three-dimensional velocity models have been derived for the upper crust of the region using 22,972 P-wave arrival times from 2242 local earthquakes recorded at 58 sites. These observations represent less than 5% of the earthquake data base and are judged to be the highest quality data available for the region. A stochastic (damped) least squares inversion procedure was used to derive the velocity models. A large number of initial one-dimensional velocity models with different starting velocities, number of layers, and depth of interfaces were examined. Results for the 1-D inversion indicate that the upper crust is best modeled by a four-layer velocity structure. This model features a near-surface layer whose thickness ranges from 0-3 km with a velocity of 5.2 km/sec, underlain by layers of 5.6 km/sec (1.37 km above S.L. - 4 km depth), 5.87 km/sec (4-20 km depth), and a mid-crustal layer having velocity of 6.1 km/sec (20-32 km depth).

The 1-D model was used as the starting point for the three-dimensional inversion, where each layer was divided into 10 by 8 blocks, each with 10 km by 10 km dimensions. The results of this inversion, an example of which is shown in Figure 1, indicate a very good correlation between velocity variation and the geology and tectonic setting of the region. The general features of the model include a zone of high velocity extending in an ENE-WSW direction in the northern part of the study area and associated with the crystalline basement rocks of the Tien Shan range, moderate velocities associated with the deformed sediments of the Peter the First Range, and a zone of low velocities associated with the thickest sediments at the southern edge of the range.

*Satellite Imagery Interpretation.* We have acquired three scenes of SPOT satellite imagery covering the entire region monitored by the Garm network. These data were analyzed using image processing equipment at the Lamont-Doherty Geological Observatory of Columbia University. This imagery was processed using (1) standard contrast and edge enhancement techniques, and (2) rotation and distortion of the imagery to allow it to be superimposed on digital topography. In this way, we were able to produce false-color stereo pairs of the processed images that display the full 3-D relationship of the images to the topography. The processed satellite imagery provided a critical data base for completion of a preliminary reconnaissance geologic map of the Peter the First Range and adjacent areas. This was particularly useful because of the combination of higher resolution of these data (compared to Landsat data used previously), the arid climate of the study area, time of year (late fall, when snow and vegetation cover is at a minimum), and the strong signature of resistant marker beds that show up in the enhanced images. The processed imagery was used to provide base maps for the six-week reconnaissance field work in the Peter the First Range (described in the following section).

*Geological Structure.* Reconnaissance mapping in the Peter the First Range revealed a system of previously unrecognized out-of-sequence thrusts that strike at an oblique angle to the mountain front (Figure 2). These thrusts are considered "out-of-sequence" because they cut across existing fold structures and locally place younger rocks on older rocks. When viewed on the scale of the entire Peter the First Range, this thrust system forms an *en echelon* array that we interpret as a consequence of dextral transpression [Pavlis *et al.*, 1991]. This interpretation--of a late-stage deformation within the interior of the fold-thrust belt--may provide a new explanation of (1) the complexity of the structures observed along the axis of the range, (2) the tendency of earthquake focal mechanisms to show compression axes at an oblique angle to the fold axes, and (3) the concentration of seismicity within the axis of the range rather than at the leading edge of the thrust system.

Interpretation of imagery in the eastern portion of the Garm region suggests that additional complexities may be occurring in that area in response to extreme shortening in the central Peter the First Range. Near the site of the area's largest historical earthquake (the 1949 Khait earthquake,  $M=7.5$ ), geomorphic evidence suggests that a major south-vergent backthrust has developed in this area. This inferred backthrust may represent an imbricate along a north-dipping thrust that forms the southern edge of the Tien Shan system, and may represent a major transfer structure between the north-directed thrusts of the Peter the First Range to south-directed thrusts of the Tien Shan system.

*Stratigraphy.* Our geologic work in the Garm region during the summer field season also included description and interpretation of lithofacies for Mesozoic and Tertiary strata in the Tien Shan, Darvaz, and Peter the First ranges. This work is an important complement to our structural work, as a constraint both on the tectonic reconstructions of the area and on the subsurface structural geometries in the region. We were able to collect an extensive sample set of Cretaceous sedimentary rocks, in anticipation of a possible provenance study of sandstone and conglomerate beds in this interval. The stratigraphic study also included detailed mapping in the Mesozoic volcanic/sedimentary sequence exposed in the Darvaz Range (northern Pamir), the first Western analysis of this tectonically important area. Extensive structural work in this area supports our earlier conclu-

sion [Pavlis and Hamburger, 1990; Hamburger *et al.*, 1991c] that the contact between Cretaceous rocks of the Tadjik Depression and older rocks in the northern Pamir must be a stratigraphic, rather than a structural, contact. Any suture between the two blocks must be situated further to the south, within the Pamir uplift itself.

**Earthquake Prediction Studies.** Two main approaches were used to evaluate variations in seismic activity of the Garm region: (1) a qualitative approach, involving examination of maps, cross sections, space-time plots, and earthquake histograms for the area identified as the rupture area of the mainshock; (2) a quantitative approach using counts of events per unit area and time within the seismic network. In the quantitative analysis, the level of seismic activity in small sub-areas is measured by a parameter  $A_2$ , defined as the  $A$  value at magnitude 2 in Gutenberg-Richter's magnitude-frequency relation  $\log N = A - bM$ . The parameter is calculated by a least-square fit to the counts of earthquakes with  $M \geq 1.5$ , judged to be complete throughout the network. The area is divided into thirty 12' x 12' cells to provide sufficient numbers of earthquakes per unit time.  $A_2$  is then calculated for every space-time cell with a time window of 5 years sliding 1 year. We examined 12 mainshocks of  $M \geq 5.0$ . Of these 12, only one event, the  $M = 6.3$  Dzhirgital earthquake of 26 October 1984, shows clearly defined quiescence prior to the mainshock. Evidence for this includes: (1) a well defined change in slope of the cumulative number of earthquakes (Figure 1a); (2) a well defined gap in space-time and magnitude-time plots; (3) a significant decrease (by a factor of 45%) in activity level (Figure 1b). Three additional events, the earthquakes of 17 January 1980 ( $M = 5.2$ ), 6 April 1983 ( $M = 5.5$ ), and 9 January 1988 ( $M = 5.3$ ), showed qualitative evidence of quiescence. However, none of these mainshocks showed significant changes in  $A_2$ . One possible explanation for this discrepancy is that the area used in calculating  $A_2$  is more than an order larger than the rupture area of those earthquakes. The results of the quantitative analysis also show strong spatial variations: the central portion of the study area, which includes the Peter the First Range fold-thrust belt, shows little long-term variation in seismic activity, the Tien Shan basement uplift in the north has a tendency of decreasing activity; and the northeastern part of the study area shows increasing activity. The October 1984 earthquake is located near the transition between the two tendencies.

## References

- Hamburger, M.W., W.A. Swanson II, and G.A. Popandopulo, 1991a, Velocity structure and seismicity of the Garm region, Soviet Central Asia, *Geophys. J. Int.*, in review.
- Hamburger, M.W., H.J. Al-Shukri, G.L. Pavlis, and G.A. Popandopulo, 1991b, P-wave velocity structure of the crust beneath the Garm region, Soviet Central Asia [abstract], *EOS, Trans. Am. Geophys. Un.*, 72, 350.
- Hamburger, M.W., D.R. Sarewitz, T.L. Pavlis, G.A. Popandopulo, 1991c, Structural and seismic evidence for intra-continental subduction beneath the Peter the First Range, Soviet Central Asia, *Geol. Soc. Am. Bull.*, in press.
- Pavlis, T. L., and M. W. Hamburger, 1990, The Jura-Cretaceous Tadjik Depression, Soviet Central Asia: Rifted margin of Asia vs. foreland basin, *Geol. Soc. Am. Abs. w/ Prog.*, 22, A144.
- Pavlis, T.L., R.D. Myers, G.L. Pavlis, J.H. Holbrook, M.W. Hamburger, A.A. Lukk, and S.L. Yunga, Transpressional tectonics in the Peter the First Range, Soviet Tadjikistan [abstract], *EOS, Trans. Am. Geophys. Un.*, 72, 514.
- Ramos, E.G., M.W. Hamburger, A.A. Lukk, and S.L. Yunga, 1991, Seismicity and stress patterns within a collisional plate boundary, Soviet Central Asia [abstract], *EOS, Trans. Am. Geophys. Un.*, in press.
- Zheng, B., M.W. Hamburger, G.L. Pavlis, and G.A. Popandopulo, 1991, Temporal variations in the Garm region, USSR: Evidence for quiescence preceding a  $M = 6.3$  earthquake [abstract], *EOS, Trans. Am. Geophys. Un.*, 72, 322.

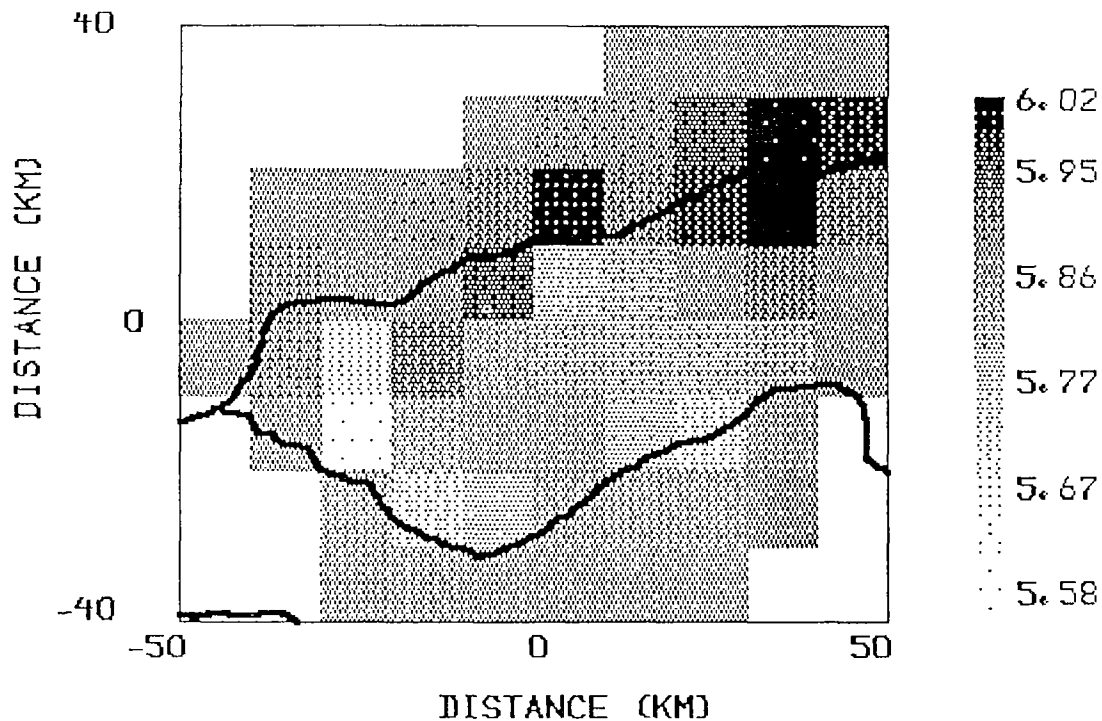


Figure 1. Velocity variation in layer 2 (depth 4 - 12 km) obtained by inverting travel-time data of P-waves from local earthquakes. Solid lines indicate rivers in the region, and unshaded areas indicate regions where no solution could be obtained.

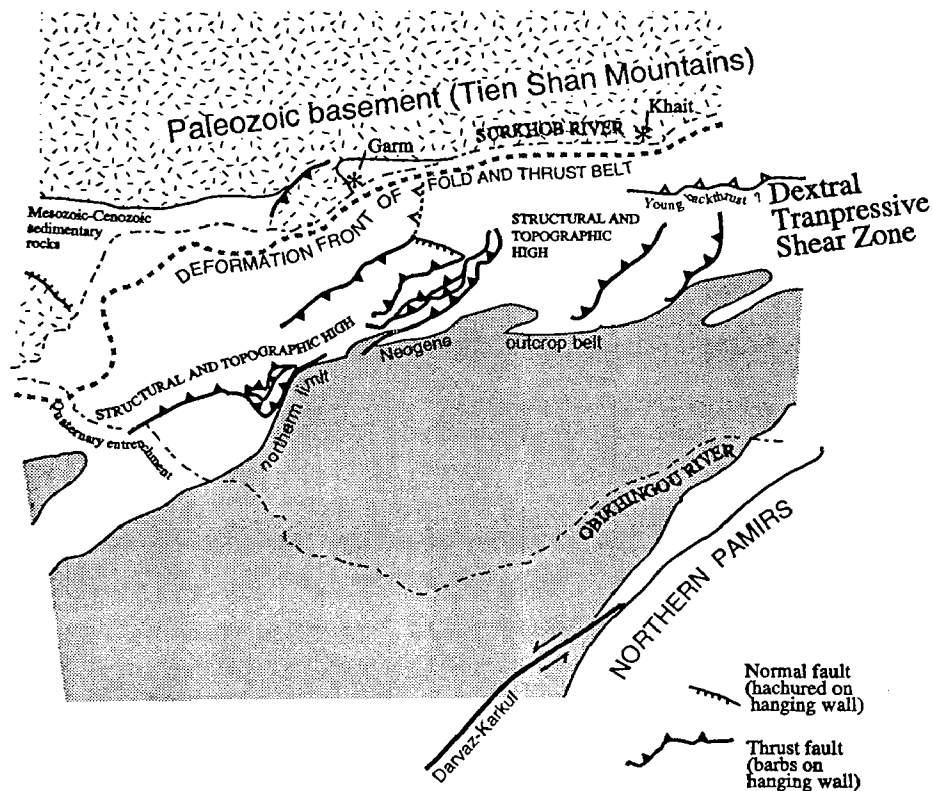


Figure 2. Tectonic map of the Garm region, showing young, "out-of-sequence" thrust faults in the interior of the Peter the First Range, developed as a result of dextral transpression against the deformation front of the fold-thrust belt.

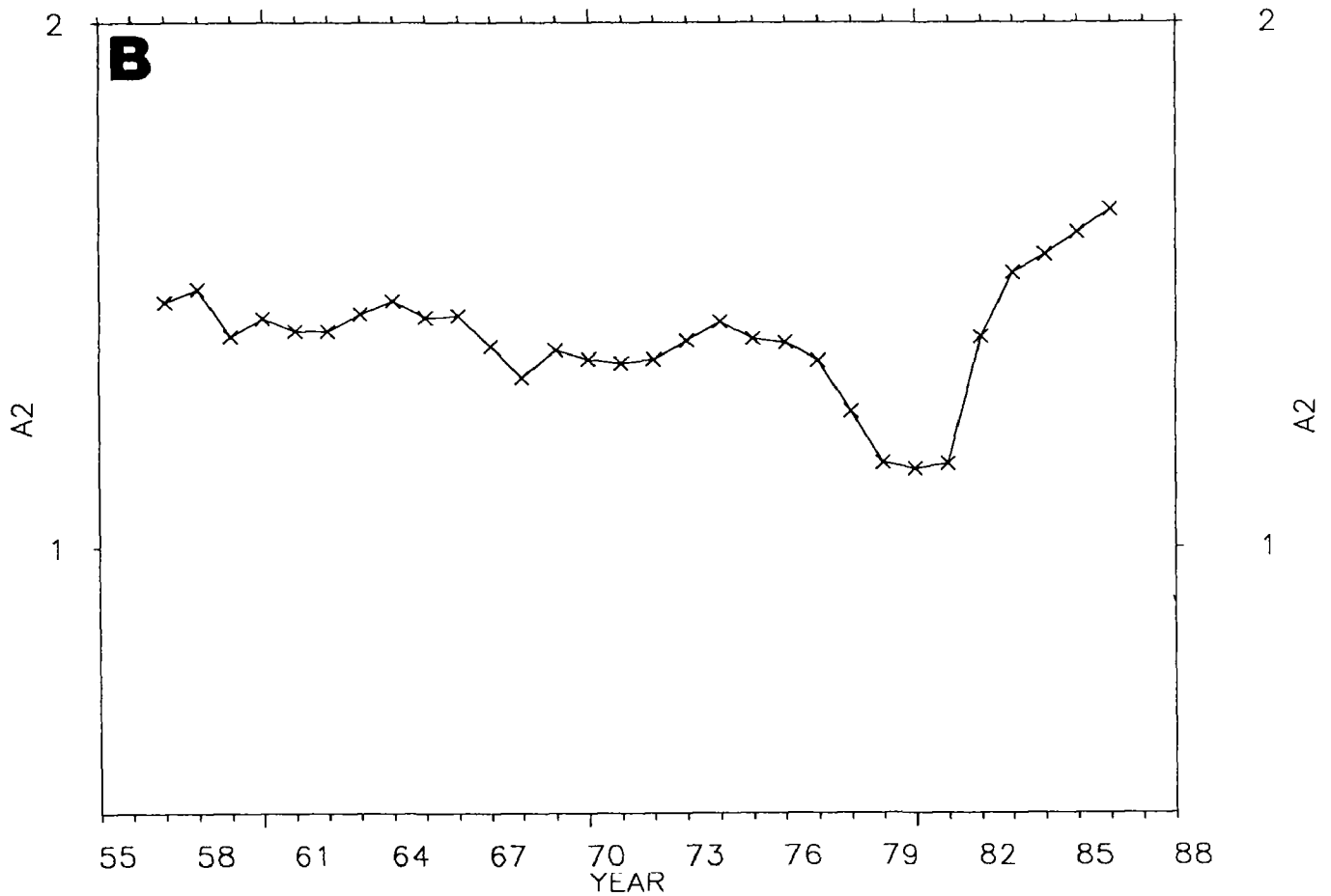
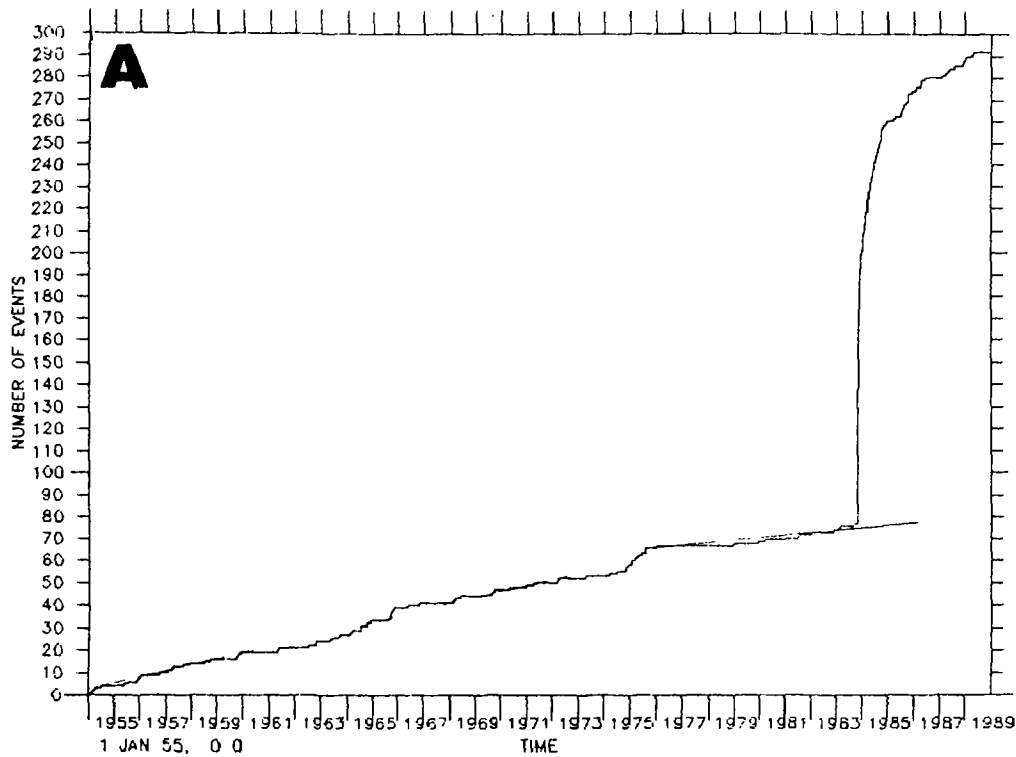


Figure 3. Evidence for quiescence preceding the  $M = 6.3$  Dzhirgital earthquake in 1984. (A) Cumulative number of events with  $M \geq 2.0$  from 1955-1988. Note the change in slope of the curve, beginning in early 1977. (B) Variations in seismic activity of the Dzhirgital area, shown as the annual variation in  $A_2$ , smoothed over a five-year interval. Note the well defined decrease (by a factor of 45%), beginning in 1977.



## Analysis of Earthquake Data from the Greater Los Angeles Basin and Adjacent Offshore Area, Southern California

#14-08-0001-G1761

Egill Hauksson

Seismological Laboratory,  
California Institute of Technology,  
Pasadena, CA 91125  
818-356 6954

### INVESTIGATIONS

Seismotectonic analysis of earthquake data recorded by the CIT/USGS and USC networks during the last 15 years in the greater Los Angeles basin. Improve models of the velocity structure to obtain more accurate earthquake locations including depth and to determine focal mechanisms. Studies of the earthquake potential and the detailed patterns of faulting along major faults in the metropolitan area and adjacent regions.

A comprehensive study entitled: *The 1988 and 1990 Upland Earthquakes: Left-Lateral Faulting Adjacent to the Central Transverse Ranges*. was reported on in USGS Open-File Report 91-352 and by Hauksson and Jones (1991).

A comprehensive study of the *the 1991 ( $M_L=5.8$ ) Sierra Madre earthquake* in southern California is in progress. Below we report some of the preliminary results.

### RESULTS

The ( $M_L=5.8$ ) Sierra Madre earthquake of 28 June 1991, occurred 18 km northeast of Pasadena at a depth of 12.5 km under the San Gabriel Mountains of the central Transverse Ranges (Figure 1). The mainshock focal mechanism, derived from first motion polarities, exhibited pure thrust faulting on a plane striking east-northeast and dipping  $50^\circ$  to the north. The event appears to have occurred on the Clamshell-Sawpit Canyon fault, an offshoot of the Sierra Madre fault system, although because all of the aftershocks are in the depth range of 9-14 km, the relation to surface faults can only be hypothesized. The Sierra Madre earthquake occurred close to where the east-northeast-striking Clamshell-Sawpit and Raymond faults join the Sierra Madre fault from the northeast and southwest, respectively. The Clamshell-Sawpit fault has sometimes been interpreted as an extension of the Raymond fault.

At least since the 1930's, prior to the occurrence of the mainshock, this region had remained quiescent at magnitude 3.0 and greater. The mainshock was followed by an aftershock sequence deficient in small earthquakes with 105 recorded aftershocks and a b-value of 0.6. Arrival time data from the mainshock, aftershocks, and two calibration blasts, recorded by the Southern California Seismographic Network, were inverted to obtain two refined crustal velocity models and station delays. Thirty single-event focal mechanisms were determined for aftershocks of  $M>1.8$  (Figure 2). These focal mechanisms and the hypocenters of all of the aftershocks outline a complex set of faults. The 4 km long fault that caused the mainshock is outlined by several thrust focal mechanisms with an east-north-east striking fault plane dipping to the north. To the west, another 3 km long fault is outlined by numerous thrust faulting aftershocks with east striking nodal planes. These events may be associated with the Sierra Madre fault itself. In addition, several strike-slip and normal faulting events occurred between and along the edges of these two thrust planes, indicating secondary tear faulting. None of these tear faults can be associated with mapped surficial faults. Stress inversion of the focal mechanisms shows that the maximum principal stress is horizontal and is rotated  $4-8^\circ$  to the

west from the ambient stress, which trends north-south. Similar change in stress state was also observed following the Whittier Narrows earthquake, suggesting that dynamic loading of these faults occurs over a fairly short time scale.

#### PUBLICATIONS and REPORTS

- Hauksson, E., Earthquakes, faulting, and stress in the Los Angeles Basin, *J. Geophys. Res.*, 95, 15365-15394, 1990.
- Hauksson, E. and S. Gross, Source Parameters of the 1933 Long Beach Earthquake, *Bull. Seismol. Soc. Amer.*, 81, 81-98, 1991.
- Hauksson, E. and L. M. Jones, The 1988 and 1990 Upland earthquakes: Left-lateral faulting adjacent to the central Transverse Ranges, *J. Geophys. Res.*, 8143-8165, 1991.
- Hauksson, E., Seismotectonics, US National Report to International Union of Geodesy and Geophysics 1987-1990, *Reviews of Geophysics*, Supplement, 721-733, 1991.
- Hauksson, E. and C. R. Allen, Seismicity and seismogenic faults in the vicinity of the Port of Los Angeles, *POLA Seismic Workshop, Proceedings*, in press, 1991.
- Hutton, L. K., L. M. Jones, E. Hauksson, and D. D. Given, Seismotectonics of southern California, *Decade of North American Geology, Neotectonics of North America*, Geological Society of America, in press, 1991.
- Hauksson, E., K. Hutton, K. Douglass, and L. Jones, Earthquake Atlas for Southern California, 1978-1990, submitted to: *Engineering Geology of southern California*, 1991.
- Hauksson, E., and L. M. Jones, The 1991 (ML=5.8) Sierra Madre Earthquake in Southern California: Seismological and Tectonic Analysis, *1991 AGU Fall Meeting*, San Francisco, CA, 1991.
- Jones, L. M., and E. Hauksson, H. Kanamori, Anomalous Earthquake Activity in the San Gabriel Valley, Southern California, 1987-1991, *1991 AGU Fall Meeting*, San Francisco, CA, 1991.

## Sierra Madre 28 June - 15 August 1991

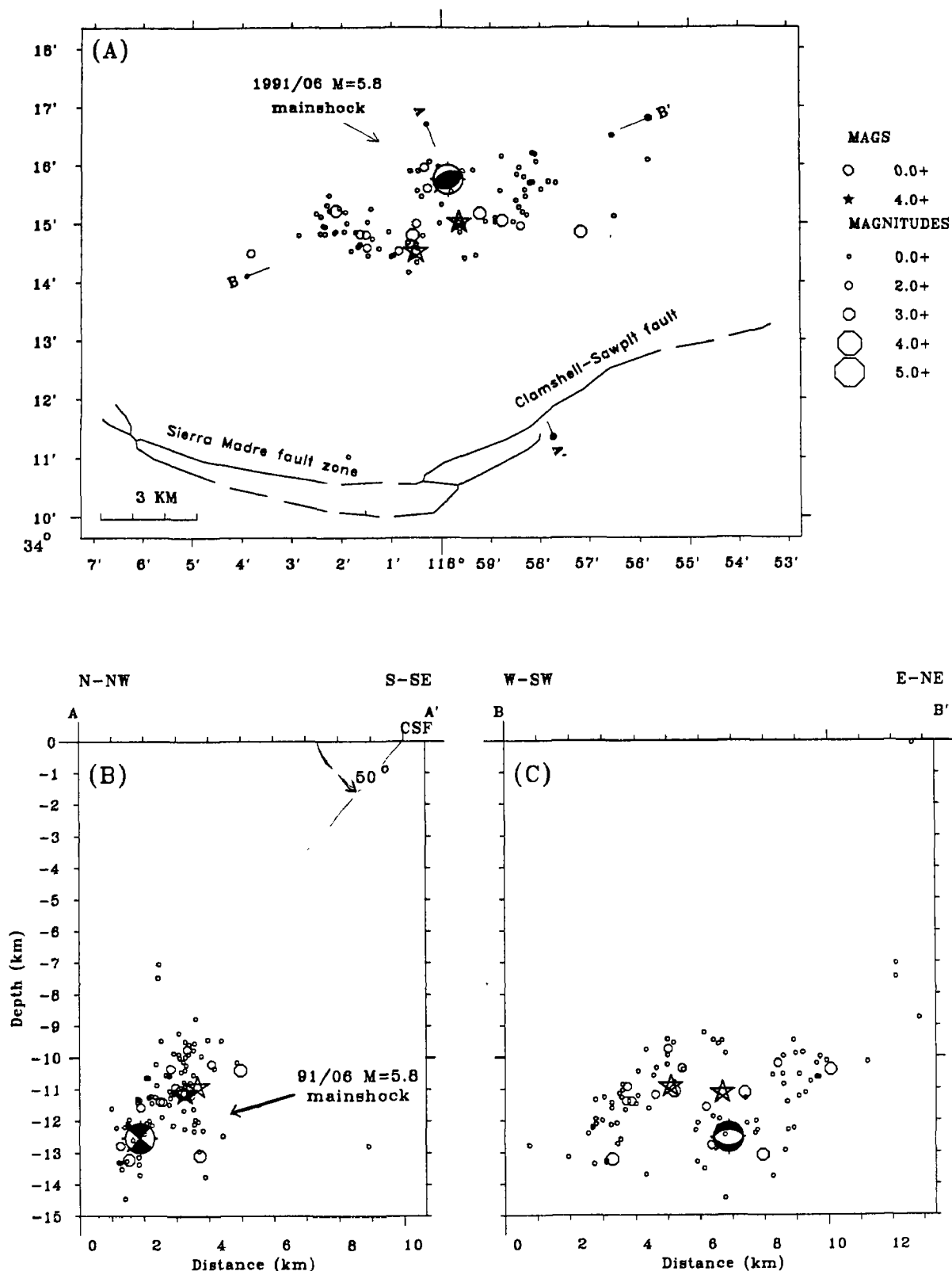


Figure. 1. The 1991 Sierra Madre mainshock-aftershock sequence. (A) map view of the sequence showing also nearby faults. The lower hemisphere focal mechanism of the mainshock is plotted. (B) north-northwest trending cross section taken normal to the preferred nodal plane of the mainshock showing the depth distribution of the activity. (C) a northeast trending cross section taken parallel to the fault.

## Sierra Madre Sequence Focal Mechanisms 1991

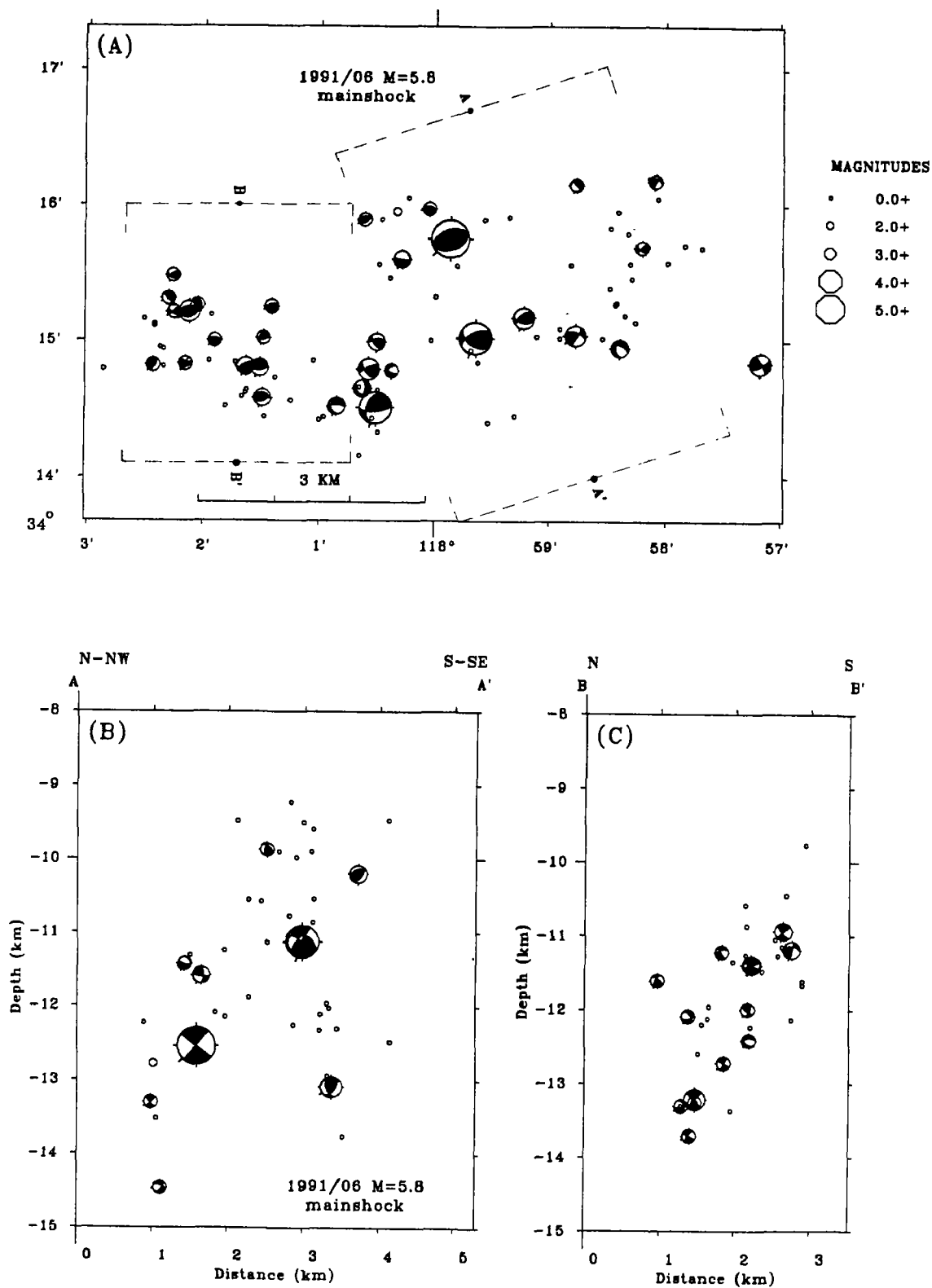


Figure 2. Lower hemisphere focal mechanisms of the mainshock and 30 aftershocks. Two groups of thrust focal mechanisms can be identified, first has a nodal plane striking east-northeast, second has a nodal plane striking east. This suggest that the rupture surface follows the curvature of the Clamshell-Sawpit and Sierra Madre faults. (A) map view of the activity; (B) a north-northwest trending cross section taken normal to the preferred nodal plane of the mainshock; (C) cross north striking section showing depth distribution of some of the aftershocks.

## Source Characteristics of California Earthquakes and Attenuation Effects

14-08-001-G1872

Donald V. Helmberger  
Seismological Laboratory  
California Institute of Technology  
Pasadena, CA 91125

(818)356-6998

### Investigations

A number of recent and historic earthquakes have occurred along the Transverse Ranges, causing significant damage to the greater Los Angeles region. Many of the historic events occurring in this region have been recorded (locally) by relatively low gain long period and short period torsion instruments operated by Caltech (1930 to 1960). Some of the larger events  $M > 5$  can be seen on the (Berkeley Galitzins) regionally while still larger events  $M > 6$  can be observed teleseismically, (De Bilt ,etc.).

To understand these seismograms or separate propagational distortions from source properties is relatively easy at teleseismic distances, but becomes more difficult at regional and local distances. Fortunately, the digital systems used in the TERRAscope array provides observations that greatly aid in establishing the nature of regional propagation. For example, the wide dynamic range allows motions from small events (aftershocks) to be compared with large events at the same site even though the motions can be different by several orders of magnitude. Signals at these distances have not suffered mantle attenuation and thus the broadband features of this system allow us to see obvious propagational effects (headwaves and critical reflections) and detailed source characteristics (near-field and source complexity).

The clearest lesson to date from our studies is that events viewed through a short-period Wood-Anderson instrument (wa-sp) for similar paths are generally similar over several magnitude units. Apparently, the largest asperity dominates the wa.sp response for the larger events. This suggests that normal scaling laws such as  $\omega^{-2}$ ,  $\omega^{-3}$ , etc. are not very dependable in characterizing earthquakes. Secondly, the propagational path is mostly responsible for the seismic signature at local and regional distances. Thus, knowledge of local seismicity and an extensive catalog of waveform data from known events for comparative analysis becomes essential.

Modeling attempts to date indicate that whole seismograms can be understood at ranges less than a few degrees with simple models. At larger ranges, the energy carried by direct S generally becomes scattered and difficult to model, presumably caused by shallow earth structure. Fortunately, at these larger ranges the mantle headwaves, Pn and Sn, become visible and we believe this beginning portion of records (excluding the surface waves) can be used in source estimation as demonstrated by our waveform inversion results.

### Results

In this summary period three studies will be emphasized; (a) on the complex faulting deduced from the broadband modeling of the 28 February 1990 Upland Earthquake ( $M_L = 5.2$ ),

- (b) strong motion and broadband teleseismic analysis of the 1991 Sierra Madre Earthquake, and
- (c) source parameters of the Sierra Madre earthquake from regional and local body waves.

The 1990 Upland earthquake was one of the first sizable local events to be recorded broadband at Pasadena, where the Green's functions appropriate for the path are known from a previous study. The synthetics developed in modeling the 1988 Upland sequence were available for use in rapid assessment of the activity. First-motion studies from the Caltech-USGS array data gave two solutions for the 1990 main shock based on the choice of regional velocity models. Although these focal mechanisms differ by less than  $5^\circ$  in strike and  $20^\circ$  rake, it proved possible to further constraint the solution using these derived Green's functions and a three-component waveform inversion scheme. We obtain from long-period waves a fault-plane solution of  $\theta = 216^\circ$ ,  $\delta = 77^\circ$ ,  $\lambda = 5.0^\circ$ ,  $M_0 = 2.5 \times 10^{24}$  dyne-cm, depth = 6 km, and a source duration 1.2 sec, for which the orientation and source depth are in good agreement with the first-motion results of Hauksson and Jones (1991). Comparisons of the broadband displacement records with the high-pass Wood-Anderson simulations suggests the 1990 earthquake was a complicated event with a strong asperity at depth. Double point-source models indicate that about 30 per cent of the moment was released from a 9-km deep asperity following the initial source by 0.0 to 0.5 sec. Our best-fitting distributed fault model indicates that the timing of our point-source results is feasible assuming a reasonable rupture velocity. The rupture initiated at a depth of about 6 km and propagated downward on a 3.5 by 3.5 km (length by width) fault. Both the inversion of long-period waves and the distributed fault modeling indicate that the main shock did not rupture the entire depth extent of the fault defined by the aftershock zone. A relatively small asperity (about  $1.0 \text{ km}^2$ ) with a greater than 1 kbar stress drop controls the short-period Wood-Anderson waveforms. This asperity appears to be located in a region where seismicity shows a bend in the fault plane.

Short period and broadband teleseismic waveform data and three-component strong motion records were analyzed to obtain the source parameters of the 1991 Sierra Madre earthquake. Close-in strong motion velocity records (analyzed from 5 sec to 5 Hz) show two distinct pulses about 0.35 sec apart, requiring some rupture complexity. The near-field shear wave displacement pulse from this event has a relatively short duration (about 1 sec) for the magnitude of the event, requiring a particularly high average stress drop. To further constrain the rupture process, the data were used in a finite fault source inversion to determine the temporal and spatial distribution of slip. Depth constraints are provided by teleseismic short period and broadband recordings which require a centroid depth of 10-11 km. Our inverse modeling results indicate that both data sets can be fit with a compact rupture area, about  $12 \text{ km}^2$ , southwest and up-dip from the hypocenter. The average slip is approximately 50 cm, and the maximum slip is 120 cm. The seismic moment obtained from either of the separate data sets or both sets combined is about  $2.8 \pm 0.3 \times 10^{24}$  dyne-cm and the potency is  $0.01 \text{ km}^3$ .

We inverted the three-component, long-period data recorded by the TERRAScope array for the June 28, 1991 Sierra Madre, California event to determine the seismic moment and source orientation of the mainshock ( $M_L = 5.8$ ). Remarkably four of the six stations were located  $159.2 \pm 0.7$  km from the epicenter. Variations in absolute traveltimes were smaller than 2% and 3% for  $P_n$  and  $S_n$ , whereas the surface waves displayed greater variation. Similarities in the waveforms and the small variance in traveltimes suggest that a common Green's function can be used to invert the data. We used the whole waveforms excluding the fundamental surface waves at the more distant stations to invert for source parameters. The results of the inversion indicated that this event is predominantly a thrust type earthquake, where the strike, rake and dip were determined to be  $235^\circ$ ,  $74^\circ$  and  $50^\circ$ , respectively. The seismic moment was determined to be  $2.5 \times 10^{24}$  dyne-cm. The source duration was found to be about 1.0 seconds by direct measurement of the direct S-wave recorded at the Pasadena station (located 20 km from the

epicenter). Considering circular rupture and a source time duration of 1 second we obtain a stress drop of 460 bars.

## References

- Bent, Allison L. and D. V. Helmberger (1991). A re-examination of historic earthquakes in the San Jacinto fault zone, California, Bull. Seism. Soc. Am. in press.
- Bent, A. and D. V. Helmberger (1991). Seismic Characteristics of Earthquakes Along the Offshore Extension of the Western Transverse Ranges, California, Bull. Seism. Soc. Am., **81**, 399-422.
- Dreger, Douglas S. and Donald Helmberger (1991). Complex Faulting Deduced from Broadband Modeling of the 28 February 1990 Upland Earthquake ( $M_L = 5.2$ ), Bull. Seism. Soc. Am., **81**, 1129-1144.
- Dreger, Douglas S. and D. V. Helmberger (1991). Source Parameters of the Sierra Madre Earthquake from Regional and Local Body Waves, submitted to Geophys. Res. Lett.
- Hauksson, E. and L. M. Jones (1991). The 1988 and 1990 Upland earthquakes: left-lateral faulting adjacent to the central Transverse Ranges, J. Geophys. Res. **96**, 8143-8165.
- Wald, David J. (1991). Strong motion and Broadband Teleseismic Analysis of the 1991 Sierra Madre, California, Earthquake, submitted to Bull. Seism. Soc. Am.
- Wald, David J. and D. V. Helmberger (1990). Rupture model of the 1989 Loma Prieta earthquake from the inversion of strong motion and broadband teleseismic data, Bull. Seism. Soc. Am. in press.

## **Pressure Solution, Crack Healing and Crustal Stress**

9960-04543

Stephen H. Hickman  
Branch of Tectonophysics  
U.S. Geological Survey  
345 Middlefield Rd., MS 977  
Menlo Park, CA 94025  
(415) 329-4807

### **Investigations**

1. As part of a cooperative program between the U.S. Geological Survey and the Soviet Ministry of Geology, we are conducting a study of stress-induced borehole breakouts in a 4-km-deep well at Tyrnauz, USSR, in the Greater Caucasus Mountains. The Tyrnauz well is located within a granitic pluton in a region of active north-south crustal shortening associated with the collision of the Arabian and Eurasian plates. The goal of this study is to improve our understanding of the mechanics of breakout formation and the state of stress in seismically active areas.

2. We are initiating (together with Colin Williams of the USGS, Menlo Park) a program to make measurements of stress orientations and magnitudes, natural fracture and fault orientations, permeability, pore pressure and heat flow within and adjacent to the New Madrid Seismic Zone (NMSZ). These measurements will be used to evaluate competing theories for the localization of seismicity within the NMSZ and provide constraints on the mechanics of intraplate earthquakes. We hope to begin this program with a series of stress and heat-flow measurements in up to eight 1.5- to 2.0-km-deep exploratory oil wells that will be drilled along the southern portion of the NMSZ in the next two years. As part of this program, we are currently developing a wireline packer system for making in-situ stress measurements using the hydraulic fracturing technique. Because this wireline system can be used without a drill rig, the cost of making in-situ stress measurements will be substantially reduced from what would be the case if standard drill-pipe-deployed packers were used. Depending upon the success of this "holes-of-opportunity" measurement program, in fiscal year (FY) 1993 we propose to drill a dedicated scientific drillhole directly within the central segment of the NMSZ.

3. We are conducting an experimental study of pressure solution and crack healing under load in simple quartz/water systems. These experiments will employ single crystals in well-controlled model geometries inside a hydrothermal vessel equipped with an optical observation port. The goal of these experiments is to constrain the mechanisms and kinetics of solution-transport creep and fault strengthening and to provide fundamental constraints on processes controlling the spatial and temporal evolution of physical properties in the earth (e.g. permeability, seismic velocities, and density).

### **Results**

1. In July of this year we conducted a borehole televiwer log in the Tyrnauz well, USSR, between the depths of 290 m and 3100 m. This televiwer log, which is being digitally processed to create oriented three-dimensional images of the borehole, reveals extensive borehole elongation throughout the well in addition to a large number of natural fractures, fault zones and dikes. Although the interaction between breakouts and drill-pipe wear in this well is quite



complex, we are able to unambiguously identify breakouts at a number of depths based upon their irregular cross-sectional geometry, bilateral symmetry and discontinuous distribution with depth. Unusually high horizontal stresses are indicated in the Tyrnauz well by the development of borehole breakouts at depths as shallow as 390 m. Breakouts were observed to terminate at natural fractures and dike contacts at some depths, suggesting either localized reductions in stress magnitudes and/or increases in rock strength. The direction of the maximum horizontal compressive stress,  $S_H$ , at Tyrnauz is approximately north-south, based upon preliminary determinations of breakout azimuths. Most of the natural fractures observed in the televiwer log strike sub-parallel to this inferred  $S_H$  direction and dip steeply to the west. The inferred  $S_H$  azimuth from the Tyrnauz well is parallel to the direction of relative motion between the Arabian and Eurasian plates and compares favorably with the NNW-NNE range of P axes from larger earthquakes in this region. Analysis and interpretation of these data will continue into FY 1992, including an exchange visit by two Soviet scientists to the USGS in Menlo Park early in 1992.

2. During the past six months, we devoted our effort on the New Madrid stress and heat flow project to three distinct objectives. First, we followed through with a proposal for hydraulic fracturing stress measurements in an approximately 2.7-km-deep hole of opportunity being drilled by the Dupont Chemical Company in western Tennessee, on the edge of the Mississippi Embayment. Unfortunately, Dupont corporate politics eventually countermanded the initially favorable response and our proposal was rejected. Second, we continued our search for holes of opportunity within the New Madrid region by contracting with a consulting geologist (Jim Howe of Boulder, Colorado) to look for planned or existing drillholes that might serve as platforms for stress and heat flow measurements. His efforts led to the successful contact with the oil exploration company that will be drilling the array of 1.5- to 2.0-km-deep exploratory oil wells referred to above. Mr. Howe was also asked to locate any existing information on stress orientations and fluid pressures from wells already drilled in the northern Mississippi Embayment. As a result, we now have in hand, or are in the process of obtaining, several oriented 4-arm caliper logs and drill stem tests from wells within or close to the NMSZ which have been heretofore unavailable. Third, approximately one fourth of the components for the wireline packer system have already been designed and purchased using FY 1991 New Madrid funds. If funding for the development of this system is continued, we will complete the design, construction, and testing of this packer system in FY 1992.

3. We are currently assembling and testing the pressure vessel, furnace, and optical equipment to be used in the single-crystal pressure solution and crack-healing experiments. We have just hired a full-time research technician to assist with this study and anticipate the initiation of experiments during the first half of FY 1992.

## Reports

Hickman, S., Stress in the lithosphere and the strength of active faults, *U.S. National Report to the IUGG, Reviews in Geophysics Supplement*, April 1991, 759-775, 1991.

Hickman, S., and B. Evans, Growth of grain contacts in halite by solution transfer: Implications for diagenesis, lithification, and strength recovery, in *Fault Mechanics and Transport Properties of Rocks*, B. Evans and T.-F. Wong (eds.), Academic Press, 1991 (in press).

Lockner, D., S. Hickman, V. Kuksenko, A. Ponomarev, A. Sidorin, J. Byerlee, and B. Khakaev, Laboratory-determined permeability of cores from the Kola Superdeep Well, USSR, *Geophys. Res. Lett.*, 18, 881-884, 1991.

**FIELD AND MECHANICAL STUDIES OF EARTHQUAKE GROUND RUPTURES**  
9980-04038

Marie D. Jackson  
Branch of Igneous and Geothermal Processes  
U. S. Geological Survey  
2255 North Gemini Drive  
Flagstaff, Arizona, 86001  
(602) 556-7186

**Investigations**

1. *Late Quaternary movement along the Hat Creek Fault, northeastern California.*

The Hat Creek fault, located about 30 km north of Lassen Peak, is composed of prominent NNW-trending escarpments that offset Quaternary and Pliocene volcanic rocks by more than 300 m. This fault, and the nearby McArthur, Pittville, and Mayfield faults (Wills, 1991) form an active system of normal faults, down-dropped to the west, that is the westernmost, and perhaps youngest, expression of Basin and Range normal faulting in northeastern California (Fig. 1). The Hat Creek escarpments, or rims, which are modified by erosion to a repose angle of about 35°, form the eastern side of an asymmetric graben, along which the Hat Creek Basalt flowed during the Late Pleistocene or Early Holocene (Fig. 1) (Muffler et al., in review). The most recent slip along the fault forms a 20-km-long, left-stepping scarp as much as 30 m high cutting the Hat Creek Basalt (Fig. 2). Stream gravels, estimated to be no more than 15,000 years old (Muffler et al., in review), overlie the Hat Creek Basalt and were offset as much as 20 m by this youngest faulting. Monoclinial flexures with S-shaped axial planes link some of the left-stepping fault segments. The average Holocene vertical displacement along the fault has been about 2 mm per year, and the existence of this prominent young scarp in an area of low modern seismicity suggests that movement has been episodic with a periodicity of hundreds, or perhaps thousands of years (Muffler et al., 1989).

This study uses field data and mechanical analysis to examine the structure of the Hat Creek fault and to evaluate its earthquake potential. I am investigating how a normal fault propagates and develops a surface rupture, and how its en echelon segments link to transfer predominantly dip-slip displacements. Field work undertaken includes 1:5000 mapping of the entire young Hat Creek scarp and detailed 1:1000 scale mapping of critical kilometer-long exposures along the scarp, and of the S-shaped monoclines at three large left-steps. Analytical work undertaken will include 1) mechanical analysis of the surface deformation over a growing normal fault and 2) analysis of interactions at left-steps using methods of elasticity and fracture mechanics.

2. *Field and mechanical study of ground cracks associated with the 1974  $M_L=5.5$  and 1983  $M_L=6.6$  Kaoiki, Hawaii, earthquakes.*

The Kaoiki seismic zone, a young tectonic feature of Mauna Loa volcano, Hawaii, is the site of recurrent moderate-magnitude earthquakes that cause serious damage. Ground rupture zones from the 1983  $M_L=6.6$  earthquake, the 1974  $M_L=5.5$  earthquake, and an older, undated earthquake, all trend N48°-N55°E, a direction that is nearly parallel to

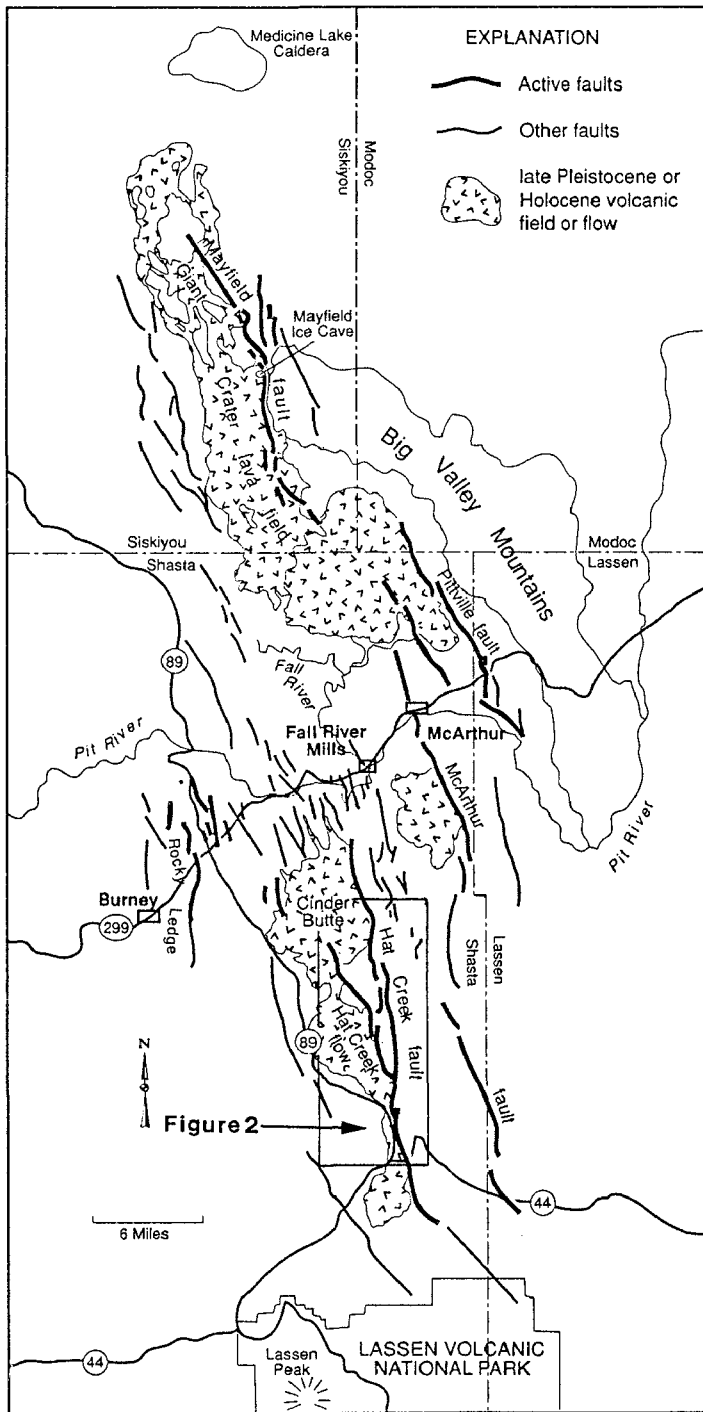


Figure 1. Simplified geologic map showing faults and young volcanic fields and flows between Lassen Peak and Medicine Lake volcano (after Wills, 1991).

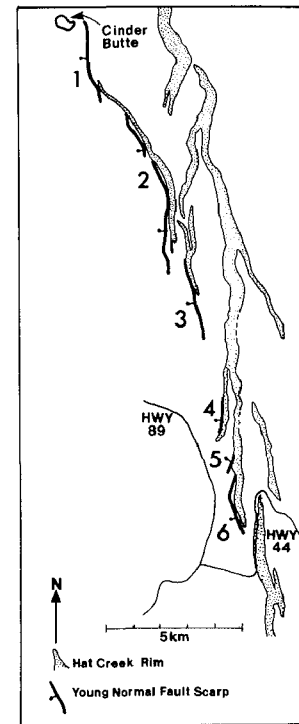


Figure 2. Sketch map of the Hat Creek Fault, showing the older escarpments and Late Quaternary ground rupture.

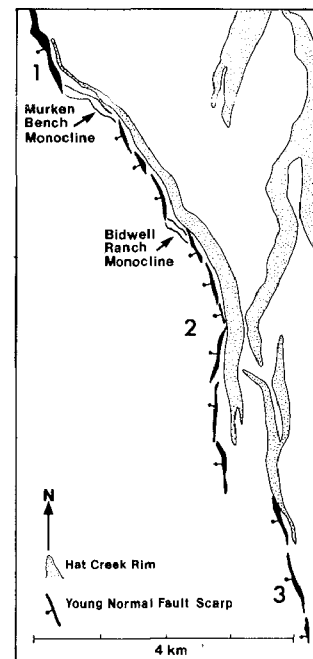


Figure 3. Left-stepping segmentation of the young Hat Creek scarp.

nodal planes of the 1983 and 1974 main shocks' focal mechanisms. Individual ruptures consist of arrays of left-stepping, en echelon cracks with predominantly opening displacements, which strike roughly EW, about 30°-50° clockwise from the overall trend of the zones.

Geologic mapping, field interpretations, and mechanical analysis of rock fracture (Jackson et al., 1988) suggest that the 1983 mainshock created a new fracture, at least near the earth's surface, rather than following the trace of an older fault. The ground cracks are part of a large zone of secondary cracking located ahead of the parent strike-slip fault, in which stresses generated during propagation of the rupture were large relative to the rock strength. First motion seismic data, estimation of the seismic moment release, and results from the analysis of geodetic data spanning the 1983 rupture substantiate our field observations that right-lateral strike-slip faulting dominated the 1983 mainshock and confirm the importance of strike-slip faulting on the SE flank of Mauna Loa.

## Results

### 1. Hat Creek Fault

This project essentially started in September 1991 because I took several months maternity leave. Prior to the leave, however, I designed and contracted for an aerial photo survey of the young scarp that was completed in July 1991. The Photogrammetry group in Flagstaff prepared two 1:1000 digital topographic base maps of two of the S-shaped monoclines from these photographs in August.

I spent nearly 3 weeks in the field, in September 1991. During this time, I mapped two-thirds of the young scarp using 1:5000 aerial photography. The most important results of this mapping are summarized below.

1) The young fault is composed of six several-km-long, left-stepping segments (Fig. 2) which offset the Hat Creek basalt. Some of these follow the older rim and others extend past the older escarpments into the valley floor. Each of these long segments is composed of two or more 0.5- to 1 km-long, left-stepping segments, as shown in Figure 3. These segments are made up of shorter, left-stepping segments, usually less than 100m in length. In this respect, the young scarp shows great similarity to the recent Kaoiki ground ruptures (Jackson et al., in review). There, a large region of secondary cracking forms a fracture-process zone ahead of the tip of the parent fault, through which displacements are transmitted from the parent fault to the earth's surface.

2) Along the left-stepping segments, the young fault is expressed as variations of three different structures: near vertical cliffs or scarps, scarp monoclines of variable amplitude and wavelength, and zones of basaltic rubble.

These structures record processes active in the development of the fault. The cliff-like scarps appear to develop from vertical extension cracks that strike parallel to the young fault. Opening displacements dominated the formation of the cracks, and subsequent west-side-down, dip-slip displacements created a steep scarp along the crack walls. The scarp monoclines appear to develop from predominantly dip-slip displacements in more-or-less intact basalt; flexure of the basalt was accommodated in part by slip along columnar joints. More detailed mapping is required to determine whether the monoclines grow in height and width

with repeated episodes of slip or if their shape is determined by the length of a particular rupture event. Zones of rubble formed as the host basalt was shaken, broken, and oversteepened within the strike monoclines. In many localities, all three structures -- cliffs, monoclines and rubble -- coexist together.

3) **S**-shaped monoclines link all scales of the left-stepping segments. The most prominent of these -- for example, the monoclines at Murken Bench and Bidwell Ranch (Figure 3) -- and their smaller equivalents record how dip-slip displacements were transferred along segments at all scales. I began 1:1000 scale mapping of these monoclines, this field season, but further work is needed to understand the complexity of these structures.

This Fall, I began compiling a map of the young scarp at 1:15,000 scale, using the new aerial photography with a PG-2 stereoplotter. This map shows many detailed structures within the several-km-long segments and is permitting me to accurately measure displacements along the young fault.

## 2. Kaoiki Seismic Zone

I have nearly completed work on a manuscript returned from review by Journal of Geophysical Research for minor final revisions. This paper describes the structure and propagation paths of the 1974 and 1983 Kaoiki ground ruptures, and their relation to the long-term geologic history and recent seismicity of Mauna Loa's SE flank. Summaries of the data presented in this paper have appeared in previous EQHRP reports. The paper will be ready for publication next month when Paul Delaney (U.S.G.S.) and Thora Arnadottir (Stanford) complete their analysis of trialteration data spanning the 1983 rupture. 20 baselines have deformations that are well-explained by a right-lateral strike-slip fault in the vicinity of the mapped rupture.

## References cited

- Endo, E. T., 1985, Seismotectonic framework for the southeast flank of Mauna Loa volcano, Hawaii: Ph.D. Thesis, Univ. of Wash., Seattle.
- Jackson, M. D., E. T. Endo, P. T. Delaney, 1988, Ground rupture from the 1983 Kaoiki earthquake, Mauna Loa volcano, Hawaii (Abs.): Seismological Research Letters, v. 59, p. 35.
- Jackson, M. D., and E. T. Endo, 1989, Genesis of a strike-slip fault zone: the 1974 and 1983 Kaoiki ground ruptures, Mauna Loa Volcano, Hawaii (Abs): EOS, v. 70, p. 1409.
- Muffler, L. J. P., M. A. Clynne, and D. E. Champion, in review, Late Quaternary faulting of the Hat Creek Basalt: to be submitted to Geology.
- Wills, C. J., 1991, Active faults north of Lassen Volcanic National Park, northern California: California Geology, p. 51-58.

## Reports

- Jackson, M. D., E. T. Endo, P. T. Delaney, and T. Arnadottir, submitted, The 1974 and 1983 Kaoiki earthquake ground ruptures, Mauna Loa volcano, Hawaii: Journal of Geophysical Research, 33 ms. p., 18 figs., 1 table. Director's approval 3/12/91.

**State of Stress in the Rupture Zone of Large Earthquakes**

Agreement No. 14-08-0001-G1773

Hiroo Kanamori  
Seismological Laboratory, California Institute of Technology  
Pasadena, California

(818) 356-6914

**Investigation**

The 1990 Rudbar-Manjil earthquake, Iran.

**Results**

The June 1990 Rudbar earthquake is remarkable in that it was a major strike-slip event in a region which is dominated by thrust faults and in which thrusting has been found to be the predominant mode of seismicity. The surface fault has been mapped by Berberian et al. (1991), and consists of three very steeply dipping en-echelon fault strands with ESE strike. The total length of the surface fault amounts to 80 kilometers. The length of the individual segments and the amount of displacement increase from the WNW to the ESE. Remarkably, there was a vertical displacement of up to a meter with the southside uplifted as opposed to a left-lateral displacement of only 60 centimeters. This is at odds with the seismic observations which indicate pure left-lateral strike-slip. Also, the fault that ruptured did not have any evidence for previous activity contrary to nearby faults.

**1. Body-wave analysis**

The waveforms at teleseismic distances look quite complex indicating that the rupture consisted of several subevents. The records from various stations for this earthquakes show that the rupture started off with a small subevent and that the energy release increases towards the end of the rupture. The initial NEIC location for this event was off by about 100 kilometers which may be due to misidentification of first arrivals because of the very emergent onset of the records.

The body-wave inversion method used here has been described in detail in Kikuchi and Kanamori (1991). It solves for the spatial and temporal distribution of subevents as well as for their mechanism by iteration. In this particular inversion the subevents were constrained along a fault segment with a strike of 110 degrees and a vertical fault plane. We used eight nodes along the fault with a separation of 15 kilometers. The depth of the subevents were constrained initially between 5 and 25 kilometers with a separation of 5 kilometers but on the basis of these earlier inversion runs we constrained the depths between 7.5 and 17.5 kilometers. The only constraint on the mechanism of the subevents was a double couple constraint. Because of the gradual build-up of energy release we had to impose a time window for the first subevent to occur, but even then, the very first beginning of the rupture remains unsolved. The subevent distribution is given in Figure 1 with the corresponding subevents given in Table 1, and it is clear that the largest energy release occurred in the SE part of the fault zone. In order to explain the data we need at least four subevents which are all strike-slip but with slight variations in strike. Because of

the strike-slip mechanism we have several stations which are close to a nodal plane and therefore their waveforms are very sensitive to small changes in focal plane parameters. We therefore think that these variations in strike are significant. The locations of the subevents and their sizes agree well with the surface observations (Berberian et al., 1991). There is however no evidence for any significant vertical movement.

The results from our CMT inversion using long-period surface waves agree quite well with the body-wave results apart from the dipping secondary fault plane.

## 2. Discussion

When we compare the results from our body-wave inversion and the observations on the surface rupture we can see that there is generally good agreement between the two. The increase in moment release towards the east matches the increased fault length and offset. This and the variation in strike between the different subevents suggest that the observed segmentation of the fault extends to the depth at which most of the seismic energy was released. The segmentation on the surface, called Riedel faulting, has been studied extensively in sand-box (Naylor et al. 1986) and in the field (e.g. Harding, 1973). Riedel faulting is generally associated with a buried wrench fault which imposes movement on the overburden. This particular Riedel pattern, generally designated 'R' or synthetic Riedel, is characteristic for faults with a very low strain rate or faults in their early stages of development. We may therefore expect this kind of source complexity for faults in their early stages.

## References

- Berberian, M., Qorashi, M., Jackson, J. A., Priestly, K., Wallace, T., 1991. The Rudbar-Tarom earthquake of 20 June 1990 in NW Persia: preliminary field and seismological observations, and its tectonic significance. In prep.
- Harding, T. P., 1973. Newport-Inglewood Trend, California - an example of wrenching style deformation. AAPG bull., 57(1), 97-116.
- Kikuchi, M., Kanamori, H., 1991. Inversion of complex body-waves III. In press.
- Naylor, M. A., Mandl, G., Sijpestein, C.H.K., 1986. Fault geometries in basement-induced wrench faulting under different initial stress states. J.Struct.Geol., 7 (8), 737-752.

Table 1

sub-event	time after JB	depth	Moment, 10 <sup>25</sup> dyne- cm	strike	dip	slip
1	4.0	12.5	8.73	281.5	73.7	1.8
2	7.0	15.0	10.40	297.1	70.8	7.1
3	17.5	10.0	46.53	295.5	81.2	1.5
4	25.0	7.5	24.78	130.7	80.6	-3.8
Total			84.89	298.5	84.1	1.3
CMT			120.	117.4	89.5	-26.5

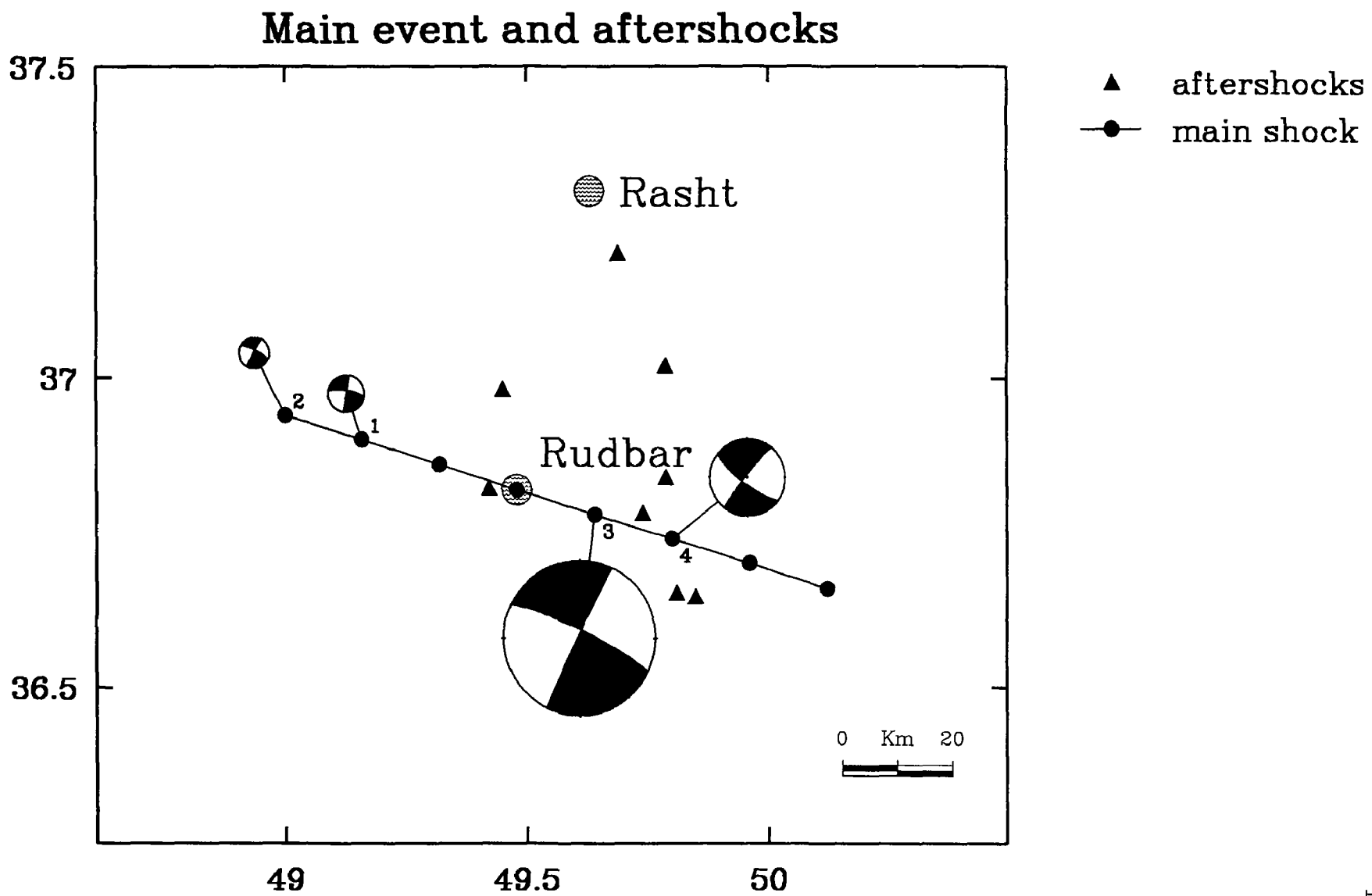


Figure 1



**Earthquake and Seismicity Research Using SCARLET and CEDAR**

Agreement No. 14-08-0001-G1774

Hiroo Kanamori and Robert W. Clayton  
 Seismological Laboratory, California Institute of Technology  
 Pasadena, California  
 (818) 356-6914 and (818) 356-6909

**Investigation**

Mechanism Determination of Local Earthquakes Using Waveform and First-Motion Data.

**Results**

The Pasadena TERRAscope station recorded many small earthquakes around Pasadena. The records can be deconvolved into displacement records. We have developed a method to use these waveform data to determine the mechanism of small events for which first-motion data are incomplete. First-motion data are often incomplete, but they are good enough to constrain the range of allowable solutions. In contrast, the waveform data are of high-quality, but are not enough to determine the mechanisms uniquely. We can combine these two sets of data to determine the mechanisms.

Figure 1 shows the results for the aftershocks of the 1988 Pasadena earthquake.

The P, SV, and SH far field displacements,  $U_r$ ,  $U_\theta$ , and  $U_\phi$ , from a double-couple point source are given by

$$\begin{bmatrix} U_r \\ U_\theta \\ U_\phi \end{bmatrix} = \frac{M_0 s(t)}{4\pi\rho r\alpha^3} \begin{bmatrix} R^P \\ (\alpha/\beta)^3 R^{SV} \\ (\alpha/\beta)^3 R^{SH} \end{bmatrix} \quad (1)$$

where  $s(t)$  and  $M_0$  are the unit moment rate function and the seismic moment, respectively. Here,  $\rho$ ,  $\alpha$ , and  $\beta$  are density, P velocity, and S velocity, and  $R^P$ ,  $R^{SV}$ , and  $R^{SH}$  are P-wave, SV-wave and SH-wave radiation patterns, respectively. The radiation patterns are functions of the fault parameters: dip  $\delta$ , rake  $\lambda$ , and strike  $\phi$ .

Let  $U_P$ ,  $U_{SVZ}$ ,  $U_{SVR}$ , and  $U_{SH}$  be the displacements of the P wave on the vertical component, the SV wave on the vertical component, the SV wave on the radial component, and the SH wave on the tangential component, respectively, observed at the free surface. If we ignore the P-SV conversion at the free surface, then

$$\begin{aligned} U_r &= U_P / (2 \cos i_o) \\ U_\theta &= U_{SVZ} / (-2 \sin i_o) = U_{SVR} / (2 \cos i_o) \\ U_\phi &= U_{SH} / 2, \end{aligned}$$

where  $i_0$  is the incidence angle.

Although the solution of equation (1) is nonunique, we can determine the range of allowable solutions that explain the observed amplitudes and polarities of P, SV, and SH waves. Figure 1 shows the loci of the P and T axes (hereafter called the inversion P-T loci) of the allowable solutions determined by inverting equation (1). Any solution with a pair of P and T axes on the loci yields the correct amplitudes and polarities of P, SV and SH waves.

The first-motion data were analyzed with the program FPFIT (Reasenber and Oppenheimer, 1985). The program FPFIT uses a grid-search procedure to find a mechanism by minimizing the normalized, weighted sum of the discrepancies between the observed and theoretical polarity at each station. The program also determines the ranges of P and T axes of mechanisms that fit the first-motion data equally well. These ranges, here called the first-motion P-T ranges, are shown in Figure 1. Since the quality of the first-motion data is limited, the allowable P-T ranges are generally large. Any solution in these ranges are considered acceptable. If the inversion P-T loci pass through the first-motion P-T ranges, any solution for which the P and T axes lie in the overlapping region can satisfy both the first-motion and waveform data. If the inversion P-T loci do not pass through the first-motion P-T ranges, we choose a point on the inversion P-T loci that is closest to the first-motion P-T ranges. Figure 1 shows the points chosen this way, and the resulting solutions (dashed curve); these solutions are compared with those (solid curve) picked by FPFIT using the first motion data alone.

These results will be published in a paper by Ma and Kanamori (1991).

## Reference

Ma, K.-F. and H. Kanamori, Aftershock Sequence of the December 3, 1988 Pasadena Earthquake, Bull. Seismol. Soc. of Amer., in press, 1991.

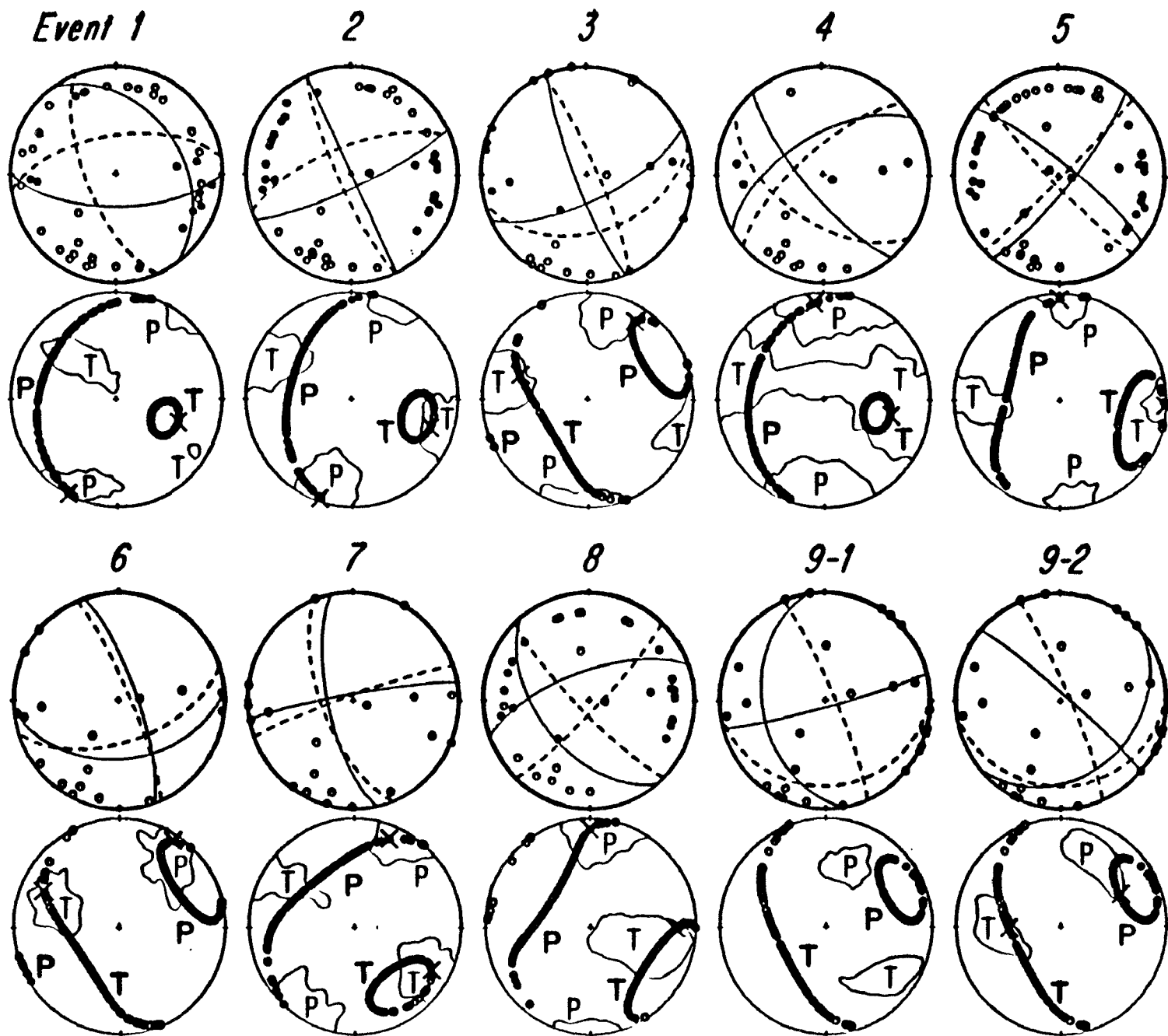


Figure 1

## Seismicity Patterns and the Stress State in Subduction-Type Seismogenic Zones

Grant Number 14-08-0001-G1810

Carl Kisslinger and Susanna Gross  
Cooperative Institute for Research in Environmental Sciences  
Campus Box 216, University of Colorado  
Boulder, Colorado 80309-0216  
(303)492-6089

Research during the current grant year was directed to following problems: (1) the effects of stress redistribution by moderate earthquakes on the spatial distribution of smaller earthquakes in the neighborhood, with possible applications to prediction; and (2) modelling aftershock decay as a relaxation process, with a comparison of the modified Omori relation and the Williams-Watts relaxation function.

### Influence of Earthquake-produced Stresses on Seismicity Distribution

The hypothesis tested in this research is that the influence of an earthquake on subsequent nearby activity can be quantitatively assessed by examining the modifications of the stress field caused by the slip. Specifically, we test whether the seismicity (mostly microearthquakes) increases where the earthquake-related stress acts to increase the greatest principal stress. We assume that any effect will be independent of the orientation of the faults being influenced as long as the contribution to the stress field due to the moderate earthquake is not large enough to change the orientation of the faults most likely to slip.

Seventy-six earthquakes with teleseismic body wave magnitudes from 3.9 to 5.7 that had been located by the Central Aleutians Seismic Network were selected as the "target events". Events with fairly well-determined focal mechanisms were chosen. This is a non-trivial criterion for events in the Central Aleutian Islands, for which the distribution of seismic stations makes the determination of reliable focal mechanisms of moderate events a challenge. A combination of teleseismic and local network first motion polarities was used. After an initial determination of best-fitting focal mechanisms, those teleseismic stations for which the polarity picks fit fewer than one-half of these mechanisms were eliminated, and the mechanisms redetermined. This left an average of 37 first motions per event. A systematic search through all strikes, dips and rakes was executed to find the best-fitting mechanism. A map of the epicenters and best focal mechanism for a sample of the target events is shown in Figure 1.

# Target Events

I

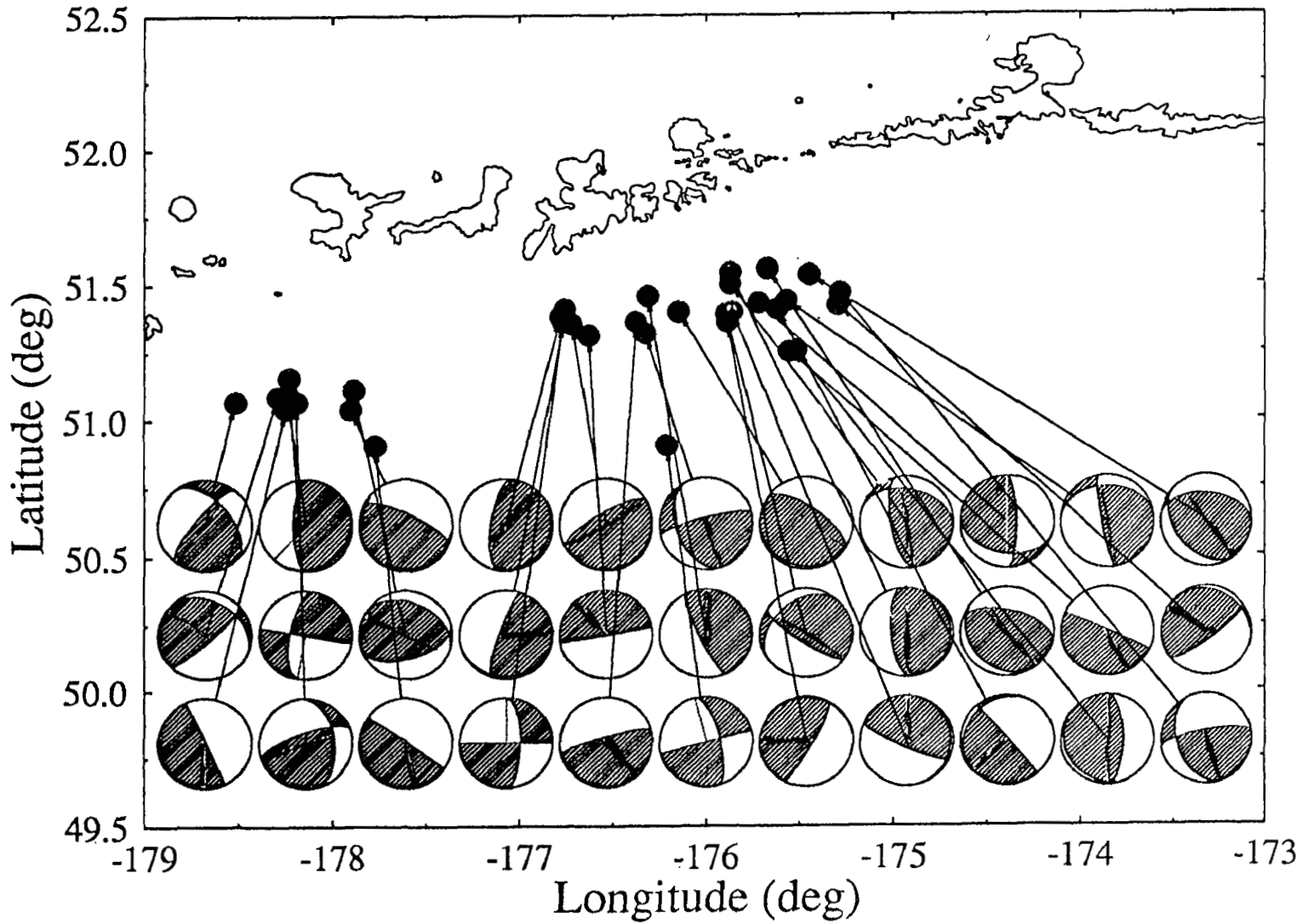


Figure 1: Map of the central Aleutian islands with focal mechanisms from some of the target events used in this study

With the focal mechanism determined, the standard equations for the stress components due to a double-couple in an infinite elastic medium were used to calculate the static stress field associated with each target event.

Time windows defined by 1000 events before and after each target event (about 16 months in the CASN catalog) were selected as including a sufficient number to define a spatial distribution of seismicity. The spatial ranges were concentric shells 10 km thick, centered on the target event. The smallest shell extended from 5 to 15 km; the largest from 75 to 85 km. The components of the earthquake-generated stress tensor were calculated at each hypocenter in the designated distance ranges, and the traction in the direction of the greatest principal stress of the ambient regional stress field calculated. In this way, the stress tensor was replaced by a single scalar value, the magnitude of this traction.

Figure 2 shows a horizontal slice through the calculated increment to the greatest principal stress for a typical target event, with some of the surrounding pre- and post-event seismicity. The azimuth of the greatest principal stress is taken as the direction of the velocity of the Pacific plate relative to the mantle, 30° E, from Minster and Jordan. The plunge is assumed to be the orientation of the Wadati-Benioff zone defined by the hypocenters in the CASN catalog.

**Results of the Investigation to Date.** The calculated stresses at hypocenters of the surrounding activity before and after each target earthquake were compared by computing a t-statistic for each distance range. The t-statistic used in this work is defined by:

$$t = \frac{\bar{\tau}_1 - \bar{\tau}_2}{\sqrt{(\frac{\sigma_1^2}{N_1} + \frac{\sigma_2^2}{N_2})}},$$

where  $\bar{\tau}_1$  and  $\bar{\tau}_2$  are the mean values of the calculated stress changes defined above, evaluated at the hypocenters of the events in each shell, before, 1, and after, 2, the target event.  $N$  and  $\sigma$  are the number of events and the standard deviation of the stress change in each of these data sets.

The t-statistics were then compared with synthetic data to evaluate their significance. With 76 target events, it was simplest to compare the distribution of observed t-statistics with a distribution expected for the null hypothesis, that the earthquake-related stress changes have no effect on the subsequent seismicity. Since negative t-statistics would be observed if increases in the greatest principal stress caused increases in seismicity, the measure of significance chosen for this work was the number of t-statistics more than one standard deviation below zero.

If the t-statistics fit the t-distribution, each one has roughly a 15% chance of being more than one  $\sigma$  less than zero. Are the t-statistics distributed this way? Since we wish to use

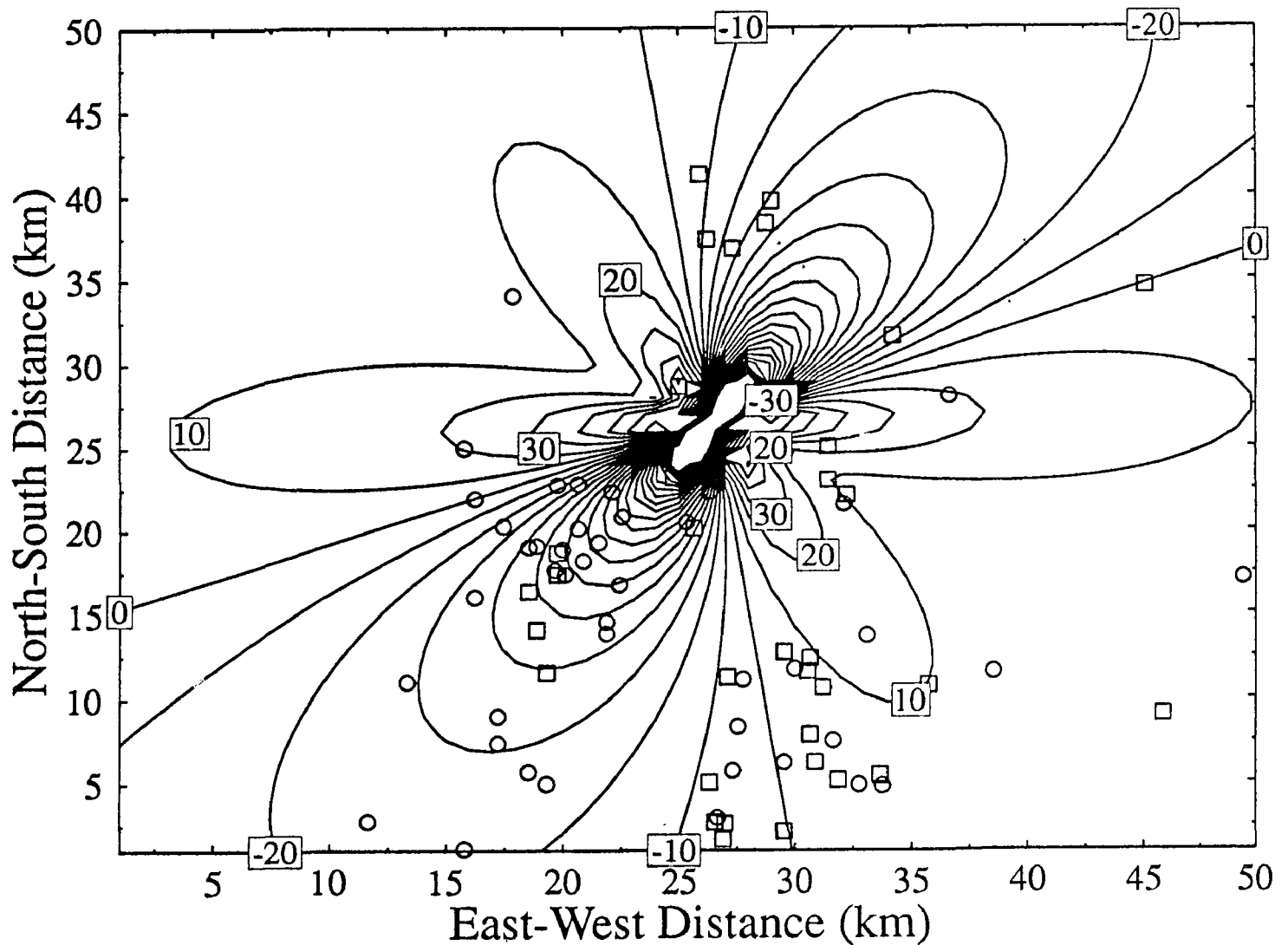


Figure 2: Contribution to the greatest principal stress made by a particular target event, a magnitude 4.8 which occurred on August 2nd, 1978. It has a strike slip mechanism. A horizontal slice through the stress field has been plotted with seismicity having depths within 5 km of the target event. Pre-event seismicity is plotted with circles and post event seismicity with squares.

them to test the hypothesis that the target events are influencing the nearby seismicity, it is important to find out what the distributions of t-statistics would be if there was no such influence. We generated a synthetic data set that is as realistic as possible, but in which there is no influence of the occurrence of target events. In this way, the statistical test can be made sensitive to the quantity we most wish to measure.

The times of the target events in the catalog were scrambled, so that each target event was given a random time, but kept its the hypocenter location and focal mechanism. In the numerical experiment, the seismicity surrounding the synthesized sequence of target events was real seismicity in all respects, except there could be no influence of the target upon its surrounding seismicity. One hundred sets of synthetic seismicity were generated and t-statistics computed assuming the theoretical greatest principal stress direction mentioned above, in order to find the probability of a t-statistic being less than  $-1 \sigma$ . The average result of these computations showed that the the probability of having a t-statistic significantly negative by this measure ranged from 15% to 21% as the distance went from 5km to 55km. These probabilities become distinctly greater than the 15% estimate from theory as the distance increased.

Using the binomial theorem and the probability of a single t-statistic being less than  $-\sigma$  as derived from the computations with synthetic data, it is easy to find the likelihood of a given number of these t-statistics arising by chance. The numbers of t-statistics more than one standard deviation negative and their associated probabilities of arising by chance are listed in Table 1.

The result for the distance slice from 15 to 25 km away from the hypocenter is significant at the 0.8% level. The t-statistics resulting from changes in spatial distribution of seismicity in various distance ranges are expected to show the strongest effects near the target events, since the stress pulse is largest there. However, the result for the distance range from 5 to 15 km, closest to the target event is not at all significant. Several factors may be causing this. The source model is not accurate at distances comparable to the source dimension. Earthquake location error would blur out any changes in spatial distribution smaller than the event-to-event relative location error. If the size of the stress pulse is great enough, assumptions made about the principal stress direction being unchanged may be incorrect. Several of these factors may be operating here.

All of the above calculations have been repeated for assumed ambient principal stress directions at  $5^\circ$  intervals of azimuth and plunge, in order to evaluate the sensitivity of the conclusions to this fundamental parameter in the problem. A wide range of principal stress directions give essentially the same result.



T Statistics Found with the Theoretical Principal Stress Direction				
Distance Range	5-15km	15-25km	25-35km	35-45km
Number of t's $< -\sigma$	9	21	15	11
Random t's $< -\sigma$	11.6	13.1	14.7	14.7
Probability of Randomness	74%	0.8%	40%	82%
Distance Range	45-55km	55-65km	65-75km	75-85km
Number of t's $< -\sigma$	14	13	17	18
Random t's $< -\sigma$	16.2	16.2	13.9	14.9
Probability of Randomness	67%	77%	14%	15%

Table 1: Information about the distributions of t-statistics computed to compare modeled stresses at the hypocenters of seismicity surrounding 76 moderate earthquakes in the Central Aleutians. If increases in stress cause increases in seismicity, than the t-statistics should be negative. The largest number of strongly negative t-statistics is found for the distance range 15 to 25 km.

**Conclusions.** Stress pulses from moderate earthquakes appear to significantly change the spatial distribution of nearby seismicity. The effect is most noticeable in the 15-25 km range. The ambient maximum principal stress must be fairly uniform, consistent with a simple subduction model and the Minster and Jordan velocity. This technique provides opportunities to investigate stresses in seismically active areas that are not accessible to in-situ stress measurements. Since this technique focuses on the spatial and temporal variability of the stress field, it compliments the analysis of Gephardt and Forsyth, which determines the directions and relative magnitudes of the principal stresses.

## Modelling Aftershocks as a Relaxation Process

The spatial and temporal distributions of aftershocks contain information about the physical properties of the fault zone, ambient physical conditions, and the nature of the earthquake nucleation process. In this study, supportive of our work on seismogenesis in subduction zones, the decay of aftershock activity with time after a mainshock is considered as a relaxation process. This type of model postulates that the slip during the mainshock applies a stress step to unbroken sites on the mainshock rupture surface or in its immediate vicinity and that rupture eventually occurs at these sites to produce the aftershocks. The sequence may progress because stress is transferred to the remaining "strong points", or

asperities, or these points may lose strength in a time-dependent manner. The sequence is usually considered to have ended when the rate of activity has returned to the long-term background rate in the seismic zone, a time that is difficult to fix with confidence for real data. The creation of new aftershock sites due, for example, to the action of ambient tectonic processes is assumed to be negligible over the duration of the sequence, though the regional stresses continue to act.

The physical mechanism by which sequential aftershocks are triggered is not known, but seems to involve a combination of the action of the initial stress step on sites with time-dependent strength, re-distribution of stress by creep in the weakened portions of the fault, and the recovery of strength on the fault surface. The diffusion of pore fluids may play an essential role in the process. Whether the aftershocks occur on the same fault surface that broke in the mainshock or in newly strained material in a narrow zone on either side of and around this surface is not easily resolvable with present seismic data and is not important for this discussion.

Because relaxation processes occur in a wide variety of physical systems, a large literature exists in which mechanisms by which relaxation occurs and alternate forms of the relaxation time function are discussed. Little of this work has been examined for applicability to the aftershock problem. In this paper, an alternative to the conventional modified Omori relation is examined. The model investigated is the stretched exponential function, also called the Williams-Watts relaxation function. The theoretical basis is from work by others using continuous-time random walks.

**The Stretched Exponential Relaxation Function.** The conventional way of modeling aftershock decay is by the the modified Omori relation (MOM),

$$n(t) = \frac{K}{(t + c)^{-p}}, \quad (1)$$

where  $n(t)$  is the rate of occurrence of aftershocks at time,  $t$ . This is an empirical extension by Utsu of Omori's original form,  $n(t) = K/t$ . Ogata developed the widely used algorithm for calculating the maximum likelihood estimates of  $K$ ,  $p$ , and  $c$  for a given data set. The modified Omori relation has been used by many authors to model aftershock sequences, and many sequences are described well by it, with a value of  $p$  near 1. In recent work, the differences in  $p$ -values among sequences have been examined in an attempt to relate the rate of decay of aftershocks to ambient physical or geological conditions.

Of the forms investigated as alternatives to power law or exponential relaxation, the stretched exponential function,

$$N^*(t) = N(0)\exp[(-t/t_0)^q], 0 \leq q \leq 1 \quad (2)$$

emerges as "...a universal function that slow relaxations obey. If the system is driven ... out of equilibrium, it returns according to the formula" given in eqn (2) (quoted in Scher, et al., *Physics Today*, January, 1991).  $N^*(t)$  is the number of "survivors" at time  $t$  (unrelaxed polarized molecules in a dielectric, oriented magnetic domains, unbroken stressed asperities that will produce aftershocks in this study, etc.), starting with  $N(0)$  initially. Because this form has been found to describe relaxation in a wide variety of physical systems, it seems worthwhile to test it for applicability to aftershocks.

We first recast the modified Omori relation slightly to facilitate the comparison with the usual formulation of the stretched exponential function. Again, we assume a finite number of potential aftershock sites,  $N(0)$ , are present when the process begins. Write the number of aftershock sites that have not yet failed at  $t$  (the survivors) in the conventional form for a relaxation function,

$$N^*(t) = \frac{N(0)}{(1 + t/c)^s}, \quad (3)$$

where  $c$  and  $s$  are parameters that depend on the physical conditions in the fault zone. Then, the cumulative number of events that have occurred up to time  $t$ , starting from time  $T_s$ , is

$$\begin{aligned} N(t|T_s) &= [N(0) - N^*(t)] - [N(0) - N^*(T_s)] \\ &= N(0)c^s[(T_s + c)^{-s} - (t + c)^{-s}] \end{aligned} \quad (4)$$

$T_s$  can, of course, be chosen as 0.

The rate of occurrence is

$$n(t) = dN/dt = N(0)sc^s(t + c)^{-(s+1)}.$$

This is the modified Omori relation, (1), with  $p = s + 1$ , and  $K = N(0)sc^s$ . A relation useful for generating synthetic sequences is the time to a given cumulative number, with  $T_s = 0$ :

$$t = [K^{-1}(1 - p)N + c^{1-p}]^{1-p} - c \quad (5)$$

For the special case,  $p = 1$ , the original Omori relation,

$$N(t|T_s) = K[\ln(t + c) - \ln(T_s + c)].$$

This case was not considered further.

A problem with the MOM relation that apparently was recognized implicitly by Utsu, but which appears to have been ignored in applications, is that if  $p < 1$  ( $s < 0$ ), the

cumulative number of aftershocks diverges, so that the total number of aftershocks does not approach asymptotically a limiting value at very long times after the mainshock. Values of  $p < 1$  (slowly decaying sequences) are found when the MOM relation is fit to real data, though values greater than 1 may be more common. An unbounded cumulative number of aftershocks contradicts the postulate that a finite number of sites are loaded at the instant of the mainshock and that these fail at a decreasing rate to produce a sequence with a finite number of aftershocks, toward which the sequence converges more or less slowly. There is no problem for  $p > 1$ , as  $N_S$  converges to  $N(0)$  at very long times.

For the stretched exponential,  $N^*(t)$  is given by equation (2). Then,

$$N(t|T_s) = N(0)\exp[-T_s/t_0]^q - \exp[-(t/t_0)^q] \quad (6)$$

$$n(t) = qN(0)t^{q-1}t_0^{-q}\exp[-(t/t_0)^q]. \quad (7)$$

This may be put in a form similar to the MOM relation by letting  $K' = qN(0)t_0^{-q}$  and  $p' = 1 - q$ , so that

$$n(t) = K't^{-p'}\exp[-(t/t_0)^{1-p'}]. \quad (8)$$

For  $q = 1$ ,  $p' = 0$ , this becomes ordinary exponential decay (Debye relaxation), which has also been used to describe aftershock decay (Mogi, 1962). For  $q$  close to 0 ( $p'$  close to 1), this becomes the Omori relation with a large  $N(0)$ . Large values of  $t_0$  correspond to slowly decaying sequences, for which the MOM  $p$ -values are less than 1, but here there is no problem with the convergence of the cumulative sequence. The time to occurrence of a given cumulative number of aftershocks, comparable to equation (5) is

$$t = t_0[-\ln(1 - N/N(0))]^{1/q} \quad (9)$$

C. H. Scholz found for sequences of aftershocks in some laboratory experiments that, when he allowed the machine to continue to load the sample after rupture, after a short interval of time the cumulative number of events fits equation (6), with  $q = 0.5$  and  $t_0 = 8.2$  and 25 for the two examples he showed. Values of  $q$  near 0.5 appear frequently in the sequences of natural aftershocks examined in this study.

The time,  $t_0$ , is the relaxation time for the overall process and has not yet been related to a specific physical mechanism. It is expected that it represents the combined effects of the factors mentioned above, stress relaxation, time-dependent shear strength, and fluid diffusion, as well as the heterogeneity of the strength distribution. Ambient temperature should be an important factor governing this parameter.

**Comparative Behavior of the Two Functions.** The behavior of the two relaxation functions, Equations (2) and (3), is compared in Figure 3, for typical values of the parameters

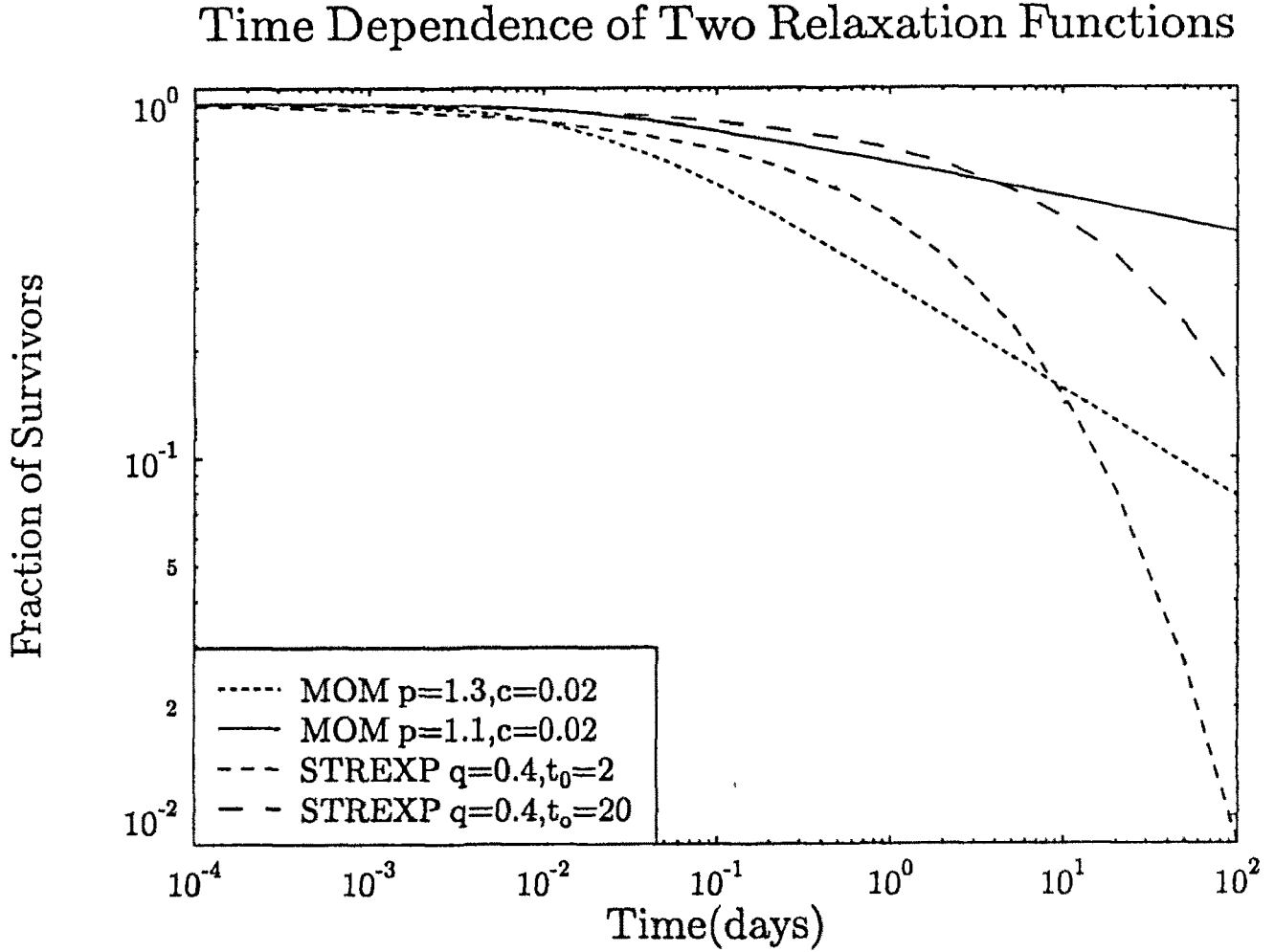


Figure 3: Comparison of the modified Omori function (MOM) and the stretched exponential function (STREXP) for a normally decaying sequence ( $p=1.1$ ,  $t_0 = 20$ ) and a rapidly decaying sequence ( $p=1.3$ ,  $t_0 = 2$ ). The fraction of events that have not yet occurred is plotted against time from the mainshock. The differences are not great until times greater than about 20 days are exceeded, for these examples.

derived from the analysis of real "normally" and rapidly decaying sequences. The MOM  $p$ -value 1.1 is the mean value for many sequences in southern California and is contrasted with a stretched exponential with a relaxation time of 20 days. A rapidly decaying sequence is illustrated by  $p = 1.3$ ,  $t_0 = 2$  days. No example of a slowly decaying sequence is shown because the total number of possible aftershocks,  $N(0)$ , is not defined. The differences during the first 10 days are not great; it is the long-time behavior that is most easily distinguishable, with the stretched exponential falling off more rapidly for similar early behavior. For the rapidly decaying sequences, 92% of the aftershocks have occurred at 100 days by the MOM relation, 99.2% by the stretched exponential. For the moderately decaying sequences, 57% of the aftershocks have occurred at 100 days by MOM, 85% by the stretched exponential. For a slowly decaying sequence,  $t_0 = 10,000$  days, only 15% of the events have occurred at 100 days. As pointed out above, for  $p < 1$ , the MOM relation is not appropriate in principle, even though a good fit to a catalog of finite duration can be achieved.

Further comparisons of the two models were carried out by generating time sequences for a specified number of events using Equations (5) (Omori) and (9) (stretched exponential). Sequences were generated with parameters corresponding to "normal", fast and slow decay rates. In each a case, as sequence was first generated based on Equation (5) and then modelled by both the modified Omori relation and the stretched exponential. Then values of the stretched exponential parameters close to those from the fit to the Omori-generated sequence were used to generate a new sequence by Equation (9) and this was modelled by the two functions. The total number of events chosen for each sequence was controlled by the requirements that the number be big enough that the numerical fits were sufficiently constrained, and that the time to reach the number had to be finite (controlled by MOM for fast decay (large  $p$ ) and STREXP for slow decay (large  $t_0$ )), but not be too short. From equation (4) the maximum number of events allowed by the MOM relation, with  $p > 1$ , is  $N_{max} = c^{1-p}K/(p-1)$ , for which the time to occurrence is infinite. There is no maximum number for  $p < 1$ . From equation (9), the time to reach 63.2% of a given  $N(0)$  is equal to  $t_0$ , and increases rapidly for larger fractions of  $N(0)$ .

The value of the Akaike Information Criterion, AIC, (Akaike, 1974) is given for each model fit. This measure, which is based on the maximum likelihood value of the fit, is used to judge which of two models fits a given data better. The algebraically smaller value is the better score. The values used and results of the modelling are given in Table 2.

As seen in Figure 3 and expected from the Shlesinger-Montroll (1984) theory, the biggest differences in the two models should be seen at long times after the onset of the sequence. The long-time behavior of the interevent times for the synthetic sequences was examined. On the basis of this test, it appears practically impossible to distinguish the two models

Table 2

- (1) "normal" decay: total number of events = 100.  
 MOM input:  $p=1.05$ ,  $c=0.03$ ,  $K=10.1$ .  
 Results of fitting:  
     MOM:  $p=1.049$ ,  $c=0.032$ ,  $K=10.196$ ,  $AIC=45.406$   
     STREXP:  $q=0.307$ ,  $t_0=25.35$ ,  $N(0)=103.46$ ,  $AIC=65.497$   
 STREXP input:  $q=0.3$ ,  $t_0=28$ ,  $N(0)=103$   
 Results of fitting:  
     STREXP:  $q=0.303$ ,  $t_0=30.65$ ,  $N(0)=103.21$ ,  $AIC=88.280$   
     MOM:  $p=0.917$ ,  $c=0.00036$ ,  $K=6.136$ ,  $AIC=102.318$
- (2) fast decay: total number of events = 90.  
 MOM input:  $p=1.3$ ,  $c=0.03$ ,  $K=10.1$ .  
 Results of fitting:  
     MOM:  $p=1.292$ ,  $c=0.030$ ,  $K=10.11$ ,  $AIC=-391.619$   
     STREXP:  $q=0.338$ ,  $t_0=1.421$ ,  $N(0)=90.13$ ,  $AIC=-360.076$   
 STREXP input:  $q=0.34$ ,  $t_0=1.42$ ,  $N(0)=90.1$   
 Results of fitting:  
     STREXP:  $q=0.334$ ,  $t_0=1.591$ ,  $N(0)=90.20$ ,  $AIC=-367.039$   
     MOM:  $p=1.060$ ,  $c=0.00176$ ,  $K=7.056$ ,  $AIC=-343.832$
- (3) slow decay: total number of events = 210.  
 MOM input:  $p=0.75$ ,  $c=0.03$ ,  $K=10$ .  
 Results of fitting:  
     MOM:  $p=0.752$ ,  $c=0.040$ ,  $K=10.13$ ,  $AIC=652.917$   
     STREXP:  $q=0.388$ ,  $t_0=1280.6$ ,  $N(0)=349.32$ ,  $AIC=659.977$   
 STREXP input:  $q=0.39$ ,  $t_0=1280.6$ ,  $N(0)=349$ .  
 Results of fitting:  
     STREXP:  $q=0.399$ ,  $t_0=1150.0$ ,  $N(0)=340.48$ ,  $AIC=675.999$   
     MOM:  $p=0.0703$ ,  $c=0.0014$ ,  $K=8.080$ ,  $AIC=677.665$ .

Table 2: This test shows that the AIC is effective in selecting the model. In every case, the better AIC score is for the model by which the time sequence was originally generated. The difference is not very large for the slowly decaying case, but is still definite. The first values under each result show how well the programs return the known input values, in the absence of noise (other than roundoff) in the input time sequence. This comparison shows that the Omori  $p$ -value and the relaxation time  $t_0$  value for a given sequence are inversely related, as expected.

for the case of slow decay out to 210 events (about 1000 days), as already suggested by the similar AIC values in Table 2. There are large differences only in the times to the first few events, to about 0.3 days, with the stretched exponential earlier, and also for numbers greater than about 300, not shown here, for which the times exceed 3000 days, with the stretched exponential later. The first few hours of many aftershock lists are not reliable (discussed below) and after eight or nine years, we can expect the seismicity rate to be close to that of background, independent of the aftershocks. The interevent times are essentially indistinguishable.

The two models are more easily distinguished for the moderate and fast decay cases, as expected from the AIC values in Table 2. The good separation at the beginning is not very useful because it extends only to the first 15-20 events, less than 0.1 days. The times and interevent times are separated by a factor of about 3 in the mid-range of these sequences.

**Applications to Some Sequences.** The principal objective of this study was to investigate which of the two models fits real data better. One problem in carrying out such tests is the inherent constraint imposed by the quality of earthquake catalogs. A large fraction of the total number of aftershocks in a sequence occurs in a relatively short time after the mainshock. This is the part of the list of aftershocks that is most likely to be incomplete, because of the difficulty of identifying small events in the coda of the mainshock and possible limitations on the resources available to the analysts to locate all of the many events.

In many cases, the cumulative number of events starts rather slowly and builds rapidly to a level from which it follows a more-or-less smooth curve. A question as yet unresolved is whether this behavior is due to missed events in the earliest times, or is a real phenomenon, such that aftershocks do start out rather slowly and build up to the rate modelled by relations such as those examined here. All that can be said now is that the beginnings of sequences often do not fit either of the relations tested here very well.

The maximum likelihood estimates of  $p'$ ,  $t_0$ , and  $K'$ , eqn.(7), from which  $N(0)$  may be calculated, are found for a given sequence by applying Ogata's algorithm, but with the modified Omori rate function, eqn (1), replaced by  $n(t)$  for the stretched exponential function. The fit by the stretched exponential function was tested on a number of crustal sequences for which the modified Omori parameters had previously been computed. Most of these were in southern California. The unpublished data for one Japanese intraplate earthquake (Narugo Town, March, 1985) were also used. Sequences were selected for which the catalog was considered reliable and for which the modified Omori p-values covered a wide range, from 0.71 to 1.8. A variety of tests were performed on these data, the results of which are summarized.

The sequences for which results are presented are listed in Table 3. The parameters



TABLE 3  
The Sequences Tested

Sequence	Date and location		MAG	MMIN	Nmin	tend
1	05/18/40	34.08N 116.30W	5.4	3.5	42	110.2
2	07/13/86	32.98N 117.86W	5.4	2.2	1248	501.3
3	02/21/73	34.10N 119.00W	5.5	2.8	16	23.4
4	06/28/66	35.92N 120.53W	5.6	3.6	12	4.3
5	11/04/49	32.20N 116.55W	5.7	3.1	29	10.3
6	12/04/48	33.93N 116.50W	6.0	2.8	94	663.9
7	09/04/81	33.67N 119.11W	5.3	1.9	157	182.3
8	05/19/40	32.73N 115.50W	6.9	3.5	34	19
9	05/02/83	36.22N 120.32W	6.5	3.1	269	773.5
10	08/04/85	36.15N 120.05W	5.8	2.2	193	24.7
11	05/02/83	36.22N 120.32W	6.5	3.1	184	76.8
12	10/15/79	32.63N 115.33W	6.6	2.9	23	25
13	03/15/79	34.32N 116.45W	5.2	2.2	323	509
14	08/13/78	34.35N 119.70W	5.1	2	229	149.7
15	04/10/47	34.98N 116.55W	6.2	3	124	443.1
16	10/01/87	34.06N 118.08W	6.0	1.8	197	35.8
17	07/21/52	35.00N 119.02W	7.7	4	224	3329.2
18	03/19/54	33.28N 116.18W	6.2	3.3	80	72
19	02/25/80	33.53N 116.55W	5.5	2.1	58	157.9
20	05/02/49	34.02N 115.68W	5.9	3	107	183
21	07/24/47	34.02N 116.5 W	5.5	2.7	79	125.4
22	03/11/33	33.62N 117.97W	6.3	4	132	2525.6
23	03/28/85	38.89N 140.71E	4.7	2	68	93
24	04/26/81	33.10N 115.63W	5.7	2.6	62	7.1
25	06/09/80	32.22N 114.98W	6.1	3	32	14.9
26	02/07/87	32.39N 115.31W	5.4	2.4	65	54.9
27	10/15/79	32.63N 115.33W	6.6	2.9	393	466.
28	10/15/79	32.63N 115.33W	6.6	2.9	360	466.
29	03/15/46	35.73N 118.06W	6.3	3.5	95	418.

Table 3: Date, epicentral coordinates, and magnitude are for the mainshock. Mmin is the minimum magnitude chosen for completeness of the catalog; Nmin, the number of aftershocks retained at this minimum magnitude. tend is the time, in days, from the mainshock to the end of the data set, at the minimum magnitude. The sequences are arranged in order of increasing Omori p-value (see Table 2). All sequences except No. 23 (Narugo Town, Japan) occurred in southern California. No. 9 and No. 11 are the Coalinga sequence, with No. 11 truncated at an earlier end-time. No. 27 is the Imperial Valley sequence of 1979; No. 12 and No. 28 are geographical subsets, as explained in Kisslinger and Jones (1991), where additional details on all of these sequences (except No. 23) are given.

TABLE 4  
Modified Omori p-values and Stretched Exponential Parameters for  $T_S = 0$

Sequence	PMOM	q	$t_0$	$N(0)$	AICMOM	AICSTR	$N(0)/N$	tend/ $t_0$
1	0.71	0.712	23.19	44.13	117.27	111.68	1.05	4.75
2	0.737	0.486	248	1652.39	-1781.89	-1774.04	1.32	2.02
3	0.772	0.395	32.1	27.29	18.09	19.2	1.71	0.73
4	0.826	0.32	303	53	-23	-21.32	4.42	0.01
5	0.884	0.419	3.94	37.4	-64.79	-61.2	1.29	2.61
6	0.93	0.333	61.18	105.55	137.7	147.41	1.12	10.86
7	0.937	0.418	20	170.71	-156.29	-148.3	1.09	9.11
8	0.94	0.404	8.5	45.35	-49.05	-42.72	1.33	2.24
9	0.953	0.327	68	302	-149.1	-109.68	1.12	11.37
10	0.984	0.507	4.01	209.93	-859.3	-840.16	1.09	6.17
11	1.039	0.41	6.8	197.26	-625.87	-596.77	1.07	11.30
12	1.019	0.395	2.69	25.26	-27.68	-23.39	1.10	9.29
13	1.024	0.398	25.67	335.57	-494.57	-463.66	1.04	19.83
14	1.041	0.378	6.61	238.21	-841.02	-802.46	1.04	22.65
15	1.05	0.32	15.78	131.15	-149.75	-120.99	1.06	28.08
16	1.099	0.428	1.69	202	-1137.8	-1107.81	1.03	21.17
17	1.107	0.339	27.12	225.37	-62.24	-56.66	1.01	122.76
18	1.119	0.357	1.21	81.15	-370.46	-352.99	1.01	59.50
19	1.121	0.336	4.9	60.43	-102.78	-81.54	1.04	32.22
20	1.174	0.603	15.67	108.2	27.83	26.01	1.01	11.68
21	1.208	0.465	5.91	80.28	-93.68	-81.68	1.02	21.22
22	1.282	0.29	6.62	132.58	-317.03	-245.43	1.00	381.52
23	1.27	0.403	1.4	68.3	-252.58	-234.36	1.00	66.43
24	1.45	0.588	0.61	62.9	-320.99	-310.54	1.01	11.69
25	1.495	0.56	1.39	32.25	-62.61	-60.11	1.01	10.76
26	1.518	0.502	1.62	65.19	-207.8	-192.17	1.00	33.86
27	1.686	0.403	1.06	393	-3064	-2879	1.00	439.58
28	1.74	0.398	0.997	360	-2806	-2610	1.00	467.36
29	1.812	0.552	11.52	95.07	-4.05	21.2	1.00	36.28

Table 4: Sequence numbers are from Table 3, PMOM are Omori p-values,  $q$ ,  $t_0$ ,  $N(0)$  are the parameters in the stretched exponential function, (2), AICMOM and AICSTR are the Akaike Information Criterion values for the two fits to the data set, Nmin and tend are from Table 3.

TABLE 5  
Modified Omori p-values and Stretched Exponential Parameters for  $T_S > 0$

Seq	$T_S$	PMOM		q	$t_0$	N(0)	AICMOM	AICSTR	Comments
3	0.051	0.90	(0.77)	0.453	44.0	26.94	35.3	36.1	
4	0.006	0.65	(0.83)	0.384	10E07	2736.	4.04	4.02	two models almost identical
5	0.019	0.88	(0.88)	0.274	100.0	74.25	-21.3	-20.9	$t_0$ not well-determined
6	0.044	0.93	(0.93)	0.211	220.0	150.5	213.5	213.3	STR fit good, back to $t=0$ .
16	0.090	1.09	(1.10)	0.384	2.57	185.5	-375.2	-378.3	
17	0.326	1.27	(1.17)	0.229	7.88	302.3	280.3	290.4	no improvement over $T_S=0$
18	0.088	1.20	(1.12)	0.179	0.20	134.6	-40.2	-40.5	
20	0.322	1.53	(1.17)	0.610	16.46	103.3	98.2	93.0	neither model is a good fit
21	0.037	1.24	(1.21)	0.342	3.97	95.0	-56.0	-53.6	
23	0.026	1.30	(1.27)	0.221	0.21	109.6	-132.7	-130.8	

for the two models are listed in Table 4 for  $T_S = 0$ . The sequences are listed in the order of increasing Omori p-value. In all but two of the cases, the MOM fit scores better than the stretched exponential, implying a better overall fit to the data. Further investigation revealed some factors that contribute to this result. Visual examination of plots of the data and the two fits shows that the stretched exponential often fits the beginning of a sequence poorly. Although the time duration of the misfitted segments is short, a relatively large fraction of the events occur during this interval, so the effect on the AIC value is large. The modified Omori relation can adjust for unreliable data at the earliest times by the parameter  $c$ ; the stretched exponential has no corresponding parameter. It was deemed undesirable to introduce an artificial fourth parameter into the stretched exponential, thereby destroying the clear physical interpretation of the parameters, so an alternative way of compensating for missing events during the initial, very active interval was tested.

A start time,  $T_S$ , was picked subjectively from a plot of cumulative number of events vs. time on which the MOM and stretched exponential fits for  $T_S = 0$  were superimposed. In general, the time was picked for which the trend of the data changed from a steeply rising, often concave upward growth curve to a more smoothly decaying rate of occurrence. In all cases, the times picked were short relative to the total duration of the sequence, from about 15 minutes to 2.5 hours. As shown in Table 5, the stretched exponential fit improved much more than to MOM with these later start times, and was superior in half of the ten cases.

For some slowly decaying sequences the best stretched exponential fit was for  $t_0$  tending to infinity (the calculation was stopped at  $t_0 = 10^7$ ).  $N(0)$  became correspondingly large, and the resulting fit was indistinguishable from the MOM fit (eqn (7)). The explanation

of this class of sequences was found in the long-time behavior of the mean interevent time. For those sequences with a finite  $t_0$ , the mean interevent time is seen to grow without limit up to the end of the data set. For those sequences for which  $t_0$  tends to infinity, the mean interevent time levels off, or increases at a decreasing rate, before the end of the catalog. The observation that a bounded mean interevent time corresponds to a power-law relaxation function, while mean interevent times that are unbounded at long times lead to a stretched exponential function with a finite  $t_0$ , is in accord with the theoretical results of Shlesinger and Montroll.

The question remains in each case whether the trend of the long-time mean interevent time is a true property of the sequence or an effect of the catalog of events. The examination of more well-documented sequences should lead to a resolution of this question. A possible explanation is that by the end of the data set, the rate of aftershock activity has decayed to, or is approaching, the normal rate of background seismicity in the particular seismic zone. If so, the levelling off to a finite mean interevent time is what would be expected.

**Conclusions.** From tests on a small number of sequences, some preliminary conclusions are:

- 1) The exponent  $q$  in the stretched exponential form is close to 0.4 for many of the cases. This value should be directly related to the long-time behavior of the pausing time distribution of aftershocks.
- 2) The process relaxation time,  $t_0$ , tends to be inversely related to the Omori p-value for a given sequence. Because the relaxation time has a definite physical meaning, even though the governing physics of the aftershock process is not yet well understood, the determination of this parameter as a descriptor of sequence decay should be useful in relating the temporal behavior of the process to fault zone properties and ambient conditions in the neighborhood of the hypocenters.
- 3) The apparent preference of many of the sequences tested for the power law decay may be the result of inadequacy of the list of events in the early part of the sequences. The choice of a starting time for the sequence is important, because there is no adjustable parameter in the stretched exponential form that can compensate for events missing from the catalog during the earliest times, 15 minutes to 2 hours for the cases analyzed.
- 4) The difference between the two models becomes important only at long times. Robust tests of the superiority of one or the other can only be made on long sequences with reliable listing of late aftershocks. The absolute time to make a sequence long depends on whether the decay is fast or slow. One measure is whether time length of the catalog is long compared to  $t_0$  in the stretched exponential model. The preference for an Omori relation fit or the

stretched exponential appears to be determined by the long-time behavior of the mean interevent time, and for the few examples is in accord with the Shlesinger-Montroll theory.

5) The stretched exponential has one obvious advantage: it eliminates the divergence of the aftershock series for slowly decaying sequences.

6) The ratio of  $N(0)$  to the observed total number of aftershocks approaches 1 for times long compared to  $t_0$ . This property may be useful for predicting or detecting the end of a sequence.

7) The stretched exponential function merits further testing as a model for aftershock decay because of its demonstrated utility in describing relaxation in other, unrelated, physical systems. If more work shows that it is a satisfactory model, aftershock occurrence would be more clearly associated with a broad class of thoroughly studied physical phenomena.

### **Publications and Presentations Based on the Research**

Gross, S. J. and C. Kisslinger, A seismicity-based stress model applied to the central Aleutians (abs), *Seism. Res. Lett.*, **62**: 31, 1991. Presented at 1991 meeting of Seismological Society of America.

Kisslinger, C. and L. M. Jones, Properties of aftershock sequences in Southern California, *J. Geophys. Res.*, **96**: 11,947- 11,958, 1991.

Kisslinger, C. and A. Hasegawa, Seismotectonics of intermediate-depth earthquakes from properties of aftershock sequences, *Tectonophysics*, **197**, in press, 1991.

Kisslinger, C., The stretched exponential as a model for aftershock rate decay (abs), *IASPEI Program and Abstracts*, 139, 1991. Presented at IASPEI Assembly, Vienna.

Kisslinger, C., Application of the stretched exponential relaxation function to modeling aftershock rate decay, *EOS*, **72**: 291, 1991.

## **LOMA PRIETA AFTERSHOCKS: Joint 3-D Structure and Hypocenter Inversion**

**14-08-0001-G1840  
01Jan90-30June91**

Thomas V. McEvilly  
Seismographic Station  
Dept. of Geology and Geophysics  
University of California  
Berkeley, CA 94720

Phone: (510) 486-7347  
FAX: (510) 486-5686  
e-mail: tvmceville@lbl.gov

### **Project Description**

This project involved the analysis of the Loma Prieta aftershock sequence as recorded by CALNET and portable local stations in the two months following the 18 Oct (UTC) mainshock. The approach to be used was an application of the joint hypocenter/velocity structure estimation method as implemented in 3-D by Michelini and McEvilly (1991) for studies at Parkfield. The goal was the estimation of the three-dimensional P- and S-wave velocity structure in the aftershock zone of the Loma Prieta earthquake sequence.

The LP earthquake occurred at the end of the southeastern rupture segment of the great 1906 earthquake, and at the final transition northwestward from the central creeping section of the San Andreas fault (SAF) to the locked 1906 segment. We are, therefore, able to investigate, qualitatively at this stage, several aspects of the earthquake process, including the nature and location of the asperity responsible for the 1989 earthquake, quasi-static loading of this asperity by the arrest of stable sliding, arrest of the dynamic rupture of the 1906 earthquake, and the interrelationships between these processes in determining the rupture characteristics of the earthquake.

The intense pre-main-shock seismicity of the creeping section in the southeastern part of our model volume and the many aftershocks of the 1989 earthquake that occurred in the central and northwestern part, together with the relatively dense regional seismographic network provide abundant data with which to constrain the three-dimensional P-velocity model. In particular, seismicity on the Sargent fault and on the dipping aftershock plane provide a three-dimensional source distribution.

### **Project Accomplishments (through 30June91)**

#### Inversion details

The three-dimensional tomographic inversion method and the data used in deriving the crustal velocity model for Loma Prieta are described in Michelini and McEvilly, 1991 and Michelini, 1991. The inversion used 5422 P-wave arrival times from 173 earthquakes, aftershocks and pre-mainshock 'background' events recorded at a minimum

of 25 and 30 local stations, respectively, of the USGS CALNET central California network. We estimate the accuracy of these well-recorded P-wave onsets to be  $\pm 0.02$  sec. The starting model for the 3-D inversion was a 1-D inversion result using the linear B-splines method of Thurber (1983), a model which yielded a weighted RMS residual of 0.236 sec.

The model is discretized in the 9x11x6-point (XxYxZ), 596-node grid shown in Figure 1. Node spacings are 3, 7, and 3 km, respectively, in the X, Y, and Z directions. The XY coordinate system is rotated 45° counterclockwise, aligned approximately along the SAF trace. Figure 1 also shows the 173 earthquakes and the stations used in the velocity inversion. After seven iterations the final 3-D model yields a weighted RMS residual of 0.092 sec. The stability of the inversion was demonstrated by Michelini (1991) through the use of a number of grid geometries which produced very similar models. In addition, the local quality of the inversion can be incorporated into the displays of the velocities by superposition of the spread function to show resolution throughout the model space. Interpretations are conservatively based on the well-determined aspects of the model.

More than 700 earthquakes (background seismicity events and aftershocks) in the Loma Prieta region were relocated with the 3-D model determined from the simultaneous inversion exercise. Figure 2 presents the full data set of relocated hypocenters which lie within the model volume. This rotated X-Y (NE-NW) position convention is used in this work, for simplicity and consistency in viewing specific features of the model or the seismicity.

#### The velocity model

The three-dimensional P velocity model is shown in map view in Figure 3 for several depths. Figures 4 and 5 are across-strike (southwest-northeast) and along-strike (southeast-northwest) depth sections through the velocity model at specified y and x values, respectively. The hypocenters shown on Figures 3 - 5 are projected on to the planes of section as described in the individual figure captions. The good correlation of the near-surface features of the velocity model with the surface geology allows us to extend our interpretation to the well-resolved parts of the model at depth with a high degree of confidence. To do this we identify the major subsurface geological contacts by comparing the three-dimensional model with published seismic refraction models. We also make use of published laboratory velocity versus pressure and velocity versus temperature data for specific Franciscan and Gabilan rocks, and for other rocks that are thought to be representative of possible constituents of the central California Coast Ranges. These laboratory data are converted to velocity-depth profiles assuming hydrostatic overburden pressure and SAF geotherm "A" of Lachenbruch and Sass (1973), which are then compared with profiles through the model at various locations.

Apart from the major surface-outcropping units described thus far, the most striking feature imaged by the three-dimensional model is the large, southeast-northwest elongated dome of high velocity rock protruding from below to depths as shallow as 7-8 km within the southwestern two-thirds of the model (Figures 3 and 4). Perhaps the most clear view of this high-velocity rock mass is on the longitudinal cross-section at  $x = 0.6$  km, shown in Figure 5. A high-velocity body was also imaged in this vicinity by Michael and Eberhart-Phillips (1991). At depths greater than 8 km, the body extends to the northeast, crossing beneath the trace of the SAF. Profiles in Figure 4 southwest of the SAF and to the northeast show that the well-resolved velocities within this body are much too high for both granite and Franciscan rocks. We can assert

with confidence the existence of this high-velocity rock mass at depths as shallow as 7-8 km. A clue to the composition of the high velocity body may be provided by surface geology and magnetic data. The only outcrop of basement rocks between the Zayante-Vergeles and San Andreas faults is not Salinian basement but is a 0.5 to 1 km wide outcrop of hornblende and anorthositic gabbro on the southwest side of the SAF near Logan. This Logan gabbro body was originally identified as a fault sliver that is correlative with a sliver of similar composition to the southwest at Gold Hill, near Cholame (Ross, 1970), on the Parkfield segment of the SAF.

In summary, the three-dimensional velocity model images a rock mass having anomalously high velocity in the mid and upper crust that apparently underlies both the Salinian and Franciscan basements within the hypocentral zone of the Loma Prieta earthquake. This body is seen in the upper, middle and probably in the lower crust in a regional tomographic model and its existence, at least southwest of the SAF, is also suggested by magnetic and gravity data. The origin and full extent of the body are not constrained by our model nor is the body well resolved by the regional model. Present evidence favors this massive body being an up-thrust section of sub-basement rock. The rather tenuous link between the buried high-velocity body and the unusual outcrop of gabbro southeast of Logan suggests that it may be composed of gabbro, in which case it may be of similar composition to the sub-basement underlying the Franciscan assemblage. The velocity model also allows a variety of alternative explanations, including an intrusive body. This massive body appears to play an important role in dictating the mode of strain release within the southern Santa Cruz Mountains segment of the SAFZ. Our present lack of knowledge of the origin and composition of the high-velocity body notwithstanding, we are able to build a picture of how the fault zone behavior is controlled in this segment by along-strike changes in lithology.

#### Aftershock distribution

The velocity model covers the final transition from the central creeping section of the SAFZ on the southeast to the locked 1906 segment to the northwest. The fault creep rate drops from 14 mm/yr at San Juan Bautista to less than 1mm/yr at Pajaro Gap. The Loma Prieta rupture zone occupies the southeastern end of the locked 1906 segment. Background seismicity on the SAFZ falls off northwest of San Juan Bautista.

Background activity revives northwest of the high-velocity body in the form of the tight cluster of earthquakes near Lake Elsmar. Low-level activity persists on a long-term basis in this vicinity but the cluster of earthquakes here also includes the M5.0 earthquake of June 27, 1988 and the M5.2 earthquake of August 8, 1989 and their aftershocks.

Coincident with the abrupt cessation of SAF creep-related seismicity where the fault encounters the high-velocity body at Pajaro Gap there is an equally abrupt increase in aftershock activity as we enter the aftershock zone proper. At this southeastern end of the aftershock zone, the aftershocks define a plane that is a continuation, to depths greater than 7 km, of the plane defined by the creep-related seismicity and triggered aftershocks to the southeast. The main concentration of aftershocks forms a belt that plunges northwest to a maximum depth near 19 km, southeast of the mainshock hypocenter. The main concentration of aftershocks northwest of the mainshock hypocenter, and presumably the mainshock rupture plane, occurs well to the northwest of the end of the high-velocity body and on the Salinian/Franciscan contact at the SAF.



## Conclusions and model implications

The three-dimensional velocity model is in good agreement with the surface geology and with available models from refraction surveys, and was in this study calibrated against laboratory P-velocity data for representative rock types found on both sides of the SAF in the region. Furthermore, the well-resolved portions of the model are delineated explicitly in the inversion calculation. We are thus able to define with a high degree of confidence a large, anomalous high-velocity body associated with the rupture zone of the Loma Prieta earthquake. This high-velocity body appears to play a profound role in controlling the transitions in slip behavior of the San Andreas fault zone (SAFZ) under the southern Santa Cruz Mountains. By interpreting the spatial distributions of background and aftershock seismicity in relation to the three-dimensional velocity model, we are able to construct a model of the Loma Prieta earthquake rupture that is a simple extension of the classical single asperity model (Kanamori, 1986). This model appears to be in good agreement with a kinematic model of the earthquake rupture (Beroza, 1991). Because our model is based in part upon consideration of the rupture of the 1906 earthquake, we are able to draw tentative conclusions about the earthquake cycle in the southern Santa Cruz Mountains which may be of help in determining the potential for future damaging earthquakes in that region.

## **Remaining Steps**

A full paper is in the final stages of preparation for the USGS Professional Paper on the Loma Prieta earthquake. It will be submitted for the Spring, 1992 deadline, and it contains the complete development of the asperity model for the fault zone. What remains to be done that could provide substantially more insight into the earthquake dynamics is an analysis of the S-waves parallel to that we (and others) have completed for the P waves. This will require a comprehensive collection of all the portable three-component data and local strong-motion data acquired in the aftershock sequence. Noone has been able to accomplish this to date, due to various instrumental, logistics, manpower and political problems. It is worth an infusion of some resources to accomplish - there has been a large investment of public research funds toward this end, and perhaps a serious community approach to the problem is warranted.

## **References**

- Beroza, G (1991). Near-source modeling of the Loma Prieta earthquake: Evidence for heterogeneous slip and implications for earthquake hazard, submitted to *Bull. Seism. Soc. Am.*, **82**, in press.
- Choy, G.L. and J. Boatwright (1990). Source characteristics of the Loma Prieta, CA, earthquake of October 18, 1989, from global data, *Geoph. Res. L.*, **17**, 1183-1186.
- Kanamori, H. (1986). Rupture process of subduction zone earthquakes, *Ann. Rev. Earth Planet. Sci.*, **14**, 293-322.
- Lachenbruch, A.H. and J.H. Sass (1973). Thermomechanical aspects of the San Andreas fault system, in Kovach, R.L. and Amos Nur, eds., *Proc. Conf. Tect. Problems of the San Andreas fault system*, Stanford, CA, Stanford Univ. Pub. Geol. Sci., **13**, 192-205.
- Michael, A.J. and D. Eberhart-Phillips (1991). Relations among fault behaviour, subsurface geology, and three-dimensional velocity models, *Science*, **253**, 651-654.
- Michellini, A. (1991). Fault zone structure determined through the analysis of earthquake arrival times, Ph.D. Thesis, Univ. CA, Berkeley.

- Michellini, A. and T.V. McEvilly (1991). Seismological studies at Parkfield: I. Simultaneous inversion for velocity structure and hypocenters using B-splines parameterization, *Bull. Seism. Soc. Am.*, **81**, 524-552.
- Ross, D.C. (1970). Quartz gabbro and anorthositic gabbro: Markers of offset along the San Andreas fault in the California Coast Ranges, *Geol. Soc. Amer. Bull.*, **81**, 3647-3662.
- Thurber, C.H. (1983). Earthquake locations and three-dimensional crustal structure in the Coyote Lake area, central California, *J. Geoph. Res.*, **88**, 8226-8236.

## LOMA PRIETA BASE MAP

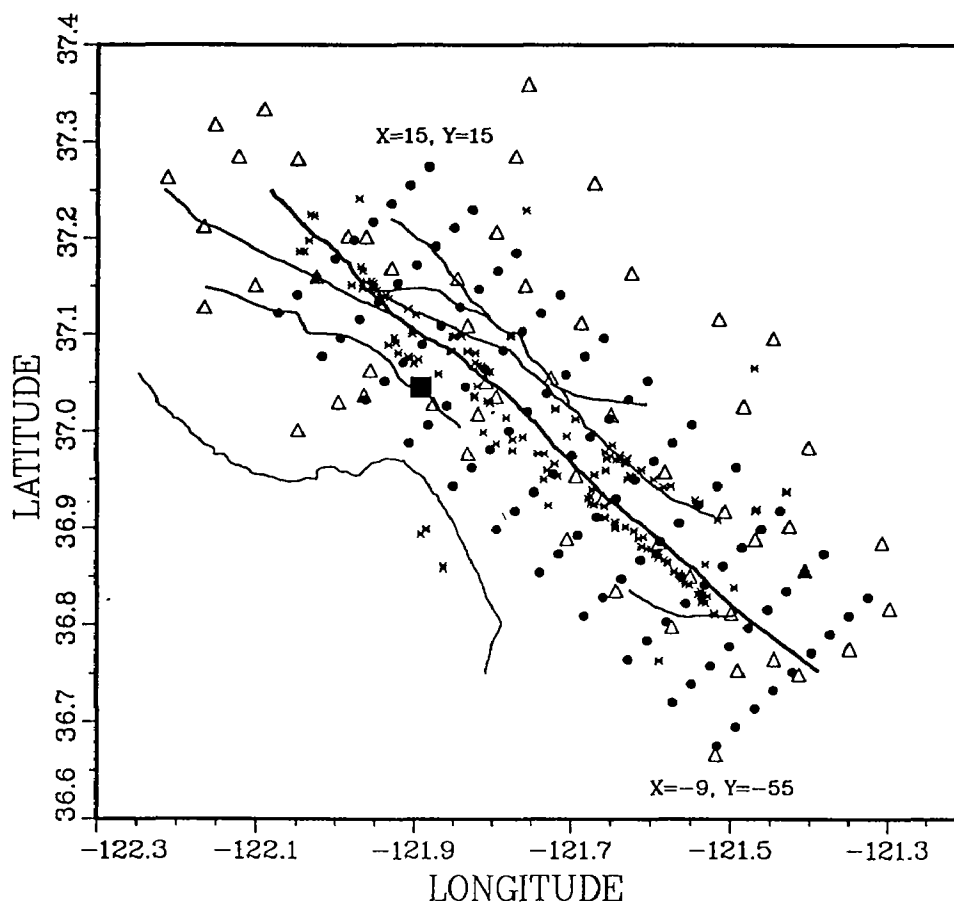


**Figure 1.** Loma Prieta base map showing inversion grid (solid dots), CALNET stations (triangles), mainshock epicenter (solid square), major fault traces, epicenters of the 173 earthquakes used in the joint inversion (crosses), and corner coordinates for the 45° rotated grid reference system (used in subsequent figures).

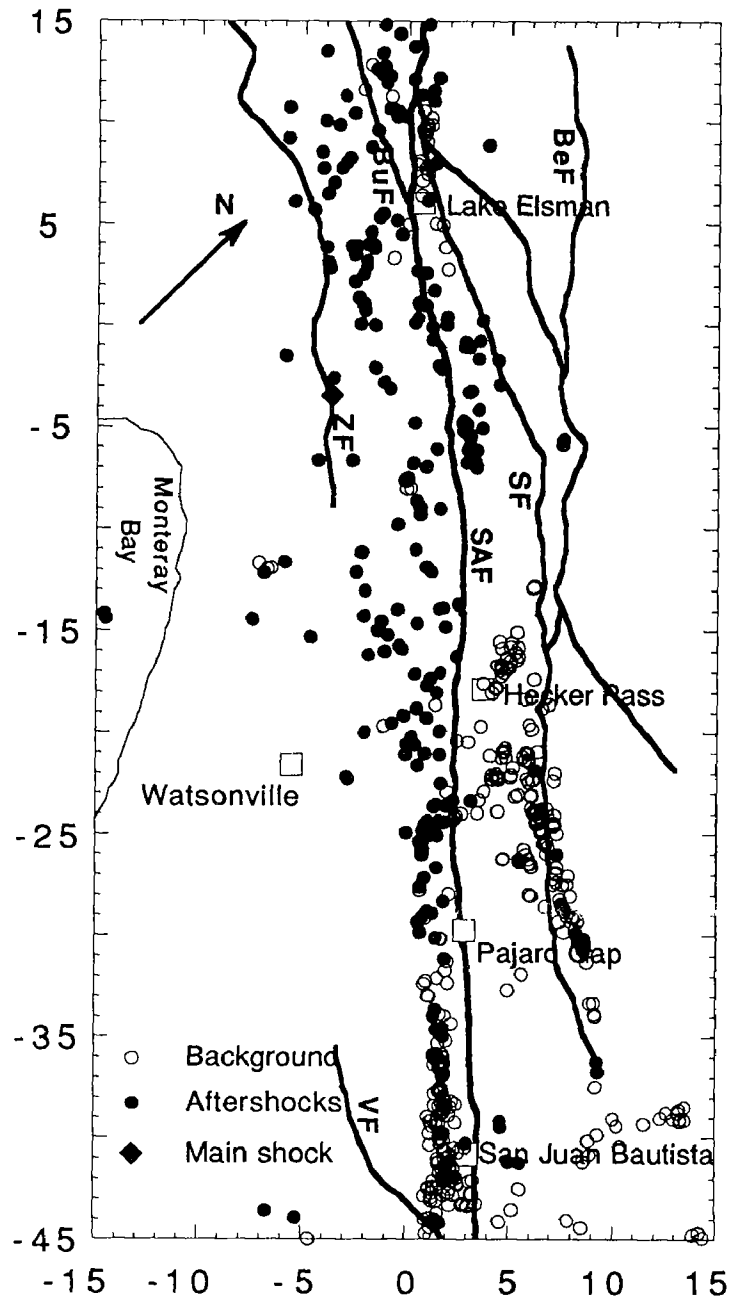


**Figure 2.** Relocated epicenters for 700+ earthquakes in the Loma Prieta area, including background (pre October 1989) seismicity and 1989 aftershocks. The coordinate system is that defined for the inversion grid in Figure 1. Major faults in the area are shown: SAF=San Andreas, SF=Sargent, BeF=Berrocal, BuF=Butano, ZF=Zayante, VF=Vergeles.

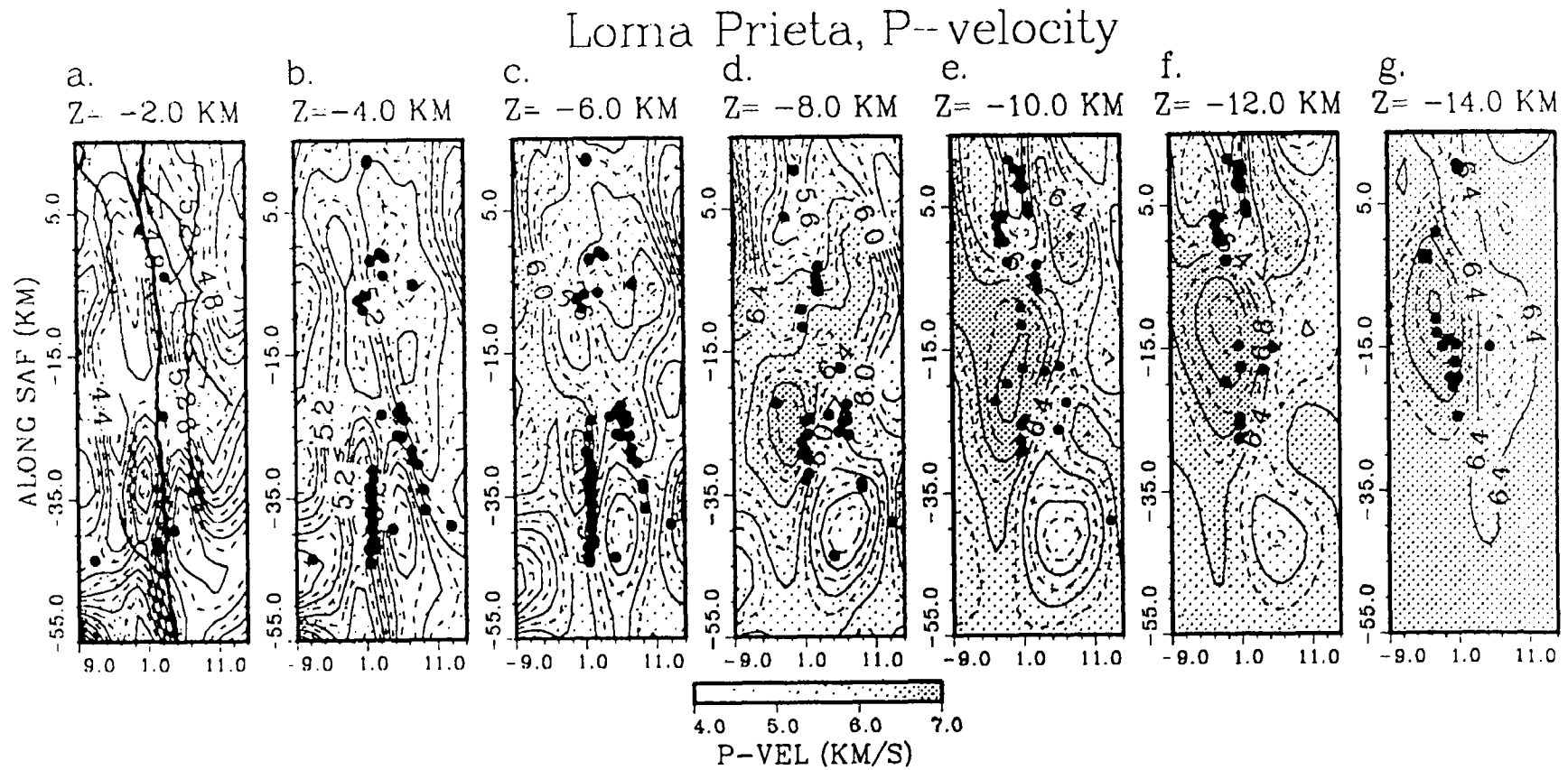


**Figure 3.** Final P-velocity model for Loma Prieta region, displayed in horizontal plan-view sections from 2-km depth to 14-km depth and extending horizontally over the grid in Figure 1, from  $x,y=-9,-55$  to  $x,y=15,15$ . Velocity values are contoured and shaded, with higher values more darkly shaded. Hypocenters determined in the joint inversion are plotted on their appropriate levels.

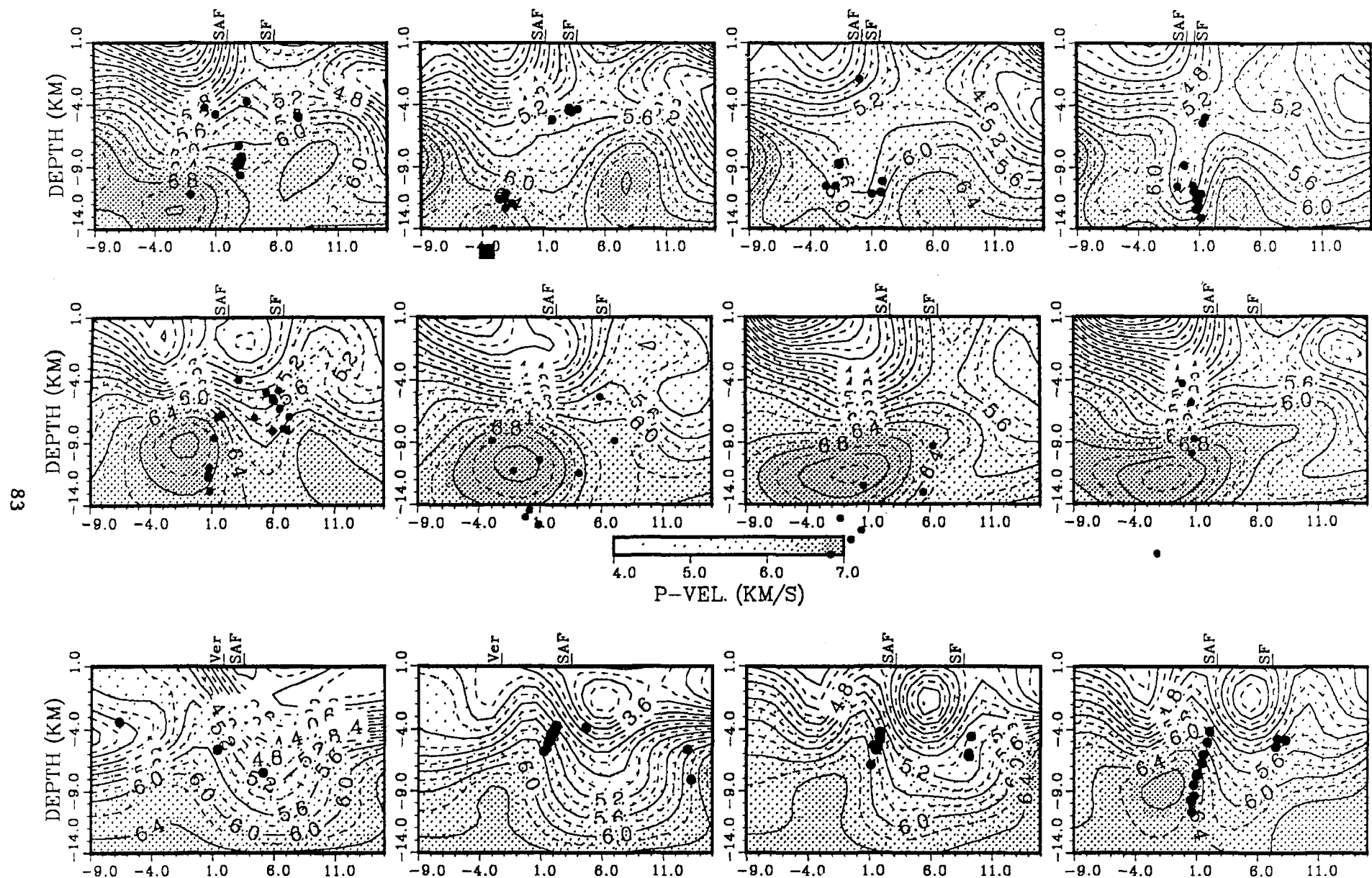


**Figure 4.** Final P-velocity model for Loma Prieta region, displayed in twelve fault-normal sections from  $y=-45$  km (southeast, lower left frame) to  $y=+10$  km (northwest, upper right frame) at 5 km intervals along the fault. Velocity values are contoured and shaded, with higher values more darkly shaded. Hypocenters determined in the joint inversion are plotted on their appropriate sections.

## Loma Prieta, P-velocity

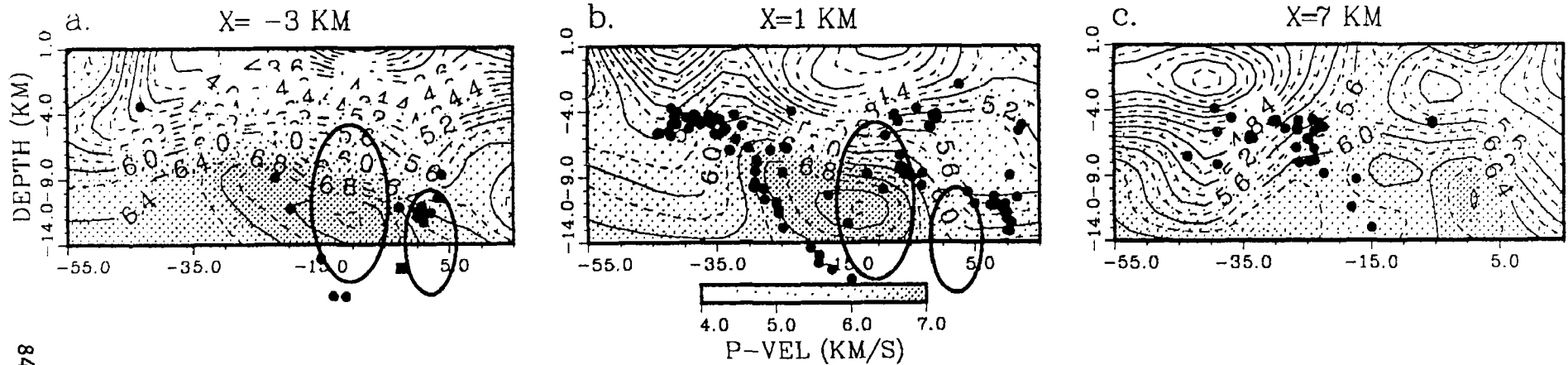


**Figure 5.** Final P-velocity model for Loma Prieta region, displayed in three fault-parallel sections at  $x=-3, +1, +7$  km. View is from the northeast (northwest is to the right). Velocity values are contoured and shaded, with higher values more darkly shaded. Hypocenters determined in the joint inversion are plotted on their appropriate sections. Ellipses are the inferred fault zone asperities from the Loma Prieta mainshock source study of Choy and Boatwright (1990).

## **OEEV Drilling Project**

9960-01176

Thomas H. Moses, Jr.  
Branch of Tectonophysics  
U.S. Geological Survey  
345 Middlefield Road  
Menlo Park, CA 94025-3591  
(415) 329-4870  
FTS: 459-4870

The primary focus for the current year has been to close down the Santa Nella, California, drilling facility by transferring, surplus, selling, and/or junking all non-usable or serviceable pieces of equipment, including removal of all hazardous wastes. Additional efforts were devoted to assisting or managing Division drilling projects, including the development of drilling programs, cost estimates, and contracts.

### **Results include:**

- 1) Closing of Santa Nella facility.
- 2) Successful completion of Test Hole Program in support of NEHRP SF Bay studies.
- 3) Successful completion of Creede, Colorado, Research Drilling Project for the ICG of the Continental Drilling Program.

## Fault Interaction, Segmentation, and Geometry along the San Andreas Fault System, Southern California

14-08-0001-G1984

Craig Nicholson  
Institute for Crustal Studies, University of California  
Santa Barbara, California 93106  
805-893-8384  
*craig@quake.crustal.ucsb.edu*

### **PROJECT PLAN**

1) Convert the analog FM-tapes from the 5-day portable recorders deployed in the epicentral region of the 1986 North Palm Springs (NPS) earthquake into digital data and incorporate the digital data into the event database. This requires the use of the USGS playback system in Menlo Park. The digital data will then be examined to determine accurate arrival times and polarities of P- and S-waves, and better spatial resolution of aftershock source characteristics. This task can only be performed if the playback system is operational, and the converted digital data are made available to this project. Arrival times for both P- and S-waves from the portable GEOS instruments have already been determined [*Nicholson et al.*, 1986].

2) Invert the phase data from all the portable and permanent regional stations for improved station corrections, revised earthquake hypocenters, and the local 3-dimensional velocity structure in the northern Coachella Valley. Analyze the resulting improved earthquake hypocenters and single-event focal mechanisms to identify patterns of interacting subsurface faults involved in the 1986 NPS sequence.

3) Examine available historical records of the 1948 Desert Hot Springs (DHS) earthquake to improve our understanding of the location, magnitude, moment and possible fault geometry involved during this earlier seismic rupture of the southern San Andreas fault.

### **PROGRESS**

This project began on 1 March 1991; this report documents progress through 31 October 1991.

1) The Branch of Seismology in Menlo Park has been contacted repeatedly regarding the digitization of the NPS 5-day analog tapes. The original playback system is now defunct, but a second playback system is marginally operational. However, this second system is fully utilized with the playback of tapes from Loma Prieta and other studies. Thus, I am still awaiting confirmation from Menlo Park to determine exactly if and when the NPS data can be digitized, and if a specific time period can be scheduled for use of the Menlo Park playback system.

2) A preliminary high-resolution tomographic inversion for 3-D P-wave velocity perturbations in the vicinity of the NPS earthquakes has been performed and submitted for publication [*Nicholson and Lees*, 1991]. The inversion was based largely on data from the regional network of telemetered stations and the portable GEOS recorders. I am awaiting the digital data from the eight 5-day analog recorders to expand the data set, increase resolution, and perform a similar inversion using S-wave arrivals. The preliminary tomographic images of velocity perturbation within the northern Coachella Valley reveal high-velocity anomalies in the region along the fault responsible for most of seismic slip during the NPS mainshock [*Hartzell*, 1989] and most of the aftershock hypocenters [*Nicholson et al.*, 1986], suggesting that the distribution of high-velocity anomalies outline the asperity responsible for the earthquake. Revised aftershock hypocenters using improved velocity models and station corrections suggest that the segment of the Banning fault that



slipped in 1986 may be listric, and may be truncated at depth by a low-angle northeast-dipping detachment surface (Figure 1). A revised hypocenter for the NPS mainshock suggests a slightly shallower focal depth (10.4 km) than reported earlier (implying that dynamic rupture may have propagated nearly equally both up and down dip), and confirmed that the initial sense of slip based on the P-wave first-motion focal mechanism was pure strike-slip ( $300^\circ$  - strike,  $40^\circ$  - dip;  $180^\circ$  - rake), although with a slightly shallower dip than reported earlier [Jones *et al.*, 1986].

3) Requests for copies of historical seismograms of the 1948 DHS earthquake have been sent to nearly all observatories that recorded the event. Nearfield records at Berkeley and Caltech—particularly from the portable stations deployed by Caltech in the epicentral region immediately following the 1948 event—have already been examined [Nicholson *et al.*, 1987]. Copies of regional and teleseismic records at stations SEA, VIC, OTT, HAL, FLO, SLM, CLE, WES, NOL, LPZ, and DBN have been received. There has been no response from repeated requests to the USGS regarding availability of historical seismograms or microfilm of various regional station records archived in Denver. These later stations include: TUO, SIT, COL, SLC, BUF, BER, and SJP, as well as possible records from PFA, BDA, BCN, BUT, BZM, RCD, CHK, PHI, and CSC. A working system for seismogram digitization was developed, but appropriate instrument responses for some of the old recording systems (needed to invert the data for mainshock source characteristics) are still uncertain.

Preliminary results indicate that the 1948 DHS event likely ruptured the adjacent segment along the Banning fault to the southeast of the 1986 NPS earthquake. Based on P-wave first-motions and long-period surface waves, the preliminary focal mechanism of the DHS mainshock is oblique strike-slip with a small reverse component ( $305^\circ$  - strike;  $75^\circ$  - dip;  $170^\circ$  - rake); the moment magnitude is more likely  $M_w$  6.2 than 6.5; and the mainshock focal depth is approximately 12 km [Nicholson, 1987; Nicholson *et al.*, 1987].

## REFERENCES

- Hartzell, S. (1989). Comparison of seismic waveform inversion results for the rupture history of a finite fault: Application to the 1986 North Palm Springs, California, earthquake, *J. Geophys. Res.*, **94**, 7515-7534.
- Jones, L.M., K.L. Hutton, D.D. Given, and C.R. Allen, The North Palm Springs, California, earthquake sequence of July 1986, *Bull. Seismol. Soc. Am.*, **76**, 1828-1843 (1986).
- Nicholson, C., Seismic slip on the southern San Andreas fault: 1948 and 1986 (abstract), *Seismol. Res. Lett. (Earthquake Notes)*, **58**, 14 (1987).
- Nicholson, C., H. Kanamori and C.R. Allen, Comparison of the 1986 and 1948 earthquake along the southern San Andreas fault, Coachella valley, California (abstract), *EOS Trans. AGU*, **68**, 1362 (1987).
- Nicholson, C. and J.M. Lees, High resolution travel-time tomography in the northern Coachella Valley from inversion of aftershock arrival times of the 1986  $M_L$  5.9 North Palm Springs Earthquake, *Geophys. Res. Lett.*, submitted 1991.
- Nicholson, C., R.L. Wesson, D. Given, J. Boatwright and C.R. Allen (1986). Aftershocks of the 1986 North Palm Springs earthquake and relocation of the 1948 Desert Hot Springs earthquake sequence (abstract), *EOS Trans. AGU*, **67**, 1089--1090.

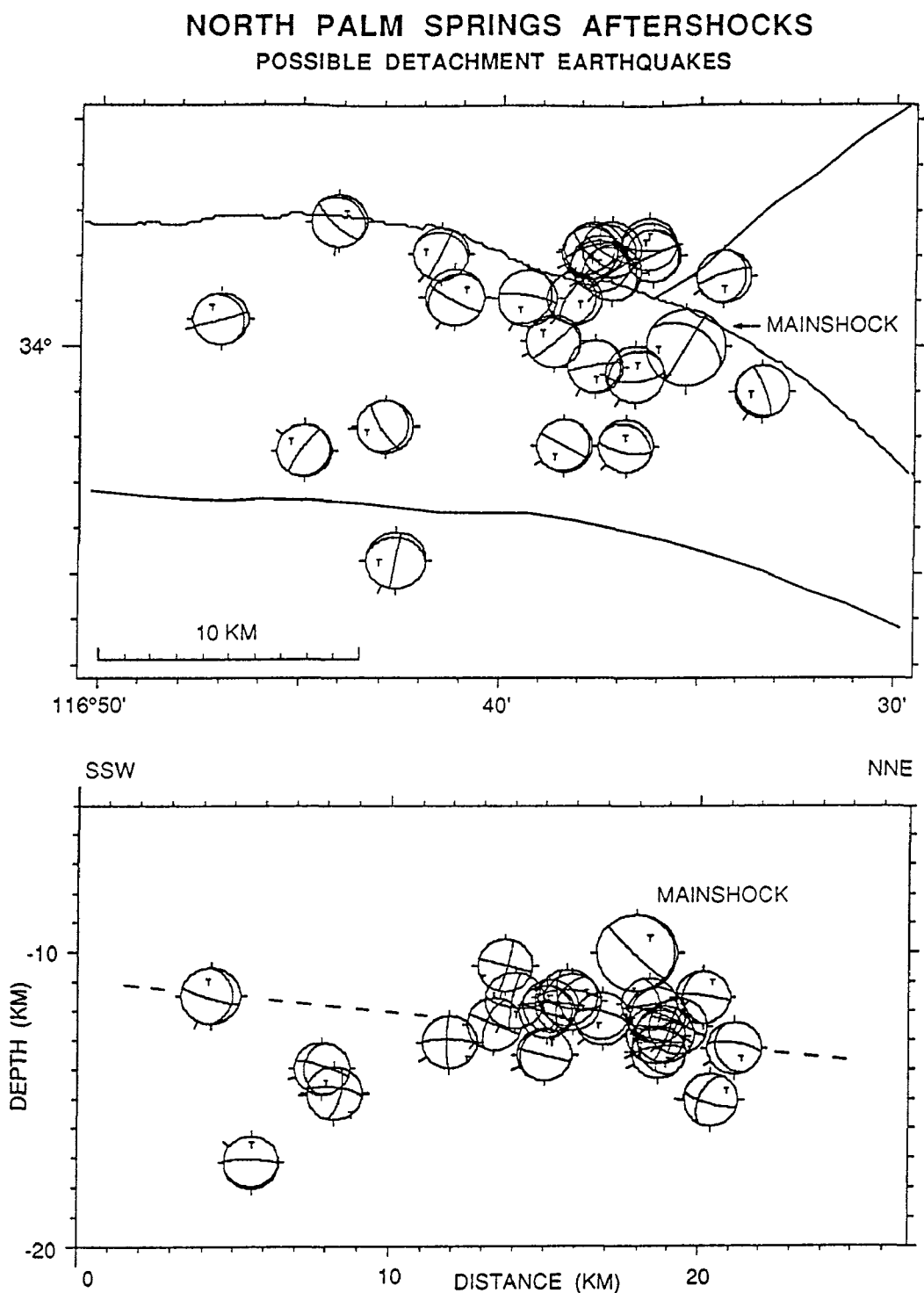


Figure 1. (top) Map showing lower-hemisphere focal mechanisms of selected aftershocks of the 1986 North Palm Springs mainshock (large symbol) that exhibit a low-angle nodal plane ( $< 20^\circ$ ). (bottom) Cross section showing back-projections of the same focal mechanisms. Although slip directions are not all the same, most of the earthquakes occur west of the Banning fault, between depths of 10–14 km, and define a low-angle structure dipping to the northeast, consistent with slip along a detachment that truncated the down-dip extent of the 1986 mainshock rupture.

# CONSTRAINTS ON TECTONIC DEFORMATION IN THE SOUTHERN ALASKA SUBDUCTION ZONE FROM HISTORICAL SEISMICITY

USGS Contract 14-08-0001-G1952

Emile A. Okal and Seth Stein

Northwestern University

*Department of Geological Sciences, Northwestern University, Evanston, Illinois 60208*

[708] 491-3238

## *General Purpose and Background*

The purpose of the project is to reassess the historical seismicity of the Central part of Alaska. This area, which in principle, should be considered intraplate, is the site of significant seismicity, leading to the possibility of a diffuse plate boundary, such as has been documented elsewhere, for example in the Indian Ocean.

In particular, the central part of Alaska features intriguing historical earthquakes, for which magnitudes as large as  $M = 7.3$  have been proposed. As always the case when dealing with historical events, the location, size, depth and focal geometry of these events are generally imprecise, and must be carefully re-assessed with the full power of modern day seismological techniques. What makes this endeavor particularly crucial is the regular operation of a VLBI station at Fairbanks in the immediate vicinity of the reported epicenters of major earthquakes in 1937 and 1947. It is generally assumed by Space Geodesists that Fairbanks, several hundred km North the plate boundary, is firmly anchored to the North American continent, and can be viewed as a genuine sampling of the stable North American plate.

## *Investigations Undertaken and Results Obtained*

We have undertaken to study approximately 30 historical earthquakes, with dates ranging from 1916 to 1960†. These events were selected on the basis of having at least one magnitude reported as  $M \geq 7$ , in various catalogues including the NEIC tape and the International Seismological Summary [ISS]. Our investigation is directed along several fronts: (i) relocation of the earthquakes; (ii) reassessment of their size; and (iii) evaluation of their focal geometry.

### • *Relocation*

The basic dataset for relocation consists of the arrival times listed in the ISS. Because the ISS starts reporting systematically around 1915, our first event goes back to 1916. We use a computerized iterative algorithm, satisfactorily developed in previous investigations (and applied to many hundreds of events) by the investigators. The algorithm can improve the old ISS locations for two fundamental reasons: we include  $S$  times, which the ISS lists, but does not use in locating; and the computerization of the process allows us to test, identify, and eventually reject data of lower quality, which either prevent convergence, or result in excessive standard

---

† “Historical” earthquakes have traditionally been taken as those predating the establishment, in 1963, of the World Wide Standardized Seismographic Network, which for the first time allowed the routine and precise location of earthquake foci worldwide.

residuals. In addition, we conduct statistical tests of the solution, by artificially injecting noise into the data, and studying its influence on the resulting locations.

In general, the 29 events relocated by this procedure were not significantly displaced from their original locations (an average of 40 km). In several instances, we were able to obtain some constraints on depth, and in the case of the 1916 event, suggest that the earthquake is probably shallow.

Probably the most important result of this part of the investigation is that the large earthquakes of 1937 and 1947 in the vicinity of Fairbanks actually took place South of the city; indeed, both events relocated South of their original epicenters. This crucial result validates the assumption, tacitly used in Space Geodesy, that no large scale crustal deformation takes place between Fairbanks and the bulk of the North American continent, in other words that Fairbanks does represent a stable benchmark in the North American plate.

- *Magnitudes*

An attempt was made to reassess the magnitudes of some of the more significant events in the dataset. A large collection of records were inspected, and when feasible, digitized at the University of Uppsala, Sweden, which maintains one of the best archives of Wiechert seismograms; at the Caltech archives in Pasadena; and at the USGS Historical Seismogram Facility in Denver. In many cases, standard surface wave magnitudes appear to have been overestimated (see Table 1). We are presently researching the origin of this bias, which may lie in the use of a variable period in the early magnitude measurements.

Whenever possible, we conducted a measurement of the mantle magnitude  $M_m$ , measured at very low frequencies, and representative of the seismic moment of the source, as introduced by us in earlier investigations. Given the above remark regarding  $M_s$ , the generally lower than expected level of the seismicity resulted in only a small number of  $M_m$  values: there was just not enough energy at long periods in most old records to obtain a reliable measurement (see Table 2).

- *Focal Mechanisms*

We are presently investigating the focal mechanism of the central Alaskan events of 1937 and 1947. Because of the paucity of records available for this study, we have to rely on special techniques. We are using the three-component Benioff 1-90 records at Pasadena, which have the double advantage of providing good recording characteristic throughout a broad frequency spectrum, and of having been continuously used up to the present, allowing for direct comparison with modern earthquakes. Since the historical events were not truly gigantic, their spectrum is concentrated in the 20–70 s period range, in which the influence of lateral heterogeneity on the dispersion characteristics of surface waves is primordial. In order to eliminate this unknown parameter, we use modern earthquakes traveling over a similar path (Northwestern Alaska to California), and whose focal solutions have been published as part of the CMT dataset, in order to retrieve the Love and Rayleigh dispersion along the source-to-receiver path, and in turn extract the focal parameters of the historical earthquake (moment and geometry) from the complex spectra of its Love and Rayleigh waves at a single station. This work is presently being performed with Graduate Student Wei-chuang Huang.

Table 1: Alaskan Historical Earthquakes Relocated in This Study

Date D M Y	Initial Location					Relocation				
	Time (GMT)	Lat. °N	Long. °W	Depth (km)	$M$	Time (GMT)	Lat. °N	Long. °W	Depth (km)	$M_s$ (UPP)
18 4 1916	04:01:48.0	53.25	170.00	170	7.5	04:01:44.9	53.66	170.00	33.0	
04 5 1923	16:26:39.0	55.50	156.50	25	7.1	16:26:42.2	55.29	156.67		
24 10 1927	15:59:55.0	57.50	137.00	25	7.1	15:59:51.8	57.67	136.80		6.7
21 6 1928	16:27:13.0	60.00	146.50	25	7.0	16:27:14.9	60.21	147.09		6.6
07 3 1929	01:34:39.0	51.00	170.00	50	8.6	01:34:39.3	50.66	169.69		7.6
26 5 1929	22:39:54.0	51.00	131.00	0	7.0	22:40:03.0	50.76	130.80		
27 4 1933	02:36:04.0	61.25	150.75	25	7.0	02:36:05.3	61.04	151.10		
04 5 1934	04:36:07.0	61.25	147.50	80	7.2	04:36:05.4	61.40	147.74		6.5
22 7 1937	17:09:29.0	64.75	146.75	25	7.3	17:09:30.7	64.52	146.77		6.9
10 11 1938	20:18:43.0	55.50	158.00	25	8.7	20:18:40.1	55.35	158.38		8.2
22 8 1940	03:27:18.0	53.00	165.50	25	7.1	03:27:13.6	52.17	165.36		6.8
09 9 1942	01:25:26.0	53.00	164.50	80	7.0	01:25:22.5	52.95	166.19		5.8
03 11 1943	14:32:17.0	61.75	151.00	25	7.3	14:32:18.4	61.75	150.88		7.0
27 7 1944	00:04:23.0	54.00	165.50	70	7.1	00:04:25.2	54.05	165.47	22.9	
12 1 1946	20:25:37.0	59.25	147.25	50	7.2	20:25:38.2	58.95	147.25		6.2
01 4 1946	12:28:54.0	52.75	163.50	50	7.4	12:29:01.5	52.94	163.20		
16 10 1947	02:09:47.0	64.50	147.50	50	7.0	02:09:46.6	64.01	147.50		7.0
14 5 1948	22:31:43.0	54.50	161.00	25	7.5	22:31:43.4	54.55	161.00		7.5
22 8 1949	01:01:11.0	53.75	133.25	25	8.1	01:01:14.2	53.56	133.28		
27 9 1949	15:30:45.0	59.75	149.00	50	7.0	15:30:44.9	60.03	149.11		6.6
13 2 1951	22:12:57.0	56.00	156.00	0	7.0	22:12:55.6	55.57	156.29	2.7	7.0
02 1 1957	03:48:44.0	53.00	168.00	0	7.0	03:48:43.4	52.68	167.98		
09 3 1957	20:39:16.0	52.30	169.00	0	7.1	20:39:17.8	52.45	169.57		
22 3 1957	14:21:10.0	53.74	165.66	20	7.0	14:21:11.0	53.58	165.81	10.1	
10 4 1957	11:30:00.0	55.96	153.86	0	7.1	11:29:59.5	55.82	153.86	3.5	
19 4 1957	22:19:26.0	52.00	166.50	0	7.3	22:19:29.3	52.01	166.37	4.6	
07 4 1958	15:30:40.0	66.03	156.59	0	7.3	15:30:41.3	65.82	156.41	3.1	7.0
10 7 1958	06:15:51.0	58.60	137.10	0	7.9	06:15:57.2	58.13	136.35	7.7	7.8
13 11 1960	09:20:32.3	51.40	168.80	32	7.0	09:20:33.6	51.10	168.75	7.7	

Table 2: Estimates of Seismic Moments Obtained in This Study

Date	Estimate	
	Mantle magnitude	Seismic Moment
	$M_m$	( $10^{27}$ dyn-cm)
07 3 1929	8.0	10
10 11 1938	8.7	46
22 8 1949	8.4	23
10 7 1958	7.8	6

Earthquake Research in the Eastern Sierra Nevada  
Western Great Basin Region

Contract 14-08-0001-C1524, 1 Nov 1990 - 30 Mar 1991

W.A. Peppin and D.M. dePolo  
 Seismological Laboratory, MS 168  
 University of Nevada  
 Reno, NV 89557  
 (702) 784-4218

### Investigations

This contract supports continued research focused on the eastern Sierra Nevada and western Great Basin region. We have investigated: (1) site characteristics at Mammoth Lakes as related to inferred source parameters; (2) RMS S to P spectral ratios of downhole instruments near Long Valley caldera for fundamental source characterization; (3) source finiteness of the 1980 Mammoth Lakes earthquakes; and (4) mantle anisotropy under the western U.S. Some of these results are described below.

### Results

#### (1). Site Characteristics at Mammoth Lakes

Peppin (1991) summarized the strong influence of site effects on inferred source parameters of the 1980 Mammoth Lakes sequence using the University of Nevada wideband array of digital seismographs. While it is now generally known that site effects are quite strong, this study shows that significant reduction of the spectral corner frequency (and therefore the inferred stress drop) extends to the highest on-scale events recorded, of magnitude ML 5.0. The results of this study concur with the recent work of Lindley and Archuleta (1990).

#### (2). RMS S to P Spectral Ratios.

Lawrence Berkeley Laboratory operated an array of downhole digital seismographs from 1989 to 1990. Peppin (1991) has computed RMS S to P spectral ratios from these downhole data. Looking at the long-period spectral ratios, evidence is fairly strong that one event (25 May 1990, 0235 GCT) has a strong component of nonshear motion. We are now producing theoretical seismograms using the PROSE wavenumber integration program to explore the expected behavior of these RMS ratios, and assist in the characterization of these sources.

Looking at the high-frequency RMS spectral ratios, we find almost universally that, at frequencies exceeding about 10 Hz, the S to P ratio shows a marked and rapid falloff. Castro (1991) argues that a similar 10-Hz falloff on the Guerrero Mexico strong-motion data originates in part at the source,

and interprets the source effect as motion perpendicular to the slip plane. However, because the earthquakes in Long Valley caldera show about the same onset of S to P falloff (10 Hz), and are very much smaller in magnitude ( $M 2 - 2.5$  versus 4 to 7 for the Guerrero events), it seems probably that in both cases this is a near-receiver site effect, and is not related to excessive P energy leaving the source at high frequencies. Work is underway also with the Parkfield downhole data to bring more information to bear on this question.

### (3) Source Complexity of the 1980 Mammoth Lakes earthquakes

An  $w-1$  slope above the lowest corner frequency is expected for a complex multiple event source or an "abrupt locking" or "self healing" model (Brune, 1970; Smith and others, 1989, 1991; Heaton, 1990; Wennerberg, 1990), or equivalently from a barrier model of the type proposed by Papageorgiou and Aki (1983). If the complex source interpretation is correct for the larger 1980 Mammoth events, we might expect the strong motion accelerograms from the larger events to be much more complex than the accelerograms for smaller events, and this is generally the case, but some of the aftershock records at the same stations also appear complex, either because they are on a node for the main radiation, or because the source is more complex.

We (Priestley and Brune) have attempted to synthesize waveform and spectra of a larger event by randomly summing accelerograms for 3 smaller events of magnitude about 4.5, sufficient in number to give the same moment. This procedure is similar to that employed by Munguia and Brune (1984). In this technique we make no attempt to model the exact waveform or phase of the larger signal, but rather only the general amplitude envelope and spectrum. Using this technique, the two spectra averaged over the whole frequency band 1.5 to 6 Hz are not greatly different. The differences in spectra can be attributed to the fact that the average spectra of the aftershocks used in the summation are not exactly the same shape as the spectra of the main shock, but it is perhaps surprising that the average spectra are so close, and no strong filter effect between low and high frequencies is required.

When we consider the longer periods, 10 - 20 seconds, the results are quite different. The moment for the larger event determined from surface waves is almost an order of magnitude larger than the moment given by Archuleta and others (1982). This might suggest that we should have summed ten times as many events, but here we suggest the other alternative, namely that the majority of slip occurred at a time scale with predominant frequencies lower than adequately recorded by the strong motion instruments. This may be typical of events which occur in a high heatflow, magmatic region like the Mammoth Lakes area.

We conclude that we can approximately represent high frequency (> 1 Hz) part of the observed spectrum for the larger event as a sum of accelerograms from smaller events, thus lending strength to the interpretation of the large event as a complex, multiple event superposition of smaller events. However, at lower frequencies there is apparently a considerable amount of low frequency (low velocity) slip on the fault which is not adequately sampled by the strong motion instruments, but shows up in the higher moment determined from the surface waves.

#### (4). Anisotropy Studies.

Martha Savage and coworkers continue their study of upper-mantle anisotropy under the western United States using data from the UNR, Berkeley, and Caltech networks. Their work has been summarized in the abstracts given below.

##### Written Submittals, This Contract Period

Brune, J.N., W.F. Nicks and A.A. Aburto, 1991. Microearthquakes at Yucca Mountain, Nevada, Bull. Seism. Soc. Am., submitted.

Ozalaybey, S., M.K. Savage, and P.G. Silver, 1991. Regional variation in teleseismic shearwave splitting in east-Central California and southern Nevada, EOS, Trans. Am. Geophys. Un., in press.

Peppin, W.A., 1991. Evidence for non-shear motions accompanying microearthquakes in the south moat of Long Valley caldera, California, Earthquake Notes, in press.

Peppin, W.A., 1991. High-frequency RMS S to P spectral ratios: evidence on non-shear source motions, EOS, Tran. Am. Geophys. Un., in press.

Peppin, W.A., 1991. Real time analog and digital data acquisition through CUSP, Seis. Res. Letters, submitted.

Peppin, W.A., 1991. The effects of site response on source parameters deduced for the 1980 Long Valley, California earthquake sequence, Geophys. Res. Lett., 18, 1905 - 1908.

Savage, M.K. and P.G. Silver, 1991. Teleseismic shear-wave splitting and mantle anisotropy from western North America, Int. Union Geodesy Geophysics, August.

Savage, M.K. and P.G. Silver, 1991. Teleseismic shear-wave splitting from western North America, Int. Workshop Seis. Anisotropy in the Mantle and Geodynamics Orogenic Belts.



**Micromechanics of Rock Friction**  
USGS 14-08-0001-G1668

C. H. Scholz, R. L. Biegel, W. Wang, and N. Yoshioka

*Lamont-Doherty Geological Observatory and  
Department of Geological Sciences Columbia University  
Palisades, New York 10964*

Two manuscripts reporting the results from the initial slip experiments have been accepted for publication in JGR and are now in press. Synopsis of these papers are in USGS Open File Report 91-352, page 500. In the first paper, *Biegel et al.* (1991) reported observing a roughness dependence in the evolution of friction. During the first several hundred microns of displacement they identified two stages of development which were called initial slip and slip hardening. In Paper 2, *Boitnott et al.* (1991) introduced an elastic contact model which successfully predicted the friction response of rough granite samples in the initial stages of slip.

Currently, we are conducting a detailed investigation of the mechanics of asperity scale adhesion and mechanisms of slip hardening such as ploughing and interlocking. Friction experiments with different roughnesses of quartzite and granite on surfaces of optically flat sapphire are being performed. Results now indicate that slip hardening mechanisms are active at the beginning of slip and that the initial stiffness observed in the rough granites (*Biegel et al.*, op. cit.) is attributable to slip hardening mechanisms active at the start which was previously unsuspected. The absence of slip hardening mechanisms leads us to conclude that an adhesion strength exist for elastically contacting materials which is a substantial part of the total friction. The shear model of *Boitnott et al.* does not distinguish between adhesion and slip hardening and so must be modified. We are testing two methods to do this, one of which incorporates an area of contact dependent adhesion in the model, and the second involves scaling the radii of curvature of the asperities to the height. Both steps will probably be necessary to model the sapphire data. Finally, a detailed investigation of the different slip hardening mechanisms is being carried out by sliding contrasting roughnesses of sapphire and quartzite to isolate the ploughing and interlocking effects. The data on the adhesion mechanism will be used to the effects of adhesion from slip hardening.

In a related project, we have nearly completed scaling the shear model to crustal dimensions. Experiments have shown that following a step jump in velocity contacting surfaces must slide a critical length to achieve a new equilibrium friction and this distance is equal to the distance necessary to completely change the population of contacting asperities (*Dieterich*, 1979a,b; *Tullis and Weeks*, 1986). *Boitnott et al.*, (op. cit.) calculated that essentially all of the asperities should be fully sliding after a displacement which compared favorably with Dieterich's critical slip distances. The comparisons suggest that 1) the same mechanism which determines the critical length in rate stepping experiments,  $L_c$ , also determines the initial slip distance in our experiments, and 2) is equivalent to the distance necessary to fully change the population of contacting asperities. Therefore,  $L_c$  and the initial slip distance predicted by the model should be equivalent. In the parameter study in *Boitnott et al.*, (op. cit.), the initial slip distance was predominantly dependent on the roughness, all other parameters having only second order effects. *Brown and Scholz* (1985) found that rock surfaces are fractal over several orders of magnitude. Thus, scaling the model requires scaling the roughness parameters to the required length using the cutoff frequency of the power spectrum. In this way we obtained the required topographic parameters as input to the model.

We are now turning our attention to modelling the entire rate/state variable friction law based on a micromechanical contact model. This involves determination of the dependence of contact state on normal load and slip velocity through a combination of closure measurements and instantaneous normal and shear compliance data from 'glitch' experiments. Results to date suggest that both transient and steady state effects can be modelled with an elastic contact model for the path of increasing normal load then increasing shear stress. However, for the path of decreasing normal load, an additional 'memory' term, perhaps due to adhesion, needs to be included. The steady state velocity effect on contact state can also be observed through closure measurement and is consistent with the steady state velocity effect on friction, but the transient

behavior on a step change of velocity also requires the memory term. Experiments are underway to further explore the properties of the memory effect. The effects of roughness and normal stress on both running in and steady state wear have been studied. A contact model which incorporates a criteria for asperity fracture has been developed that is consistent with the experimental observations.

### References

- Biegel, R. L., W. Wang, C. H. Scholz, G. N. Boitnott, and N. Yoshioka, Micromechanics of friction in rock: 1. Effects of surface roughness on initial friction and slip hardening in Westerly granite, submitted, *J. Geophys. Res.*
- Boitnott, G. N., R. L. Biegel, C. H. Scholz, W. Wang, and N. Yoshioka, Micromechanics of friction in rock: 2. Quantitative modeling of initial friction with contact theory, submitted, *J. Geophys. Res.*
- Brown, S. R. and C. H. Scholz, Broad bandwidth study of the topography of natural rock surfaces, *J. Geophys. Res.*, *90*, 12575-12582, 1985.
- Buckley, D. and K. Miyoshi, Tribological properties of structural ceramics, *Structural Ceramics*, J. Watchman ed., Academic Press, pp. 293-365, 1990.
- Dieterich, J. H., Modeling of rock friction, 1. Experimental results and constitutive equations, *J. Geophys. Res.*, *84*, 2161-2108, 1979a.
- Dieterich, J. H., Modeling of rock friction, 2. Simulation of preseismic slip, *J. Geophys. Res.*, *84*, 2169-2175, 1979b.
- Tullis, T. E. and J. D. Weeks, Constitutive behavior and stability of frictional sliding of granite, *Pure Appl. Geophys.*, *124*, 383-414, 1986.

# Quantitative Analyses of Shear-wave Polarizations and Inversion for Shear-wave Splitting Parameters

14-08-0001-G1767

Peter M. Shearer  
Institute of Geophysics and Planetary Physics  
Scripps Institution of Oceanography  
University of California, San Diego  
La Jolla, CA 92093  
(619) 534-2260

## Investigations

Our research in the last year has focused on applying quantitative methods for analyzing shear-wave polarizations to data from three-component surface and borehole seismometer arrays, comparing these results to local stress orientations obtained from focal mechanisms, and studying similar earthquake pairs to constrain temporal variations in seismic Green's functions. Results of this work are described in detail in Aster et al. (1990, 1991) and Aster and Shearer (1991*a,b*; 1992). Abstracts for the latter three papers are listed below.

## Results

Two borehole seismometer arrays (KNW-BH and PFO-BH) have been established in the Southern California Batholith region of the San Jacinto Fault zone by the U.S. Geological Survey. The sites are within 0.4 km of Anza network surface stations and have three-component seismometers deployed at 300 m depth, at 150 m depth, and at the surface. Downhole horizontal seismometers can be oriented to an accuracy of about 5° using regional and near-regional initial P-wave particle motions. Shear waves recorded downhole at KNW-BH indicate that the strong alignment of initial S-wave particle motions previously observed at the surface KNW Anza site (KNW-AZ) is not generated in the near-surface weathered layer. The KNW-BH surface instrument, which sits atop a highly weathered zone, displays a significantly different (~20°) initial S-wave polarization direction from that observed downhole and at KNW-AZ, which is bolted to an outcrop. Although downhole initial shear-wave particle motion directions are consistent with a shear-wave splitting hypothesis, observations of orthogonally polarized slow shear waves are generally elusive, even in seismograms recorded at 300 m. A cross-correlation measure of the apparent relative velocities of  $S_{\text{fast}}$  and  $S_{\text{slow}}$  horizontally polarized S waves suggests shallow shear-wave anisotropy, consistent with the observed initial S-wave particle motion direction, of  $2.3 \pm 1.7$  per cent between 300 and 150 m and  $7.5 \pm 3.5$  per cent between 150 and 0 m.

We examine surface and downhole P- and S-wave spectra from local earthquakes recorded at two borehole seismometer arrays (KNW-BH and PFO-BH) installed in the Southern California Batholith region of the San Jacinto Fault zone by the U.S. Geological Survey to assess the influence of the weathered layer on the spectral content of high-frequency (2 to 200 Hz) seismic signals. Earthquake signals recorded downhole at both sites show significantly improved seismic bandwidth due to both a reduction in ambient noise levels and (especially) to dramatically increased levels of high-frequency signal. Significant seismic signal is observed up to approximately 190 Hz for P waves at KNW-BH. Stacked spectral ratios from these signals indicate that the highly weathered near-surface (between 0 and 150 m) at KNW-BH and PFO-BH exerts a much larger influence on seismic signals than deeper (between 150 and 300 m) material. Modeling of

uphole/downhole spectral ratio data suggests  $Q_\alpha \sim 6.5$  and  $Q_\beta \sim 9$  between 0 and 150 m, increasing to  $Q_\alpha \sim 27$  and  $Q_\beta \geq 26$  between 150 and 300 m. An outcrop-mounted Anza network station, deployed approximately 0.4 km from KNW-BH, displays roughly similar high-frequency content to the KNW-BH downhole sensors, but it exhibits spectra that are significantly colored by directional resonances. Low-Q and low-velocity near-surface material forms a lossy boundary layer at these borehole sites that is advantageous to the high-frequency borehole environment; not only are noise levels reduced, but reflections from the surface and near-surface are greatly attenuated. As a result, high-frequency recordings from below the weathered zone more nearly resemble those recorded in a whole space than would otherwise be expected.

We use focal plane solutions to constrain principle stress directions in the vicinity of six Anza Network stations which show evidence for shallow shear-wave anisotropy in the vicinity of the Anza seismic gap region of the San Jacinto fault. Faulting near all stations is consistent with approximately N-S maximum compressive stress. Five of these stations show nearly N-S initial particle motion alignment, consistent with the anisotropy-stress relationship expected for stress-aligned microcracks. However, one station (KNW) has a well-defined preferred initial shear-wave polarization direction of N40°W. Although this polarization direction differs dramatically from the local maximum compressive stress direction, it is consistent with the anisotropy expected due to a local alignment of anisotropic bedrock minerals, particularly biotite. Thus, anisotropy observed at this station most likely reflects a fixed, paleostain alignment of anisotropic minerals and/or microcracks and does not require a dependence on the current stress field.

## Reports

- Aster, R., Shearer, P., Berger, J., Quantitative measurements of shear-wave polarizations at the Anza Seismic Network, Southern California — implications for shear-wave splitting and earthquake prediction, *J. Geophys. Res.*, **95**, 12449-12474, 1990.
- Aster, R., Shearer, P., Berger, J., Reply to "Comment on 'Quantitative measurements of shear-wave polarizations at the Anza Seismic Network, Southern California — implications for shear-wave splitting and earthquake prediction'", *J. Geophys. Res.*, **96**, 6415-6419, 1991.
- Aster, R., Shearer, P., High-frequency borehole seismograms recorded in the San Jacinto Fault Zone, Southern California, Part 1: Polarizations, *Bull. Seismol. Soc. Am.*, **81**, 1057-1080, 1991a.
- Aster, R., Shearer, P., High-frequency borehole seismograms recorded in the San Jacinto Fault Zone, Southern California, Part 2: Attenuation and site effects, *Bull. Seismol. Soc. Am.*, **81**, 1081-1100, 1991b.
- Aster, R., Shearer, P., Initial shear-wave particle motions and stress constraints at the Anza Seismic Network, *Geophys. J. Int.*, in press 1992.

## **Seismotectonic Framework and Earthquake Source Characterization (FY91) Wasatch Front, Utah, and Adjacent Intermountain Seismic Belt**

14-08-0001-G1762

R.B. Smith, W.J Arabasz, and J.C. Pechmann\*

Department of Geology and Geophysics

University of Utah

Salt Lake City, Utah 84112-1183

(801) 581-6274

### **Investigations: April 1 - September 30, 1991**

1. High-resolution seismic imaging and gravity analysis of deformation across the Wasatch fault near Kaysville, Utah.
2. Source dependency of site amplification in the Salt Lake Valley, Utah.
3. Space-time patterns of main shock occurrence and precursory seismicity in the Utah region.

### **Results**

1. High resolution seismic reflection and gravity data were acquired at a trench site across an exposure of the Wasatch fault near Kaysville, Utah. Primary objectives of the high-resolution seismic study included: 1) testing the ability of reflection seismology to delineate unconsolidated stratigraphic units of Quaternary age in the upper 50 m of the study area; and 2) developing seismic processing techniques to suitably enhance the nonconventional, high-resolution data. Gravity data complemented the seismic data and provided a constraint on the fault zone interpretation. These data revealed major fault locations in the unconsolidated sediment; however, gravity was more helpful in mapping the location of the sediment-bedrock interface across the Wasatch fault zone.

Specialized seismic acquisition equipment recorded signals up to 400 Hz. The 12-fold, high-resolution data were processed using methods similar to those of the oil industry. Static shifts (due in part to the over 35 m of topographic relief along the 154-m seismic profile) were a major interpretation problem that was solved by refraction statics analysis. After processing, stratigraphic resolution was around 1 m, with Fresnel zone radii of 5 m on the deepest reflecting interfaces, at 40 m depth. Good resolution (80-300 Hz dominant bandwidth) in the stacked seismic data permitted a direct trench log-seismic profile comparison (Figure 1). The seismic data delineate fault locations and unconsolidated, displaced sediments as well as colluvial material abutting the main fault zone. The Wasatch fault is imaged as three diagonal

---

\*W.J. Stephenson, J.R. Pelton, S.J. Nava, and D.J. Trentman also contributed significantly to the work reported here.

traces offsetting gently dipping reflectors. Dip of the Wasatch fault is  $70^{\circ}\text{W}$  at the surface, and is estimated from the seismic data to be  $45^{\circ}\text{W}$  at 25 m depth. A cumulative displacement of 2 m across the antithetic fault system is observed in both the seismic data and the trench. Agreement between the trench log and the seismic data suggests the seismic reflection method is a viable investigative tool in faulted, unconsolidated sediments.

2. To gather some data on the variability of site amplification in the Salt Lake Valley with source location, frequency, and incident wave type, we augmented the Utah seismic network for  $7\frac{1}{2}$  months with two short-period, three-component, analog telemetry stations in the Salt Lake Valley. One station was located on Quaternary alluvium in a quiet residential neighborhood, and the other was located 8 km away on a Paleozoic quartzite outcrop in the Wasatch Range near the eastern edge of the valley. These stations successfully recorded teleseisms, nuclear blasts in southern Nevada, and local earthquakes and blasts of  $M > 2$ .

Examination of the data from these stations indicates that the amount of apparent site amplification at the alluvium site (BRO) relative to the rock site (MHD) varies strongly with source location and, to a lesser extent, with wave type and component. Recordings of nuclear blasts at the Nevada Test Site show time domain amplification of up to a factor of ten, depending on the component and the time within the record. The Pn phase shows the least amplification, less than a factor of two. Similarly, recordings of a local blast southwest of the Salt Lake Valley (Figure 2) show a significant amount of amplification, up to a factor of ten, on all three components over nearly the entire record. In contrast to the data from these blasts, data from a  $M_c$  2.1 earthquake east of the valley stations show *smaller* ground velocities at the alluvium site than the rock site, except for the S wave on the N-S components (Figure 2). These smaller ground motions at the alluvium site can be at least partially explained by geometrical spreading, since its hypocentral distance is 28 km compared to 22 km for the rock site. Seismograms of teleseismic P waves show relatively modest amplification of the direct P wave (a factor of two or less) at the alluvium site relative to the rock site, but considerable amplification of the P-wave coda, especially on the horizontal components.

These observations imply that the two- and three-dimensional structure of the Salt Lake Basin has a strong influence on site amplification, in agreement with numerical simulations. An expanded study using ten portable digital seismographs is now underway.

3. It has been recognized for some time that notably fewer instrumentally-recorded main shocks occur in the Wasatch Front area of north-central Utah than in neighboring parts of the Intermountain Seismic Belt. For this same area, an apparent decrease has been noted in the number of main shocks of  $M \geq 3.0$  since the mid-1960s along a zone more than 200 km long between about  $39.5^{\circ}\text{N}$  and  $41.5^{\circ}\text{N}$ —encompassing the most geologically active parts of the Wasatch fault (see our last project summary, *USGS Open-File Rept. 91-35*, p. 142-146). We have analyzed the temporal occurrence of independent main shocks in this region to test for non-Poisson behavior. Specifically, we analyzed samples of earthquakes consisting of  $M \geq 5.0$ , 1900-1990,  $M \geq 4.3$ , 1938-1990, and  $M \geq 3.0$ , 1962-1990. For each sample, given  $n$  observed events in  $t$  years, we used a normalized likelihood function to estimate  $\lambda$ , the rate

parameter of a Poisson process, together with the 95-percent-confidence estimates of its lower and upper bounds. We then applied the Kolmogorov-Smirnov test to determine whether one could reject the null hypothesis that an observed distribution of interevent times is Poisson. We could not reject the null hypothesis for any of the nine cases (three respective size-time samples of main shocks, each having a most-likely, an upper-bound, and lower-bound estimates of  $\lambda$ ). Thus, apparent changes that have been noted in the pattern of main-shock occurrence in the vicinity of the Wasatch fault aren't necessarily inconsistent with a Poisson process.

A period of relative seismic quiescence within 50 km began about 6½ years before the 1975  $M_L$  6.0 Pocatello Valley (Idaho-Utah border) earthquake and lasted for 4½ years. The main shock was also preceded by preshocks ( $\Delta < 10$  km;  $10 \text{ d} < t < 1 \text{ yr}$ ) and foreshocks ( $\Delta < 10$  km,  $t \leq 10 \text{ d}$ ). The case history of the Pocatello Valley earthquake sequence motivated a comparative study of seismicity prior to five recent main shocks in the Utah region ( $4.8 \leq M_L \leq 5.4$ , 1987-1989). Coincidentally, all five of these main shocks were preceded by foreshocks. At least two, and possibly four of the studied main shocks were preceded by significant *decreases* in background seismicity, within 25 km, that began 7 to 8 years before the main shock and lasted about 4 to 7 years. The two earthquakes for which there is good evidence of a precursory decrease in seismicity are the  $M_L$  5.3 San Rafael Swell earthquake of August 1988 and the  $M_L$  4.8 Bear Lake earthquake of November 1988. Both earthquakes also had preshocks.

## Reports and Publications

- Olsen, K.B., G.T. Schuster, and J.C. Pechmann (1991). Finite difference simulation of three-dimensional elastic wave propagation in the Salt Lake Basin (abstract), *EOS, Trans. Am. Geophys. Union* 72 (Supplement), 327.
- Peyton, S.L., R.B. Smith, and J.C. Pechmann (1991). Seismotectonics of the Yellowstone-Hebgen Lake region from earthquake focal mechanisms and stress field inversion (abstract), *EOS, Trans. Am. Geophys. Union* 72 (Supplement), 335.
- Stephenson, W.J., R.B. Smith, and J.R. Pelton (1991). High resolution seismic imaging and gravity analysis of deformation across the Wasatch fault, Kaysville, Utah (abstract), *EOS, Trans. Am. Geophys. Union* 72 (Supplement), 327.
- Stephenson, W.J. (1991). Near surface, high-resolution seismic and gravity study across the Wasatch fault, Utah, *M.S. Thesis*, University of Utah, Salt Lake City, Utah, 86 pp.
- Sylvester, A.G., J.O.D. Byrd, and R.B. Smith (1991). Geodetic evidence for aseismic reverse creep across the Teton fault, Teton Range, Wyoming, *Geophys. Res. Lett.* 18, 1083-1086.

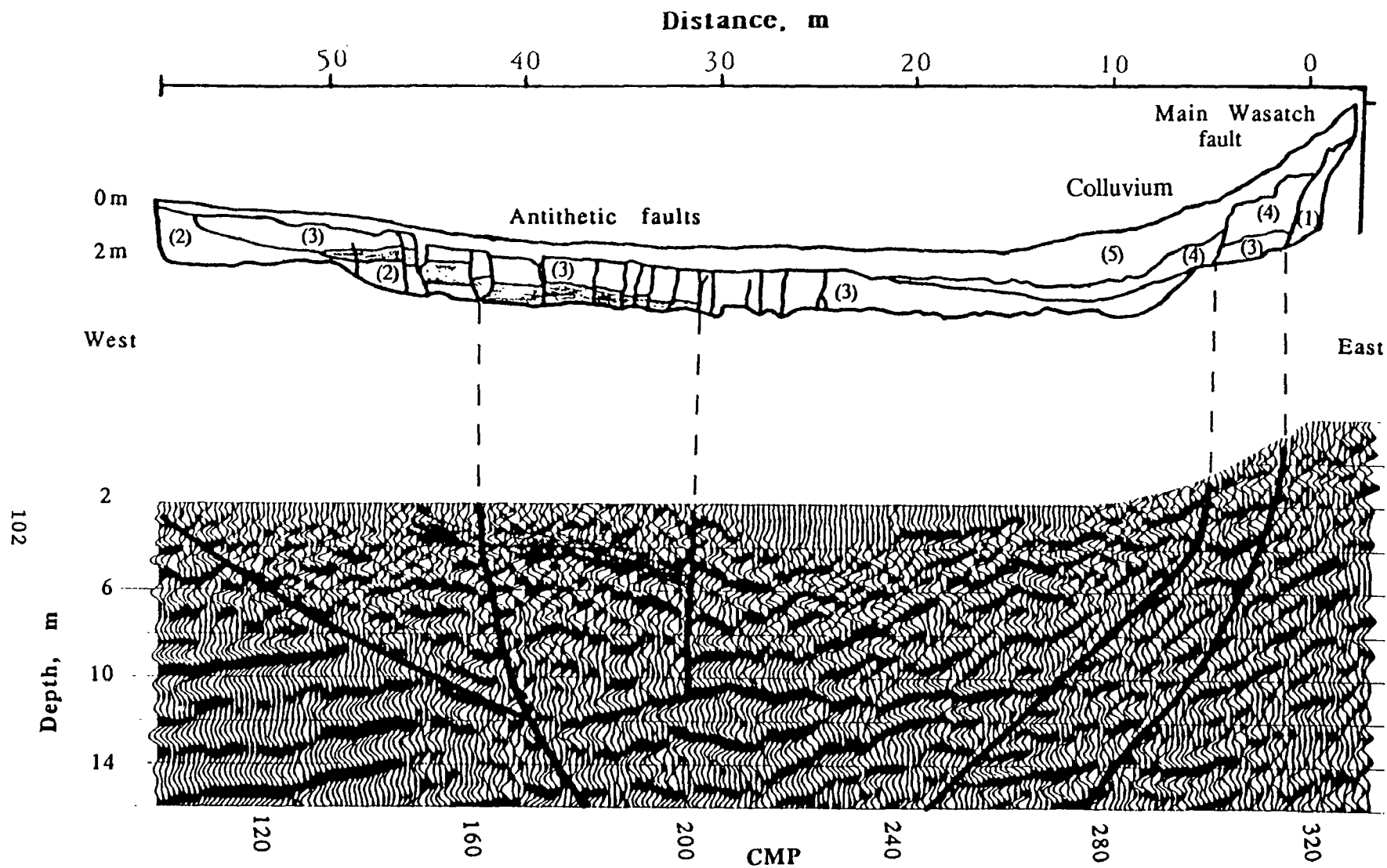
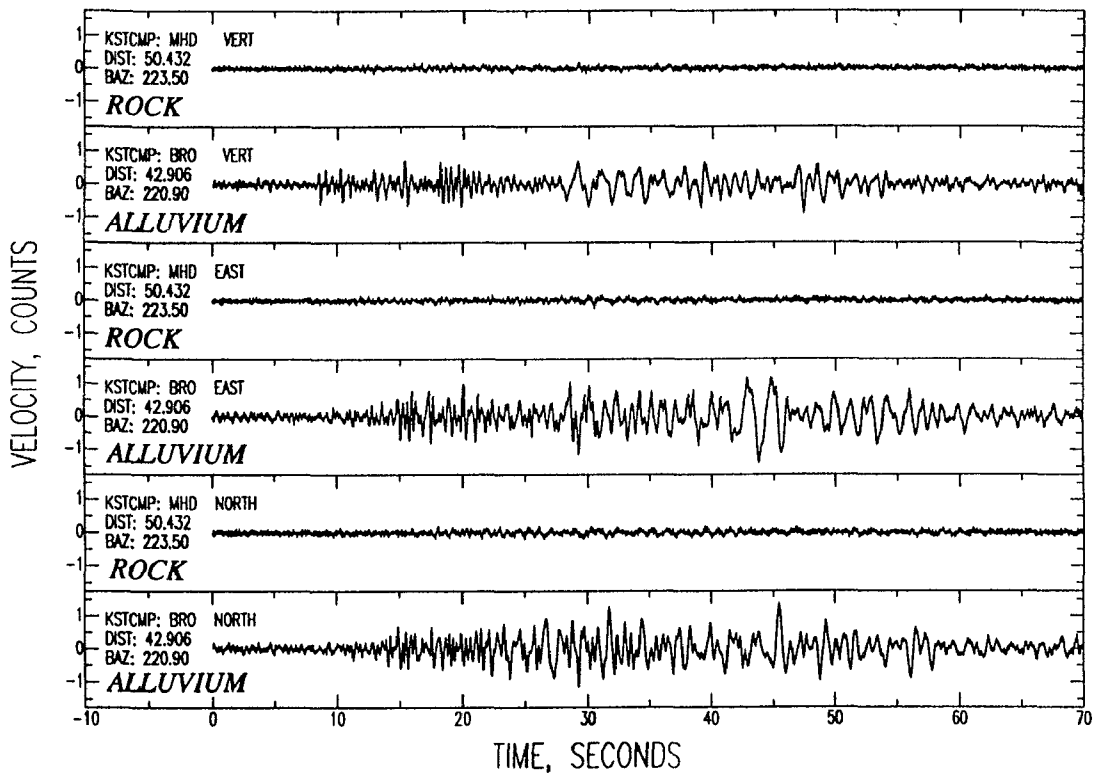


Figure 1. Direct comparison of the stacked seismic data to the trench log of Swan et al. (1980, BSSA 70, 1431-1462). A marker bed is shaded from 30 to 50 m distance on both the trench log and the seismic section. The faults as well as the lacustrine, alluvial, and colluvial deposits that were mapped in the trench are imaged on the seismic section. There is a third trace of the Wasatch fault to the east of the section.



Mc 2.5 BLAST, MERCUR MINE,  
NOVEMBER 5, 1990, 23:13:57



Mc 2.1 EARTHQUAKE, WASATCH MTS,  
DPT 11.7 KM, OCTOBER 11, 17:18:47

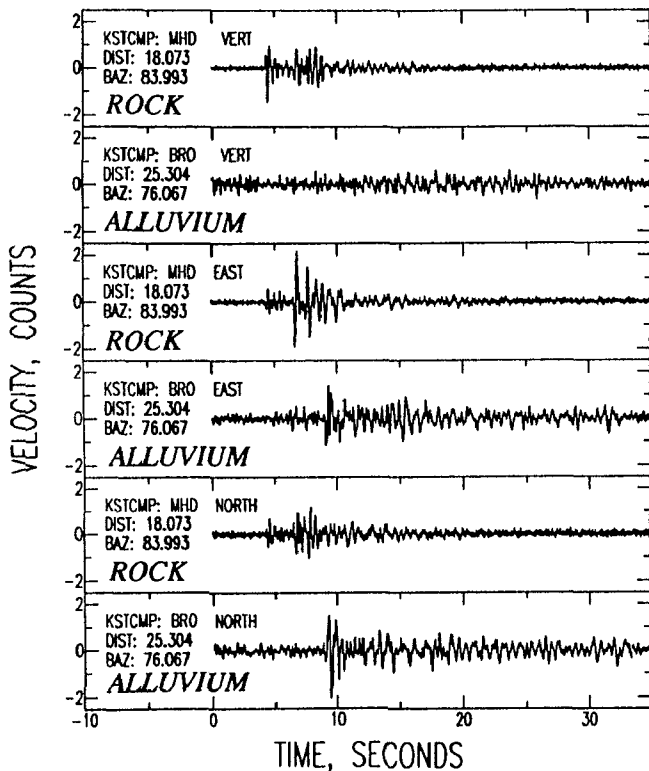


Figure 2. Sample three-component data from two temporary stations of the University of Utah regional seismic network: BRO, which is located on Quaternary alluvium in the Salt Lake Valley, and MHD, which is located 8 km ENE of BRO on a Paleozoic quartzite outcrop overlooking the valley. The station name and component (kstcmp) are given at the left of each seismogram, along with the epicentral distance in km (dist) and the back azimuth in degrees (baz). The time given at the top of each set of plots is the origin time of the seismic event in UTC, which corresponds to the origin of the time axis. The relative amplitudes of the velocity seismograms in each set of plots are correct. The seismometers at each site are Geotech S-13 velocity transducers, with the free periods set to  $\sim 0.6$  sec. The data are filtered at the recording sites using lowpass Butterworth filters with corner frequencies of 2.5 Hz.

# MECHANICS OF LITHOSPHERE PLATES

9960-03419

William D. Stuart and Ruth A. Harris  
 Branch of Tectonophysics  
 U. S. Geological Survey  
 Pasadena, California 91106  
 818 405-7816  
 FTS 961-7816

## Investigations

### Pacific-North America Plate Interaction

This work is an attempt to derive from mechanical principles the locations, slip rates, and lifetimes of major plate boundary faults in central and southern California since late Oligocene time. A special case is the present set of faults. The data most useful for testing the models for earlier times are measured offsets, rotations, and vertical motions of geologic units and crustal blocks. Results of this study may help explain average slip rates on modern seismically active faults, as well as apparent brittle strength variations along strike.

### Interaction of Plates on a Sphere

The goal here is to construct a mechanical model using the theory of spherical elastic shells to simulate motions of the major tectonic plates. Shell fragments (plates) are in static equilibrium and subject to forcing by excess mass at subduction zones. Stresses resisting motion satisfy a time-dependent constitutive relation at plate bottoms and lateral boundaries. The first application of the model will be to simulate the current (Quaternary) motions of plates on the earth. The second application will be to simulate motions of plates in the Pacific basin since late Mesozoic time (e.g. Engebretson et al., GSA Spec. Paper 206). Results of the above investigation of Pacific-North America plate interactions for late Tertiary faults should help constrain constitutive laws at plate margins and bottoms. This work is a collaboration with Philip O. Banks (CWRU).

### Dynamic Fault Interaction - Parallel Strike-Slip Faults

The magnitudes of most strike-slip earthquakes are controlled by their rupture lengths, therefore if one could determine what controls the rupture length, one could determine the magnitude of an upcoming earthquake. The object of this study is to determine how fault geometry affects a propagating earthquake rupture. We specifically study the case of parallel (non-collinear) strike-slip fault segments. This initial study is performed using numerical simulations assuming plane strain conditions (a two-dimensional calculation).

The calculations simulate spontaneously propagating shear fractures. This work is being done by Ruth Harris, in collaboration with Steve Day (SDSU).

## Results

### Pacific-North America Plate Interaction

In a two-dimensional stress model starting with only a bent San Andreas fault, it is possible to derive approximately the location, slip rate, and length of the Garlock fault. The computed stress field in the area corresponding to the Owens Valley to Death Valley region is extensional to the northwest, as observed. In this region the observed extensional rate is the highest of all in the northern Basin and Range. The model explains this observation if the extension due to Garlock slip is regarded as superimposed on more widespread extension of the Great Basin due to another cause, presently uncertain. The Garlock may be indirectly due to large scale Great Basin extension if that extension caused the bend in the San Andreas.

### Interaction of Plates on a Sphere

Simple models of plates on a sphere are being analyzed. No reportable results.

### Dynamic Fault Interaction - Parallel Strike-Slip Faults

The results to date demonstrate that spontaneously propagating shear fractures can jump both dilational and compressional steps in vertical strike-slip faults. It also appears that wider dilational steps can be jumped (up to 5 km wide). This result is supported by field data which show that the maximum dilational step-width, which has been jumped by a strike-slip earthquake, was approximately 5 km wide (this occurred during the great M8 Erzincan earthquake of 1939). The widest known case for a compressional step is the 1891 Nobi earthquake (also M8) which jumped a 3-km wide compressional step. Additional results are that dilational steps appear to slow the propagating rupture more than compressional steps do, leading to a slower apparent rupture velocity. In FY92 these studies will be continued, using 3D numerical models.

## Reports

Banks, P. O., W. D. Stuart, and S. -W. Liu, 1991, Piezomagnetic fields of screw dislocation fault models, *Jour. Geophys. Res.*, 96(13), in press.

Harris, R. A., 1991, Dynamic interaction of parallel strike-slip fault segments: some implications for the San Francisco Bay area (abs.), *Second Conference on Earthquake Hazards in the Eastern San Francisco Bay Area*, accepted.

Stuart, W. D., 1991, Cause of the Garlock fault (abs.), *GSA Abstracts with Programs*, 23(5), 198.

## **STUDY OF THE CORRELATION BETWEEN WATER LEVEL FLUCTUATION AND RESERVOIR INDUCED SEISMICITY - PHASE I**

14-08-0001-G-1713

Pradeep Talwani  
Department of Geological Sciences  
University of South Carolina  
Columbia, SC 29208  
(803) 777-6449

**Objective:** To study the role of lake level fluctuations on the mechanism of reservoir induced seismicity (RIS) by monitoring of groundwater and seismicity at the Bad Creek pumped storage facility in northwestern South Carolina.

### **Investigations**

Impoundment of the reservoir started on January 6, 1991. Since then seismicity and lake levels have been monitored continuously. In addition, the hydraulic head expressed as elevation above mean sea level, has been monitored in three observation wells, OW1, OW2 and OW3. The locations of the wells are shown in Figure 1.

The seismicity is monitored on stations of the Bad Creek-Lake Jocassee network and recorded at Jocassee hydro station. Since September 13, 1991, data from BC (Bad Creek) station are telemetered by telephone to Columbia.

We are also carrying out two theoretical studies aimed at calculating the coupled response of the earth to reservoir impoundment.

### **Results**

The preliminary results of these investigations are summarized below.

#### **a. Groundwater Monitoring**

The hydraulic head expressed as height of water above the mean sea level in the three observation wells OW1, OW2 and OW3, are shown in Figure 2.

Both OW1 and OW2 are within the reservoir area and show immediate response to changes in the reservoir level. OW3 is located outside the reservoir area and there is a time delay in its response to the reservoir changes. Lightning strikes appear to have damaged the pressure transducers in OW1 and OW2, these are being replaced.

#### b. Seismicity Monitoring

The seismicity in the vicinity of Bad Creek has been monitored for several years prior to impoundment. Although a minor increase in seismicity occurred soon after impoundment, a major burst of seismicity has not occurred yet. Most of the earthquakes recorded near Bad Creek are of magnitude  $<0.0$ . After filling the largest event had a magnitude of 0.6. The cumulative seismicity curve shows an increase in seismicity rate during initial filling (Figure 3).

#### c. Modeling Studies

Two one dimensional models (one numerical using finite differences and one analytical) have been developed to study coupled response of elastic effects and pore pressure diffusion and its correlation with seismicity. Variations in hydraulic parameters and physical properties of materials are being analyzed to study their sensitivity. We plan to develop a two dimensional model which accounts for lateral inhomogeneities in space.

Another theoretical study is aimed at understanding the influence of rate of loading on the growth of the pore pressure field. We have computed the contribution due to undrained (increase in pore pressure due to elastic compression of rocks) and drained response (diffusion of pore pressure under the influence of a changing head) for various loading rates. For the elastic properties assumed for Bad Creek the undrained response is about 53% on the total pore pressure, if monotonic growth of pore pressure is assumed. Our computations also suggest that rapid loading results not only in an instantaneous increase in pore pressure but also in a faster pore pressure build up due to diffusion.

We plan to develop numerical models elucidating coupled pore pressure field due to rapid fluctuations, and also the effect of heterogeneity in the hydraulic properties.

## **Reports**

Pradeep Talwani and Kusala Rajendran, Long term response of seismogenic reservoirs. Presented at the 63rd Annual meeting of the Eastern Section of the Seismological Society of America, October, 1991.

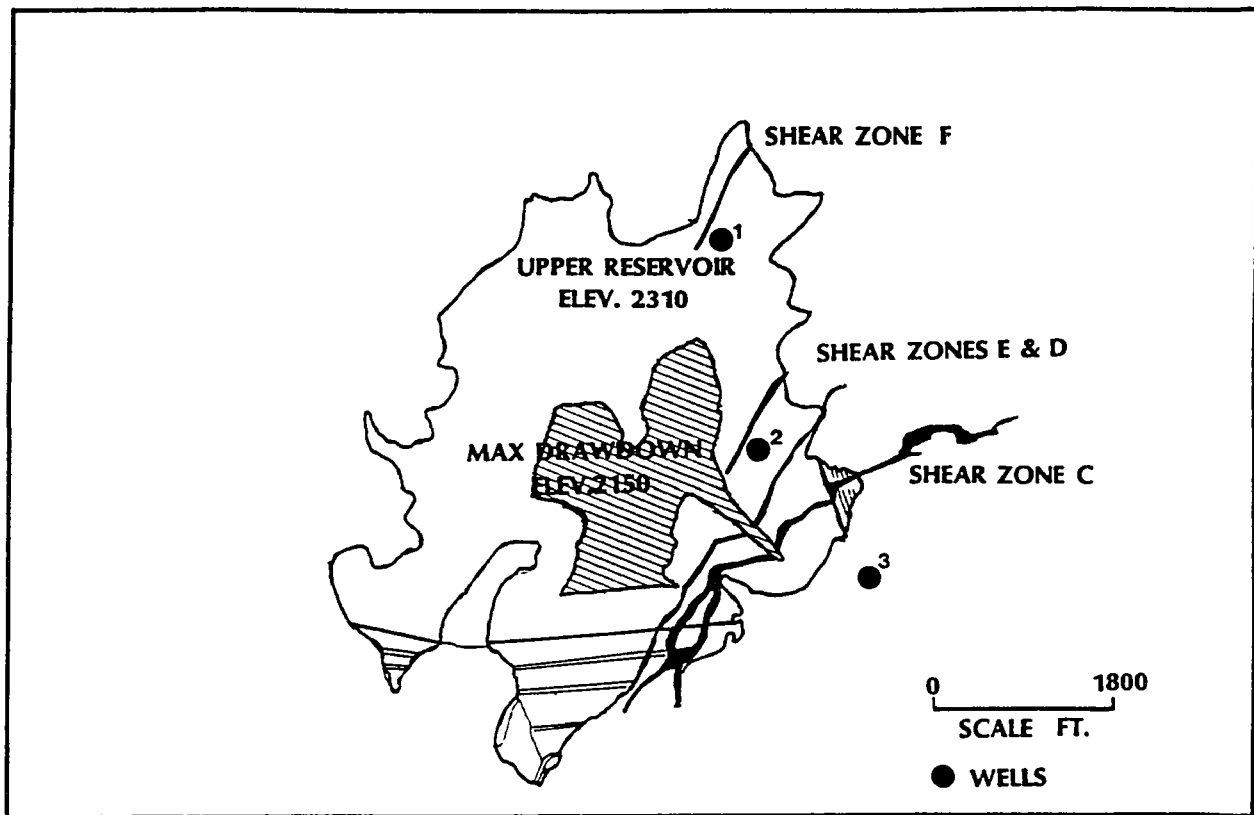


Figure 1. Location of shear zones in Bad Creek area. The lake outline shows the extent of full pond (2310 ft) and stippled pattern shows the maximum drawdown (2150 ft). The numbers show the locations of observation wells.

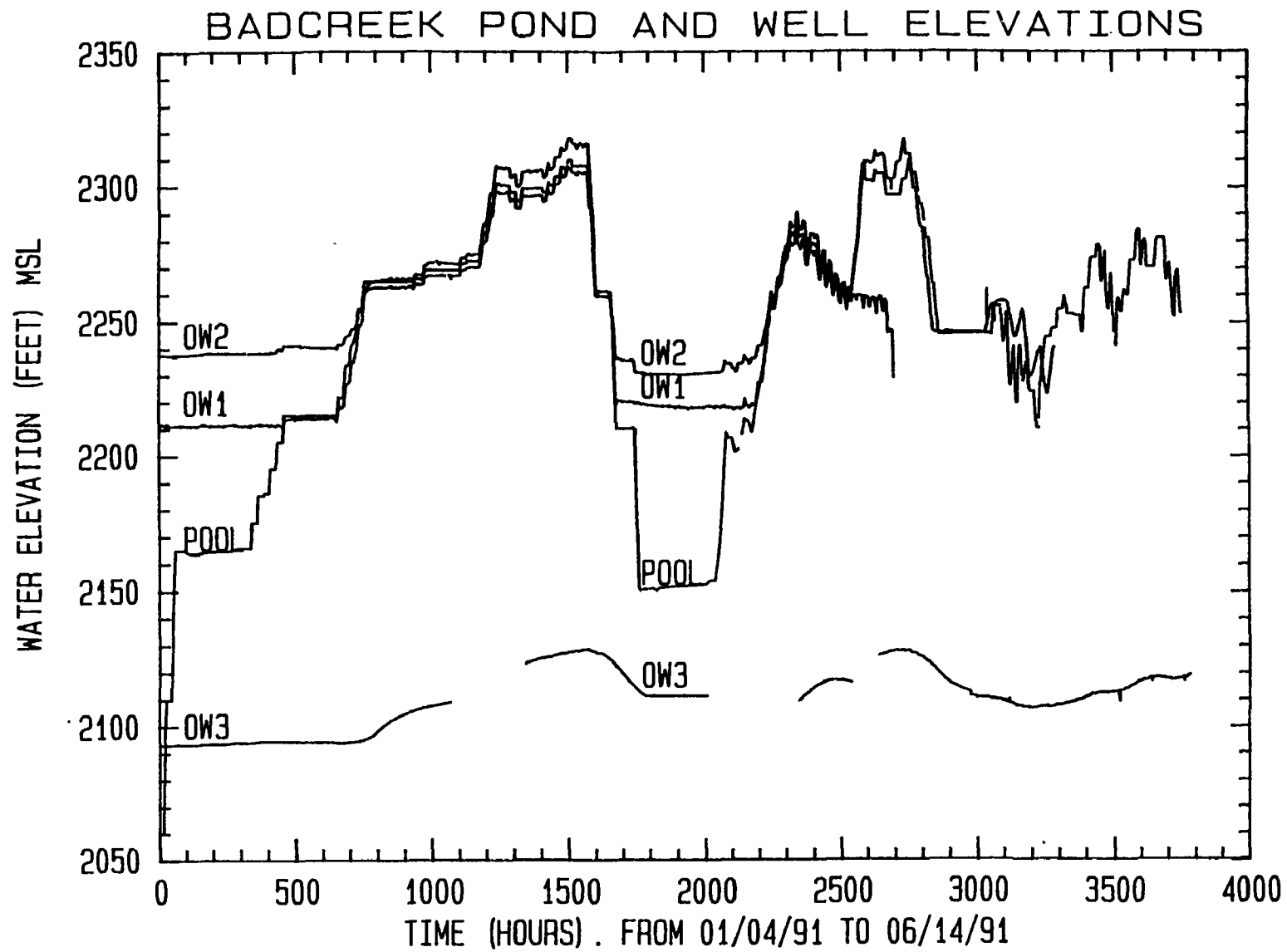


Figure 2. Elevation of water in the pool and three observation wells at Bad Creek.



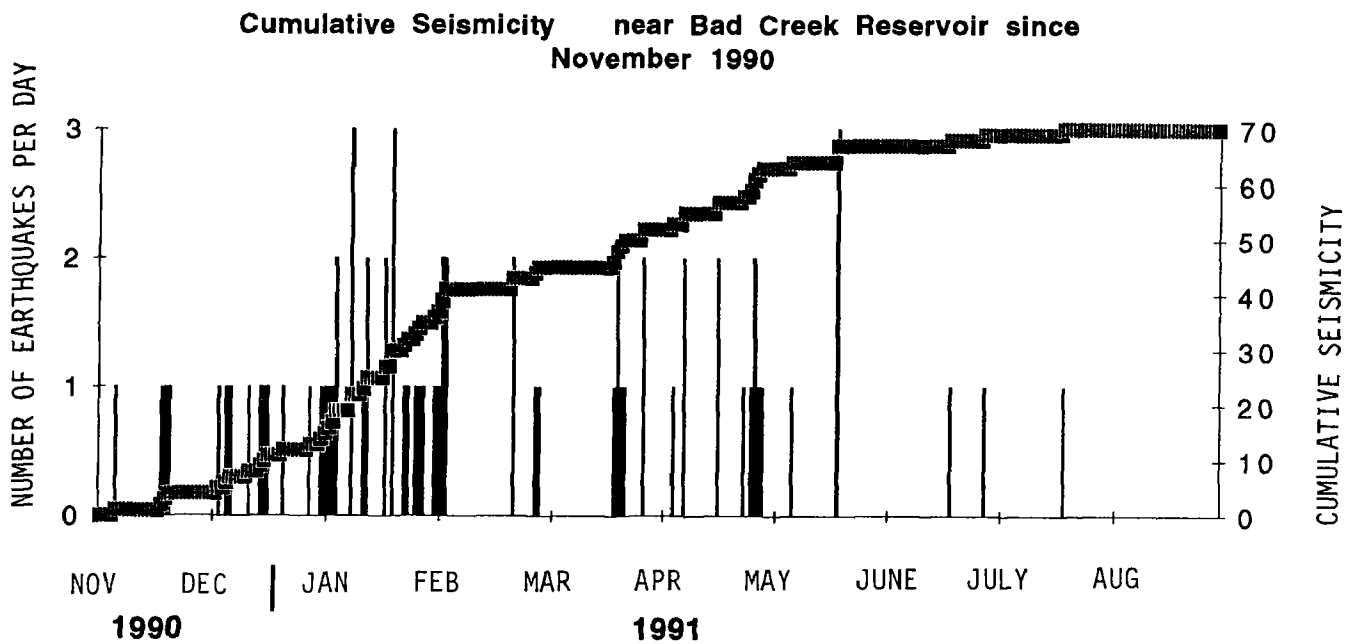


Figure 3. Number of earthquakes per day and cumulative seismicity near Bad Creek reservoir from November 1990 through August 1991. The filling started in January 1991 .

## QUATERNARY BLIND THRUSTING IN THE SOUTHWESTERN SACRAMENTO VALLEY, CALIFORNIA

Contract # 14-08-0001-G2059

Jeffrey R. Unruh (Dept. of Geology; 916-752-4950)  
Lewis P. Munk (Dept. of Land, Air and Water Resources; 916-752-1406)  
Eldridge M. Moores (Dept. of Geology; 916-752-0352)  
Randal J. Southard (Dept. of Land, Air and Water Resources; 916-752-7041)

*all at:* University of California, Davis      95616

### OBJECTIVES

The goal of this investigation is to study Quaternary surface deformation related to movement on potentially seismogenic blind thrust faults in the Dunnigan Hills region, southwestern Sacramento Valley, California. Our approach is to combine analysis of seismic reflection data with mapping of Quaternary tectonic-geomorphic features to infer the rate, timing and kinematics of late Cenozoic shortening.

### INVESTIGATIONS UNDERTAKEN

Our study has pursued several complementary tracks intended to relate patterns of surface deformation to the kinematics and mechanics of blind thrusting. To date, we have obtained over 75 km of high quality seismic reflection data from industry sources. We are using these data to interpret stratigraphic and structural relationships beneath the Dunnigan Hills. Using well-established depth-velocity relationships for the southwestern Sacramento Valley, we have derived depth sections from interpreted migrated time sections. Where possible, we have verified the derived depths to critical stratigraphic horizons with published drill-hole data from the Dunnigan Hills region. Using the depth sections as a guide, we have tested several forward models for the evolution of the blind thrust system. Our approach is to construct a series of kinematically restorable cross-sections that account for both progressive movement on the thrusts and syntectonic sedimentation in the ancestral Sacramento Valley forearc basin.

Our study of late Cenozoic surface deformation includes mapping tectonic-geomorphic features such as uplifted and tilted surfaces, quantitative analysis of drainage system development in the actively growing Dunnigan Hills anticline, and soil stratigraphic studies to infer relative ages of deformed surfaces.

During reconnaissance field studies of the Dunnigan Hills and surrounding regions, we observed numerous perennial saline springs emerging along east-dipping thrusts in Upper Cretaceous strata. The springs are cold, near neutral, chloride-rich, chemically reduced, and locally discharge at high elevations and along ridgetops. The springs occur in areas of the western Sacramento Valley and eastern Coast Ranges known to have anomalously high fluid pressures at depth. We have performed stable-isotope analyses of the spring waters in order to determine their origin, and explore possible relationships between the springs, anomalously high subsurface fluid pressures and active crustal shortening.

### RESULTS OBTAINED

Seismic reflection data reveal that the northeastern Coast Ranges mountain front and the Dunnigan Hills are underlain by a system of northeast-vergent blind thrusts. The style of mountain front deformation is similar to the growth and propagation of "triangle zones" found at the leading edges of many fold and thrust belts (Unruh and Moores, in press). Based on analysis of stratigraphic and structural relationships visible in seismic reflection profiles, initial thrusting occurred during late Cretaceous time or earlier (Unruh and Moores, 1990b; also, in prep.). The early thrusting occurred during plate convergence and east-dipping subduction beneath the ancestral Sacramento Valley forearc basin. Geophysical studies in the western San Joaquin Valley south of the study area suggest that accretionary prism rocks of the Franciscan assemblage may

have been thrust beneath the Great Valley group forearc strata as an eastward-tapering tectonic wedge (Wentworth et al., 1984). Similar patterns of arcward-vergent thrusting have been reported in other forearc regions (Silver and Reed, 1988). In particular, arcward-vergent underthrusting of accretionary prism rocks was proposed by Torrini and Speed (1989) for the Tobago trough forearc basin, Lesser Antilles. If so, the Lesser Antilles arc-trench system may be useful tectonic analogue for inferring the deep structure beneath the Coast Ranges and western Great Valley of California (Unruh et al., 1991).

The blind thrusts beneath the Dunnigan Hills are reactivated structures. Stratigraphic and structural relationships provide evidence for several episodes of deformation. Forward kinematic modeling of the thrust system suggests an interplay between thrusting and forearc sedimentation. The models also suggest that cumulative shortening can not be accurately modeled by strict application of fault-bend fold geometries.

Tectonic-geomorphic studies indicate that Quaternary folding of the Dunnigan Hills above the blind thrusts has uplifted fluvial terraces and strongly influenced drainage system development (Munk et al. 1991a; 1991b; in prep.). Topographic profiles drawn on smoothed contours of the Dunnigan Hills reveal that the shape of the modern antiform is similar to the profile of a folded angular unconformity between Upper Cretaceous and Eocene strata visible in seismic reflection profiles. The elevation of the modern Dunnigan Hills is much less than the total tectonic relief on the folded unconformity, suggesting that similar episodes of shortening have occurred in this region during the Tertiary.

We have mapped and correlated deposits and geomorphic surfaces in key areas of the Dunnigan and Rumsey Hills. We have sampled and described soil profiles representative of the soils forming in deposits of varying age (30 backhoe pits). Field and laboratory investigations pertinent to the soil stratigraphy are on-going. Preliminary results of the soil stratigraphic study indicate that the modern Dunnigan Hills are probably late Pleistocene in age. In addition to soil morphologic properties, age estimates are supported by radiometric dating of Pleistocene fossils (U/Th/Pa), charcoal ( $^{14}\text{C}$ ) and tephrochronology. Andre' Sarna-Wojcicki (USGS) has provided valuable support by sampling and correlating tephra beds located during the field investigations. We anticipate this study will produce a well constrained soil stratigraphy for the southwestern Sacramento Valley, and will provide a benchmark for future studies of Quaternary deformation and landscape evolution in this region.

Stable isotope data indicate that fluids from perennial saline springs emerging along thrust faults in the study area are indistinguishable from oil field waters, but are clearly distinct from local meteoric waters (Unruh et al., in review). We conclude that the springs represent formation waters from the Cretaceous Great Valley strata. Given the non-meteoric character of the fluids, the cold temperature of the fluids and perennial flow at high elevations and near ridgetops, we propose that the waters are being expelled under the anomalously high pressures reported at shallow depths in drill holes. The general coincidence of high fluid pressures with late Cenozoic uplift, folding and thrusting in the study area is consistent with models that relate excess fluid pressures to the movement of large thrust sheets. Further study of the relationship between perennial saline springs, thrust faults and active crustal shortening in the northern California Coast Ranges is planned.

## REFERENCES

- Wentworth, C.M., Blake, M.C. Jr., Jones, D.L., Walter, A.W., and Zoback, M.D., 1984, Tectonic wedging associated with emplacement of the Franciscan assemblage, California Coast Ranges, in Blake, M.C. Jr., ed., *Franciscan Geology of Northern California: Pacific Section, Society of Economic Paleontologists and Mineralogists*, v. 43, p. 163-173.
- Silver, E.A., and Reed, D.L., 1988, Backthrusting in accretionary wedges: *Journal of Geophysical Research*, v. 93, p. 3116-3126.
- Torrini, R. Jr., and Speed, R.C., 1989, Tectonic wedging in the forearc basin-accretionary prism transition, Lesser Antilles forearc: *Journal of Geophysical Research*, v. 94, p. 10,549-10,584.

## REPORTS

### Abstracts

- Unruh, J.R., and Moores, E.M., 1990a, Kinematics of Quaternary blind thrusting in the southwestern Sacramento Valley, California: Abstracts with Programs, Geological Society of America Annual Meeting, Dallas, Texas, p 224.
- Unruh, J.R., and Moores, E.M., 1990b, Three-dimensional internal structure of a reactivated triangle zone, southwestern Sacramento Valley, California: EOS (Transactions, American Geophysical Union), v. 71, no. 43, p. 1632-1633.
- Unruh, J.R., Moores, E.M., and Verosub, K.L., 1991, Quaternary blind thrusting and potential seismic hazards in the southwestern Sacramento Valley, California: Geological Society of America Abstracts with Programs, Cordilleran Section, p. 105.
- Phipps, S.P., Unruh, J.R., and Moores, E.M., 1991, Young crustal wedging and imbricate thrusting, Sacramento Valley and northern Coast Ranges, California: Geological Society of America Abstracts with Programs, Cordilleran Section, p. 89.
- Munk, L.P., Unruh, J.R., Moores, E.M., and Southard, R.J., 1991, Fluvial geomorphic indicators of neotectonism in the southwestern Sacramento Valley, California: Geological Society of America Abstracts with Programs, Cordilleran Section, p. 82.
- Munk, L.P., Unruh, J.R., and Southard, R.J., 1991, Drainage development in the Dunnigan Hills and implications for blind thrust faulting in the southwestern Sacramento Valley, California: Geological Society of America Annual Meeting Abstracts with Programs, p. A432.
- Munk, L.P., and Southard, R.J., 1991, Morphology and composition of non-calcareous silica pendants in a California Paleixeralf: Proceedings, Soil Science Society of America, Annual Meeting, Denver, Colorado, p. 317.
- Unruh, J.R., Ramirez, V.R., Phipps, S.P., Moores, E.M., and Davis, D.L., 1991, Tectonic wedging beneath forearc basins: ancient and modern examples from California and the Lesser Antilles: EOS (Transactions, American Geophysical Union), Fall Meeting Program and Abstracts, p. 443.
- Davisson, M.L., Unruh, J.R., Criss, R.E., and Moores, E.M., 1991, Stable isotope characteristics of perennial saline springs and their implications for abnormally high fluid pressures and active thrusting, southwestern Sacramento Valley, California: EOS (Transactions, American Geophysical Union), Fall Meeting Program and Abstracts, p. 485.

### Papers

- Unruh, J.R., Ramirez, V.R., Phipps, S.P., and Moores, E.M., 1991, Tectonic wedging beneath forearc basins: ancient and modern examples from California and the Lesser Antilles: GSA Today, v. 1, p. 185-190.
- Unruh, J.R., and Moores, E.M., in press, Quaternary blind thrusting in the southwestern Sacramento Valley, California: to be published in *Tectonics*, 1992.
- Unruh, J.R., Davisson, M.L., Criss, R.E., and Moores, E.M., in review, Implications of perennial saline springs for abnormally high fluid pressures and active thrusting in the southwestern Sacramento Valley, California: submitted to *Geology*, August 1991.
- Munk, L.P., and Southard, R.J., in review, Pedogenic and mineralogical implications of non-calcareous opaline pendants in some late-Pleistocene California Paleixeralfs: submitted to Journal of the Soil Science Society of America.
- Unruh, J.R., Munk, L.P., and Moores, E.M., in prep., Kinematics and timing of blind thrusting beneath the Dunnigan Hills, southwestern Sacramento Valley, California.

## Coherence and Empirical Green's Functions from ANZA Data

14-08-0001-G1959

Frank Vernon and Guy Masters  
Institute of Geophysics and Planetary Physics  
Scripps Institution of Oceanography  
University of California, San Diego  
La Jolla, CA 92093  
(619) 534-5537

A three-dimensional P-wave velocity model for the San Jacinto fault zone has been constructed using traveltimes data from local earthquakes in the Anza region. The purpose of this study is to improve the quality of small earthquake locations to facilitate similar-earthquake studies of source characteristics, to investigate the structure of the fault zone by revealing the geometry of fracture planes that are delineated by the earthquakes, and to acquire new information about the structure of the seismic gap through interpretation of the velocity model itself.

Modeling of the one-dimensional velocity structure revealed that most of the variation in seismic velocity was lateral rather than depth-dependent. A simultaneous inversion for earthquake locations and velocity structure was done using 9300 P-wave arrival times and 4700 S-wave arrival times from 560 events (figure 1). Arrival times at stations of both the Anza Seismic Network and the Caltech-USGS Southern California Array were used. Constraints were applied that required velocity to increase with depth, minimized the second-derivative of the velocity function with depth, and satisfied borehole velocity measurements. It was found that by including station corrections in the model parameters, the variance of the traveltimes data was reduced 350% over that of the best fitting model with no station corrections. The improvement in location precision decreases accordingly. It was also found that some tradeoffs exist, with the size of the station corrections correlated with an offset in velocity as a function of depth. Figure 2 shows this tradeoff in misfit as a function of model norm.

Traveltimes residuals calculated from the one-dimensional model are roughly 1.5 times the picking error and show coherent variation due to lateral variations of velocity that cannot be compensated using station corrections alone. 3D variations in the velocity model are required to fit the data. The picking error was evaluated by comparing multiple estimates of the pick time for a subset of the data and turns out to be approximately .02 seconds for P-waves and .05 seconds for S-waves. We have developed an algorithm to solve simultaneously for earthquake locations and the 3D P-wave velocity structure with the smoothest perturbation to the 1D structure. Station corrections were included as free parameters in order to evaluate their tradeoff with near surface structure. The algorithm allowed the influence of the constraints on the size of the station corrections to be adjusted relative to the constraints on the smoothness of the velocity functional so that a range of models could be recovered that satisfied the data. Figure 3 shows this tradeoff of misfit as a function of model norm. It was found that with lateral perturbations of velocity on the order of 8%, the traveltimes data could be predicted to the accuracy of the picking errors. In the limit where all the station corrections are near zero, the roughness of the velocity model near the surface increases drastically and relatively large anomalies appear directly beneath some stations indicating that some of the traveltimes variation is most likely due to local site structure. Between 3 and 9 km below sea level the resolution is adequate for reliable reconstruction of features on the order of 4-6 km size. In this region the relative lateral perturbations of the model are independent of the size of the station corrections. The most prominent feature at a depth of 3 km is a lower velocity region that runs subparallel to the fault (figure 4). This could be due to rocks being fractured in the fault zone. There is another distinct low velocity feature in the southeast, most obvious at 6 km depth, that cannot be explained by any obvious relation to fault structure. Between 6 and 9 km depth the relatively linear low velocity feature visible at 3 km appears to be broken up by a higher velocity

feature that extends into the fault zone from the northeast side of the fault. This feature happens to coincide with a 6 km segment of the fault that has a conspicuous absence of events. This may be evidence for high seismic velocities to indicating regions where the fault is locked at depth.

The earthquake locations calculated with the three-dimensional structure show that the predominant effect of the lateral variations is to shift the locations approximately 400-600 meters to the northeast and to shift shallow events about 1 km deeper (figure 5). The coherent shift in locations allows us to conclude that when spatial patterns of events are used to examine fault structure, a one-dimensional algorithm that includes station corrections is sufficient to characterize the fine-scale details of the seismicity. For studies in this region that depend on high precision locations to discriminate events that are suitable for similar earthquake comparisons, the correlated offset of events in an earthquake cluster show that relocating the events with station corrections preserves the same interevent distance as calculated using the full three-dimensional algorithm.

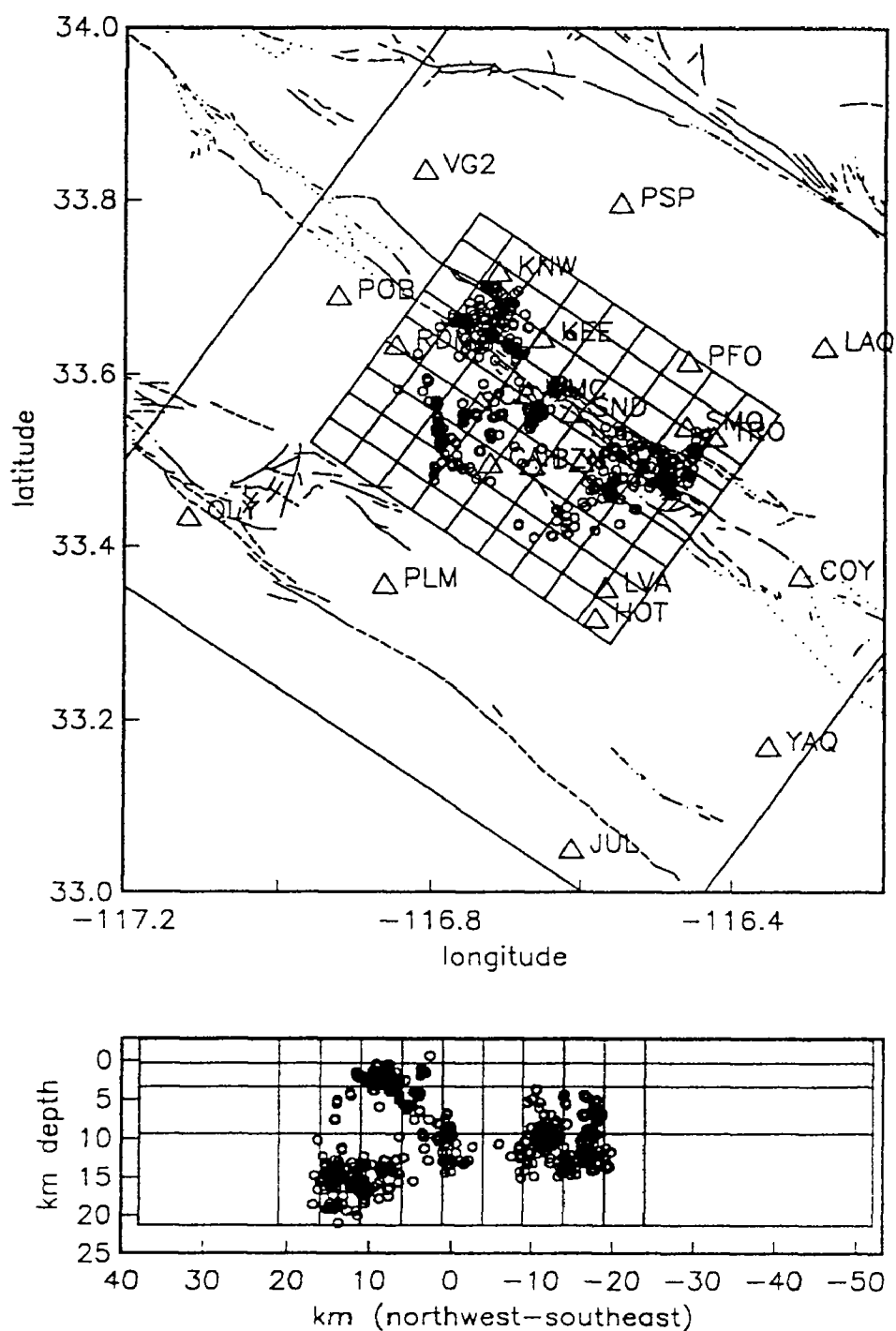


Figure 1. Map showing the events and the stations used in the velocity inversions. The grid shows the region of the San Jacinto fault zone that was modeled with a 3D structure.

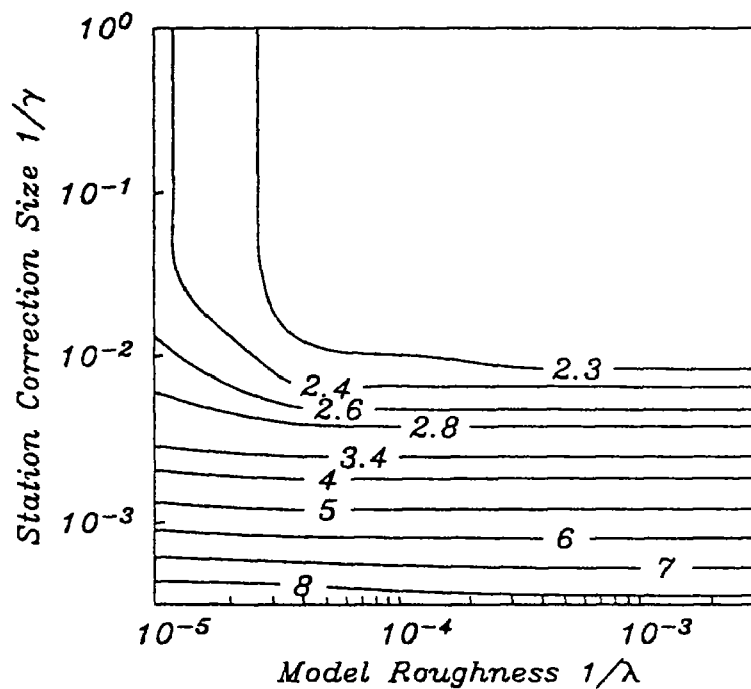


Figure 2. Tradeoff curve for 1D inversion showing contours of the  $\text{CHI}^{**2}$  measure of misfit of the traveltime data as a function of the tradeoff parameters for model roughness and station correction size. Note that most of the decrease in misfit can be accomplished by applying station corrections to a very simple (i.e. small norm) model.

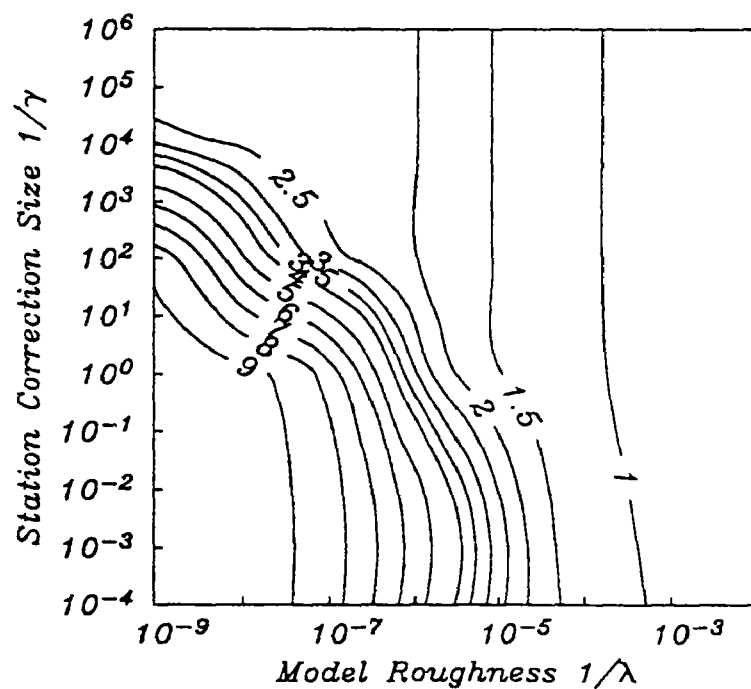


Figure 3. Tradeoff curve for 3D inversion showing contours of the  $\text{CHI}^{**2}$  measure of misfit of the traveltime data as a function of model roughness and station correction size. Note that some lateral variation is required to fit the data to  $\text{CHI}^{**2} = 1$ .



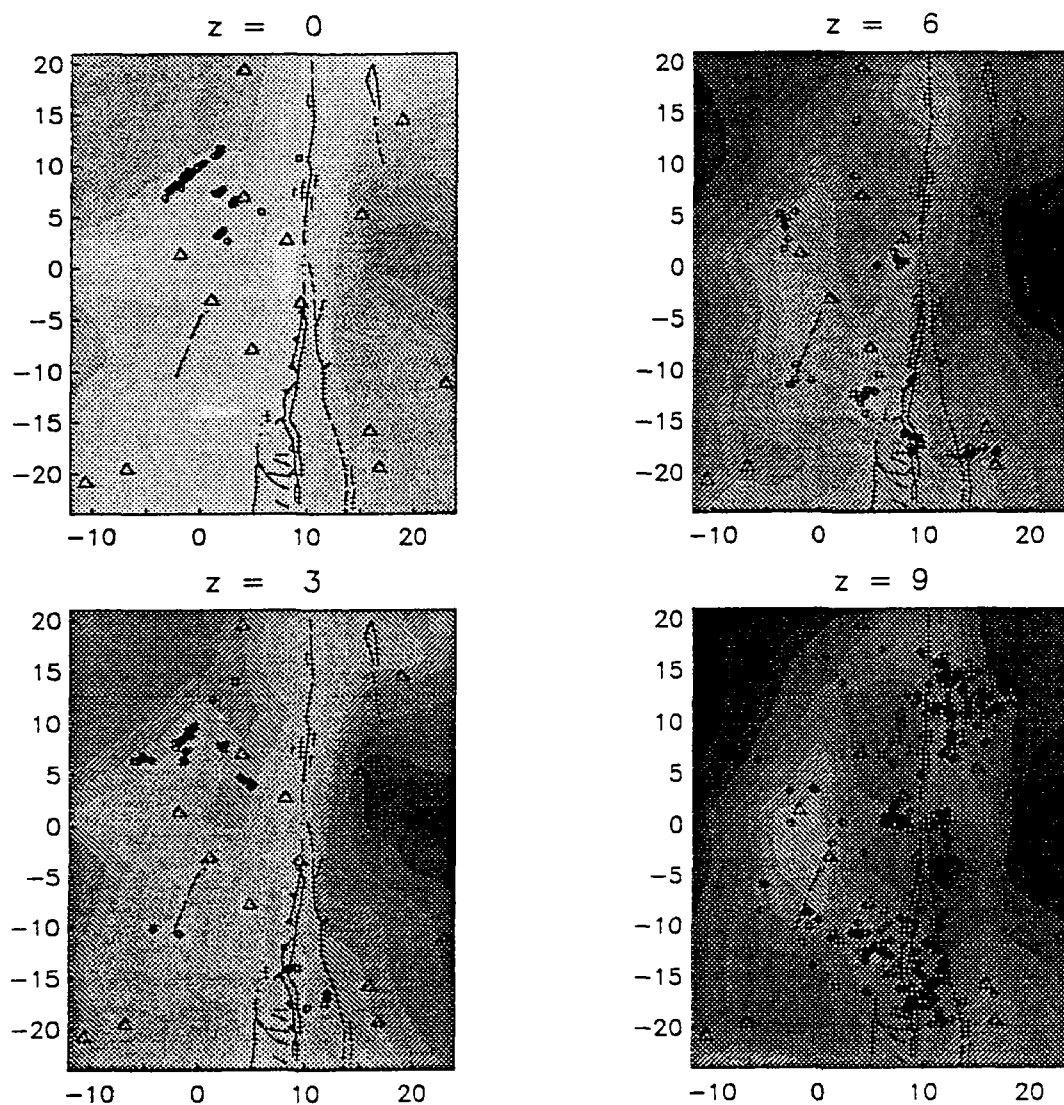


Figure 4. Horizontal cross-sections through the 3D P-wave velocity structure with the surface traces of the branches of the San Jacinto Fault superimposed. The scale is in kilometers and the map is rotated 50 degrees east of north and depths are referenced to sea level. Events are plotted at the level closest to their depth. Features at 0 km depth are very poorly determined, as well as features near the edges of the grid in the cross-sections at 3, 6, and 9 km depth.

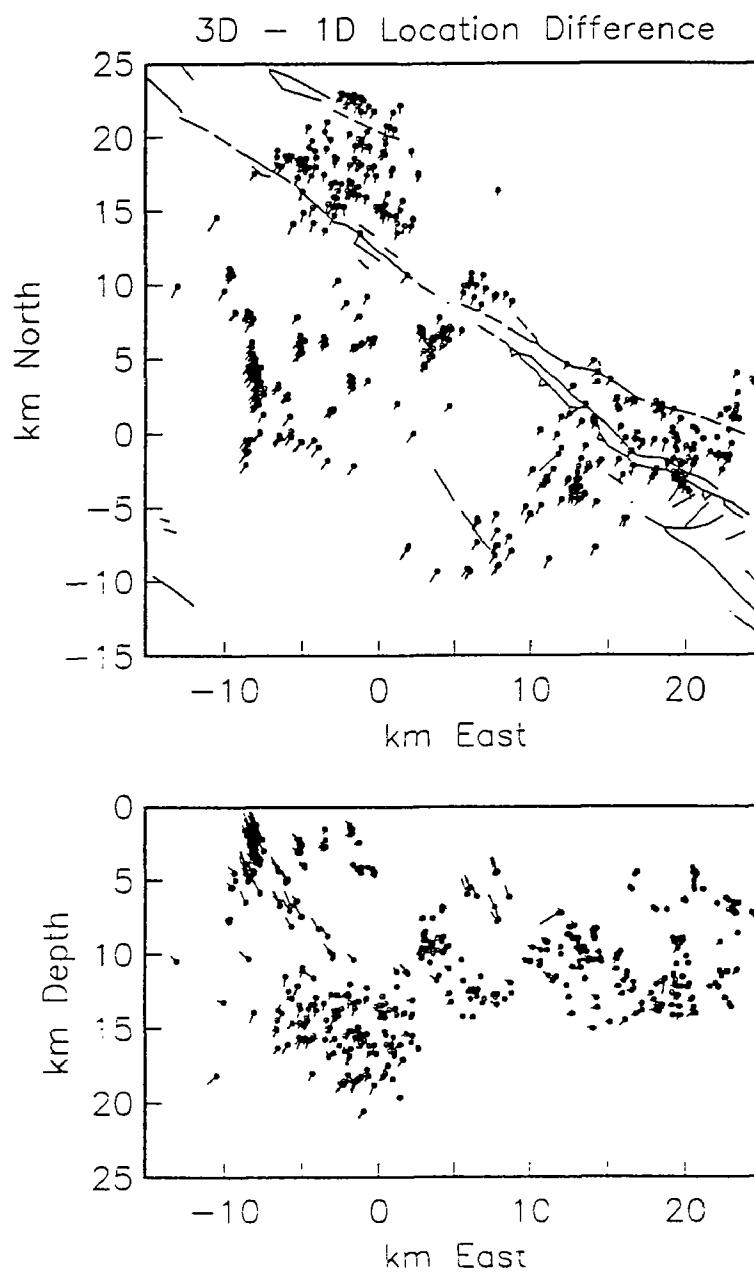


Figure 5. Difference in locations calculated for events in the 3D model vs those calculated in the 1D model. 3D location is at the circle and the length of the line is plotted to the same scale as the axes.

## Seismic Monitoring of the Shumagin Seismic Gap, Alaska

# 14-08-0001-A0616

Geoffrey A. Abers  
Lamont-Doherty Geological Observatory of Columbia University  
Palisades, New York 10964  
(914) 359-2900

### Investigations

Seismic data from the Shumagin seismic network were collected and processed to obtain digital waveforms, origin times, hypocenters, and magnitudes for local and regional earthquakes. The data are used for earthquake source characterization, determination of earth structure, studies of regional tectonics, analysis of possible earthquake precursors, and seismic hazard evaluation. Yearly bulletins are available starting in 1984.

### Results

The USGS decided in early 1991 to cease support for Aleutian network operations. Accordingly, all remote stations in the Shumagin Seismic Gap were removed during the 1991 field season and network operations ceased at that time. Only one high-gain station remains, the broadband station in Sand Point, which was moved to a new, quieter site on land owned by the Sand Point School (informally referred to as SPS). In addition to this station, digital strong-motion instruments continue to be operated by Lamont in Sand Point and Dutch Harbor, and analog strong-motion instruments were left at four remote sites in the Outer Shumagins (BKJ, CNB, NGI, and SIM). Thus, the 1991 field season marks the end of eighteen years of near-continuous monitoring of the Shumagin Seismic gap. Following removal of USGS-supported networks, the entire Aleutian arc is monitored by three stations east of Kodiak (~2500 km of plate boundary): SDN, 160.5°W; ADK, 176.5°W; and SMY, 174°E.

Shumagin network data were used to locate 121 earthquakes from January 1 to June 30, 1991, bringing the total number of digitally recorded events in Shumagin network catalog to 5926 since 1982. As the network was removed in the summer of 1991 (telemetry ceased on June 28), no further event locations from this project are anticipated. This number is somewhat lower than in previous years, because a substantial part of the network was removed in the summer of 1990. The seismicity for the first half of 1991 is shown in map view on Figure 1 and in cross section on Figure 2. Events shown by solid symbols are those events that meet the following quality criteria: located by 8 or more *P* or *S* arrivals, vertical error from *Hypoinverse* less than 10 km, and horizontal error less than 5 km. The same criteria were used for the comparison with the PDE catalog, discussed below (Figure 3). Other events are shown by open symbols. These criteria provide a rough indication of the location quality, and show that epicenters more than 100 km from the nearest station are rarely well determined. Additional numerical tests of hypocenter stability show that when the entire network is operating, shallow events west of 166°W, east of 156°W, or seaward of the trench can not be reliably located. Also, depths of shallow earthquakes are only well-determined beneath the Shumagin Islands.

The overall pattern in Figures 1-2 resembles the long term seismicity. Seismicity is concentrated near the base of the main thrust zone between 25 and 40 km depth, and immediately above it within the overriding plate. Seismicity contours below 30 km depth parallel the volcanic arc, rather than the trench, and become closer to the trench west of the network (Figure 1). Seismicity appears to be sparse where the main thrust zone is shallower than 35 km, between the Shumagin Islands and the trench. Deeper seismicity extends to depths of 200 km. Some locations near 100 km depth on Figure 2 correlate with the lower plane of the double seismic zone seen in long-term seismicity.

The most significant activity in the Shumagin area was a  $M_S = 6.7$  event on May 30, 1991. The event was located in the Sanak basin, in a region characterized by persistent localized low-level seismicity; this cluster has been evident throughout the period of network operations. The May 30 event was determined to have a shallow thrust mechanism from teleseismic body-wave inversion, at a depth of  $30 \pm 5$  km. The mechanism, depth, and location are all consistent with this earthquake being due to thrusting on the main plate interface. The surface-wave magnitude (6.7) formally makes this event the largest to have been recorded in the Shumagin region since the advent of regional monitoring in 1973, although the event is not significantly larger than  $M_S = 6.5$ -6.6 events in 1983, 1985, and 1987, and is significantly smaller than major regional events of 1917 ( $M_S = 7.4$ ), 1946 ( $M_S = 7.4$ ), and 1948 ( $M_S = 7.5$ ).

Three primary tasks were accomplished in the Summer 1991 field season. First, all telemetered equipment was removed and remote sites (all in wildlife refuges) were cleaned up. The only exceptions are the four analog strong-motion recorders (SMA-1's) mentioned above, and physical structures for 4 sites near volcanoes left for the Alaska Volcano Observatory. Second, locations were redetermined using GPS surveying equipment at all sites not previously removed (Table 1). All locations are single-station 3D locations made with Trimble recorders made while Selective Availability was turned off. Differences with previous locations were a few to a couple tens of meters at most, except for one site (BKJ) whose previous location was in error by  $\sim 600$  m.

The third significant accomplishment of the 1991 field season was the successful moving of the Sand Point broad-band station to a new, quiet site at the town school (SPS). The Guralp CMG-4 sensors were placed a pier poured directly on bedrock, enclosed in a small, low structure. Recording is done continuously at the school on a Sun-based system, where data is available via modem for up to one week. After that, data is written to tape and mailed to Lamont. Broad-band data is digitized at two gains at 20 samples per second, 12 bit samples, producing 6 continuous records. The local school district plays an active role in station operations. The station would make a good site for National Network deployment in the Aleutians. This instrument has provided high-quality records since late July, 1990 when it was configured in this mode at the old Sand Point station, and provides data that are being used for detailed source and propagation studies.

Now that future monitoring will be done solely by teleseismic recording, it is worthwhile to assess differences between local and teleseismic locations. We have correlated the Shumagin catalog with the PDE catalog from 1982 to 1990 (Figure 3; see caption for details). The most significant differences are a location bias and a magnitude bias. PDE locations are systematically located arcward relative to Shumagin Network locations, probably because of the high-velocity downgoing slab. Events beneath the Shumagin Islands ( $159^\circ\text{W}$  -  $161^\circ\text{W}$ ) are located to within a few km by the local network; here PDE locations are 25-50 km closer to the arc. Events lower in the slab (near  $56^\circ\text{N}$ ) and farther from the network show larger biases (40-100 km). Location biases for earthquakes directly beneath the Shumagin Islands are probably most reflective of systematic errors in teleseismic locations, rather than in Network locations, and indicate that teleseismic locations cannot be relied upon to better than 25-50 km. These biases are generally attributed to the effect of the high-velocity slab on travel times.

The Shumagin magnitudes are systematically lower than the PDE magnitudes, by 0-1 units but with significant scatter. Shumagin magnitudes are based upon maximum peak-to-peak amplitudes in the early part of the  $P$  wavetrain, corrected for the instrument response at the dominant frequency. It is not known what causes this discrepancy, but we suspect that it may be due to scale saturation for Shumagin stations above magnitude 4; for these events the high-gain stations are on scale but the  $P$  wavetrain shows significant energy over several cycles. The high-gain channels are off-scale for larger events, and Shumagin magnitudes are based upon other measurements.

TABLE 1. Shumagin Seismic Network, Stations 1982-1991

Station	Latitude	Longitude	Elev. (m)	Method	Instruments
bal	55°11.60'N	162°47.21'W	366		SPZ
bkj	55°09.64'N	159°33.99'W	170	GPS	SPZ, <u>SMA</u>
blh	55°42.15'N	162°03.95'W	390		SP3
cdb	55°11.50'N	162°42.00'W	25		SMA
cnb/cnf	54°49.22'N	159°35.37'W	100	GPS	SP3;FBA; <u>SMA</u>
dlg	55°08.39'N	161°50.15'W	350	GPS	SPZ;SMA
drd	54°55.44'N	162°17.07'W	390	GPS	SPZ;SMA
dutf	53°54.00'N	166°32.00'W	25		<u>SSA</u>
fsp	54°56.44'N	163°27.72'W	275		SPZ
ivf	55°53.75'N	159°31.80'W	275		SPZ;SMA
ngi	55°02.37'N	160°04.18'W	270	GPS	SPZ; <u>SMA</u>
pn6	55°27.12'N	161°54.89'W	814		SPZ
pn8	55°26.62'N	162°01.25'W	605		SPZ
ps1	55°25.41'N	161°44.20'W	300	GPS(2D)	SPZ
ps4	55°21.23'N	161°52.12'W	560	GPS	SPZ
pvv	55°22.45'N	161°47.45'W	180	GPS	SP3
sas/sai	55°20.36'N	160°29.91'W	23	GPS	SP3;BB; <u>SSA</u>
sps	55°21.05'N	160°28.48'W	90	GPS	BB
sgb	55°32.76'N	160°27.30'W	290	GPS	SP3;SMA
sim	55°55.20'N	159°15.50'W	500		<u>SMA</u>
snk	54°28.44'N	162°46.52'W	159		SPZ;SMA
sqf/sqh	55°13.23'N	160°33.86'W	310	GPS	FBA
dt2	55°09.91'N	162°13.83'W	660	(AVO Station)	SPZ
zkb	55°19.16'N	160°45.08'W	250	GPS	SPZ

Instruments: SPZ, short-period vertical velocity sensor (Geospace HS-10, 1 Hz); SP3, short-period 3-component sensors (Geospace HS-10, 1 Hz); SMA, analog strong-motion accelerometer (Kinematics SMA-1); FBA, telemetered 3-component force-balance accelerometer (Kinematics FBA-3/FBA-13); SSA, digital strong-motion accelerometer (Kinematics SSA-1); BB, 3-component broad-band (Guralp CMG-4; 0.05 Hz corner). Underlined instruments remain deployed as of July, 1991.

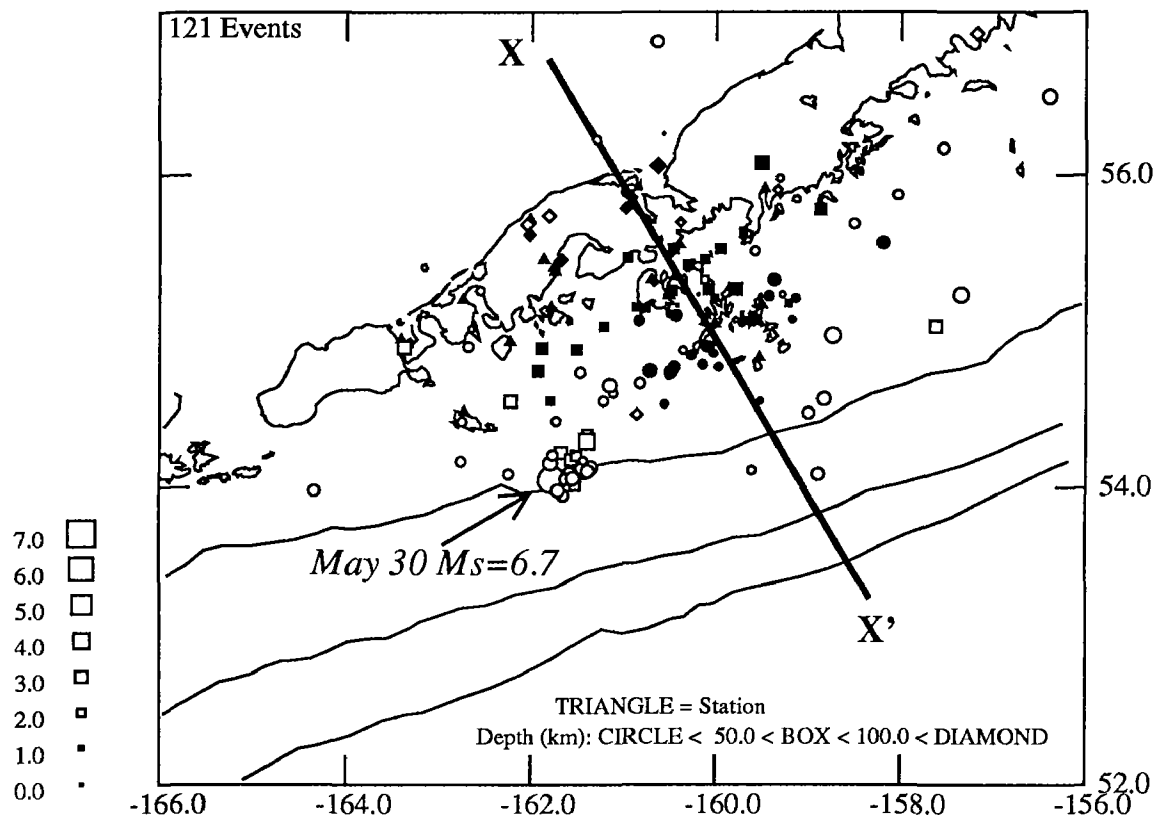


Figure 1. Map of seismicity located by the Shumagin seismic network from January to June, 1991. Symbol shapes show depths, sizes show magnitudes. Filled symbols meet criteria for well-located events, described in text.

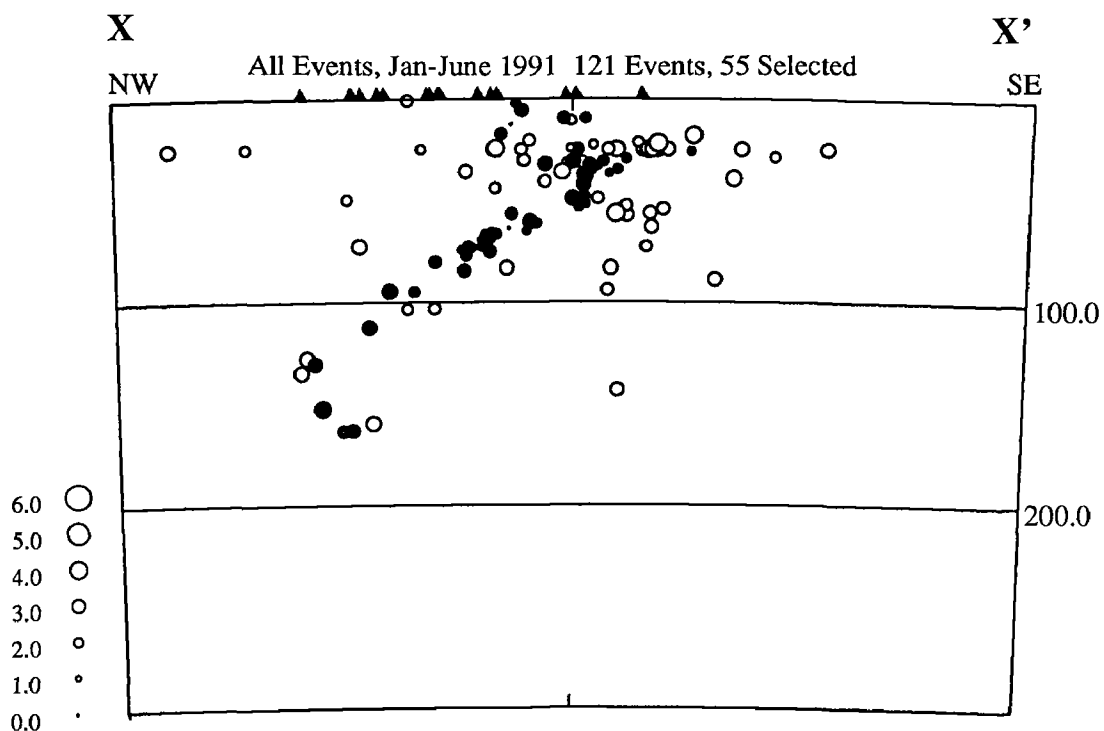


Figure 2. Cross-section of all Shumagin Network seismicity January to June, 1991, located in Figure 1. Triangles are station locations.

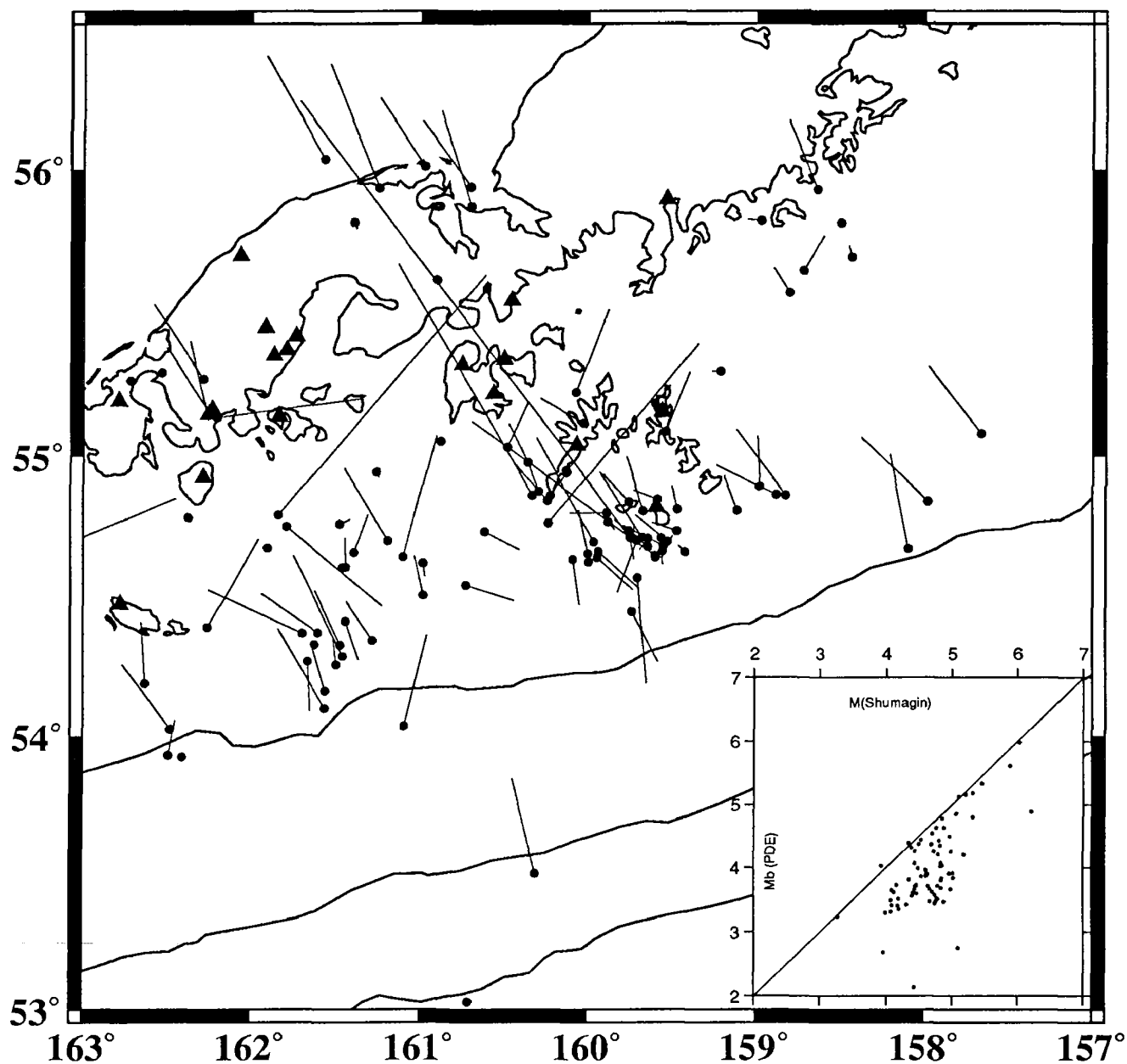


Figure 3. Comparison of Shumagin catalog data, 1982-1990, with the PDE catalog. A total of 260 matching events are found with PDE locations between 164°W and 204°W, of which 120 have Network locations that meet the quality criteria discussed in text. Only these 120 events are plotted, and the subset of these with magnitudes is shown in the inset. Solid circles are Network locations, vector tips are PDE locations. Triangles are Network stations. Inset shows comparison of body wave magnitudes between Shumagin catalog and PDE (each magnitude is randomly perturbed by up to 0.05 units, for display purposes).

**Piñon Flat Observatory:  
Comparative Studies and Geophysical Investigations**

14-08-0001-G1763

Duncan Carr Agnew, Frank K. Wyatt,  
James W. Happer, and Hadley O. Johnson  
Institute of Geophysics and Planetary Physics  
Scripps Institution of Oceanography  
University of California, San Diego  
La Jolla, CA 92093-0225  
(619) 534-2411

This grant provides support for collaborative studies with several USGS-sponsored investigators conducting research at Piñon Flat Observatory (PFO). The initial aim of this work was to evaluate instrumentation developed for the measurement of ground deformation, the idea being to operate simultaneously a number of continuously recording sensors and small geodetic arrays, and, by direct intercomparison, to identify the merits and limitations of the various techniques. Good progress has been made in evaluating the instruments in a common setting and in establishing better bounds on the behavior of the crust in this tectonically active area. As instrument work has progressed the focus of the work has naturally shifted to the use of the combined results to learn more about the earth.

One of our current efforts is a cooperative project with Dr. John Langbein, and involves the USGS two-Color EDM data from the networks around Pinyon Flat (shown as solid lines in the top panel of Figure 1). Over its range ( $< 10$  km) the two-color EDM has an error of 0.3 to 1.0 mm, lower than any other so far established or even expected in the near future. At these levels, we would expect monument motion to become a source of error, as has indeed occurred at the two-color network in Parkfield. There is clear evidence for similar difficulties in the nominally much-better-rock at PFO. The bottom panel of Figure 1 shows the line-length changes on two nearly parallel lines in the Pinyon two-color network, which run from the central mark (Green) to colocated monuments PF5 and PF5A. Since both these lines run nearly NW-SE, we can compare length changes in them with the NW-SE laser strain data; rather than scaling the length changes to strain we have scaled the strainmeter data to equivalent length changes over the geodetic line. It seems clear that the geodetic data have fluctuations of several mm; these are much larger than the error in the measurement (which is shown by the error bars, and confirmed by the small scatter of points taken close together in time), and very much larger than what the strainmeter shows. We attribute this error to monument motion, probably at the far ends of the lines, since if the central point were to move the changes would be the same for both. Such monument motion is potentially a significant part of the error budget for many other techniques. With proper anchoring, however, monument motions can be greatly reduced, as the laser strainmeter data show.<sup>1</sup>

---

<sup>1</sup> Note that because of the scaling of the strainmeter data, the physical displacement of its monuments are about one fifth of the of what indicated on the figure, and amounts to only  $\sim 0.2$  mm.



This network also gives us a chance to compare GPS with other types of measurements. The two-color networks around Pinyon Flat offer many lines that can be occupied by both systems. As mentioned earlier, over the span of this network (and the other ones nearby), the two-color system is the most precise available—with 1 mm or better precision, it's better than has been shown for GPS. A systematic comparison of the two should teach us about both systems. Even though length scales of ~10 km are extremely relevant to fault-mechanics studies, achieving the maximum possible accuracy with GPS over these distances is relatively neglected. At very short distances (< 1 km), mm-level GPS repeatabilities can best be gotten with a weighted combination of the solutions of the two frequencies  $L_1$  and  $L_2$ ; the differential ionospheric contribution is so small that the ionosphere-free observable  $L_C$  adds noise. At 10 km or more, use of  $L_C$  starts to become advisable (Y. Bock, pers. comm.); the appropriate weighting of different observables over spans of several km, and the accuracies that can be attained, are still matters of open research. Such studies can be best pursued if there is a standard of comparison available, and the two-color data provide us with this—indeed one that is potentially good to 0.5 mm or so.

The comparison is not straightforward, however, because of the nature of the two-color Terrameter measurements. This system does not in fact measure the absolute distance; unlike most EDM's it does not measure the phase of a signal modulated at different frequencies, but varies the modulation frequency until a null is found, meaning that there are an integer number of wavelengths,  $K$ , in the optical path. This is done for two colors, red and blue, giving two frequencies  $f^r$  and  $f^b$ . If  $f^r$  and  $f^b$  are separated by ~42 kHz (which is what is done),  $K$  is the same for both. The relationship between the line distance  $D$  and the measurements is then

$$D = \frac{Kc}{2} \left[ \frac{1}{f^r} - A^r \left( \frac{1}{f^b} - \frac{1}{f^r} \right) \right] + C_\tau$$

where  $c$  is the speed of light,  $A^r$  is related to the ratios of the index of refraction of red and blue light (and is found from end-point meteorological data) and  $C_\tau$  is an instrument (and reflector) constant. If the instrument is used to find only changes in  $D$  (as it usually is),  $C_\tau$  drops out and one needs only a rough estimate of  $K$ ; this is done using a measurement over a nearby line with an HP3808 EDM. However, if we seek to compare absolute lengths, we need to know both of these, neither of which is usually found. We believe that combined measurements over a number of lines will enable us to adjust for these quantities, thus learning something about the Terrameter as well as about GPS. Our goal is to combine these data to determine absolute distance on the 2-color lines to within the submillimeter precision of the Terrameter measurements.

We have already made one trial comparison over two of the lines of the Pinyon network. Last summer we measured the two lines from the two-color mark at Green (the center station) to PFO with Trimble receivers, and also the (2 meter) offset from the two-color to the HP3808 mark. The resulting line lengths (both about 4.5 km) can be compared to the HP3808 values, corrected for index of refraction using the two-color data; the numbers agree to within 1 mm in one case and 3 mm in the other; in terms of proportional line-length,  $2 \times 10^{-7}$  and  $7 \times 10^{-7}$ . This level is perhaps better than we have any right to expect, but very encouraging: it implies that we are headed in the right direction.

Since the spring of 1990 a continuously-operating GPS network (the PGGA) has been running in Southern California over baselines of ~100 km. A somewhat shorter scale is of interest for fault studies, and we, like many others, have been eager to try the experiment of a

“GPS strainmeter”: two receivers, operating continuously, separated by about 10 km. Together with Dr. Yehuda Bock, we have begun such measurements with the goal of interpreting the results in terms of the deformation patterns already known for the area from USGS Geodolite, USGS Two-Color and UCSD laser strainmeter records.

The upper panel of Figure 1 shows the location of our new GPS line, extending west from PFO to a site at Pine Meadow, 14.124401 km away. The Pine Meadow installation was made permanent at the beginning of Spring 1991, and since then we have been running one of our SIO Trimble receivers there, connected to a PC which, using software from Trimble, operates it as a continuous tracker; a high-speed modem is used to download the data nightly into the same computer at IGPP which collects the PGGA data. Another Trimble (on loan from Dr. Jackson of UCLA, another collaborator in this study) is installed at PFO, on the secondary deeply-anchored mark there.

Processing of these data has proceeded fairly smoothly; as often is the case in GPS studies, the biggest difficulties have come with the data from the other (fiducial) stations needed to constrain the satellite orbits. We have therefore focussed on a period of the summer of 1991 for which precise orbits were generated by Dr. Bock as part of the PGGA project, using data from a global network of P-code receivers. We are investigating a variety of processing options (e.g., using broadcast orbits, different observables, and different constellations); once the data have been cleaned, this is easy to do, and the large number of days of data available means that we can have a high level of confidence in any changes that appear as a result. Figure 2 shows some results for the line from the Trimble tracker at PFO to the station at Pine Meadow, and also the 50-meter line between the Trimble and Rogue continuous trackers (both on anchored monuments) at PFO. Over the longer line the standard deviation of the North-South relative displacement is 8 mm; for the East-West (and length) it is 5 mm, and 14 mm for the vertical. For the shorter line the equivalent numbers are 0.7 mm, 1.0 mm and 1.3 mm. All these numbers are somewhat preliminary; as they stand (i.e., even after considerable effort in data processing), they do not appear to give length measurements quite comparable to the observed repeatability of Geodolite measurements over 10-15 kilometers. There is also some hint of correlation from day to day (especially in the vertical); it may be that GPS, like other deformation measurement techniques, has more noise at low frequencies than high.

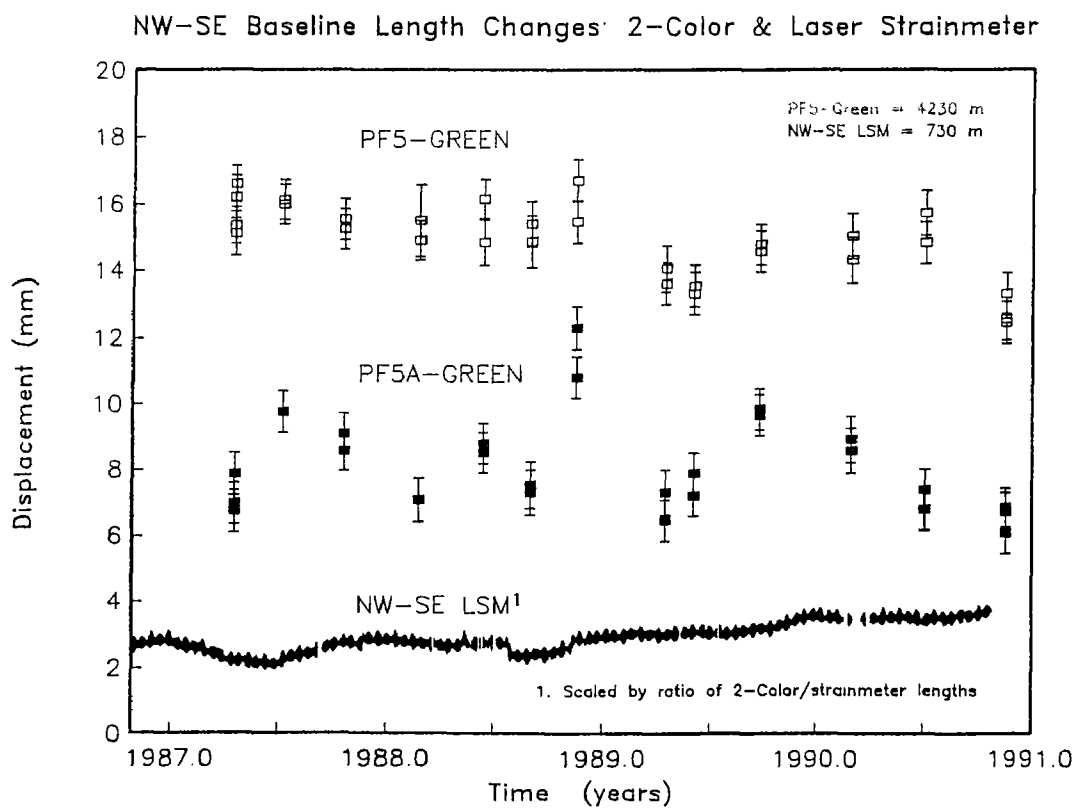
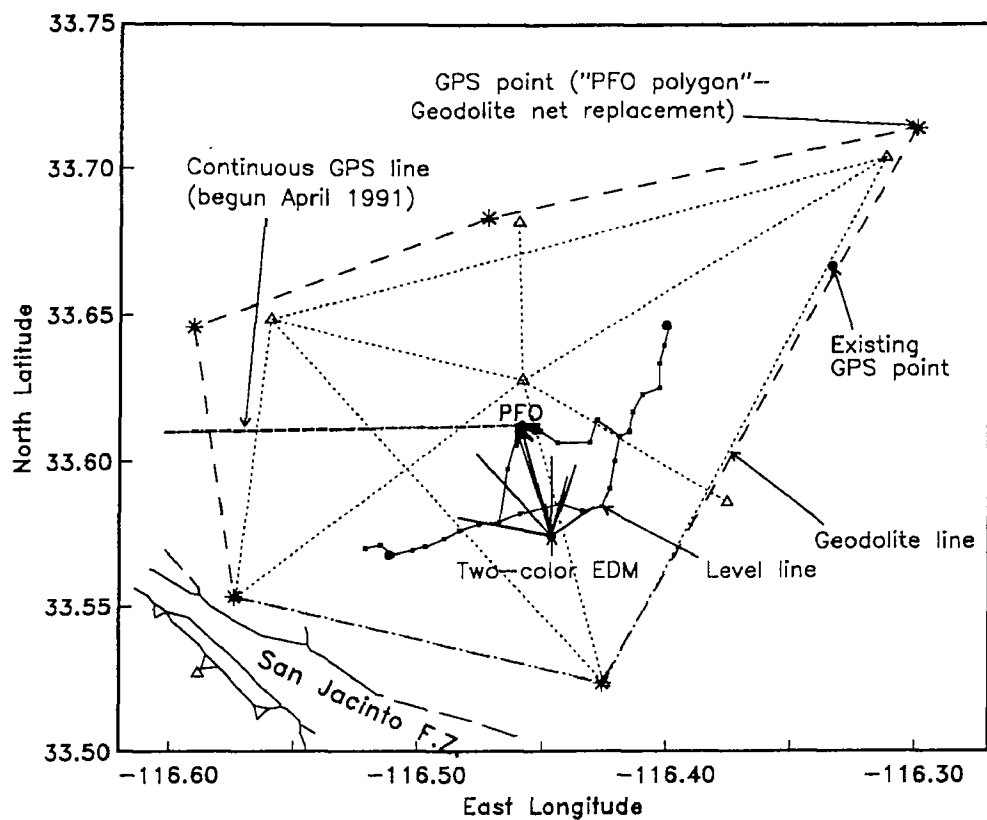


Figure 1

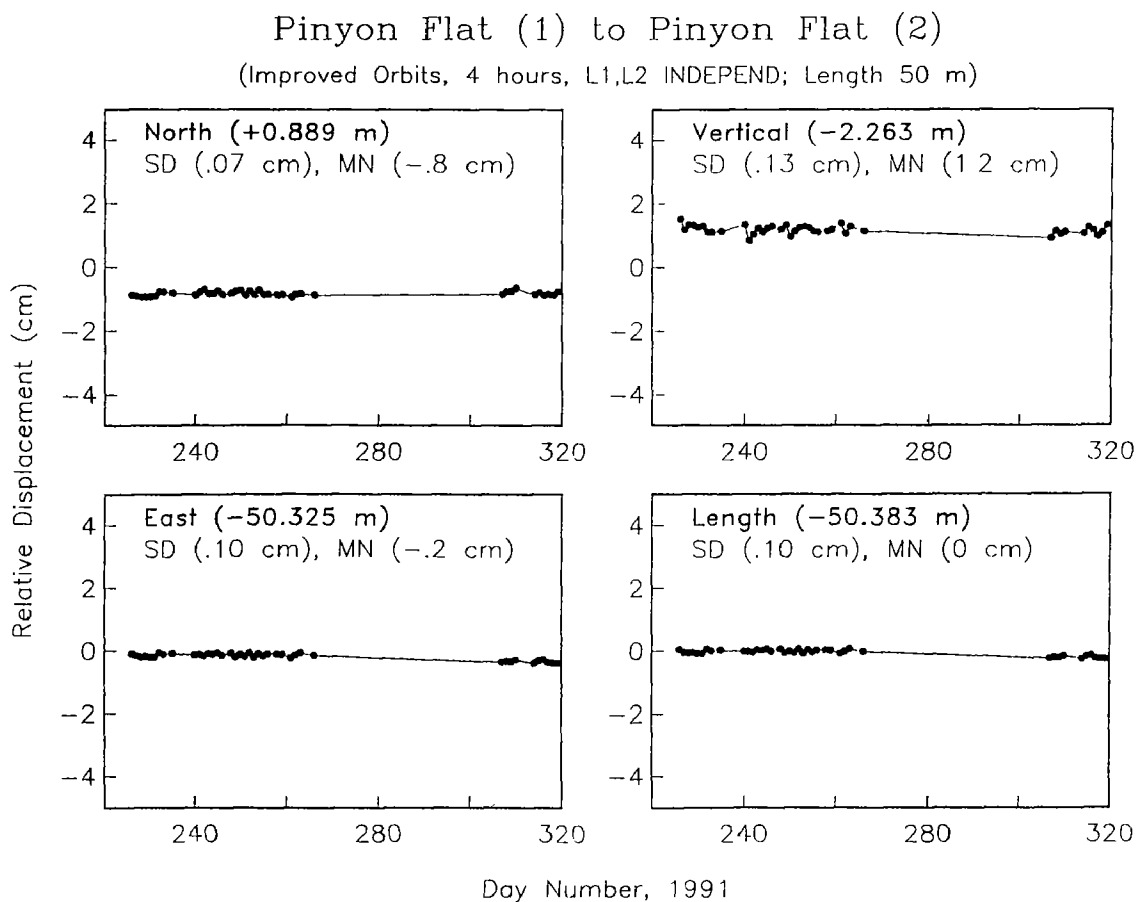
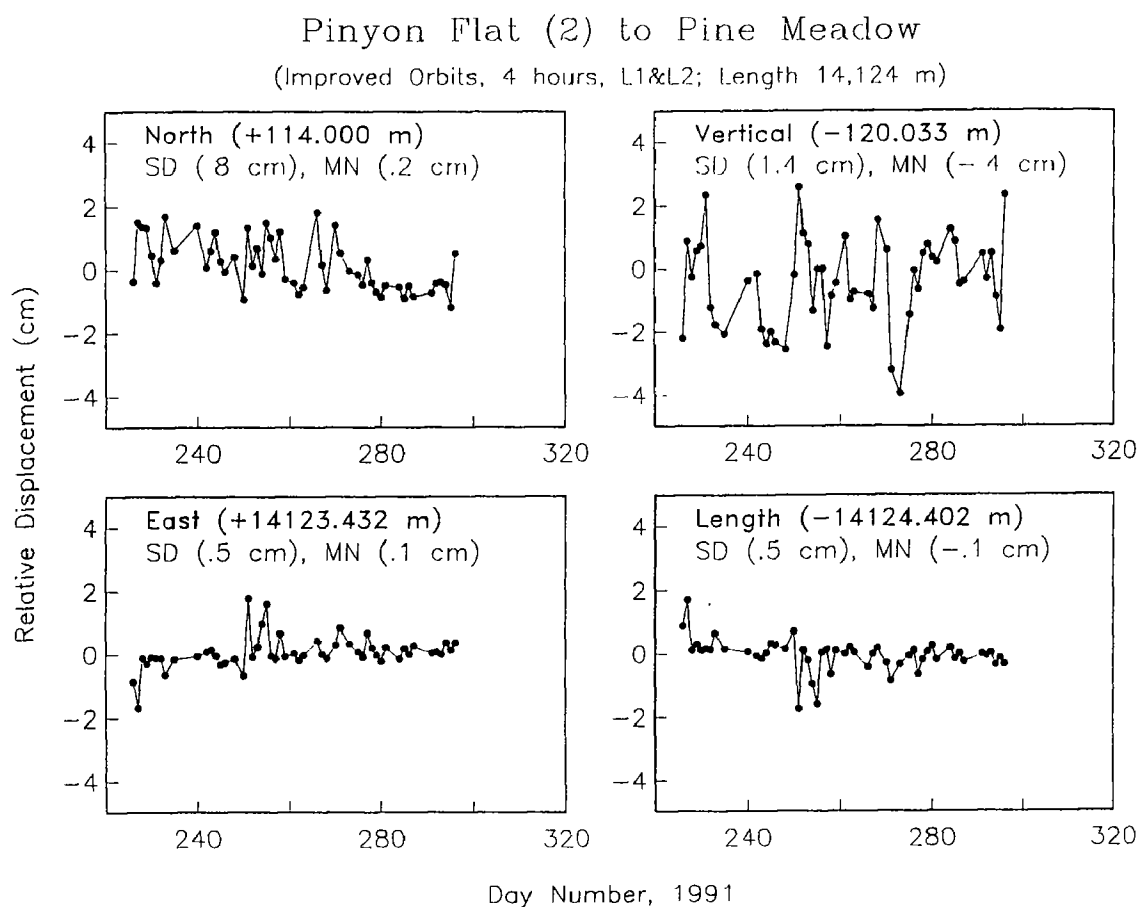


Figure 2

## Seismological Data Processing

9930-03354

Greg Allen, Moses Smith

Branch of Seismology  
U.S. Geological Survey  
345 Middlefield Road, MS 977  
Menlo, Park, Ca. 94025  
(415) 329-4695

### INVESTIGATIONS

This project provides services for UNIX computers and PCs in the areas of network management and maintenance, computer system management, installation, backups, maintenance, and user assistance. There are currently 21 UNIX computers in the Branch of Seismology: an Integrated Solutions Inc., multi-user system; a SUN 4/280 fileserver; 6 SUN SPARCstation 1s; 6 SUN 3/60 workstations; 2 SUN 3/50 workstations; 1 SUN 3/80 workstation; 1 SUN SPARCstation SLC; 2 SUN SPARCstation 2s; 1 SPARCSTATION ELC. This project also maintains a NOVELL network of 7 PCs (MS-DOS), for the branch administrative staff.

### RESULTS

Gave general user assistance with the use of UNIX systems.

Did monthly and nightly backups of the ISI and SUN computers.

Maintained the RTP data system buffer service to branch UNIX and VAX computers.

Maintained the branch administrative office's Novell PC network.

Prepared computer hardware and software maintenance contracts.

Maintained and upgraded UNIX application software.

Arranged for various hardware repairs for the UNIX computers.

Extended the SUN data communication sub-net from building 7 to building 8.

Upgraded the SUN 4/280 file server hardware by adding a 1 gigabyte, SCSI disk, and 32 serial ports.

Upgraded the operating system of SUN workstations to SUN OS 4.1.1

Participated in the preperation of the new computer room facilities, and moved the SUN 4/280, ISI UNIX computer and the RTP monitoring workstation into the new computer room.

Installed 2 SUN SPARCstation 2 and 1 SUN SPARCstation ELC computers.

## REGIONAL AND LOCAL HAZARDS MAPPING IN THE EASTERN GREAT BASIN

9950-01738

**R. Ernest Anderson**  
Branch of Geologic Risk Assessment  
U.S. Geological Survey  
Box 25046, MS 966, Denver Federal Center  
Denver, Colorado 80225  
(303) 236-1584

### INVESTIGATIONS

Although funded primarily by a Gilbert Fellowship, the following investigations contribute to the NEHRP in terms of understanding the attitude, geometry, and interconnectedness of potentially active normal fault systems.

1. Prepared report detailing investigations of the three-dimensional Neogene strain field in the Mormon Mountains area, Nevada-Utah.
2. Conducted field studies of selected aspects of the three-dimensional Neogene strain field in the Lake Mead area, Nevada-Arizona.

### RESULTS

1. The Mormon Mountains area is one of the "breeding grounds" for modern concepts of extensional deformation--in particular, the concept that large-magnitude extension takes place by uniform-sense displacements on stacked systems of regionally distributed low-angle detachment faults. This concept does not agree with the historic record of large normal-faulting earthquakes, which lacks conclusive evidence of displacements on low-angle normal faults, and is inconsistent with measured and assumed stress conditions in the upper crust. A field study of these "breeding grounds" was conducted to evaluate whether or not the concept is well-founded. Many results of the study are at variance with the concept. In particular, we find no evidence in either the geologic or geophysical data for the high degree of lateral continuity and interconnectedness of faults required by the concept and purported by fault correlations over long distances. Instead, we find extreme lateral heterogeneity in deformational style and magnitude. This heterogeneity includes abrupt lateral contrasts in vertical structural relief as well as in the distribution of strike-slip faulting and associated folding. A surprising outcome of our study is that the strain field includes major elements of plan-view contraction normal to the direction of extension. Preliminary analysis indicates that the amount of this contraction, when combined with the more widely known vertical contraction (structural attenuation) may equal the amount of extension, thus revealing balanced three-dimensional coaxial strain.
2. Preliminary results of field studies in the Lake Mead area indicate that synorogenic magmatism played a critical role in Neogene crustal rifting and extensional deformation. Although the large-volume inflation of the upper crust by plutons allows us to estimate the direction, amount, and age of two-dimensional rifting, it precludes understanding the three-dimensional strain partitioning from analysis of faults and folds. However, major postintrusion faulting and folding provide clues suggesting that meridional collapse and extension-normal contraction are important elements of the Neogene strain field in the Lake Mead area.

**REPORTS**

- Anderson, R.E., 1991, Relationship between Miocene plutonism, uplift, and extension, Lake Mead area, northwesternmost Arizona and adjacent Nevada: Geological Society of America Abstracts with Program, v. 23, no.5, p. A245.
- Barnhard, T.P., and Anderson, R.E., 1991, Tectonic significance of dike orientations in the Lake Mead area of Nevada and Arizona: Geological Society of America Abstracts with Program, v. 23, no. 5, p. A233.
- Anderson, R.E., and Barnhard, T.P., in press, Heterogeneous Neogene strain and its bearing on horizontal extension and horizontal and vertical contraction at the margin of the extensional orogen, Mormon Mountains area, Nevada and Utah: U.S. Geological Survey Bulletin 2011, 80 ms p., 31 figs.



## Regional Seismic Monitoring Along The Wasatch Front Urban Corridor And Adjacent Intermountain Seismic Belt

14-08-0001-A0621

W. J. Arabasz, R. B. Smith, J. C. Pechmann, and S. J. Nava

Department of Geology and Geophysics

University of Utah

Salt Lake City, Utah 84112

(801) 581-6274

### Investigations

This cooperative agreement supports "network operations" associated with the University of Utah's 81-station regional seismic telemetry network. USGS support focuses on the seismically hazardous Wasatch Front urban corridor of north-central Utah, but also encompasses neighboring areas of the Intermountain Seismic Belt. Primary products for this USGS support are quarterly bulletins and biennial earthquake catalogs.

### Results (April 1 - September 30, 1991)

**General accomplishments.** During the report period, significant efforts related to: (1) implementation of a distributed computer system (4 SUN Sparc 2 workstations with optical-disk data storage) for processing and analysis of network data and data from portable seismographs; (2) experimental use of 4 REFTEK digital recorders for supplementing regional-network data collection; and (3) continued upgrading of site hardware and electronics at field stations that have been operating since the mid-1970s.

**Network Seismicity.** Figure 1 shows the epicenters of 440 earthquakes ( $M_L \leq 3.8$ ) located in part of the University of Utah study area designated the "Utah region" (lat.  $36.75^\circ$ - $42.5^\circ$ N, long.  $108.75^\circ$ - $114.25^\circ$ W) during the six-month period April 1 to September 30, 1991. The seismicity sample includes eight shocks of magnitude 3.0 or greater (labeled in Fig. 1) and five felt earthquakes ( $M = 3.8, 2.9, 2.8, 2.6, 2.5$ ).

The largest earthquake during the six-month report period was a felt shock of  $M_L 3.8$  on April 20, 1991 (12:56 UTC), located 4 km north of Paragonah, in southwestern Utah. This earthquake was part of a swarm of 119 earthquakes that occurred mostly in late April 1991. Swarm activity such as this has been observed in southwestern Utah in the past and is not considered unusual. Approximately twenty-five percent of the seismicity detected during the report period was associated with an area of ongoing coal-mining related seismicity, located 20-90 km SW of Price in east-central Utah (100 shocks,  $1.6 \leq M \leq 2.9$ ).

### Reports and Publications

Nava, S.J. (1991). Earthquake Activity in the Utah Region, July 1 - September 30, 1990, *Survey Notes (Utah Geological and Mineral Survey)* 24, no. 3, 19; October 1 - December 31, 1990, *Survey Notes (Utah Geological and Mineral Survey)* 24, no. 3, 32.

Nava, S.J. (1991). Earthquake Activity in the Utah Region, January 1 - March 31, 1991, *Survey Notes (Utah Geological and Mineral Survey)* 24, no. 4, 10.

Nava, S.J. (1991). Earthquake Activity in Utah, October 1 - December 31, 1990, *Wasatch Front Forum (Utah Geological and Mineral Survey)* 7, no. 2, 2.

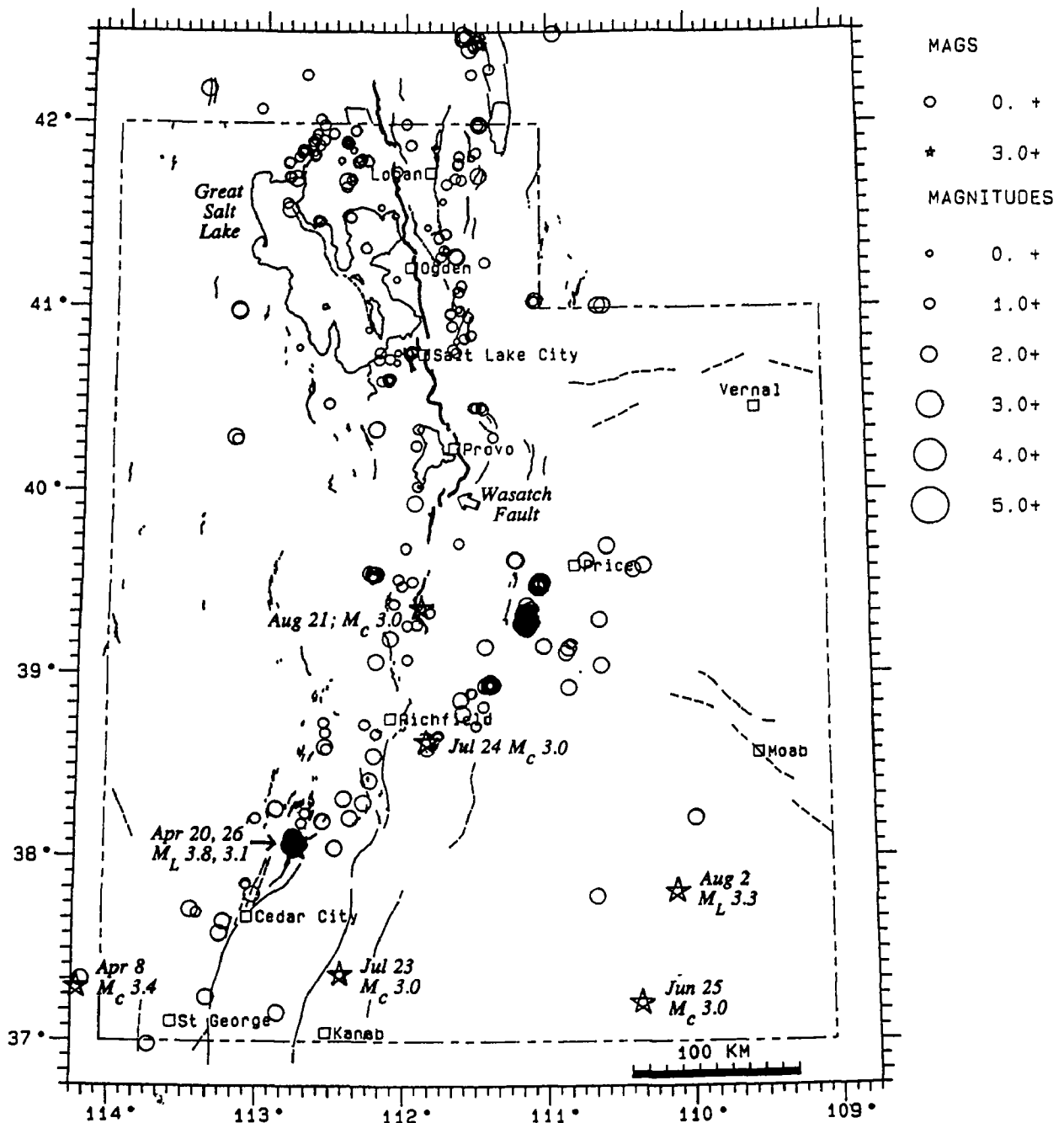


Figure 1. Earthquake Activity in the Utah Region, April 1, 1991, through September 30, 1991. Stars indicate shocks of magnitude 3.0 or greater.

## Holocene Paleoseismology in Western Washington State

Projects 9540-04004 (fiscal year 1991), 9540-10180 (1992)

Brian F. Atwater

U.S. Geological Survey at University of Washington AJ-20

Seattle, WA 98195

(206) 553-2927 FTS 399-2927

### INVESTIGATIONS

**Alaskan archives of a great earthquake.** A ten-day field study near Anchorage focussed on the geologic record of the 1964 Alaskan earthquake. Members of the field party included a dendrochronologist (Dave Yamaguchi), a micropaleontologist (Eileen Hemphill-Haley), and visitors (Gary Carver, Rod Combellick, Lou Gilpin, Mark Hemphill-Haley, Gordon Jacoby). Records studied included killed and surviving trees, intertidal silt that has accumulated on 1964 soils, and gravelly intrusions.

**High-precision dating of coastal subsidence about 300 years ago along the Cascadia coast.** A report on such dating in Washington was finalized and published. New samples were cut from spruce stumps at the Nehalem River estuary, in northern Oregon. Rings from previously collected samples from Humboldt Bay, California, were removed and then submitted to the isotope lab at the University of Washington.

**Study of vented sand in southern coastal Washington.** The timing of venting was studied in 18 trenches with total length of 135 m, at a diked tidal marsh along the Copalis River. The source of the sand was studied through drilling of 60 boreholes, the longest 43 m deep.

### RESULTS

The most surprising--yet frustrating--results came from the study of vented sand along the Copalis River. This sand provides no conclusive evidence either for or against strong Holocene shaking along the subduction-zone coast in Washington.

As interpreted in 1990 (Atwater, in press), the vented sand indicates earthquake-induced liquefaction about 1100 years ago. Extensive trenching and hand-coring in 1991 confirmed this age and further showed that the venting was copious: 50,000 cubic meters of sand across an area 1/2 km on a side. But hand coring and power drilling in 1991 showed that the sand has no likely source shallower than 35 m. By contrast, earthquakes up to magnitude 7.5 are not generally regarded as capable of causing sand to vent from depths greater than 10 or 15 m. If the 1100-year-ago venting along the Copalis River resulted primarily from shaking during an earthquake, that earthquake was probably much larger than magnitude 7.5. But the likely depth to the sand source is so great that the venting probably resulted less from shaking than from crustal deformation that squeezed deep aquifers, uncorked water already at high pressure, or liquefied sand through crustal faulting.

One could argue against strong Holocene shaking in coastal Washington by citing an absence of recognized evidence for earthquake-induced liquefaction features in the area of 1100-year-ago venting along the Copalis River. Little if any sand vented in this area during inferred plate-boundary earthquakes 300 and 1700 years ago. But with a source sand more than 35 m deep, copious venting along the Copalis either requires shaking so extreme, or has so little relation to shaking, that earthquakes 300 and 1700 years ago still could have been strong.

## REPORTS

Atwater, B.F., Stuiver, M., and Yamaguchi, D.K., 1991, Radiocarbon test of earthquake magnitude at the Cascadia subduction zone: *Nature*, v. 353, p. 156-158.

Atwater, B.F., 1992, Earthquake-induced subsidence and liquefaction along the Copalis River, southern coastal Washington: *Journal of Geophysical Research* (in press).

Atwater, B.F., Nunez Jimenez, H., and Vita-Finzi, C., 1992, Net late Holocene emergence despite earthquake-induced submergence, south-central Chile, in Ota, Y., Nelson, A.R., and Berryman, K., eds., *Impacts of Neotectonics on Quaternary Coastal Evolution: Quaternary International* (in press).

## Long Baseline Tiltmeters: Southern California

Grant No. 14-08-0001-G1790

John Beavan

Lamont-Doherty Geological Observatory of Columbia University, Palisades, New York 10964

Tel: (914) 359-2900; Fax: (914) 359-5215; e-mail: beavan@lamont.lamont.columbia.edu

### Investigations

We are analysing data from a 535 m long-baseline half-filled water tube tiltmeter that has operated for eight years at Piñon Flat Observatory (PFO) in the San Jacinto Mountains of southern California. This analysis, in conjunction with analysis of data from a similar instrument by the University of California, San Diego (UCSD), is used to investigate:

- (1) sources and magnitudes of noise affecting the tilt signal;
- (2) methods of referencing tiltmeters to depth;
- (3) interpretation of tilt signal.

We also work on the development of improved water level sensors for future tiltmeter installations, and are testing prototype sensors on the Mammoth Lakes long baseline tiltmeter.

### Results (November, 1991)

#### *1. Tiltmeter Sensor Development*

Development of a prototype simple absolute sensor (USGS Open File Report 90-54, pp 163-165, 1989) is complete, and two prototypes have been installed at Mammoth Lakes, California. The power requirements have been reduced to about 250 mA at 12 V; since most of the electronics can be turned off between samples this makes the instrument potentially operable from batteries for extended periods of time.

The CCD sensors were installed in vaults B and C on the E-W (N100°E) arm of the Mammoth Lakes long fluid tiltmeter, in parallel with the existing interferometer sensors. Early data from the CCD sensors are compared with the interferometer data in Figures 1 through 3. As expected, the noise level on the CCD sensors is somewhat higher than on the interferometers (Figure 1). However, it generally appears to be much better than the design goal of 0.2 pixel (2  $\mu\text{m}$  on CCD, 1.4  $\mu\text{m}$  water height). There have been a couple of teething problems with the Mammoth installation, though neither were connected with the CCD part of the system, which so far has performed flawlessly. The long gap in the vault C water height data (Figure 2) was the result of a manufacturing defect in the single-board computer that controls the data sampling. (This defect was the subject of a manufacturer recall, and the offending board has now been replaced.) The shorter data gap in vault B was the result of corrosion in the anodized aluminum end reservoirs that we had used to reduce costs in the development of the prototype sensors. In both cases the measurement datum was preserved across the data gap, giving a striking indication of the value of the "absolute" measurement provided by the CCD sensors. The tilt derived from the CCD sensors is compared with that from the interferometers in Figure 3. The long wavelength differences between the two signals is probably a result of the different temperature coefficients of the CCD and interferometer end reservoirs. This problem will be addressed when a field version of the CCD sensor is constructed.

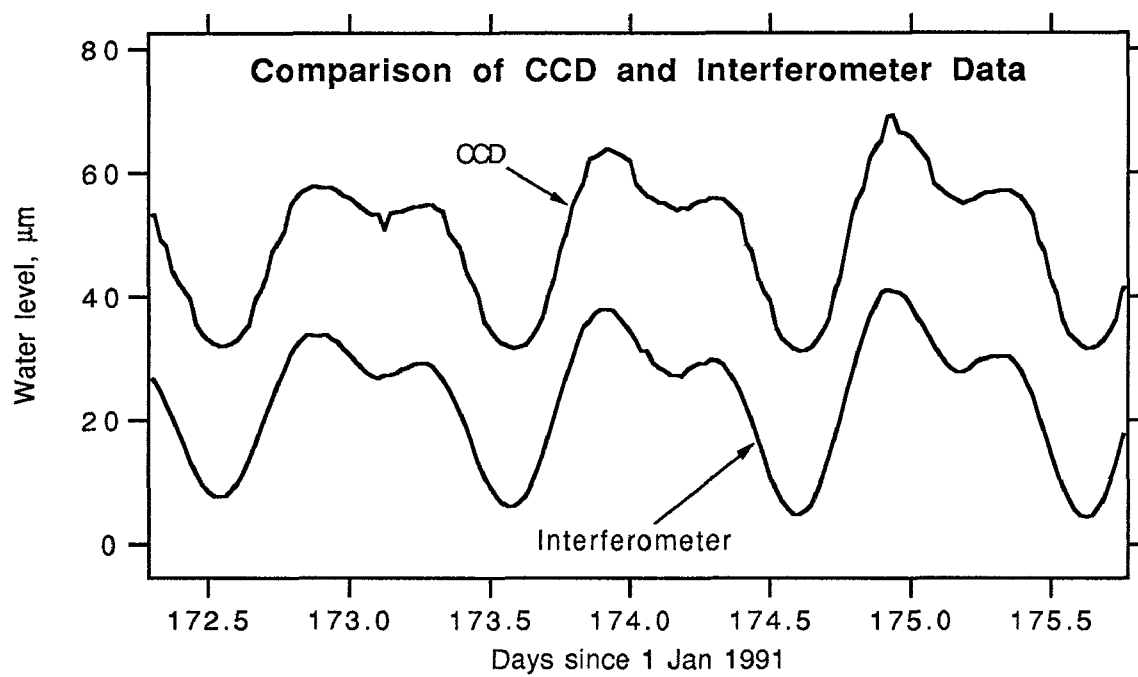


Figure 1. Comparison of data from CCD and interferometer sensors, showing the good quality of data from the CCD sensor.

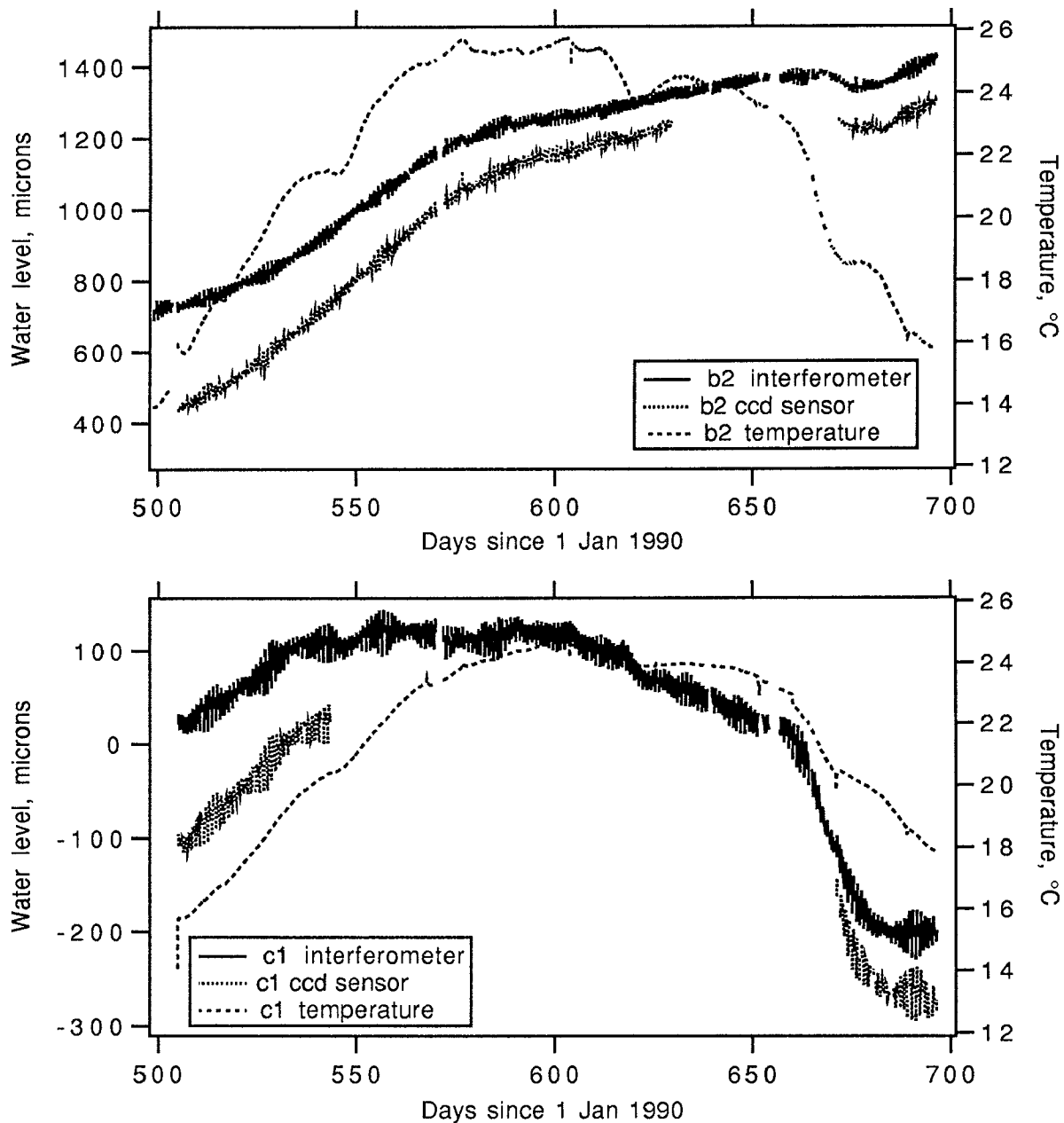


Figure 2.

Comparison of data from interferometer and CCD sensors at Mammoth Lakes between May and November 1991. Upper plot: vault B; lower plot: vault C. The B-C arm of the tiltmeter is oriented  $80^{\circ}\text{W}$ .

The very long gap in the vault C CCD data was due to a defective computer. However, the great advantage of the CCD sensor is that the datum of the water level record has been preserved across this long gap. The shorter gap in the vault B CCD data was due to corrosion in the CCD end reservoir, but the datum has likewise been preserved across the gap. Gaps in the interferometer data have been treated in the traditional fashion of matching data by eye across the gap.

The long term differences between the CCD and interferometer data in each vault look very much as though they are correlated with temperature. This is not surprising since the sensors are made of different materials, and no attempt has yet been made to minimise the temperature coefficient of the CCD sensor.

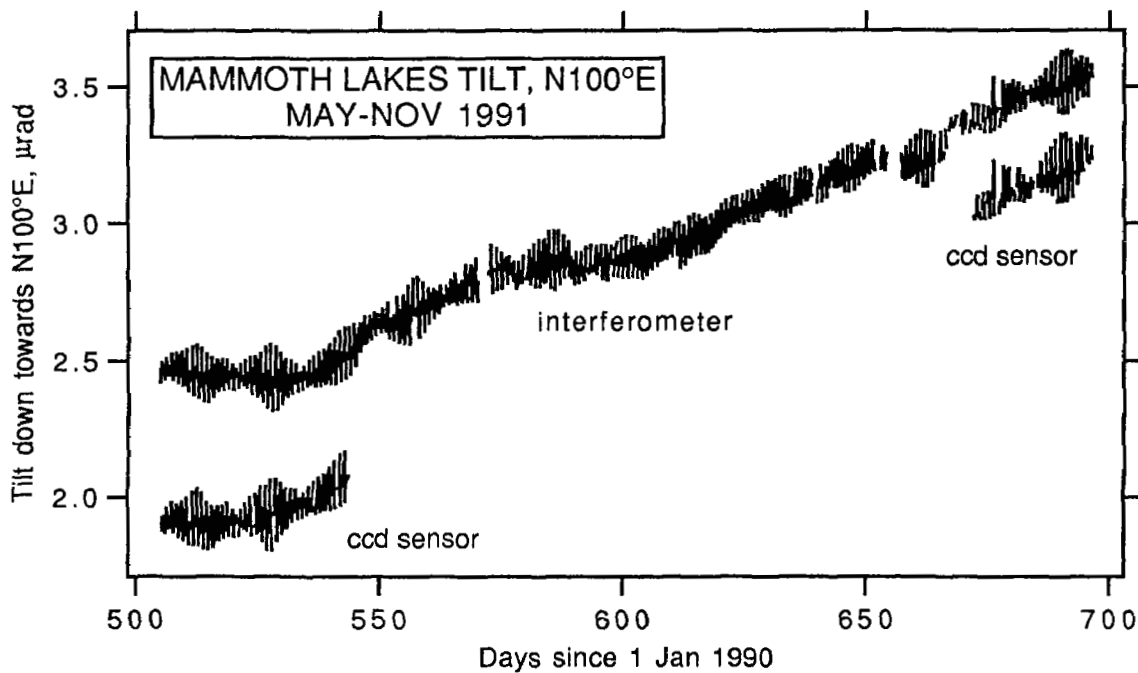


Figure 3.

Mammoth Lakes tilt in azimuth N100°E derived from interferometer sensors, and from CCD sensors. Both data sets have been corrected for vault instability using the vertical strain signal between the vault and the bottom of a borehole. Note that the datum of the CCD-derived tilt is preserved despite the long data gap.

The thickness in the lines is caused by the tidal signal, whose peak-peak amplitude can reach about 0.2  $\mu\text{rad}$ .

The "long-term" tilt rate appears somewhat higher in the CCD-derived data. This may result from the high temperature coefficient of the CCD end reservoir, a problem that will be addressed in the next version of the sensors.



## 2. Mammoth Lakes Tilt Data

The past two years of tilt data from the long base tiltmeter at Mammoth Lakes, as edited and corrected at Lamont, is illustrated in Figure 4. Corrections for vertical strain (i.e., vertical motions of the end piers relative to the bottoms of the boreholes) have been made using data from the vertical strainmeters installed by Roger Bilham in late 1989. No temperature corrections have yet been made, but these do not appear to be particularly significant. Figure 4a shows corrected and edited data from the individual tilt components. Figure 4b is a presentation of the tilt vector data that shows the monthly-averaged path that the point of a freely hanging pendulum would describe with respect to the ground. These plots all demonstrate the rapid deformation episode that has been occurring since late 1989 (Langbein et al., 1990). The data describe a tilt rate of  $\sim 5 \mu\text{rad/yr}$  at the start of 1990, decreasing to  $\sim 2 \mu\text{rad/yr}$  later in the year. The deformation episode had more or less ceased by early 1991, but appears to have picked up again later in 1991. The azimuth of the tilting has been fairly constant near  $130^\circ$  throughout the episode. This is consistent with the model developed by Langbein (1990) to fit the 2-color geodimeter data.

## 3. PFO Tiltmeter Data Analysis

The analysis of the Piñon Flat tiltmeter data was discussed in USGS Open File Report 90-334, pp 165-168. The micrometer intercomparison experiment between the LDGO and UCSD tiltmeters has now been terminated. The LDGO interferometers at PFO continue to collect data in a zero-maintenance mode. We are embarrassed that the results from this experiment have not yet been published, but we are taking concrete steps to see that this happens: during the Fall of 1991, Duncan Agnew is planning to spend part of his sabbatical at Lamont, and this will present a golden opportunity to wrap up the analysis and writing up of the tiltmeter intercomparison experiment.

## References

Langbein, J.O., D.P. Hill, T.N. Parker, S.K. Wilkinson and A.M. Pitt, Renewed inflation of the resurgent dome in Long Valley Caldera, California, from mid-1989 to mid-1990, *Eos*, **71**, 1466.

## Publications during this reporting period

Pratusevich, G., J. Beavan, J. Behr and R. Bilham, CCD Sensors and Mammoth Lakes Tilt Data (abstract), *EOS*, **72**, 505, 1991.

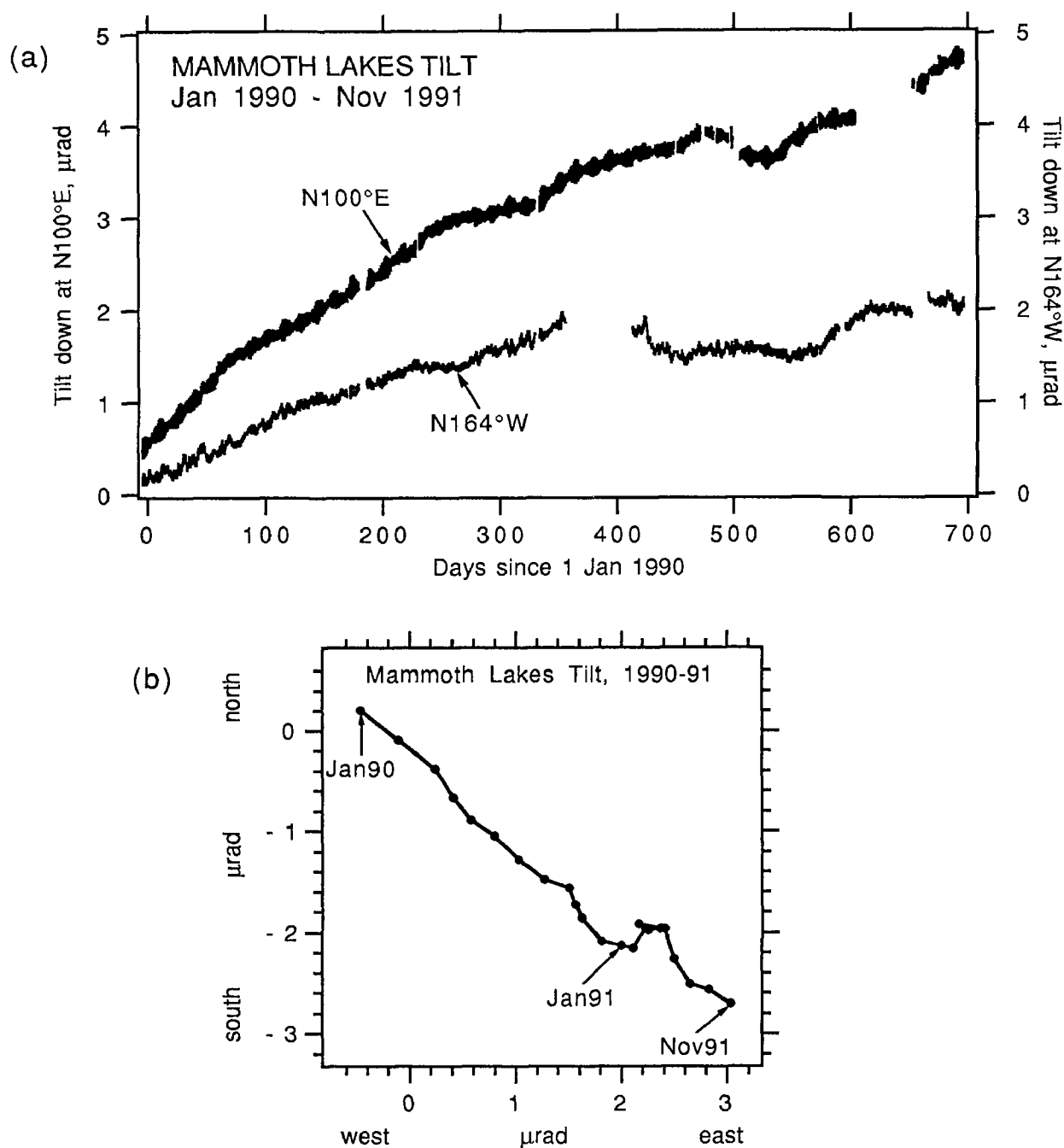


Figure 4.

1990-91 data recorded by long baseline tiltmeter at Mammoth Lakes, Ca. (a) edited and vertical-strain corrected data from the two tilt components. (b) evolution of tilt vector throughout 1990 and 1991, represented as monthly means of tilt. The inflation episode that began in late 1989 had more or less died out by early 1991, but appears to have regenerated to some extent later in the year. The tilt direction remains consistent at about N130°E, indicating that the signal probably results from continuing inflation centered on the resurgent dome.

## Crustal Deformation Measurements in the Shumagin Seismic Gap, Alaska

Grant No. 14-08-0001-G1792

John Beavan

Lamont-Doherty Geological Observatory of Columbia University, Palisades, NY 10964

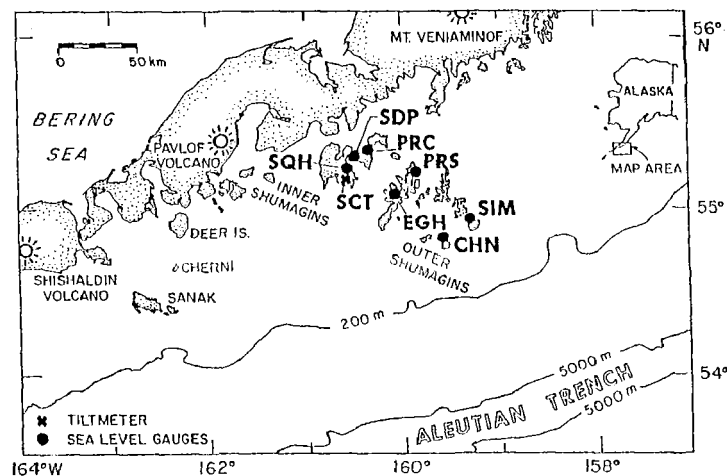
Tel: (914) 359 2900; Fax: (914) 359 5215; e-mail: beavan@lamont.lidgo.columbia.edu

### Investigations

1. Twelve short (~ 1 km) level lines are measured every one to three years within the Shumagin seismic gap, Alaska (Figure 1). Surface tilt data are interpreted in terms of tectonic deformation and earthquake hazard at the Pacific-North American plate boundary.
2. Six absolute-pressure sea-level gauges (Figure 1) are operated in the Shumagin Islands in an attempt to measure vertical deformation associated with the Aleutian subduction zone.
3. The sea-level data are transmitted by satellite in near real time, and are examined for possible tectonic signals. Noise studies are used to determine the relative usefulness of different types of measurement, and to evaluate the minimum size of tectonic signal visible above the noise. Our data are compared with other crustal deformation data from the Shumagin gap.
4. In cooperation with USGS Menlo Park scientists, we are making GPS survey measurements in the Shumagin Islands.

### Results (November 1991)

Figure 1a. Location of the Shumagin Islands with respect to the trench and the volcanic arc. Depth contours are in metres. The seismic gap stretches from approximately Sanak Island in the west to about 30 km east of the Shumagin Islands. Also shown are the sites of six sea-level gauges operated by LDGO and one by the National Ocean Survey (at SDP). Level lines of approx. 1 km aperture are located on many of the Shumagin Islands, and on Sanak Is.

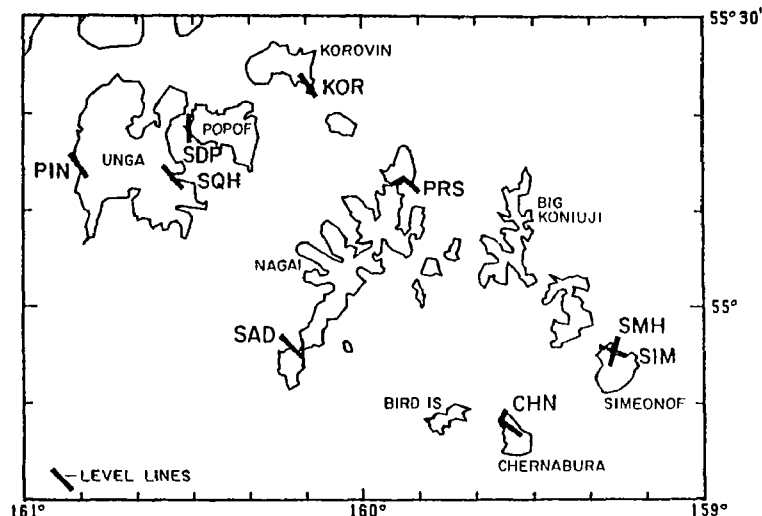


### *Self-contained sea level gauges*

The self-contained sea level gauges that we started to deploy in 1990 were recovered in the summer of 1991 after their first year of operation. The rationale behind these gauges is that they remove the weakest link in our previous system - the cable running through the surf zone from the underwater gauge to the electronics and data transmission system on land. The cable system will be retained at the more sheltered sites (PRC, EGH, SIM) in order to provide near-real-time data from a subset of sites.

One of the self-contained gauges was unfortunately washed away during the winter due to corrosion of the bolts used to attach the gauge to the rock. We improved the mounting system in our 1991 installations. Data were recovered from the other two self-contained gauges, and our electronics and recording system had behaved flawlessly in both cases.

Figure 1b. The Shumagin Islands, showing the locations and directions of first-order level lines, whose lengths vary between 600m and 1200m. The resultant of the data from lines SDP and SQH is used to estimate the tilt direction in the Inner Shumagins. The resultant of SIM and SMH is used for Simeonof Island. The lines at CHN and PRS each consist of two approximately straight sections in different azimuths, with benchmarks at the junction. This non-linear geometry allows tilt direction to be estimated at these sites. Two sets of perpendicular level lines have also been installed on Sanak Island, at the western end of the seismic gap (see Fig. 1). One of these, at the SE end of the island was measured in 1988 and 1990. The other, at the NW end, was first measured in 1990.



### *Level Lines*

Due to exceptionally good weather during the 1991 field season, a large subset of the Shumagin Island level lines were measured during 1991 (Figure 2). The Sanak lines were not measured, and these will be given top priority during the 1992 field season. The data, particularly from the outer islands (Figure 2b) showed some interesting changes from their previous behaviour. Until next year's measurements we cannot unequivocally determine whether these changes are a result of statistical variability, or whether they represent real tilt signals. An overall view of the data still appears to indicate arcward tilting in the outer islands (Fig. 2b), and trenchward tilting in the central and inner islands (Fig. 2a), though this conclusion is less convincing with the addition of the 1991 data.

### *Differential Sea Level*

All available differential sea level data from the 1976-91 period have been reanalysed. Results from the sites with the longest history are shown in Figure 3. Each plotted point represents the average sea level difference over a 3 month interval. If the data are interpreted by a constant differential uplift rate, then the outer islands appear to have been subsiding relative to the inner islands at about  $4 \pm 1$  mm/yr. If only the higher quality post-1985 data are used, there is still an apparent relative subsidence of the outer islands at  $1.8 \pm 1.2$  mm/yr. These motions are in the same sense as are predicted by simple models of strain accumulation at a locked subduction zone [e.g., Savage, 1983], but are almost an order of magnitude smaller. All other deformation data collected in the Shumagins have likewise shown rates smaller, sometimes much smaller, than the rates expected on the basis of the simplest model [e.g., Lisowski et al., 1988; Beavan, 1988, 1989, 1990; Ma et al., 1990]. A satisfactory explanation has not yet been given for the discrepancy between these low deformation rates and the high seismic potential [Boyd et al., 1988; Nishenko and Jacob, 1991] deduced from seismic observations.

### *References*

Beavan, J., 1988. Crustal Deformation Measurements in the Shumagin Seismic Gap, Alaska, USGS Open File Report, 88-673, 183-188.

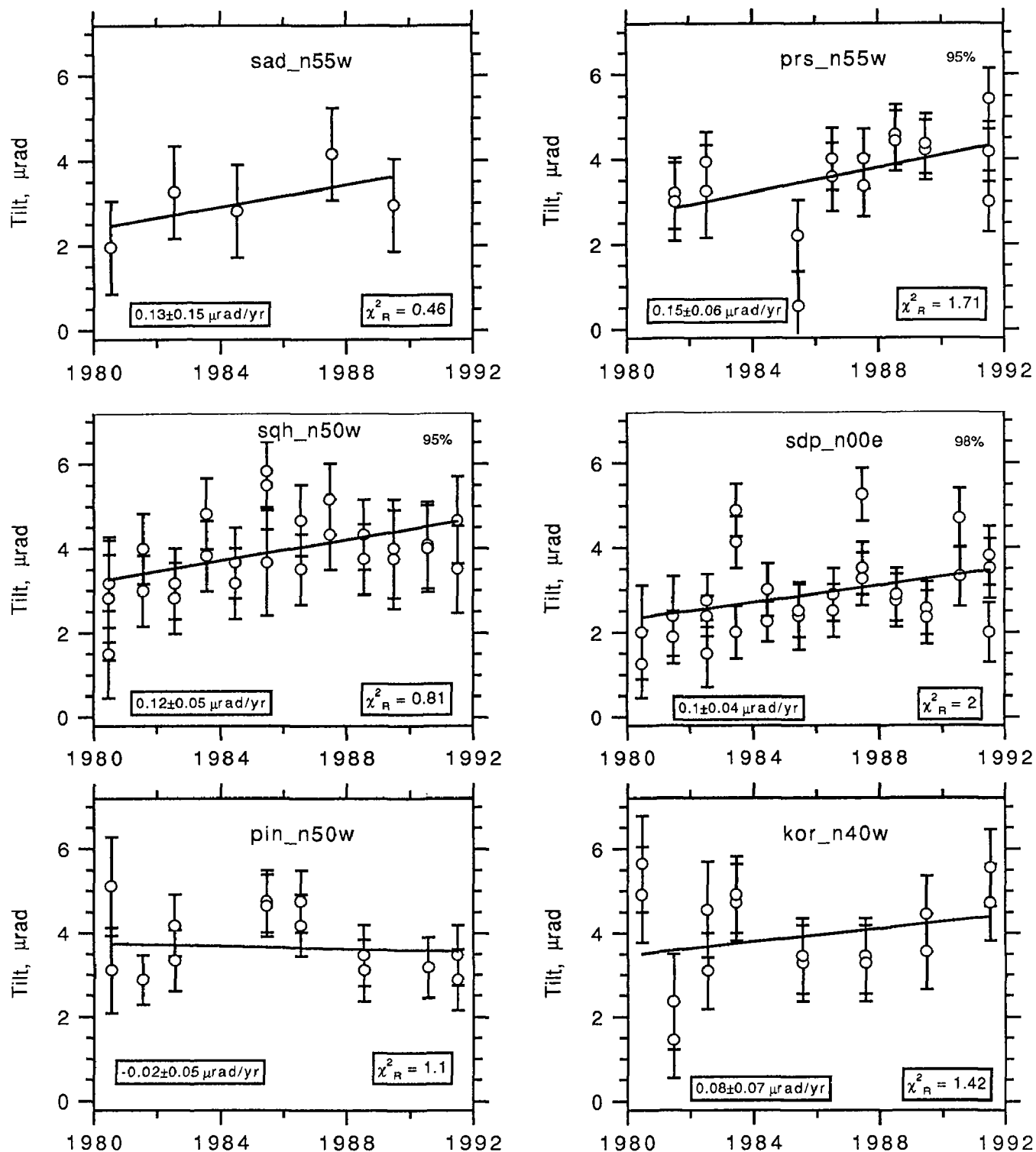


Figure 2a

1980-91 data from level lines in the Inner and Central Shumagin Islands. See Figure 2b caption for explanation of plots.

There appears to be a tendency for trenchward tilting in these data; i.e., relative ground subsidence towards the south-east.

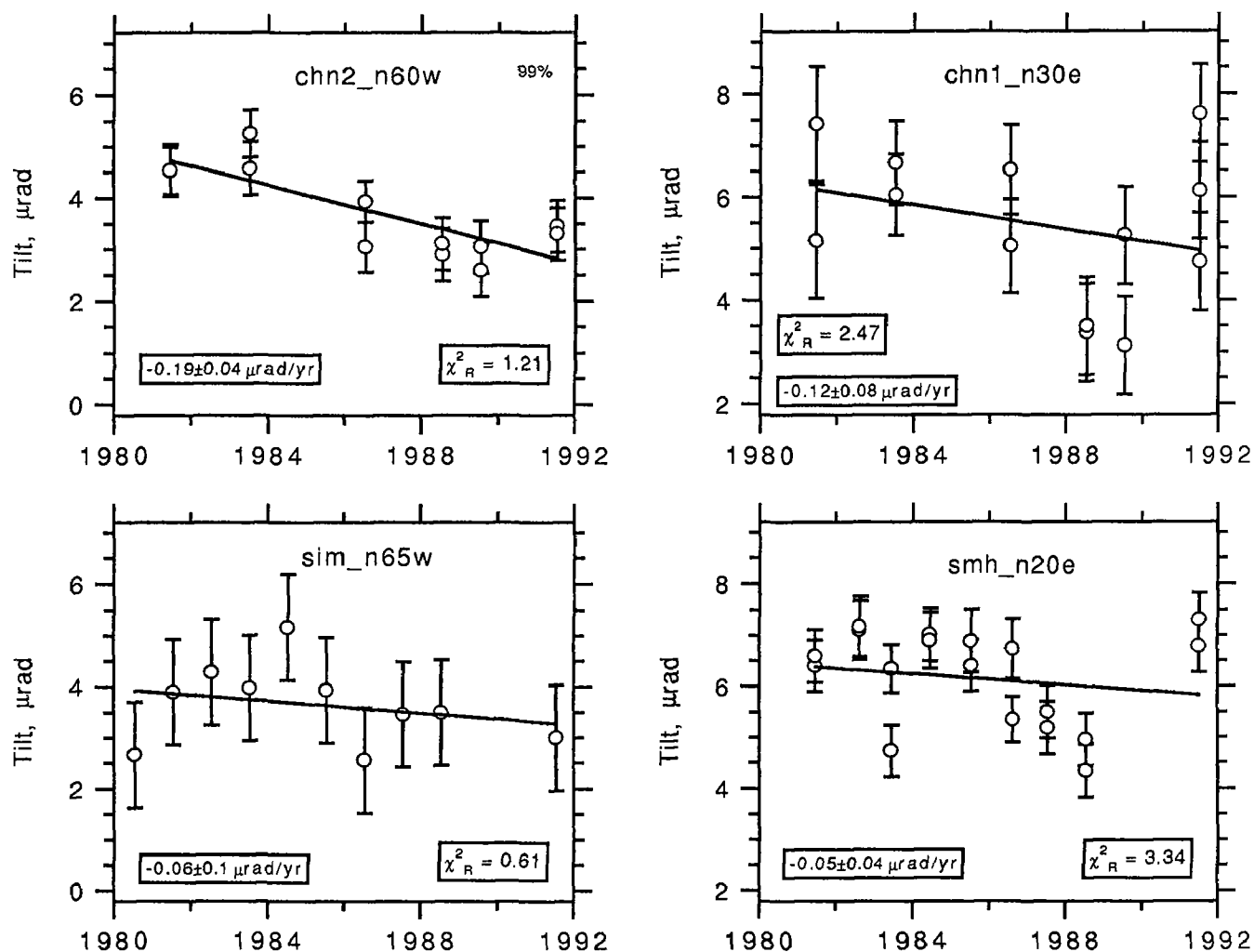


Figure 2b

1980-91 data from level lines in the Outer Shumagin Islands. Positive excursions on the plots indicate relative uplift in the direction indicated in the plot title. Error bars are  $\pm 1\sigma$ . The slope and  $1\sigma$  error of the best-fit weighted linear regression line are indicated on each plot, together with the reduced  $\chi^2$  "goodness of fit" statistic. When the slope of the regression line is different from zero with 95% or higher confidence, this is indicated in the upper right corner.

There appears to be a tendency towards arcward tilting in these data; i.e., relative ground subsidence towards the north-west.

The addition of the 1991 measurements has made the inferred tilt rates somewhat less pronounced than was indicated by the 1980-90 data. This is probably the result of statistical variability in the data, but could also signify a real change in tilt rate.

## SHUMAGIN ISLAND SEA LEVEL DIFFERENCES: 1976-1991

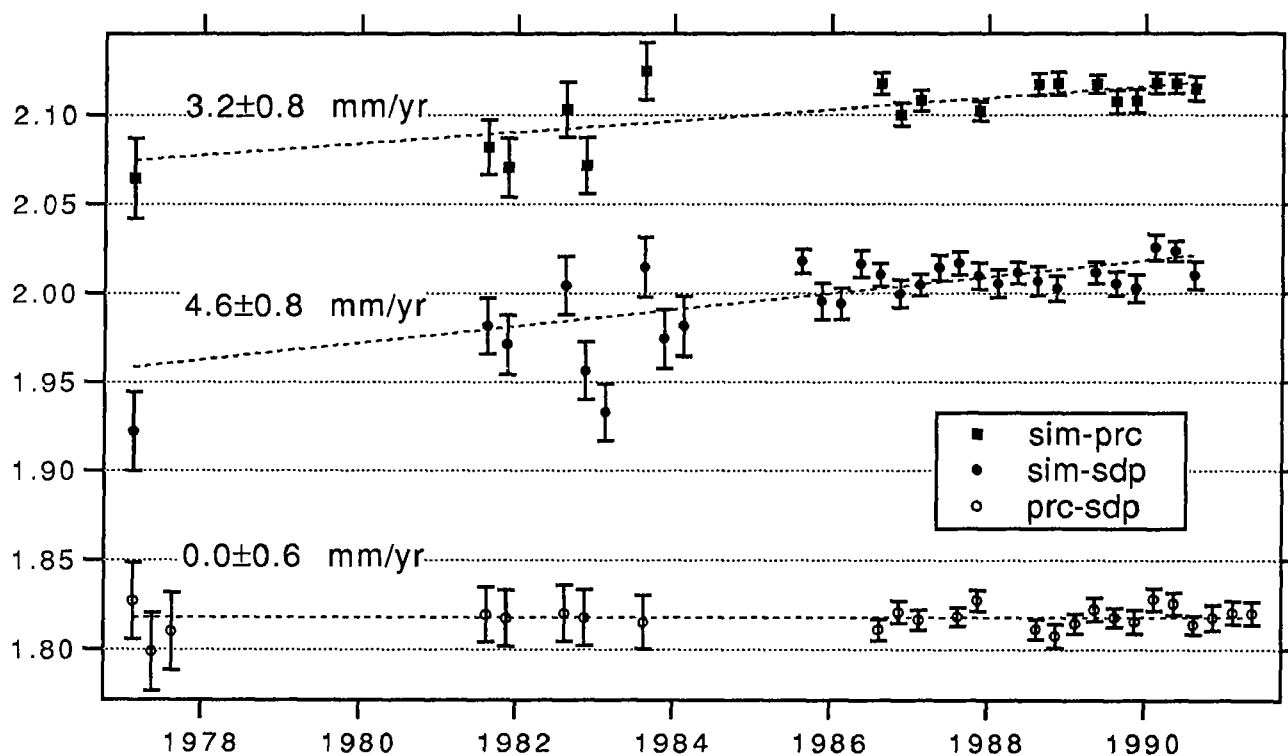


Figure 3.

**Data**

1976-77: Mean-sea-level-indicator at PRC, SIM. NOS gauge at SDP.  
 1981-84: Ceramic pressure gauge at PRC, SIM. NOS gauge at SDP.  
 1985-91: Paros quartz pressure gauge at PRC, SIM. NOS gauge at SDP.

**Location**

SIM is 80 km trenchward of PRC and SDP. PRC and SDP are close together and are expected to show little or no differential motion.

**Tectonic Interpretation**

If the 1976-91 data are interpreted as constant tilt rate, then SIM is subsiding relative to PRC/SDP at about  $4 \pm 1$  mm/yr.

If fit is made only to the 1985-91 data, then SIM appears to be subsiding relative to PRC/SDP at  $1.8 \pm 1.2$  mm/yr.

- Beavan, J., 1989. Crustal Deformation Measurements in the Shumagin Seismic Gap, Alaska, USGS Open File Report, 89-453, 181-184.
- Beavan, J., 1990. Crustal Deformation Measurements in the Shumagin Seismic Gap, Alaska, USGS Open File Report, 90-334, 169-174.
- Boyd, T.M., J.J. Taber, A.L. Lerner-Lam and J. Beavan, 1988. Seismic rupture and arc segmentation within the Shumagin Islands seismic gap, Alaska, Geophys. Res. Lett., 88, 201-204.
- Lisowski, M., J.C. Savage, W.H. Prescott and W.K. Gross, 1988. Absence of strain accumulation in the Shumagin seismic gap, Alaska, 1980-1987, J. geophys. Res., 93, 7909-7922.
- Ma, C., J. Sauber, L.J. Bell, T.A. Clark, D. Gordon, W.E. Himwich and J. Ryan, Measurement of horizontal motions in Alaska using Very Long Baseline Interferometry, J. geophys. Res., 95:B13, 21991-22012, 1990.
- Nishenko, S.P. & K.H. Jacob, 1991. Seismic Potential of the Queen Charlotte-Alaska-Aleutian Subduction Zone, J. geophys. Res.
- Savage, J.C., 1983. A dislocation model of strain accumulation and release at a subduction zone, J. geophys. Res., 88, 4984-4996.

*Publications during this reporting period*

- Abers, G.A. and J. Beavan, Seismic deformation and structure of an interplate thrust zone: seismicity in the Shumagin region, eastern Aleutian arc (abstract), EOS, 72, 460, 1991.



Late Quaternary Recurrence Intervals on the Owens Valley Fault  
Zone, Lone Pine, California

14-08-0001-G1783

Paul Bierman and Alan Gillespie  
Department of Geological Sciences, Mail Stop AJ-20  
Seattle, WA 98195

(206) 543-2079

Objectives: Our investigation has two main objectives: to constrain more tightly current estimates of recurrence intervals and fault slip rates for the Lone Pine fault, a subsidiary strand of the Owens Valley Fault Zone and to evaluate rigorously the accuracy, precision, and utility of rock varnish dating methods.

Results Obtained: Since the preparation of the last report we have done the following:

Continued processing thermoluminescence samples with Dr. G. Berger, Western Washington University. We are dating 12 samples from the two trenches opened across the colluvial wedge shed from the Lone Pine fault. Samples of 1872 colluvium collected several meters from the scarp have effective TL ages from hundreds to thousands of years.

Collected 44 varnished cores from a granodiorite boulder sequentially exposed on the fault scarp at Lone Pine. We have analyzed varnish on the cores using an SEM and techniques presented in Bierman and Kuehner (in press). These data suggest that the concentration of K and Ca are higher in analyses of younger varnish and that the concentration of Ti and Fe are higher in the analyses of older varnish. The cation ratio of the younger varnish appears to be higher than that of the older varnish. We are testing these observations by analyzing varnish from several other sites where the varnish should be of two distinct ages. We are unsure of the role that substrate plays in our findings.

Collected rock varnish samples from geomorphic features of known age for the purpose of testing sample preparation methods for  $^{14}\text{C}$  analyses of rock varnish. We have run several line and method blanks to verify that our line and chemical preparation methods are not contaminating the small amounts of organic material present in varnish. We hope to complete our  $^{14}\text{C}$  analyses in 1992.

Led a fieldtrip to the Lone Pine Scarp during the 1991 Geological Society of America national meeting. During this trip we presented the results of our research.

Results Published:

Bierman, P. and Kuehner, S., *in press*, Accurate and precise measurement of rock varnish chemistry using SEM/EDS: Chemical Geology.

Bierman, P. and Gillespie, A., 1991, Range Fires: A significant factor in exposure-age determination and geomorphic surface evolution: *Geology*, v. 19, p. 641-644.

Bierman, P. and Gillespie, A., 1991, Accuracy of rock varnish chemical analyses: implications for cation ratio dating: *Geology*, v. 19, p. 196-199.

Bierman, P., Kuehner, S., and Gillespie, A., 1991, Precision of rock varnish chemical analyses and cation-ratio ages: *Geology*, v. 19, p. 135-138.

Bierman, P. and Gillespie, A., 1990, Range Fire: A dramatic and significant factor in the dating and evolution of Geomorphic Surfaces: Geological Society of America Abstracts with Programs, v. 22, n. 7, p. A110.

Bierman, P. and Gillespie, A., 1990, An independent evaluation of the potential precision and accuracy of rock-varnish cation ratio dates: Geological Society of America Abstracts with Programs, v. 22, n. 7, p. A270.

Bierman, P. and Gillespie, A., 1990, Varnish cation-ratio ages - How precise can they be? Geological Society of America Abstracts with Programs, v. 22, n. 3, p. A8.

Bierman, P. and Gillespie, A., 1989, Rock varnish, alluvial fans, and tectonism in the southern Owens Valley, CA: Geological Society of America Abstracts with Programs, v. 21, n. 6, p. A343.

## Creepmeters on California Faults

USGS 14-08-001-G1876

Roger Bilham

CIRES University of Colorado,  
Boulder, CO 80309-0250  
303 492 6189

### Investigations:

1. We maintain 13 digital creepmeters across active faults in California (Figure 1). The creepmeters are designed to record data once per minute during creep or seismic slip of the fault and once per hour during times of fault inactivity. A decision to retain high data-rates is made if the mean fault slip velocity exceeds  $500 \mu\text{m}/\text{hour}$ . The creepmeters have a resolution of 10 microns and a minimum range of 15 cm. Creepmeters in selected seismic gaps, at the southern end of the Parkfield region, and near Anza have ranges up to 1 m. The creepmeters are typically 5-10 m long, but one creepmeter monitors the 110-m-long abutment-separation of Chittenden bridge across the San Andreas fault south of Loma Prieta. The instruments are visited three times each year to collect their recorded data.
2. We have designed experiments to distinguish between soil processes and displacement on surface faults. The experiments are also designed to search for the existence of strain stored close to the fault which may be released during creep events. These experiments use co-linear pairs of identical extensometers, one of which is installed across the fault and one is not. The difference signal, in principle, contains only fault slip.
3. We have examined published accounts of vertical and sinistral creep data from the Xianshuihe fault in eastern Tibet to test the possibility that creep on this fault is similar to steady state creep in central California.
4. We retain four creepmeters in readiness for monitoring afterslip in a future earthquake. Each creepmeter can be installed within 24 hours of an earthquake in California. To facilitate early alert of a California event we have implemented in Boulder the Caltech PDE active display system for earthquakes in southern California.

### Results:

1. Episodic afterslip continues on the Superstition Hills fault at approximately 28 mm/year (Figure 2). Creep episodes consist of three or more events with individual slip amplitudes of more than 8 mm and cumulative amplitudes of up to 14 mm (Figure 3). We have recorded creep events on the Imperial fault south of the Mexican Border at Saltillo, on the San Andreas fault 2 km south of Highway 46 near Parkfield, and at Nyland Ranch north of San Juan Bautista. Nyland Ranch fault creep continues at a rate of 20 mm/year which is approximately 3 times higher than the mean creep rate for the past 20 years (Figure 4). No significant cumulative creep has been recorded at Indio or Durmid Hill on the southern San Andreas fault. Creep events with amplitudes  $>2$  mm have been detected on the San Andreas fault south of Highway 46. Although a cumulative dextral offset of 4 mm has occurred since Dec18 1990, we observe two episodes of sinistral slip in March (0.7 mm) and May (1 mm).
2. Slip on the Superstition Hills fault between creep events occurs at a rate of roughly 2.4 mm/year, a factor of ten slower than the annual rate attributable to episodic slip. We suggest that this background slip occurs near the surface, and that deeper parts of the surface fault creep episodically. The ratio of velocities is proportional to the ratio of base depths of these two processes. Thus if episodic creep

extends 3 km from the surface to the top of the coseismic rupture zone, steady state creep is limited in depth to approximately 300 m (Figure 5).

We observe that background creep is a common attribute of many creeping faults. Two properties of our model may prove useful for monitoring time-dependant variations in strain and stress applied to a creeping fault: the background creep signal is a linear measure of strain applied to the fault, and the ratio of the episodic to background creep velocity may depend on, among other variables, the amplitude of in-situ fault normal stress.

We report further that we observe less than 1  $\mu$ strain of linear strain release close to the fault zone at the time of creep events with slip more than 1 cm, suggesting block-like motion of the surface fault. We conclude that fault-normal stresses are essentially zero at the surface.

3. Although recent creep data from the Xianshuihe fault suggest steady-state sinistral creep, an alternative and more likely interpretation is that surface creep was initiated as afterslip following the 1973 Luhuo earthquake and is currently decaying slowly. Supporting this view we observe that creep measurements prior to the earthquake do not exist, and that creep is restricted to parts of the fault that have slipped recently during earthquakes. The sinistral creep data, unlike the dip-slip data, were not recorded for the first four years following the Luhuo earthquake. However, we found that the horizontal and vertical slip signals are related by a linear  $\sim 8.3$  scaling factor for the eleven years for which they are available simultaneously (Figure 6). By assuming that this correlation holds for the missing early years of sinistral slip we infer that up to 24 cm of slip may have occurred on the fault since the Luhuo earthquake (more than doubling previous estimates), and that this slip is a manifestation of afterslip. The absence of steady-state creep on the Xianshuihe Fault leaves the San Andreas system a unique location for this style of aseismic slip.

4. A display of southern California earthquakes is currently operating on an IBM compatible system under control of software developed by Caltech and loaned to us by Egill Hauksson. The data are forwarded to us from Caltech using an E-mail scheme into which address we also receive worldwide PDE data from the Global Seismology branch of USGS Denver. We envisage developing a future display that will alternate between a world map and a California map showing significant earthquakes within minutes of a PDE availability. We wish to thank Egill Hauksson and Waverly Person for their assistance in facilitating these displays.

#### Publications:

- Behr, J., R. Bilham, P. Bodin, R. Burgmann and R. O. Burford (1990). Aseismic slip on the San Andreas fault south of Loma Prieta, *Geophys. Res. Lett.* **17**, 9, 1445-1448.
- Behr, J. and R. Bilham (1991). A two layer model for fault creep; Background Creep Velocity as a measure of local stress and strain. *Eos Trans. Amer. Geophys. Un.* **72**, 44, 444
- Bilham, R, Surface Slip Subsequent to the 24 November 1987 Superstition Hills, California, Earthquake Monitored by Digital Creepmeters (1989). *Bull. Seism. Soc. Amer.*, **79**, 2, 424-450.
- Bilham, R. Sinistral Creep on the Xianshuihe Fault at Xialatuo in the 17 years Following the 1973 Luhuo Earthquake. Proc. PRC/US Bilateral Symposium on the Xianshuihe fault Sept 22-30, (1991) in the press.
- Bilham, R and J. Behr (1991). A two layer model for aseismic slip on the Superstition Hills fault, submitted to *Bull. Seism. Soc. Amer.*
- Bürgmann, R., J. Behr and R. Bilham (1989). Creep events and interevent slip on the Superstition Hills fault, California, *Eos Trans. Am. Geophys. Un.* **70**, 1348.
- Marone, C. J., C. H. Scholz, and R. Bilham (1991). On the mechanics of earthquake afterslip, *J. Geophys. Res.*, **96**, 8441-8452.
- Sylvester A., S. Barrientos, R. Bilham, and M. Jackson (1991). Shear, Uplift and Shortening across Durmid Hill: Interseismic Transpression on the Southern San Andreas Fault, California. *Eos Trans. Amer. Geophys. Un.* **72**, 44, 497

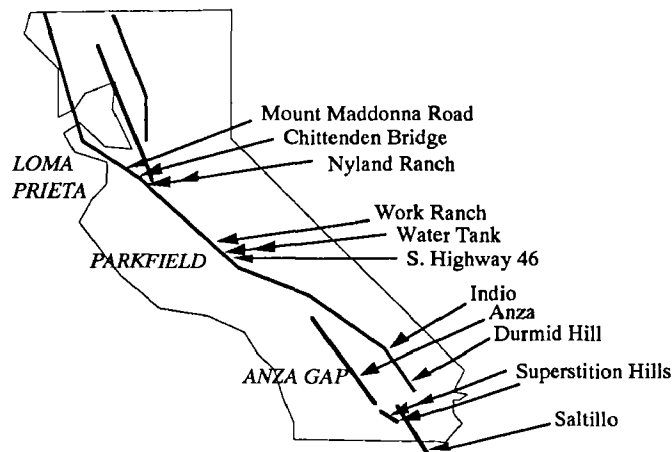


Figure 1 Locations of digital creepmeters. Three instruments currently operate on the Superstition Hills fault, three on the San Andreas fault south of Loma Prieta, three on the southern part of the Parkfield region, two on the southern San Andreas fault and one each on the southern Imperial and the San Jacinto fault. Pairs of creepmeters indicated by double arrows.

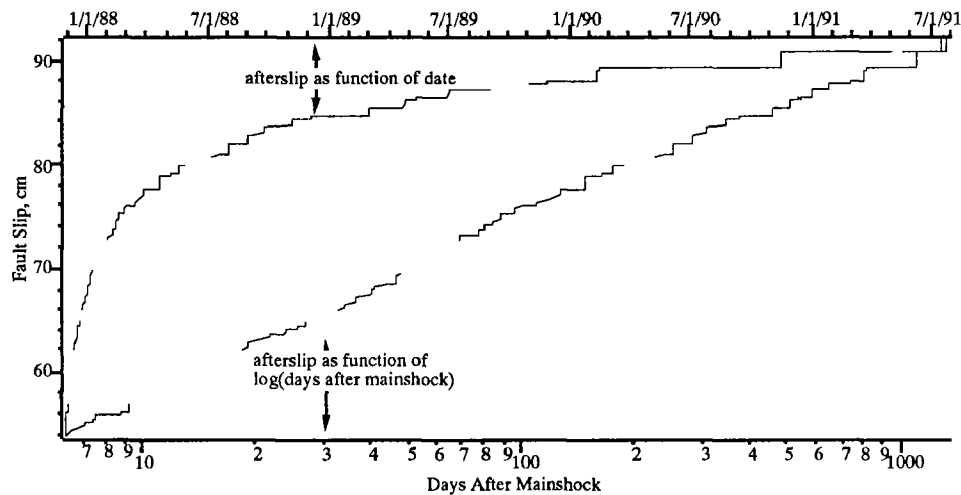


Fig. 2. Afterslip data from Site 1 near Imler Road on the Superstition Hills fault for 3.6 years after the mainshock. Afterslip remains a factor of two higher than the mean slip rate in the 30 years prior to the mainshock.

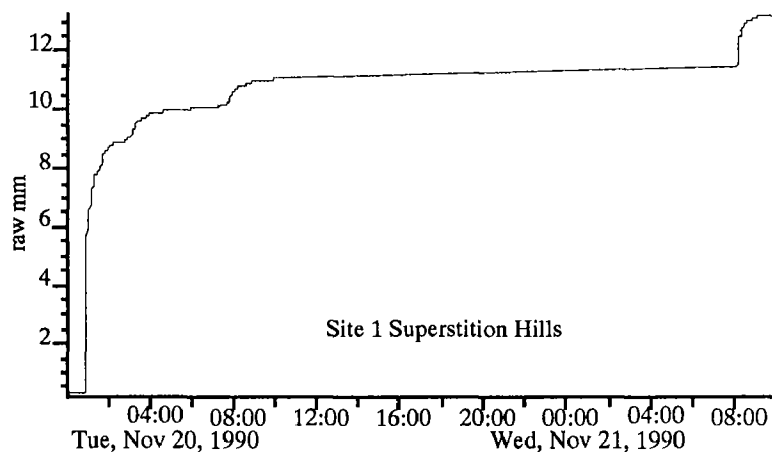


Figure 3 The largest creep sequence on the Superstition Hills fault was recorded on 21/22 Nov 1990. Dextral slip is obtained by multiplying the above values by 1.26. This creep event and the following 9 Feb event consisted of four subevents. Maximum fault slip velocity occurred in the second minute of the 21 Nov event and was not preceded by any slow acceleration in creep or by the release of strain on an adjoining extensometer. The preceding interval was the largest interval between events in the afterslip process. Sharp (personal communication, 1991) reports that slip in November propagated the entire length of the Superstition Hills fault.

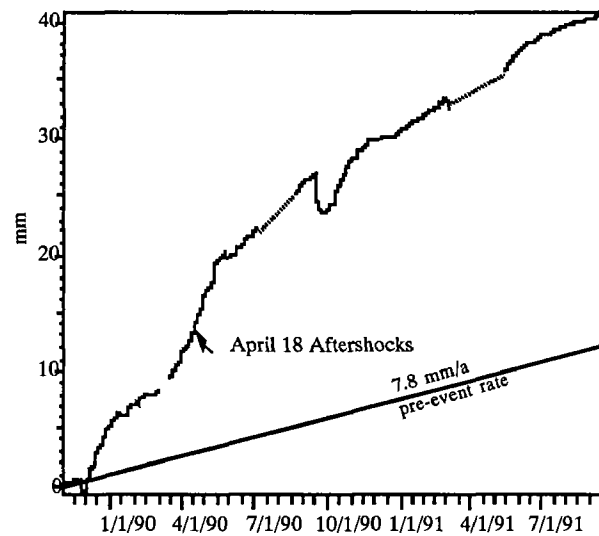


Figure 4 Data from Nyland Ranch after the Loma Prieta earthquake show continued creep at rates several times higher than that observed in the preceeding thirty years. Creep did not commence at Nyland ranch for more than a week following the mainshock. Mt. Madonna Road creep is insignificant after an initial settlement in the week following the event

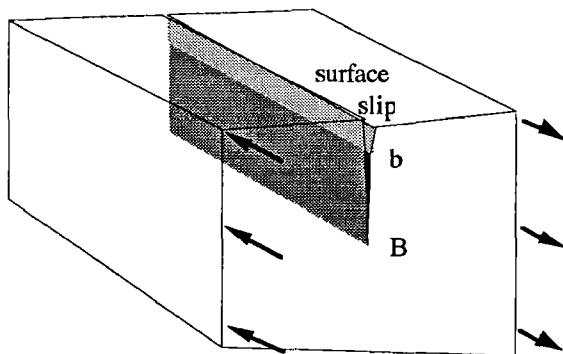


Fig. 5. Proposed two depth model for aseismic surface slip. Slip proceeds steadily on the surface in response to applied antisymmetric strain. Although the displacement rate is low, its measurement as across-fault strain offers an amplified signal compared to strain in the adjacent materials. Episodic slip occurs below a transition depth,  $b$ . The transition depth is presumably partly controlled by fault normal stress, hence, variations in the ratio of background creep to episodic creep may reveal changes in in-situ stress.

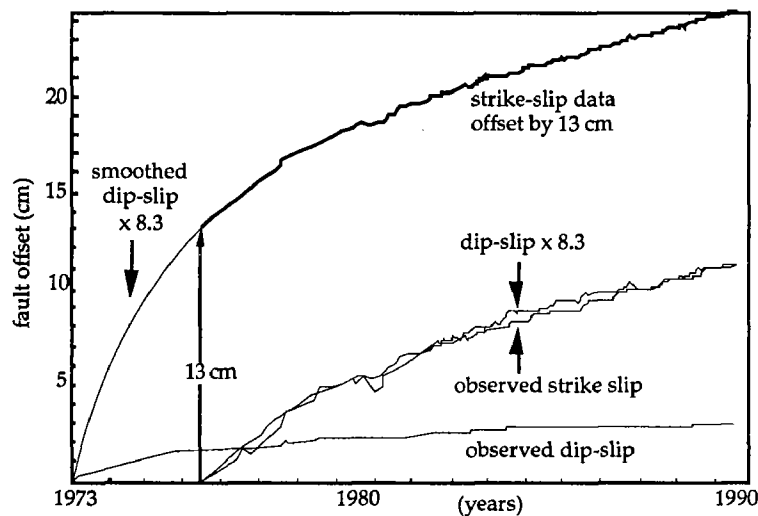


Fig. 6 Proposed reconstruction of the first four years of afterslip on the Xianshuihe fault at Xialatuo based on an observed linear scaling relationship between sinistral and dip-slip fault creep between 1976 and 1990.

## Mammoth Lakes Michelson Tiltmeter

USGS 14-08-0001-G6170

Roger Bilham

CIRES University of Colorado,  
Boulder, CO 80309-0250  
303 492 6189

### Investigations:

A pair of Michelson tiltmeters are maintained within the Long Valley Caldera 1 km north of the Mammoth Lakes airport. The tiltmeters are modelled after one designed by Michelson in 1914 and consist of two horizontal water pipes each with a continuous water surface, terminated by optical interferometer transducers.

Location	37°37'58"N, 118°50'01" West (center vault) See Fig. 1.
East/West tiltmeter	length 423.3 m, azimuth 280°, least count 0.57 nanoradians
North/South tiltmeter	length 449.2 m, azimuth 16°, least count 0.53 nanoradians
Pipe	20 cm diameter bell-ended PVC at a mean subsurface depth of 1.5 m.
Water level detectors	1. Equal-arm Michelson-Interferometers powered by polarized He/Ne lasers. Resolution 0.25 $\mu\text{m}$ , range 1 cm. 2. Experimental LCD sensors on East West arm.
Surface displacement sensors	10 mm diameter invar rods to 26 m maximum depth. LVDT sensors with accuracy $\pm 1 \mu\text{m}$ and range 3 mm.

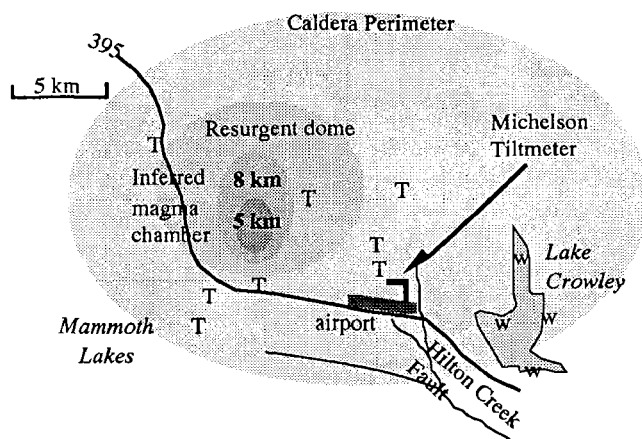


Figure 1 Sketch of location of biaxial Michelson tiltmeter. Borehole tiltmeters (T) and Lake Crowley water sensors (W) provide alternative measures of caldera tilt. A level line exists along Highway 395.

### Results:

1. Tilt in the floor of the Caldera appears to have stabilised in the past year with a tilt down to the SE of approximately 1  $\mu\text{rad}$ . From late 1989 to late 1990 an inflation event NW of the tiltmeter has caused a 3  $\mu\text{rad}$  tilt down to the south and 4  $\mu\text{rad}$  tilt to the east. Data from the instrument are shown in Figures 2 and 3.

2. Microseismic activity close to the tiltmeter has resulted in frequent loss of counts on the interferometers. In conjunction with J. Beavan (Lamont-Doherty) a prototype water surface monitoring system using Charge Coupled Detectors has been installed on the east-west sensor. The sensor is unaffected by water surface vibration and promises to provide a reliable  $\pm 1 \mu\text{m}$  monitoring system (Pratusevitch G, J. Beavan, J. Behr and R. Bilham, CCD Sensors and Mammoth Lakes tilt data(1991) *Eos Trans. Am. Geophys. Un.* 70, 505.

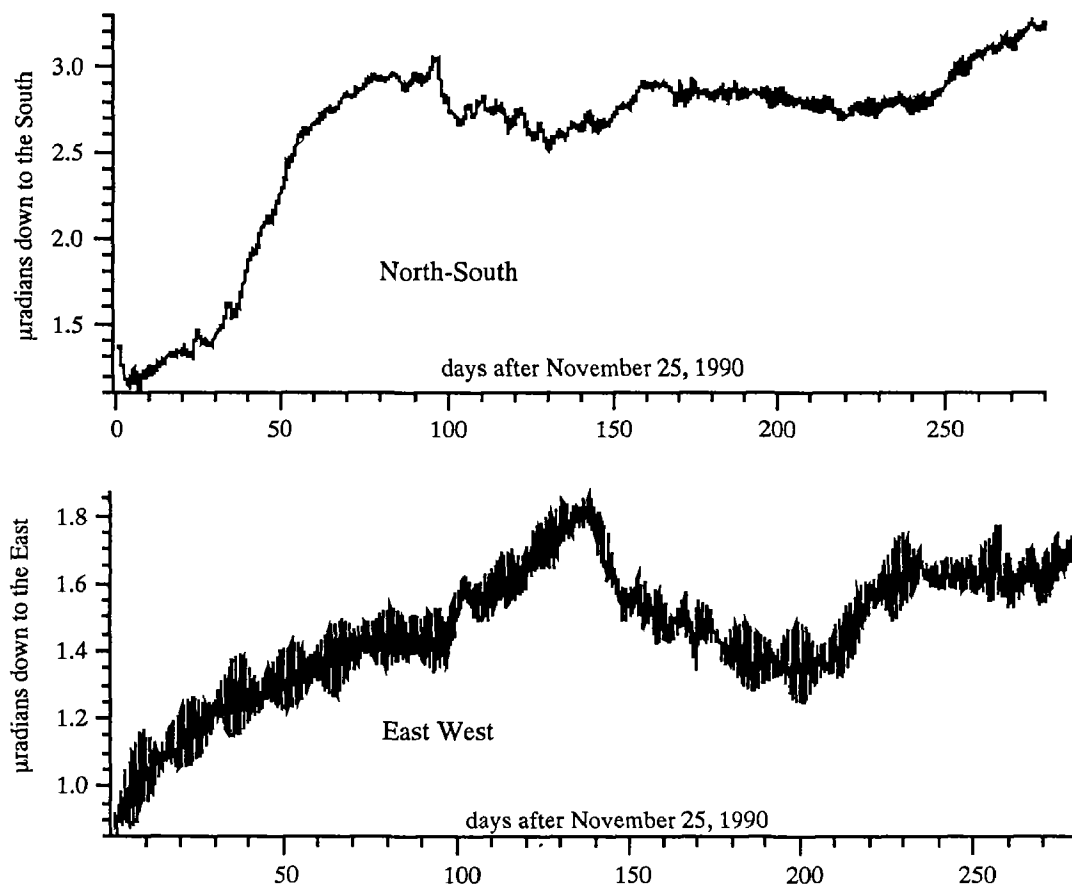


Figure 2 Tilt relative to base of boreholes for the period Nov 25 1990 to Sept 1 1991. The thickness in line is caused by the daily tide which is approximately a factor of three higher in the east west than in the north south direction.

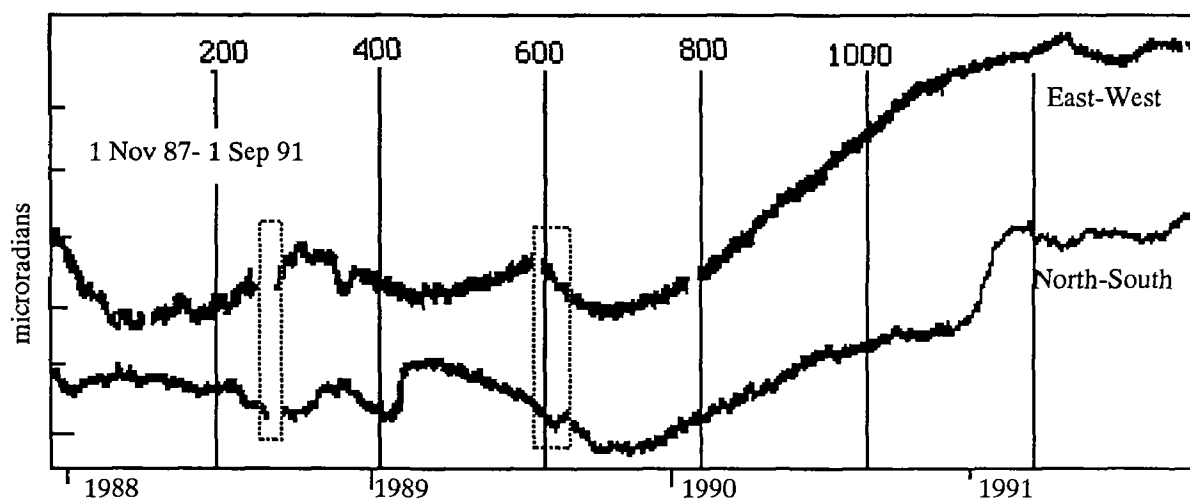


Figure 3 Cumulative tilt from the biaxial Michelson tiltmeter for the period 1987-1991. Two dotted boxes indicate times of major disturbance to the instrument. Vertical extensometers were installed in late 1989.



## Finite Element Modeling of the California Fault System

Agreement No. 14-08-0001-G-1947

Peter Bird  
Department of Earth and Space Sciences  
University of California  
Los Angeles, CA 90045

(310) 825-1126

### Investigations Undertaken:

1. The rewriting of the finite element code FAULTS was completed; this code predicts steady-state (cycle-averaged) slip-rates of faults, anelastic strain-rates of blocks, and vertically-integrated stresses, based on plate-tectonic velocity boundary conditions and an assumed crustal rheology. The convergence properties of the code have been studied and optimized.

2. A finite element grid representing California and its faults (with accompanying elevation, heat-flow, and crustal-thickness datasets) was prepared, based on an earlier version created in 1984.

3. A preliminary set of 10 models was run without any tractions on the base of the crust; the single variable was the amount of friction on faults.

4. Results of the models were scored according to their ability to predict 3 datasets: geologic estimates of slip-rates on faults (collected from the literature by the author); stress directions (collected by Mary Lou Zoback); and VLBI baseline rates (published by NASA).

5. The thermal model parameters and the dislocation creep constants for the crust were then adjusted so that the depths of the brittle/ductile transition on the faults in the model matched the maximum depths of seismicity in 16 different regions (from the literature).

6. While keeping the brittle-ductile transitions at the depths calibrated by data, we adjusted the activation-energy and pre-exponential constant of the crustal creep law in concert so as to vary the amount of coupling between the crust and the upper mantle. The pattern of upper-mantle flow assumed was that of Bird and Rosenstock (1984). (While mantle drag was applied to the Pacific and North American plate regions, no drag was applied to the Sierra Nevada/Great Valley block, because the velocity of the upper mantle is unknown in this region.) The amount of coupling of crust to mantle became a second master parameter (the first being the level of friction on faults). A set of 81 models (9 values of fault friction  $\times$  9 values of coupling) was computed.

7. Finally, some experiments were conducted in which the fault elements did not all have equal friction. The motivation for this was the concept advocated by James Byerlee and James Rice, that faults of large net offset have thick gouge zones, in which high pore pressures can be supported indefinitely by non-Darcy permeability. We are

investigating the specific hypothesis that effective fault friction may be reduced by some coefficient multiplied by net slip. Since this coefficient cannot be predicted, the model parameter space is now three-dimensional, and many calculations are required to span it.

#### Results Obtained:

1. With the newly rewritten program, monotonic convergence of the predicted (steady-state) velocities and stresses can be achieved (Figure 1). A tradeoff was discovered between the asymptotic convergence limit (measured as the relative mean size of the velocity changes between iterations) and the maximum stiffness permitted in "rigid" blocks and "locked" faults. Some degree of artificial viscous compliance is required for convergence, because otherwise the condition number of the stiffness matrix is too large and pseudo-random numerical noise prevents convergence. However, if artificial viscous compliance is permitted to grow too large the realism of the models will obviously be compromised. We discovered that if the integral (across California) of the artificial viscous strain-rate is restricted to 1 mm/year, we can achieve convergence of the solution to 0.01% velocity change and 0.1% stress error.

2. A grid of 994 nodes, 147 fault elements, and 314 continuum elements originally prepared in 1984 was corrected with some new information on fault dips (e.g., vertical along the southernmost San Andreas, but  $70^{\circ}$  SW in the Loma Prieta segment). The grid extends from Point Arena southeast to the head of the Gulf of California, and east to the Death Valley-Furnace Creek-Fish Lake fault zone, and includes all faults with slip rates of over 1 mm/year. Heat-flows were assigned to each node based on hand-contouring of a regional compilation of data. Crustal thickness beneath each element was obtained from the seismic-refraction compilation of Mooney (1990). Velocity boundary conditions were taken from the NUVEL-1 model of DeMets et al. (1990), and Basin/Range extension (integrating to 10 mm/year) was assumed along the NE boundary.

3. In the first set of 10 models, there were no tractions on the Moho except for isostatic support. The friction within continuum elements was fixed at 0.85. However, the friction on faults was assumed to be 100%, 90%, 80%, ..., 10% of this value. All models converged well. Subjectively, the most realistic appeared to be the one with a fault friction of 0.17. At higher frictions, almost all faults (except the central San Andreas) slipped too slowly or were locked. At 0.085, unrealistic gravitational slumping of the Transverse Ranges blocks occurred.

4. A dataset of 79 geologic estimates (or limits) on mean slip-rates of California faults has been collected. Only offset distances of more than 20 m and offset times of 5 Ma or less were included in this dataset. The predictions of each finite element model were compared to these rates or rate limits, and the discrepancy was expressed as the RMS error. The best match achieved was an RMS error of 6 mm/year, and this occurred for the model with fault friction 0.17 (Figure 2).

Second, a dataset of 221 stress-directions in the model region was extracted from the compilation by Mary Lou Zoback on the *Geophysics of North America* compact disk and compared to the model

predictions. The best model according to this test was the same one, with an average discrepancy of  $24^{\circ}$  (Figure 3). Although this is not an impressive match, it should be remembered that the scatter in the data is so great that even a "perfect" model would probably have a mean discrepancy of  $18^{\circ}$ . Also, any attempt to fit a uniform regional stress field results in a mean error of at least  $28^{\circ}$ ; so, at least some of the variations predicted by the model are real.

Finally, a dataset of 45 geodetic baseline-rates between VLBI benchmarks was extracted from NASA Technical Memorandum TM-100765, with formal errors for each rate. This dataset was compared to a modified form of the finite element model predictions, in which elastic anti-dislocations of steady rate were added on the brittle upper parts of all model faults to temporarily lock them during the epoch of VLBI observations. Because the baseline rates have widely varying errors, these errors were used as (inverse) weights in the calculation of the average discrepancy of each model. The best result was a weighted-mean discrepancy of 3.0 mm/year, and again this best result was from the model with fault friction of 0.17 (Figure 4).

For each dataset, the range of scores is not great; this is due to some stubborn errors which occurred in all 10 models, such as too much slip on the Elsinore-Whittier faults, and on the Hayward-Calaveras faults. However, the agreement of all three datasets in selecting the best model is very strong evidence that the mean effective friction of California faults is much lower than that exhibited by rocks in the laboratory (even hydrated clays). This may be due to high pore pressures localized along major faults, or to some other unknown cause.

5. From the seismological literature, maximum depths of California earthquakes were obtained for 16 regions within the finite element model domain. Plotting these depths against estimated heat-flow gave an inverse relation, suggesting that in California the brittle-ductile transition takes place at  $350-410^{\circ}\text{C}$ . The dislocation creep law used in these finite element models was adjusted by trial and error to give the best possible match of predicted and actual transition depths. If the creep law is expressed as:

$$(\text{shear-stress}) = A (\text{strain-rate})^E \exp(B/T),$$

where  $E = 0.333$ , and  $T$  is Kelvin temperature, then the best-fitting results are obtained when:

$$\log_{10}(A) = 12.2 - 7 \times 10^{-4} B$$

for  $A$  in  $\text{Pa s}^E$ , and  $B$  in Kelvin.

6. The addition of varying amounts of mantle drag improved the scores of some models, but did not change the conclusion that (most) faults must have low friction. As shown in Figure 5, the RMS prediction error for fault slip rates can be reduced below 5 mm/year if fault friction is low and mantle drag is strong. (A low activation energy for creep in the crust implies strong mantle drag, and vice versa.) The stress directions have a minimum error of about  $23^{\circ}$  for fault friction values near 0.2 (Figure 6). The RMS prediction error for the 45 VLBI baseline rates can also be reduced slightly (Fig. 7), and also shows a minimum for friction of 0.2, although the preference for

these models is very weak.

7. As scoring of this set of models is not completed, results will be presented at the December 1991 AGU meeting.

#### Reports Published:

1. Bird, P., and X. Kong (1991) First accurate thin-plate models with faults (abstract), Eos (Trans. Am. Geophys. U.), 72, Nov. 1991 (in press).

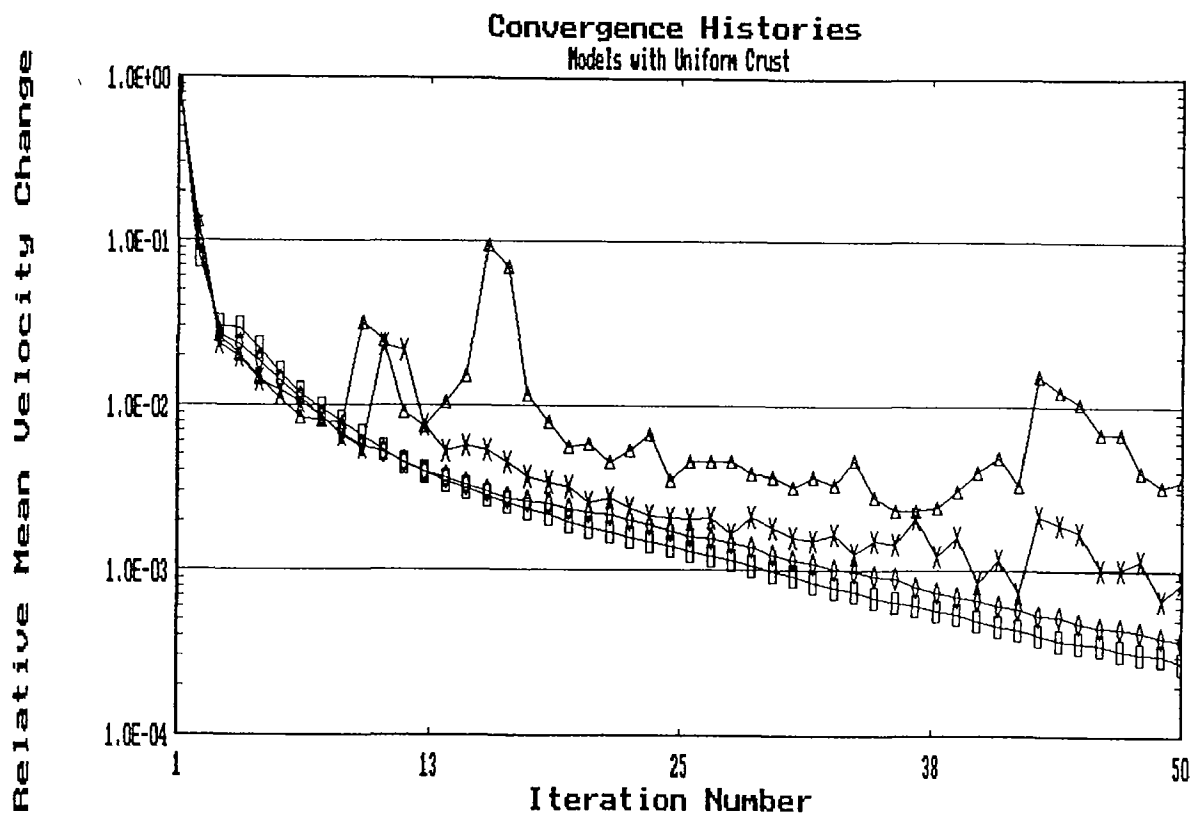


Figure 1. Convergence histories of four calculations with different upper limits on stiffness: (box) integrated viscous compliance  $\approx 3$  mm/year; (diamond) integrated viscous compliance  $\approx 1$  mm/year; (x) integrated viscous compliance  $\approx 0.3$  mm/year; ( $\Delta$ ) integrated viscous compliance  $\approx 0.1$  mm/year.

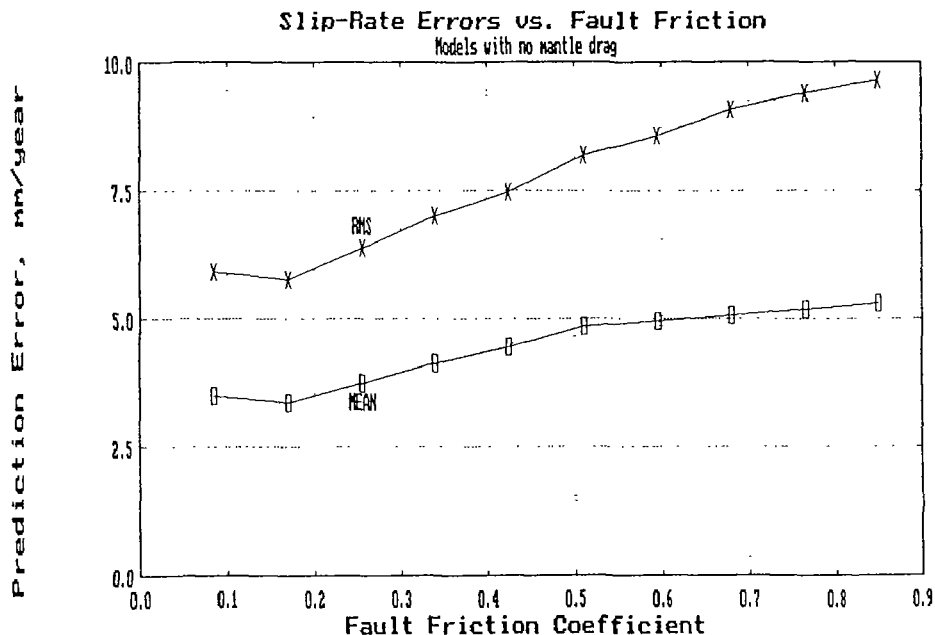


Figure 2. Mean and root-mean-square (RMS) error in prediction of geologic slip rates on faults, as a function of the coefficient of friction of all faults. In these models, there are no shear tractions on the Moho, and the friction of crustal blocks is 0.85.

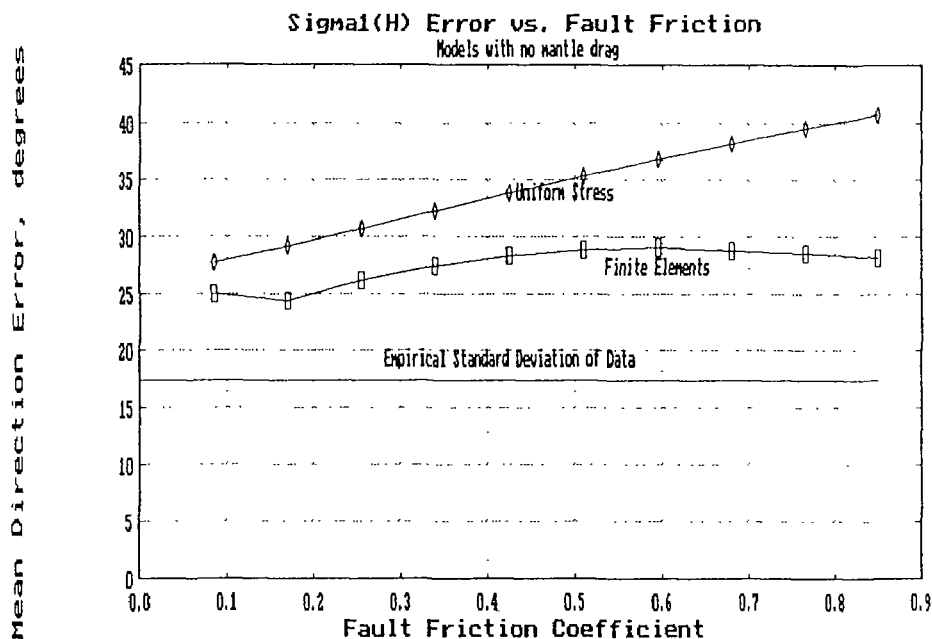


Figure 3. Mean error in the predicted direction of horizontal greatest principal compression as a function of assumed fault friction coefficient. "Empirical standard deviation of data" is derived from the intercept of a variogram of stress azimuth. "Uniform stress" curve is error relative to a constant stress direction for all of California, which is determined by the friction on the central San Andreas fault.

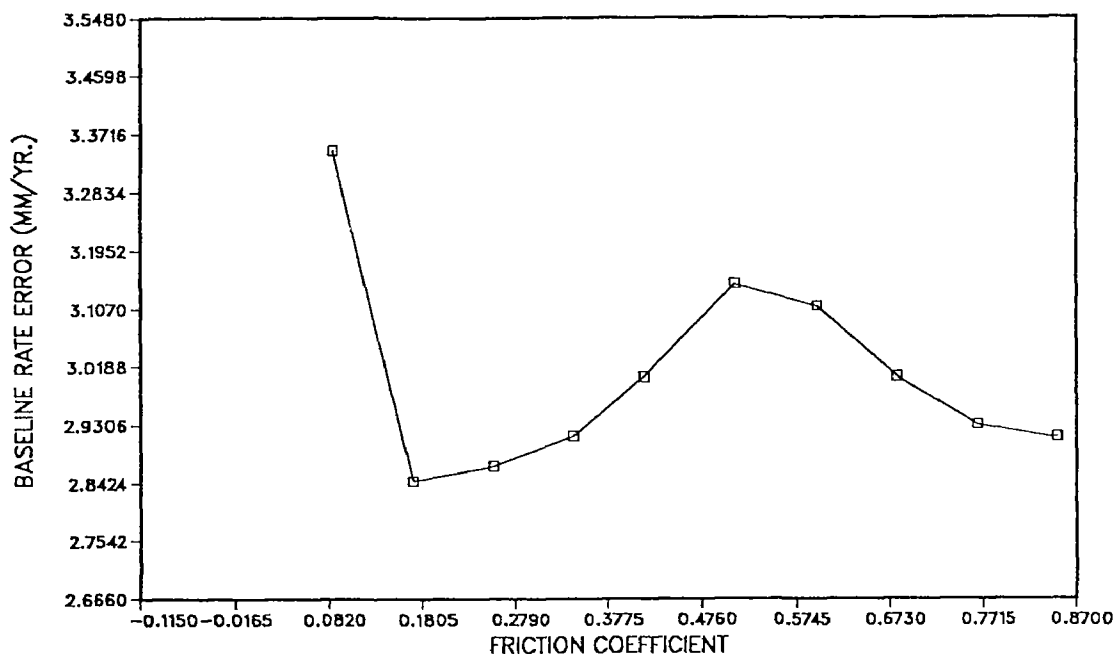
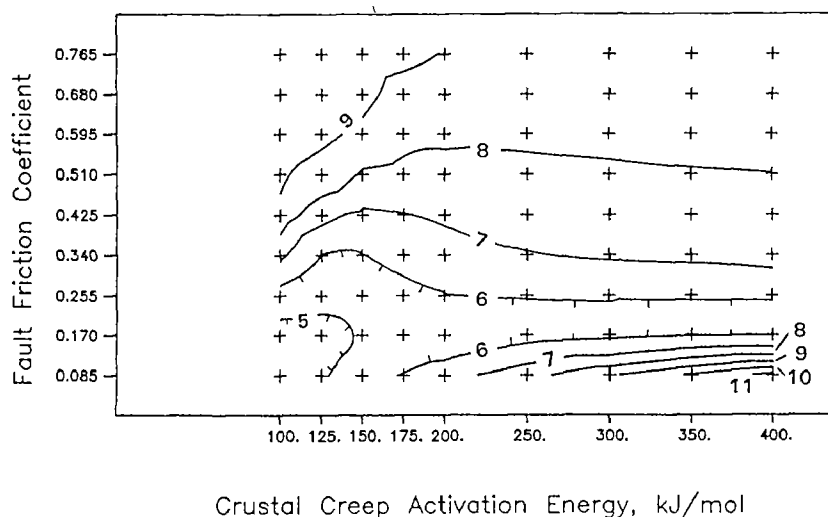
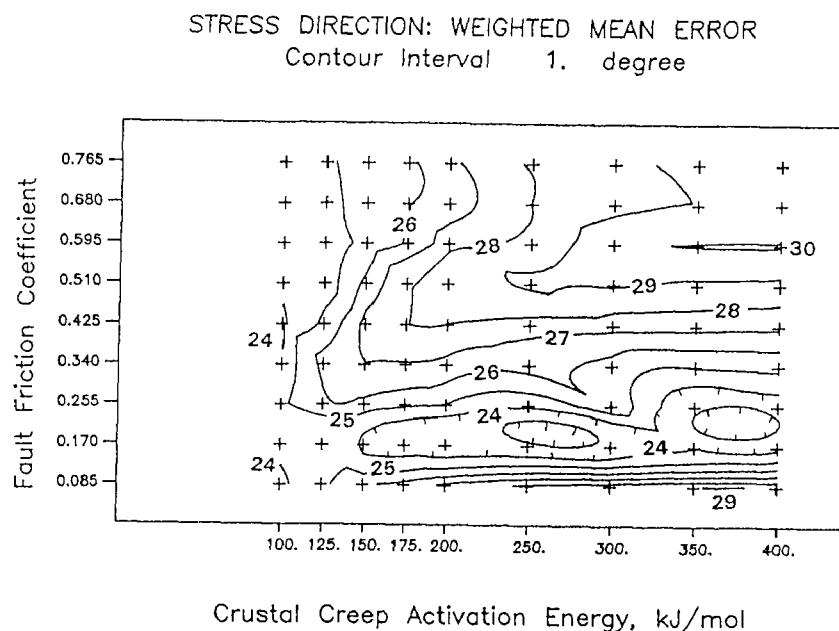


Figure 4. Weighted mean error in the prediction of 45 VLBI baseline rates, as a function of assumed fault friction. While the differences in the errors are small, note that the same model is preferred as in Figures 2 and 3.

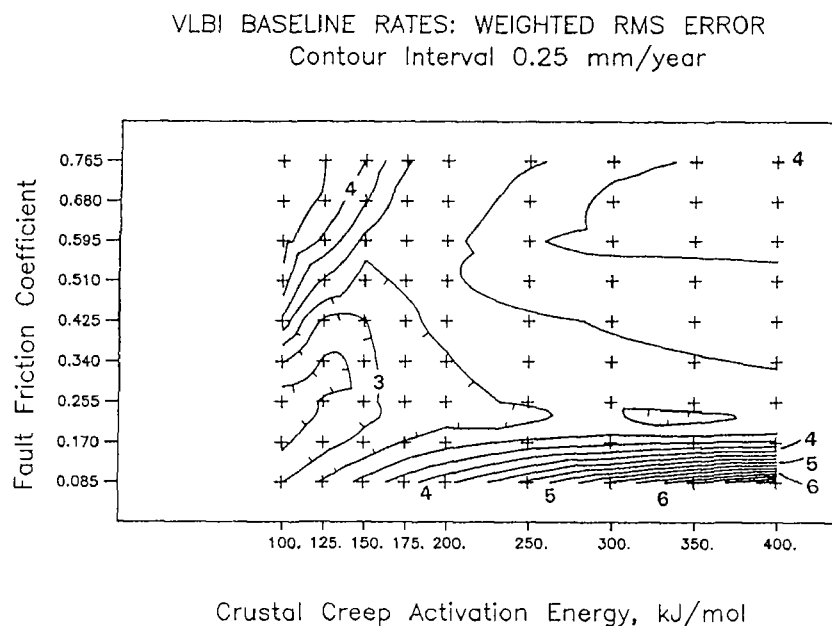
FAULT SLIP-RATES: RMS PREDICTION ERROR  
Contour Interval 1. mm/year



5. RMS prediction errors for 79 fault slip-rates, in mm/year. The vertical axis is fault friction, in increments of 0.085. The horizontal axis is the activation energy for creep in the lower crust; hence the intensity of mantle drag increases toward the left.



6. Weighted mean prediction errors for 221 principal stress directions, in degrees. The horizontal axis is the activation energy for creep in the lower crust; hence the intensity of mantle drag increases toward the left.



7. Weighted RMS prediction errors for 45 VLBI baseline rates, in mm/year. The horizontal axis is the activation energy for creep in the lower crust; hence the intensity of mantle drag increases toward the left.

## High Temporal and Spatial Resolution of Crustal Deformation with GPS

14-08-0001-G1673

Yehuda Bock  
Institute of Geophysics and Planetary Physics  
Scripps Institution of Oceanography  
La Jolla, CA 92093  
(619) 534-5292  
E-Mail: BOCK@BULL.UCSD.EDU

### Objectives

GPS surveying has the potential to provide crustal deformation precursors for the prediction of large earthquakes and, in particular, to allow *frequent and dense* monitoring of coseismic and postseismic strain transients which would add to our fundamental understanding of the physics of the earthquake process. The goal of this research is to develop and evaluate the capability of surveying *spatially dense, small and medium-aperture, three-dimensional geodetic networks, in near real-time with several millimeter-level accuracy* using GPS in continuously operating ("strainmeter") and kinematic-type modes.

### Investigations Undertaken and Data Collected

#### *Imperial Fault Kinematic Survey*

In May 1991, we surveyed a large portion of the Imperial College network across the northern part of the Imperial Fault near El Centro. This network has been surveyed since the early 1970's with very precise EDM instruments (first the Kern Mekometer and then the Kern Geomensor) [Mason, 1987]. The Geomensor measures distances with an accuracy of  $\pm (0.1 \text{ mm} + 0.1 \text{ ppm})$ . The network consisted of approximately 300 stations at the time of the October 15, 1979 Imperial Valley earthquake, with stations about 800 meters apart at road intersections, about half of which lay in an 8x10.5 km block extending more than 6 km on either side of the surface break. In January-April 1991 the network was leveled by Imperial College using trigonometric leveling with a mean standard error of 1.8 mm. In addition, all fault crossing lines were re-surveyed with a Kern DM503 EDM indicating  $55.7 \pm 11.5 \text{ mm}$  of fault slip since 1987 [Mason et al., 1991].

The network is ideal for kinematic-type GPS surveying. The terrain is flat and there are very few obstructions which in most cases can be easily avoided. We deployed 4-5 Trimble 4000 SST receivers for four days (5-6, 8-9 May). Two receivers were used in kinematic mode while the remaining 2-3 receivers were deployed as base stations in static mode. To obtain redundancy we surveyed crossover points. Furthermore, the roving receivers moved from site to site synchronously. Typically, each kinematic site was surveyed for 10 minutes in order to average out multipath errors. Each roving team was able to survey about 10 points during two kinematic windows (five or more satellites) of 75 and 60 minute duration. We are currently comparing our results with the conventional horizontal and vertical measurements. [Mason et al. 1991].

#### *Strainmeter-type Surveys near Parkfield*

We surveyed the USGS Kennedy Ranch Alignment Array located 10 km southeast of Parkfield using kinematic GPS. On 11 November 1990, we observed the ten points of the 258 m long array with one hour of observations using three Trimble 4000 SST receivers. On 8-10 February 1991, we reobserved the array for one hour on each day using three Ashtech XII receivers. The data at the two end points of the array were collected at a 1 second sampling rate for the entire one hour



period for all surveys. A roving receiver measured the intermediate points with repeated 3 minute occupations sampled at a 15 second sampling rate.

### *Permanent GPS Geodetic Array*

The Permanent GPS Geodetic Array (PGGA) has been operated as a NASA pilot project since the spring of 1990 by Scripps Institution of Oceanography (SIO) and the Jet Propulsion Laboratory, with assistance from Caltech, MIT and UCLA. The objectives are to monitor crustal deformation continuously, in near real-time and with millimeter accuracy, using a fully automated and economically feasible system. The development and operations of the PGGA have been described by Bock and Shimada [1990], Bock et al. [1990], Bock [1991a,b] and Bock and Genrich [1991]. We are using the PGGA data to support our investigations of the spatial and temporal resolution of GPS.

### Results Obtained

#### *Implications for GPS Strainmeters and Kinematic GPS*

We have reported on the results of the Kennedy Alignment Array Survey in Bock [1991], Bock and Genrich [1991], and Genrich and Bock [1991]. We reiterate our conclusions which provide guidelines for precise continuously monitoring and kinematic-type GPS surveys:

- (1) Multipath effects interfering with the incoming radio signal will tend to average out over a period of several minutes. Therefore, to achieve one millimeter level precision with kinematic GPS a site should be occupied for about ten minutes. Several millimeter to one centimeter precision can be achieved with shorter occupations.
- (2) In order to increase the resolution of millimeter-level position for a continuous GPS strainmeter, it is necessary to model the effect of multipath on the position components.
- (3) Multipath effects can be modeled for GPS strainmeters to an rms of a millimeter or two at a resolution of about one minute.

#### *Results from Permanent GPS Geodetic Array*

We have been estimating the position of the SIO-JPL-PFO triangle (Figure 1) daily since September 1991. We perform, at twenty-four intervals, a simultaneous weighted least squares adjustment of the station positions and improved satellites ephemerides using the PGGA data and data from a global set of tracking stations. As an example, the time series of positions of the JPL to Scripps baseline are shown in Figure 2, indicating an rms scatter of approximately 3 mm in the north, 6 mm in the east and 10 mm in the vertical. Considering the length of the PGGA baselines, we estimate that the daily orbits are precise at no worse than the 20-30 parts per billion level. We are investigating various approaches to improving the repeatability, particularly in the east and vertical components and performing tests at observation windows less than 24 hours. We also are examining the time series of a continuously operating GPS baseline from Piñon Flat Observatory to a site 14 km away [Happer, et. al., 1991]

We are also evaluating the precision of our satellite parameters based on overlapping orbital arcs. We are able to extrapolate several meter-level precise orbits twenty-four hours ahead of the time of collection. Although we typically perform solutions about 4-5 days after collection (primarily waiting for global tracking data that are downloaded by others), we now have all the components required to maintain a near-real time crustal motion monitoring array.

Our orbital ephemerides should be sufficiently precise to support most crustal deformation GPS surveys in California. Furthermore, our entire data base of orbital tracking data since April 1990, is on-line and accessible to investigators via anonymous ftp over Internet.

In Figure 3, we show the daily solutions of the Goldstone to JPL (Pasadena) baseline during the period of the Sierra Madre earthquake. We detect no significant deformation in the baseline

(from a distance of 180 km) with a precision of several mm. This result agrees with horizontal and vertical displacements computed from earthquake dislocation models (D.C. Agnew, personal communication).

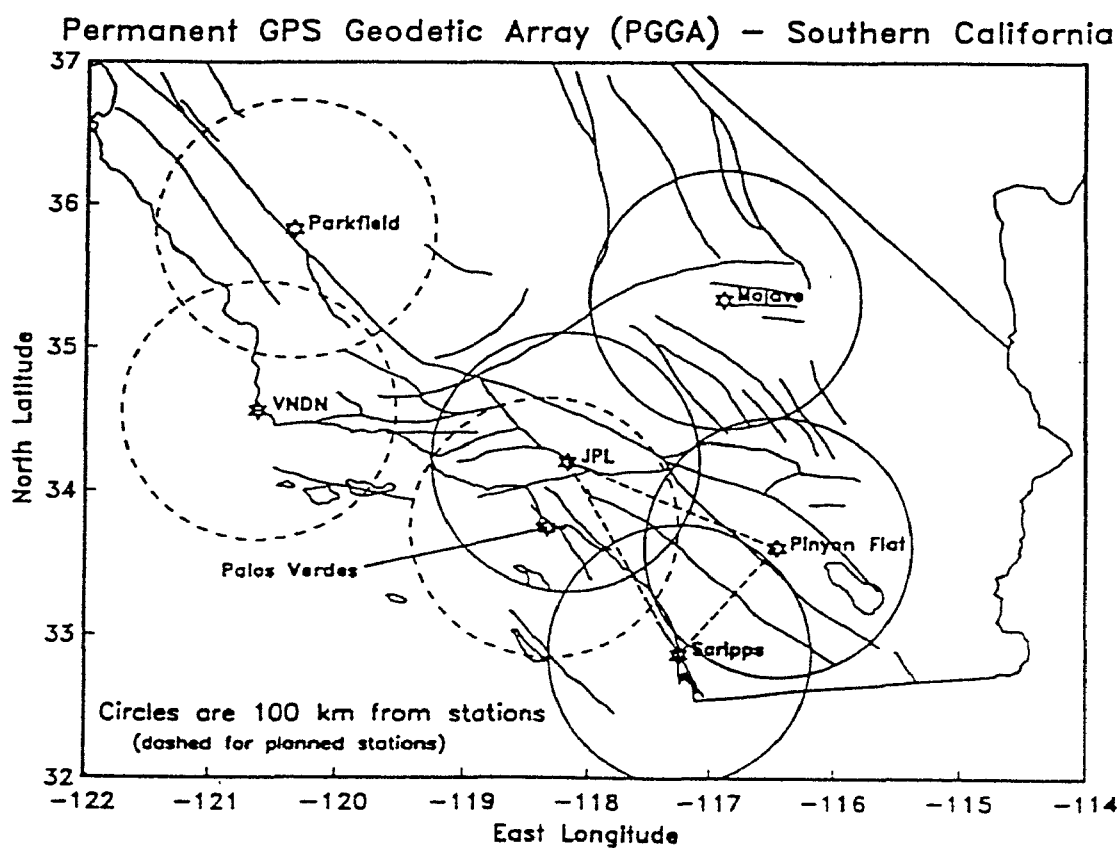
### Reports Published

- Bock, Y. and S. Shimada (1990a), Continuously monitoring GPS networks for deformation measurements, in Global Positioning System: An Overview, Y. Bock and N. Leppard (eds.), Springer Verlag, 40-56.
- Bock, Y., F. Wyatt, D.C. Agnew, J.-B. Minster, W. Gurtner, P. Henkart, S. Shimada, S.S.O. Puntodewo, K. Stark, D. Rosenblatt, Z.-K. Chen and P. Worcester (1990b), "Continuous monitoring of crustal strain using GPS in Southern California", GPS '90 meeting, Ottawa, Canada, September 3-7, 1990, 853-865.
- Bock, Y. (1991a), Continuous monitoring of crustal deformation, *GPS World*, 2, 40-47.
- Bock, Y. (1991b), Continuous GPS monitoring for crustal deformation in southern California: Status and Prospects, *EOS Trans. AGU*, 72, 119.
- Bock, Y. and J. Genrich (1991), NEHRP Summaries of Technical Reports, Vol. XXXII.
- Genrich, J.F. and Y. Bock (1991), Rapid resolution of crustal motion with short-range GPS, *J. Geophys. Res.*, in press.
- Happer, J., D.C. Agnew, Y. Bock, H. Johnson, K. Stark, and F. Wyatt (1991), Results from continuous GPS measurements over a 14-km line, *EOS Trans. AGU*, 72, 118.
- Mason, R., Y. Bock, J.F. Genrich and K. Grist (1991), Crustal deformation across the Imperial Fault: Results from kinematic GPS, trilateration and leveling of a densely-spaced, small-aperture network, *EOS Trans. AGU*, 72, 117.
- Shimada, S. and Y. Bock (1991), Crustal deformation measurements in central Japan determined by a GPS fixed-point network, *J. Geophys. Res.*, in review.

### References:

- Mason, R.G., Geomensor surveys in the Imperial Valley, California, report to the U.S. Geological Survey, 1987.

# SOUTHERN CALIFORNIA PERMANENT GPS GEODETIC ARRAY (PGGA) BULLETIN



Volume 1	July 1991	No. 1
----------	-----------	-------

**Figure 1:** Map of the Permanent GPS Geodetic Array (PGGA) in southern California taken from the cover page of the first issue of the PGGA bulletin. The sites at VNDN, Parkfield and Palos Verdes are expected to come on line in the first quarter of 1992.

# JPL to Scripps

(PGGA Solutions; Length 171,195.727 m)

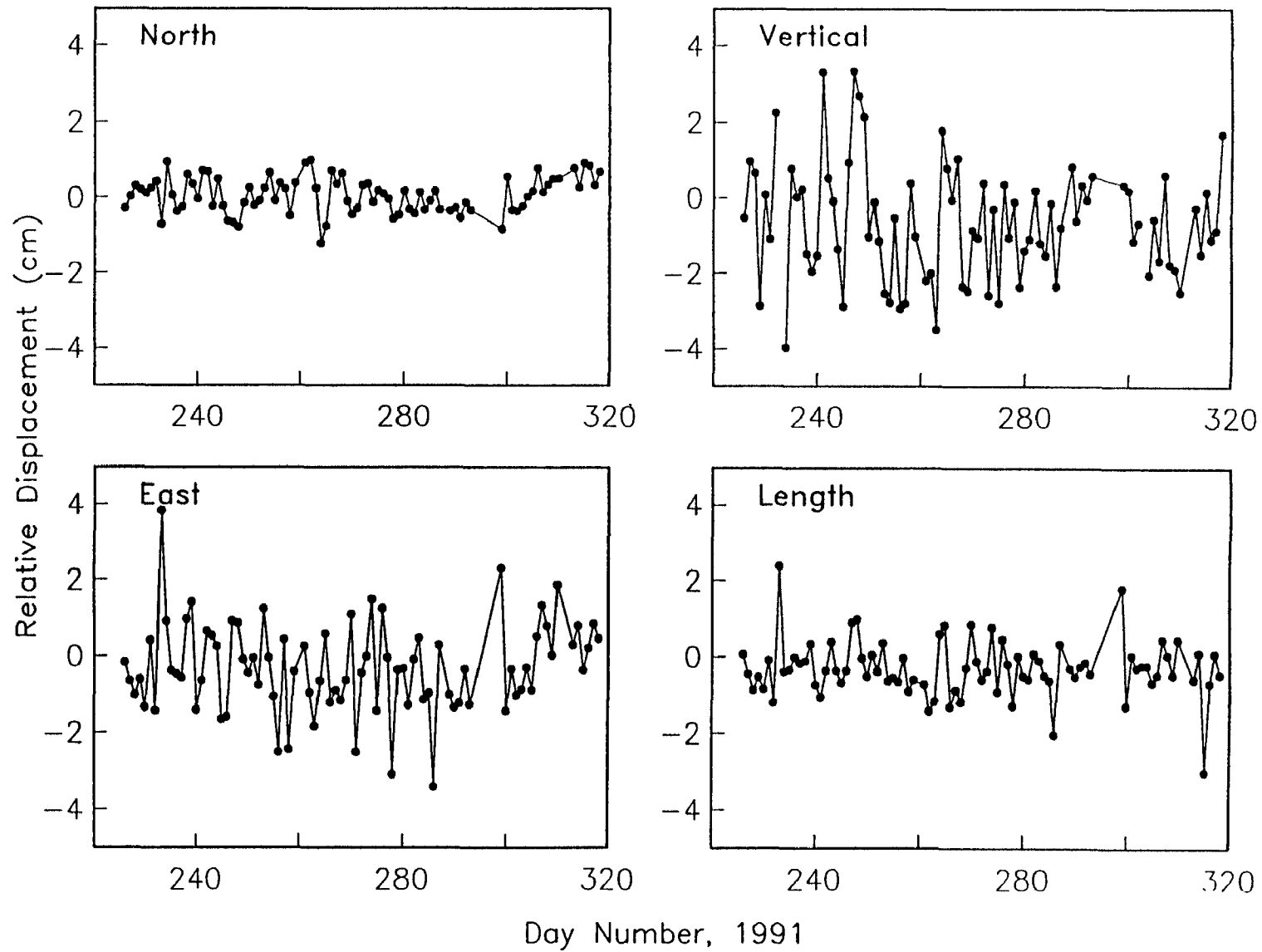


**Figure 2:** Daily PGGA solutions for the JPL to Scripps baseline for days 226-318.

# Goldstone to JPL

(PGGA Solutions; Length 179,254.461 m)

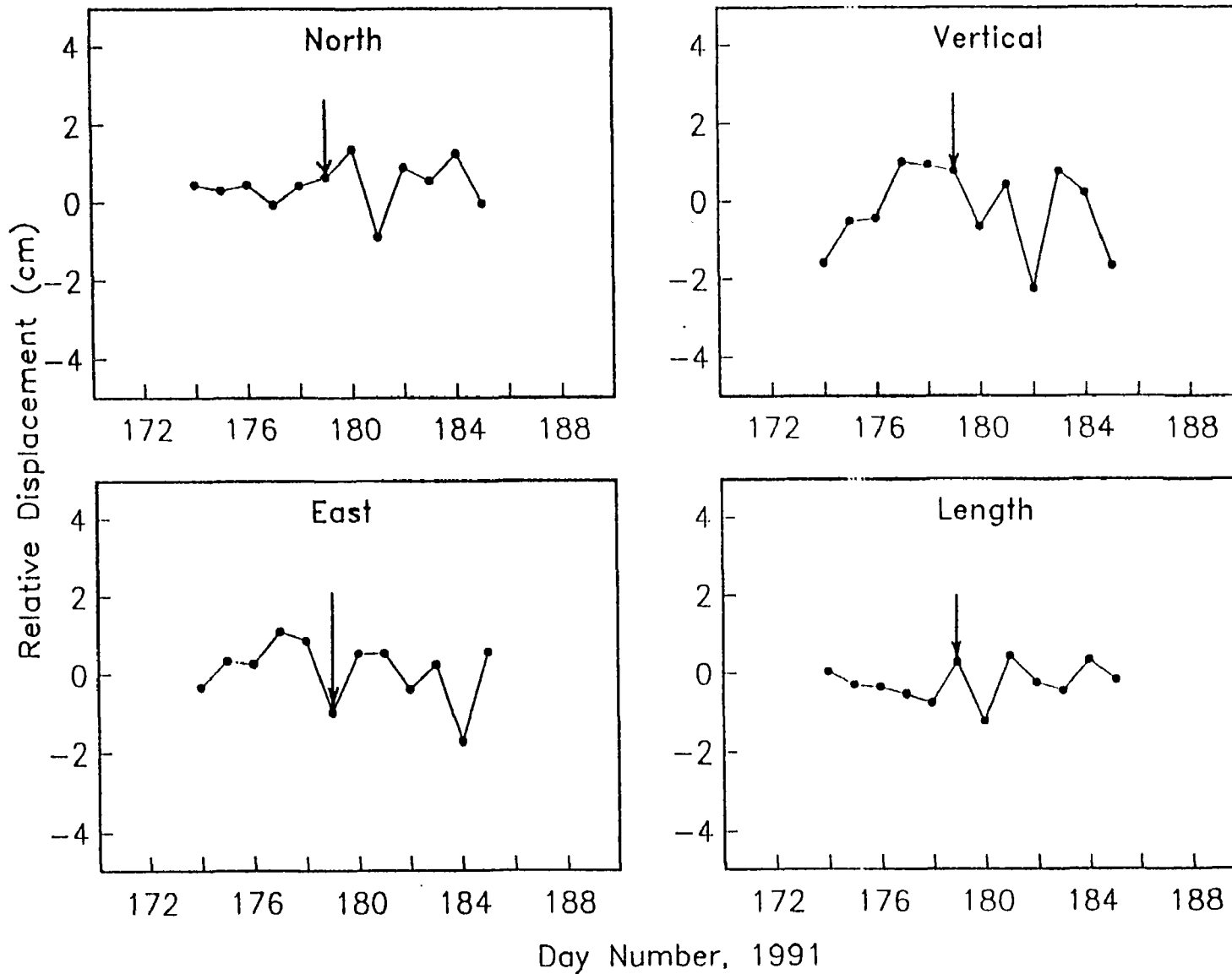


**Figure 3:** Daily PGGA solutions for the Goldstone to JPL baseline during the period of the Sierra Madre Earthquake (day 179). The vertical arrow indicates the first solution after the earthquake.

## Surface Faulting Studies

9910-02677

M.G. Bonilla  
Branch of Engineering Seismology and Geology  
U.S. Geological Survey  
345 Middlefield Road, MS 977  
Menlo Park, CA 94025  
(415) 329-5615

### Investigations

Study of the geology of the Marina District to better understand the distribution and causes of the severe earthquake damage there. Maps dating back to 1851, archival materials including photographs, logs of borings made from 1912 to 1990, and published reports on the history, geology, and earthquake damage were used in the study.

### Results

Maps and cross-sections showing the geology, distribution of soft bay mud, and depth to water table were prepared. A map showing contours on the buried surface of the bedrock was made based on borings, offshore geophysical data, and geologic interpretations. The general form of the bedrock surface is of a northwest-trending valley whose elevation ranges from sea level to about 90 m below sea level. The valley in the bedrock surface is buried by firm Pleistocene bay clay, a dense Pleistocene sand layer, soft Holocene bay sediments, loose to dense Holocene beach and dune sands, and artificial fill that have an aggregate maximum thickness of about 90 m. Artificial filling of a cove at the site of the Marina District proceeded gradually from the late 1860s to 1912, when major hydraulic filling was done for the Panama-Pacific International Exposition. The remains of thousands of piles driven for the Exposition very probably still exist and have had unknown effects on long-term ground settlement and earthquake-related ground displacements.

Intensity maps of the 1906 earthquake, and seismic recordings and severe building damage in 1989, reported by others, indicate that ground motion was amplified on both natural and artificial ground. This suggests that the configuration of the bedrock surface and the location and thickness of various clay and sand deposits underlying the artificial fill had an important effect on the shaking. However, most of the settlement and liquefaction and the damage to pipelines, building foundations, streets, sidewalks and curbs occurred in areas of artificial fill consisting mainly of loose sand.

Manuscripts describing the results of the study were prepared for the Bulletin of the Seismological Society of America and a USGS Professional Paper chapter. In collaboration with others, a display on earthquake effects in the Marina District was prepared for the USGS open house in Menlo Park, and the display has been shown in the Marina District.

### Reports

- Bennett, M.J., Bonilla, M.G., and Holzer, T.L., 1990, Liquefaction in the Marina District, San Francisco, California, during the Loma Prieta earthquake [abs.]: Geological Society of America Abstracts with Programs, v. 22, no.7, p. A188.
- Bonilla, M. G., 1990, Historical faulting, *in* Moore, G.W., Bonilla, M. G., Rapp, R. H., Rinehart, W. A., Liebert, Lee, Simkin, Tom, Soller, D. R., and Zoback, M. L., Geodynamic Map of the Circum-Pacific Region, Arctic Sheet: U.S. Geological Survey Circum-Pacific Map Series, Map CP-38, scale 1:10,000,000.

- Bonilla, M. G., and Lienkaemper, J. J., 1991, Factors affecting the recognition of faults exposed in exploratory trenches: U. S. Geological Survey Bulletin 1947, 54 p.
- Bonilla, M. G., 1991, The Marina District, San Francisco, California: Geology, history, and earthquake effects: Seismological Society of America Bulletin, v. 81, no. 5, p. 1958-1979.

## **Holocene Slip Rate of the Hayward Fault, Union City, California**

Agreement No. 14-08-0001-G2078

Glenn Borchardt  
Soil Tectonics  
P.O. Box 5335  
Berkeley, California 94705

(510) 654-1619

### **Objectives**

This project is a cooperative effort with Jim Lienkaemper of the USGS to complete the Union City project which was initially funded by the California Division of Mines and Geology. At Union City a stream cuts through the uplifted northeastern side of the fault near Masonic Home and debouches onto an alluvial fan on the southwest side of the fault during flood stage. In 1989, our 130-m trench across the fan and parallel the fault uncovered an extremely complicated series of channel fills and interleaved soils. We had initially expected a simple record of successively older buried channel deposits laid down as the debouchment point moved to the northwest. Instead, the record shows a complex of relatively well developed buried alluvial fans having projected apexes of increasing age and offset. The relatively stable points of debouchment apparently were established in conjunction with an offset in the thalweg of the stream.

Preliminary slip rates for carbon-14 dated apexes between 4 ka and 14 ka were between 7 and 9 mm/yr. During the first phase of the work the projections were necessarily based on logs of trench walls only 0.9 m apart. Channel margins had to be projected 20 m toward the fault plane. During the 1990 field season we excavated a parallel trench 10-m further to the southwest. Most of the channel fills identified in the Holocene portion of the 1989 trench also appeared in the 1990 trench. Preliminary evaluation of the extremely detailed logs confirms our earlier estimates of the amount of offset. However, to increase the precision of the slip rate measurement, we need to improve our knowledge of the precise time when each of the stream offsets was initiated.

Fortunately, the site contains much datable charcoal and at least a dozen paleosols which will help in unraveling the depositional sequence. The paleosols formed on the stable portions of former fan surfaces at the same time as the channels were cutting still other portions of the same fans. In the interpretation of



such alluvial systems we use the paleosols as stratigraphic markers that constrain the ages of the channel fills that we use as piercing points. Many of these fills are by no means easy to recognize from trench-to-trench. When the size, morphology, and contents of a fill do not suffice, its relationship to the paleosol of the same age becomes the deciding factor in its identification. In studies of this type, the precision of the age and measurement of the offset improve as our knowledge of the paleosols and depositional sequence increases.

We obtained 115 soil samples and performed 55 particle size analyses on 11 vertical sections taken the 130-m trench. The objectives of this project are to provide complete soil descriptions and interpretations of the soil data in the context of the channel-fill sequence and the C-14 dates.

## Results

Unlike the 9-ka soils at the Fremont site, 9-ka soils at Union City have blocky structure and contain extensive clay film development, apparently because they are derived from fine smectitic clays of the Orinda Formation that dominates the drainage. Paleosols formed during the Early Holocene have unique Bk horizons containing nodular calcite--apparently as a result of an especially dry climate. Holocene soils at the site are gray brown and associated with varying fluvial conditions, while the Pleistocene soils are yellow brown and associated with relative landscape stability. The further analysis and study of these well-dated paleosols will be of utmost importance in determining the relative age of movement along faults throughout the Bay Area. We are now in the process of choosing still more charcoal samples to obtain the precise dates for the initiation of the two Holocene fan apexes.

## Reports Published in FY91

Borchardt, Glenn, 1991 (in press), Liquefaction and shaking damage in the Watsonville and Oakland areas and its implications for earthquake planning scenarios, in Baldwin, J.E., and Sitar, N., eds., Loma Prieta earthquake: Engineering geologic perspectives: Association of Engineering Geologists Special Publication No. 1.

Borchardt, Glenn, 1991, Preparation and use of earthquake planning scenarios: California Geology, v. 44, p. 195-203.

- Borchardt, Glenn, 1991, Vertical crustal stability between Point Pinole and Carquinez Strait during the Late Quaternary: EOS, Transactions of the American Geophysical Union, v. 72, no. 44, p. 446.
- Borchardt, Glenn, and Rogers, J.D., 1991 (in press), Earthquake potential along the Hayward fault, California, in Prakash, Shamsher, ed., Second International Conference on Recent Advances in Geotechnical Earthquake Engineering and Soil Dynamics, St. Louis, Missouri, March 11-15, 1991: Rolla, MO: University of Missouri-Rolla, 3.
- Borchardt, Glenn, and Seelig, K.A., 1991, Soils, paleosols, and Quaternary sediments offset along the Hayward fault at Point Pinole Regional Shoreline, Richmond, California, in Sloan, Doris and Wagner, D.L., eds, Geologic excursions in northern California: San Francisco to the Sierra Nevada: California Division of Mines and Geology Special Publication 109, p. 75-83.
- Lienkaemper, J.J., and Borchardt, Glenn, 1990, Holocene slip rate, historic creep rate, and the potential for large earthquakes on the Hayward fault, California: EOS, Transactions of the American Geophysical Union, v. 71, no. 43, p. 1645.
- Lienkaemper, J.J., and Borchardt, Glenn, 1991, Holocene slip rate of the Hayward fault at Union City, California: Geological Society of America Program with Abstracts, Cordilleran Section, v. 23, no. 2, p. 73.
- Lienkaemper, J.J., Borchardt, Glenn, and Lisowski, Michael, 1991, Historic creep rate and potential for seismic slip along the Hayward fault, California: Journal of Geophysical Research, v. 96, no. B11, p. 18261-18283.
- Wills, C.J., and Borchardt, Glenn, 1990, Holocene slip rate and earthquake recurrence on the Honey Lake fault zone, northeastern California: EOS Transactions, American Geophysical Union, v. 71, no. 43, p. 1608.

# ACCELERATION, VELOCITY, AND VOLUMETRIC STRAIN FROM PARKFIELD GEOS NETWORK

**9910-02089**

Roger D. Borchardt, Malcolm J. Johnston,  
C. Dietel, G. Glassmoyer, and Allan Lindh  
Branch of Engineering Seismology and Geology  
U.S. Geological Survey  
345 Middlefield Road, MS 977  
Menlo Park, California 94025  
415/329-5619 or FTS 459-5619

## Investigations

- \* Maintain GEOS array near Parkfield, CA, to provide broad-band, high-resolution measurements of the mainshock as well as an array to provide measurements of pre-, co-, and post-seismic strain and displacement field perturbations for purposes of earthquake prediction.
- \* Maintain up-to-date archive of all events recorded in anticipated rupture zone.
- \* Develop theoretical basis and models to interpret co-located measurements of volumetric strain and seismic displacement fields.

## Results

- \* An array of 15 stations has been maintained at 95% or greater reliability since July, 1987. Array maintenance is being conducted by C. Dietel. He is also maintaining an up-to-date digital data archive and providing summaries for monthly internal USGS reports. (See previous reports for detailed description of the array.) Events recorded along Parkfield segment of study zone during time interval indicated are summarized according to magnitude and depth (Table 1, Figure 1). Ground velocity (Figure 2, Figure 3; traces 4, 5, and 6), and ground acceleration (Figure 2, traces 4, 5, and 6; Figure 3, traces 1, 2, and 3) for a magnitude 3.1 event are shown.
- \* An example of magnitude 3.1 event recorded at all stations is shown in Figures 2, 3, 4, and 5. Co-located measurements of ground acceleration (traces 1-3) and ground velocity (traces 4-6) are shown in Figures 2 and 3. Co-located measurements of volumetric strain at 3 gain levels (traces 1-3) and ground acceleration or velocity (traces 4-6) are shown in Figures 4 and 5.

### Reports

(See projects Borchardt et al., [9910-02689 and 9901-03009] and Johnston for related reports.)

TABLE 1

HYPO-71 LISTING: PARKFIELD EARTHQUAKES RECORDED ON ONE OR MORE GEOS STATIONS  
FROM OCTOBER 1, 1990 THROUGH AUGUST 11, 1991.

9010	1	224	11.41	35	58.04	120	30.56	7.99	1.49	6	214	1.6	0.01	1.8	1.4				
9010	3	1449	47.59	36	2.31	120	35.05	2.71	1.47	6	207	6.1	0.01	1.0	4.4				
9010	6	325	0.83	35	55.70	120	28.52	9.95	2.56	39	92	3.0	0.11	0.3	0.3	S			
9010	8	1350	42.98	35	59.53	120	34.02	4.99	1.64	23	122	3.2	0.09	0.3	0.4	S			
9010	8	2026	30.51	35	59.61	120	33.79	5.03	1.67	22	124	3.6	0.10	0.3	0.4	S			
901020	531	38.62	36	0.88	120	34.62	6.41	1.64	23	164	4.0	0.06	0.4	0.4	S				
901021	1555	17.56	35	55.67	120	28.45	4.72	1.57	18	147	3.1	0.04	0.3	0.5					
901023	7	3	55.14	35	55.78	120	28.54	4.71	1.32	16	147	2.9	0.03	0.4	0.5	S			
901024	1647	47.15	35	55.72	120	28.43	4.88	1.22	11	148	3.1	0.03	0.5	0.6					
901026	2157	37.01	35	56.10	120	38.75	7.52	1.83	19	54	4.9	0.15	0.4	1.1					
901028	814	17.33	35	41.13	120	14.28	8.99	1.46	8	105	4.2	0.04	0.4	0.7					
901028	1217	2.82	35	40.97	120	14.15	9.21	1.44	10	72	3.8	0.06	0.4	1.0					
901028	1748	11.84	36	2.46	120	35.32	5.27	1.53	13	181	6.3	0.03	0.6	0.6					
901030	148	44.65	36	1.55	120	35.18	5.82	2.25	29	152	4.7	0.08	0.3	0.3					
901030	529	53.98	36	1.55	120	35.03	5.82	1.59	16	176	4.8	0.06	0.5	0.4					
9011	4	1532	40.25	35	55.78	120	28.51	5.42	1.72	21	147	3.0	0.03	0.3	0.3				
901114	1934	14.09	35	57.88	120	30.92	7.92	3.12	42	135	1.9	0.09	0.3	0.2					
901116	057	12.53	35	58.00	120	31.19	7.87	2.45	34	134	2.3	0.07	0.3	0.2					
901117	1	7	38.05	36	3.91	120	36.86	7.63	2.16	30	128	8.9	0.07	0.3	0.4				
901122	1156	10.58	35	59.52	120	33.78	5.93	2.06	28	91	3.6	0.07	0.3	0.2					
901123	726	32.46	35	59.60	120	33.76	5.81	2.17	28	93	3.6	0.09	0.3	0.2					
901128	342	54.73	35	57.18	120	29.43	13.51	2.23	30	138	0.7	0.07	0.4	0.3					
901130	425	59.35	35	56.85	120	29.77	11.60	3.09	44	69	1.0	0.11	0.2	0.3	S				
901130	428	8.02	35	56.89	120	29.43	10.90	2.08	26	135	1.1	0.06	0.3	0.3					
9012	4	1313	59.23	35	56.17	120	31.75	9.98	1.89	29	70	1.6	0.13	0.4	0.4	S			
9012	4	1332	25.72	35	56.31	120	31.12	10.78	1.86	25	77	1.4	0.12	0.4	0.5				
901218	630	52.68	36	0.13	120	34.56	5.22	1.66	15	129	3.0	0.11	0.4	0.7					
901226	23	0	29.12	36	0.62	120	34.43	5.18	2.19	26	130	3.7	0.08	0.3	0.3				
901226	23	2	4.09	36	0.53	120	34.56	4.95	2.53	31	130	3.5	0.10	0.3	0.3				
901226	23	7	18.50	36	0.71	120	34.03	5.33	2.19	23	132	4.3	0.07	0.3	0.3				
901228	614	57.65	35	53.33	120	26.08	10.82	1.44	18	139	3.2	0.03	0.4	0.6	S				
91	1	4	026	16.06	36	0.22	120	33.88	5.53	2.57	36	132	3.9	0.08	0.2	0.2			
91	1	5	833	8.03	35	53.51	120	26.06	10.23	1.43	18	143	3.3	0.04	0.3	0.5	S		
91	1	9	22	9	4.81	35	54.23	120	26.99	6.40	3.11	38	129	4.8	0.08	0.2	0.3		
91	119	739	6.47	35	59.00	120	33.66	5.97	1.55	13	114	3.7	0.06	0.3	0.3				
91	119	838	15.63	35	59.05	120	33.60	5.87	1.68	17	86	3.8	0.07	0.3	0.3				
91	121	247	27.00	35	46.84	120	20.03	8.36	2.90	40	57	7.0	0.10	0.2	0.3	S			
91	128	1554	4.81	35	44.34	120	17.90	12.24	1.83	25	49	4.5	0.05	0.2	0.4				
91	2	4	2	7	21.04	35	46.80	120	20.13	8.17	2.79	38	57	6.9	0.10	0.2	0.4	S	
91	2	4	2	8	46.95	35	46.96	120	19.97	8.39	2.06	28	59	7.3	0.06	0.2	0.4	S	
91	2	5	437	25.68	36	0.95	120	33.89	5.32	1.88	21	134	4.8	0.05	0.3	0.3			
91	2	5	1121	18.58	35	58.69	120	31.66	11.27	2.09	32	135	3.6	0.06	0.2	0.3			
91	210	038	24.89	35	57.43	120	30.38	9.13	1.99	28	112	0.8	0.08	0.3	0.3				
91	216	1232	55.82	36	0.10	120	34.52	6.62	1.67	18	98	3.0	0.10	0.4	0.5				
91	228	15	2	57.00	35	57.33	120	30.97	5.90	2.20	35	51	1.7	0.14	0.3	0.3			
91	3	8	133	11.02	36	0.49	120	33.87	5.74	1.92	21	133	4.2	0.06	0.4	0.3	S		
91	311	2248	30.27	35	58.84	120	31.49	11.43	1.76	24	136	3.7	0.04	0.5	0.4				
91	322	1121	52.84	35	57.72	120	31.12	11.09	2.51	35	65	2.0	0.12	0.3	0.5				
91	329	610	17.64	35	59.53	120	32.91	5.56	1.93	14	180	4.9	0.07	0.5	0.4				
91	4	3	530	14.26	35	56.43	120	29.00	6.51	1.57	16	151	2.2	0.03	0.3	0.4			
91	4	9	14	0	22.95	35	51.27	120	23.80	5.59	2.94	39	93	3.1	0.12	0.2	0.3		
91	410	333	44.77	35	51.28	120	23.91	4.62	2.35	30	91	3.0	0.08	0.2	0.4	S			
91	410	4	0	55.08	35	51.13	120	23.92	3.15	1.87	19	88	3.3	0.06	0.2	0.6	S		
91	412	629	14.75	35	58.07	120	30.61	11.22	2.13	24	162	1.7	0.05	0.4	0.3				

91	412	947	15.41	35	57.95	120	31.12	11.48	2.21	33	148	2.2	0.10	0.3	0.3	
91	421	5	5	2.35	35	45.13	120	18.11	8.02	1.56	19	57	5.3	0.06	0.2	0.5
91	421	547	38.77	35	45.14	120	18.12	8.20	1.73	18	57	5.3	0.07	0.3	0.5	
91	423	1319	40.24	35	58.99	120	32.98	5.82	1.71	27	113	4.7	0.09	0.3	0.3	
91	426	943	57.52	35	58.33	120	30.93	11.21	1.84	25	136	2.4	0.05	0.3	0.3	
91	429	3	8	38.13	35	58.40	120	31.85	12.13	1.19	17	162	3.5	0.07	0.7	0.5
91	5	6	859	38.59	35	57.77	120	31.20	10.75	2.10	35	123	2.2	0.11	0.3	0.4
91	5	7	115	39.97	36	2.30	120	35.34	5.57	1.67	25	166	6.0	0.06	0.4	0.3
91	5	8	20	1	55.10	35	56.24	120	29.53	11.02	33	126	1.7	0.13	0.3	0.4
91	5	8	20	3	54.12	35	56.58	120	28.80	11.55	12	163	2.2	0.03	0.6	0.8
91	519	322	17.18	36	1.96	120	35.54	6.24	1.41	28	165	5.3	0.07	0.4	0.6	
91	529	1641	46.83	35	53.66	120	26.56	6.42	2.04	35	119	4.0	0.10	0.3	0.4	
91	613	0	0	50.32	35	59.58	120	33.72	5.46	1.13	18	123	3.7	0.12	0.4	0.5
91	7	7	124	58.52	35	58.26	120	30.64	11.11	0.65	17	164	2.0	0.04	0.5	0.4
91	711	1049	54.70	35	57.93	120	31.33	11.21	2.20	28	155	2.4	0.09	0.4	0.3	
91	722	2351	31.32	35	58.20	120	31.17	11.03	1.11	22	162	2.5	0.04	0.3	0.3	S
910806	0103	55.00	36	3.29	120	36.70	7.84	3.7	40	86	8.	0.08	0.2	0.3	B	

# PARKFIELD

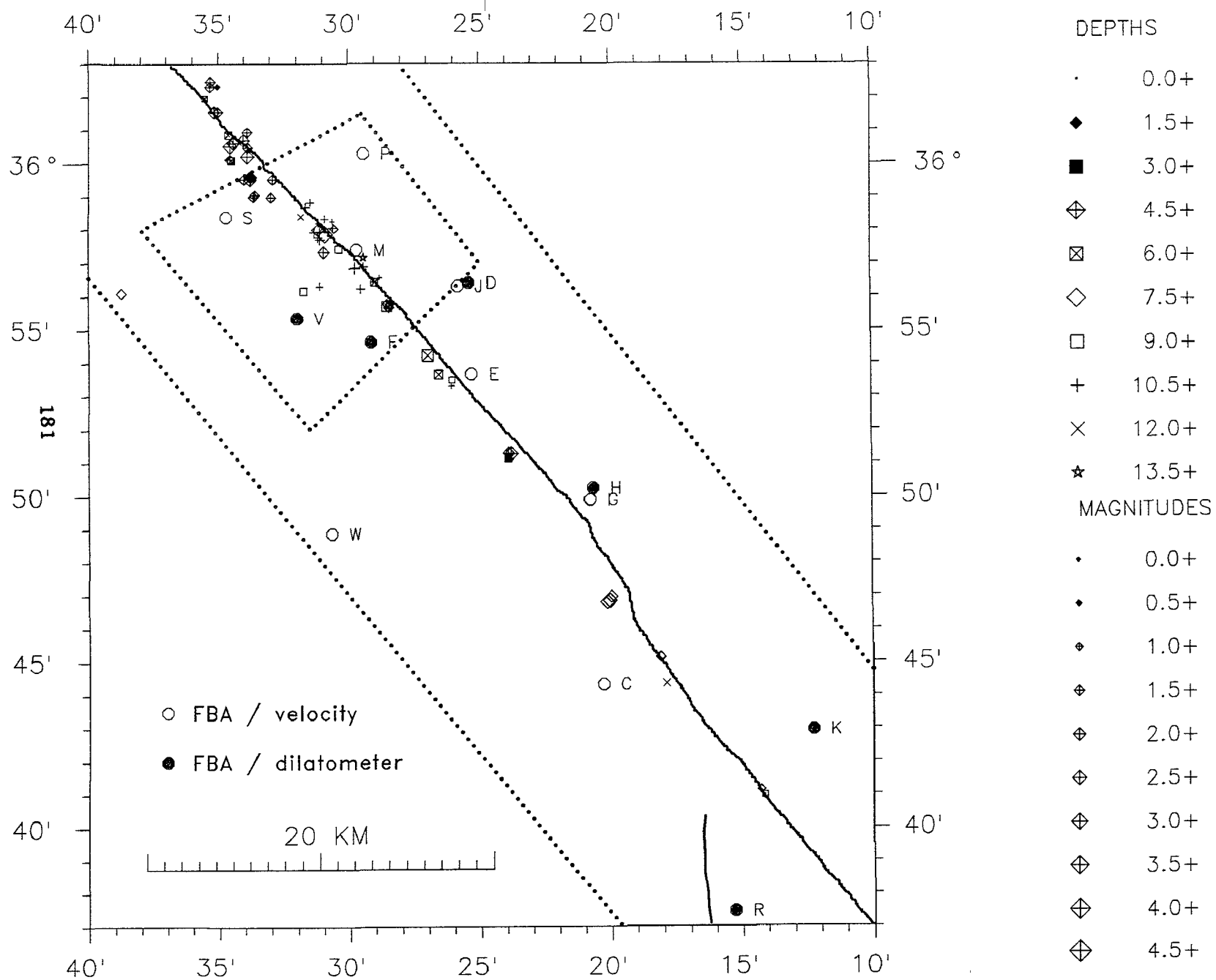


Figure 1

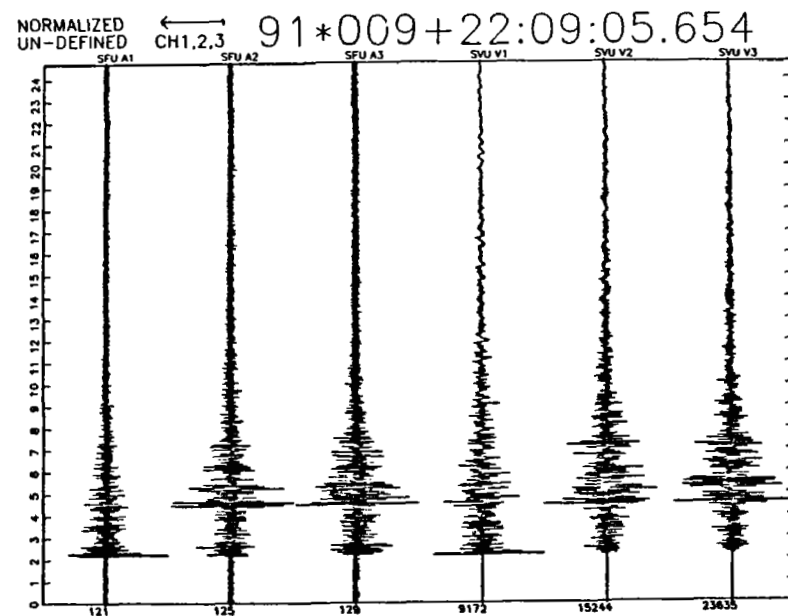
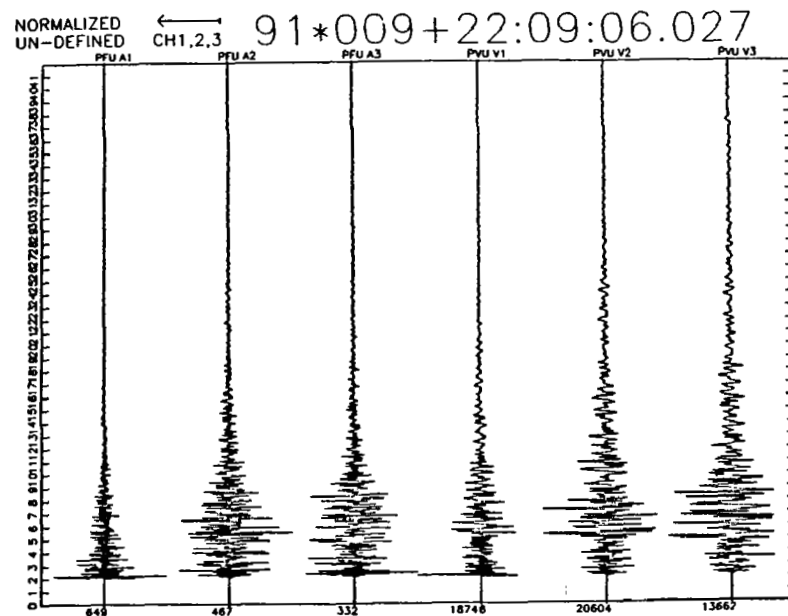
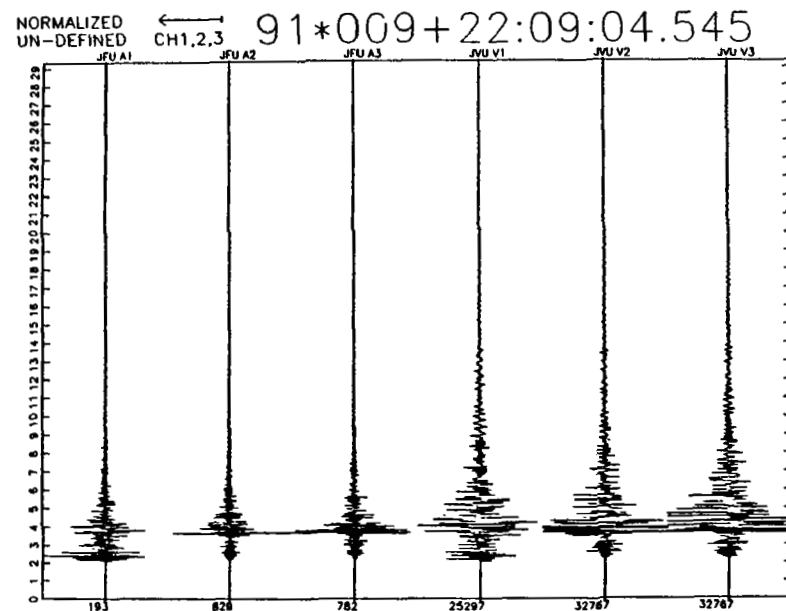
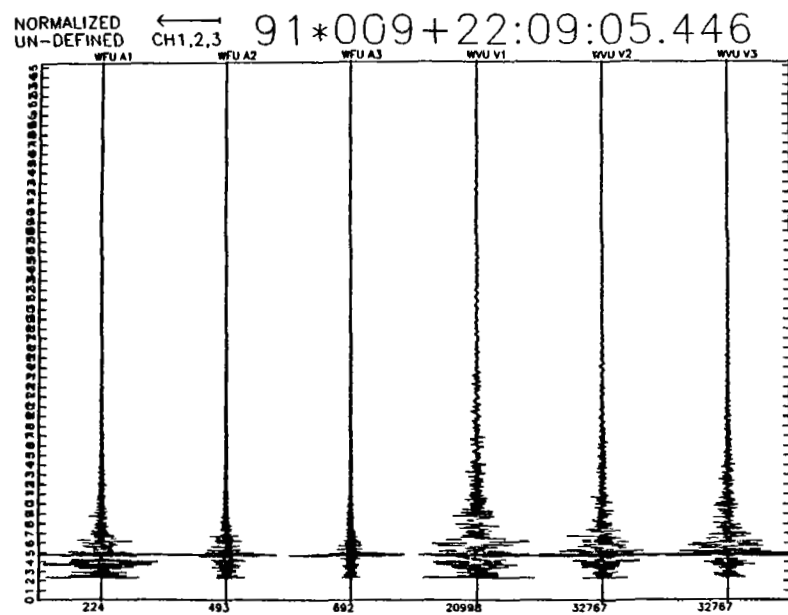


Figure 2



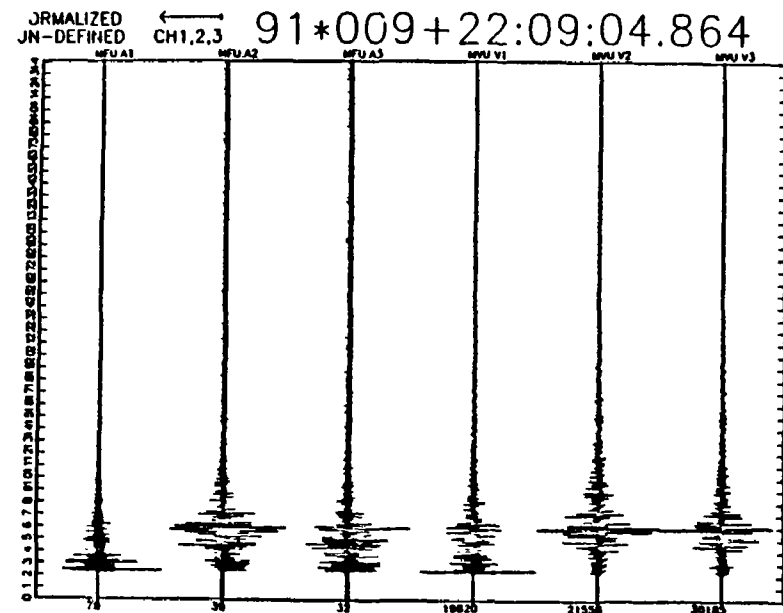
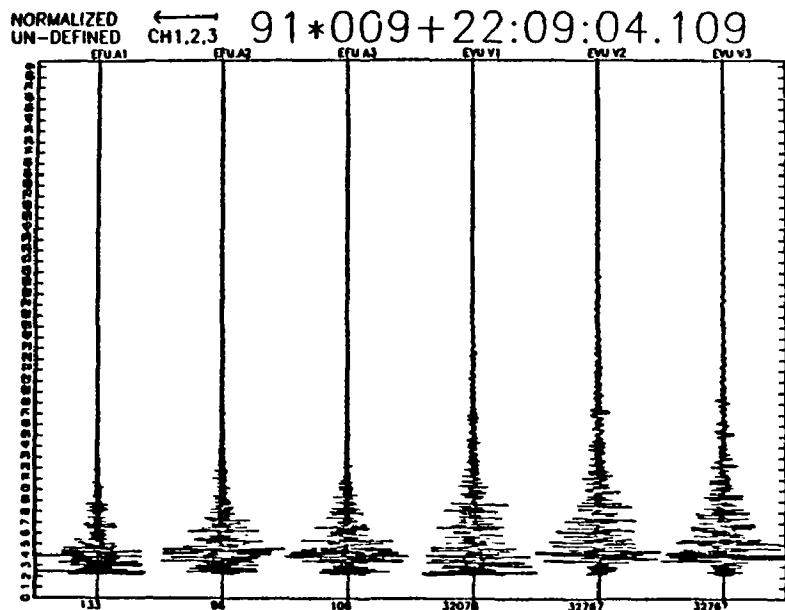
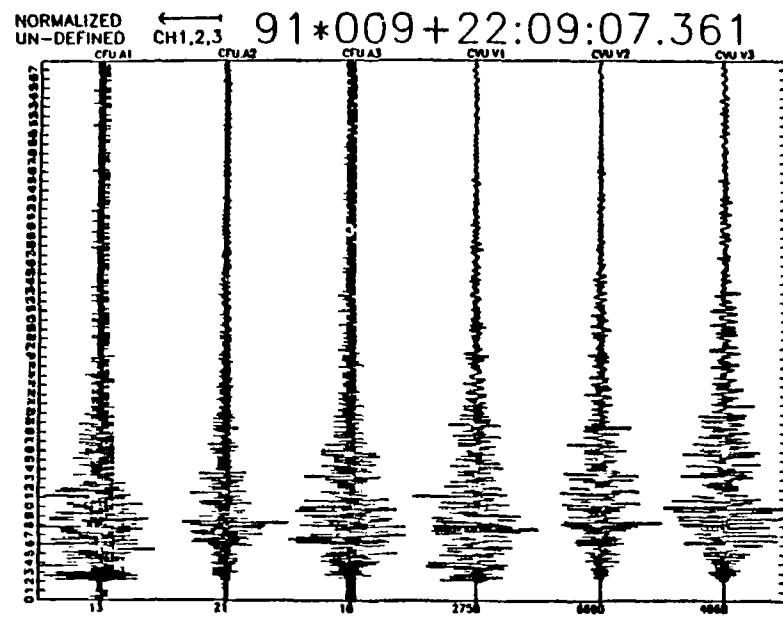
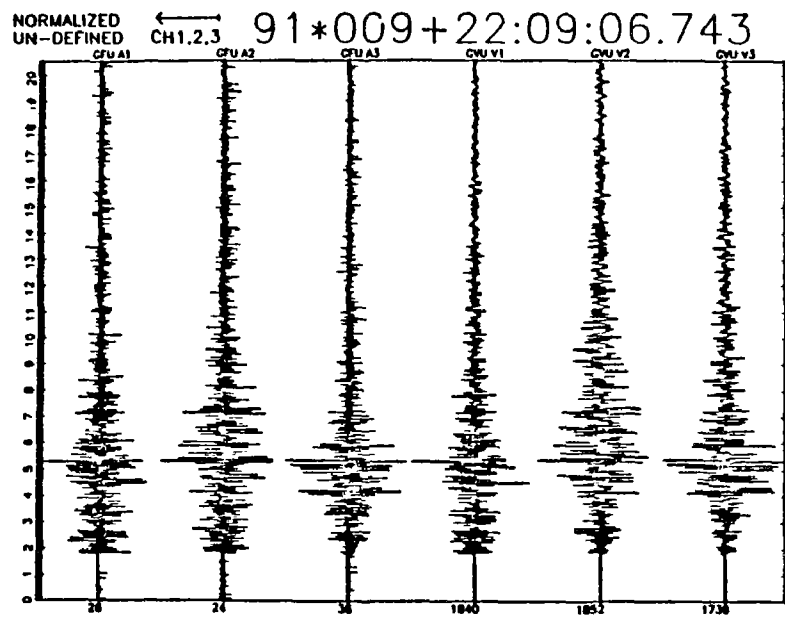


Figure 3

II

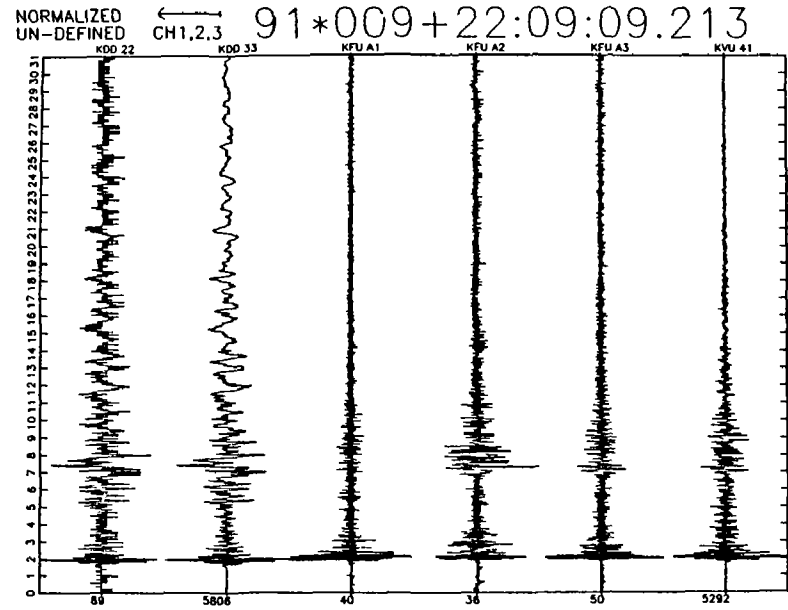
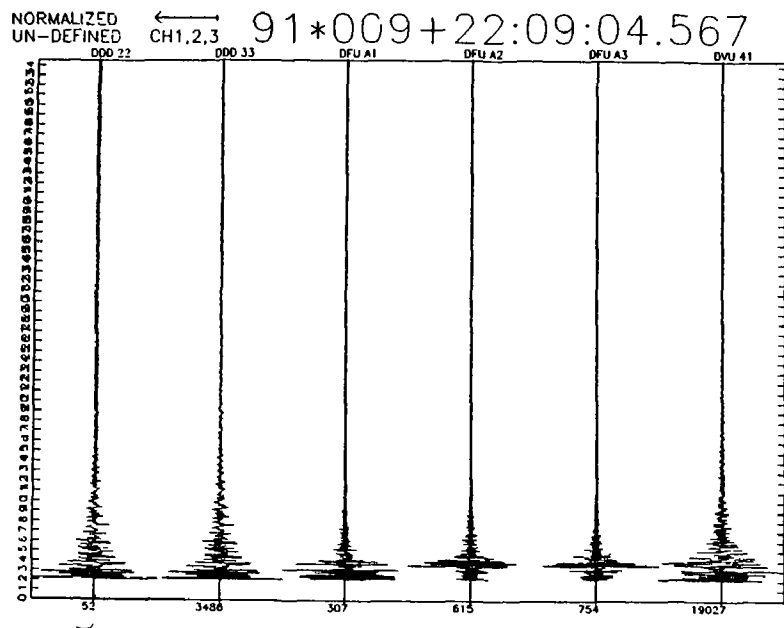
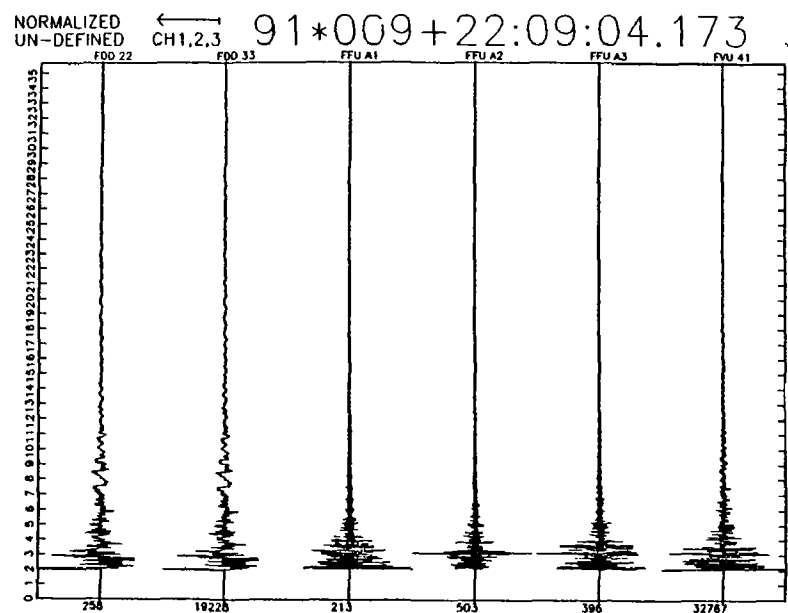
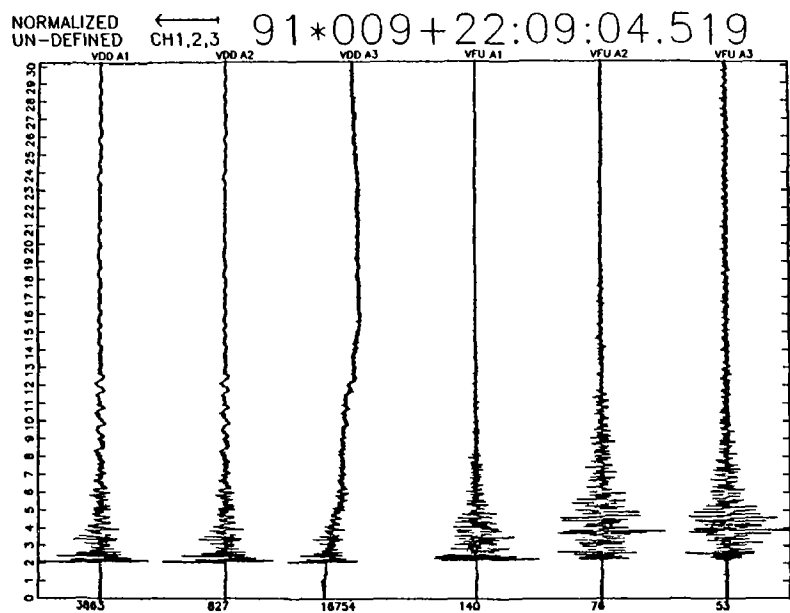


Figure 4

II

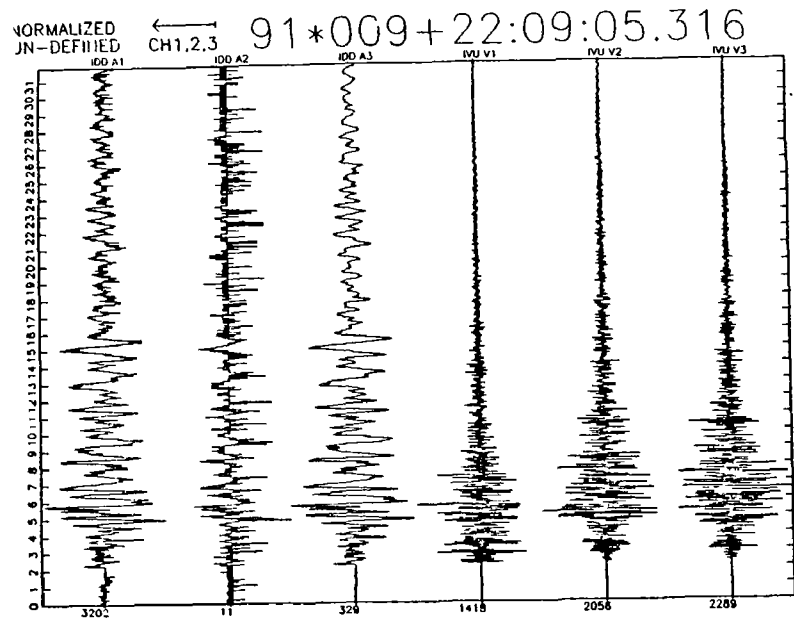
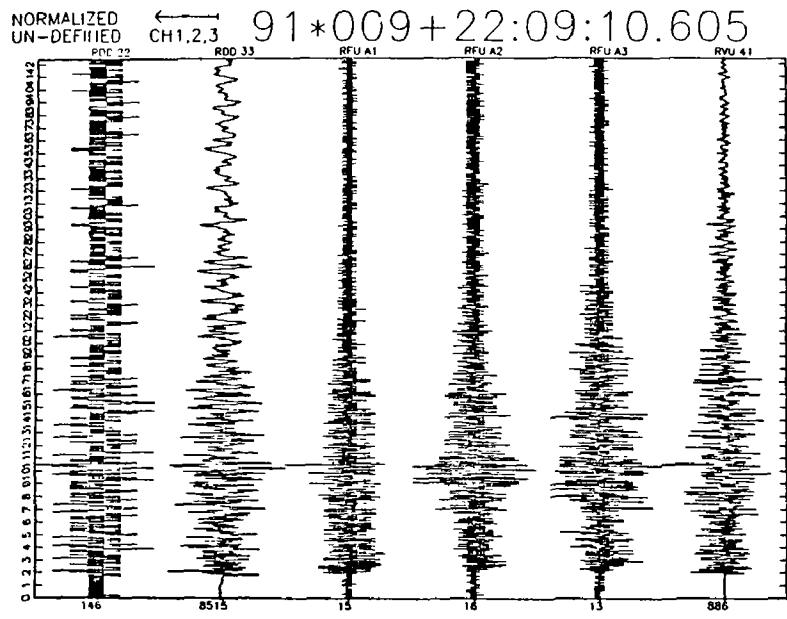


Figure 5

## Northern San Andreas Fault System

9910-03831

Robert D. Brown  
Branch of Engineering Seismology and Geology  
U.S. Geological Survey  
345 Middlefield Road, MS 977  
Menlo Park, California 94025  
(415) 329-5620

### Investigations

1. Synthesis studies of the geology, seismology, and tectonics of the San Andreas fault system, especially in northern California.
2. Advisory activities for Bay Area Regional Earthquake Preparedness Project (BAREPP) and San Francisco Bay Conservation and Development Commission (BCDC), both of which are state agencies.
3. Research and review of work by others on the tectonic setting and earthquake potential of Diablo Canyon power plant (DCPP), near San Luis Obispo, California. Activities were in an advisory capacity to the Nuclear Regulatory Commission (NRC) staff and were chiefly to review and evaluate data and interpretations obtained by Pacific Gas and Electric Company (PG&E) through its long-term seismic program.

### Results

1. Completed report reviewing geology, seismology, and tectonics near Diablo Canyon. This report was submitted to NRC in February, 1991, and was released as a part of NRC's Safety Evaluation Report, NUREG-0675, in June, 1991.
2. Completed chapter, with D. Hill and R. Wallace, on the San Andreas fault system. Chapter is planned for publication in a book, *The Geological Character of Active Fault zones*, edited by R. Bucknam and P. Hancock, and sponsored by the International Geological Correlation Program.
3. Evidence acquired from several onshore and offshore geologic investigations documents the structural complexity of the San Andreas fault in the northern San Francisco peninsula and Marin County. South of the Golden Gate, the predominantly strike-slip fault appears to dip westward and to possess a modest reverse-slip component of displacement. To the north, some of the strike-slip displacement west of the San Andreas fault may be accommodated by northward underthrusting along the onshore extension of the Point Reyes thrust fault in a region marked by extensive recent landsliding, overturned folds in stratified sedimentary rocks, and an anomalously thick middle and upper Miocene (Monterey Formation and younger) marine sequence.

## Reports

1. U.S. Geological Survey staff, 1991, Review of geological and geophysical interpretations contained in Pacific Gas and Electric Co. final report of the Diablo Canyon Long Term Seismic Program for the Diablo Canyon power plant--A report to the staff of the U.S. Nuclear Regulatory Commission *in* U. S. Nuclear Regulatory Commission, Safety evaluation report related to the operation of Diablo Canyon nuclear power plant, units 1 and 2, NUREG-0675, Supplement no. 34, Appendix C, 27 p.
2. Brown, Robert D., 1990, Quaternary deformation *in* Wallace, R. E., ed., The San Andreas fault system, California: U.S. Geological Survey Professional Paper 1515, p.83-113.
3. Brown, Robert D., 1991, Seismicity and geologic structure, San Francisco bay region, California [abst.]: Geological Society of America Abstracts with Programs, v. 23, no. 2, p. 9.

11/91

## PUGET SOUND PALEOSEISMICITY

9950-04484

ROBERT C. BUCKNAM  
U.S. Geological Survey  
M.S. 966, Federal Center  
Denver, Colorado 80225  
(303) 236-1604

### INVESTIGATIONS:

This project is aimed at defining the character, timing, and extent of an area of late Holocene (ca. 1,500 - 1,000 years ago) uplift in the central Puget Sound region, Washington.

Fieldwork during the reporting period was done at Alki Point (western Seattle), at a marsh near Winslow (Bainbridge Island), at Lynch Cove (Hood Canal near Belfair), and at Oakland Bay (near Shelton). The sites are shown on figure 1.

Paleontological analysis of plant macro and microfossils at sites under study by this project was initiated during the reporting period by Estella B. Leopold (Dept. of Botany, University of Washington). Changes in relative sea level as recorded in the strata of coastal marsh sequences is the primary basis for inferring prehistoric vertical deformation. The paleontological analyses will provide a rigorous basis for detailed interpretation of paleoecological conditions at the sites and permit development of detailed histories of relative sea level.

### RESULTS:

#### 1. *Minimum estimate of amount of uplift at Alki Point, western Seattle.*

In June 1991, an excavation for a new building provided a rare exposure of near surface stratigraphy at Alki Point, an area virtually completely covered by urban construction. Steeply dipping Tertiary siltstone of the Blakeley Formation is exposed near the site in the coastal intertidal zone and on a nearby steep hillslope. The excavation, which was studied with Brian Atwater (USGS), showed a planar surface (platform) sloping 4° seaward that was cut on fractured siltstone. The platform is overlain by about a meter of medium- to coarse-grained sand that is gravelly at the base. The highest point exposed on the planar bedrock surface is 4.3 meters above mean higher high water (MHHW), which is taken as a minimum measure of the amount of uplift at the site since the platform was cut.

The bedrock surface is interpreted to be a raised marine platform similar to that at Restoration Point, which is less than 5 km west of Alki Point and directly across Puget Sound. About 7 meters of uplift occurred at Restoration Point less than 1,550-1,350 years ago. No material suitable for radiocarbon dating was found in the excavation at Alki Point. However, the similar character of and proximity to the uplift at Restoration Point suggests that the raised platform at Alki Point is a result of the same tectonic event.

#### 2. *Cores collected from Winslow marsh.*

Two continuous 7.5 cm-diameter, 3-meter-long cores were collected in plastic pipe from a small coastal salt marsh near Winslow. Previous work has shown that the marsh was present when the 7 meter uplift occurred at Restoration Point, 5 km to the south. Preliminary study of the Winslow section indicates that any vertical displacement at the site was dramatically less

than that at Restoration Point. The cores were collected for paleontological and radiocarbon analysis to establish details of the relative sea level history at the site. The results will provide a basis for determining the deformation gradient associated with the uplift and, thus, give some insight into the structural controls of the deformation.

### 3. *Paleontological analysis of peat at Lynch Cove marsh.*

Peat containing abundant wood fragments and overlying material believed to be tideflat mud at Lynch Cove has previously been interpreted as evidence of abrupt uplift that raised the mudflat above tidal range and permitted the growth of freshwater plants. Radiocarbon data indicates that the uplift occurred about 1,230-980 years ago.

Preliminary study by Estella Leopold, assisted by Jill Suhy, of several samples of the peat overlying the mud at the Lynch Cove marsh shows that seeds of the heath family — *Vaccinium* (blueberry) or *Gaultheria* (salal), *Urtica* (nettle), Umbelliferae (*Angelica* type), Juncaceae (*Juncus* type), and Rosaceae (*Rubus* type) are abundant in the peat. The assemblage indicates that the peat formed in moist upland meadow and freshwater marsh environments, above tidal range. The contact at the base of the peat and its vertical relief indicates that the amount of uplift of the prehistoric tideflat was greater than 1.1 meters. The rise in relative sea level since the uplift has been at least 1.8 meters (1.5-1.8 mm/yr).

### 4. *Evidence for late Holocene uplift at Oakland Bay.*

Study of a coastal salt marsh at the head of Oakland Bay in the southwestern Puget Sound region shows a stratigraphic sequence similar to that at Lynch Cove. At the Oakland Bay site, dark fibrous peat abruptly overlies muddy silt and sand. Locally, roots of woody shrubs are preserved in the mud immediately below the peat. The basal 2 cm of the peat has a  $^{14}\text{C}$  age of 1,180-1,060 cal yr B.P. (tree ring calibrated years before present). It is likely that the section records the same uplift event as that at Lynch Cove or one closely spaced in time. Additional on-going field study and paleontological and radiocarbon analyses will clarify the timing and nature of deformation at the site.

Taken together, information collected through this project from sites in central Puget Sound indicate the presence of an area of uplift extending at least 60 km southwesterly from Alki Point at Seattle to Oakland Bay near the southeastern foot of the Olympic Mountains. The uplift occurred within the past 1,500-1,000 years, possibly as the result of a single event, with vertical displacements of as much as 7 meters.

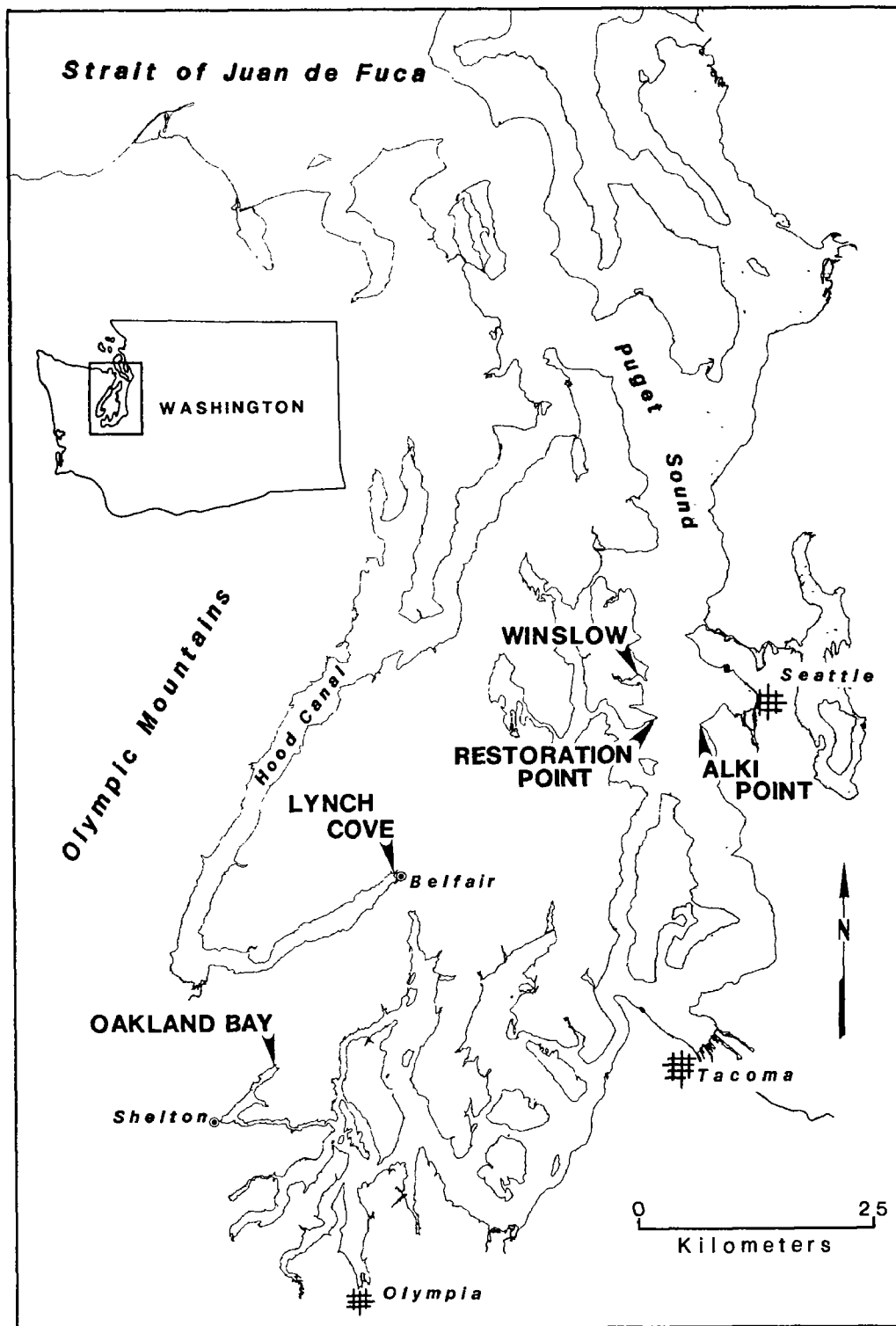


Figure 1. Map of Puget Sound region, Washington. Localities discussed in text labeled with arrows.



## Global Seismograph Network

9920-02398

Howell M. Butler  
Branch of Global Seismology and Geomagnetism  
U.S. Geological Survey  
Albuquerque Seismological Laboratory  
Building 10002, Kirtland AFB-East  
Albuquerque, New Mexico 87115  
(505) 844-4637

### Investigations

The Global Seismograph Network (GSN) presently consists of 7 SRO/ASRO, 9 DWSSN, 70 WWSSN, 6 IRIS-I, and 6 IRIS-2 type recording stations located in 58 countries and islands throughout the world. The primary objective of the project is to provide high-quality digital and analog seismic data for fundamental earthquake investigations and research, enhancing the United States capabilities to detect, locate and identify earthquakes and underground nuclear explosions in support of test ban issues. Technical and operational support is provided as funds permit to keep the GSN operating at the highest percentage of recording time possible. This support includes operational supplies, replacement parts, repair service, modifications of existing equipment, installation of systems and on-site maintenance, training and calibration. A service contract provides technicians to perform the support requirements as well as special projects such as on-site noise surveys, site preparations, and evaluation and testing of seismological and related instrumentation.

### On-site Station Installation/Maintenance

IRIS-2 seismograph systems were installed at Charters Towers, Australia (CTAO); Guam, Mariana Islands (GUMO); Kongsberg, Norway (KONO); and Toledo, Spain (TOL). Chiang Mai, Thailand (CHTO); College, Alaska (COL); Albuquerque, New Mexico (ANMO) and Guam, Mariana Islands (GUMO) required maintenance visits.

The systems located at Bogota, Colombia (BOCO); Bangui, Central African Republic (BACO); South Karori, New Zealand (SNZO); and Lembang, Indonesia (LEM) have discontinued operations and will remain inoperative until an IRIS or a GTSN system is installed.

### Results

The Global Seismograph Network continues with a combined total of 98 WWSSN/SRO/ASRO/DWSSN/IRIS-I/IRIS-2 stations. The main effort of this project, as funding permits, is to furnish the types of support at a level needed to keep the GSN at the highest percentage of operational time in order to provide the improved geographical coverage with analog and digital data from highly sensitive short-period and broadband seismic sensor seismograph systems.

## **Paleoseismicity of Kodiak Island Alaska**

Agreement No. 14-08-0001-G2121

Gary Carver - Geology Dept. Humboldt State University  
Arcata, CA 95521 (707) 826-3950

L. M. Gilpin - Earth Sciences University of California,  
Santa Cruz, CA 95064 (415) 383-0801

### **Field Work 1991**

We were in the field during the months of July and August 1991 and we plan to return in May or June 1992. Field work in the spring will enable us to observe more surficial features on the islands without the heavy late summer vegetation.

We completed a reconnaissance of the road system that crosses the NE end of the island and trends approximately parallel to the plate margin convergence direction. In addition, we visited sites further NW, toward the arc on the Shelikoff Strait side of the island. The most productive sites included Big Bay on Shuyak Island, Afognak River mouth on Afognak Island, and the Sturgeon River mouth near Karluk on the SW coast of Kodiak Island.

Collaboration with Rick and Philomena Knecht (Kodiak Area Native Association), archeologists studying historic and prehistoric cultural changes on the island, resulted in the identification of two uplifted paleo-lagoon surfaces along the road system. We hope to excavate for driftwood which would determine the ages of lagoon emergence. The following section is excerpted from our American Geophysical Union 1991 Fall Meeting Abstract.

### **Results**

The Kodiak archipelago subsided up to 2 meters along a NE-SW trending axis, as a result of the 1964 Ms 9.2 Aleutian Megathrust event. Evidence of earthquake events prior to the 1964 event allow us to constrain the long term crustal response to repeated great thrust earthquakes.

The orientation of the island and the intensely embayed coastline provide an excellent opportunity to document surface deformation with changes in the coastal datum.

During a transect of the NE part of Kodiak Island archipelago, perpendicular to the Aleutian Megathrust we found evidence for up to three paleoseismic events and long term ( $10^3$ yr BP) coastal tectonic movements indicative of combined coseismic and interseismic surface deformation.

Evidence for paleoseismic events is preserved in tidal marsh stratigraphy as sequences of salt water plant species (predominantly triglochin) overlying fresh water species (predominantly sphagnum) commonly with an intervening sand or fine gravel layer separating the two peat deposits.

Coastal geomorphic features indicative of long term ( $10^3$  yr BP) submergence were identified from the zone of maximum 1964 coseismic subsidence to the NW extent of our transect and include: (1) peat deposits with a succession of fresh to salt water affinity; (2) single, high beach barrier berms protecting small tidal lagoons; (3) the lack of extensive Holocene abrasion platforms; and, (4) river delta plain graded to present sea level lacking both entrenched tidal mouths and abandoned shoreline features. Long term ( $10^3$  yrs) tectonic subsidence reflects the dominance of coseismic deformation over interseismic rebound in the area arcward of the surface projection of the 1964 rupture zone.

Coastal geomorphic features indicative of long term emergence are constrained to the SE portion of the transect from the zone of maximum 1964 coseismic subsidence, SE to the shorelines closest to the trench. The evidence for emergence includes emergent lagoon and beach barrier berms, coastal embayments and, post-glacial shoreline deposits. Long term vertical tectonic uplift in a zone characterized by coseismic subsidence reflects the dominance of interseismic crustal rebound over coseismic deformation in the area of the surface projection of the fault rupture zone.

The tectonic setting, paleoseismic record, co- and interseismic deformation as inferred from geomorphic features and measured with pre- and post-1964 earthquake geodetic observations in

the Kodiak archipelago of the Eastern Aleutian arc, may provide insight to the Cascadia margin earthquakes.

### Radiocarbon Dating

Samples were collected from the exposed tidal banks where possible, however several samples were collected with a soil auger. The samples were air dried soon after collection. We submitted 10 samples to a commercial lab and will be submitting 20 more to the University of Washington Radiocarbon Lab. Results from the commercial lab will be available for a presentation at the 1991 Fall American Geophysical Union Meeting. The remaining dates will not be available for 6 months.

## **SEISMIC REFRACTION/REFLECTION INVESTIGATIONS IN THE S. F. BAY AREA**

<i>Project Number:</i>	<i>1-9930-02102</i>
<i>Investigator:</i>	<i>R. D. Catchings</i>
<i>Institution:</i>	<i>U.S. Geological Survey, OEVE 345 Middlefield Rd., MS 977 Menlo Park, CA 94025 FTS 459-4749; (415) 329-4749</i>

### **Investigations Undertaken**

In May 1991, the Crustal Studies group acquired a 200-km-long seismic refraction profile over the epicenter of the 1989 Loma Prieta (L. P.) earthquake, along the San Francisco (S. F.) and Marin Peninsulas. In addition, a perpendicular seismic reflection profile was recorded across the epicenter of the 1989 Loma Prieta earthquake epicenter. The objective of these investigations were to: (1) determine the velocity structure of the area around the L. P. earthquake epicenter, (2) determine the regional velocity structure (to be used in regional earthquakes), (3) investigate the role of critical-angle reflections in producing destruction in the S. F. Marina and Oakland areas, (4) provide an image of the crust beneath the epicenter of the 1989 L. P. earthquake, (5) determine some of the physical properties of the hypocentral region, and (6) investigate attenuation as a function of depth and distance,.

### **Results Obtained**

Data from the May 1991 seismic investigations have been collected and processed. Seismic records have been plotted to provide velocity and visual images of the crust within the L. P. fault zone (Fig. 1). The data are in the process of being analyzed and interpreted, but from the raw data, several observations are evident. (1) The Earth's crust beneath the epicenter of the L. P. earthquake is unusually high in velocity at shallow depths. (2) Regionally along the Peninsulas, the crustal velocity is also relatively high. The depth to the Moho is only about 20-22 km beneath the epicenter and varies laterally. (3) The S. F. Marina is at a critical distance from the L. P. epicenter where there is strong focussing of seismic energy. This suggests that the destruction in the Marina area may have been caused in part by strong reflected energy. Areas between S. F. and L. P. with similar types of soil were apparently not significantly affected. (4) Images of the crust show that there are strong reflectors at the approximate hypocentral depth of the 1989 L. P. earthquake.

These reflectors are not continuous laterally. (5) The hypocenter of the 1989 earthquake is apparently within a mafic or ultramafic layer. This has strong rheological implications, suggesting that the brittle part of the crust includes the lower crust or that there is more than one brittle layer in the crust.

These data are being compared with similar data from the New Madrid region and a comparison of attenuation for both regions will be made. This will help to predict the effects of a 7.1 magnitude earthquake in the New Madrid region.

#### Reports Published

Since these data are new, funds were not allocated for analysis, and the data are being analyzed on a part-time basis, no journal reports have been produced. However, an AGU abstract and presentation have been submitted. Published reports are expected during the coming year.

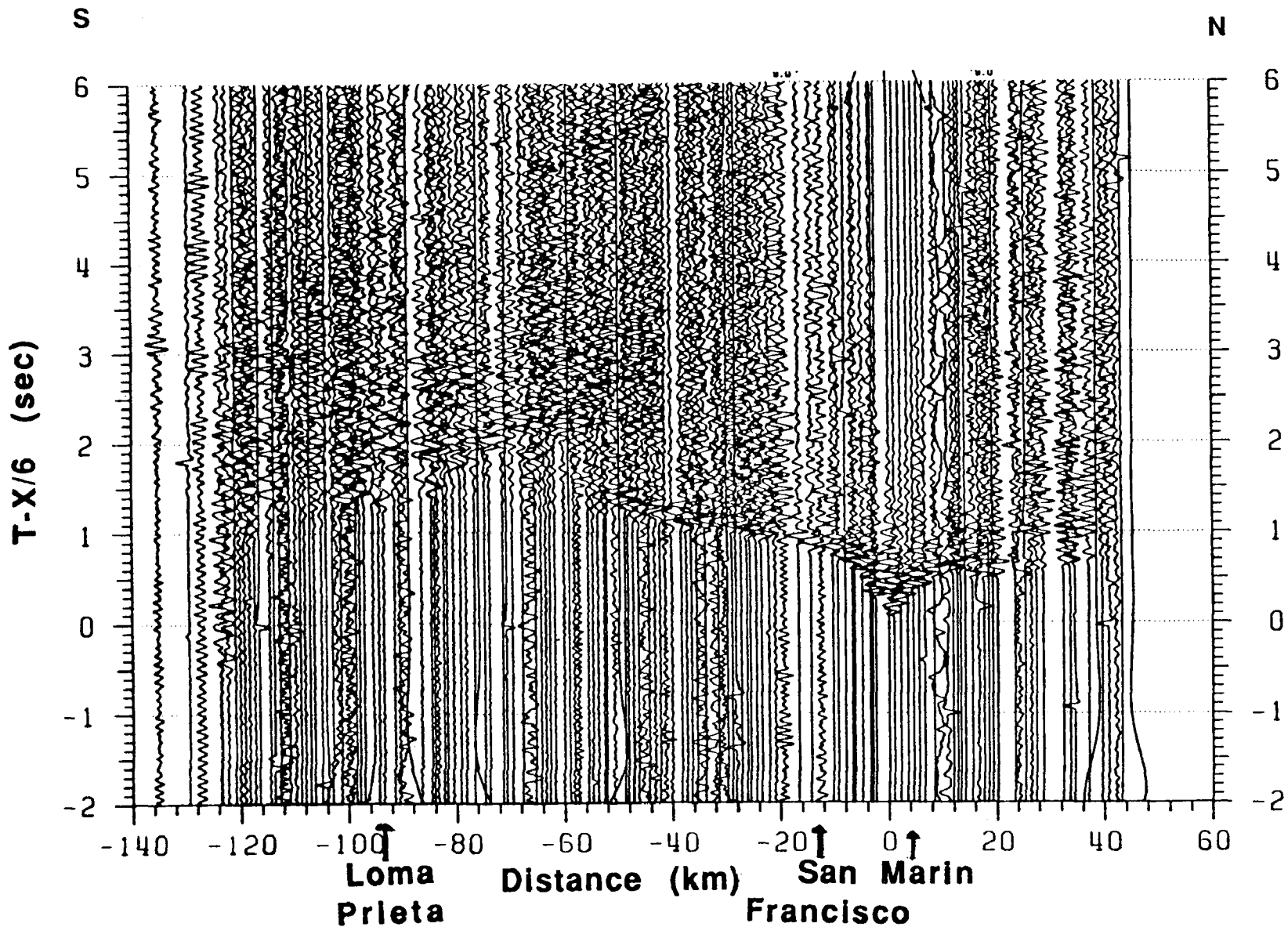


Fig. 1 (a) An unprocessed seismic shot gather from the refraction line along the San Francisco and Marin Peninsulas. This shot gather is the reversal of the approximate path from Loma Prieta to San Francisco. It shows that there are high-amplitude arrivals and an extended coda for reflections from crustal layers and the Moho. Such reflected, focussed energy may have accounted for the destruction in the S. F. Marina and Oakland areas during the 1989 earthquake while similar areas along the S. F. Peninsula were largely unaffected

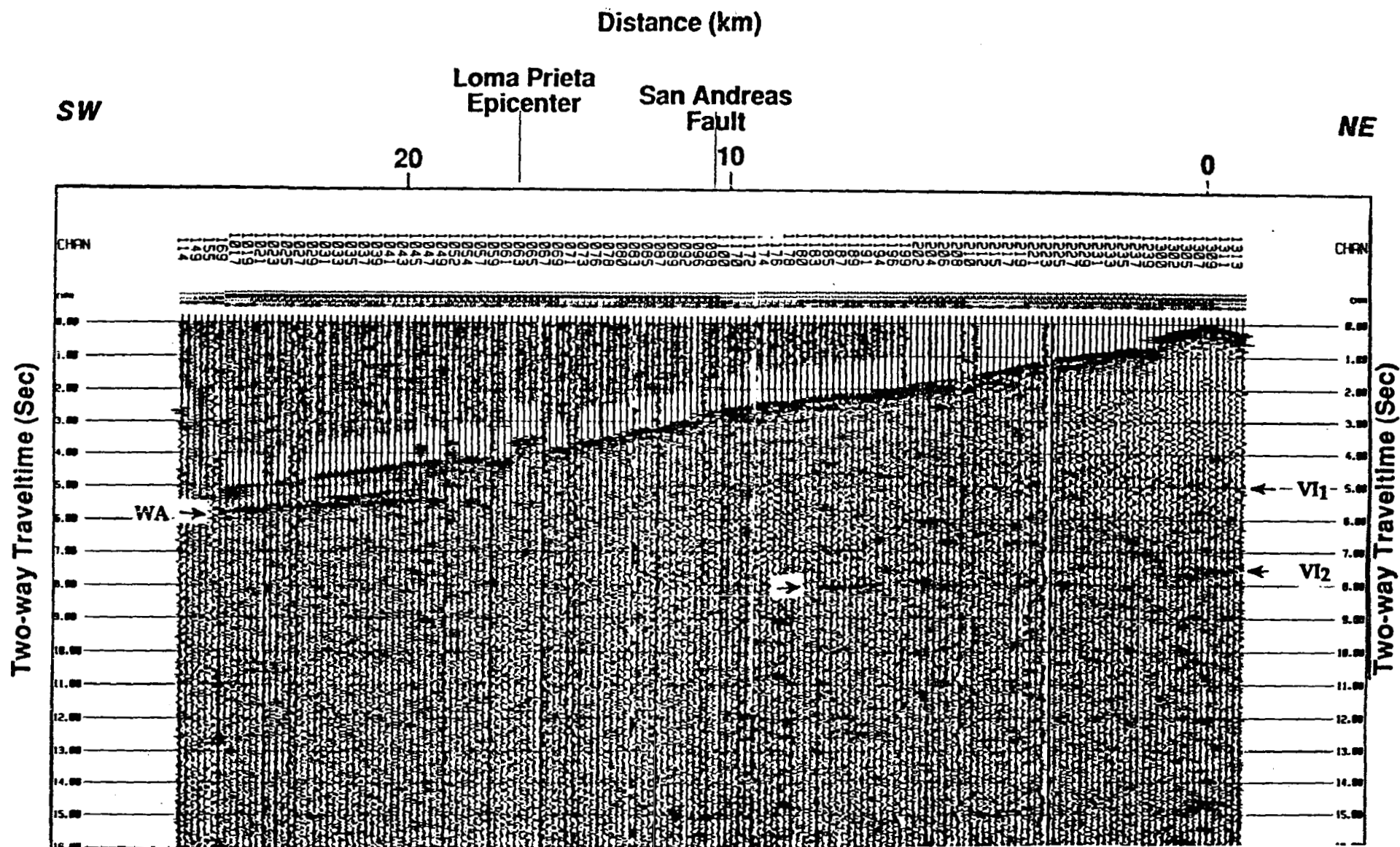


Fig. 1 (b) A reflection shot gather over the epicenter of the 1989 earthquake epicenter (total distance ~ 25 km). Reflectors between 5 and 10 seconds vary in strength, but some of the brighter reflectors are at the approximate depth of the 1989 earthquake hypocenter. These reflectors are being correlated with the refraction profiles in order to estimate gross compositions and improve the structural images.



## **INSTRUMENTATION OF STRUCTURES**

**9910-04099**

Mehmet Çelebi  
Branch of Engineering Seismology and Geology  
U.S. Geological Survey  
345 Middlefield Road, MS 977  
Menlo Park, California 94025  
415/329-5623 or FTS/459-5623

### Investigations

1. The process of selection of structures to recommended for strong-motion instrumentation has continued in Hawaii, Puget Sound (Seattle), Reno (Nevada), and Puerto Rico. This effort has also been extended to Salt Lake City.
2. The process to design instrumentation schemes has continued. Permits for a structure in Orange County, California, have been obtained. Permits for a structure in each of Orange County, California, Hawaii, and Seattle (Washington) have been obtained.
3. The process of implementation of instrumentation for those structures for which instrumentation schemes have been designed has been completed in Anchorage, Alaska, and Orange County, California. A base isolated structure in Los Angeles and in the Marina District of San Francisco have been permitted and instrumented. The strong-motion recording systems in these buildings are now operational. Also, permit efforts have been made for a structure in New Madrid area as a result of new EHRP funding.
4. Non-destructive dynamic testing of Salt Lake City and County Building is to be carried out progressively to evaluate the dynamic characteristics of the building before and after rehabilitated by base isolation.
5. The minimal instrumentation in a building in Alhambra, Southern California, has been upgraded to contain extensive instrumentation to acquire sufficient data to study complete response models of the building. A set of records is obtained during the Uplands earthquake. This will be compared with the Whittier (October 1, 1987) earthquake data which was code-type. Instrumentation at 575 Market Street, in San Francisco, California, has also been upgraded.
6. Agreements have been made with UCLA to convert the wind-monitoring system in the Theme Building in Los Angeles (previously financed by NSF) into a strong-motion monitoring system. Plans are being made to implement the conversion.

7. Studies of records obtained from instrumented structures are carried out. In particular, the records obtained during the October 21, 1987 Whittier Narrows earthquake from 1100 Wilshire Finance Building (Los Angeles), the Bechtel Building (Norwalk), and the Santa Ana River Bridge (base-isolated) are being investigated. Data obtained during the October 17, 1989 Loma Prieta earthquake from the Transamerica Building (San Francisco) and Pacific Park Plaza Building (Emeryville) have been studied.
8. Studies of records obtained from instrumented structures during the October 17, 1989, Loma Prieta earthquake are carried out. In particular, Transamerica Building in San Francisco and Pacific Park Plaza in Emeryville have been investigated. Papers are prepared.
9. Cooperative project with NIST on low-level amplitude tests of instrumented structures carried out.

### Results

1. The Hawaii Committee on strong-motion instrumentation of structures has completed its deliberations and a draft report is being prepared.
2. As final report of the Puget Sound (Seattle) advisory committee for strong-motion instrumentation has been completed.
3. Papers resulting from study of records obtained from structures are prepared.
4. An invited talk given on "Responses of structures during the Loma Prieta earthquake" at ASCE Structures Congress in San Francisco, California (November, 1990).
5. Invited talk on "Response of structures during the Loma Prieta earthquake" at ASCE Structures Congress in Indianapolis, Indiana (April, 1991).
6. Invited talk in Golden, Colorado (march 1991), "Researches on Strong-Motion Records from Instrumented Structures."

### Reports

- Çelebi, M., Şafek, E., and Youssef, N., 1991, Torsional response of a unique building: ASCE, STD, May 1991.
- Çelebi, M., and Şafak, E., 1991, Recorded seismic response of Transamerica Building—Part I: Data and preliminary analysis: ASCE, August 1991.
- Şafak, E., and Çelebi, M., 1991, Recorded seismic response of Transamerica Building—Part II: System identification: ASCE, August 1991.

- Çelebi, M., and Şafak, E., 1991, Recorded seismic response of Pacific Park Plaza—Part I: Data and preliminary analysis: in print, ASCE.
- Marshall, R.D., Phan, L.T., and Çelebi, M., 1990, Measurement of structural response characteristics of full-scale buildings: Selection of structures: U.S. Geological Survey Open-File Report 90-667. [Also Interagency NIST Report.]
- Şafak, E., and Çelebi, M., 1990, Recorded seismic response of Pacific Park Plaza—Part II: System identification: in print, ASCE.
- Çelebi, M., and Şafak, E., 1991, Recorded responses of two tall buildings during the 10/17/89 Loma Prieta (California) earthquake: ASCE Structures Congress, April 29-May, 1991, Indianapolis, Indiana, invited paper.
- Şafak, E., and Çelebi, M., 1991, Analyses of recorded responses of two high-rise buildings to Loma Prieta mainshock: Bulletin of the Seismological Society of America.
- Çelebi, M., Phan, L.T., and Marshall, R.D., 1991, Comparison of responses of a select number of buildings to the 10/17/89 Loma Prieta (California) earthquake and low-level amplitude test results: UJNR Proceedings, May 1991.
- Çelebi, M., Phan, L.T., and Marshall, R.D., 1991, Dynamic characteristics of five buildings determined from their response to the 10/17/1989 Loma Prieta (California) earthquake and low-level amplitude tests: in review, ASCE, 1991.
- Çelebi, M., 1991, Coherency of free-field motions near a structure—a case study: (invited paper) ASCE Structures Congress, April, 1991.

## LATE QUATERNARY SLIP RATES ON ACTIVE FAULTS OF CALIFORNIA

**9910-03554**

Malcolm M. Clark  
Branch of Engineering, Seismology and Geology  
U.S. Geological Survey  
345 Middlefield Road, MS 977  
Menlo Park, California 94025  
415/329-5624 or FTS/459-5624

### Investigations

1. Recently active traces of the Calaveras fault zone at Tres Pinos and San Felipe Creeks, California (K.J.Kendrick, J.W. Harden, M.M. Clark).
2. Recently active traces of Owens Valley fault zone, California (Sarah Beanland (NZGS), Clark).
3. Degradation of fluvial terrace risers along Lone Pine Creek, San Bernardino County (Kendrick, in conjunction with J.B.J. Harrison, L.D. McFadden (UNM), and R.J. Weldon (University of Oregon)).
4. Revision of slip-rate table and map of late Quaternary faults of California (Clark, Kendrick, J.J. Lienkaemper, K.R. Lajoie, C.S. Prentice, M.J. Rymer, D.P. Schwartz, R.V. Sharp, J.D. Sims, J.C. Tinsley, R.J. Weldon).
5. Late Quaternary evolution of the San Timoteo Badlands region, southern California (Kendrick, in conjunction with D.M. Morton and L.D. McFadden).

### Results

2. The right-lateral Owens Valley fault zone extends  $100 \pm 10$  km from near the northwestern edge of Owens Lake through Big Pine. It passes through Lone Pine near the eastern base of the Alabama Hills and the follows the floor of Owens Valley northward to Poverty Hills, where it steps 3 km left and continues northwest across Crater Mountain to Big Pine. The fault has an overall strike of N20W and a dip of  $85 \pm 10$  degrees ENE. Surface Ruptures associated with the 1872 earthquake occurred along the whole length of the fault zone. The right lateral component of offset in 1872 averaged  $6 \pm 2$  m and reached a maximum of 10 m at Lone Pine, whereas the subordinate vertical component, normal, was  $1 \pm 0.5$  m and variable in sense. Average and maximum net slip values of  $6.1 \pm 2.1$  m and 11 m indicate a seismic moment of 1.8 to  $4.4 \times 10^{27}$  dyne cm. The associated moment magnitude is 7.5-7.7, slightly lower than previous estimates.

Data from one site suggest an average slip rate for the Owens Valley fault zone since 300 ka of  $1.5 \pm 1$  mm/yr. Data from several other sites indicate an average Holocene slip rate of  $2 \pm 1$  mm/yr. Owens Valley fault zone apparently experienced three Holocene earthquakes. At the Lone Pine fault the minimum average recurrence interval is 5 ky, whereas elsewhere in the Owens Valley fault zone it is 3.3-5 ky. None of these paleoearthquakes is dated, so an average recurrence interval need not apply. The Owens Valley fault zone did, however, appear to generate approximately equal (characteristic) amounts of displacement in each Holocene earthquake.

The Owens Valley Fault zone apparently accommodates some of the relative motion between the North American and Pacific plates along a discrete structure. This dextral shear occurs within the dominantly normal Basin and Range province, although within its Walker Lane Belt, which includes other strike-slip faults. In Owens Valley strike slip and normal faulting are to a large degree partitioned between the Owens Valley and the subparallel and purely normal Independence Faults. The Holocene dip-slip rate along the Independence Fault is about one-tenth the Holocene strike slip rate along the Owens Valley fault. Contemporary activity on faults of such contrasting styles suggests large temporal fluctuations in the relative magnitudes of the maximum and intermediate principal stresses, while the extension direction remains consistently east-west.

3. Fluvial terrace risers along Lone Pine Creek provide an excellent opportunity to evaluate the current models of scarp degradation. These terraces are relatively well-dated, are formed in similar parent material, and the initial angles of the associated risers can be inferred due to their mode of formation. Thirty four slope profiles were measured on the terrace risers between six terraces. These profiles were coordinated with the description and analysis of degree of soil development. This provided the opportunity to compare the sediment erosion and transportation, as predicted by the scarp degradation model, with the actual accumulation and stripping of the soil profiles. The model generally predicts this accurately, though the upper parts of the slope, which would be expected to experience stripping, have accumulated eolian fines.

The soil development on the slopes was compared to the soils of the same age on the lower terrace. These soils are experiencing the same soil forming factors (time, parent material, climate, vegetation, *etc.*), with the exception that the soils on the slope are affected by the slope degradation processes. The variability of soil development is greater on the flat-lying, stable surface of the lower terrace than it is for the soils associated with the terrace riser. The variability of the soil development along the terrace riser is less than the variability of predicted model ages from the non-linear scarp degradation model of Hanks and Andrews (1990), suggesting that the variability is inherent in the model, and represents the method uncertainty. The evaluation of both the scarp-degradation models and the use of soils on slopes is critical because both are being employed to assess seismic hazard. This study attempts to combine these two approaches in order to understand the benefits and limitations of both.

4. We are in the process of revising, updating, and publishing (as a USGS Bulletin) the slip-rate table and map of late-Quaternary faults of California (USGS OFR 84-106). Our aim is to review all entries in OFR 84-106 and add all new data generated since its release. We welcome any relevant unpublished data from workers in this field.
5. Kendrick has mapped Quaternary units and described twenty soils in San Timoteo and Reche Canyons, San Bernardino and Riverside Counties. Three surfaces and two paleosurfaces have been defined in San Timoteo Canyon, and one major, complex surface is recognized in Reche Canyon. The soils are helpful in determining the effect of the adjacent San Jacinto Fault on the patterns of aggradation and erosion on the two canyons. The soils are being compared to regional soils described by L.D. McFadden, including the Cajon Pass chronosequence described by McFadden and Weldon. Preliminary analysis indicates that these soils are similar to those at Cajon Pass, only 40 km to the northwest, though eolian input is less. The deformation of the paleosurfaces is being measured using altimeters and drilling, and will define the long-term activity of the fault.

### Reports

None this reporting period.

# LATE CENOZOIC DEFORMATION OF THE NORTHERN CALIFORNIA-SOUTHERN OREGON CONVERGENT MARGIN

9460-11031

by

Samuel H. Clarke, Jr<sup>1</sup>, and Gary A. Carver<sup>2</sup>

<sup>1</sup>Branch of Pacific Marine Geology  
U.S. Geological Survey  
345 Middlefield Road, MS-999  
Menlo Park, California 94025  
(415) 354-3091 - FTS 459-3091

<sup>2</sup>Department of Geology  
Humboldt State University  
Arcata, California 95521  
(707) 826-3950

## **Investigations**

Principal research objectives are to characterize the late Cenozoic structural architecture and tectonic history, to document the history of late Holocene paleoseismicity, and to determine the seismic potential of the southern Cascadia subduction zone (SCSZ) of central-southern Oregon and northern California. These studies are of particular importance to an understanding of Cascadia subduction zone tectonics because only in this region does the active accretionary fold and thrust belt overlying the subduction zone extend onland (fig. 1). The unique geometry of the convergent margin in the SCSZ thus allows 3-dimensional offshore seismic-reflection studies of accretionary margin structure and the relationship of this structure to the subduction zone to be linked directly with detailed studies on land of the deformational styles and rates, and paleoseismic histories of the principal seismogenic structures.

Seismic-reflection studies of offshore northern California and southern Oregon show that the SCSZ is dominated by northwest- to north-northwest-trending, west-verging thrust and reverse faults (and related folds) that form imbricate thrust fans (fig. 1). Many faults merge downward into sole thrusts that extend to or near the Gorda-North America plate interface. This compressive deformation expresses Gorda-North America plate convergence, strong interplate coupling, and contraction across the North America plate margin. Deformation and paleoseismicity associated with two of the principal thrust systems, the Mad River and Little Salmon fault zones (fig. 1), have been extensively studied on land in the Arcata, California, area. Two faults in the Mad River fault zone (MKF and MRF, fig. 1) record eight coseismic slip events averaging 3.5 m of dip slip per event during late Pleistocene and Holocene time. The Little Salmon fault zone (LSF, fig. 1) has experienced at least three slip events of as much as 4.5 to 6.5 m per event at intervals ranging from 300 to 560 years during the past 1,700 years. The most recent event occurred about 300 y BP. At the Mad River Slough and Clam Beach (MRS and CB, fig. 1), as many as 4 or 5 episodes of sudden, coseismic subsidence and uplift are recorded by buried marsh peats and fossil forests and by uplifted late Holocene marine terraces. <sup>14</sup>C dates suggest that these fault offset, subsidence and uplift events were synchronous (within the range of <sup>14</sup>C age uncertainty). The Little Salmon fault zone, onshore and offshore, is about 100 km long and relationships between rupture area and magnitude indicate that these events, if of local origin, had magnitudes of about 7.8. However, it is probable that these events actually reflect episodic deep subduction earthquakes and that magnitudes were much greater.

Work conducted during the past year was directed at expanding knowledge of the tectonic framework and Quaternary structure of the region between Coos Bay, Oregon, and Eureka, California, and of the coseismic deformation history of major structures of the southern Cascadia folded thrust belt, and at using these and related data to estimate the breadth of the coupled and

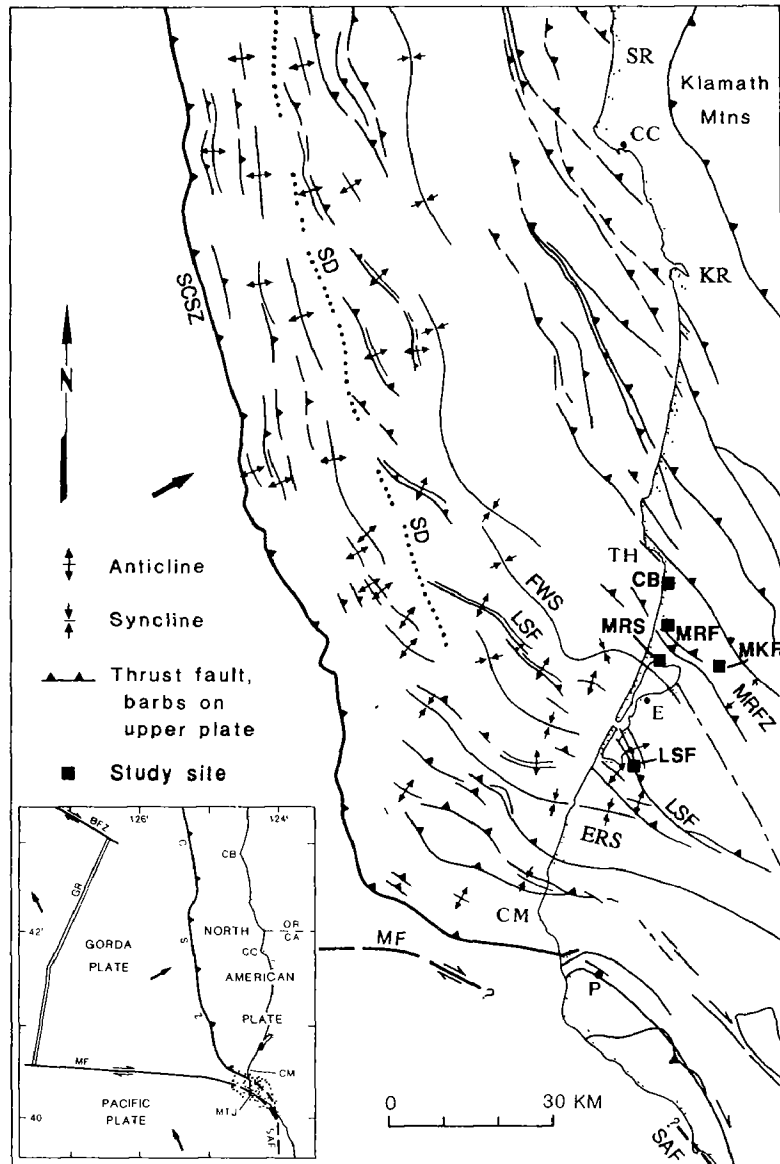


Figure 1. Plate tectonic setting of the northwestern California continental margin. Arrows indicate oceanic-plate motions relative to North American plate. Barbed line shows the base of the continental slope--the approximate boundary between the Gorda and North American plates. Half arrows on inset map indicate relative motions along the Blanco fracture zone and the Mendocino fault. Abbreviations are as follows: Locations, CB = Cape Blanco; CC = Crescent City; CM = Cape Mendocino; E = Eureka; KR = Klamath River; SR = Smith River; TH = Trinidad Head. Structural features, BFZ = Blanco fracture zone; CSZ = Cascadia subduction zone; ERS = Eel River syncline; GR = Gorda Ridge; LSF = Little Salmon fault; MF = Mendocino fault; MRFZ = Mad River fault zone; MTJ = area of Mendocino triple junction; SAF = San Andreas fault; SCSZ = Southern Cascadia subduction zone; SD (heavy dotted line) = Structural discontinuity mentioned in text. Study sites, CS = Clam Beach; LSF = Little Salmon fault; MKF McKinleyville fault; MRF = Mad River fault; MRS = Mad River Slough.



presumably seismogenic part of the Gorda-North America plate interface and the likely magnitudes of paleoseismic events in the SCSZ.

## **Results**

### **1. *Structure and late Cenozoic tectonic framework between Crescent City, California, and Coos Bay, Oregon.***

In northern California, the Franciscan Central and Coastal belts are separated by a pre-Miocene suture—the Coastal belt fault—that extends seaward near Arcata (fig. 2). North of Cape Blanco, Oregon, the Siletz River Volcanics and Fulmar terrane are similarly separated by a lengthy late Eocene or Oligocene suture, the Fulmar fault (Snively, 1987). The Fulmar fault lies mostly offshore but extends onland south of Coos Bay. Varied permissive evidence suggests that the Fulmar terrane and Franciscan Coastal belt are correlative. If so, the Fulmar fault and Coastal belt fault originated as a simple north-trending colinear suture marking a late Eocene or Oligocene accretionary event that affected most of the northern California-Oregon margin. As such, it would provide a valuable structural piercing point throughout this region; study of the manner in which this suture has been disrupted by younger faulting would yield critical and definitive evidence concerning the Neogene tectonic history of the region.

We have mapped the Coastal belt fault offshore northward to the extended California-Oregon border, and Snively<sup>1</sup> has mapped the Fulmar fault southward to south of Coos Bay. Alternate hypotheses exist concerning fault location in the intervening region of southern Oregon between 42°N and 43°N (fig. 2). The Coastal belt fault may parallel the coastline offshore, as suggested by regional aeromagnetic data, or it may join the onland Whalehead fault, which forms the eastern boundary of the allochthonous Gold Beach terrane in southern Oregon. The latter alternative has a significant neotectonic implication—that the Crescent City platform is underlain by a series of youthful duplexed thrust sheets.

Field reconnaissance and reexamination of offshore seismic-reflection and aeromagnetic data from southern Oregon suggest, but do not establish, that the Coastal belt and Whalehead faults join offshore southern Oregon. Coordinated onshore and offshore studies may be required to wholly resolve this issue, which is critical to the completion of work to determine the regional neotectonic fabric of the northern California-Oregon margin. Critical gaps in offshore seismic-reflection data coverage in southern Oregon between about 42°N (California-Oregon border) and 42°50'N (Cape Blanco), especially inshore, and the lack of aeromagnetic data from offshore northern California hamper onshore-offshore correlations in a structurally complex area. These gaps may be filled in FY 93 or later in conjunction with offshore EDGE/DCS studies of this region, coupled with small boat high-resolution seismic-reflection profiling in nearshore areas. Continued field study of this region and interpretation of a small number of newly acquired industry seismic-reflection lines is planned for the current year.

---

<sup>1</sup>Snively, P.D., Jr., 1987, Tertiary geologic framework, neotectonics, and petroleum potential of the Oregon-Washington continental margin, in Scholl, D.W., Grantz, A., and Vedder, J.G., eds., *Geology and resource potential of the continental margin of western North America and adjacent ocean basins-Beaufort Sea to Baja California: Circum-Pacific Council for Energy and Mineral Resources, Earth Science Series*, v. 6, p. 305-335.

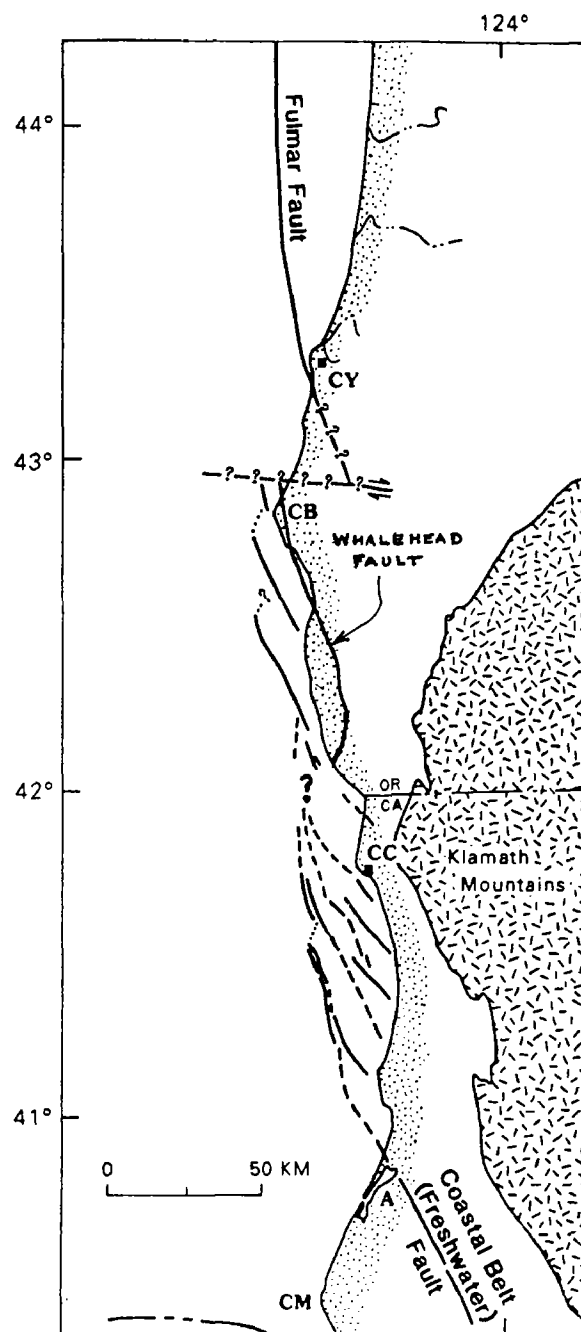


Figure 2. Sketch map showing postulated extension of the Coastal belt (Freshwater) fault from near Arcata, California, to the central Oregon offshore. Locations: A - Arcata; CB - Cape Blanco; CC - Crescent City; CM - Cape Mendocino; CY - Coos Bay. Fulmar terrane lies west of the Fulmar fault in the Oregon offshore north of Cape Blanco. Franciscan Coastal belt lies west of the Coastal belt fault on land and offshore in the vicinity of Arcata, California.

2. *Previously unmapped faulting onland in the Patricks Point-Crescent City area, northern California.*

Many structures mapped from offshore seismic-reflection data project landward between Patricks Point, California, and the California-Oregon border (fig. 1). These structures are suggested on land by up-to-the-east steps in accordant ridge summits, deformed marine terrace deposits and geomorphic lineaments, but remain largely unstudied because they lie principally in forested, landslide-prone and extensively sheared Franciscan bedrock.

Field reconnaissance in the coastal segment south of Crescent City has produced evidence that at least four thrust faults cut the coast in the vicinity of the Klamath River. Although the faults were not exposed in densely vegetated areas, apparent vertical separations of the base of the Pleistocene Gold Bluffs sediments are generally <90 m, suggesting that the large fault systems mapped offshore have considerably reduced vertical separations landward along the eastern margin of the southern Cascadia fold and thrust belt. This observation, that the fold and thrust belt dies out eastward, is consistent with seismicity data from the Eureka to Cape Mendocino area that show an eastward decrease in North America plate seismicity associated with Gorda plate convergence (McPherson<sup>2</sup>).

Field reconnaissance in the Crescent City-Smith River area indicates that the complex system of thrust, back thrusts, and fault-related folds offshore is represented on land by marine-terrace deformation similar to that mapped farther south in the Humboldt-Arcata Bay area near Eureka. Marine-terrace deposits (thought to be 83 to 130+ ka) have been tilted and warped across broad folds that probably overlie buried thrust tips. It is probable that soil chronosequences can be developed and dated in the Crescent City area, and that these data can be used to establish Quaternary terrace deformation styles and rates. In addition, coring in the axis of a prominent northwest-trending syncline north of Crescent City is likely to yield high-marsh peats and intertidal mud sequences that record late Pleistocene coseismic subsidence events.

3. *Late Holocene subsidence history of the Eel River syncline.*

Displaced dated soil horizons together with dated evidence of coseismic uplift and subsidence have established the paleoseismic history of the 100-km-long Little Salmon fault (LSF, fig. 1)—the principal thrust fault of the SCSZ. Three Little Salmon fault offsets have been dated, the most recent at about 300 y BP. Determination that a separate major structure—the Eel River syncline—moved synchronously with the Little Salmon fault during one or more of these events would strengthen arguments that the Little Salmon deformation involved multiple major structures and that it records intermittent slip on the underlying SCSZ megathrust.

Reconnaissance mapping (by hand-auger coring) of late Holocene coastal environments in the Eel River delta along the axis of the Eel River syncline (fig. 1) was conducted by Wen Hao Li of Humboldt State University. At least two peats representing former high-marsh surfaces were widely encountered. The uppermost buried peat has yielded a tentative <sup>14</sup>C age of about 290 y BP, suggesting that this event was synchronous (within the range of <sup>14</sup>C age resolution) with the youngest event associated with the Little Salmon fault, thus supporting the thesis that the Little Salmon events reflect SCSZ megathrust displacements at depth. Vibracoring to obtain undisturbed 3" cores for microstratigraphic, micro-paleontologic, and paleobotanic study was subsequently carried out along two north-south traverses across the flanks of the syncline, and several suitable cores were collected.

---

<sup>2</sup>McPherson, R.C., 1989, Seismicity and focal mechanisms near Cape Mendocino, northern California, 1974-1984, MS thesis, Humboldt State University, 75 p.

Study of these cores, presently underway, should also help establish both short-term subsidence and interseismic uplift rates of the Eel River syncline. Extrapolated offshore, this information can be combined with known rates of deformation on the major thrust systems to produce an actualistic, three-dimensional model of sudden seafloor deformation leading to tsunami generation in this region.

4. *Breadth of the coupled zone between the Gorda and North America plates, and implications for paleoseismic magnitudes.*

The absence of historic (~ 200 years) subduction-related earthquakes along the southern Cascadia subduction zone together with clear evidence of late Quaternary convergence-related compressive deformation of the northern California margin supports the conclusion that the Gorda and North America plates are coupled, or "locked," across the SCSZ megathrust. This conclusion is bolstered by evidence of episodic large late Holocene earthquakes derived from studies of coseismic deformation in near coastal Washington, Oregon and northern California. Determination of the area of the coupled zone, the zone over which elastic strain is stored and released, is fundamental to the estimation of the magnitudes of past seismic events in this region. Evidence from the SCSZ suggests that the breadth of the coupled zone is 70-80 km, and permits estimates of magnitudes to be made using various rupture-length scenarios.

The west edge of the coupled zone is determined by the coincidence of: (a) a discontinuity in the trends of youthful structures on the outer margin of northern California (SD, Fig.1). Folds and thrust faults west of this discontinuity trend N to NNW, parallel to the CSZ deformation front and non-orthogonal to the direction of Gorda plate convergence. Structures east of the discontinuity trend NW to NNW, approximately orthogonal to the direction of plate convergence. This discontinuity is interpreted as the boundary between, to the west, young relatively water-saturated offscraped Gorda plate cover sediment that lacks the strength to deform brittly and, to the east, the older, thickened part of the accretionary wedge that has acquired sufficient strength to transfer compressional stress from the subducting plate, to which it is coupled, upward through the overlying strata. (b) the approximate western limit of shallow, compressive North American plate seismicity. The region west of the discontinuity is essentially aseismic, consistent with decoupling, whereas the region to the east is seismic, consistent with coupling to Gorda plate.

The east edge of the coupled zone is less sharply defined, but is determined by the approximate coincidence of: (a) the eastern margin of the fold-and-thrust belt that is orthogonal to Gorda plate convergence and that is believed to express in interplate coupling; (b) a bend in the subducted Gorda plate (determined from seismicity data) at which the plate dip increases from  $10^{\circ}$  -  $11^{\circ}$  (to the west) to about  $25^{\circ}$  (to the east) (fig. 3); and (c) the eastern extent of compressive seismicity at or near the Gorda-North American plate interface. North America plate seismicity to the west is compressional and is believed to express interplate coupling. Seismicity to the east is tensional, and is believed to be associated with normal faulting in the sinking Gorda slab.

The western edge of the coupled zone (i.e. the structural discontinuity) lies about 20 km landward of the CSZ deformation front in northern California (Fig. 1), and the eastern edge of the zone is about 90 + km landward of deformation front. Thus, the coupled zone averages about 70-80 km in breadth in this region. Depths to the coupled zone range from about 6 1/2 km on the west to about 20 km on the east.

Various scenarios concerning rupture length can be proposed. If one presumes the CSZ to be segmented, and the southern CSZ (between the Blanco transform fault and the Mendocino triple junction) to act independently of the rest of the CSZ, the length of the southern segment

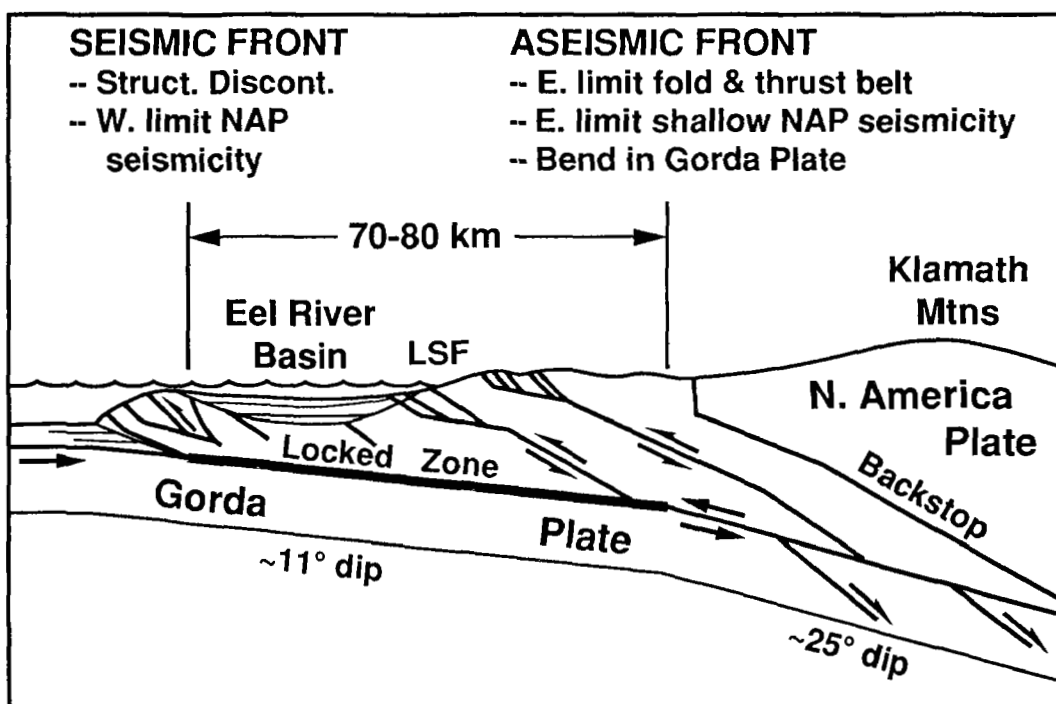


Figure 3. Sketch showing breadth of zone of Gorda-North America plate coupling off northern California.

of the CSZ is about 240 km. The resulting rupture area would be about 17,000 - 19,000 km<sup>2</sup>, and would yield an earthquake magnitude of about 8.4.

While possible, this scenario suffers from the observation that subduction zone earthquake sequences elsewhere in the world commonly propagate across apparent structural boundaries, such as the Blanco fault, in the downgoing plate. If the events recorded in Washington and northern California prove to be synchronous, then a much greater length, perhaps 900 km or more, of the CSZ may have ruptured in a single event in the past. If the breadth of the coupled zone remains about 70-80 km throughout the Oregon and Washington margin, the resulting rupture area would be 63,000 - 72,000 km<sup>2</sup> or larger, and the corresponding magnitude would be about 9, or greater. While this scenario is speculative, it is not contraindicated by the data now available.

### **Reports**

- Clarke, S.H., Jr., 1990, Map showing geologic structures of the northern California continental margin, *U.S. Geological Survey Miscellaneous Field Studies Map*, MF 2130, scale: 1:250,000, with interpretive text.
- Clarke, S.H., Jr., in press, Geology of the Eel River basin and adjacent region: Implications for late Cenozoic tectonics of the southern Cascadia subduction zone and Mendocino triple junction, *American Association of Petroleum Geologists Bulletin*, 53 p., 10 figs.
- Clarke, S.H., Jr., and G.A. Carver, in press, Late Holocene tectonics and paleoseismicity, southern Cascadia subduction zone, *Science*, 15 p., 5 figs.
- Snively, P.D., and R.E. Wells, 1991, Cenozoic evolution of the continental margin of Oregon and Washington, *U.S. Geological Survey Open-File Report* 91-441B, 34 p.

## Partial Support of Joint USGS-CALTECH Southern California Seismographic Network

#14-08-0001-A0613

Robert W. Clayton  
Egill Hauksson

Seismological Laboratory,  
California Institute of Technology  
Pasadena, CA 91125 (818-356-6954)

### INVESTIGATIONS

This Cooperative Agreement provides partial support for the joint USGS-Caltech Southern California Seismographic Network. The purpose is to record and analyze data from more than 10,000 local earthquakes every year and generate a data base of phase data and digital seismograms. The primary product derived from the data base is a joint USGS-Caltech catalog of earthquakes in the southern California region. We also provide rapid response to media and public inquiries about earthquakes.

For more detailed information about data access, please contact:

Dr. Kate Hutton at (818)-356-6959;  
or with E-mail: [kate@bombay.gps.caltech.edu](mailto:kate@bombay.gps.caltech.edu).

### RESULTS

#### Network Operation

*Southern California Seismographic Network.* The SCSN has 220 remote sites (with 300 components) and gathers data from local, regional and teleseismic earthquakes. These data are used for earthquake hazards reduction as well as for basic scientific research. The earthquake hazards reduction effort has become more important as moderate-sized earthquakes continue to occur within densely populated areas in southern California. The last damaging earthquake to occur was the ( $M_L=5.8$ ) Sierra Madre earthquake of 28 June 1991, located 20 km northeast of Pasadena. It caused over \$40 million in damage.

The average rate of 15 publications per year over the last 10 years using the network data illustrates the strength of the ongoing research activities that use the network data. Continued efforts to improve data quality and accessibility have created the arguably best regional earthquake data base in the world. The ongoing upgrading of the quality of the waveforms recorded by the short-period network and the addition of low-gain seismometers and accelerometers provide numerous new avenues of research. Most important of these is analysis of on-scale waveforms to determine source, path and site effects.

The USGS operates most of the remote stations in the SCSN. Caltech operates: 1) 24 short period telemetered stations; 2) 7 stations with local photographic recording of Wood-Anderson seismometers; and 3) 5 very broadband TERRAscope stations; in 1992 we plan to install 10 more TERRAscope stations. Caltech also maintains drum recorders and other equipment at the central site located in the Seismological Laboratory at Caltech.

The computer equipment at the central site is being upgraded and a switch-over to the new computers is planned in January 1992. The SCSN data will be recorded by two microVAX-III computers and the data processing will be done on three VAX workstations

using a VAX-4000 as a central server. The operation of this equipment is shared by Caltech and USGS personnel. To avoid duplication, software development is done in cooperation with the USGS in Menlo Park.

More than 10,000 earthquakes are entered into the southern California earthquake catalog every year. Approximately 1.0-1.5 Mbytes of phase data and 10-15 Gbytes of seismograms are archived every year. In addition to the data analysis we carry out software maintenance, hardware maintenance and other tasks necessary to complete the catalog. Caltech and USGS maintain a data base that includes: 1) earthquake catalog (1932-present); 2) phase data (1932-present); 3) photographic paper seismograms (1930-present); and 4) digital seismograms (1977-present). The earthquake catalog (1932-present) and phase data (1960-present) are available via dial-up and over INTERNET. Other data are available upon request. This data base is being made available to the DC/SCEC and will be the most voluminous part of the data stored in the DC/SCEC.

Near real-time reporting to USGS in Reston and the Governor's Office of Emergency Services and other response to any felt or damaging earthquake activity is provided by network personnel.

*The Data Center of the Southern California Earthquake Center.* This center will significantly increase the use of the data from SCSN for scientific research. The mass-store system, which became operational on 1 October 1991, provides on-line storage for more than 300 Gbytes of data. The availability of 60 years of catalog, 30 years of phase data, and 14 years of digital seismograms on both UNIX and VMS computers and on-line over INTERNET/NSFNET improves the access to the data.

#### Seismicity October 1990 - September 1991

The Southern California Seismographic Network (SCSN) recorded 9094 earthquakes during the 12 months from October 1990 through September 1991, an average of 758 per month, making it a quiet reporting period (Figure 1). There were six events of  $M_L \geq 4.0$  and 23 events of  $M_L \geq 3.5$  in southern California during the last 12 months.

The largest event was the ( $M_L=5.8$ ) Sierra Madre earthquake of 28 June 1991, which occurred 18 km northeast of Pasadena at a depth of 12.5 km under the San Gabriel Mountains of the central Transverse Ranges (Figure 2b). The mainshock focal mechanism, derived from first motion polarities, exhibited pure thrust faulting on a plane striking east-northeast and dipping  $50^\circ$  to the north. The event appears to have occurred on the Clamshell-Sawpit Canyon fault, an offshoot of the Sierra Madre fault system, although because all of the 104 recorded aftershocks are in the depth range of 9-14 km, the relation to surface faults can only be hypothesized. The largest aftershock had a magnitude of  $M_L$  4.3 and a similar focal mechanism (Figure 2b).

Two events originated in the southern San Joaquin Valley. The first a  $M_L$  4.2 earthquake occurred on 18 December 1990 and was located, 8 miles east of Bakersfield (Figure 2a). The second occurred on 3 April 1991 and was located near the northeast end of the White Wolf fault. Two earthquakes were located southwest of Los Angeles, one was a  $M_L$  3.8 event, located in the Costa Mesa area, near the Newport-Inglewood fault on 17 October, 1990, the second occurred 9 miles north-northeast of Avalon, Catalina Island on 9 April 1991. In May, July and early August 1991 five events occurred along the San Jacinto fault.

During the last 12 months the prominent areas of microseismicity were the usual ones: the Coso and Kern River areas, the San Jacinto fault, the southern Elsinore fault, the Imperial Valley and the San Bernardino and Little San Bernardino Mountain areas. Aftershocks continued at a rate clearly higher than background in the Oceanside sequence ( $M_L$  5.3 on July 13, 1986) and the Coalinga sequence ( $M_L$  6.3 on May 3, 1983).

#### *Focal Mechanisms*

The focal mechanism for earthquakes of  $M \geq 3.5$  are shown in Figure 2a and 2b. A total of 23 events of  $M \geq 3.5$  were recorded in southern California from 1 October 1990 to 30



September 1991 and reliable focal mechanisms could be determined for 18 events. One  $M_L 3.5$  event (31 January 1991) for which a focal mechanism was not determined, occurred at a shallow depth (probably less than 1 km) in the Orcutt Oil Field in the Santa Maria basin. This event was most likely induced in the oil field. Several other events are either preceded by immediate foreshocks or only a few first motion polarities are available because they are located near the edges of the network. Strike-slip faulting is observed in the southern San Joaquin Valley. The western and central Transverse Ranges are dominated by reverse faulting while the eastern Transverse Ranges and the Peninsular Ranges are dominated by strike-slip faulting. Three events showing strike-slip faulting occurred in the San Bernardino Mountains. Five events showing strike-slip faulting occurred along the San Jacinto fault zone. One event (14 December 1990) showing strike-slip faulting was recorded north of the Coso Geothermal Area.

#### *Weekly Seismicity Report*

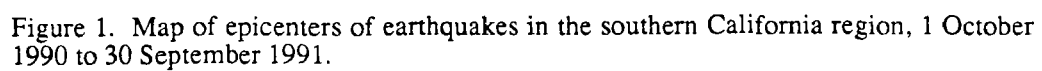
In January 1990, the Seismographic Network initiated a weekly seismicity report, patterned after a similar report issued by the U.S. Geological Survey in Menlo Park. The language of the "earthquake report" is aimed at the general public. The report has been enthusiastically received. A few members of the local media have started basing regular news features on it.

TABLE . Locations and Focal Mechanisms of  $M \geq 3.5$  Earthquakes that Occurred During October 1990 - September 1991

Origin Day	Time UT	Latitude N	Longitude W	Mag $M_L$	Depth km	CUSP-ID	Focal Mechanisms		
							Ddir	Dip	Rake
901018	1721 56.0	33 38.24	-117 52.68	3.8	3.24	2006524	95	75	-150
901109	0711 19.8	34 25.66	-116 48.52	3.5	3.74	1062836	115	80	0
901115	1738 18.2	35 55.43	-117 42.28	3.5	5.55	2007530			
901214	1422 33.0	36-33.60	-117-55.82	3.6	6.0	2008930	330	60	-20
901217	1744 21.2	34 12.40	-117 01.28	3.7	5.96	2009059	310	45	0
901218	1656 43.0	35 22.45	-118 50.75	4.2	6.00	688784	185	80	-140
910131	0039 05.3	36 03.20	-121 41.74	3.5	6.00	2011299			
910131	2328 18.0	34 49.23	-120 23.00	3.5	1.00	2011371			
910308	0927 35.5	34 09.00	-116 43.11	3.7	11.16	2013964	70	90	170
910403	1729 46.9	35 27.86	-118 19.45	3.5	8.91	2015771	215	55	170
910409	0751 20.1	33 28.25	-118 15.76	3.5	6.92	2016096	160	80	40
910412	1945 6.7	34 30.51	-119 00.92	3.5	3.76	694013	110	80	-20
910520	1500 53.4	33 46.88	-116 56.08	3.7	12.77	695381	300	60	-30
910520	1504 10.0	33 46.74	-116 56.01	3.5	12.39	695382	135	80	30
910530	0647 59.2	32 50.92	-116 39.80	3.7	6.00	2019878			
910628	1443 54.5	34 15.69	-117 59.97	5.8	10.53	2021449	165	40	100
910628	1700 55.5	34 15.18	-117 59.52	4.3	9.47	2021473	215	50	140
910629	1753 39.6	34 55.32	-116 32.47	3.6	6.00	51520	70	55	-140
910629	1753 52.0	34 54.51	-116 34.76	4.0	6.00	2021565			
910705	1741 57.1	34 29.82	-118 33.33	4.1	10.90	2022113	210	60	100
910709	0906 11.5	33 29.49	-116 25.45	3.7	7.35	2022070	135	70	30
910719	0241 36.8	33 12.75	-115 58.09	4.0	3.10	697556	225	80	150
910803	0959 49.8	34 05.61	-117 18.73	3.5	17.28	698180	150	70	0

# **PUBLICATIONS USING NETWORK DATA (ABSTRACTS EXCEPTED)**

- Agnew, D. C., and L. M. Jones, Prediction probabilities from foreshocks, *J. Geophys. Res.*, 96, 11,959-11,971, 1991.
- Bryant, A. S., and L. M. Jones, Anomalous deep crustal earthquakes in the Ventura Basin, California, *J. Geophys. Res.*, 1991, in press.
- Hauksson, E., and S. Gross, Source parameters of the 1933 Long Beach earthquake, *Seismol. Soc. Am., Bull.*, 81, 81-98, 1991.
- Hauksson, E., and L. M. Jones, The 1988 and 1990 Upland earthquakes: Left-lateral faulting adjacent to the Central Transverse Ranges, *J. Geophys. Res.*, 96, 8143-8165, 1991.
- Jones, L. M., K. E. Sieh, D. Agnew, C. Allen, R. Bilham, M. Ghilarducci, B. Hager, E. Hauksson, K. Hudnut, D. Jackson, A. Sylvester, K. Aki, and F. Wyatt, Short-term Earthquake Alerts for the Southern San Andreas Fault, *U. S. Geological Survey Open File Report 91-32*, pp., 1991.
- Kisslinger, C., and L. M. Jones, Properties of aftershock sequences in southern California, *J. Geophys. Res.*, 96, 11,947-11,958, 1991.
- Michael, A. J., Spatial variations in stress within the 1987 Whittier Narrows, California, aftershock sequence: New techniques and results, *J. Geophys. Res.*, 96, 6303-6319, 1991.
- Mori, J., Estimates of velocity structure and source depth using multiple P waves from aftershocks of the 1987 Elmore Ranch and Superstition Hills, California, earthquakes, *Seismol. Soc. Am., Bull.*, 81, 508-523, 1991.
- Sen, M. K., Modeling of Wave Propagation in northern Los Angeles Basin, *Bull. Seismol. Soc. Amer.*, 81, 751-768, 1991.
- Su, F., K. Aki, and N. N. Biswas, Discriminating quarry blasts from earthquakes using coda waves, *Seismol. Soc. Am., Bull.*, 81, 162-178, 1991.



FOCAL MECHANISMS  $\geq 3.5$   
OCTOBER 1990 - APRIL 1991

II

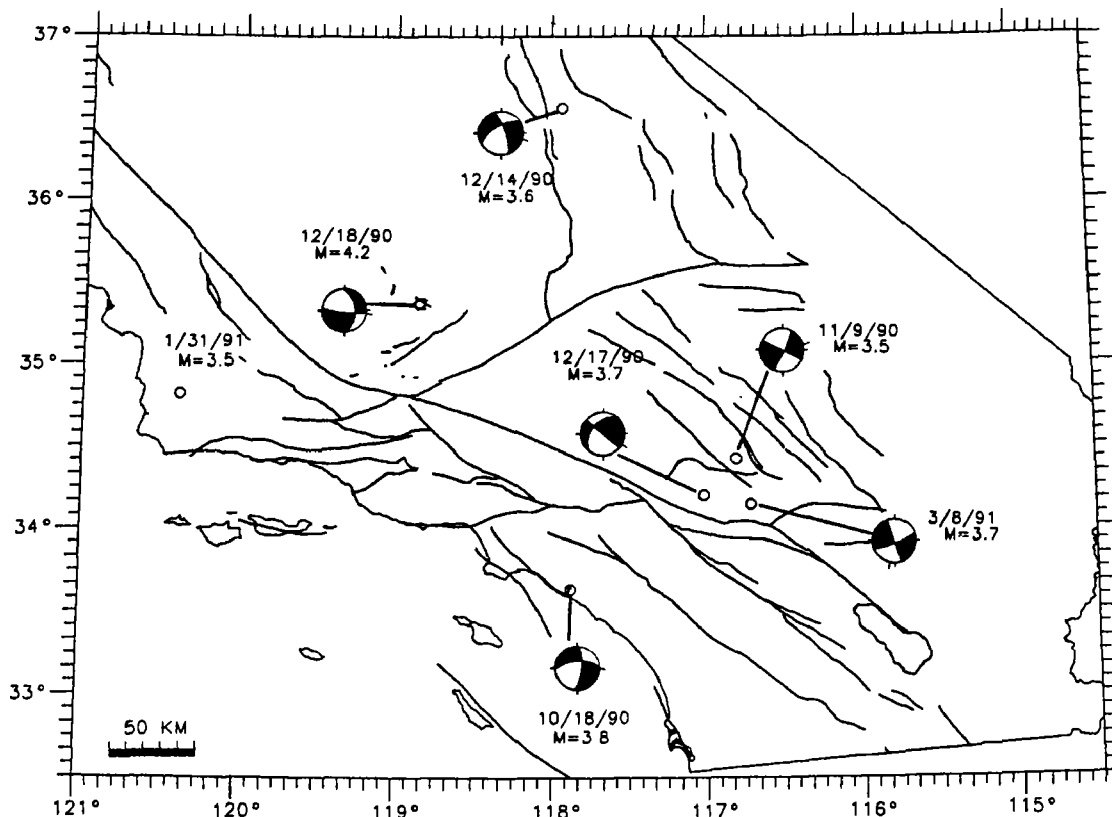


Figure 2a. Focal mechanisms of earthquakes of  $M \geq 3.5$  that occurred in southern California from 1 October 1990 to 30 March 1991. (See also enclosed table).

FOCAL MECHANISMS  $\geq 3.5$   
April - September 1991

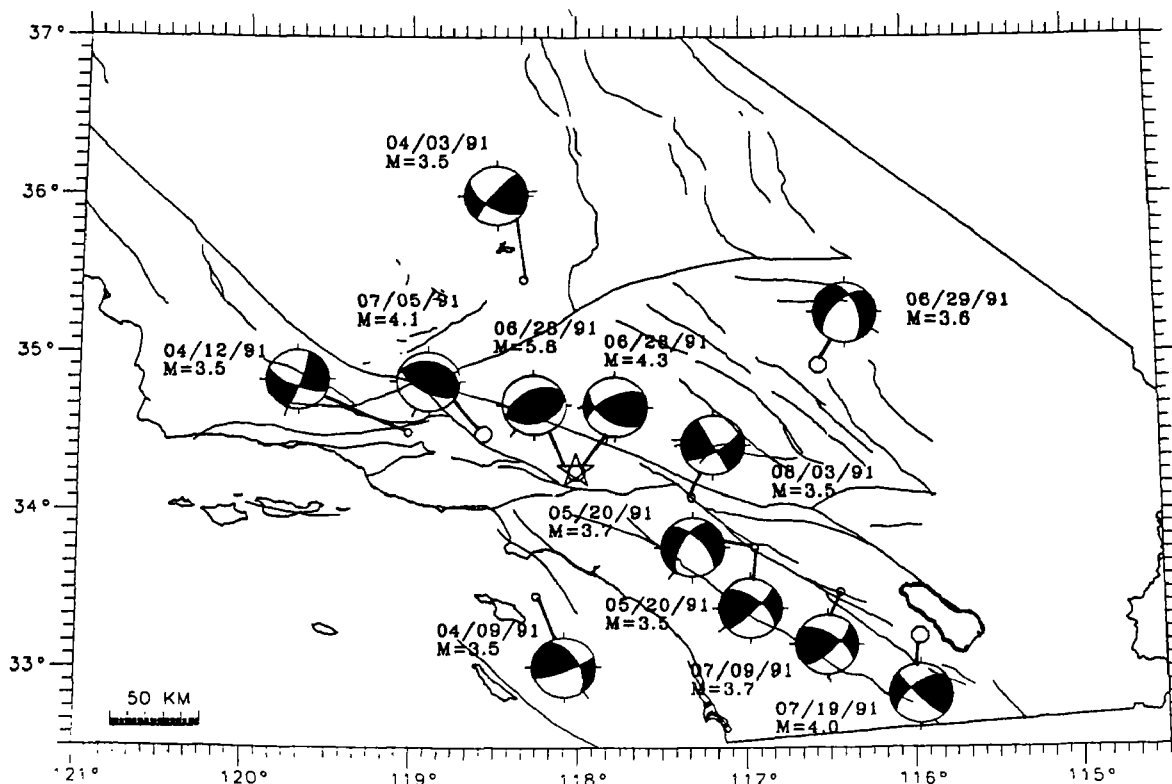


Figure 2b. Focal mechanisms of earthquakes of  $M \geq 3.5$  that occurred in southern California from 1 April to 30 September 1991. (See also enclosed table).

# INVESTIGATION OF PEAT STRATIGRAPHY IN ESTUARINE FLATS NEAR ANCHORAGE, ALASKA, AS A MEANS OF DETERMINING RECURRENCE INTERVALS OF MAJOR EARTHQUAKES

14-08-0001-G1949

Rodney A. Combellick and Richard D. Reger  
Alaska Division of Geological & Geophysical Surveys  
794 University Ave., Suite 200  
Fairbanks, Alaska 99709  
(907) 474-7147

## Investigations

We are conducting borehole drilling with continuous core sampling at three estuaries along the eastern shore of Cook Inlet south of Anchorage, Alaska (fig. 1), to determine cycles of late-Holocene estuarine deposition and coseismic subsidence in the Cook Inlet region. Our goal is to obtain subsurface data from as many estuaries as possible in the Kenai Peninsula portion of the region that subsided during the great earthquake of 1964. The resulting database should help to provide a regional chronology of coseismic subsidence during the late Holocene.

Our previous drilling along Turnagain and Knik Arms in upper Cook Inlet revealed multiple submerged peat layers, possibly associated with six to eight coseismic subsidence events during the past 4,700 calendar years, which corresponds to a recurrence interval of 590 to 780 years (Combellick, 1990). The current program involves drilling and examination of tidal-channel exposures in estuaries of Fox River (Kachemak Bay), Kasilof River, and Kenai River.

## Results

As indicated in our April 1991 project summary, we drilled nine boreholes to a maximum depth of 12 m at Fox River flats near Homer (fig. 1) in February 1991. Although the estuarine muds contained some horizons with abundant plant debris, none of the boreholes revealed distinct peat-silt couplets similar to those we observed in Turnagain and Knik Arms. We returned to Fox River flats in May 1991 to drill eight additional shallow holes with hand auger and to examine bluff exposures more closely. Fox River flats appears to be devoid of buried peat layers or other strong evidence of pre-1964 coseismic subsidence. However, the estuarine muds locally contain distinct layered concentrations of salt-marsh plant fossils, well below modern ordinary high water, which may have been submerged and buried as a result of coseismic subsidence. We are currently evaluating these data and processing samples for textural analysis, radio-carbon dating, and possible microfossil study to develop a model for the sedimentology of Fox River flats and to determine possible implications for paleoseismicity of the area.

In May and June 1991, we examined extensive river-bluff exposures at Kenai and Kasilof River flats (fig. 1). Additionally, we drilled four boreholes to a maximum depth of 10.4 m at Kenai River flats and two boreholes to a maximum depth of 8.2 m at Kasilof River flats. Thick (1.5-m) grassy and woody peat is exposed along the river channels near the mouths of both Kenai and Kasilof Rivers and contains up to three horizons of rooted tree stumps. These forest horizons may relate to changes in land elevation, but may alternatively be due to other climatic or hydrological changes.

Boreholes at Kenai and Kasilof River flats reveal as many as three deeper peat layers that may have been buried as a result of subsidence during earthquakes. The deepest

of these is a thick (1 m) grassy and woody peat buried under about 6 m of estuarine mud at Kasilof. We have finished describing, photographing, and sampling these cores and are preparing the samples for radiocarbon dating, textural analyses, and possible microfossil identification.

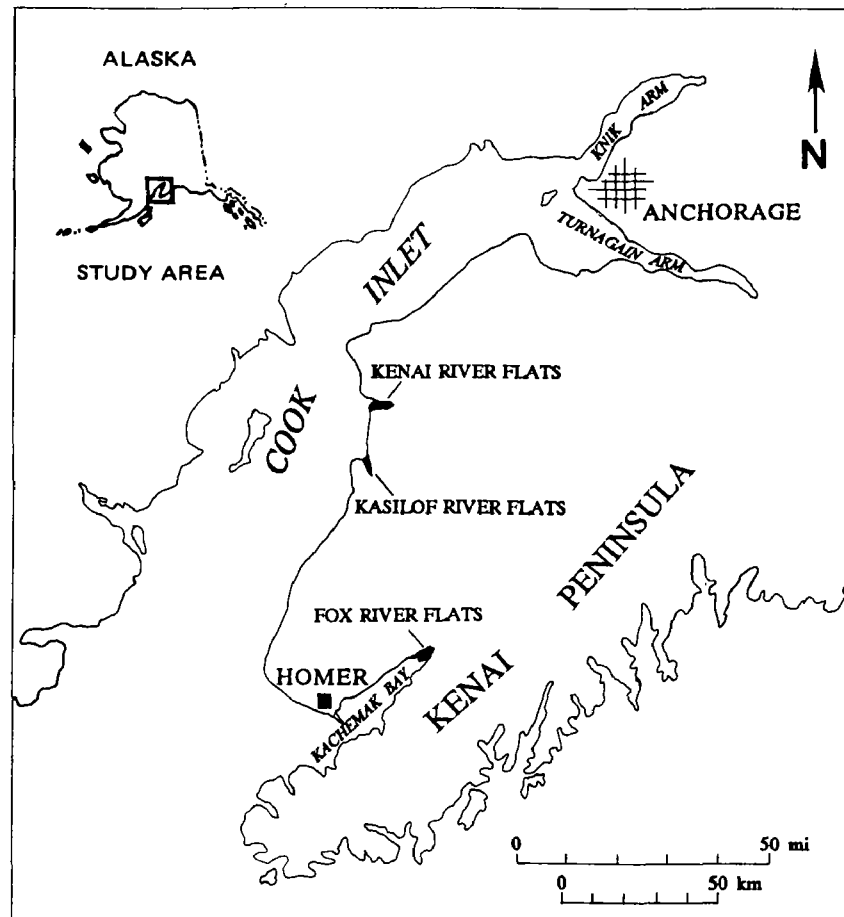


Figure 1. Cook Inlet region, Alaska.

## Reports

- Combellick, R.A., 1986, Chronology of late-Holocene earthquakes in southcentral Alaska: Evidence from buried organic soils in upper Turnagain Arm: Geological Society of America Abstract with Programs, V. 18, no. 6, p. 569.
- Combellick, R.A., 1990, Evidence for episodic late-holocene subsidence in estuarine deposits near Anchorage, Alaska: Basis for determining recurrence intervals of major earthquakes: Alaska Division of Geological & Geophysical Surveys Public-Data File 90-29, 67 p.
- Combellick, R.A., 1991, Paleoseismicity of the upper Cook Inlet region, Alaska, as recorded by peat stratigraphy in nine tidal-flat boreholes: Geological Society of America Abstracts with Programs, v. 23, no. 2, p. 15.
- Combellick, R.A., 1991, Paleoseismicity of the upper Cook Inlet region, Alaska: Evidence from peat stratigraphy in Turnagain and Knik Arms: Alaska Division of Geological & Geophysical Surveys Professional Report 112, in press.

## TECTONICS OF SEISMIC SOURCE ZONES, CENTRAL INTERIOR OF THE UNITED STATES

9950-04542

ANTHONY J. CRONE  
Branch of Geologic Risk Assessment  
U.S. Geological Survey  
Box 25046, MS 966,  
Denver, Colorado 80225  
(303) 236-1595

### PURPOSE OF PROJECT

This large multidisciplinary project is designed to provide basic geologic and geophysical information on the distribution, characteristics, and frequency of large earthquakes in the central interior of the United States and contribute to a better understanding of the structural features that might produce large, potentially damaging intraplate earthquakes. Project members are: Donley S. Collins, Anthony J. Crone, Richard L. Dart, Sharon F. Diehl, William L. Ellis, Meridee Jones-Cecil, Donald T. Rodbell, and Henri S. Swolfs.

### INVESTIGATIONS

#### Subsurface Stratigraphy and Structure—New Madrid Seismic Zone (NMSZ)

R.L. Dart revised a series of previously finalized subsurface geologic maps of Paleozoic rocks in the New Madrid region to incorporate additional drill-hole data that was acquired as a result of recent visits to State Geological Survey offices in the region. Much of the new data is from drill holes located beyond the boundary of his original study area, which extended from 34°30' to 37°45' N. and 88° to 91°30' W. He is also converting his comprehensive catalog of subsurface geologic data in the New Madrid region to the GIS ARCINFO system. This work should be completed in early 1992.

D.S. Collins continued to analyze insoluble residues of cuttings from important deep drill holes throughout the New Madrid region to assist in correlating and clarifying the structural relations between Lower Paleozoic rocks in the Reelfoot rift. He is currently processing selected samples of cuttings from the Strake Petroleum #1 Russell drill hole (Pemiscot Co., southeastern Missouri) to examine the stratigraphy, depositional history, and tectonic framework of Lower Paleozoic rocks near the apex of the Pascola Arch.

S.F. Diehl has continued her petrographic and scanning electron microscope (SEM) analyses of core and cuttings from significant deep drill holes in and adjacent to the Reelfoot rift. Diehl and F. A. McKeown have plotted hydrologic data (Brahana and Mesko, 1987), such as fluid pressure and water temperature from drill holes in the Mississippi Embayment, on a structural map of the New Madrid region to examine the relation between areas of high fluid pressure and earthquakes.

H.S. Swolfs continued his analyses of structural features in the Dow Chemical Co. #1 Garrigan drill hole in Mississippi County, Arkansas, to clarify the origin, evolution, and extent of deep-seated seismogenic structures that underlie and are perhaps associated with structurally high features in the Reelfoot rift. This drill hole is on the southeastern flank of the Blytheville Arch, a major structural feature that coincides with the narrow, 120-km-long (74.4 mi) trend in seismicity between Marked Tree, Arkansas and Caruthersville, Missouri. He prepared a manuscript summarizing the results of these investigations for publication in *Seismological Research Letters*.

A.J. Crone completed a preliminary analysis of about 135 km (83.7 mi) of seismic-reflection data across the southeastern margin of Reelfoot rift to clarify the geologic history and the earthquake potential of the rift-bounding faults, particularly near to Memphis, Tennessee. He prepared a draft of a manuscript summarizing the results of this analysis for publication in *Seismological Research Letters*.

Crone also finalized the purchase of 75 km (46.2 mi) of Vibroseis™ seismic-reflection data near the southwestern end of the Blytheville Arch to precisely define the extent of the arch, and thereby determining the areal limits of a major seismic source zone in the New Madrid region.

#### Quaternary Deformation and Paleoseismicity—NMSZ

D.T. Rodbell began two interrelated investigations of Quaternary deposits in western Tennessee. One investigation involves mapping and determining the age and gradient of alluvial terraces along the Obion River in northwestern Tennessee to identify areas of possible Quaternary deformation related to the NMSZ. The second investigation focuses on determining the distribution of liquefaction features on terraces of various ages, and attempting to identify and date liquefaction features that predate the 1811-12 earthquakes. This effort seeks to provide paleoseismologic data of the recurrence of large earthquakes in the region.

#### Distribution of Stress—NMSZ

W.L. Ellis completed his compilation and review of published stress indicators and stress-measurement data for 36 locations within a radius of approximately 250 km of the NMSZ. He also began assembling data to compare the results of shallow (<0.3 km) versus deep (>1 km) stress measurements and other stress indicators (*i.e.*, borehole breakouts and earthquake focal mechanisms) in areas where both shallow and deep stress data are available. The goal of this study is to determine if shallow stress measurements can reliably reflect deep-seated regional stresses in the crust and, as a result, evaluate the relative merits of shallow and deep stress measurements as means of improving our understanding of the mechanisms that control intraplate seismotectonics. He prepared a draft of a manuscript summarizing stress-measurement data in the New Madrid region for publication in *Seismological Research Letters*.

#### Investigations of the Meers Fault, Southwestern Oklahoma

M. Jones-Cecil continued her geophysical investigations of the Meers fault to assess its seismic potential. The fault is a rare example of an exposed, recently reactivated and probably seismogenic fault in the central and eastern United States. Hence, understanding its role in the structural framework of the more extensive Frontal Wichita fault zone and characterizing the deformation and properties of rocks associated with the Meers fault may clarify why some intraplate faults have the potential to generate earthquakes. The geophysical study seeks to define the geometry of the Meers fault in the upper crust and the interaction of the Meers fault with other faults in the Frontal Wichita fault zone. Jones-Cecil, assisted by L.-A. Bradley (Branch of Geologic Risk Assessment), collected detailed ground-magnetic data along three profiles across the Meers fault and magnetic susceptibility data at several other sites to supplement existing geophysical data. The existing data include a USGS aeromagnetic survey, eight ground-magnetic profiles, *in situ* and laboratory magnetic-susceptibility and density measurements (in collaboration with L.-A. Bradley), regional and detailed gravity data (compiled and collected in collaboration with S.L. Robbins and C. Williamson, Branch of Sedimentary Processes), and reconnaissance VLF (very low frequency) data. In addition, Jones-Cecil is conducting paleomagnetic, petrologic, and shear-plane analyses of drill core (provided courtesy of Kenneth V. Luza, Oklahoma Geological Survey) from a series of core holes adjacent to the Meers fault to examine the characteristics and properties of the rocks in the fault zone.

In conjunction with Jones-Cecil's work, D.S. Collins has examined the petrology of 28 thin sections and hand samples of core from three holes drilled adjacent to the fault to provide data on



the lithologies and mineral alteration of igneous rocks adjacent to the fault zone. These petrologic investigations will refine models of potential-field data near the fault and will help clarify the structural relations between rocks across the fault zone.

### Related Investigations

Although not directly funded by NEHRP, Crone and M. N. Machette (Branch of Geologic Risk Assessment) prepared a draft of a manuscript during the reporting period, in which they describe the results of their G.K. Gilbert Fellowship field studies of the paleoseismicity of the 1988 Tennant Creek, Australia intraplate earthquakes. The manuscript, which has been submitted for publication as a USGS Bulletin, contains lithologic/structural logs of four trenches, detailed site maps, plots of scarp profiles, and preliminary results of thermoluminescence and electron-spin resonance dating. They also submitted two abstracts summarizing their Australian studies for presentation at the Geological Society of America 1991 annual meeting. They compiled and began analysis of the data from their field studies of the 1986 Marryat Creek, South Australia fault scarps. Their Australian studies are being conducted in collaboration with J. Roger Bowman (Australian National University, Canberra), who has studied the seismology of earthquakes.

## **RESULTS**

### Subsurface Stratigraphy and Structure—NMSZ

Dart has updated and expanded the subsurface database for Paleozoic rocks in the New Madrid region by including data from an additional 54 drill holes in the New Madrid region. The subsurface structure-contour and isopach maps in the map series had contours that did not represent the actual subsurface data in places near the map edges. This edge-contouring problem will be remedied by using newly acquired drill-hole data in the surrounding 1°-wide perimeter of the established map boundaries. A series of northwest-oriented cross-strike profiles and northeast-oriented strike-parallel profiles of the Paleozoic strata, constructed from the previously mapped subsurface data, revealed some overlapping contacts of Paleozoic units. These erroneous overlaps commonly occurred where mapped units thinned near the northwestern and southeastern borders of the Mississippi Embayment or where these contacts are shallow or at the ground surface in southeastern Missouri, southern Illinois, or west-central Kentucky. Ground-surface elevation data from topographic maps and ground-surface geologic data of Paleozoic outcrops are being added to increase the control for contouring the subsurface data in these areas. A revised version of these subsurface geologic maps will be in review by early 1992.

Dart presented updated versions of the subsurface geologic maps in a poster session at the Louis Unfer, Jr., Conference on the Geology of the mid-Mississippi Valley at Southeast Missouri State University, Cape Girardeau, Missouri in June, 1991.

Collins' analysis of the insoluble heavy minerals from the Strake Petroleum #1 Russell drill hole indicates that medium- to high-grade metamorphic rocks were exposed in the source area during deposition of the Early Paleozoic clastic rocks in southeastern Missouri. The heavy minerals include kyanite, zoisite, and staurolite, which indicate a metamorphic source area. Heavy minerals from a metamorphic terrain were not found in the Dow Chemical Co. #1 Garrigan drill hole, which is about 90 km to the south of the Strake drill site. This indicates that isolated depocenters having different source terrains were present within the Reelfoot rift during Paleozoic time.

In cooperation with John Repetski and Michael Taylor (Branch of Paleontology and Stratigraphy), Collins has used paleontological data from core samples to refine stratigraphic and structural relations between the Dow Chemical Co. #1 Garrigan and Dow Chemical Co. #1 Wilson drill holes. An assemblage of Late Cambrian trilobites from 2,434 m (7,986 ft) in the Garrigan drill hole is roughly correlative with a similar assemblage from a depth of 3,273-

3,383 m (10,740-11,100 ft) in the nearby Dow Chemical Co. #1 Wilson drill hole. This correlation implies that about 858-949 m (2,754-3,114 ft) of structural relief is present between the two drill holes, which are about 27 km apart. Preliminary analysis of conodont assemblages places the upper boundary of Ordovician rocks at about 1,109 m (3,640 ft) in the Garrigan drill hole and at 2,743 m (9,000 ft) in the Wilson drill hole. The combined trilobite and conodont age assignments suggest that 1,325 m (4,346 ft) of calcareous siliciclastic rocks in the Garrigan are equivalent in age to about 549 m (1,800 ft) of carbonate rocks in the Wilson drill hole. Thus, Late Cambrian and Ordovician rocks in the Garrigan drill hole were deposited in a deep basin, whereas, the equivalent rocks in the Wilson hole were likely deposited in shallower water and are less than half as thick. The difference in thickness of similar-age rocks in these two holes indicates a comparatively high sedimentation rate at the Garrigan drill-hole site, which may reflect Late Cambrian/Early Ordovician subsidence in an intra-rift basin.

Diehl's preliminary investigations of ground-water conditions in the rift, conducted in collaboration with F.A. McKeown, have revealed that the areas of highest hydrologic head (high fluid pressure) coincide with the major seismicity trends in the NMSZ and with the fault zones that bound the rift (fig. 1). Areas of low fluid pressure are located away from both the seismic zone and Reelfoot rift. Unusually high fluid pressure in hydraulically connected Cretaceous and Paleozoic aquifers in the Upper Mississippi Embayment is well documented in the literature. The abnormal pressures seem to be controlled by the thickness of confining layers in the Paleocene Midway Group and are highest in the parts of Reelfoot rift where the seismicity in the NMSZ is most abundant. This observation indicates that a potentially significant relationship exists between the seismicity and areas of high fluid pressure and intensely fractured and sheared rock in the Blytheville-Pascola Arch complex. The available data suggest that the seismicity occurs mainly where both fluid pressure is high and the rocks at seismogenic depths are pervasively fractured.

During visits to the Missouri and Arkansas Geological Survey/Commissions in Rolla, Missouri, and Little Rock, Arkansas, respectively, Diehl obtained samples of drill cuttings from several deep drill holes in the New Madrid region, including the Cockrell Corp. #1 Carter, Strake Petroleum #1 Russell, and Houston Oil and Minerals #1 Singer. Petrographic analyses of these samples will permit the comparison of structural fabrics and the paragenesis and composition of fracture-filling minerals in the subsurface from deep drill holes throughout the New Madrid region. The majority of the samples are still being prepared for analysis, but preliminary examination of samples of mafic rocks from a depth of 4,267 m (14,000 ft) in the Cockrell Corp. #1 Carter drill hole revealed the presence of copper and iron sulfides. If an adequate amount of sulfide minerals is available, sulfur-isotopes measurements of these samples may determine if these mafic intrusives in the Reelfoot rift could be a source of metals for Mississippi-Valley-type ore deposits to the northwest of the rift. Also, analysis of the copper and iron sulfides might indicate if metallic ore deposits could be present within the rift. Petrographic analysis of the mafic rocks may also aid in interpreting aeromagnetic data.

The preliminary results of Diehl and McKeown's examination of overpressure conditions in the Reelfoot rift were presented in an oral presentation at the 1991 meeting of the Eastern Section, Seismological Society of America in Memphis, Tennessee.

Swolfs' analyses of cores and borehole geophysical logs of the Dow Chemical Co. #1 Garrigan hole suggest the following sequence of paleotectonic events after the formation of the Reelfoot rift in Late Proterozoic or Early Cambrian time.

1. A thick sequence of black shale (now at a depth of 2,585-3,669 m in the Garrigan hole) was deposited in an anoxic central basin and was later tilted about 20° to the southeast during an early phase of deformation in the rift. This tilting could be related to diapiric uplift or to some other tectonic process that led to structural inversion of the central basin. This early phase of deformation was virtually complete by Late Cambrian time.

2. The tilted shale was capped or perhaps truncated by a sequence of subhorizontal sandstone, interbedded sandstone and shale (turbidites), and mudstone (now at a depth of 795-

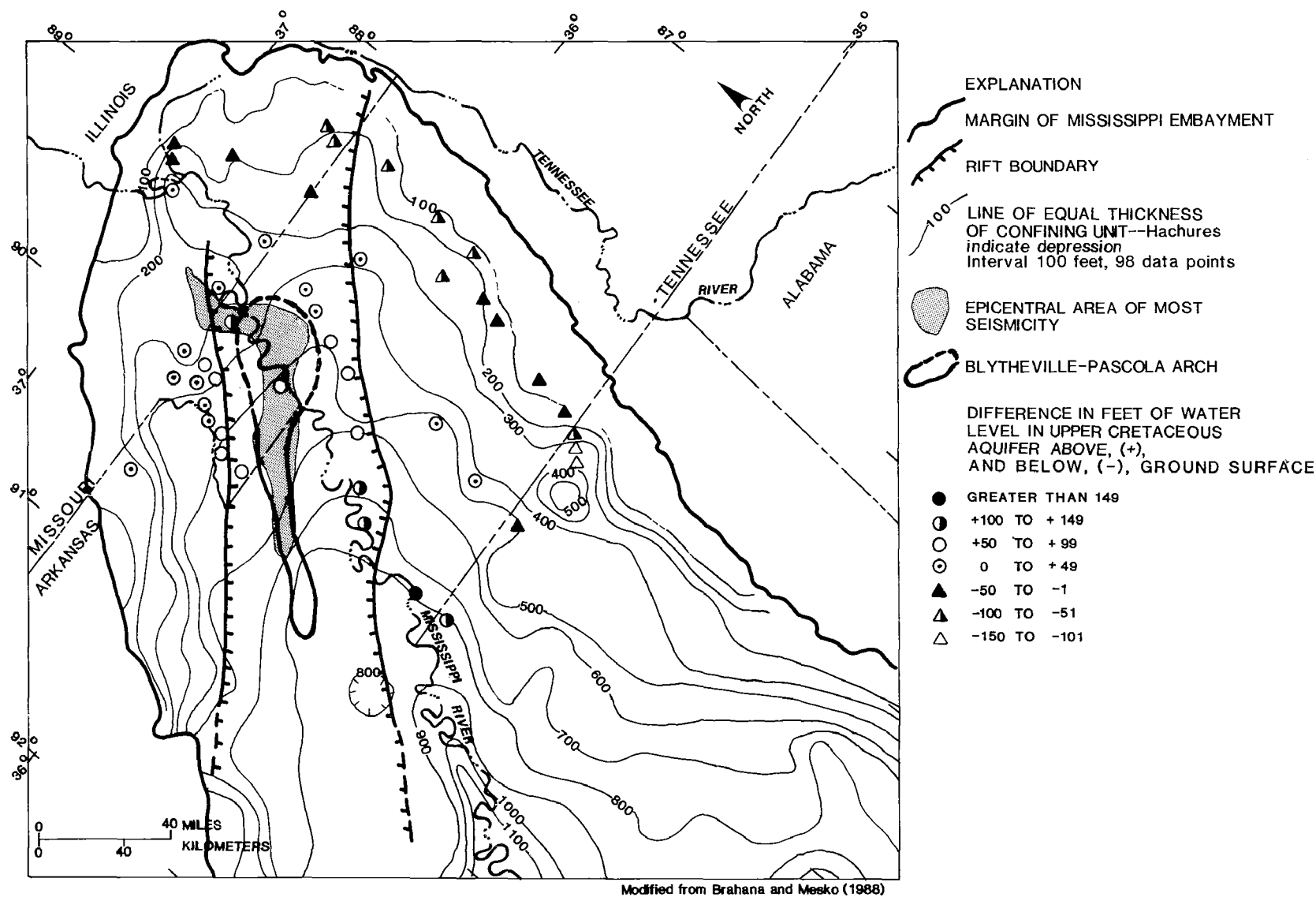


FIGURE 1. EXTENT AND THICKNESS OF THE MIDWAY GROUP CONFINING UNIT, WATER LEVELS, RIFT, BLYTHEVILLE-PASCOLA ARCH, AND SEISMICITY

2,585 m in the drill hole) of Late Cambrian to Early Ordovician age that signals a renewed episode of subsidence in the central basin. A distinctive but poorly understood stratigraphic boundary at a depth of 2,858 m corresponds to a lithologic and a structural contact, and is tentatively identified as an unconformity.

3. The first and most extensive system of extensional veins, which strike northwest and dip southwest in all three cores from the Garrigan hole, developed perhaps in association with the uplift of the northwest-trending Pascola Arch, which is located 50 km to the northeast of the drill hole. The attitude and orientation of this vein set is uniform above and below the unconformity, which means that it postdates the early deformation phase that involved the tilting of the black shale and its subsequent truncation by the overlying strata.

4. A younger system of extensional veins developed in compacted, lithified, and brittle sandstone. This set is only present only above the unconformity and may have developed in response to local faulting associated with the uplift of the Blytheville Arch sometime after Early Ordovician time. The nearest fault reported in the drill hole is 25 m above the top of the core.

Swolfs presented the results of this study at the 1991 meeting of the Eastern Section, Seismological Society of America, Memphis, Tennessee.

Crone's preliminary interpretation of about 135 km of seismic-reflection data provides new information on the structural characteristics of the southeastern margin of Reelfoot rift and about the relations between the Crittenden County fault zone (CCFZ) and the subjacent rift-bounding faults. On the reflection data, the southeastern boundary of the rift is characterized by a 4- to 8-km-wide zone of incoherent reflected energy and disrupted reflectors that extend down to at least 12 km. In places, disrupted reflectors at the rift margin extend upward into the Upper Cretaceous and Tertiary rocks that fill the Mississippi Embayment. The CCFZ is interpreted as a northwest-dipping, high-angle reverse fault with a northwest-side-up sense of throw, which is opposite to the net structural relief in the underlying graben. Most faults in the CCFZ are apparently ancient rift-margin normal faults that have been reactivated as reverse faults in the Mesozoic and Cenozoic. The reflection data show that the CCFZ coincides with rift-bounding faults that extend down to hypocentral depths. However, the CCFZ is unfavorably oriented for reverse slip in the present stress field and may not be capable of generating damaging earthquakes. Source-parameter information for earthquakes along the southeastern margin of the rift is needed to clarify earthquake hazard associated with the CCFZ. The results of this study were presented at the 1991 meeting of the Eastern Section, Seismological Society of America in Memphis, Tennessee.

Crone has also completed the purchase of about 75 km of additional seismic-reflection data near the southwestern end of the Blytheville Arch, which is the only distinctive geologic structure known to be directly associated with one of the major trends in seismicity in the NMSZ. These data will permit the southwestern limit of the arch to be mapped and thus determine the precise location of a major earthquake source zone with respect to major metropolitan areas.

#### Distribution of Stress—NMSZ

Ellis' compilation of the available stress data and stress indicators around the NMSZ provides insight into the distribution of crustal stress in the region. Most of the data are consistent with an ENE-WSW direction of maximum horizontal stress, which is characteristic of the midcontinent, but earthquake-focal mechanism data indicate local variations in the horizontal stress orientation that may be related to the intersection of seismogenic structures near the central left-stepping part of the NMSZ between Dyersburg, Tennessee and New Madrid, Missouri. This area may be part of a transitional zone between (1) thrust and strike-slip faulting in the southern Illinois Basin, (2) predominantly strike-slip faulting near and to the southwest of the NMSZ, and (3) normal faulting in the Ozark Uplift to the northwest. The available data indicate little variation in the horizontal stress orientations with depth, which suggests that shallow stress measurements can realistically reflect stress directions in the

upper crust. The results of this analysis were presented at the 1991 meeting of the Eastern Section, Seismological Society of America in Memphis, Tennessee.

An initial review of published shallow stress measurements shows that horizontal stress trajectories are commonly consistent with deeper stress indicators. In some cases, multiple shallow measurements of horizontal stress directions are more consistent with the regional stress directions inferred from deep earthquake focal mechanisms than the directions measured at depths of a kilometer or more. The detailed distribution of stress trajectories near earthquake source zones may help identify potentially seismogenic faults and help distinguish between various models used to explain the origin of intraplate seismicity. The finding that multiple shallow stress measurements commonly reflect the orientation of the regional stresses in the upper crust emphasizes the value of using shallow stress measurements to map stress trajectories throughout the New Madrid region. Understanding the characteristics of the stress field in the New Madrid region and the surrounding midcontinent could provide a better understanding of the forces that affect intraplate seismogenesis.

#### Quaternary Deformation and Paleoseismicity—NMSZ

Rodbell has identified and mapped (scale 1:24 000) three terrace levels along the Obion River, a major tributary to the Mississippi River in western Tennessee. The identification of three sets of fluvial terraces corroborates the reconnaissance work of Saucier (1987). Three parameters are useful in distinguishing the terraces: (1) their elevation above the modern river channel, (2) the number of late Quaternary loess units that mantle a terrace surface, and (3) the degree to which the terrace has been dissected by tributary streams. These parameters provide a basis for accurately correlating fragments of terraces in the Obion River drainage and determining if tectonism has produced anomalous terrace gradients. Several cores of the Quaternary deposits from these terraces have been obtained using a hydraulically powered drill rig. Samples from the base of the loess mantle in some cores contained material that is being radiocarbon dated. One radiocarbon date indicates that the youngest terrace along the Obion River formed about 20,000 yr BP.

The proximity of the terrace surfaces to the modern water table and the presence of 1811-12 liquefaction features on the terraces strongly suggests that large pre-1811-12 seismic events in the region probably would have produced prehistoric liquefaction features on these deposits. However, trenching of one large sandblow on the lowest Obion River terrace has revealed no conclusive evidence of prehistoric liquefaction. Future efforts will continue to search for pre-1811-12 liquefaction features.

#### Investigations of the Meers Fault, Southwestern Oklahoma

Jones-Cecil's previous interpretations of magnetic and gravity data have identified structural features in the Paleozoic rocks that bear on the seismic potential of the Meers fault. In particular, a distinct left step in the trace of the fault and the presence of several splays at the stepover (located approximately 8 km northwest of the end of the Holocene scarp) probably mark the location of a barrier to rupture propagation along the reactivated segment of the fault. Furthermore, modeling of both ground-magnetic and aeromagnetic data show a probable near-vertical dip on the fault down to at least 1-km depth, in contrast to the moderate southward dip inferred by other workers in previously published studies. Jones-Cecil's original models, however, assumed only induced magnetization of the source rocks, but access to the Oklahoma Geological Survey drill core gave us the opportunity to directly measure magnetic properties of source rocks in the fault zone and ultimately refine the models. Koenigsberger ratios on 34 paleomagnetic samples from the drill core are generally less than 0.5, indicating that, as a first approximation, the assumption of induced magnetization is appropriate. Inclinations from the core, measured both before and after alternating-field demagnetization, are shallow and indicate that the magnetization was probably acquired during either Cambrian or Carboniferous tectonism. Incorporating the measured magnetization and inclinations of the unoriented core and

a range of probable Early and Late Paleozoic declinations will further refine the magnetic models and place better limits on the attitude of the fault.

In addition to its value in magnetic modelling, petrologic and structural data from the cores provide insight into the characteristics of the Meers fault zone. A dike-like body has been interpreted to be present directly south of the fault and extend along almost half of the Quaternary scarp on the basis of a prominent, narrow magnetic anomaly (Purucker, 1986). Southward, away from the Meers fault scarp, core samples have a high magnetic susceptibility that is at the appropriate depth and location to be the probable source body of the magnetic anomaly. D.S. Collins' petrologic studies of core samples has revealed that the dike-like body of igneous rock is probably composed of extensively sheared and altered meta-gabbro, meta-andesite, diorite, and an unknown rock-type of probable intermediate composition. The amount of alteration and fracturing in the core samples progressively increases in the holes south of the fault scarp, which suggests the presence of significant fault south of the Meers fault. This observation is consistent with the results of a recent ground-magnetic profile between the core-hole locations, which suggests the presence of a parallel fault that may be close to the southernmost core hole (about 75 m south of the scarp). The core from the southernmost hole is very intensely altered, sheared, and has a high clay content. Significant amounts of kaolinite and montmorillonite are present in the entire fault zone but seem to be present in greater quantities near this probable parallel fault. If similar quantities of these clay minerals are present along the fault zone at seismogenic depths, then they might make the fault zone relatively weak and thus may explain why a specific section of the Meers fault was selectively reactivated in the late Holocene.

#### Related Investigations

Preliminary results of Crone and Machette's Gilbert Fellowship research on the Marryat Creek and Tennant Creek scarp in Central Australia (Crone and others, 1991; Machette and others, 1991) show that these historic intraplate earthquakes reactivated ancient faults. However, there was no clear evidence of fault-scarp derived colluvium in the Quaternary deposits in any of the six trenches, and there is no compelling geomorphic evidence of prehistoric fault scarps at any of the sites. The oldest age estimate that John Prescott (University of Adelaide) has obtained on the eolian sand at Tennant Creek is  $61 \pm 5$  ka. These relations indicate that the historical earthquakes were associated with faults that had ruptured in the past, but that the recurrence interval for surface-rupturing earthquakes on these faults is probably measured in time increments of tens of thousands of years and possibly hundreds of thousands of year or more (millions of years?). These investigations of historical intraplate faulting and our brief observations of a trench across the 1968 Meckering (Western Australia) fault scarp suggest that Australian intraplate faults have very long repeat times; with this in mind, the concept of recurrence intervals may not be appropriate for earthquakes that occur in the 'stable' interiors of continents. Perhaps hazard assessments in Australia and other continental interiors should be based on models in which moderate- to large-magnitude earthquakes can occur at any time on faults that are suitably oriented in the contemporary stress field, rather than only on faults that have demonstrable Quaternary movement.

## REFERENCES CITED

- Brahana, J.V., and Mesko, T.O., 1987, Hydrogeology and preliminary assessment of regional flow in the Upper Cretaceous and adjacent aquifers in the northern Mississippi Embayment: U.S. Geological Survey Water-Resources Investigations Report 87-4000, 65 p.
- Purucker, Michael, 1986, Interpretation of an aeromagnetic survey along the Wichita Frontal fault zone *in* Gilbert, M.C., ed., Petrology of the Cambrian Wichita Mountains igneous suite: Oklahoma Geological Survey Guidebook 23, p. 129-136.
- Saucier, R. T., 1987, Geomorphological interpretations of late Quaternary terraces in western Tennessee and their regional tectonic implications: United States Geological Survey Professional Paper 1336-A, 19 p.

## REPORTS

- Collins, D.S., 1991, Insoluble residue of selected samples from the Dow Chemical B.L. Garrigan #1 drill hole, Blytheville, Arkansas: Program with Abstracts, Louis Unfer, Jr., Conference on the Geology of the Mid-Mississippi Valley. Southeast Missouri State University, Cape Girardeau, Missouri, 6 p. (unnumbered)
- Crone, A.J., 1991, Structural relations between the Crittenden County fault zone and the southeastern margin of Reelfoot rift near Memphis, Tennessee: Program and Abstracts, Eastern Section, Seismological Society of America, 63<sup>rd</sup> Annual Meeting, Memphis, Tennessee, October 13-16, 1991, p. 62.
- Crone, A.J., Machette, M.N., and Bowman, J.R., 1991, Surface faulting and earthquake recurrence in 'stable' continental interiors—Examples from Australia and North America: Geological Society of America Abstracts with Programs, v. 23, no. 5, p. A431.
- Dart, R.L., 1991, Paleozoic subsurface mapping of the Upper Mississippi Embayment from drill-hole and seismic-reflection data: Program with Abstracts, Louis Unfer, Jr., Conference on the Geology of the Mid-Mississippi Valley, Southeast Missouri State University, Cape Girardeau, Missouri.
- Diehl, S.F., and McKeown, F.A., 1991, Evidence of paleo- and recent fluid overpressure in the New Madrid seismic zone of the Reelfoot rift, southeast Missouri and northeast Arkansas: Eastern Section, Seismological Society of America, Program and Abstracts, 63<sup>rd</sup> Annual Meeting, Memphis, Tennessee, October 13-16, 1991, p. 68.
- Ellis, W.L., 1991, Stress distribution in south-central Oklahoma and its relationship to crustal structure and contemporary seismicity, *in* Roegiers, J.-E., ed., Rock mechanics as a multidisciplinary science--Proceedings of the 32<sup>nd</sup> U.S. Symposium: 1991 Proceedings, A.A. Balkema, Rotterdam, p. 73-83.
- Ellis, W.L., 1991, Stress distribution in the region of the New Madrid seismic zone, east-central United States: Program and Abstracts, Eastern Section, Seismological Society of America, 63<sup>rd</sup> Annual Meeting, Memphis, Tennessee, October 13-16, 1991, p. 46.
- Jones-Cecil, Meridee, *in press*, Total-field aeromagnetic and derivative maps of the Lawton area, southwestern Oklahoma: U.S. Geological Survey Geophysical Investigations Map GP-998-A, 2 sheets, scale 1:100 000.
- Jones-Cecil, Meridee, and Robbins, S.L., *in press*, Bouguer and isostatic residual gravity anomaly and derivative maps of the Lawton area, southwestern Oklahoma: U.S. Geological Survey Geophysical Investigations Map GP-998-B, 3 sheets, scale 1:100 000.

- Machette, M.N., Crone, A.J., Bowman, J.R., and Prescott, J.R., 1991, Surface ruptures and deformation associated with the 1988 Tennant Creek and 1986 Marryat Creek, Australia, intraplate earthquakes: Geological Society of America Abstracts with Programs, v. 23, no. 5, p. A224.
- Robbins, S. L., Williamson, Courteney, and Jones-Cecil, Meridee, 1991, Principal facts for gravity stations in Oklahoma and southern Kansas established in 1987, 1988, and 1989: U.S. Geological Survey Open-File Report 91-335, 80 p., one 5<sup>1</sup>/<sub>4</sub>" diskette.
- Swolfs, H.S., 1991, Deformation features in cores from the Dow Chemical B.L. Garrigan #1, Mississippi County, Arkansas: Program and Abstracts, Eastern Section, Seismological Society of America, 63<sup>rd</sup> Annual Meeting, Memphis, Tennessee, October 13-16, 1991, p. 61.
- Swolfs, H.S., in press, Structural features in the Dow Chemical B.L. Garrigan No. 1, Mississippi County, Arkansas, and their paleotectonic implications: *Seismological Research Letters*.
- Taylor, M.E., Collins, D.S., Palmer, A.R., and Repetski, J.E., 1991, Upper Cambrian biostratigraphic correlations in the Reelfoot basin, northeastern Arkansas: Program with Abstracts, Louis Unfer, Jr., Conference on the Geology of the Mid-Mississippi Valley. Southeast Missouri State University, Cape Girardeau, Missouri, 5 p. (unnumbered)



**1. Regional Seismic Monitoring in Western Washington**

**14-08-0001-A0622 R.S. Crosson, P.I.**

**and**

**2. Seismic Monitoring of Volcanic and Subduction Processes in Washington and Oregon**

**14-08-0001-A0623 S.D. Malone and A.I. Qamar, P.I.s**

R.S. Crosson, S.D. Malone, A.I. Qamar and R.S. Ludwin

Geophysics Program

University of Washington

Seattle, WA 98195

(206) 543-8020

April 1, 1991 - Sept. 30, 1991

## **Investigations**

Operation of the Washington Regional Seismograph Network (WRSN) and preliminary analysis of earthquakes in Washington and Northern Oregon continue under these contracts. Quarterly bulletins which provide operational details and descriptions of seismic activity in Washington and Northern Oregon are available from 1984 through the third quarter of 1991. Final published catalogs are available from 1970, when the network began operation, though 1986.

The University of Washington operates 81 stations west of 120°W under these agreements, 28 are supported under A0622, 51 under A0623, and 2 are operated jointly. This report includes a brief summary of significant seismic activity. Additional details are included in our Quarterly bulletins.

## **Network Operations**

In August and September 1991, under JOA 14-08-0001-A0623 4 new stations in Oregon (SSO, FBO, WMO, and RNO) were added to the network. Station GRO in Oregon was resited and renamed TKO. APW, funded under A0622, was removed in March due to blasting at a nearby quarry and will be resited. Locations of recent significant earthquakes located by the WRSN can be obtained over the ethernet using the utility "finger quake@geophys.washington.edu".

## **Seismicity**

Figure 1 shows earthquakes ( $M_c \geq 2.0$ ) located in Washington and Oregon during this reporting period. Excluding blasts, probable blasts, and earthquakes outside the U. W. network, a total of 794 earthquakes west of 120.5°W were located between April 1 and Sept 30, 1991. Of these, 279 were located near Mount St. Helens, which has not erupted since October of 1986. East of 120.5°W, 121 earthquakes were located.

During this reporting period there were 6 earthquakes reported as felt west of the Cascades, and 1 reported as felt to the east of the Cascades. No damage was reported. The largest earthquake within the area shown in Fig. 1 was a  $M_c$  3.9 earthquake which occurred on April 15 (UTC) at a shallow depth ( $< 5$  km) in the north Cascades approximately 35 km NE of Chelan and was felt in Chelan and Douglas Counties. An earthquake sequence in the Portland area between July 17 and August 3 included two felt earthquakes and 18 others larger than magnitude 1., most at depths between 10 and 20 km. Both felt earthquakes occurred on July 22 with  $M_c$  3.5 and 2.2 at 09:04 and 09:11 UTC respectively.

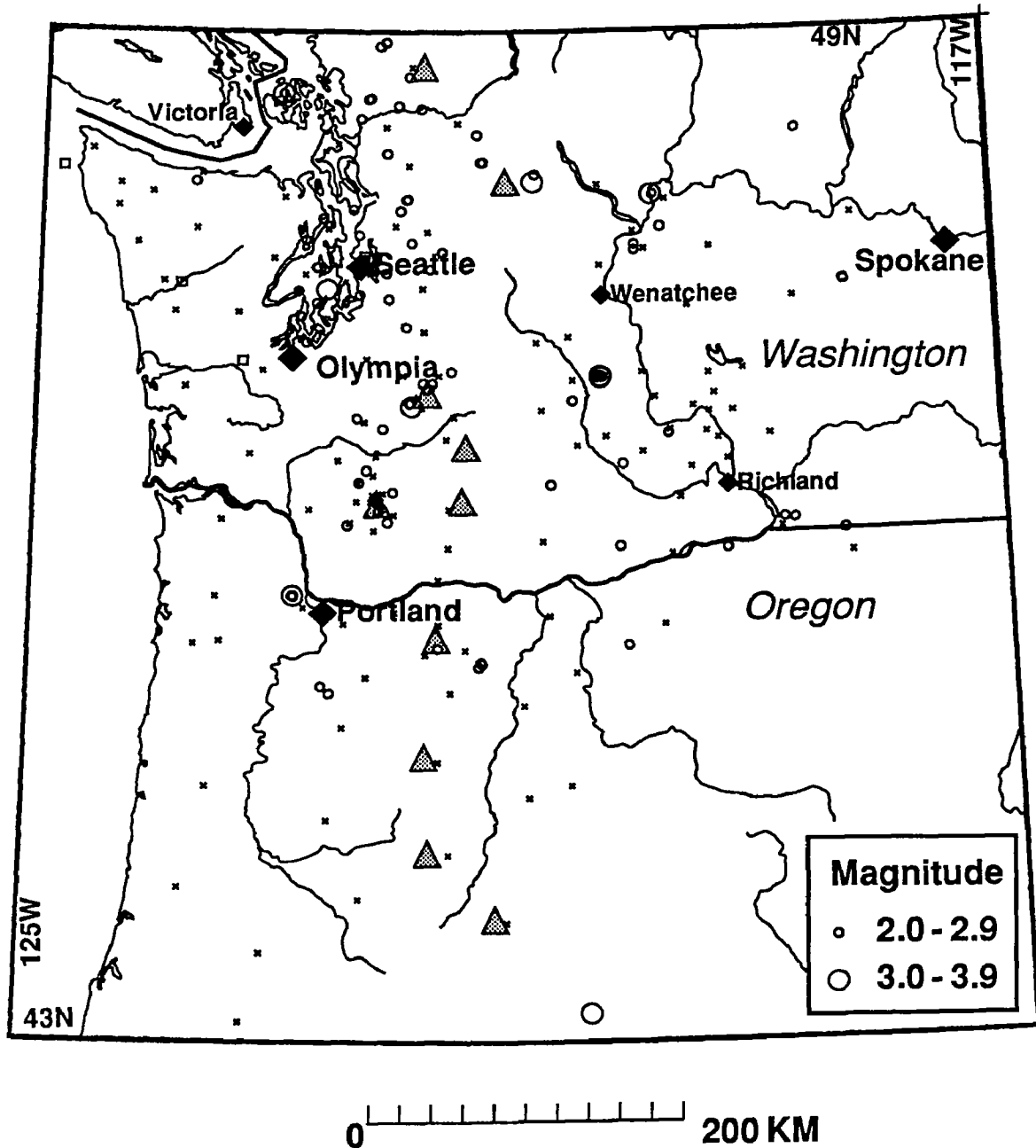


Figure 1. Map view of Washington and Oregon showing locations of earthquakes ( $M_c \geq 2.0$ ) that occurred between April 1 and September 30, 1991. Earthquakes shallower than 30 km are shown as circles, while deeper events are indicated by squares. Shaded triangles represent Cascade volcanos, and seismic stations operated by the WRSN are indicated by "x".

## Publications

- Barker, S.E. and S.D. Malone, Magmatic system geometry at Mount St. Helens modeled from the stress field associated with post-eruptive earthquakes, *JGR*, V. 96, pp. 11883-11894.
- Ludwin, R. S., S.D. Malone, R.S. Crosson, A.I. Qamar, (in press), Washington Earthquakes 1986, *in* U.S. Earthquakes
- Ludwin, R. S., S.D. Malone, R.S. Crosson, A.I. Qamar, (in press), Washington Earthquakes 1987, *in* U.S. Earthquakes
- Ludwin, R. S., S.D. Malone, R.S. Crosson, A.I. Qamar, (in preparation), Washington Earthquakes 1988, *in* U.S. Earthquakes
- Ludwin, R. S., S.D. Malone, R.S. Crosson, A.I. Qamar, (in preparation), Washington Earthquakes 1989, *in* U.S. Earthquakes
- Ludwin, R. S., C.S. Weaver, and R.S. Crosson, (in press), Seismicity of Washington and Oregon, *in*: Slemmons, D.B., E.R. Engdahl, D. Blackwell and D. Schwartz, editors, Decade of North American Geology associated volume CSMV-1; Neotectonics of North America.
- Ma, Li, R.S. Crosson, and R.S. Ludwin, (submitted), Preliminary Report on Focal Mechanisms and stress in western Washington, *in*: USGS Professional Paper "Assessing and Reducing Earthquake Hazards in the Pacific Northwest")
- Thompson, K.I., (in preparation), Seismicity of Mt. Rainier - a detailed study of events to the west of the mountain and their tectonic significance,
- Univ. of Wash. Geophysics Program, 1991, Quarterly Network Report 91-A on Seismicity of Washington and Northern Oregon
- Univ. of Wash. Geophysics Program, 1991, Quarterly Network Report 91-B on Seismicity of Washington and Northern Oregon
- Univ. of Wash. Geophysics Program, 1991, Quarterly Network Report 91-C on Seismicity of Washington and Northern Oregon

## Abstracts

- Jiang, Y, A.I. Qamar, and S.D. Malone, 1991, Earthquake relocation near the Blanco fracture zone, *EOS*, V. 72, # 44, p. 605.
- Jonientz-Trisler, C. B. Myers, and J. Power, 1991 (in press), Seismic identification of gas-and-ash explosions at Mount St. Helens: capabilities, limitations, and regional application, presented at "First International Symposium on Volcanic Ash and Aviation Safety" Seattle WA, July 8 through 12, 1991.
- Malone, S.D., S. Moran and S. Barker 1991, Magma system evolution at Mount St. Helens, Washington as determined from seismicity, presented at 1991 IUGG meeting, Vienna Austria, IAVCEI Program and Abstracts p. 36
- Moran, S., S.D. Malone, and S. Barker, 1991, Deep earthquakes at Mt. St. Helens: evidence for a collapsing and dilating magma chamber, *EOS*, V. 72, # 44, p. 523.
- Qamar, A.I., R.B. Benson, and R.S. Ludwin, 1991, Recent seismicity in the Pacific Northwest since 1986, *EOS*, V. 72, # 44, p. 603.

## Characterization and Seismic Potential of Blind Thrusts along the Northern Margin of the Los Angeles Basin

Agreement No 14-08-0001-G1965

Thomas L. Davis and Jay S. Namson  
Davis and Namson Consulting Geologists  
25600 Rye Canyon Road, Suite A  
Valencia, CA 91355

(805) 257-6870

### Introduction

The Transverse Ranges of southern California are undergoing active north-south shortening as documented by late Miocene and Quaternary age folds, thrust faults, and reverse faults, geodetically measured north-south convergence and numerous compressive earthquake events with north-south directed P-axes. We have proposed that the compression has resulted in an actively developing fold and thrust belt in which the high level thrusts root into a mid-crustal detachment at 12-15 km. These interpretations are based on the integration of surface, subsurface, seismic reflection and earthquake data into retrodeformable cross sections that can be used to determine slip rates and seismic potential of thrust faults. We also suggest that zones of high seismicity and moderate to large compressive earthquakes of the Transverse Ranges occur in the ramp areas of the major thrusts (1930 Santa Monica earthquake,  $M=5.5$ ; 1952 Kern County earthquake,  $M=7.7$ ; 1971 San Fernando earthquake,  $M=6.6$ ; 1972 Point Mugu earthquake,  $M=6.0$ ; 1978 Santa Barbara earthquake,  $M=5.0$ ; 1979 Malibu earthquake,  $M=5.0$ ; 1987 Whittier Narrows earthquake,  $M=5.9$ ). An important element of these interpretations is that many of the thrusts do not reach the surface (blind thrusts) but terminate in folds or reach the surface by complicated trajectories.

These destructive earthquakes underscore the need for detection and study of the geometry, slip rates and seismic potential of thrust faults. The most useful approach in assessing the seismic potential of active thrusts involves the integration of geological and geophysical surface and subsurface data into balanced cross sections and subsurface maps on key stratigraphic horizons. Our recent work has identified large blind thrust faults that underlie the northern margin of metropolitan Los Angeles that are responsible for the recent uplift of the Santa Monica Mountains. This fault trend poses one of the most serious earthquake hazards in the United States because it passes directly under a densely populated area, the fault(s) have high slip rates, and tentative recurrence and segmentation analysis suggests the faults may generate future earthquakes larger than the magnitude 5.9 Whittier Narrows earthquake.

In past studies we have constructed three regional cross sections across the northern margin of the Los Angeles basin. These three regional cross sections show changes in thrust geometry, structural style and slip rate estimates for the trend that must be resolved and understood to accurately assess the seismic potential of active thrusting.

## Research Objectives

The objective of this study is to resolve the three dimensional structural geometry of the fault zone and determine the fault slip history so that the seismic potential of active thrust faults along the northern margin of the Los Angeles basin can be more fully evaluated. To accomplish these objectives the structural style and growth history of the deformation must be determined. The main approach is to construct: 1) a series of balanced cross sections across the northern margin of the basin and 2) a set of subsurface maps of the basin's northern margin on critical late Cenozoic-age stratigraphic horizons. These products, when integrated with our existing analyses and existing Quaternary surface studies, will provide a detailed picture of the three-dimensional geometry and growth history of the faults responsible for the active uplift and deformation of the Los Angeles basin's northern margin. This type of three-dimensional analysis is the most effective way to minimize the uncertainties of structural interpretation when applying the balanced cross section approach to earthquake hazards.

## Research Status

Our research status is in the compilation phase. Two new cross sections are currently being constructed. One of the new cross sections traverses the Montebello Hills and central Los Angeles Basin and the second new cross section traverses the Puente Hills and eastern portion of the Los Angeles Basin. For these two cross sections we are constructing topographic profiles, integrating surface geology, interpreting and correlating subsurface lithologic, structural and paleontologic data from oil and gas wells. We have also begun posting subsurface data on key stratigraphic horizons for constructing the regional structure contour maps.

## Reports Published

Namson, Jay and Davis, Thom L., 1991, Structural styles across a transpressive plate boundary examples from central and southern California: Geological Society of America (abst), v. 23, n. 5, p. 256.

# Reanalysis of Instrumentally Recorded United States Earthquakes

9920-01901

J. W. Dewey

and

William Spence

Branch of Global Seismology and Geomagnetism

U.S. Geological Survey

Denver Federal Center

Box 25046, Mail Stop 967

Denver, Colorado 80225

(303) 236-1506

## Investigations

1. Describe the seismicity before and after the  $M_w$  8.7, 1957 Aleutian arc earthquake to better understand the earthquake cycle in subduction zones. This major undertaking also will answer numerous questions concerning the size and probable rupture characteristics of this important earthquake (William Spence with T. Boyd and E. R. Engdahl).
2. Interpret the seismicity before and after the  $M_s$  7.8, 1974 Peru earthquake to clarify the nature of subduction at this complex convergence zone (William Spence with C. J. Langer).
3. Prepare report on public response to Iben Browning's prediction of an earthquake to occur in the region of New Madrid, Missouri on about 4 December 1990 (William Spence with R. B. Herrmann, A. C. Johnston, and G. Reagor).
4. Determine the tectonic consequences of a stalled Farallon plate that is heated by the underlying asthenosphere, as an explanation for the regional tectonic origins of modern western North America (William Spence).
5. Relocate epicenters, recompute magnitudes, and evaluate the tectonic implications of teleseismically recorded earthquakes from Yellowstone Park, Wyoming, and adjacent Montana and Idaho, including shocks associated with the Hebgen Lake earthquake ( $M_s$  7.5) of August 1959 (J. W. Dewey).
6. Numerically model temperature distributions within a subducting plate with the objective of calculating the extent of phase changes, plate rheology, and, ultimately, the magnitude of slab pull force. Numerically model the dynamics of delivery of the slab pull force into shallow subduction zones with the objectives of improved understanding of how the slab pull force contributes to causing both major subduction earthquakes and other dynamic processes at subduction zones (Steve Mueller with W. Spence).

## Results

1. Magnitudes and relocations have been determined for nearly 7000 earthquakes in the region of the great 1957 Aleutian arc earthquake for the period 1950-present. The catalog for the 1957 aftershocks is complete above magnitude 5.5.
2. Most aftershocks of the 1974 Peru earthquake have been relocated to verify focal depths and space-time development of the aftershock series, as earlier done with another velocity model and another location algorithm. This aftershock data set remains one of the most detailed and precise for any great subduction earthquake and thus is of particular significance in interpretation of the earthquake cycle in subduction zones. Composite focal mechanisms indicate thrust faulting for aftershocks downdip of the main shock's rupture at the plate interface section analogous to that which spawned the great 1940 Peru earthquake. Additionally, one concentration of aftershocks shows that the Nazca plate underwent localized internal deformation.
3. Photos and newspaper clippings have been assembled into a source document for researchers on the sociological impact of this failed earthquake prediction. These materials and an accompanying report have been submitted for publication as a USGS Circular.
4. Spence's model postulates that a large subhorizontal segment of the subducting Farallon plate stalled beneath western North America at the end of the Laramide orogeny (50-45 Ma). Subsequently, the plate has translated southwestward with the North American plate, the former being continually heated by the underlying asthenosphere. The low velocity zone that underlies much of the western United States is the partially melted relict Farallon plate, whereas the asthenosphere is beneath this low-velocity zone for P waves. Spence proposes that the thermal evolution of the stalled Farallon plate has determined the tectonic evolution of the post-Laramide, overriding continental lithosphere.
5. Short-period magnitudes ( $m_{Lg}$ ) have been computed for 225 shocks of the Yellowstone/Hebgen Lake region based on amplitudes of the Lg phase measured on microfilmed seismograms. The  $m_{Lg}$  magnitudes are calculated using source-station attenuation parameters that account for regional variations in Lg attenuation. These parameters are held constant for all Yellowstone/Hebgen Lake earthquakes recorded at a single station, but the parameters are, in general, different for different stations. The attenuation parameters are based on, but modified slightly from, attenuation parameters implied by a map of crustal Q published by Singh and Herrmann (1983, Journal of Geophysical Research, v. 88, p. 527-538). With a single attenuation parameter at all stations,  $m_{Lg}$  computed at individual stations would be highly dependent on epicentral distance and azimuth, and the average  $m_{Lg}$  for each earthquake would depend on the stations that provided Lg amplitude data for the earthquake. The use of station-dependent attenuation parameters substantially reduces the scatter of individual station  $m_{Lg}$  about the mean  $m_{Lg}$ , and it allows valid comparison of earthquakes recorded by different sets of

stations. The computed  $m_{Lg}$  agree well with  $m_b$  magnitudes determined for Yellowstone/Hebgen Lake shocks using only P-wave amplitudes recorded at epicentral distances of more than  $15^\circ$ .

Considering the magnitude ( $m_{Lg}$ ) versus frequency distribution of the teleseismically recorded shocks as well as the extent to which the earthquakes were recorded at teleseismic distances, it appears that the catalog of shocks is essentially complete for  $m_{Lg} \geq 4.6$  since the mid-fifties. The earliest teleseismically recorded event from the Yellowstone/Hebgen Lake region occurred in 1947.

Previous catalogs of shocks for the region for 1947-1989 are extremely heterogeneous, reflecting changes that have occurred through the decades in magnitude computing practice. Considering earthquakes from 1947-1962 for which magnitudes were computed in the present study, less than 25 percent have magnitudes assigned to them in the hypocenter data files of the National Earthquake Information Center (NEIC). For 1962-1977, the number of events with previously computed magnitudes rises to 80 percent of the total, but most of the previous magnitudes are  $m_b$  magnitudes that were calculated by applying formulas of Gutenberg and Richter (e.g., C. F. Richter, Elementary Seismology, p. 688) to amplitudes obtained at epicentral distances of less than  $15^\circ$ . It is now recognized that Gutenberg and Richter's formulas are unsatisfactory for computing  $m_b$  at small epicentral distances in many areas; in the Yellowstone/Hebgen Lake region,  $m_b$  computed with data from distances less than  $15^\circ$  are systematically high with respect to  $m_b$  computed with data from distances greater than  $15^\circ$ . After 1977,  $m_b$  for Yellowstone/Hebgen Lake shocks have generally been computed using only amplitudes recorded at  $\Delta > 15^\circ$ , and most shocks have had a type of  $M_L$  computed for them.

The existence of magnitudes computed with a common procedure should allow study of the evolution of Yellowstone/Hebgen Lake seismicity since 1947 with a confidence that has not previously been warranted. The revised magnitudes imply that since 1964 the frequency of shocks having short-period magnitudes of 4.6 and greater is lower by a factor of 10 than implied by previously catalogued  $m_b$  magnitudes. Since 1964, the frequency of shocks having  $m_{Lg}$  of 3.8 and greater is lower by a factor of three than implied by previously catalogued  $m_b$ .

6. An existing computer program for calculating mantle convection has been adapted for numerical calculations of the thermal evolution of subducted lithosphere. Early results show the temperature distributions within subducting plates of arbitrary descent velocities to match those determined by Dan McKenzie, who used more limited analytic methods. These results are being input into a program coded by Mueller and R. Phillips to calculate deformations within a plate of elastic-plastic rheology.

### Reports

Bowman, J. R., and Dewey, J. W., 1991, Relocation of teleseismically recorded earthquakes near Tennant Creek, Australia--Implications



- for midplate seismogenesis: *Journal of Geophysical Research*, v. 96, p. 11,973-11,979.
- Boyd, T., Engdahl, E. R., and Spence, W., 1991, Aleutian earthquake catalog--1957 through 1989 [abs.]: EOS (American Geophysical Union, Transactions) (in press).
- Dewey, J. W., 1991, Joint epicenter determination for earthquakes occurring over several decades--A case history from northern Algeria, in Mezcua, J., and Udias, A., eds., *Seismicity, seismotectonics and seismic risk of the Ibero-Maghrebian region*: Monografia 8, Instituto Geografico Nacional, Madrid, Spain, p. 51-63.
- Spence, W., 1991, Tectonic origins of the modern American West [abs.]: EOS (American Geophysical Union, Transactions), v. 72 (in press).
- Spence, W., Herrmann, R. B., Johnston, A. C., and Reagor, G., 1992, Responses to Browning's prediction of a 1990 New Madrid, Missouri, earthquake: U.S. Geological Survey Circular (submitted).

## Seismic Studies of Fault Mechanics

9930-02101

William L. Ellsworth  
Lynn Dietz and David A. Castillo

Branch of Seismology  
U.S. Geological Survey  
345 Middlefield Road - MS 977  
Menlo Park, California 94025  
415-329-4784

### Investigations

1. Analysis of preshocks and aftershocks of the 1989 Loma Prieta earthquake.
2. Nucleation and growth of the 1989 Loma Prieta earthquake.
3. Seismotectonics of the San Andreas fault system in northern California.
4. Earthquake monitoring along the Hayward fault.

### Results

1. Continuing analysis of the locations and focal mechanisms of the Loma Prieta earthquake and regional activity underscores our earlier conclusions about the absence of activity along the rupture zone in the decades prior to the earthquake (Figure 1). Comparisons between the prior activity associated with the San Andreas fault and Loma Prieta aftershocks show that the Loma Prieta event forms a distinct plane along most of its length. At the southeastern end of the sequence, however, it merges smoothly with the San Andreas, near the prominent cluster of deep activity at km 47 in Figure 1. This suggests that the Loma Prieta fault plane branches continuously from the San Andreas at this position.

New results for the aftershocks, obtained from the first 10½ months of the sequence reveal surprisingly little activity in the vicinity of the main shock. This is somewhat surprising, give results from modelling of mainshock seismograms which indicate little slip in this region. If this were a region of low slip, then numerous aftershocks could be expected, by analogy with other well-studied earthquakes such as the 1984 Morgan Hill, California, earthquake. Results described below, however, raise questions about the interpretation of small slip, and suggest substantial displacements in the hypocentral region during the 1.6 s interval between the initiation of faulting (in a foreshock) and the high-frequency main shock origin time.

2. High frequency seismograms of the 1989 Loma Prieta, California earthquake ( $M_w$  6.9) indicate that it initiated with a foreshock 1.6 s before the main shock. P and S phase arrivals for both events are seen on the 1 Hz USGS Calnet stations, on the U.C. Berkeley broad band stations, and on strong motion accelerographs operated by U.C. Santa Cruz and CDMG. A magnitude of 5.0 is estimated for the foreshock from the peak amplitude of the S wave velocity as measured on 26 strong motion instruments, and by comparison

of P wave amplitudes with the 1989 Lake Elsinore, Calif., earthquake (Figure 2). A JHD solution for the foreshock and mainshock hypocenters places the mainshock about 1-1½ km above the foreshock. This result, however, depends critically upon the proper identification of phases, and consequently mainshock nucleation at the foreshock hypocenter cannot be rejected.

Broad band displacement seismograms recovered from five digital accelerographs with pre-event memory, all located in the near field of the earthquake, tell a different story. They show that the earthquake began very smoothly starting from the time of the foreshock (Figure 3). The initial portions of the displacement seismograms can be fit by simple synthetic seismograms from a point source with the same moment rate function as a uniformly expanding circular crack. The integrated moment accumulated in the first 1.6 s of the rupture, or by the time of the high frequency mainshock origin time, is equivalent to a  $M_w$  5.7 earthquake. These results emphasize the importance of broad band recordings in the near field of earthquakes for the interpretation of source dynamics.

3. The northernmost and relatively youthful segment of the San Andreas fault system between Point Arena and Cape Mendocino forms a ~ 100 km wide zone of northwest trending strike-slip faults centered on the Maacama fault and bounded by the San Andreas fault to the west and the Bartlett Springs fault to the east. The San Andreas fault north of Point Arena has been virtually aseismic in recent decades. In contrast, dense clusters of microearthquakes locate along the Maacama fault, and to a lesser extent, along the Bartlett Springs fault. Seismicity at the northern ends of these fault zones terminates above the southern edge of the subducted Gorda Plate. Seismic strain release along both of these faults is dominated by right-lateral shearing along fault planes that dip 60°-80° to the northeast, rather than along vertical faults which is the norm along more mature faults within the San Andreas fault system. This suggests that these youthful faults reactivate structures formed within the forearc region of the Cascadian subduction zone, specifically the Garberville and Lake Mountain fault zones located to the north. Although the Maacama and Bartlett Springs faults lie within the broad heat flow anomaly presumably due to the presence of the asthenospheric "window" beneath them, the placement of these seismically faults appears to be principally controlled by inherited structural fabric as opposed to thermal weakening of the lower crust and upper mantle.
4. As part of the Bay Area Future Earthquakes Project, a new all-digital seismic network is being installed along the Hayward fault in the eastern San Francisco Bay region. This work is being done in cooperation with Malcolm Johnston and Paul Spudich (U.S.G.S.), and Tom McEvilly and Barbara Romanowicz (U.C. Berkeley). The network will consist of high frequency seismometers installed in boreholes and force-balance accelerometers installed at the surface. Three components of ground motion will be transmitted in real time from both sets of sensors to central recording sites in Menlo Park and Berkeley. The network is designed to provide routine detection and recording of all earthquakes above about  $M$  0.5 along the fault, and to record all events on-scale through the largest anticipated ground motions, a  $M$  7 event on the Hayward fault. The network will be used to prototype algorithms for a seismic early warning system with a design response time of 2-3 seconds after the initial P-wave arrival. It will also be used to study the

characteristics of the earthquake source at frequencies up to 100 Hz.

Installation of the first four borehole sensors in core holes at borehole strainmeter sites along the southern Hayward fault is now complete. Digital field acquisition hardware and central site recording hardware has been ordered, with delivery expected in the spring of 1992.

## Reports

- Castillo, D.A., and Ellsworth, W.L., 1991, The seismotectonics of the San Andreas fault system north of Point Arena among the Coast Ranges of Northern California (abs.): *Seismological Research Letters*, v. 62, p. 11.
- Ellsworth, W.L., and Dietz, L.D., 1990, Crustal stress and seismic strain release in the 1989 Loma Prieta, California earthquake: *Proceedings of Seventh Joint Meeting the U.J.N.R. Panel on Earthquake Prediction Technology*, Tsukuba Japan: Geographical Survey Institute, Ministry of Construction, p. 67-82.
- Ellsworth, W.L., 1991, Practicing earthquake prediction: translating Earth science research into action: *International Seminar on Earthquake Prediction and Hazard Mitigation Technology*: Science and Technology Agency, Japan, p. 43-62.
- Ellsworth, W.L., 1991, Nucleation and growth of the Loma Prieta earthquake (abs): *EOS, Transactions, American Geophysical Union*, v. 72, no. 44, p. 293.

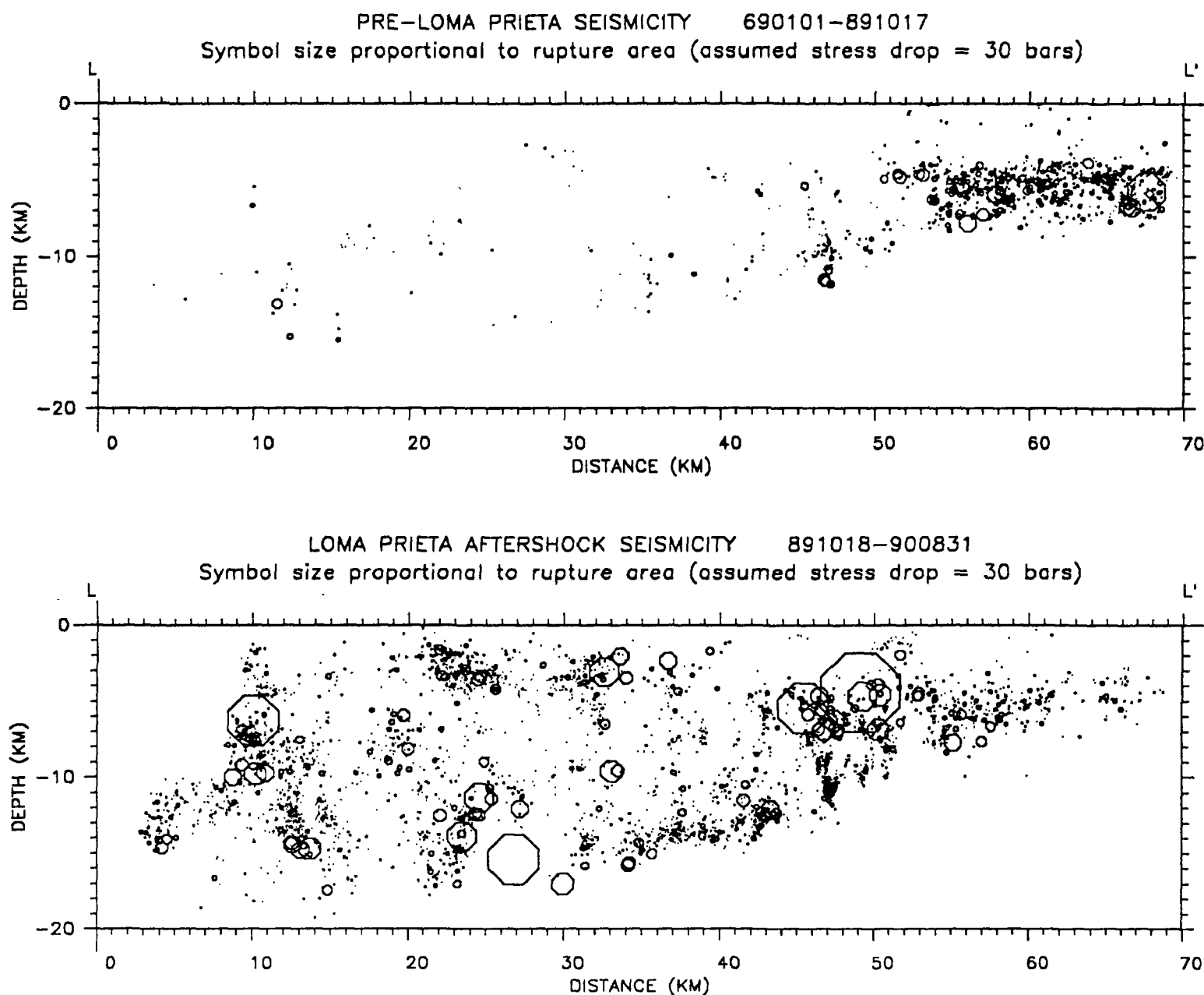


Figure 1. Cross sections of seismicity along the 1989 Loma Prieta, California, earthquake aftershock zone. Hypocenters restricted to the narrow dipping zone defined by early aftershock activity. Symbol size is equal to source dimension for a 30 bar stress drop. Top figure displays all events from January 1, 1969 until the main shock. Bottom figure displays main shock (large symbol at bottom center) and aftershocks through August 31, 1990.

## Foreshock S-Wave Amplitude Magnitude

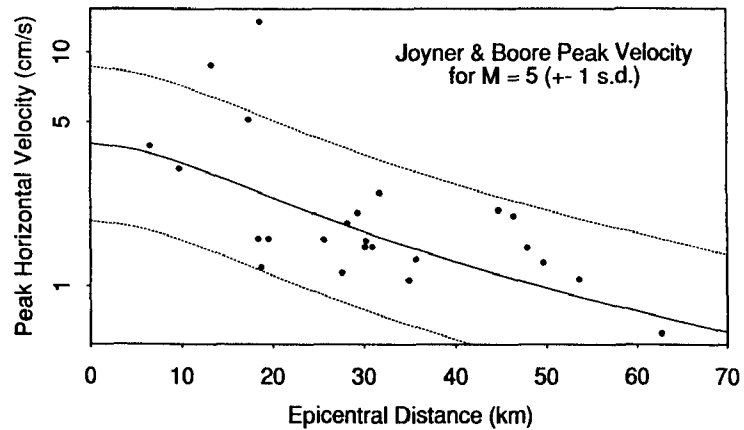


Figure 2. Comparison between peak horizontal velocity of foreshock S-wave arrival and peak velocity relation from Joyner and Boore (1988) for  $M = 5$  event. The amplitudes, measured at frequencies of 2-5 Hz, suggest a magnitude of about 5 for the foreshock.

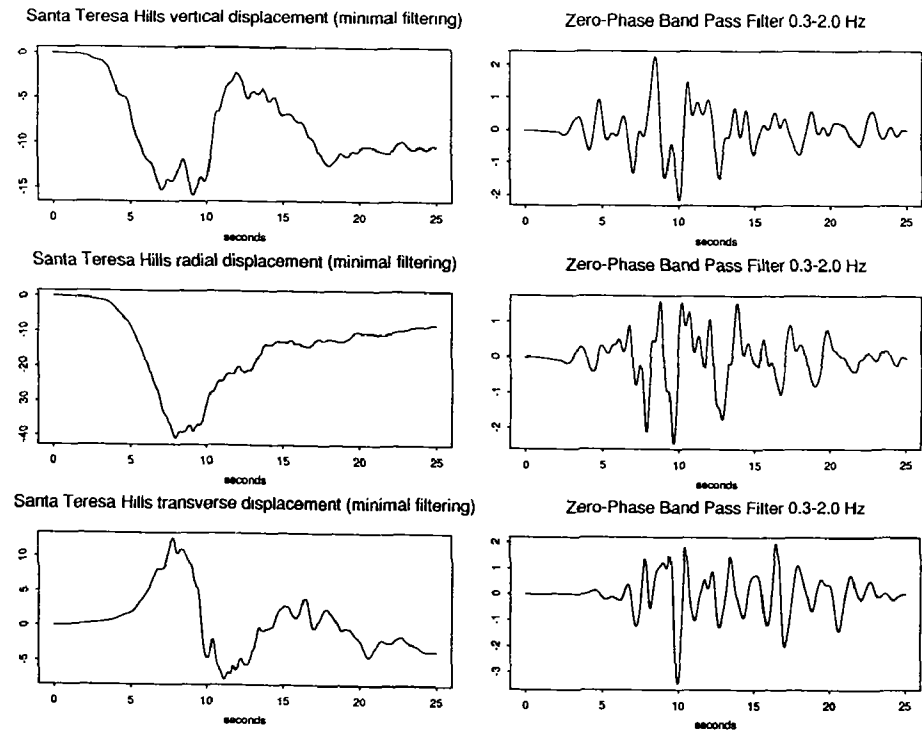


Figure 3. Displacement seismograms recovered by double integration of digital accelerogram recorded at CSMIP station 563 (Santa Teresa Hills, San Jose) at an epicentral distance of 20 km. Orientation of components is with respect to the epicenter. (Note that radial component is also essentially perpendicular to the entire rupture.) Left-hand column filtered with 1-pole high-pass Butterworth filter at 100 s period. Right-hand column filtered to simulate pass-band commonly used in strong-motion modelling of the event.

## Global Seismology

9920-03684

E. R. Engdahl

and

E. A. Bergman

Branch of Global Seismology and Geomagnetism

U.S. Geological Survey

Denver Federal Center

Box 25046, Mail Stop 967

Denver, Colorado 80225

(303) 236-1506

Investigations

1. Travel-Time Tables. Develop new standard global travel-time tables to locate earthquakes.
2. Arrival-Time Data. Coordinate planning for an International Seismological Observing Period (ISOP)--a time interval during which there would be enhanced reporting of arrival-time data.
3. Earthquake Location in Island Arcs. Develop practical methods to accurately locate earthquakes in island arcs.
4. Subduction Zone Structure. Develop techniques to invert seismic travel times simultaneously for earthquake locations and subduction zone structure.

Results

1. Travel-Time Tables. Over the last three years, a major international effort within IASPEI has led to the construction of a new set of global travel-time tables for earthquake location and phase identification (Kennett and Engdahl, 1991). The new tables are derived from a radially stratified model iasp91 which has been constructed so that the times for the major seismic phases are consistent with the times for events in the ISC catalog for the period 1964-1987. The baseline for the P-wave travel times in the iasp91 model has been adjusted to provide only a small bias in estimated origin time for well-constrained events at the main nuclear testing sites around the world. The primary form of representation of the new tables is a set of computational algorithms, but for convenient reference, a book of tables (the IASPEI 1991 Seismological Tables) has also been produced. The style of the iasp91 velocity model has been chosen to facilitate the development of travel time calculation and location schemes that allow for regional variations in the outer parts of the Earth.
2. Arrival-Time Data. The International Seismological Observing Period (ISOP) is gaining recognition as a uniting force within the seismological community. This is the overall impression after the recent ISOP workshop at the IUGG General Assembly in Vienna. This impression was well conveyed in an inspired closing address by T. H. Jordan (who proposed the project in

1986). The meeting had, in fact, several functions: (1) This was the proper place to report on the current status and future plans of ISOP. The progress report of the Chairman E. R. Engdahl highlighted the establishment of the ISOP office in Golden, Colorado, and the employment of a full-time coordinator (E. A. Bergman). Since careful planning is essential for success of the project, a definite timetable for the actual Observing Period is not yet available; certainly this period would not start before 1993 at the earliest. (2) Several ISOP-related initiatives have resulted in products such as the new IASP91 velocity model and travel-time tables (edited by B.L.N. Kennett), a competing radial velocity model (A. Morelli and A. Dziewonski), information plots for stations reporting to the ISC (L. Hwang and R. Clayton), and a seismic analysis software package (A. Plesinger et al.). (3) Research reports relevant to ISOP include the analysis of ISC data (E. R. Engdahl et al., and R. Adams and V. Marza), the processing of global long-period digital data (P. Shearer), and the analysis of later-phase parameters (D. Doornbos and T. Rekdal).

3. Earthquake Location in Island Arcs. Within a 30-year period, portions of the Aleutian arc have ruptured twice in great earthquakes. The first, in March 1957 ( $M_W=8.5$ ), ruptured no less than 900 km of the arc. The second, in May 1986 ( $M_W=8.0$ ), nucleated close to the epicenter of the 1957 event and reruptured a 250-km long portion of the arc. We have relocated and cataloged seismicity recorded from 1957 through 1989 (March) that is located between  $175^\circ\text{E}$  and  $160^\circ\text{W}$ . This catalog contains observations for the only complete seismic cycle bounded by two instrumentally recorded great earthquakes along the Alaska-Aleutian arc.

Our relocations include epicenter-dependent, P-wave station corrections that account for near source velocity structure. These corrections are calculated for 686 stations using a slab geometry detailed in a recent travel-time study and the iasp91 travel-time model. Unless other information is available, source depths are constrained to 35 kilometers. For deeper events occurring within the Wadati-Benioff zone, station corrections are not used and depths are allowed to change. Travel-time observations for events occurring between 1957 through 1963 are obtained from the bulletins of the ISS and the BCIS. For this time period, these catalogs provide magnitudes for only a small percentage of the events. We calculated magnitudes for as many of the events as possible using amplitudes recorded at Pasadena. For events occurring from 1964 through 1989, travel times and magnitudes are obtained from the ISC phase tapes.

The completed catalog consists of approximately 7300 events. Of these, approximately 5000 have 90-percent error vectors of less than 25 km. The homogeneous magnitude cutoff of the catalog appears to be about 5.5. Our relocations are compared with previously published relocation efforts, and the limitations of the data set imposed by the quantity and quality of the observations are determined.

4. Subduction Zone Structure. In tomographic studies, the signal in residual data reported by agencies such as the ISC is usually assumed to be largely the result of 3-D structure. However, a substantial part of the data scatter can be explained by inaccuracies in the reported earthquake



locations and by incorrect assumptions about the 1-D variation of P-wave velocity with depth. P and later arriving phases were used with the iasp91 travel times to relocate ISC hypocenters and reassociate phases prior to inversion for 3-D Earth structure. Upon relocation, structurally related signal that had been absorbed in the inaccurate ISC earthquake locations was recovered in the new travel-time delays. Subsequent tomographic inversion revealed that the addition of this previously missing information resulted in significantly better resolution of velocity anomalies. Tomographic inversions for mantle structure beneath northwestern Pacific island arcs using this approach provides new information about the morphology of subduction zones in this region (Van der Hilst et al., 1991). In particular, the tomographic images show that slabs beneath the Japan and Izu Bonin island arcs are deflected at the boundary between the upper and lower mantle, whereas those beneath the northern Kuril and Mariana arcs sink into the lower mantle.

### Reports

- Hwang, L. J., and Clayton, R. W., 1991, A station catalog of ISC arrivals-- Seismic station histories and station residuals: U.S. Geological Survey Open-File Report 91-295, 3187 p.
- Kennett, B.L.N., and Engdahl, 1991, E. R. Travel times for global earthquake location and phase identification: *Geophysical Journal International*, v. 105, p. 429-465.
- Van der Hilst, R. D., and Engdahl, E. R., 1991, On the use of PP and pP data in delay time tomography: *Geophysical Journal International*, v. 106, p. 169-188.
- Van der Hilst, R. D., Engdahl, E. R., Spakman, W., and Nolet, G., 1991, Tomographic imaging of subducted lithosphere below northwest Pacific island arcs: *Nature*, v. 353, p. 37-42.

## SEISMOTECTONIC RESEARCH STUDIES

9950-04556

A.F. Espinosa, H.R. Schmoll, L.A. Yehle  
 Branch of Geologic Risk Assessment  
 U.S. Geological Survey  
 Box 25046, MS 966, Denver Federal Center  
 Denver, Colorado 80225-0046  
 (303) 236-1597

### Investigations

1. Post-earthquake investigations were undertaken after the damaging Limón, Costa Rica Earthquake of April 22, 1991, with an  $M_s = 7.5$ . Follow-up field investigations have been conducted in the eastern part of Costa Rica and in the northwestern part of Panamá. The post-earthquake field work consisted of video-capturing the intensive damage sustained by the environment and by man-made structures in the meizoseismal region. Direct field observations were made on three occasions in Costa Rica and Panamá. The intensity-damage assessment and geologic field studies were partially funded by AID/OFDA, the Organization of American States, and the governments of Costa Rica and Panamá. The Limón earthquake is a very significant event since it is an intraplate earthquake located on the Caribbean plate.

2. The analysis of earthquake seismicity and focal mechanism solutions have been compiled for Alaska and the Aleutian Island region, for events recorded in the region from 1960 through 1991. The data base is being used to determine  $M_o$  vs magnitude ( $M_L$ ,  $m_b$ ,  $M_s$ ) relationships for events with different source characteristics (thrust, normal, and strike-slip) and for different depth distribution. These relationships will be used to determine the scalar seismic moment for all earthquakes recorded in the region. This program has been initiated after editing a very large data-base for the region. The maximum horizontal stress components for all the significant earthquakes in the region are being determined and mapped in a three-dimensional spatial representation in order to ascertain the spatial characterization of the earthquake potential in said area.

3. Field investigations in the Anchorage A-8 SE quadrangle, Alaska, resulted in numerous improvements to the mapping of that area. Much suburban development has occurred in the past 10 to 15 years since the area was last under detailed investigation, and this has given access to areas not previously visited. Many new roadcuts and excavations have provided new insights into the nature of materials in the area and provided support for or limitations on interpretations of the geology that are currently undergoing revision as a result of the upgrading of the previous mapping.

### Results

1. Results (preliminary) from the intensity (MMI) distribution post-earthquake study in Costa Rica and Panamá shows a very substantial number of observations on the existing inconsistencies in the Modified Mercalli Intensity scale, and they are very similar in nature to the earlier documented problems after the Peruvian, Guatemalan, Nicaraguan, Ecuadorian, and Algerian earthquakes.

2. A seismicity and tectonic stress distribution on the Eurasia-Africa plate boundary has been completed and is in the process of being released for publication.

3. Work in completing geologic mapping of the Anchorage lowland metropolitan area has been underway for several years, bringing up to date mapping that started following the 1964 Alaska earthquake. The ultimate aim is to publish completed maps of the entire area in the I- or GQ- map series at a scale of 1:25,000 on the present topographic base maps. These topographic maps are currently being upgraded by National Mapping Division, and the revised maps should be used for the final publications. Of the 12 geologic quadrangle maps that cover the area, 6 have now been published as surficial geologic or geologic (in areas lacking bedrock) maps in the open-file series; these are the Anchorage B-7 NE, NW, SE, and SW and the Anchorage B-8 SE and SW quadrangles. The latter is the most recently published of these, and involved new mapping in areas on the west side of Knik Arm not previously mapped. Evidence for a later estuarine incursion of the area than that represented by the Bootlegger Cove Formation, resulting from either isostatic or tectonic processes, was developed as a result of that mapping, resolving stratigraphic problems that previously had remained enigmatic. Work on the next map in the series, of the Anchorage A-8 SE quadrangle, is nearly complete, and work on the following map, of the Anchorage A8-NE quadrangle, is under way. In these areas, new more detailed mapping has led to the establishment of two additional morainal systems that were not previously recognized, resulting in more refined categorizations of geologic materials, particularly in the Hillside area, an important suburban residential area.

4. Work has been completed on two reports resulting from investigations of intertidal deposits (interbedded silt and peat) in both Alaska and Chile. These deposits have been recognized as having the potential for providing dates on and recurrence intervals for previous great earthquakes in those areas. The work in Chile did not reveal conclusive evidence for such events. The Alaska work indicated that many such events might have taken place, but unequivocal evidence that the burial of peat deposits by intertidal silt was earthquake related in all cases, and as well as the precise dating of such events, has proved elusive. Nevertheless, recurrence intervals on the order of 400-800 years can be suggested as possible.

5. Geologic mapping previously undertaken in areas of potential coal-mining development on the west side of Cook Inlet has been prepared for open-file release, following requests for this information because of renewed interest in opening of coal mines in that area. The report is presently undergoing revision following technical review. Revision of a surficial geologic map of the Eklutna valley area, Municipality of Anchorage, has been completed following technical review; the map is to be included in a Water Resources Division report currently in preparation.

### **Reports**

Bartsch-Winkler, Susan, and Schmoll, H.R., (in press), Evidence for Late Holocene relative sea level fall from reconnaissance studies in an area of earthquake-subsided intertidal deposits, Isla Chiloé, Chile: International Association of Sedimentologists Special Publication "Sedimentation and Tectonics," R. Steel and others, editors.

Bartsch-Winkler, Susan, and Schmoll, H.R., (in press), Utility of radiocarbon-dated stratigraphy in determining Late Holocene earthquake recurrence intervals, upper Cook Inlet region, Alaska: Geological Society of America Bulletin.

Espinosa, A.F., and Rukstales, K.S., 1991, Geometry, Mode of Subduction and Stress distribution of the Wadati-Benioff Zone beneath western South America, (poster), International Union of Geodesy and Geophysics, International Association of Seismology and Physics of the Earth's Interior, Vienna, Austria.

Espinosa, A.F., and Shedlock K.M., 1991, Stress distribution and seismic deformation in the Alaska and Aleutian Islands Wadati-Benioff Zone (abs.): International Union of Geodesy and Geophysics, International Association of Seismology and Physics of the Earth's Interior, Vienna, Austria.

Yehle, L.A., Schmoll, H.R., and Dobrovolsky, Ernest, 1991, Geologic map of the Anchorage B-8 SW quadrangle, Alaska: U.S. Geological Survey Open-File Report 91-143, 30 p., scale 1:25,000.

## Teleseismic Tomography

9930-01172

John R. Evans, David Croker, H. M. Iyer  
U.S. Geological Survey  
Branch of Seismology  
345 Middlefield Road, MS-977  
Menlo Park, California 94025  
415-329-4753

### Investigations

This Project is performing two relatively distinct tasks for NEHRP: (1) a teleseismic tomography study of the Loma Prieta region, and (2) creating a new teleseismic triggering system for CUSP.

Understanding the lower crust and upper mantle is an element of causality necessary for NEHRP framework studies. The plates are driven by deep circulation patterns; the San Andreas is a plate boundary driven at mantle depth and modified by processes and structures at all depths. Understanding the detailed structure and state of the lower crust and upper mantle are prerequisite to understanding the shallow fraction of the plate boundary responsible for earthquake hazards.

Loma Prieta teleseismic tomography largely targets the middle and lower crust of this major seismogenic zone, below the resolvable depths for local-earthquake tomography. We aim to clarify the condition and location of the controlling plate boundary and to delineate the root structure of the imbricate thrust system bounding the Santa Clara Valley. This thrust system is now recognized as both a major unresolved structural issue and a likely seismogenic zone in its own right.

The second, operational task is applicable to a wide range of studies beyond teleseismic tomography. It will result in a routine flow of teleseismic and distant regional events to CUSP archives, the IRIS data center, and possibly other fora chosen to make these data widely available. CalNet is the largest short-period network in the world and will yield a uniquely powerful teleseismic data set for source studies and Earth structure studies at many scales. These data are now going largely unrecorded.

### Results

1. *Teleseismic tomography:* We successfully operated a 31-site portable seismograph network through December, 1990. This network augmented CalNet in the target region around Loma Prieta, forming nested oval shaped networks centered on the seismogenic zone (Figure 1). The larger network was 30x50 km with 6-km station spacing. Data from this network will be used to image lower crustal and upper mantle structure to delineate primary plate structures and the imbricate thrust system, which it encompasses. The center of this network was further augmented in a 10x30 km region to reach 3-km station spacing. This network will be used to unravel the complex intersection of the Sargent and San Andreas faults and to determine whether two "San Andreas faults" are present, one dipping and one vertical, as inferred from other studies. It is widely believed that some such structures limited fault rupture, but the responsible structure is ill defined. Local-earthquake data recorded on these networks also will be used for upper-crustal tomography, improving existing *P*-wave results and providing the first comprehensive *S*-wave data set.

Three types of seismographs were used in this study, but most of the the data were recorded by the old "5-day" recorders. Digitizing and processing these data is very labor intensive and consumed most of our efforts in FY91. At this writing, the data are 65% digitized and 19% analysed. Reaching this point consumed approximately 1.5 person-years of effort. We anticipate completion of digitizing and most analysis in FY92. We also hope to produce a preliminary result for the Loma Prieta volumes now in preparation by many authors.

2. *CUSP Teleseismic Triggering:* In FY91 we began the design and testing of a PC-based teleseismic triggering system to be installed on CUSP in FY92. An IBM PC compatible dedicated computer will monitor three or more subnets of CalNet, and run a special, highly optimized teleseismic trigger. This system was originally built for the Loma Prieta teleseismic tomography study, and is now being extended for this new use. The event log from the PC will be relayed to CUSP computers, which will then save teleseismic and distant regional events for the entire network.

A great deal of progress has been made to date but several major tasks remain. We have designed the overall system, in consultation with CUSP and Branch experts; defined necessary PC software and hardware changes and obtained the first round of these changes; determined the PC's computational limits (3.5 subnets of 16 stations); assisted the creation of a CUSP2AH decimator/translator (used for dissemination and analysis); systematically selected trigger subnets; and had the subnets wired up to the PC's patch panel and tested. We are now well into tuning the first subnet, including writing two significant pieces of software to support this evaluation.

Remaining tasks are completion of software changes for the PC, tuning the remaining subnets, building the necessary CUSP software, and developing a routine processing and archiving scheme to make the data widely available without significantly impacting normal CalNet operations. This work is likely to be completed in FY92. A remaining problem of uncertain solution is the discovery of numerous microwave telemetry drop outs, probably caused by atmospheric refraction on links near the Bay Area. These multi-channel pulses easily trigger the exquisitely sensitive PC algorithm and pose a potentially serious editing load for CalNet operations. An anticipated beam widening program is likely to help this problem. The larger conclusion must be that new things will be discovered with new triggers, and these seem destined to improve network maintainability and data quality. Trigger performance, aside from these network problems, has been superlative—both sensitive and highly resistant to false alarms. We are likely to reach a limiting magnitude of less than 5.0 for teleseismic  $P$ .

## Reports

No reports were produced in FY91. All resources were applied to processing the largest teleseismic tomography data set yet collected by this Project, and to the operational task of designing, testing, and tuning the new teleseismic trigger system for CUSP.

# Seismic Network for the Loma Prieta Teleseismic Experiment 1990

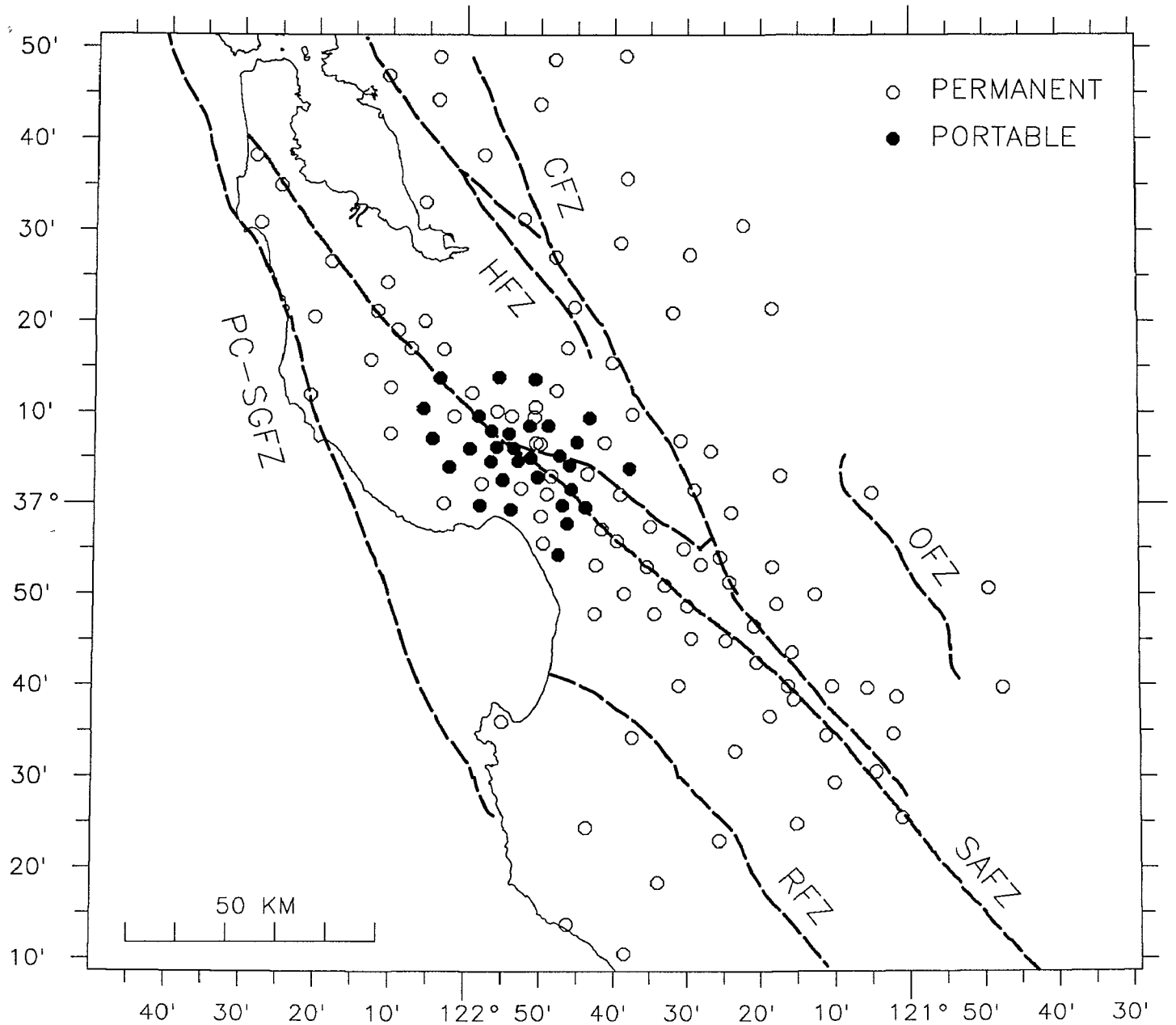


Figure 1: Map of CalNet permanent seismographs (open circles) and temporary seismographs (solid dots) used for both teleseismic tomography and local-earthquake tomography. Temporary stations operated from August through December, 1990, mostly in continuous recording modes.

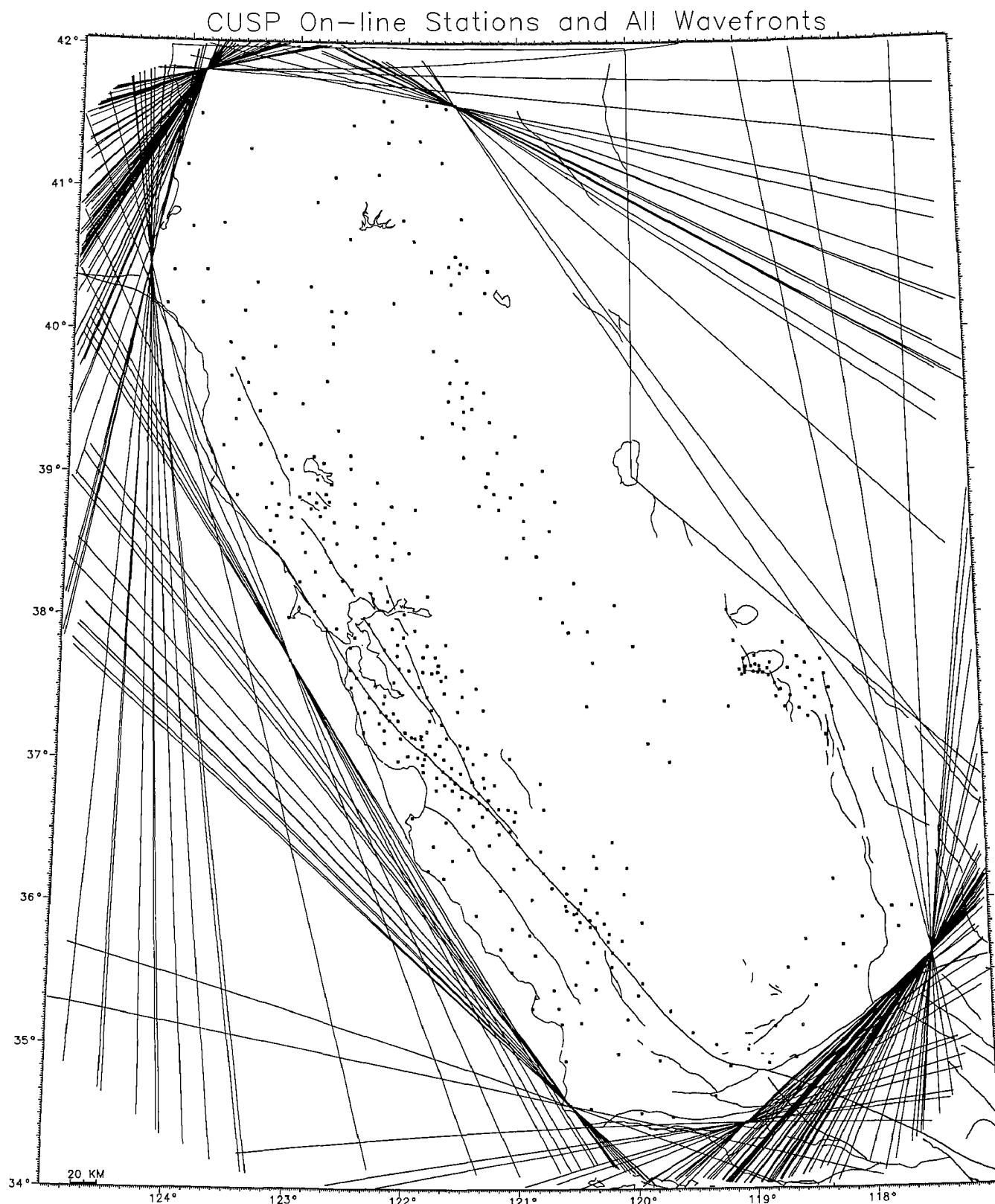


Figure 2: Teleseismic wavefronts from all Flinn-Engdahl geographic regions producing recordable teleseismic-*P* events in 1990. Each wavefront is plotted as it impinges the CalNet station closest to the event. Three or more subnets near the periphery of CalNet will be monitored by a PC-based teleseismic trigger. The same type of PC system is readily applicable to the southern California network and all other NEHRP-funded networks for about \$10K each.

### **On-Line Seismic Processing**

9930-02940

Fred Fischer (for Rex Allen)  
Branch of Seismology  
U.S. Geological Survey  
345 Middlefield Road, MS 977  
Menlo Park, California 94025  
(415) 329-4724

#### **Investigations and results (November, 1991)**

The INMOS based RTP is still under development. A second 286 PC was purchased for backup and overlapping development. The current INMOS RTP system requires 2 PCs. Tests with 5 linked processors were at first slowed with the retirement of Rex Allen, then halted with the loss of a suitable digitizer. Continuation of this project will depend on the acquisition of a Tustin or National Instruments class A/D converter.

Gray Jensen and Jim Ellis have nearly completed the C language software to interface a time code, a Tustin A/D converter with the INMOS RTP.

The Mk I (TI 990) and Mk II (Motorola 6800) RTPs in Menlo Park continue to function satisfactorily, with maintenance by Sam Rodriguez and Jim Ellis.



## Analysis of Natural Seismicity at Anza

9910-03982

Joe Fletcher, and Lawrence M. Baker  
Branch of Engineering Seismology and Geology  
U.S. Geological Survey  
345 Middlefield Road  
Menlo Park, CA 94025  
(415) 329-5628, 5608

### Investigations:

- 1). Incorporation of broadband sensors into the Anza array.
- 2). Provide access to the Anza wave form data in nearly realtime over Internet.

### Results:

1). Two sensors were considered: the Guralp CMG-4 and Streckeisen STS-2. Both have responses to well below the 2 Hz natural frequency of the HS-10s now in use. CMG-4s were used to record aftershocks of the Loma Prieta earthquake at Corralitos, a station near the epicenter. Streckeisen STS-2s have been used recently at Pinyon Flat Observatory in short-baseline array experiments. Records from these instruments demonstrate their increased sensitivity to long periods (120 s for the STS-2 and 30s for the Guralp) and they are also low noise. Their response to high frequency waves of 40 to 50 Hz was judged to be good enough to be compatible with the existing instrumentation. STS-2s have an auto-centering system so that DC offsets should not be a problem. Both appear sensitive to temperature changes (Vernon, personal communication).

In conjunction with Jon Berger and Frank Vernon at IGPP/UCSD 11 STS-2s were purchased for the Anza array. The STS-2s have the widest bandwidth currently available especially at long periods (120 s to 50 Hz) in a package that would not require an extensive vault. The auto-centering system is a distinct advantage for realizing the most dynamic range from the sensor.

2). A MicroVAX-II computer system is now being used as a front-end file server to the VAXStation currently performing the realtime data acquisition. Two dual-ported 1GB disks are attached between the MicroVAX and the VAXStation and serve as temporary data storage and isolate the realtime system from network traffic. With the addition of the front-end file system event files, which were written originally to tape, are now stored on disk. In addition, an erasable optical disk has been attached to the MicroVAX for archiving the data. DECnet/Internet access is now available by the MultiNet TCP/IP software package for VMS, which is also installed on the VAXStation used for analysis of the data in Menlo Park. It is anticipated that waveform data will be routinely telemetered over the Internet to SCEC to be incorporated into the routine processing of phase times for Southern California.

## THEODOLITE MEASUREMENTS OF CREEP RATES ON SAN FRANCISCO BAY REGION FAULTS

Grant Number 14 - 08 - 0001 - G1992

Jon S. Galehouse  
Department of Geosciences  
San Francisco State University  
San Francisco, California 94132

(415) 338-1204

We began to measure creep rates on San Francisco Bay region faults in September 1979. Amount of slip is determined by noting changes in angles between sets of measurements taken across a fault at different times. This triangulation method uses a theodolite to measure the angle formed by three fixed points to the nearest tenth of a second of arc. Each day that a measurement set is done, the angle is measured 12 times and the average determined. The amount of slip between measurements can be calculated trigonometrically using the change in average angle. The precision of our measurement method is such that we can detect with confidence any movement more than a mm or two between successive measurement days.

We presently have measurement sites at 23 localities on active faults in the San Francisco Bay region (see Figure 1). We remeasure most sites about once every two to three months. Most sites span a fault width of about 50-275 m. These distances are noted on Figures 2 through 8 as the IS (Instrument Station) to ES (End Station) distances. These figures also show the average rate of movement at each site as determined by the slope of the least-squares line which also appears on each of the graphs. The graphs also show the time of the 17 October 1989 Loma Prieta earthquake (LPEQ) as a vertical line. The following is a brief fault-by-fault summary of our results through 16 November 1991.

**SAN ANDREAS FAULT** (see Figure 2) - We have been measuring horizontal slip on the San Andreas fault at Site 14 at the Point Reyes National Seashore Headquarters for 6.7 years and at Site 10 in South San Francisco for 11.5 years. Both sites have shown virtually no net slip and neither was affected by the LPEQ thus far.

In November 1989, we began measuring a USGS site (our Site 22) in Woodside that had not been remeasured for many years. Our results compared to unpublished USGS measurements in 1977 show that virtually no surface slip occurred between 16 February 1977 and 4 November 1989 and virtually none has occurred since (through 19 October 1991). We also established in November 1989 Site 23 on the San Andreas fault near the southeastern end of the LPEQ aftershock zone and northwest of San Juan Bautista. Virtually no slip has occurred at this site (through 12 October 1991). In July 1990, we established Site 25 on the San Andreas fault just southeast of San Juan Bautista and the aftershock zone. This site is on the central creeping portion of the fault and has been moving at a rate of 17.3 mm/yr for the past 1.2 years (through 12 October 1991).

Site 18 (not shown on Figure 1) in the Point Arena area has averaged less than one mm/yr of right slip in the ten years between 9 January 1981 and 12 January 1991.

In summary, the San Andreas fault at our measurement sites does not appear to have been affected by the LPEQ in the two years since October 1989. Northwest of the LPEQ aftershock zone, the San Andreas fault is still virtually locked, with less than one mm/yr of creep occurring along it.

**HAYWARD FAULT** (see Figure 3) - We have been measuring horizontal slip at five sites along the Hayward fault for 11.2 to 12.1 years and have determined that the right-lateral creep rate is about 4.5 to 4.9 mm/yr. Although the creep characteristics (steady or episodic) differ from site to site, the overall rates are quite similar. None of these five sites on the Hayward fault showed any unusual movement either before or after the LPEQ.

Since we began measuring Site 1 in Fremont in September 1979, the fault has moved rather episodically. Typical surface movement characteristics are relatively rapid right slip of about a cm over a few months time alternating with relatively slower slip over a period of two or more years. The fault at Site 1 was in one of the relatively slower phases of movement prior to the LPEQ and the slower phase has now persisted for about 3.5 years (through 9 November 1991). Over the past 12.1 years, the average of the slower and faster phases of right slip is about 4.9 mm/yr.

In February 1990 we established Site 24 on the Hayward fault on Camellia Drive in Fremont, about four km southeast of Site 1 (see Figure 1). Although relatively rapid creep had been reported for this site in recent years, we have measured virtually no creep at all (through 28 September 1991). Perhaps the fault at this site moves episodically (similarly to nearby Site 1) and has been in a slower, dormant phase since we began measuring it 1.6 years ago.

Movement along the Hayward fault at Site 2 in Union City has been much more continuous and much less episodic than movement at Site 1. Site 2 has been moving at a fairly uniform rate of about 4.6 mm/yr for the 12.1 years since we began measurements in September 1979.

Extremely uniform movement characterizes Site 12 on D Street in Hayward. Two active traces of the Hayward fault occur here and their combined movement rate has been about 4.7 mm/yr for the 11.2 years since we began measurements in June 1980. Our nearby Site 13 on Rose Street in Hayward has the same overall average rate of movement (4.7 mm/yr) since June 1980, but the movement is much more episodic than at Site 12. For the past 5.5 years (through 21 September 1991), the Hayward fault at Rose Street has been in a relatively slower phase of movement of about 3.6 mm/yr that has not been affected by the LPEQ.

In the 11.2 years since we began measurements in August 1980 in San Pablo (Site 17) near the northwesterly end of the Hayward fault, the overall average rate of right slip (about 4.5 mm/yr) has been similar to the overall rate at the other Hayward fault sites. However, superposed on the overall slip rate in San Pablo are changes between some measurement days of up to nearly a cm in either a right-lateral (more common) or left-lateral (less common) sense. This pattern was more pronounced between mid-1980 to mid-1986 and has been less pronounced since. For the past 3.3 years (through 13 October 1991), the fault in San Pablo has also been in a relatively slower phase of movement of about 2.7 mm/yr that has also not been affected by the LPEQ.

**CALAVERAS FAULT** (see Figure 4) - We have been measuring horizontal slip at two sites on the Calaveras fault in the Hollister area for over twelve years. Slip at both sites has been rather episodic with intervals of relatively rapid right slip typically lasting a couple months or less alternating with longer periods of time when little net slip occurs. The LPEQ occurred during an interval of slower movement that had persisted for about a year at Site 4. The earthquake apparently triggered up to 14 mm of right slip at Seventh Street (see Figure 4). Overall the rate of right slip is about 7.1 mm/yr for the past 12.1 years (through 16 November 1991).

Slip at Site 6 along Wright Road just 2.3 km northwest of Site 4 is also episodic. The LPEQ occurred during an interval of slower movement that had persisted for about a year at Wright Road (similar to the situation at Seventh Street). The earthquake apparently triggered up to 12 mm of right slip. The overall rate of slip at Wright Road is about 11.6 mm/yr for the past 12.1 years (through 16 November 1991). Except for our relatively new site (25) on the central creeping portion of the San Andreas fault, this rate is the fastest of any of our sites in the San Francisco Bay region. It is about 4.5 mm/yr faster than the rate at nearby Seventh Street. Either the creep rate decreases significantly from Wright Road southeast to Seventh Street or undetected surface movement is occurring outside our 89.7 m-long survey line at Seventh Street.

After the rapid slip triggered by the LPEQ, both sites in the Hollister area returned to a slower mode of movement which has now persisted for more than two years. A more detailed discussion of the effect of the Loma Prieta earthquake on the Calaveras fault in the Hollister area was published in Geophysical Research Letters (Galehouse, 1990). The paper also discusses the effect of the Morgan Hill earthquake in 1984. No immediate surface displacement had occurred at either of our Hollister area sites when they were measured the day after the Morgan Hill earthquake in 1984. However, within the following 2.5 months, both sites showed over a cm of right slip which was followed by a relatively long interval of slower slip (see Figure 4).

In contrast to our sites in the Hollister area, Site 19 in San Ramon near the northwesterly terminus of the Calaveras fault was not affected by the LPEQ. It has remained virtually locked throughout our 10.9 years of measurements.

**CONCORD - GREEN VALLEY FAULT** (see Figure 5) - We began our measurements at Site 3 and Site 5 on the Concord fault in the City of Concord in September 1979. It appears that typical movement characteristics at both sites are intervals of relatively rapid right slip of about 7-10 mm over a period of a few months alternating with intervals of relatively slower right slip of about a mm or two a year over a period of several years. The latest phase of relatively slower slip has persisted for about 3.6 years (through 29 September 1991). We think it is likely that another phase of relatively rapid slip will occur within the next year.

It appears that the LPEQ and the 1990 swarms of earthquakes near Alamo (between the southeastern end of the Concord fault and the northwestern end of the Calaveras fault) had no effect on the Concord fault at our measurement sites in the City of Concord.

We began measuring Site 20 on the Green Valley fault near Cordelia in June 1984. Large variations tend to occur at this site between measurement days, possibly because logistical considerations resulted in our survey line being particularly long (335.8 m). However, our results suggest that the Green Valley fault behaves similarly to the Concord fault i.e., relatively rapid right slip in a short period of time (months) alternating with relatively slower slip over a longer period of time (years). The Green

Valley fault was in a period of relatively slower movement for the first 20 months of our measurements, averaging a few mm per year of right slip. In early 1986, however, the fault slipped right-laterally more than a cm. This was followed by about three years in which the net slip was less than one mm/yr. Sometime after 6 August 1989, the Green Valley fault entered into another phase of relatively rapid right slip that totalled about 15 mm by 22 April 1990. For the next 1.5 years (through 13 October 1991), the rate has been less than three mm/yr. The overall average rate of movement has been about 5.6 mm/yr for the past 7.3 years.

There is a possibility that shaking from the LPEQ triggered the onset of the latest phase of relatively rapid displacement on the Green Valley fault. As mentioned, we did detect about 12-14 mm of right slip on the southern Calaveras fault in the Hollister area that was triggered by the LPEQ. However, these sites were less than 50 km from the epicenter and the same sites had slip triggered by the Morgan Hill earthquake in 1984. Our site on the Green Valley fault is more than 140 km north of the epicenter and it is probably only a coincidence that the fault began its latest phase of relatively rapid movement at a time that could be approximately related to the LPEQ. Our measurement intervals on the Green Valley fault are too far apart to pin down the exact time when relatively rapid slip started and there is no other evidence suggesting any relationship. In addition, none of our other sites on the Hayward, northern Calaveras, or Concord faults (which lie between the Green Valley fault and the epicenter) showed any significant changes in surface slip rates associated with the LPEQ.

Regarding the relationship between the Green Valley and Concord faults, the episodes of relatively rapid slip and relatively slower slip do occur at different times and the rate of slip is higher on the Green Valley fault. The episodic nature of the slip and the duration of the faster and slower intervals, however, are similar. Based on these similarities and the small step between their respective trends, we consider the Concord and Green Valley faults to be different names for the southeastern and northwestern segments of the same fault system.

**RODGERS CREEK FAULT** (see Figure 6) - We measured a site on the Rodgers Creek fault in Santa Rosa from August 1980 until we had to abandon it for logistical reasons in January 1986. During these 5.4 years of measurements, no significant surface slip occurred and we concluded that the Rodgers Creek fault was not creeping at this site.

In September 1986, we established Site 21 on the Rodgers Creek fault near Penngrove (see Figure 1). The least-squares average at Site 21 is 2.4 mm/yr for the past 5.1 years (through 26 October 1991). Because variations of several mm tend to occur from one measurement day to another, it is difficult to know whether the Rodgers Creek fault is really creeping slowly or whether it is not moving much at all and our average rate at this point in time is due to the "noise" level at this particular measurement site. Perhaps the results will become less ambiguous as we continue our measurements over a longer period of time.

The LPEQ (see Figure 6) does not appear to have had any effect on the Rodgers Creek fault at Site 21.

**WEST NAPA FAULT** (see Figure 6) - We began measurements at Site 15 in the City of Napa in July 1980. Similarly to the situation at Site 21 on the Rodgers Creek fault, there tends to be a lot of surface "noise" at this measurement site. However, the average rate of right slip on the West Napa fault over the past eleven

years is only 0.2 mm/yr. In other words, the West Napa fault is virtually locked at the surface with no creep occurring.

The LPEQ (see Figure 6) does not appear to have had any effect on our results for the West Napa fault.

**SEAL COVE-SAN GREGORIO FAULT** (see Figure 7) - We began measurements at Site 7 on the Seal Cove fault segment in Princeton in November 1979. No net slip has occurred in the past 11.8 years (through 14 September 1991).

We began measuring Site 8 on the San Gregorio fault segment in May 1982. This site shows very large variations from one measurement day to another, probably due in part to the particularly long distance (452 m) between the IS and ES. The average rate of movement is less than one mm/yr for the past 9.3 years (through 14 September 1991) and we conclude that the Seal Cove-San Gregorio fault is not presently creeping.

The LPEQ (see Figure 7) does not appear to have had any noticeable effect on the rate of movement at either of our sites on this fault system.

**ANTIOCH FAULT** (see Figure 8) - We began measurements at Site 11 in the City of Antioch in May 1980. The average rate of movement has been less than one mm/yr for the past 11.4 years (through 5 October 1991). Site 9 just south of town has shown 1.7 mm/yr for the 7.6 years through 1 July 1990. New construction has destroyed our measurement array at this site. We hope to reestablish measurements in this area during 1992 when we anticipate that the construction will be finished. We have noted that much subsidence and mass movement creep occur both inside and outside the Antioch fault zone in the area of our two measurement sites and it is quite possible that these nontectonic movements are influencing our measurement results. If any tectonic creep is occurring along the Antioch fault, it is probably at a very low rate.

The LPEQ (see Figure 8) does not appear to have had any noticeable effect on movement rates at either of our sites on the Antioch fault.

## 1990 and 1991 PUBLICATIONS

Galehouse, J.S., 1990, Effect of the Loma Prieta earthquake on fault creep rates in the San Francisco Bay region: EOS, Transactions American Geophysical Union, v. 71, no. 8, p. 288.

Galehouse, J.S., 1990, Effect of the Loma Prieta earthquake on surface slip along the Calaveras fault in the Hollister area: Geophysical Research Letters, v. 17, no. 8, pp. 1219-1222.

Galehouse, J.S., 1991, Creep rates on Bay Area faults during the past decade: Geol. Soc. Am. Abstracts with Programs, v. 23, no. 2, p. 27.

Galehouse, J.S., 1991, Present - day creep on the Green Valley fault: in *Field Trip Guide to the Geology of Western Solano County*; Figuers, S.H., editor, Northern California Geological Society and Association of Engineering Geologists Guidebook, pp. 12-16.

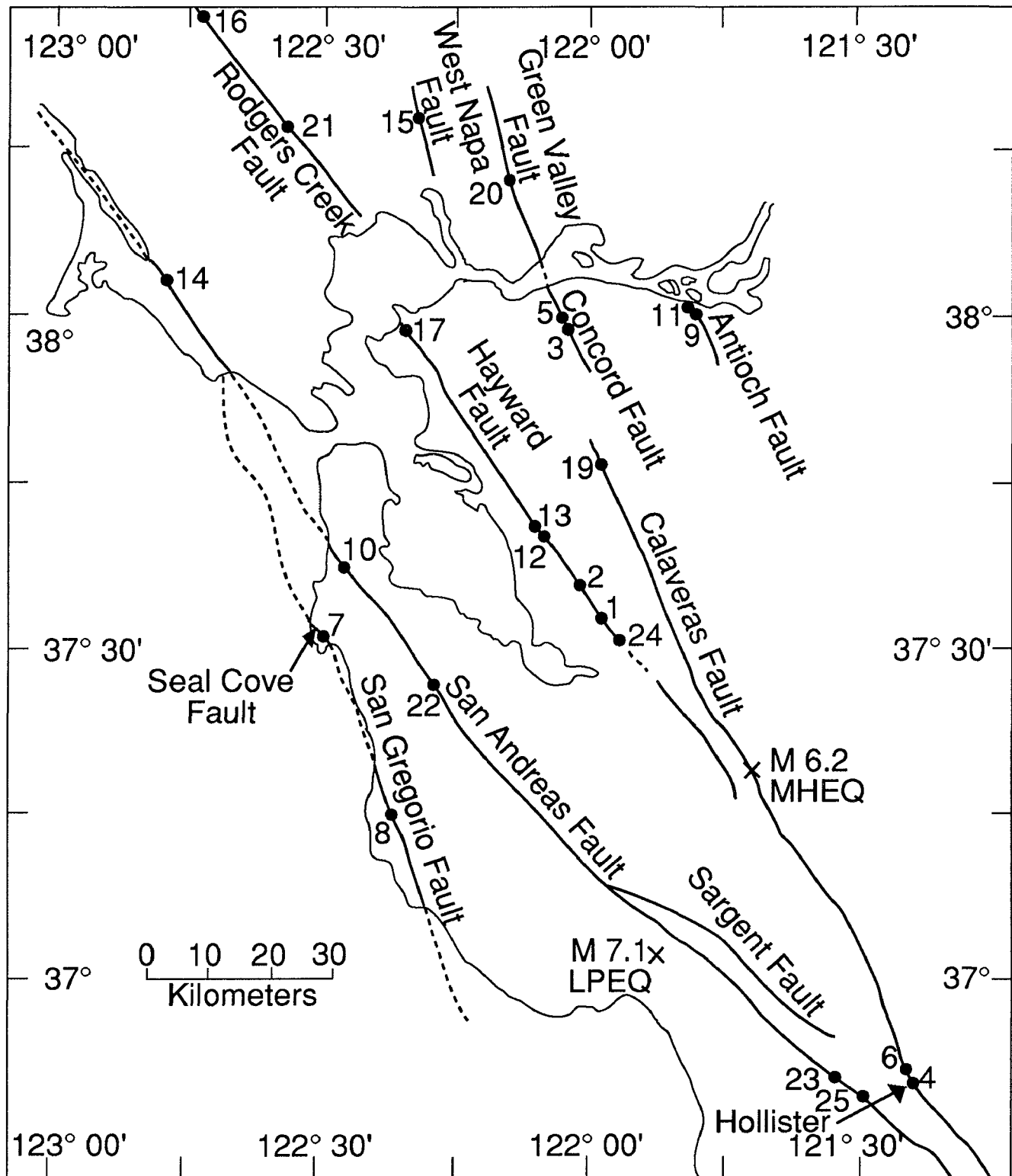
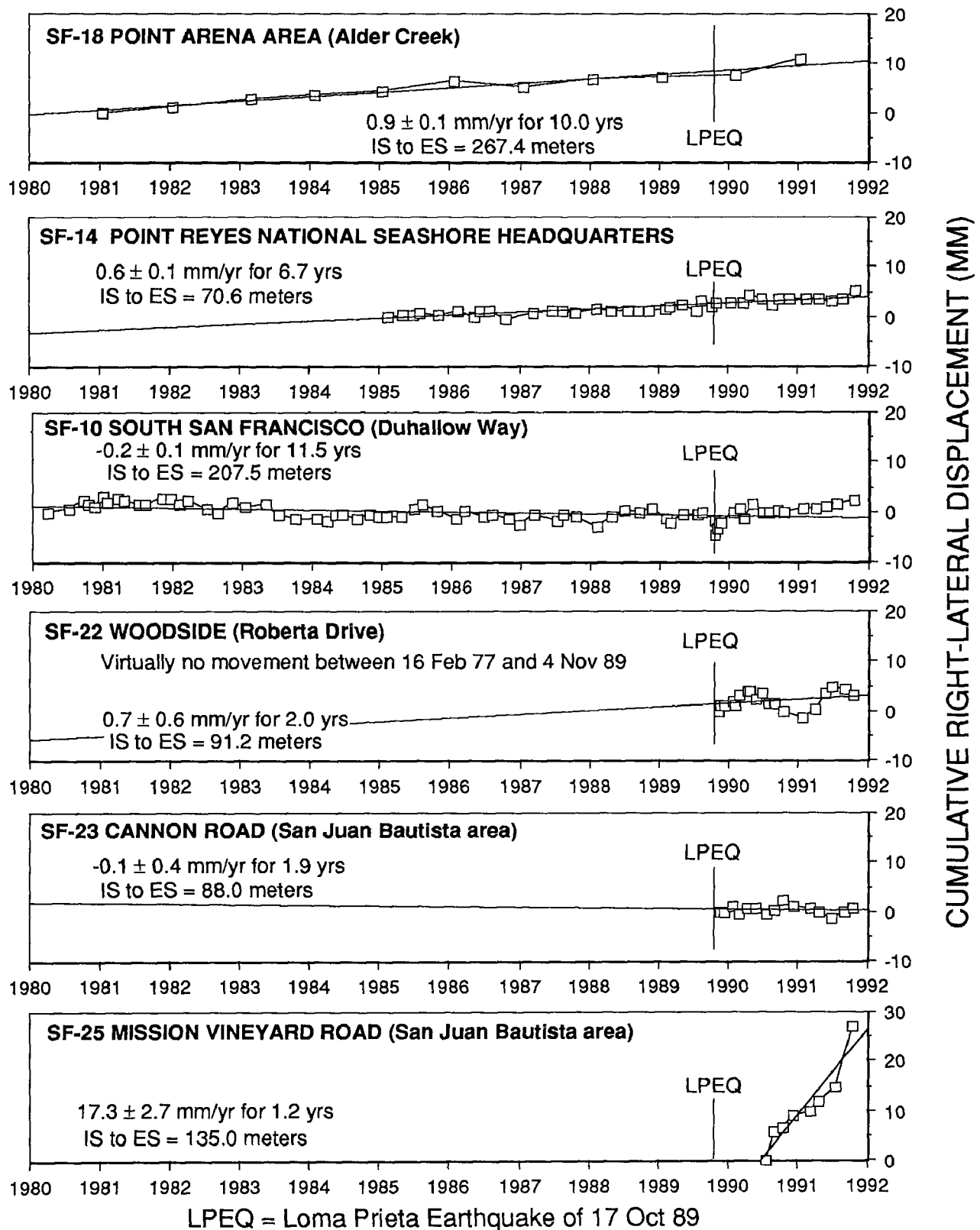


Figure 1. Numbered dots are San Francisco State University theodolite measurement sites. Epicenters and magnitudes are indicated for the 24 April 1984 Morgan Hill earthquake (MHEQ) and the 17 October 1989 Loma Prieta earthquake (LPEQ).

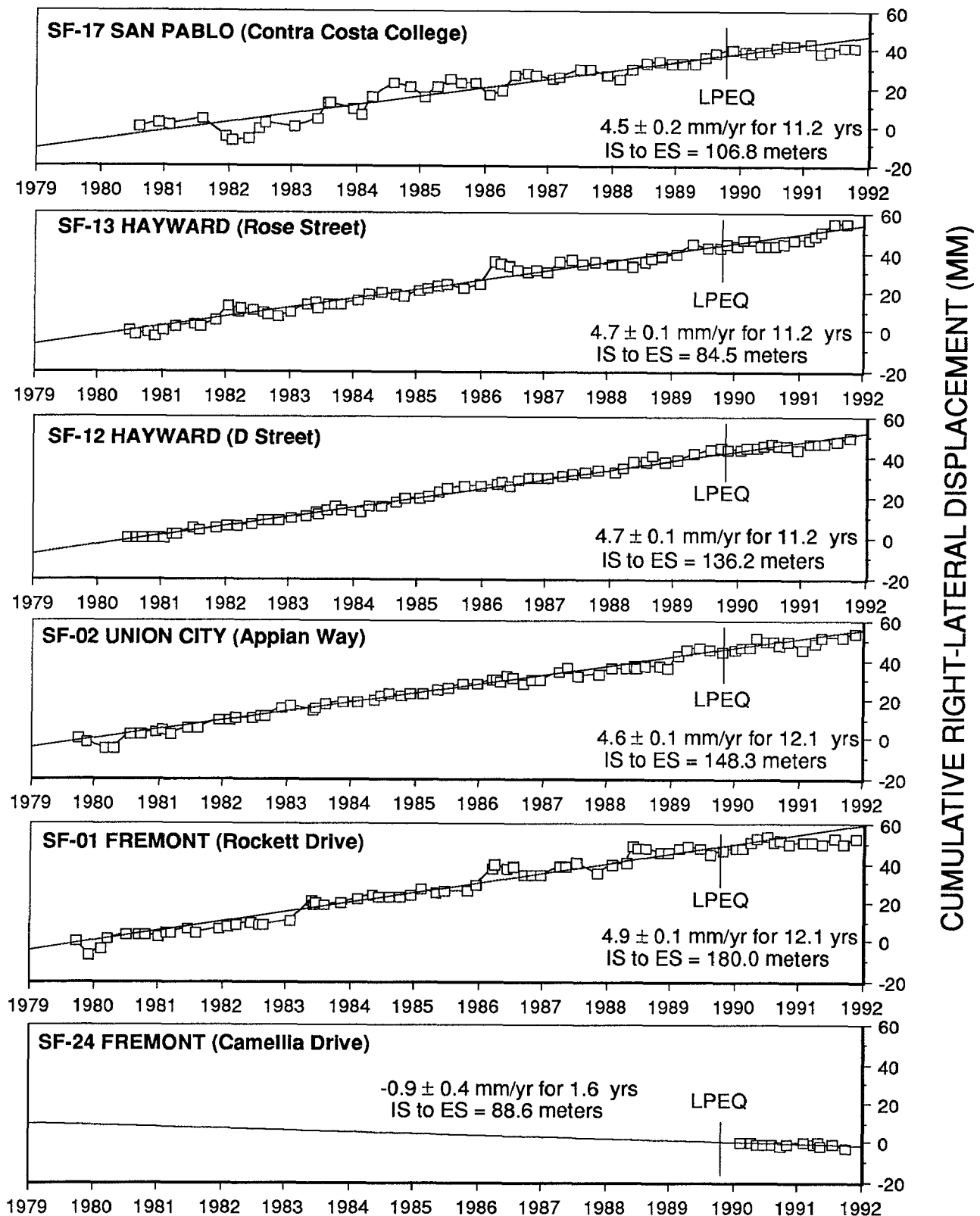
# SAN ANDREAS FAULT



**Figure 2. San Andreas Fault Displacement (1980 - 1991)**



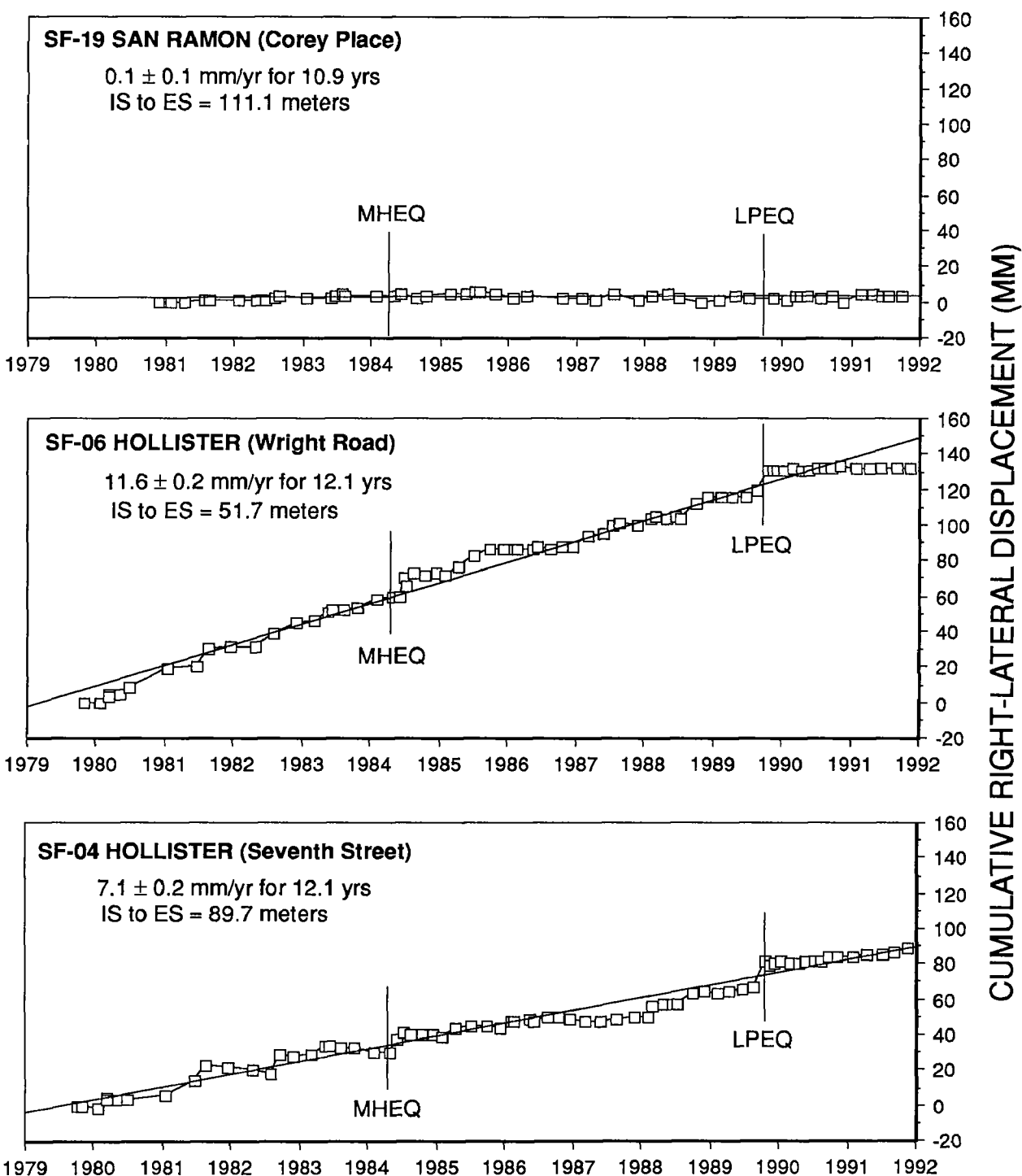
# HAYWARD FAULT



LPEQ = Loma Prieta Earthquake of 17 Oct

Figure 3. Hayward Fault Displacement (1979 - 1991)

# CALAVERAS FAULT



MHEQ = Morgan Hill Earthquake of 24 Apr 84

LPEQ = Loma Prieta Earthquake of 17 Oct 89

**Figure 4. Calaveras Fault Displacement (1979 - 1991)**

# CONCORD - GREEN VALLEY FAULT

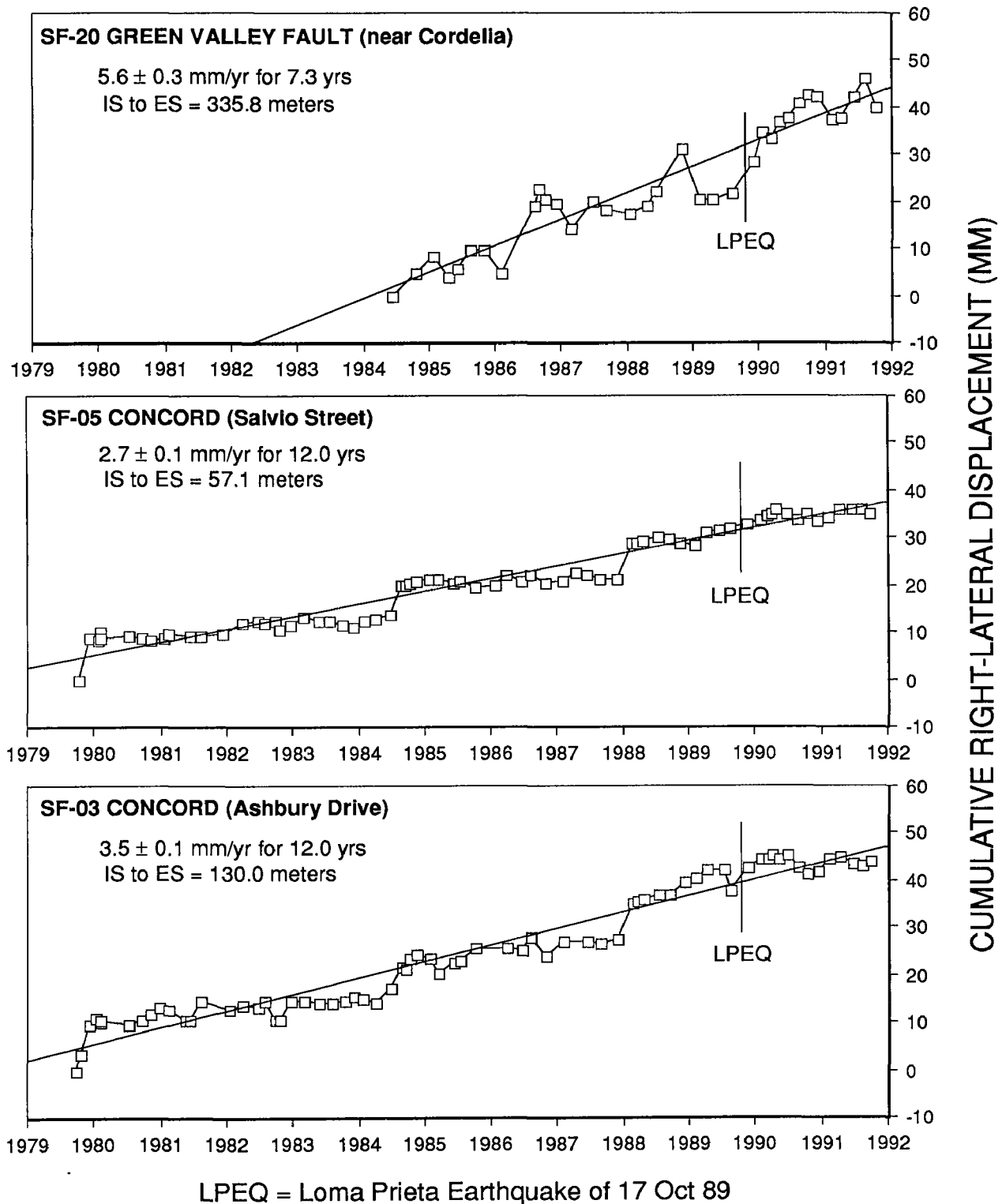
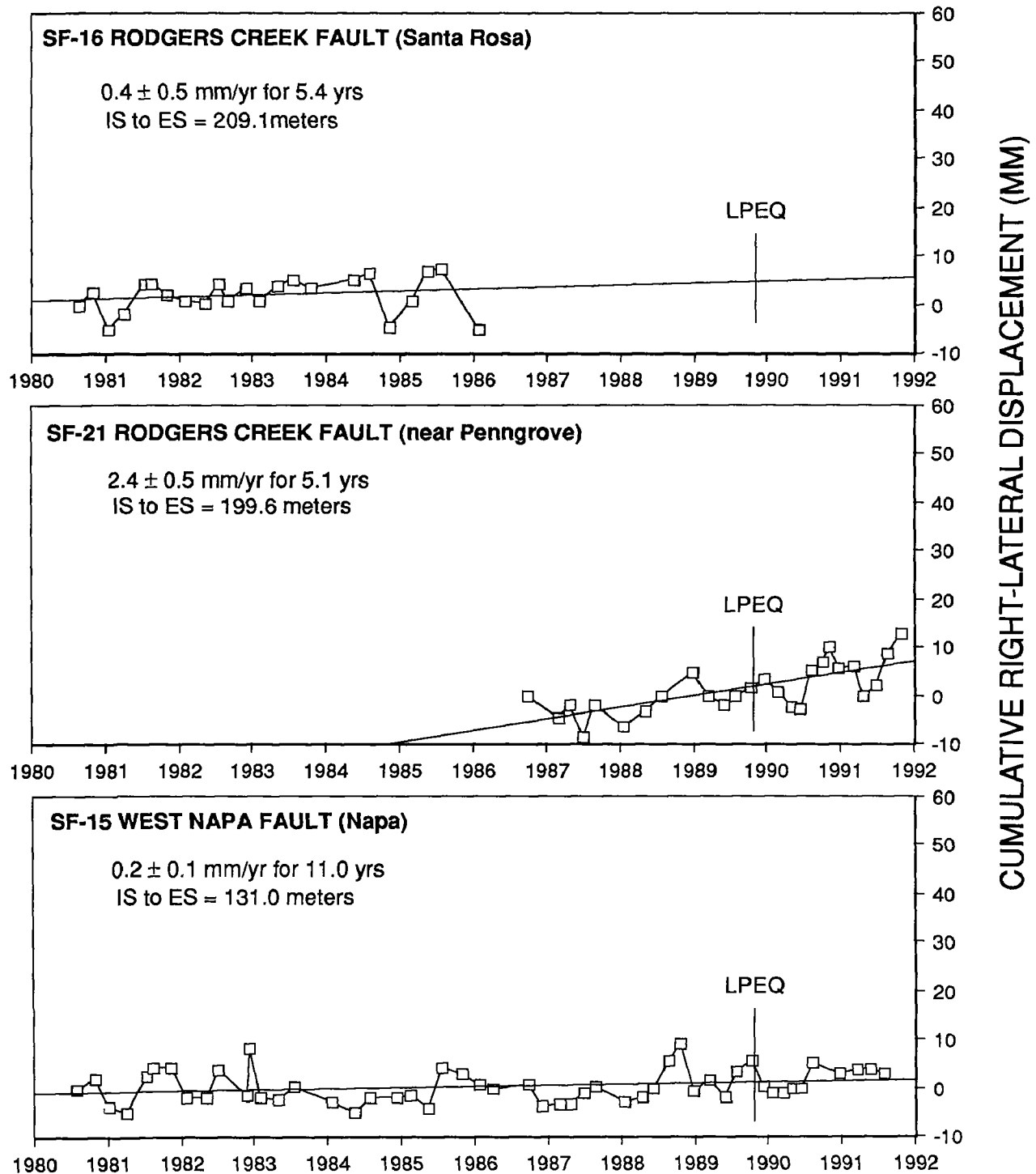


**Figure 5. Concord - Green Valley Fault Displacement (1979 - 1991)**

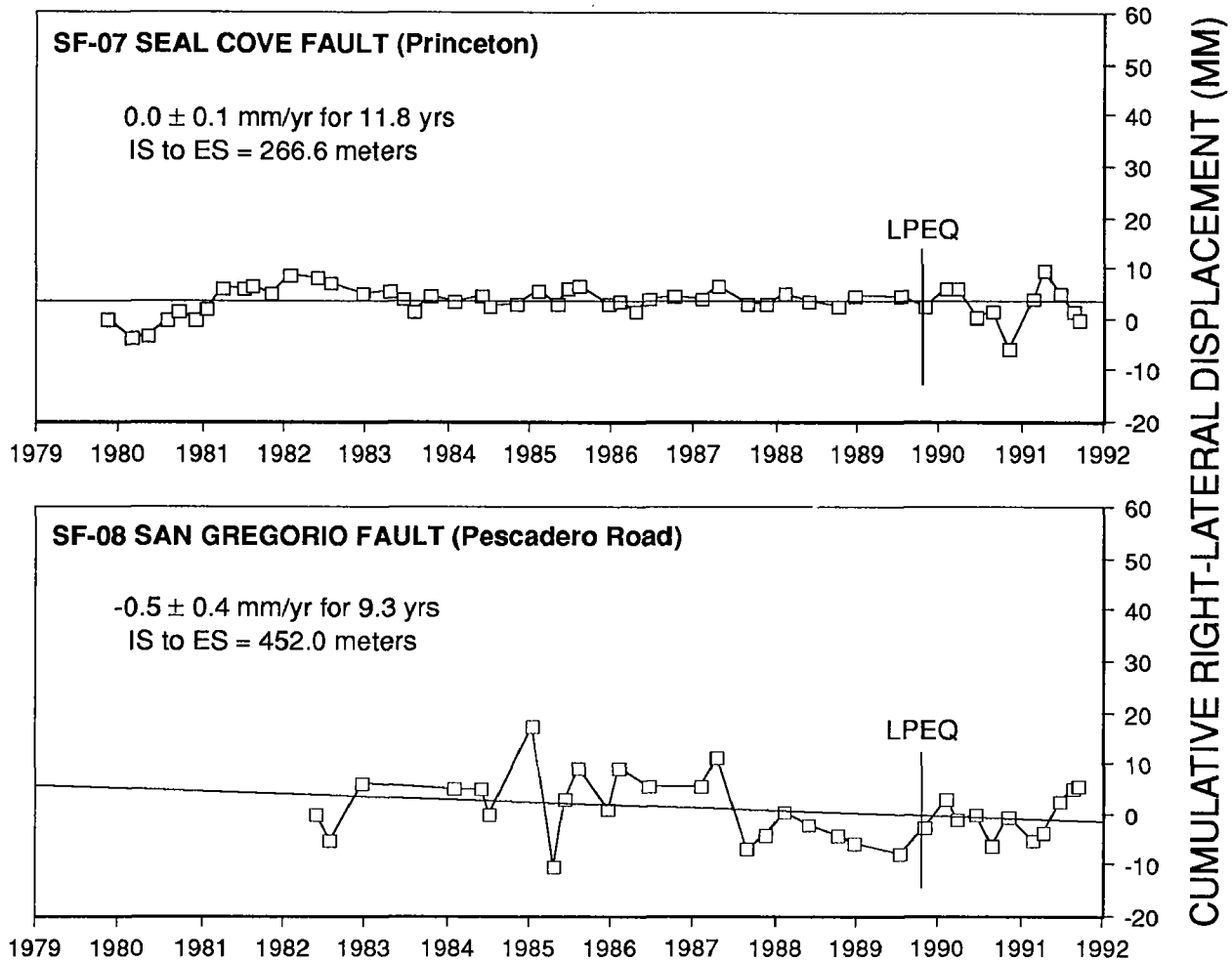
# RODGERS CREEK FAULT AND WEST NAPA FAULT



LPEQ = Loma Prieta Earthquake of 17 Oct 89

**Figure 6. Rodgers Creek Fault Displacement (1980 -1991)**  
**West Napa Fault Displacement (1980 - 1991)**

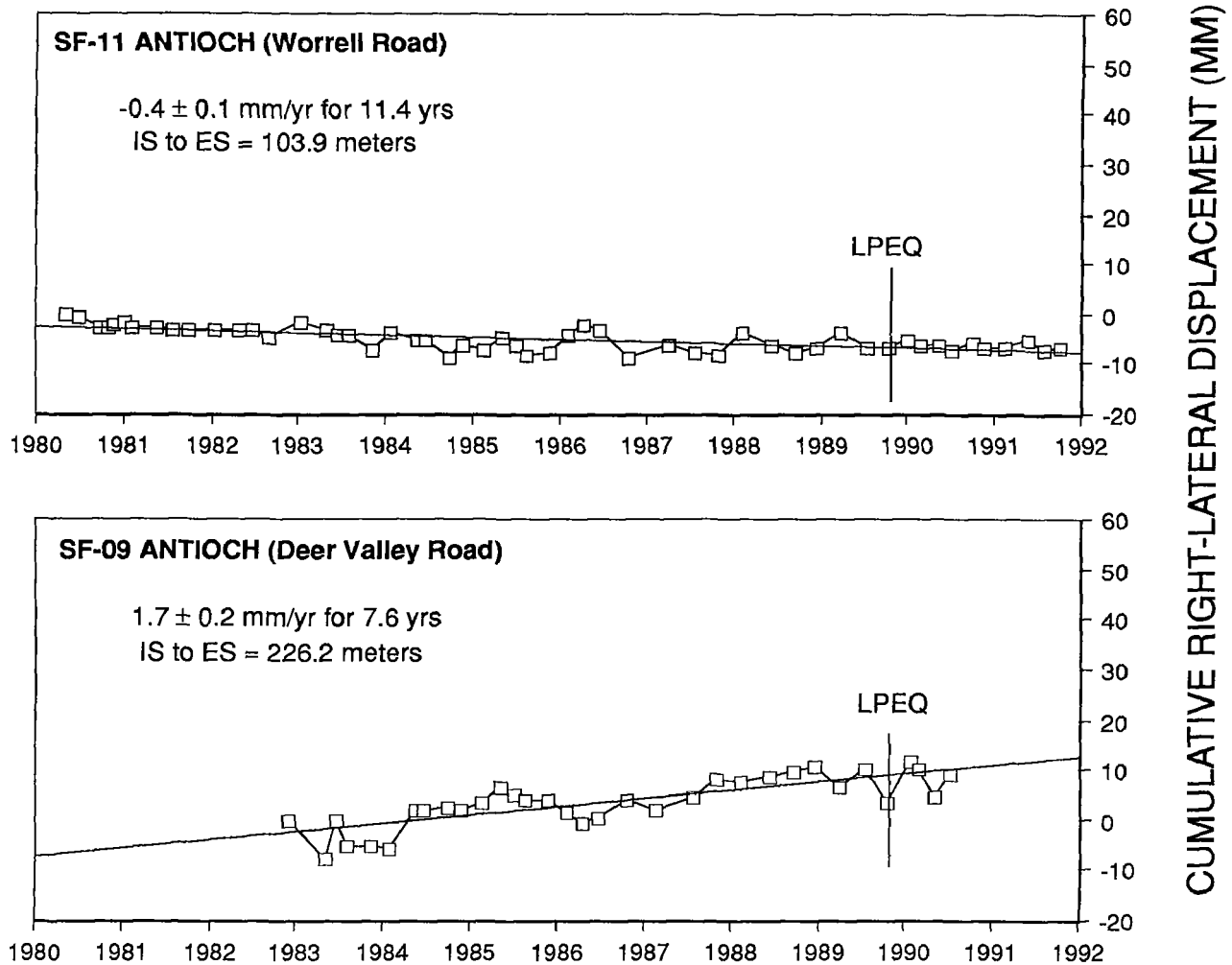
# SEAL COVE - SAN GREGORIO FAULT



LPEQ = Loma Prieta Earthquake of 17 Oct 89

**Figure 7. Seal Cove - San Gregorio Fault Displacement (1979 -1991)**

# ANTIOCH FAULT



LPEQ = Loma Prieta Earthquake of 17 Oct 89

**Figure 8. Antioch Fault Displacement (1980 - 1991)**

## Strain Rates Across California: GPS Reoccupation of an Historical Triangulation Network Between San Francisco and Lake Tahoe

Grant No. 14-08-0001-G1964

Lewis Gilbert, John Beavan, Chris Scholz

Lamont-Doherty Geological Observatory of Columbia University, Palisades, NY 10964

Tel: (914) 359 2900; Fax: (914) 359 5215; e-mail: gel@lamont.lidgo.columbia.edu

### Investigations

The part of the U.S. Primary Triangulation Arc that crosses California between the San Francisco Bay area and the Sierra Nevada is being reoccupied by Global Positioning System (GPS) surveying. The purpose is to extend the post-1906 deformation history of this network to the present; the network was measured by triangulation in 1922, 1928, ~1948 and ~1963. The derived shear-strain history will be interpreted in terms of plate-boundary models of the region, and compared with strain changes indicated by regional earthquake moment release rate variations.

### Results (as of November 1991)

#### *Background*

The transcontinental control network was completed in the late 19th century; the westernmost marks in that network span California from the Sierra Nevada to the San Andreas Fault (SAF). After the 1906 San Francisco earthquake William Bowie (then head of the Coast and Geodetic Survey) realized that the control network had been deformed, and decreed that the network from the Sierra to the SAF should be resurveyed periodically in hopes that measured deformations would lead to future earthquake predictions. Those remeasurements were carried out in increasingly haphazard fashion in roughly 1922, 1928, 1948, and 1963. The goal of our field effort is to extend the crustal deformation history of this network and to establish a high-quality regional pre-seismic baseline.

#### *Prior Results*

The existing triangulation data have been analyzed to learn about historical changes in strain rates (Gilbert et al, *EOS*, 69, p 1448, 1988; *Eos*, 70, p 1354, 1989). There is a hint of a reorientation of the strain field between the 1948 and 1963 triangulation measurements, which potentially coincides with the increase in moderate magnitude seismicity in the San Francisco vicinity (Ellsworth et al., 1981, *in* Earthquake Prediction, Maurice Ewing series vol.4, pp.126-140). The errors in the historical data are substantial, and the GPS measurements will allow us to confirm whether or not this reorientation has actually taken place.

#### *Reconnaissance*

A reconnaissance trip was made in August 1989 in order to establish the current state of the survey monuments, and to organize access and other logistical matters. All but one of the eleven historical marks had survived, or had reference marks that had survived, though a few needed repairs of various forms. The one exception was Mt. Tamalpais (Figure 1) which was destroyed around 1950 during construction of a radar facility; however, a new mark at this site has been measured since the early 1950s. Three of the old marks were inappropriate for GPS measurements because of nearby structures; these required the establishment of eccentric monuments.

### *GPS fieldwork*

The GPS campaign (entitled NCPAR91) was carried out during the period 19-28 March and 18-22 July 1991 (Figure 1) using nominal 7 hour observation sessions. The High Sierra and foothill sites were not accessible during the March campaign due to adverse weather conditions, and the network was completed during the July trip.

### *Current Status*

1) The historical network has been completely reoccupied with GPS and it has been tied into the California HPGN at two points in the Great Valley. The GPS reoccupation extends the history of this network to greater than 100 years.

2) Preliminary processing of the GPS data has been completed and day to day repeatabilities are  $\sim 1$  cm for baselines of  $\sim 100$  km. This is quite encouraging and indicates that we have collected a good set of measurements.

3) The preliminary GPS results have been combined with the triangulation data. For our initial analysis of strain rates as a function of time, the network has been broken up into two zones, the "Coast Ranges" and the "Great Valley and Foothills" (see Fig. 1). In Figure 2 we show average  $\gamma_1$  strain rate results for each zone, and over several time intervals.  $\gamma_1$  corresponds approximately to SAF-parallel shear strain. The vertical error bars correspond to  $\pm 1\sigma$  standard errors, and the horizontal bars span the time between surveys. The clearest result to date is the detection of right-lateral strain accumulation since 1922 at an average rate of  $0.3-0.4 \mu\text{rad/yr}$  over the 60 km-wide Coast Ranges zone. The average strain rate appears to be lower in the 1922-1991 interval than in the 1922-48 interval (bottom plot), suggesting a moderate decrease of strain rate with time. There are anomalies associated with the 1948-63 interval that we do not yet understand (top and middle plots).

4) Work is continuing to improve the GPS solutions and to improve the comparison between the GPS results and the historical data.

### *Publications during this reporting period*

Gilbert, L.E., J. Beavan and C.H. Scholz, Northern California Primary Arc Reoccupation 1991 (NCPAR91): GPS Reoccupation of an Historical Triangulation Network Between San Francisco and Lake Tahoe, California (abstract), EOS, 72, 116, 1991.

### *Acknowledgements*

Thanks are due to GPS operators Steve Jaumé, Chris Marone, Russell Such, Wei-hau Wang and Jerry Svarc; to Bob King, Ken Hudnut and UNAVCO for loan of GPS equipment; to Don D'Onofrio and Mike Lisowski for assistance with connecting the historical data-set to the California HPGN survey.



# *Index Map for Northern California Primary Arc Reoccupation*

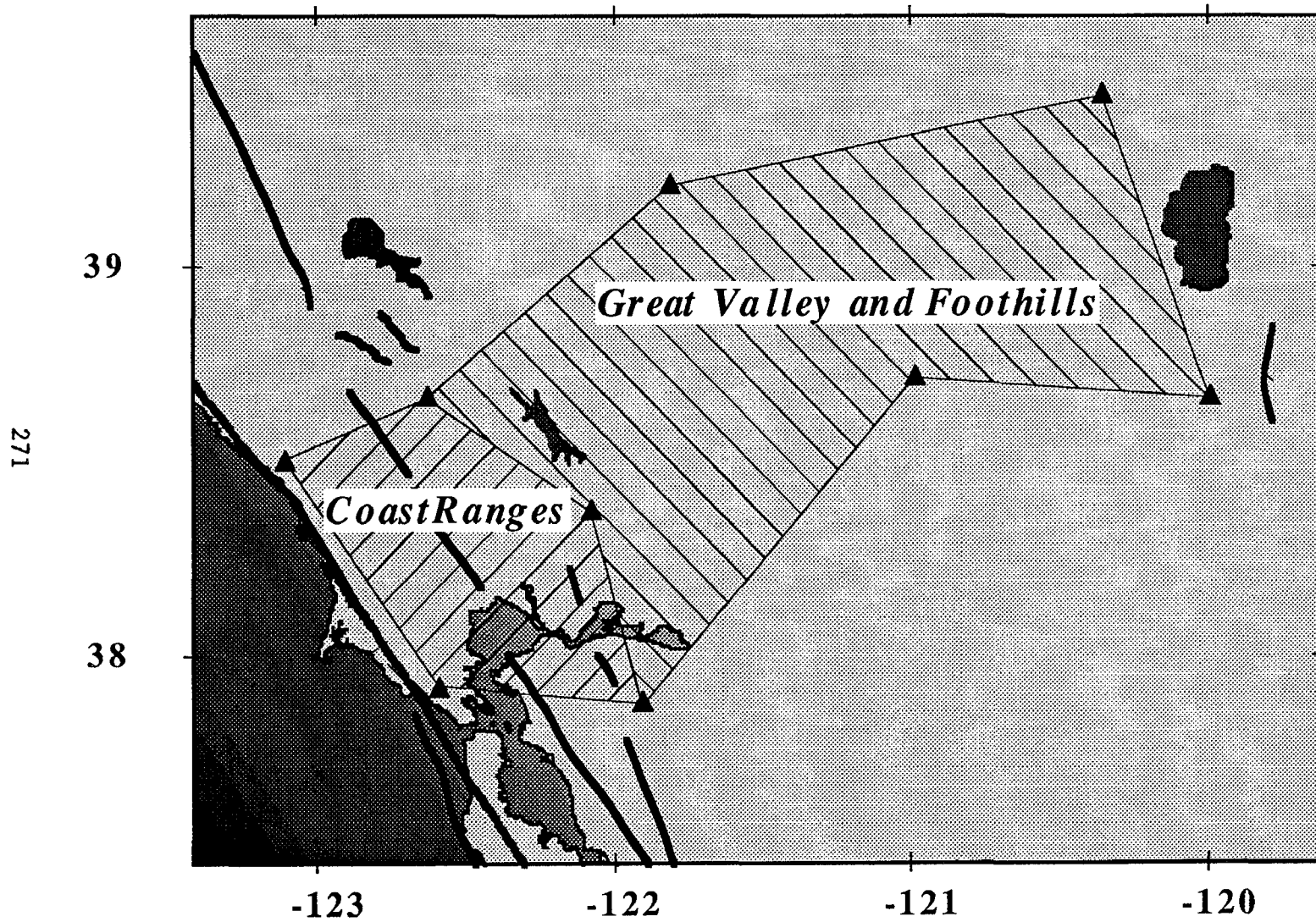


Figure 1

$\gamma_1$ ;  
*Coast Ranges / Great Valley and Foothills*

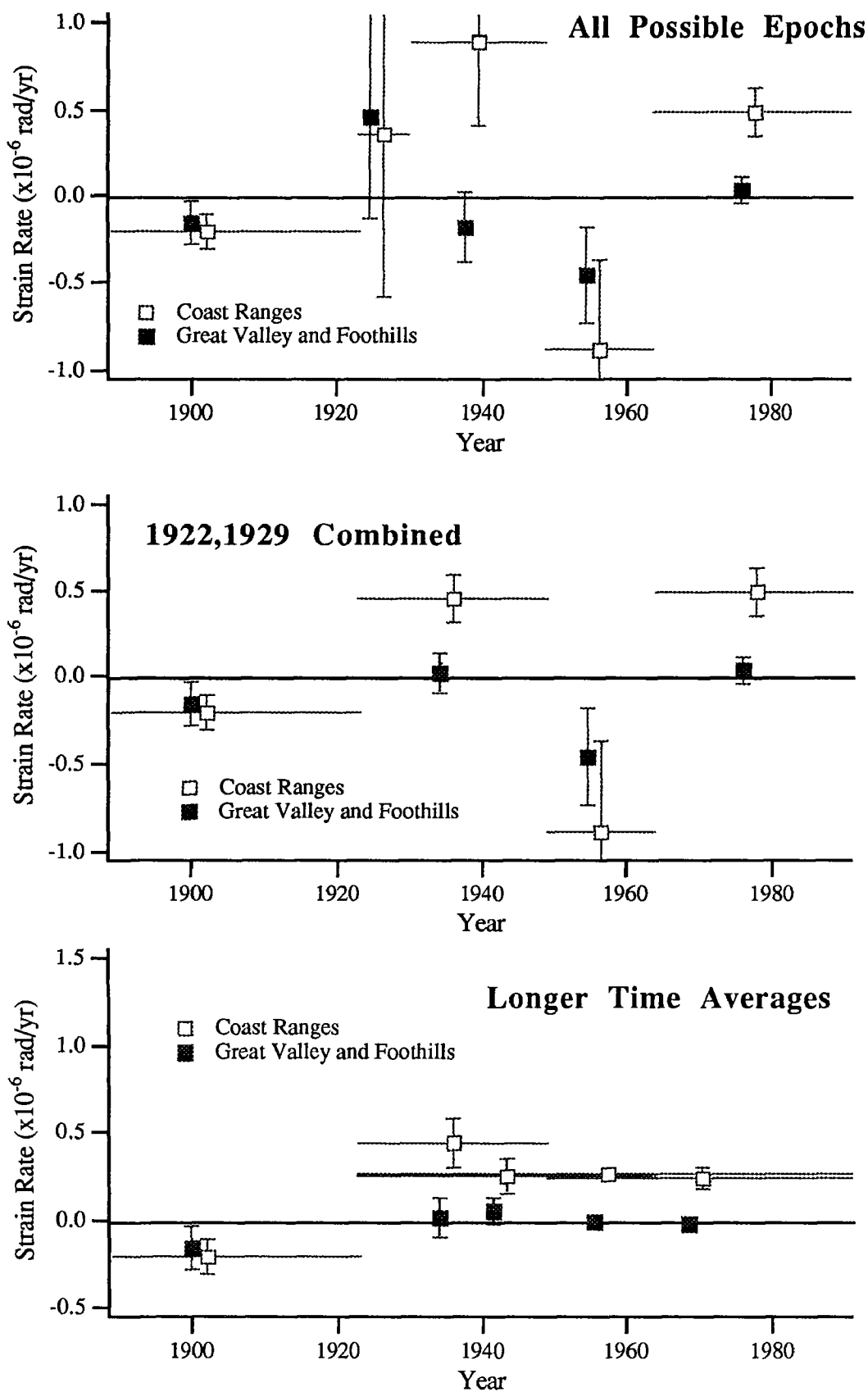


Figure 2

## DEEP BOREHOLE PLANE STRAIN MONITORING 14-08-0001-G1812

*Michael T Gladwin,*  
Department of Physics  
University of Queensland  
St. Lucia, 4067  
AUSTRALIA.  
ph. (+ 617) 3652473

### ACTIVITIES

1. An investigation of both the long term strain anomalies and details of short term changes of level in the strain data from San Juan Bautista has been carried out. These data have been compared with long term and short term creepmeter data from sites along the San Andreas fault in the region of San Juan (provided by K. Breckenridge). Models of possible common source regions for similar creep and strain signals have been investigated. Papers reporting the results of these investigations (including collaborative work undertaken during a visit by Kate Breckenridge of the U.S.G.S., Menlo Park in July, 1991) have been prepared for the Fall, 1991 AGU and have also been submitted for publication.

2. Valuable collaborative work was undertaken during an extended visit by Dr. Alan Linde (D.T.M., Carnegie Inst. of Washington) in 1991. Investigations were completed of amplitude of tidal components of the strain record for the periods before and after Loma Prieta earthquake. A paper reporting the results of this work has been submitted. Comparison of a number of different methods of tidal analysis for use in investigating strain data was also undertaken during this visit.

3. Data from the three tensor strain sites at Parkfield has been processed regularly, and monthly reports of strain provided to the Parkfield group meetings. A number of short term (hours to days) signals evident on both a strain data record and on a nearby creepmeter in the Parkfield region have been investigated to determine the possibility of a common source region.

4. A procedure involving a plot of the two primary shear strain components  $\gamma_1$  and  $\gamma_2$  against each other has been developed, and a paper giving the details is in preparation. This procedure provides a useful means for physical interpretation of shear strain and strain changes over time.

### RESULTS

For the period 1985 - September 1991 we examined the San Juan Bautista strain (SJT) and creep (XSJ2) records independently for steps. Apart from coseismic steps which are generally seen only on the strainmeter, the most frequent event is one involving both strain and creep steps. Individual strain steps at SJT are remarkably similar and have duration of about an hour. They are followed within hours to days by right lateral creep events at XSJ2 of several mm. The creep events are much slower than the strain events, with the major offset occurring over a few days. A representative selection of the events as recorded on the strainmeter and the creepmeter at XSJ2 are shown in Figure 1.

Investigation of a wide range of dislocation models in the region of San Juan Bautista led to our conclusion that the source is a small region below XSJ2 at a very shallow depth of about .5 to 1km, and a few km at most in extent. Location of this source so close to XSJ2 by processing of totally independent strain data, suggests a causal relationship between the strain and creep events.

The long term data for these two sites was examined in the light of these conclusions (see Figure 2). Data from other creepmeters further to the south on the San Andreas was also considered. The XSJ2 creep record is seen to be dominated by the event steps, which account for 80-85% of the total creep. In the strain record the shear strain  $\gamma_1$  (approximately fault parallel) is dominated by a change of strain rate, relative to the 1987 rate, of +1 microstrain/year before Loma Prieta, and +2 microstrain/year following the earthquake. The onset time of the latter change coincided with an increased creep event frequency which began some 3 to 5 months after Loma Prieta.

The linearly increasing elastic shear strain seen by the SJT strainmeter can be explained by the dislocation stress arising from a slip deficit on a locked patch in the region. Consideration of possible source regions to account for this anomaly resulted in a model with a locked patch at least 5 kilometers long, centred south-east of San Juan Bautista, the upper boundary of which is within 1-2 km of the surface, beneath the regularly failing small region discussed above. Such a model is shallower than locked regions postulated in the literature, suggesting that either the coseismic slip propagates closer to the surface than indicated in the literature, or that the region 3 to 1 km depth is locked but fails aseismically probably as afterslip, due to a velocity strengthening mechanism.

## RELEVANT PUBLICATIONS

- Gladwin, M. T., High Precision multi component borehole deformation monitoring. *Rev.Sci.Instrum.*, 55, 2011-2016, 1984.
- Gladwin, M.T., Gwyther, R., Hart, R., Francis, M., and Johnston, M.J.S., Borehole Tensor Strain Measurements in California. *J. Geophys. Res.* 92. B8 pp7981-7988, 1987.
- Gladwin, M. T. and Hart, R. Design Parameters for Borehole Strain Instrumentation. *Pageoph.*, 123, 59-88, 1985.
- Gladwin, M. T. and Wolfe, J. Linearity of Capacitance Displacement Transducers. *J.Sc.Instr.* 46, 1099-1100, 1975.
- Johnston, M.J.S., Gladwin, M.T., and Linde, A.T. Preseismic Failure and Moderate Earthquakes. *I.A.S.P.E.I.*, Tokyo, August 19-30, S7-65, 35, 1985.
- Johnston, M. J. S., Linde, A.T., Gladwin, M.T., and Borchardt, R.D. Fault Failure with Moderate Earthquakes. *Tectonophysics*. 144, 189-206, 1987.
- Gladwin, M. T., Hart, R., and Gwyther, R. L. Continuous Deformation Measurements prior to the Loma Prieta Earthquake. *EOS, (Trans. Am. G. Un.)* 71, p 1461, 1990
- Gwyther, R. L., Gladwin, M.T. and Hart, R., A New Shear Strain Anomaly Following the Loma Prieta Earthquake. (*Submitted for publication*).
- Linde, A.T., Gladwin, M.T. and Johnston, M.J.S. The loma Prieta Earthquake, 1989 and Earth Strain Tidal Amplitudes: An Unsuccessful search for Associated Changes. *Geo. Res. Lett.*, (in press).
- Gladwin, M.T., Gwyther, R.L., Higbie, J.W. and Hart, R.G., A Medium Term Precursor to the Loma Prieta Earthquake? *Geo. Res. Let.* 18 #8 pp 1377-1380, 1991.
- Gladwin, M. T., Breckenridge, K.S., Hart, R., and Gwyther, R. L. Recent Acceleration of Characteristic Creep-Strain Events at San Juan Bautista. *EOS, (Trans. Am. G. Un.)* 72 p 484, 1991.
- Gwyther, R. L., Gladwin, M.T. and Hart, R., Interpretation of Continued Shear strain anomalies of the Loma Prieta Earthquake. *EOS, (Trans. Am. G. Un.)* 72 p 310, 1991.

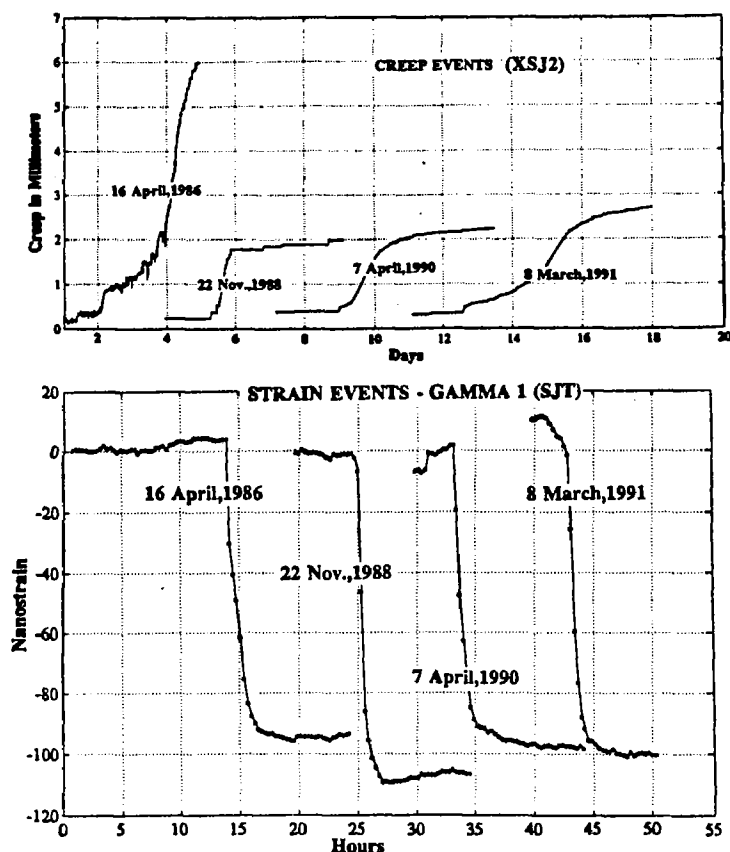


Figure 1. A Some representative samples of creep/strain events observed in the data from creepmeter XSJ2 (located on the San Andreas Fault on the southern outskirts of San Juan Bautista) and tensor strainmeter SJT (located 2 km to the west of XSJ2). Note the striking similarity of events over a 5 year timespan.

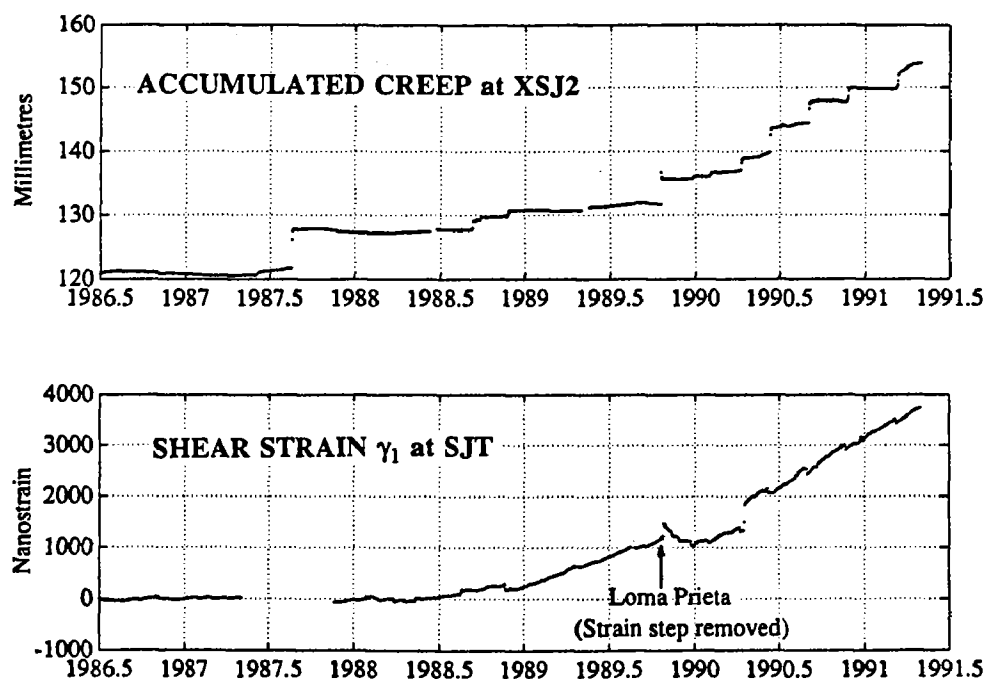


Figure 2. A comparison of the shear strain anomaly before and following the Loma Prieta event with the creep at XSJ2 (data courtesy of Ms K. Breckenridge, USGS). The creep retardation characteristic of the pre Loma period has changed to an above average creep rate with similar time signature to the observed shear strains at the San Juan tensor strain instrument.

Origin and Age of the "Sunklands" Using Drainage Patterns,  
Sedimentology, Dendrochronology, Archeology, and History

Interim Report

Agreement No. 14-08-0001-G1997

Margaret J. Guccione and Roy B. VanArsdale,  
Geology Department;  
(501) 575-3354  
David Stahle and Malcolm Cleaveland,  
Geography Department  
(501) 575-3159  
Charles R. Ewen, Arkansas Archeological Survey  
(501) 575-6547  
University of Arkansas  
Fayetteville, Arkansas 72701

PURPOSE

Surface evidence of faults in the New Madrid Seismic Zone are rare, despite three major earthquakes in 1811 and 1812. The "sunklands" of northeast Arkansas have been attributed to subsidence associated with these earthquakes. The "sunklands" are lakes or swampy areas that occur along streams that have locally low gradients. An alternative hypothesis attributes the "sunklands" to alluvial drowning at least a thousand years ago. This alluvial drowning occurred where a major crevasse channel of the Mississippi River has aggraded faster than smaller tributary streams. The purpose of this study is to determine which, if either, hypothesis is correct by determining the date and origin of the lake or "sunkland" using its sedimentologic, biologic, and historic records.

DATA COLLECTION AND ANALYSES

Geology

Lake coring of Big Lake in northeastern Arkansas was conducted during May, 1991. A total of 26 cores were collected. Of these, three cores ranged from 5 to 7 m in length and the remaining cores ranged from 1 to 2 m in length. The cores were described and sampled for textural analyses. To date grain size analyses have been completed on 10 of the cores, including all of the long cores. Organics were sampled for radiocarbon dating and 8 dates have been obtained. One core was submitted for 7 Pb-210 analyses and a date has also been obtained from these samples.

Siting of a trench is in progress. Aerial photographs, digital elevation maps of the area, and historic data from the Big Lake National Wildlife Refuge have been examined. Trenching

cannot begin until water levels subside.

### Dendrochronology

Field work to core trees in Big Lake and the St. Francis Sunklands was conducted during May, 1991. Not a single living tree older than 180 years (or 1811-1812) was located and only 15 trees were sampled from this area to verify the field observations. Most of the sampling was done at the St. Francis Sunklands where an abundance of old trees and logs were located. Here 118 trees and subfossil logs were sampled. These cores are presently being dated using dendrochronology.

### History and Archeology

Early records of French, Spanish, and English settlement of the area are being collected from University of Arkansas Library Special Collections, Memphis State University Library, and the New Madrid Museum.

Historical information from Big Lake National Wildlife Refuge has been examined. These reports, maps, etc. provide information about the condition of the area at the turn of the century prior to major construction in the area and man's impact on the area since that time. This information is valuable in interpreting sedimentation patterns in the lake and distribution of the vegetation in the area.

### PRELIMINARY RESULTS

The two hypotheses that have been proposed for the "sunklands", alluvial and tectonic, are being tested using cores from Big Lake, Arkansas. Twenty-six cores were taken in the lake. These cores were described and sampled for textural analysis, total carbon,  $C^{14}$  dating, and  $Pb^{210}$ . In 24 cores up to 1 meter of silty clay lacustrine sediment was identified at the lake bottom. Commonly organics occur at the lower contact of the silty clay. Units beneath the lake sediments were variable and included bedded and laminated sand, laminated clay, massive clay, bedded sandy loam, buried soils, and a few disturbed units interpreted as liquefaction features. In the three deepest cores the pre-lacustrine deposits included 4.2 m of bedded sand, 4.4 m of interbedded sand and clay with a buried soil at 0.8 m depth, and 6.0 m of interbedded sand and clay with a buried soil at 0.8 m depth. The sand had horizontal bedding and lamination, precluding emplacement by liquefaction.

These results are not consistent with an alluvial drowning hypothesis where fine-grained laminated sediment becomes coarser grained with depth. They are consistent with a variety of fluvial and backswamp environments suddenly drowned by the formation of a lake.  $C^{14}$  dates indicate that the lake was formed between  $160 \pm 70$  years B.P. (1720-1860 A.D.). This is consistent with the formation of the lake during the New Madrid earthquakes in 1811-1812.

## REPORTS PUBLISHED

Guccione, M. J. and Hehr, L. H., 1991, Origin of the "Sunklands" in the New Madrid Seismic Zone: tectonic or alluvial drowning?: Eastern Section Seismological Society of America, Memphis, TN, p. 64.

Guccione, M. J. and Hehr, L. H., 1991, Origin of the "Sunklands" in the New Madrid Seismic Zone: tectonic or alluvial drowning?: Geological Society of America Abstracts with Programs, vol. 23, No. 5, pp. 88-89.



## **Review and Evaluation of Predictions Made Using M8**

Award No. 14-08-0001-G2061

Ray E. Habermann

Cooperative Institute For Research in Environmental Sciences

Campus Box 216, University of Colorado

Boulder, Colorado 80309

303 - 497 - 6427, (FAX) 303 -497 - 6513

### **Introduction**

M8 is an earthquake prediction algorithm which was developed by the Russian seismologist Kosobokov (Keilis-Borok and Kosobokov, 1986). The algorithm attempts to identify characteristic variations in seismicity which occur as precursors to large earthquakes. The algorithm has been applied to numerous seismicity catalogs from around the world and the authors have claimed that it correctly identifies times during which the probability of the occurrence of a large earthquake is increased (Gabrielov et al., 1986). These are called Times of Increased Probability (TIPs).

The fundamental assumptions made by M8, and other similar algorithms, are that observed variations are related to actual physical changes in the processes which are occurring in the earth and that the parameters being examined by the algorithm are consistent indicators of those processes over time. It is clear from a growing body of work (Habermann 1988, Habermann and Craig 1988, Wyss, 1992) that neither of these assumptions are true. The strongest variations observed in seismicity catalogs are nearly always related to changes in the observing system and large temporal variations exist in systematic errors in earthquake magnitudes. Neither of these facts were considered during the development and testing of M8.

We have examined 141 regions in the southwest Pacific using M8. Two types of magnitudes from each of two catalogs were used, yielding 4 data sets for each region. Our analysis revealed 189 TIPs in 78 regions. If the TIPs were natural, we would expect them to be identified by all four catalogs in each region. In fact, only 16 of 78 regions with TIPs had four TIPs identified. If we require that the TIPs occurred at the same time, only 2 of 129 possible region/time combinations include 4 TIPs. This is a clear indication that the TIPs are more closely related to the catalog choice than to variations in the seismicity of the earth.

The only difference between two of the data sets we examined was the magnitudes assigned to the events. The TIPs identified by the two catalogs were, however, very different. This suggests that TIPs are an indicator of systematic errors in

magnitudes rather than precursory variations. Examination of the temporal variations in the differences between the two magnitudes confirmed this.

### **The Catalogs**

Our analysis was carried out using two magnitude estimates from two different catalogs:

1) The NEIC catalog was obtained by Kosobokov from the CD-ROM produced by the National Earthquake Information Center in Golden, Colorado. This was the exact catalog which Kosobokov used in his recent application of M8 to the southwest Pacific. We made one data set from this catalog using  $m_b$  (NEICMB), and one using Kosobokov's common magnitude (NEICMC). The common magnitude is taken as the maximum magnitude given for each event.

2) The ISC catalog was created by the International Seismological Center in Newbury, England. We used a version from Dr. R.C. Lilwall which has two body wave magnitudes for each event. The first is the standard  $m_b$  from ISC (ISCMB). The second is an  $m_b$  calculated using the maximum likelihood technique (ISCML).

### **The Regions**

We examined 141 circular regions which covered the seismically active regions of the southwest Pacific (Figures 1A and B). The radius of each region was 427 km. The catalog of maximum likelihood magnitudes created by Lilwall spans the time period 1964 -1983, so we restricted our study to that period.

### **The TIPs**

Running M8 on these regions resulted in the identification of 189 TIPs in 78 regions. A sample of these is listed in Table 1. The region in which the TIP occurred is determined by combining 3 fields of this Table (Region:Area:Circle). We see that a TIP was identified using the set NEICMB in EAST:1:2 and that this was the only data set which included a TIP for this region. On the other hand, three data sets included a TIP in the circle EAST:1:6.

We determined the number of TIPs in each region with at least one TIP and compiled a histogram showing the distribution of these numbers. This histogram is shown as Figure 2. If the TIPs were natural we would expect most regions with TIPs to have four, one from each data set. Figure 2 shows that only 16% of the regions with TIPs have four and that most regions with TIPs have only one. The regions with more than 4 TIPs have several at different times. The counting technique for this histogram ignores all temporal aspects of the TIPs. It is, therefore, a best-case counting technique.

This analysis assumes that all of the TIPs identified in a given region begin at the same time. Table 1 indicates that this is not so. The circle EAST:1:6, for instance, has three TIPs. One begins during 1982 and two begin during 1984. Circle EAST:1:13 has 4 TIPs. It is counted as a success in Figure 2, but it can be seen that two of the TIPs begin during January 1977, one during July 1977, and one during January, 1981. Each TIP has a duration of six years, so these TIPs have substantial overlap. Our counting technique does not consider this overlap, so it represents the worst case.

When the occurrence time as well as the region are accounted for the histogram in Figure 2 changes to look like Figure 3. In this case, only 1.5% of the region/time's with TIPs have 4 and 70% of the TIPs are isolated.

### What Causes The TIPs?

The conclusion that different catalogs identify different TIPs is clear from these results. Our interpretation of this fact is that the TIPs are catalog phenomena and not natural. If this is so, what sorts of variations in the catalogs might cause the TIPs? The temporal distribution of TIPs in different data sets from both catalogs is shown in Figures 4 and 5. In the NEIC case, there are generally more TIPs when  $m_b$  is used. This is particularly true in the first several years examined. Both data sets show a clear long-term increase in the number of TIPs / year. In the ISCMB case, the average number of TIPs/year observed increases by a factor of 5 during 1981. This increase is not apparent when the maximum likelihood magnitudes are considered.

The only differences between the data sets which we examined were the magnitudes given to the events. This suggests that systematic variations in magnitudes might result in TIPs.

There is little difference between the magnitudes in the NEIC data sets because for most of the events, the only magnitude is  $m_b$ , so common magnitude equals  $m_b$ . For the events with more than one magnitude, the maximum is chosen as the common magnitude. We examined the magnitudes in these data sets and found that the common magnitude was not  $m_b$  for only 3 to 5% of the events, depending on the time period considered. The differences in TIP counts in Figure 4, therefore, are caused by differences in the magnitudes of only a very small fraction of all of the events.

Each event in the ISC data sets has two magnitudes, so there is a much stronger difference between the two data sets than in the NEIC case. Figure 6 shows the differences between the numbers of ISCMB and ISCML TIPs. Shown along with this difference is the yearly average difference between the two magnitudes. In this case we expect the maximum likelihood magnitudes to be more stable over time, so they act as a standard against which the  $m_b$ 's are compared. The maxima in these data indicates that the  $m_b$ 's were increased systematically during the latter part of the time period considered. The M8 algorithm considers data from a 3 year window and reports a value for that window at the end of it. Changes in the data, therefore, are not clearly identified

for three years. For this reason, the magnitude differences have been shifted 3 years forward in time. The maxima in the average magnitude differences clearly coincides with the maxima in the difference in the number of TIPs. This systematic increase in magnitudes is reflected in the increased number of TIPs because the functions used to identify the TIPs depend on seismicity rates and energy released. Both of these factors increase as magnitude increases.

## Conclusion

These data clearly indicate that the results of the M8 algorithm in a particular region are strongly dependent on the catalog used for the analysis. This indicates that the algorithm is more sensitive to changes in the catalogs than to real changes in the physical processes occurring in the earth. In particular, the algorithm preferentially identifies TIPs during periods of systematically increased magnitudes. This is not surprising as the magnitudes are a fundamental input to the algorithm.

These results demonstrate again that the seismicity catalogs which are presently available are inadequate for earthquake prediction studies and that a substantial effort is required to correct the errors which pervade these catalogs.

## References

Gabrielov, A.M., O.E. Dmitrieva, V.I. Keilis-Borok, V.G. Kosobokov, I.V. Kuznetsov, T.A. Levshina, K.M. Mirzoev, G.M. Molchan, S.Kh. Negmatullaev, V.F. Pisarenko, A.G. Prozoroff, W.A. Rinehart, I.M. Rotvain, P.N. Shebalin, M.G. Shnirman, S. Yu. Schreider, **Algorithms of Long-Term Earthquakes' Prediction**, International School for Research Oriented to Earthquake-Prediction Algorithms, Software and Data Handling, Ceresis, Lima, 1986.

Habermann, R.E., **Precursory seismic quiescence: Past, present and future**, PAGEOPH, 126, 279-318, 1988.

Habermann, R.E. and M.S. Craig, **Comparison of Berkeley and CALNET magnitude estimates as a means of evaluating temporal consistency of magnitudes in California**, Bull. Seismol. Soc. Amer., 78, 1255-1267, 1988.

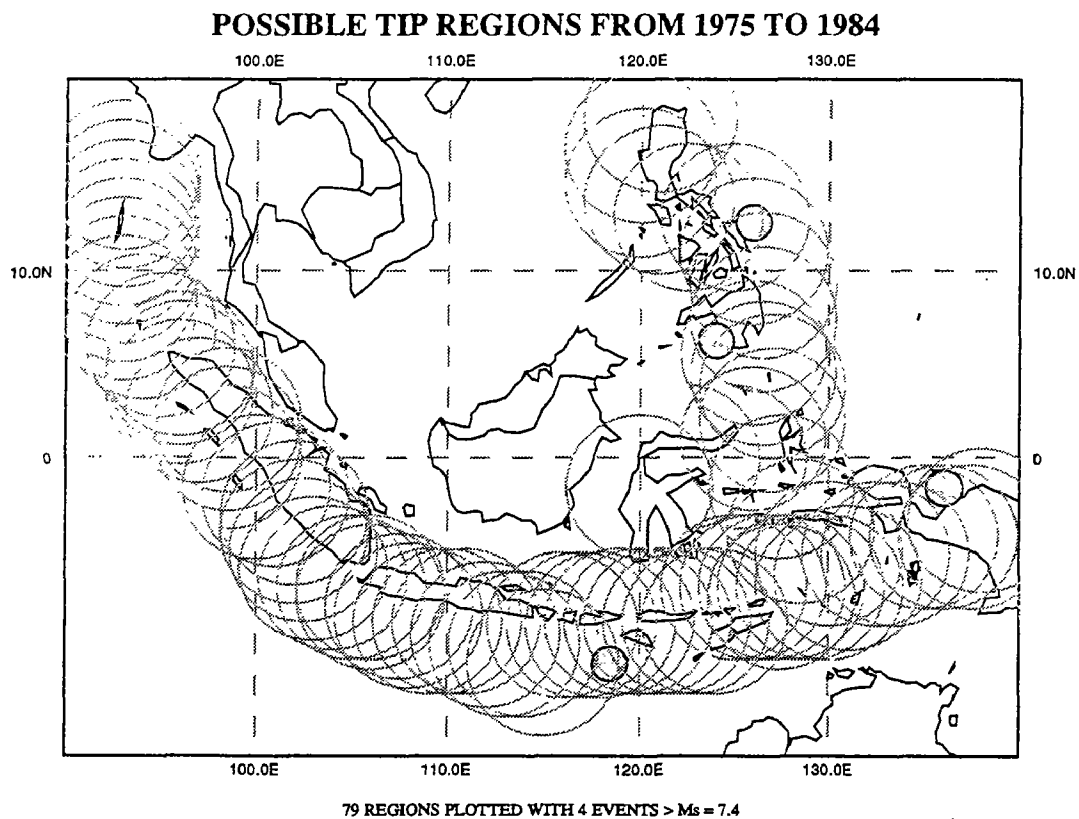
Keilis-Borok, V. I. and V.S. Kosobokov, **Times of increased probability for strongest earthquakes in the world** (in Russian), *Computational Seismology*, 19, 48-58, Moscow, Nauka, 1986.

Wyss, M., **An artificial and a precursory seismic quiescence**, in Earthquake Prediction: State of the Art, submitted, 1992.

Table 1. A sample of TIPs identified in this study.

Region	Area	Catalog	Magnitude	Type	Circle	Lat	Lon	Start
EAST	1	NEIC	MB	F	2	-6	133	Jul-78
EAST	1	NEIC	MC	C	4	-4	137	Jan-83
EAST	1	ISC	ML	C	5	-4	138	Jan-84
EAST	1	NEIC	MC	C	5	-4	138	Jan-82
EAST	1	ISC	ML	C	6	-4	140	Jan-84
EAST	1	NEIC	MB	C	6	-4	140	Jan-82
EAST	1	NEIC	MC	C	6	-4	140	Jan-84
EAST	1	NEIC	MB	C	7	-5	142	Jan-84
EAST	1	NEIC	MC	C	7	-5	142	Jul-82
EAST	1	ISC	ML	F	10	-5	148	Jan-78
EAST	1	ISC	MB	F	11	-5	150	Jan-78
EAST	1	ISC	ML	F	11	-5	150	Jan-78
EAST	1	ISC	MB	F	12	-6	152	Jan-77
EAST	1	ISC	ML	F	12	-6	152	Jan-77
EAST	1	NEIC	MB	F	12	-6	152	Jul-77
EAST	1	ISC	MB	F	13	-8	154	Jan-77
EAST	1	ISC	ML	F	13	-8	154	Jan-77
EAST	1	NEIC	MB	F	13	-8	154	Jul-77
EAST	1	NEIC	MC	S	13	-8	154	Jan-81
EAST	1	ISC	MB	F	14	-9	156	Jan-78
EAST	1	ISC	MB	C	15	-9	158	Jul-80
EAST	1	NEIC	MB	C	15	-9	158	Jul-80
EAST	2	NEIC	MB	C	1	-10.5	163	Jul-83
EAST	2	ISC	ML	F	2	-10.5	164	Jan-78
EAST	2	ISC	MB	C	3	-10.5	165.5	Jan-82
EAST	2	NEIC	MB	C	3	-10.5	165.5	Jan-84
EAST	2	ISC	MB	C	4	-12	166	Jan-82
EAST	2	ISC	ML	F	5	-13	166.5	Jan-76
EAST	2	ISC	MB	C	6	-14	167	Jul-81
EAST	2	ISC	ML	F	6	-14	167	Jan-76
EAST	2	ISC	MB	C	7	-15	167.5	Jan-82
EAST	2	ISC	ML	F	7	-15	167.5	Jan-76

The regionalization consists of three layers: Region:Area:Circle. Two catalogs were studied (NEIC and ISC). The magnitude types are described in the text. The TIP types are determined by the M8 program. They are False, Current, Successful and T, event within .5 magnitude units of target. The latitude and longitude are the center of a 427km radius circle. The TIPs last for 6 years after the start date.



1A

**POSSIBLE TIP REGIONS FROM 1975 TO 1984**

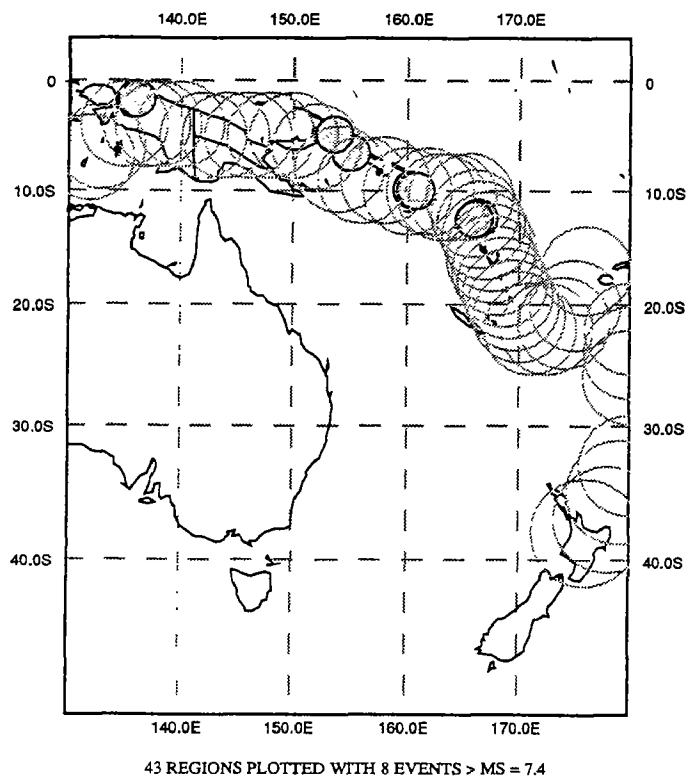


FIGURE 1B.

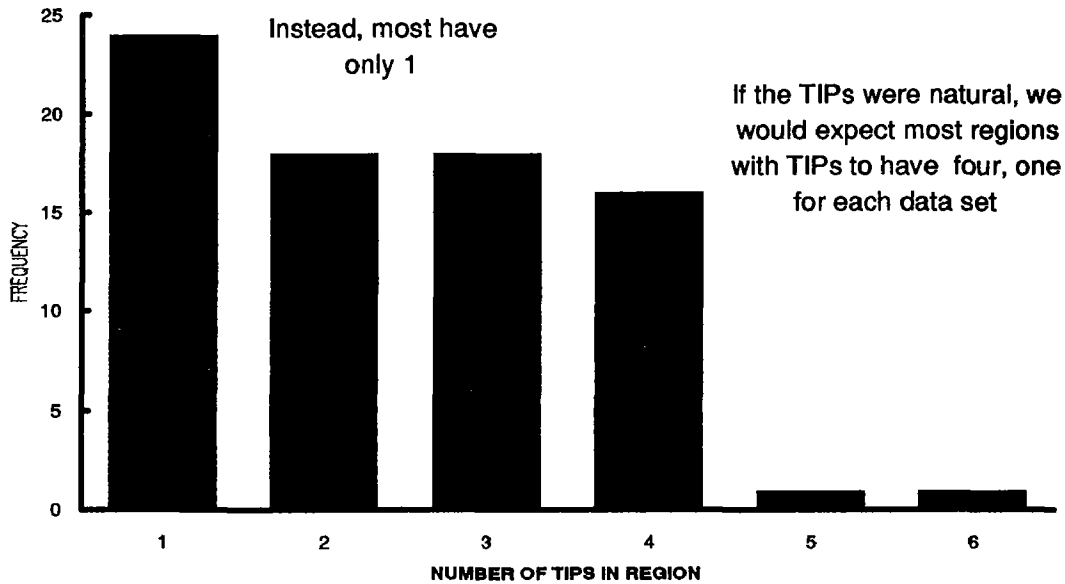


Figure 2. Histogram showing the number of TIPS in regions with at least one TIP. We would expect most catalogs to identify the TIPS if they were natural. If that were true, this histogram would be peaked at four. Instead, we see that most regions with TIPS have only one. In this case we count any TIPS in the same region as coincident, ignoring the time of the TIP. This is, therefore, a best case scenario.

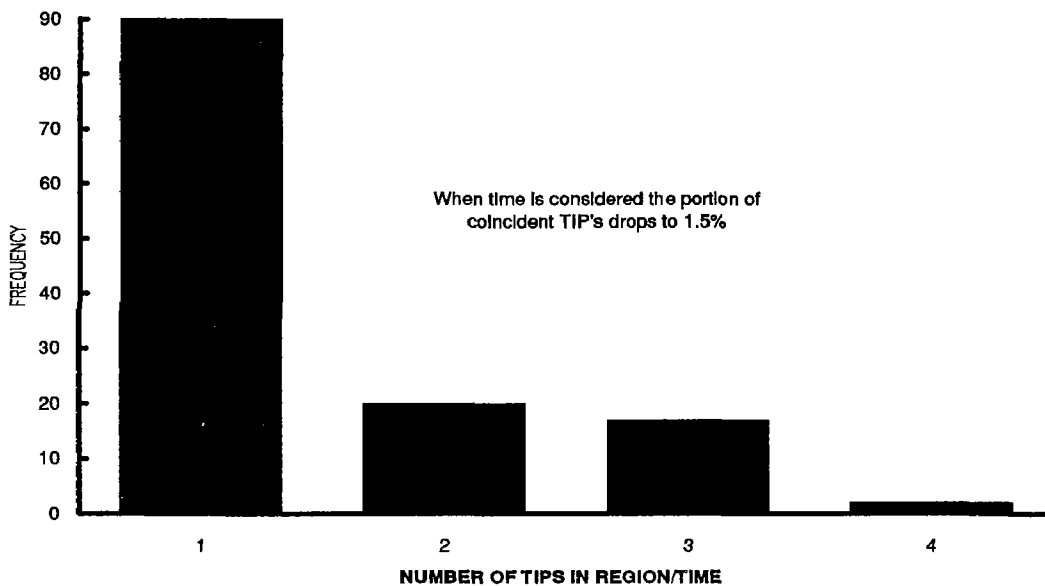


Figure 3. Histogram showing the number of TIPS in region/times with at least one TIP. This is similar to the histogram in Figure 2, but we require the TIPS to be at the same time in order to be counted as coincident. Again we would expect this histogram would be peaked at four if TIPS were real. Instead, we see that the vast majority of region/times with TIPS have only one. This is a clear indication that the TIPS are related to the catalogs, not to processes in the earth.

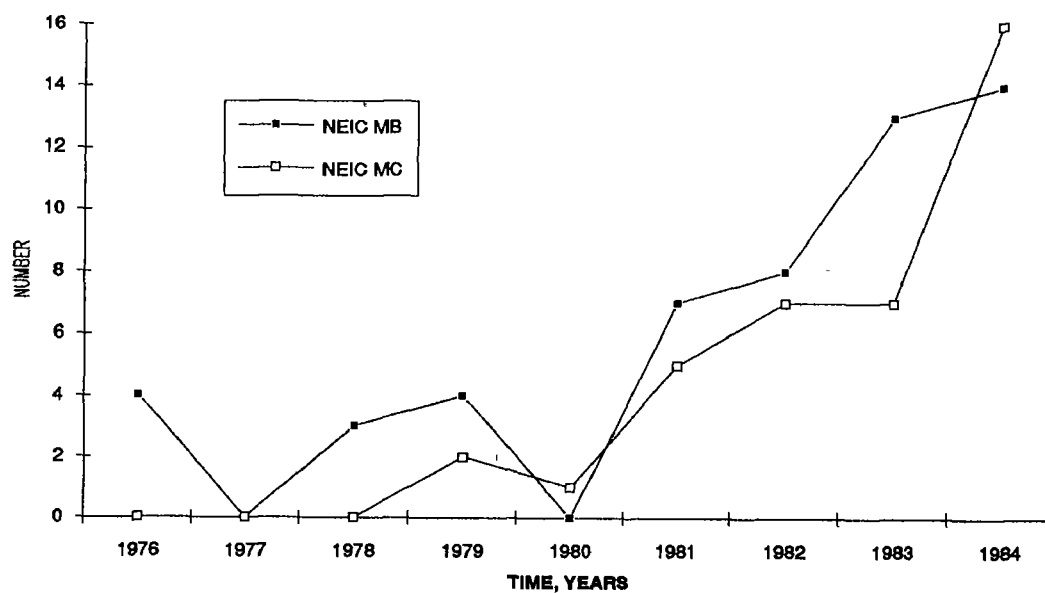


Figure 4. The number of TIPs identified in the NEIC catalog each year using two different magnitudes. Note that both magnitudes show a long-term increase in the number of TIPs.

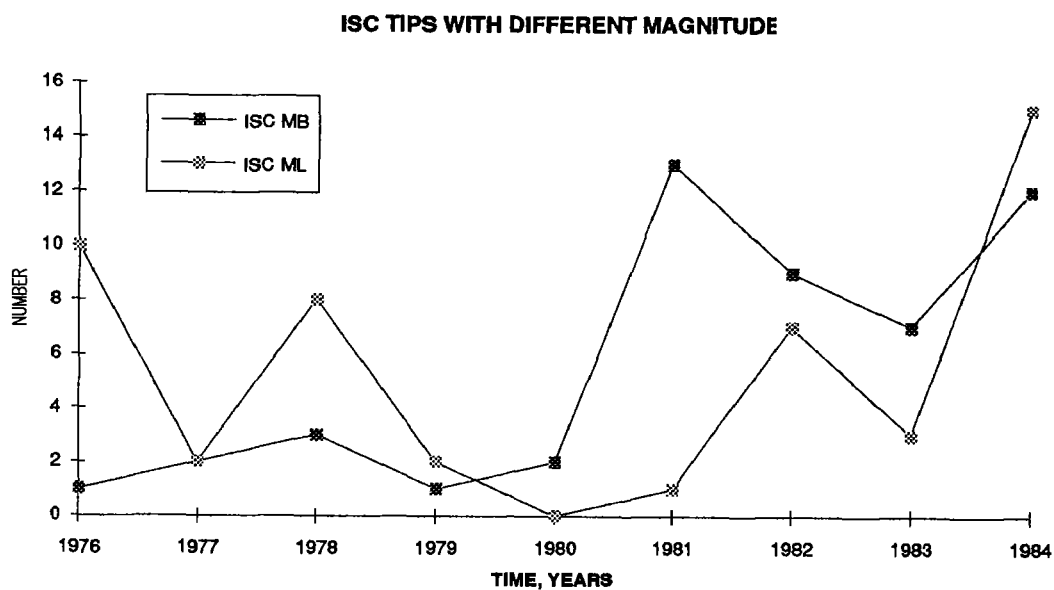


Figure 5. The number of TIPs identified in the ISC catalog each year using two different magnitudes. Note the sharp increase in the number of TIPs identified using mb during 1981 and the lack of a similar increase when the maximum likelihood magnitudes are considered. Both data sets included the same events, so the differences in the TIPs must be related to magnitudes.



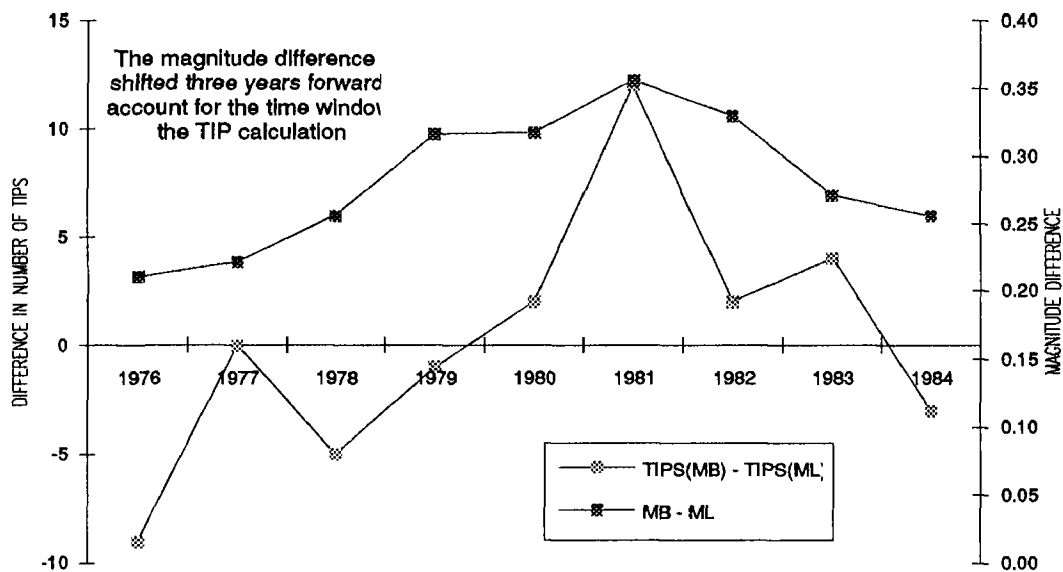


Figure 6. The difference in the number of TIPS/year in the ISC catalog with two different magnitudes. Note the sharp peak in 1981 which coincides with the peak in Figure 5. The second curve show the yearly average difference between the two magnitudes. This average is shifted 3 years forward to account for the time window used in M8.

Paleoseismic Investigations of the San Andreas  
Fault on the San Francisco Peninsula

Agreement No. 14-08-0001-G2081

N. Timothy Hall  
Geomatrix Consultants  
100 Pine Street, 10<sup>th</sup> Floor  
San Francisco, California 94111

(415) 434-9400

Research in Progress

This project is planned as a two-year investigation of the late Quaternary paleoseismic history of the San Francisco Peninsula reach of the San Andreas fault. The Phase I research, which is in progress, is designed to evaluate the paleoseismic potential of five sites that may provide an accessible, decipherable, and dateable Holocene paleoseismic history of this reach of the fault. Two are located near San Andreas and Crystal Springs reservoirs south of San Francisco; three are located farther southeast, in the town of Portola Valley. The patterns of coseismic slip recorded in 1906, physiographic expression of the rift zone, and structural characteristics of the eastern flank of the Santa Cruz Mountains suggest that a fault segment boundary may lie at the north end of Portola Valley. The sites identified for this project fall on both sides of this possible boundary.

Site Locations and Description

Of the two sites that are north of this potential segment boundary, one is between San Andreas Dam and Lower Crystal Spring Reservoir. Based on evaluations to date, this site shows promise for paleoseismic investigations. It is located where a small alluvial fan of mid- to late-Holocene age has accumulated across the major active trace of the San Andreas fault. The fan appears to have been progressively dislocated by multiple pre-1906 slip events. Another potential site, not yet evaluated, is on the Filoli Estate where an alluvial fan heads at the active fault trace, providing the potential for having preserved a record of multiple faulting events in offset channel deposits.

The three other potential sites, which are in Portola Valley, are located south of the possible fault segment boundary. One, near Portola Valley Town Center, has a well-documented record of 1906 slip. This site is underlain by

fine-grained, peaty sediments, which recently were exposed on an adjacent property in trenches excavated for a planned development. These trenches were examined, zones of deformation were logged in detail, and charcoal samples were collected. A program for future paleoseismic research has been formulated. The other sites, located on undeveloped land directly south within the rift valley, have either strong geomorphic expression or photo-documented 1906 slip. At one of these, a detailed topographic map (contour interval = 20 cm) has been prepared for a 250-m reach of the fault where features of the 1906 and earlier faulting episodes are especially well preserved. An exploratory trench that reveals the subsurface expression of the surface trace is being logged in detail. Access to the third site in Portola Valley, where young deposits have accumulated across the San Andreas fault, is being negotiated.

### Future Work

The outcome of Phase 1 will be to establish a priority ordering of the sites based on our judgment of their potential for yielding a detailed paleoseismic record. If additional funding is available, Phase 2 will involve detailed paleoseismic investigations at one or more of the sites. Methods will include backhoe trenching, detailed stratigraphic and structural analysis, and numerical (radiocarbon) analysis of key horizons. The anticipated outcome of this study is both documentation of the late Holocene slip rate and an event-by-event chronology for this currently locked segment of the fault. The detailed paleoseismic investigations we propose for the active San Andreas fault trace(s) along the San Francisco Peninsula will contribute directly to estimating when damaging earthquakes are next likely to strike this major urban center.

Paleoseismic Investigations of the San Andreas Fault  
at the Vedanta Site, Marin County, California

Agreement No. 14-08-0001-G2114

N. Timothy Hall  
Geomatrix Consultants  
100 Pine Street, 10<sup>th</sup> Floor  
San Francisco, California 94111  
(415) 434-9400

Tina M. Niemi  
Geology Department  
Stanford University  
Stanford, California 94305  
(415) 723-0507

## Introduction

An accurate estimate of the repeat time of 1906-type events is necessary to understand the earthquake cycle in the San Francisco Bay area. Unfortunately, the historical record in northern California extends only to the early 19<sup>th</sup> Century and includes no historical accounts of pre-1906 ground rupturing earthquakes on the North Coast segment of the San Andreas fault. The Vedanta research site, located near the town of Olema in Marin County, California (Figure 1), has the potential to provide data on the chronology of pre-1906 ground rupturing earthquakes.

## Research in Progress

Pre-1906 slip events were identified in four trenches excavated perpendicular to the San Andreas fault at the Vedanta site (Figure 2). The aggrading depositional environment of the Vedanta marsh, which is traversed by the 1906 fault trace, makes this a good site for paleoseismic investigations because layers of sediment accumulate across the fault after each slip event. Trench 11, located 64 m from the north end of marsh, is a shallow excavation that exposes a buried Douglas fir tree that toppled into the marsh from a nearby ridge and was subsequently displaced by the fault. Approximately 170 m farther to the south, Trench 12 contains a basal 1.5 m-thick section of clayey silts, organic-rich marsh silts, and interbedded gravel channels that are confined to a narrow trough along the fault. In the south end of the marsh, Trenches 15 and 13 are located 23 m and 70 m from the north end of the wind gap, respectively. They revealed interbedded alluvial fan gravels and fine-grained marsh sediment. Detailed logging of these trenches provides evidence for 2 to 5 pre-1906 faulting events. These events were identified on the basis of upward-terminating faults, crack fills, unconformities, and rotated and truncated blocks of sediment.

Establishing the timing of a paleoearthquake requires radiocarbon ages for both the youngest unit cut or deformed by a slip event and for the oldest layer that caps the buried earthquake feature. At present, only a limited number of radiocarbon analyses are available to bracket the precise timing of pre-1906 slip events. A burn horizon that appears in trenches both east and west of the San Andreas fault provides a stratigraphic time-line at approximately 1000 years B.P. At least three slip events including the 1906 faulting appear to cut layers higher in the section than this horizon in Trenches 13 and 15. However, in Trench 12, three events including 1906 cut layers dating to  $630 \pm 30$  years B.P. This yields a maximum recurrence of approximately 245 to 315 years and suggests the penultimate event occurred after 1591-1661 A.D.

### Future Work

In order to improve the chronology of pre-1906 events along the North Coast segment of the San Andreas fault, better age control is needed. Current NEHRP funding is providing support for AMS radiocarbon analyses of short-lived plant materials that may constrain the timing of individual paleoearthquakes at this site. Additional excavations are planned to expose the details of the fault zone at the buried fir tree in Trench 11 and to search for its truncated base. These excavations may provide the first evidence in northern California for the amount of slip that occurred on the San Andreas fault during a pre-1906 earthquake.

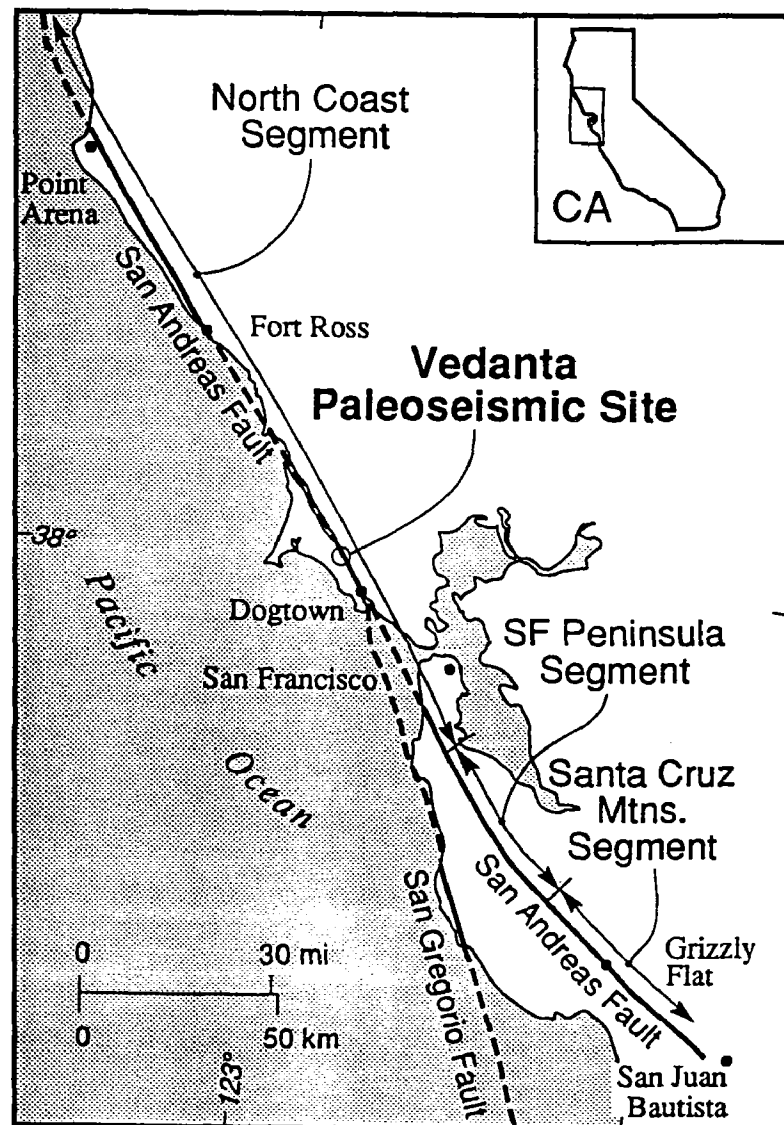


Figure 1: Paleoseismic sites along the San Andreas fault in northern California. The research site for this study is on the Vedanta Retreat property, Olema, California.

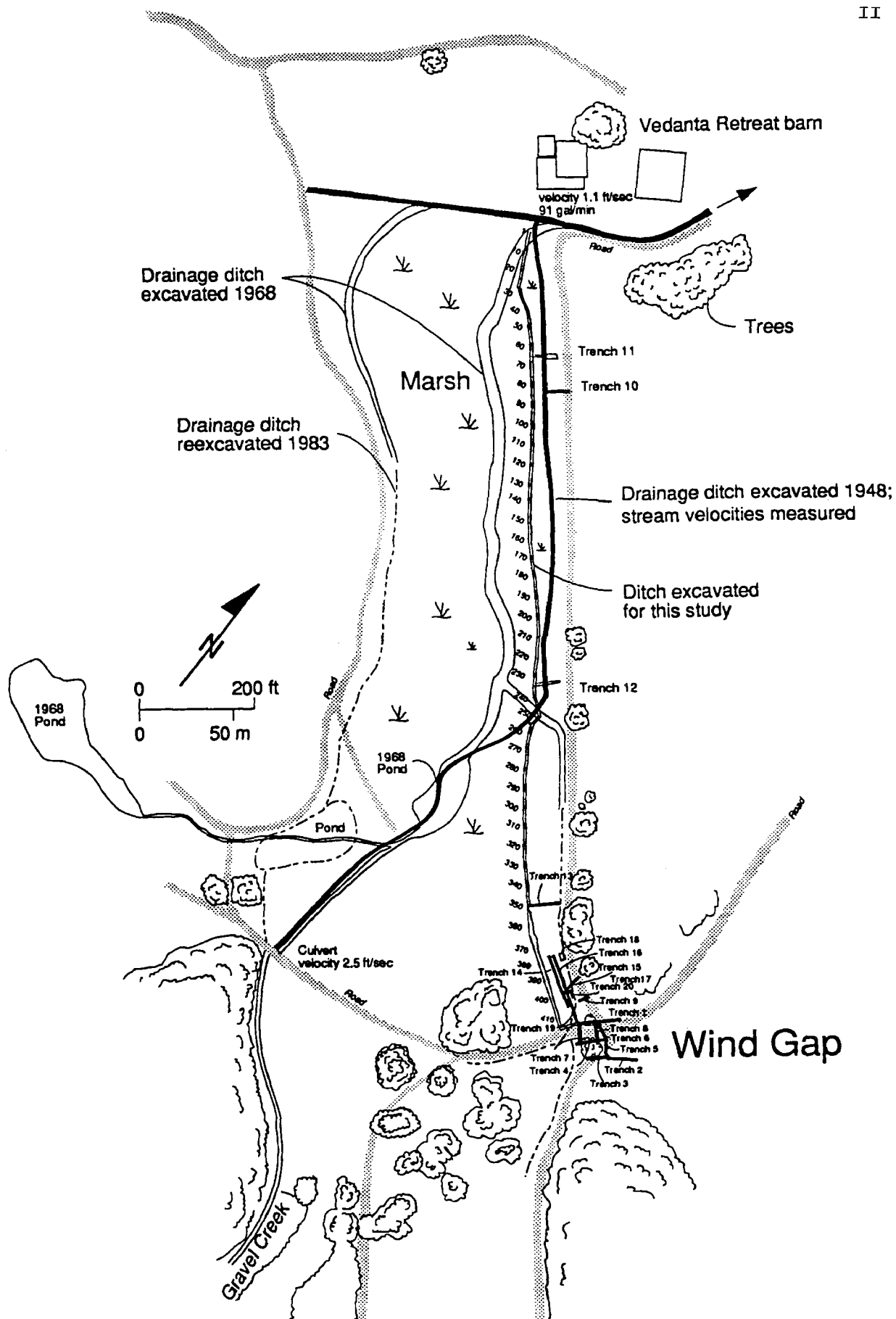


Figure 2: Map of the Vedanta marsh showing locations of trenches excavated for this paleoseismic study.

**Collaborative Research:  
Analysis of PANDA data and continuation of PANDA experiment  
in the Central New Madrid Seismic Zone**

14-08-0001-G2138

Robert B. Herrmann  
Department of Earth and Atmospheric Sciences  
Saint Louis University  
3507 Laclede Avenue  
St. Louis, MO 63103  
(314) 658-3131

### **Investigations**

The purpose of this segment of the collaborative effort is to learn as much as possible about the dynamics of the earthquake process in the New Madrid Seismic Zone by using data from the dense PANDA deployment of three component sensors on top of the seismicity in the central seismicity trend between New Madrid, Missouri, and Dyersburg, Tennessee.

### **Results**

Waveforms of 289 events that occurred during the first nine months of the PANDA deployment were examined for use in estimating  $Q$  by fitting the acceleration spectra derived from the signals in the manner of Anderson and Hough (1984). Of the 289 events, spectral analysis was applied to 63, and 55 were used in the final analysis. In general, the first 0.5 seconds of the P wave on the vertical component and the first 1.0 second of the S wave from the transverse component were used for analysis in the frequency range of 5 - 25 Hz.

The spectrum is fit using a parameter  $\kappa$  which controls the high frequency signal content by a factor  $\exp(-\pi\kappa f)$ . Given the travel time of the wave,  $T$ , and assuming that the spectral shaping is due to  $Q$ , then  $Q = T/\kappa$ . In the Mississippi Embayment, this number is strongly affected by the thick sediments ( 600 - 1000 m ). The apparent  $Q_P$  is less than 100. To isolate the effect of sediments,  $\kappa$  is plotted as a function of distance from a given station by using data from many events. This led to  $\kappa(0) = 0.05 \pm 0.01$  and the  $d\kappa/dr$  led to an estimate of  $Q_S \approx 200$ . Assuming shear velocities in the sediments, leads to an average  $Q_S = 22$  for the sediment column.

Since the M. S. Thesis of Wuenschel (1991), an additional nine months of data have been processed.

Work is beginning on modeling the PANDA waveforms by synthetic seismogram techniques, but will require a digression into anisotropy theory to see the effect of anisotropy on S-wave polarizations. This analysis will attempt to obtain focal mechanisms defined better than by using P-wave first motions alone.



### **Publications**

Wuenschel, M. E. (1991). Attenuation of body waves in the New Madrid Seismic Zone, M. S. Thesis, Saint Louis University.

Wuenschel, M. E., R. B. Herrmann, Z. Liu (1991). Attenuation of body waves in the New Madrid Seismic Zone (abs), *Seism. Res. Letters* **62**, (in press).

### Cooperative New Madrid Seismic Network

14-08-0001-G1922  
 R. B. Herrmann  
 Department of Earth  
 and Atmospheric Sciences  
 Saint Louis University  
 3507 Laclede Avenue  
 St. Louis, MO 63103  
 (314) 658-3131

14-08-0001-G1923  
 A. C. Johnston, J. M. Chiu  
 Center for Earthquake  
 Research and Information  
 Memphis State University  
 Memphis, TN 38152  
 (901) 678-2007

### Investigations

The object of this effort is to upgrade the regional seismic networks in the central Mississippi Valley to provide the data sets necessary for future research in the earthquake process and in earthquake generated ground motion.

In order to accomplish this, the satellite telemetry capability of the US National Seismic Network will be used to communicate between central data collection points at Memphis and St. Louis and the intelligent regional seismic network nodes to be placed at five sites in the region.

Major tasks involve the design and implementation of the data centers, the regional nodes at satellite uplink points, and the seismic sensors in the field. Data will be transmitted from the sensors to a node using all digital telemetry, 20 and 24 bit, to the extent possible with the present funding. The final network will consist of 5 nodes, each collecting data from a broadband sensor, an accelerometer and three-component seismometers.

### Results

Efforts to date have concentrated on the design of PC based regional nodes to communicate with the regional data centers using USNSN satellite telemetry. In addition the design of the PC systems has focused on their use as replacements for ten year old central digitizing computers of the current regional networks.

#### *Data Acquisition.*

The PC based systems run a real time UNIX product, VENIX from VenturCom, and have all the multitasking, interprocess communication and networking tools needed for an observatory and for regional nodes. This new hardware and especially a modern operating system permit processing tasks that are difficult to do on the older computers. The multiprocessing capability differentiates this system significantly from other PC based systems. The fact that it is a PC based system also has significant cost advantages with respect to repair and replacement.

In a data center environment, defined as one in which all seismic data comes to a central collection point in real time, the model used by almost all current networks, this system will perform the following tasks (items to be

implemented are indicated by an asterisk \*):

#### PC BASED ACQUISITION SYSTEM

- 1) *eqacquire* - detect earthquakes, save data on disk, notify *eqdemux* on completion of trigger. 128 input channels, subnet detection, and station dependent trigger parameters are supported.
- 2) *eqdemux* - demultiplex seismic data, create pointers to traces in binary data file, notify *eqpick* and *eqsend* upon completion
- 3) *eqsend* - send binary data files to system file server over Ethernet
- 4) *eqpick\** - pick P and S arrival times using R. Crosson's CPICK program, invoke *eqlocate* for preliminary location, robustly examine residuals to catch phase misidentification, relocate, send preliminary location over network to system file server
- 5) *eqlocate\** - robust earthquake location program that handles different earth models and locates teleseisms as well as regional seismic events
- 6) *eqtime* - read time code as it is digitized, update *eqacquire*'s concept of true time, define current A/D sampling rate, noting hourly drift.
- 7) *eqtrace\** - interactive trace analysis to correct arrival time picks
- 8) *eqmap\** - display recent earthquake locations on monitor
- 9) *eqview* - display seismic traces as they are being digitized, as a digital Develocorder (TM Geotech)
- 10) *eqmenu* - menu based system control for running individual programs listed above. Purpose is for general use (privilege protected) view of system performance. In addition permit initialization of parameters of *eqacquire*.

#### SERVER

- 1) final analysis software for catalog and archive. Programs *eqtrace\**, *eqmap\**, *eqpick\** and *eqmenu* will run as on PC. The heart of this are definitions of binary data format, and device, operating system independent graphics.
- 2) automatic notification of event occurrence
- 3) storage of all parameter and waveform data on optical disk.
- 4) waveform inversion of broadband data for significant events using IRIS, USNSN and local broadband data.

The processing steps make use of much existing code as well as analysis approaches. Operating system capabilities, such as using the line printer daemon to control processing steps, will be used to simplify the coding. Care is taken to properly define data formats and to make the analysis software as independent of specific data formats as possible. Concepts from the Center for Seismic Studies 3.0 Database will be used to characterize data and parameters. A lowest level subset will be used to permit the use of a variety of data sets, including USNSN, IRIS, strong motion data and local research network data without significant pain to the user. The code to be written will attempt to be platform independent, permitting its use not only on workstations, but also on PC's, thus fitting in with ISOP initiatives.

### *VSAT Testing*

Two VSAT's (Very Small Aperture Terminal) from Scientific Atlanta have been installed, one in Memphis at CERl, and the other in Marked Tree. The VSAT at Marked Tree will currently carry two-communications between the regional node at Marked Tree and the receiving at Memphis (and later St. Louis) via the USNSN center in Golden, Colorado. Testing of the VSAT communications network has begun. Currently, Memphis State has been successful in establishing two-way round-trip communications through the system. The current setup uses two ports on the same AD (Packet Assembler Disassembler) for testing the USNSN facilities. Both ports are presently attached to a VAX 11/785 at CERl/MSU and will be left there for the duration of the testing phase. Several sets of tests will be implemented in the immediate future. The first test will verify the integrity of the rollback system for handling data transmission problems. Once the rollback system has been verified, the full set of USNSN protocols will be implemented. The subsequent set of tests will include downloading commands to remote field sites, making data requests to the USNSN, and checking out other features of the system.

### **Publications**

Herrmann, R. B., E. J. Haug, A. C. Johnston and L.-M. Chiu, Progress in implementing the Cooperative New Madrid Seismic Network (abs), *Seism. Res. Letters* 62, (in press).

## ACTIVE SEISMIC STUDIES OF VOLCANIC SYSTEMS

9930-01496

D.P. Hill, H.M. Benz, J.A. Olson, J.E. Vidale  
 Branch of Seismology  
 U.S. Geological Survey  
 345 Middlefield Road, MS 977  
 Menlo Park, California 94025  
 (415) 329-4795

### Investigations

Over the last decade, this project has focussed on the activity in Long Valley caldera and coordination of associated monitoring research, and hazard reduction activities. Because project funding has come from the Volcano Hazards Program, the project has not been a regular contributor to the NEHERP semi-annual technical reports. For current reporting period, however, the following efforts funded under NEHERP have been administratively associated with this project in addition to the on-going coordination of Long Valley caldera monitoring and research:

- 1) Applications using the regional seismograph networks in the western United States for array studies of seismic scattering from upper mantle structures (J.E. Vidale and H.M. Benz).
- 2) Seismicity patterns associated with Loma Prieta segment of the San Andreas fault (J. Olson).
- 3) Analysis of the geometry of seismogenic strike-slip and normal faults and its significance for fault strength and stress levels in the brittle crust (W. Thatcher and D.P. Hill).

### Results

#### *Long Valley Caldera (D.P. Hill)*

Large, restless calderas pose a particularly vexing challenge for both scientists monitoring the activity and civil authorities who must respond to the threat of volcanic hazards during periods of heightened activity. Not only do we lack modern, instrumental records of eruptions and their precursors within large calderas, but the patterns of unrest documented in well-monitored calderas such as Long Valley (California), Yellowstone (Wyoming), Campi Flegrei (Italy), Rabaul (New Guinea) show episodes of intense unrest separated by years to decades of relative quiescence. This situation severely tests the ability of scientific, civil, and political institutions to maintain effective, long-term monitoring and emergency preparedness capabilities. As part of an effort to address this problem for Long Valley caldera and the adjacent Inyo-Mono

Craters volcanic chain, we (Hill and others, 1991) have developed a five-level alert system using criteria based on activity within the caldera over the last decade and on well-documented examples of activity preceding volcanic eruptions elsewhere in the world. Each of the alert levels, E (weak activity), D (moderate activity), C (strong activity), B (intense activity), and A (eruption likely) is tied to specific activity levels detected by telemetered seismic and deformation-monitoring networks maintained within the caldera as well as the results from a laser-ranging geodetic network that is measured several times a week. Each of the alert levels, in turn, triggers a specific response by the U.S. Geological Survey (USGS). Levels E through C, for example, trigger information calls to a successively wider group of federal, state, and local authorities. Level B mobilizes an intensified USGS monitoring effort from a field center established in the caldera. Level A triggers a formal Hazard Warning for the possibility of an imminent volcanic eruption. Such a system does not solve the problem of predicting volcanic eruptions nor does it eliminate the need for making tough personal judgements under difficult circumstances. It does, however, provide a stable framework for establishing and maintaining clear communication between scientists monitoring the caldera and civil authorities responsible for protecting local population centers from hazards posed by a possible volcanic eruption.

*Loma Prieta seismicity patterns (J.A. Olson)*

A Workshop on the Seismotectonic Significance of the Loma Prieta Earthquake was held at the Asilomar Conference Center, Pacific Grove, CA, on May 12-15, 1991 (Steering Committee: Bill Ellsworth, Bob Anderson, Greg Beroza, Bill Cotton, Jean Olson, and Dave Schwartz). The workshop brought researchers together to present and compare their current work on the mechanics of the earthquake and the geologic framework of the southern Santa Cruz Mountains. Extensive discussion of key issues provided a more comprehensive picture of the earthquake, a sharper focus of the outstanding controversies, and direction for further work while NEHERP projects funded in FY91 were still in progress. Olson (in press) summarizes key findings and controversies regarding the Loma Prieta earthquake that emerged from the workshop specifically including: (1) the nature of the sub-surface rupture, (2) the coseismic surface deformation, (3) the relation of the rupture surface to the San Andreas fault, (4) the long-term deformation of the southern Santa Cruz Mountains, and (5) the present earthquake potential in the southern Santa Cruz Mountains.

*Fault orientations in extensional and conjugate strike-slip environments and implications for frictional fault strength (D.P. Hill and W. Thatcher).*

In a review of the orientation seismogenic strike-slip and normal faults in regimes of distributed deformation, Thatcher and Hill (1991) find that the fault planes tend to cluster about  $45^\circ$  to the greatest principal stress direction rather than the  $\approx 30^\circ$  angle predicted by conventional Mohr-Coulomb faulting theory (also see report by Stein, Thatcher, and Grant for project no. 9960-01488). Hill and Thatcher (1992) have analyzed the energy required for slip on faults at varying angles ( $\theta$ ) to the greatest

principal stress in a fixed stress field to obtain an upper bound on the effective coefficient of friction  $\mu_d^*(\theta)$  for slip on faults misoriented with respect to the optimum angle for slip,  $\theta_0$ , given by the Coulomb criteria. They define an effective coefficient of friction as  $\mu_d^* = \mu_d(1 - P_f / \sigma_n)$ , where  $P_f$  is the pore pressure confined to the fault zone, and  $\sigma_n$  is the stress normal to the fault. The two-dimensional analysis applies to a pervasively fractured crust with heterogeneous fault strength, and the results show that 1) slip will be energetically favored on faults at  $45^\circ$  to  $50^\circ$  to the greatest principal stress if the coefficient of friction along these faults is just 20% to 25% lower than along faults at the optimum Coulomb angle ( $\theta_0 = 25^\circ$  to  $30^\circ$  for commonly accepted values of friction,  $\mu_d = 0.70 - 0.75$ , in the upper crust); 2) in the extreme case of vanishingly small frictional strength and low ambient shear stress, the  $45^\circ$  angle for optimum fault slip (parallel with the direction of maximum shear stress) is only weakly favored over a wide range of fault orientations on either side of  $45^\circ$ ; and 3) slip will be energetically feasible on strongly misoriented faults ( $\theta > 80^\circ$ ) with an intrinsic coefficient of friction of  $\mu_d \approx 0.7$  ( $\theta \approx 28^\circ$ ) if  $\mu_d^*(\theta) \leq 0.2$  along the misoriented fault. The latter implies a lower bound on the the fault-confined pore pressure of  $P_f \geq 0.8\sigma_n$ , where  $\sigma_n$  is the normal stress across the fault. This constraint has the form

$$\mu_d^* \leq \frac{r \sin 2\theta}{(1 - r \cos 2\theta)} \quad (1)$$

where  $r = \tau_m / \sigma_m$  is the stress ratio defining the threshold stress field for slip on optimally oriented faults ( $\theta_0$ ) with  $\tau_m$  and  $\sigma_m$  representing the maximum shear stress and mean stress, respectively (see Figure 1).

#### *Array Studies of Seismic Scattering (J.E. Vidale and H.M. Benz)*

See the separate summary by John E. Vidale and Harley M. Benz for project no. 9930-01496.

#### **Publications**

Hill, D.P., M.J.S. Johnston, J.O. Langbein, S.R. McNutt, C.D. Miller, C.E. Mortensen, A.M. Pitt, and S. Rojstaczer (1991): Response Plans for Volcanic Hazards in the Long Valley Caldera and Mono Craters Area, California: U.S. Geological Survey Open File Report 91-270, 64 p.

Hill, D.P., and W. Thatcher (in press), An energy constraint for frictional slip on misoriented faults: Bull. Seismol. Soc. America.

Olson, J.A. (in press), Filling in the gaps: the 1989 Loma Prieta, California earthquake: EOS, Transactions of the American Geophys. Union.

Thatcher, W., and D.P. Hill (1991), Fault orientation in extensional and conjugate strike-slip environments and their implications: Geology, v. 19, pp. 1116-1120.

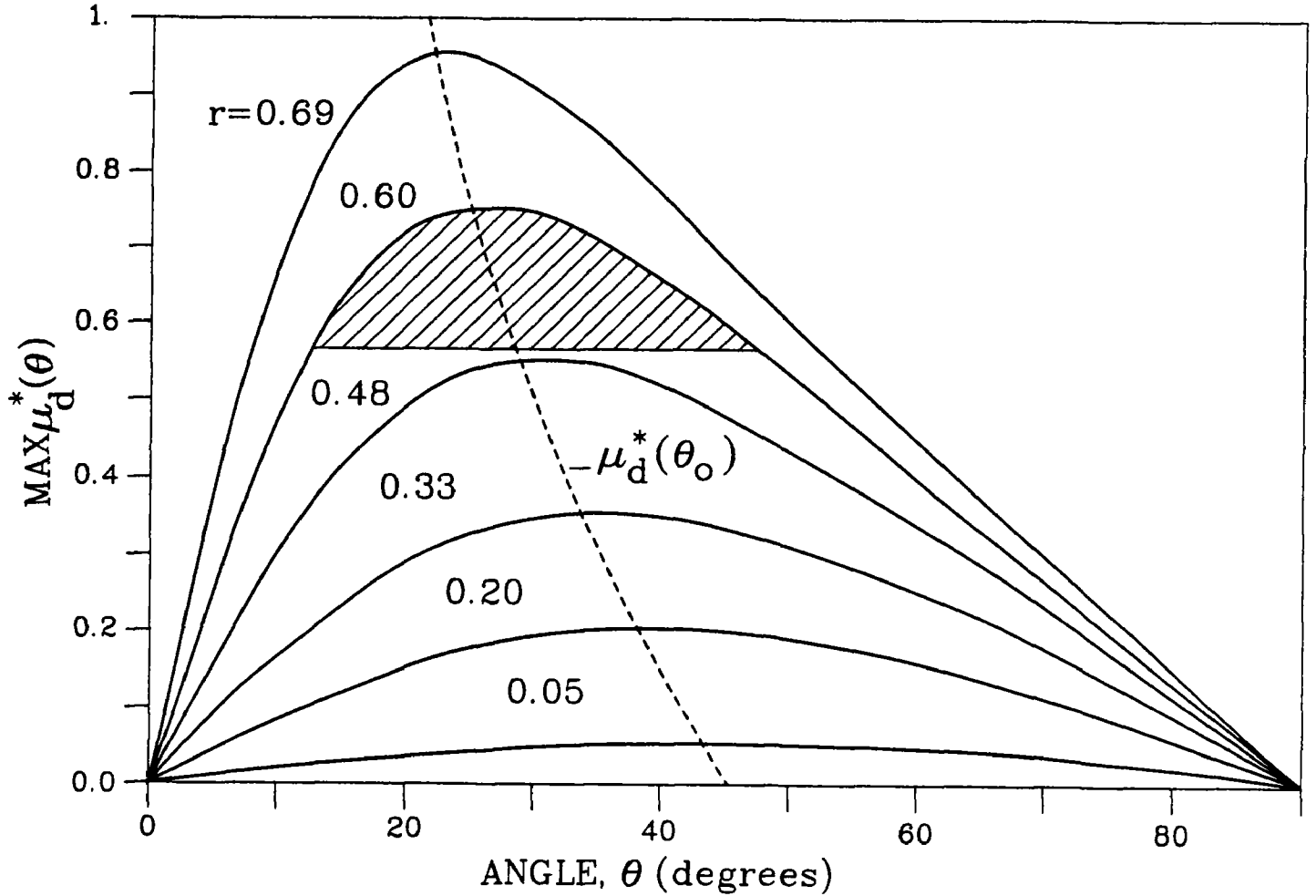


FIGURE 1. Curves from equation 1 defining the upper bound on the effective coefficient of friction,  $\mu_d^*(\theta)$ , as a function of the angle between the fault plane and the greatest principal stress direction,  $\theta$  with the stress ratio,  $r$  as a parameter. A given  $r$  corresponds to a stress field just meeting the Coulomb limit for slip on an optimally oriented, pre-existing fault along which the coefficient of friction is  $\mu_d^*(\theta_0)$ . Under this stress field, slip can occur on a misoriented fault ( $\theta$ ) if the coefficient of friction along that fault ( $\mu_d^*$ ) falls on or below the curve for  $r$  at  $\theta$ . Thus the peak for each curve corresponds to optimum Coulomb orientation,  $\theta_0$ , for the coefficient of friction  $\mu_d^*(\theta_0)$ , and the dashed line gives the locus for  $\mu_d^*(\theta_0)$ . The explicit relation between  $r$  and  $\mu_d^*(\theta_0)$ , or  $r = \mu_d^*(\theta_0) \sin 2\theta_0$ , reflects our assumption that the stress field is constant and its magnitude is limited by the strength of optimally oriented faults. The shaded area beneath the curve for  $r = 0.6$  ( $\mu_s^*(\theta_0) = 0.75$ ) illustrates the range of admissible fault orientations capable of slip for the case when the displacement-averaged dynamic coefficient of friction is limited to  $0.75 > \mu_d \geq 0.56$ .



## Systems Engineering

9920-01262

Gary Holcomb  
Branch of Global Seismology and Geomagnetism  
U.S. Geological Survey  
Albuquerque Seismological Laboratory  
Building 10002, Kirtland AFB-East  
Albuquerque, New Mexico 87115  
(505) 844-4637

### Investigations

Engineering development to improve the quality of seismic instrumentation.

### Results

Acceptance testing of the National Seismic Network (NSN) seismic sensors continued during this reporting period and will probably continue over the next several reporting periods. During this period, one borehole system was delivered and tested prior to shipment to Mexico.

Acceptance testing of the NSN 24-bit digitizers continued during this reporting period and will probably continue over the next several reporting periods. These digitizers are performing quite well and all results to date have been well within system specifications. Fifteen new systems were delivered during this period of which approximately 10 have been tested to date. Two errors were discovered in our testing operation and the test procedures are currently being modified to correct these errors.

Considerable effort was devoted to a demonstration of the capabilities of two competing digitizers for the new Global Telemetered Seismograph Network (GTSN) data acquisition system.

## Computer Support Project

9920-04559

Roger N. Hunter  
Branch of Global Seismology and Geomagnetism  
U.S. Geological Survey  
Denver Federal Center  
Box 25046, Mail Stop 967  
Denver, Colorado 80225  
(303) 236-1360

### Investigations

This project provides assistance to branch personnel in the area of IBM personal computers (hardware and software) and VAX programs. Primary focus has been on hardware procurement and graphics programs. The project also produces programs of its own as described below.

### Results

In the past year, this project has procured eight IBM PCs for the secretaries, analysts, and data entry clerks. These computers have been received and are operating correctly.

A Calera scanning system with Optical Character Recognition software was purchased and is operating. It is used to assist the data entry staff in producing ASCII text files from hard-copy originals such as telegrams and bulletins. In the past, this material was all typed in by hand. The scanner does it automatically and requires only error correction and reformatting to be used by the VAX.

Ethernet cards were procured for all branch PCs and are currently being installed. The net will link all PCs, Macintoshes, SUN workstations and VAX computers using the TCP/IP network protocol.

The Interactive Mapping Program (IMP) was completed and has been distributed worldwide. It is also being sold to the public. IMP will plot the user's data on a Mercator map with a wide range of options. Two or three world outline sets are available (depending on the version). IMP was intended as an adjunct to the EPIC CD-ROM and reads those output files by default.

Two holograms were started which will use computer-generated images to display seismic information. They will depict the seismicity in the San Francisco area. The first shows the Loma Prieta aftershock sequence and will be featured on the cover of the special edition of the Bulletin of the Seismological Society of America (BSSA) to be distributed in October 1991. The second will be a wider view of the San Francisco Bay area as seen from the northwest. These holograms are the second and third time that seismic information has been holographically displayed. (We also produced the first hologram representing seismic information.)

A PC-based Bulletin Board System (BBS) has been started which will serve as a focal point for seismic and geomagnetic information to the general public as well as participating scientists. It can be accessed by calling (303) 236-0848. We hope to add an 800 number in the future which will make the call less burdensome to the public. The BBS will be used to permit the public to access the Quick Epicenter Determination files and to leave messages to branch staff. Scientists can use it to leave seismic information or messages. The intent is to take some of the workload off of the VAX and to reduce the danger to the VAX from hackers.

In order to promote amateur seismology, we have added an area for such purposes in the BBS and have allowed Mr. Robert Samuelson of New Hope, Minnesota, to post his programs and files there. Mr. Samuelson has built his own seismometer and is recording digital waveforms on his PC. He has also written a program to display the waveforms which can then be enlarged or shifted as needed. While this may have no immediate usefulness to the branch, we feel that amateur interest in seismology should be encouraged.

# TECTONICS OF CENTRAL AND NORTHERN CALIFORNIA

9910-01290

William P. Irwin  
Branch of Engineering Seismology and Geology  
U.S. Geological Survey  
345 Middlefield Road, MS 977  
Menlo Park, California 94025  
415/329-5639 or FTS/329-5639

## Investigations

1. Preparing and revising manuscripts pertaining to the geology and tectonics of northern California and southwestern Oregon.
2. Studying distribution of oldland surfaces and glacial features for possible neotectonic information.
3. Field work to determine validity of questionable ages assigned to certain rocks of the Western Klamath terrane.

## Results

1. Much of the report period was spent preparing a description of the geology and tectonic development of the Klamath Mountains province for publication in the USGS Bulletin series. The report is designed to be supplemental to a geologic map of the Klamath Mountains, scale 1:500,000, which is now in press. In addition, an extensive revision of a preliminary geologic map of the Red Bluff 100,000 quadrangle was completed and the map resubmitted for further technical review. The preliminary version of the map, which earlier had been released as Open-File Map 84-105, covers the tectonically complex junction of the northern Coast Ranges, Great Valley, Klamath Mountains, and Cascade Ranges provinces. It is co-authored with M.C. Blake, Jr., D.S. Harwood, E.J. Helley, A.S. Jayko, and D.L. Jones, and is being prepared for publication in the USGS Miscellaneous Investigations Map series.
2. Remnants of oldland surfaces and glacial cirques in northwestern California, at the latitude of the Klamath Mountains, were plotted as an aid in studying their possible neotectonic significance. The oldland surfaces are most abundant in the Coast Ranges where many of them are elongate surfaces on northwest-trending ridges. Some of these are covered by Plio-Pleistocene gravels, and, further inland, a few are associated with small patches of shallow marine and nonmarine deposits of Miocene age. The surfaces generally are successively higher on parallel ridges to the northwest, nearer to the Klamath mountains, and attain altitudes of as

much as 1500 m. Within the Klamath Mountains the old high-level surfaces generally are not linear like those of the Coast Ranges and are restricted to the outer parts of the province. A few of these surfaces are associated with Miocene deposits, at altitudes of as much as 1200 m, but most do not have surficial deposits and are undated. The broad core area of the Klamath Mountains, which includes virtually all the high mountain ranges of the province, appears devoid of old high-level surfaces. The high mountain ranges have been glaciated as evidenced by the presence of cirques and other features along the ridge crests. The cirques in the southeastern part of the province are at a median altitude of about 2000 m, and in successive ranges to the northwest the median altitude gradually decreases to 1150 m at the northwestern edge of the province. Analysis of the neotectonic implications of these features has not been completed.

### Reports

Irwin, W.P., 1990, Geology and plate-tectonic development, in R.E. Wallace, ed., The San Andreas fault system: *U.S. Geological Survey Professional Paper 1515*, p. 60-80.

## SOUTH SAN FRANCISCO BAY AREA GEOPHYSICS

9380-03074

R. C. Jachens and Andrew Griscom  
Branch of Geophysics  
U.S. Geological Survey  
345 Middlefield Road, MS 989  
Menlo Park, California 94025  
(415) 329-5300

and R. G. Coleman  
Geology Department  
Stanford University  
Stanford, California 94305  
(415) 723-9205

### Investigations

The principal goal of this project is to construct a new, three-dimensional tectonic model of the south San Francisco Bay area based primarily on interpretations of magnetic and gravity field data supported by geologic, petrologic and other geophysical information. During FY91 the following investigations were conducted:

#### *1) Contracted for a New Detailed Aeromagnetic Survey*

In order to improve the resolution of magnetic data in the bay area, a new survey (fig. 1) was designed and bids were solicited from private contractors. This new survey complements a high-resolution aeromagnetic survey of a transect across the Coast Ranges from the Santa Cruz Mountains to the Great Valley. The former survey, completed in 1989 as part of the National Geologic Mapping Program, revealed spectacular details about the distribution of magnetic rocks in the subsurface beneath the southern San Francisco Bay area (fig. 2). Highly magnetic serpentinite bodies, which account for most of the magnetic anomalies northeast of the San Andreas fault, occupy many fault zones or are truncated by faults and thus serve as good indicators of both the locations and attitudes of faults that bound major crustal blocks. A regional compilation of lower-resolution aeromagnetic surveys north of the area shown in figure 2 (see item 2 below) indicates that other important faults (Hayward fault, northern Calaveras fault, Rogers Creek fault, etc.) also are delineated by aeromagnetic anomalies, but these surveys are too coarse to provide much information about the fault characteristics.

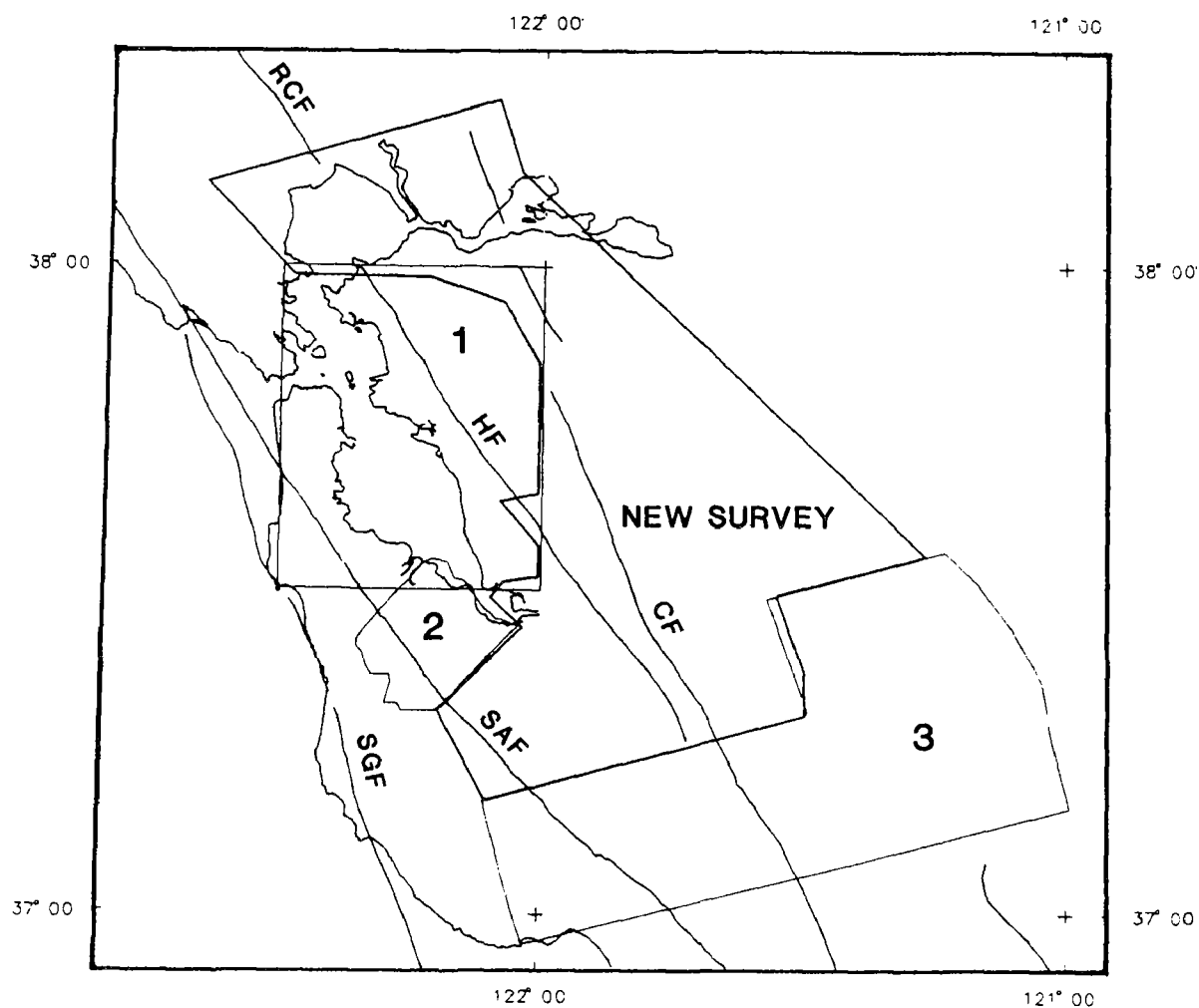


Figure 1. Index map of San Francisco Bay area and vicinity showing high-resolution aeromagnetic survey coverage. Existing surveys: 1--San Francisco; 2--Menlo Park/Palo Alto; 3--San Jose South. New Survey is being flown as of 11/91. Symbols: CF--Calaveras fault; HF--Hayward fault; RCF--Rogers Creek fault; SAF--San Andreas fault; SGF--San Gregorio fault.

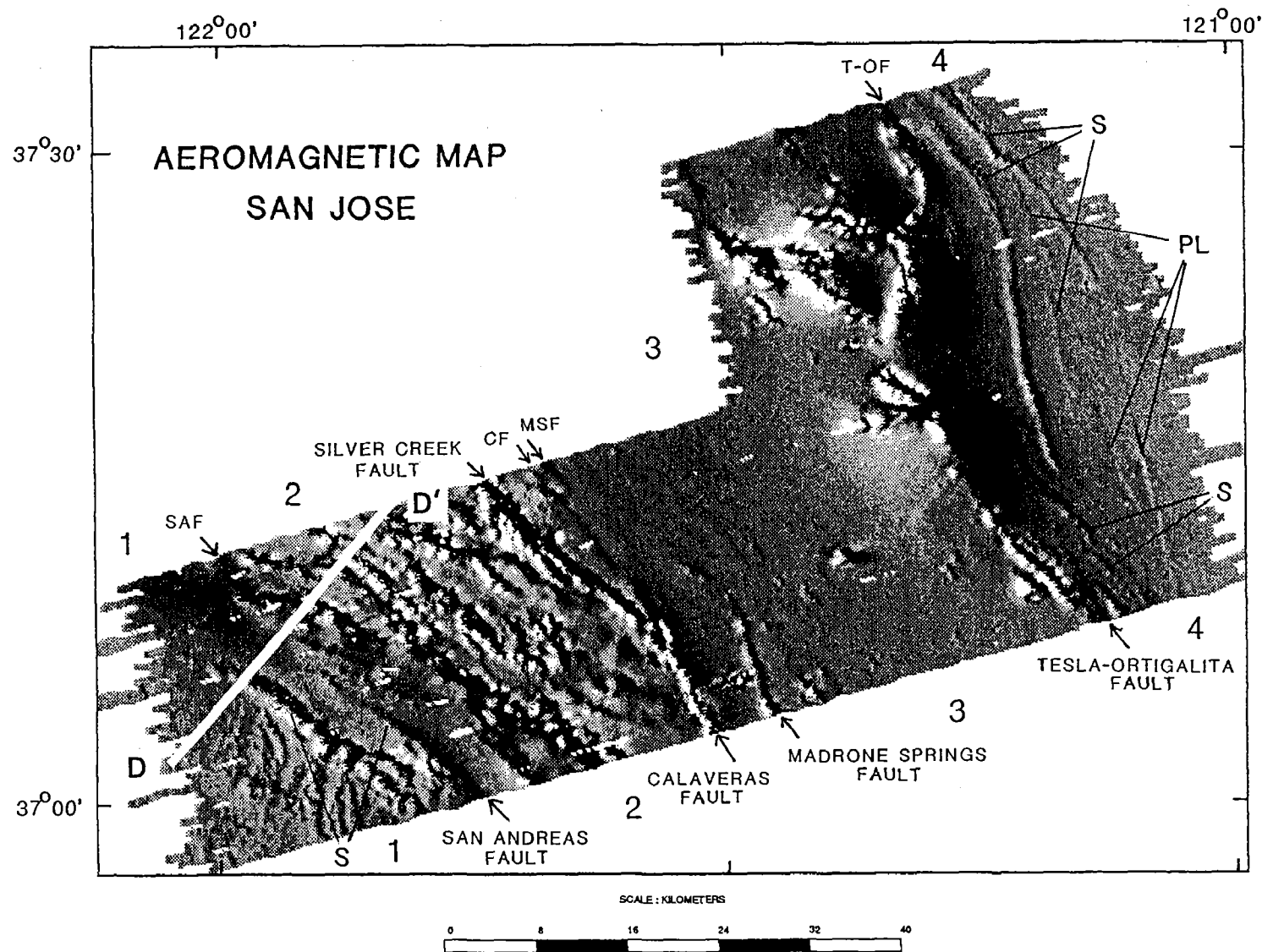


Figure 2. Shaded-relief map of the residual magnetic field along a transect of the California Coast Ranges south of San Jose, California. This presentation emphasizes short-wavelength anomalies. "Sun" azimuth--255°, height--20°. Symbols: "S" magnetic anomalies caused by sedimentary rocks; "PL" magnetic anomalies probably caused by cultural features such as powerlines and pipelines. Most of the unlabeled anomalies are caused by magnetic ophiolitic rocks and associated serpentinites. D-D' is location of modeled profile shown in figure 3.



## *2) Compiled and Composited Existing Regional Aeromagnetic Data*

Aeromagnetic coverage of the San Francisco Bay area and vicinity consists of a patchwork of small surveys flown at various flight heights and with different flight specifications. An effort was begun to construct a single aeromagnetic map suitable for defining the regional tectonic setting of the bay area by analytically continuing the individual surveys to a common height 300 m above the ground surface and then merging the individual surveys into one coherent map.

## *3) Collected and Compiled Gravity Data*

Gravity data were collected in order to fill gaps in the regional coverage and to provide detailed profiles across active faults. Updating of the regional gravity compilation covering the San Francisco Bay area and vicinity was begun.

## *4) Modeled Potential Field Data Along Profiles*

Gravity and magnetic data were modeled along profiles crossing major faults and structures in the bay area with the aim of eventually constructing a quantitative three-dimensional structural and tectonic model of the mid- to upper crust. Initial efforts focussed mainly in the Santa Cruz Mountains and adjacent Santa Clara Valley near the epicenter of the Loma Prieta earthquake; additional profiles crossing the Madrone Springs, Calaveras, and Silver Creek faults also were modeled.

## *5) Mapped Serpentinite Bodies in the South Bay Area*

Our mapping effort emphasizes establishing the structural configuration of serpentinite bodies related to present-day faults in the area. Petrological studies of the serpentine are used to establish its mantle protolith as well as to relate serpentinization to tectonic history. Physical and chemical properties of the serpentine are measured for later application to geophysical modeling.

## **Results**

1) A contract for the new aeromagnetic survey of the eastern bay area was awarded in September 1991, and flying began in late October, 1991. The new high-resolution survey (530 m linespacing, 300 m terrain clearance over populated areas and less over remote areas), when combined with adjoining high resolution surveys, will provide detailed aeromagnetic coverage of the bay area and vicinity from Santa Cruz on the south to San Pablo Bay on the north (fig. 1). The detailed coverage will extend far enough north to include the seismic reflection profile recently established through San Pablo Bay and up the Sacramento River toward Sacramento.

2) An "equivalent" 300 m draped aeromagnetic map was completed for most of the area between 36° 45' and 38° 30' N. and from the coastline to the foothills of the Sierra Nevada. Gaps exist where only widely spaced data are available. The map represents a composite of nine separate surveys.

The regional aeromagnetic map is dominated by anomalies from the ophiolite inferred to form the basement of the Great Valley, the Coast Range ophiolite, and various slivers of dismembered ophiolites embedded in the Franciscan terranes northeast of the San Andreas and Pilarcitos faults. The sources of large anomalies southwest of the San Andreas fault are mostly concealed but are inferred to be mafic plutonic bodies (possibly part of an ophiolite assemblage) similar to that exposed at Logan quarry west of Hollister. Smaller anomalies are associated with Cenozoic volcanic rocks exposed along the southern part of the Calaveras fault and in the Quien Sabe volcanic field and with isolated sedimentary units such as the Purisima Formation in the Santa Cruz Mountains and magnetic sandstone units within the Great Valley sequence. The major active faults of the San Andreas system (San Gregorio, San Andreas, Hayward, Rogers Creek, and Calaveras faults) impart a northwest to north-northwest grain to the magnetic map by truncating magnetic bodies and by enclosing highly magnetic serpentinite masses within their fault zones. The magnetic map also displays a strong, more westerly grain (N. 50°-60° W.) in the region between the San Andreas fault and the Calaveras-Hayward-Rogers Creek faults that probably reflects earlier faulting.

Comparison of the magnetic map with the distribution of epicenters in the bay area helps to explain some unusual patterns. Coherent patterns of epicenters that are not obviously associated with known faults or structures occur in the southern San Francisco Bay area near the junction of the San Andreas and Calaveras faults. Although not correlated with features in the exposed geology, the alignments do correspond with magnetic anomalies suggesting that concealed structures are influencing the release of seismic energy.

3) A new compilation of isostatic residual gravity for the bay area revealed critical gaps in the coverage over remote areas and near some of the major faults. About 130 new gravity stations were added to the data base, primarily along profiles crossing the San Andreas fault near Loma Prieta and the Calaveras-Madrone Springs faults near the southern Santa Clara Valley.

4) The main modeling effort during FY91 concentrated on interpreting magnetic data along profiles through the Santa Cruz Mountains and adjacent Santa Clara Valley, in preparation for a paper on the regional structure and tectonic setting of the Loma Prieta earthquake. Profile D-D' (fig. 2), for example, uses data taken from the 1989 high-resolution aeromagnetic survey; it strikes approximately northeast across the Zayante, Aldercroft, Berrocal, and Shannon faults. Magnetic anomalies

along this profile (fig. 3) are caused by deep gabbro(?) basement southwest of the San Andreas fault, by an ophiolite on the immediate northeast side of the San Andreas fault, and by other serpentinite masses farther to the northeast along the profile. A syncline of Purisima Formation, a Pliocene sandstone, produces an anomaly of about 100 nT near the Zayante fault. Of considerable importance are the low dips calculated for the Aldercroft (55°) and Berrocal (35°) faults. Similar models along strike yield similar low southwest dips for this set of faults that bound the east side of a 50-km long block of rocks adjacent to the San Andreas fault, and approximately centered on the latitude of the mainshock of the Loma Prieta earthquake. This set of thrust faults may be associated with many of the relatively shallow aftershocks that are located northeast of the San Andreas fault.

5) The serpentines are derived mainly from harzburgites and dunites related to the Great Valley Ophiolite of Upper Jurassic age, and contain relict textures indicating derivation from depleted oceanic mantle. Serpentinization was initiated in an oceanic environment but was completed during tectonic movements after accretion to the continent. Current modeling of aeromagnetic profiles combined with structural studies shows that the serpentines of Yerba Buena Hill, Santa Clara County, are probably thin sheets no more than 500-1000 m thick. Overthrusting of these serpentine sheets upon Santa Clara gravels of Pliocene-Pleistocene age can be seen on the west side; on the east side they are offset by strike-slip faulting along the Silver Creek fault.

### Reports

- Coleman, R.G., 1991, Serpentines of Santa Clara Valley (abs.): Geological Society of America Abstracts with Programs, v. 23, p. 17.
- Coleman, R.G., and Jove, Carlos, 1991, Geological origin of serpentines: Proceedings of the Serpentine Ecology Conference, June 1991, University of California, Davis (In press).
- Griscom, Andrew, and Jachens, R.C., 1991, Tectonic transect of the California Coast Ranges based on a new magnetic map (abs.): Geological Society of America Abstracts with Programs, v. 23, p. 31.

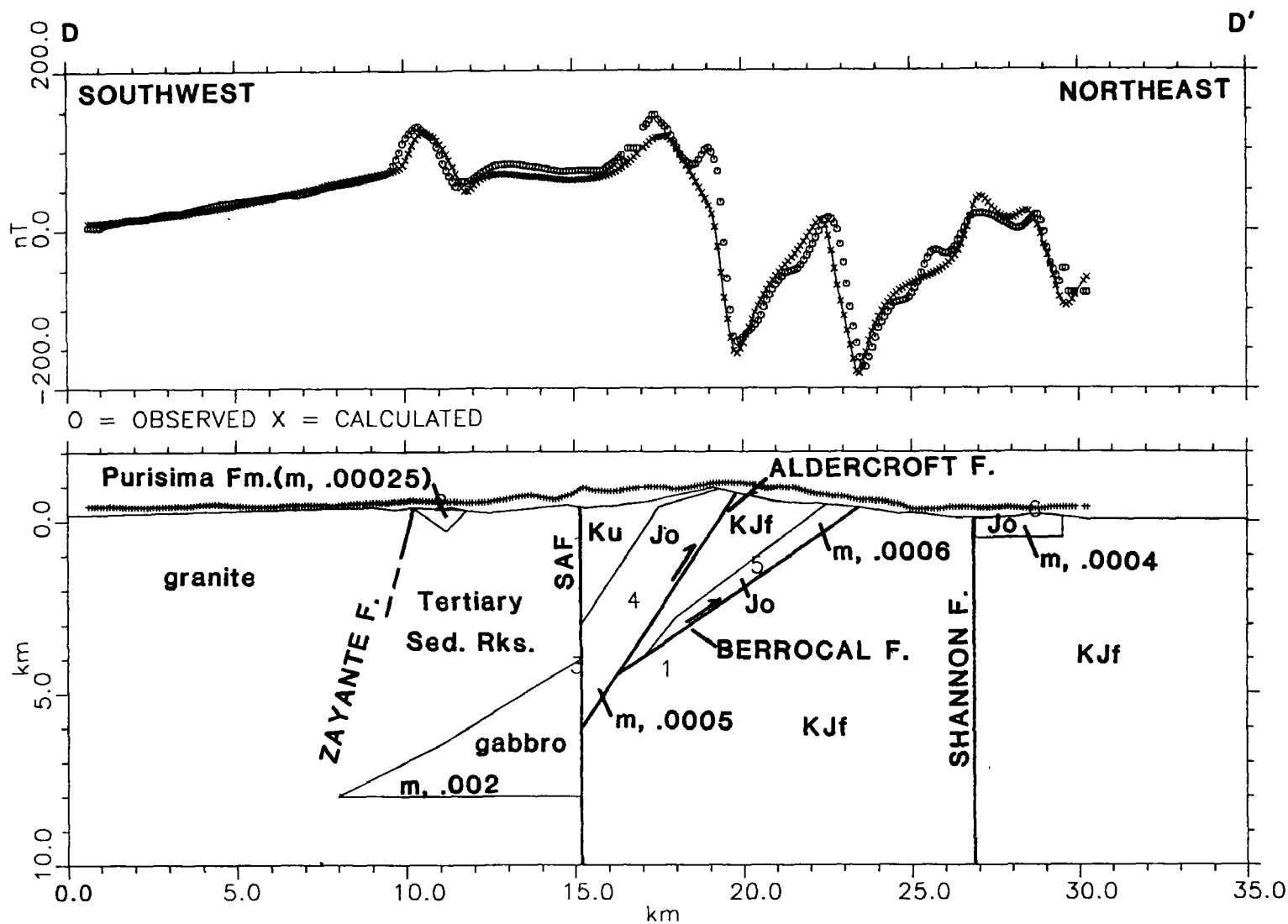


Figure 3. Magnetic model for profile D-D' across the San Andreas fault. Rock units: Jo--Jurassic ophiolite, mostly serpentinite; KJf--Franciscan complex; Ku--Great Valley assemblage, includes some Tertiary sedimentary rocks. Magnetization (m) of rock units in  $\text{emu}/\text{cm}^3$ .

**Absolute Dating of Prehistoric Earthquakes  
by Tree-Ring Analysis in California**  
EAR90-04350 (jointly with NSF)

Gordon C. Jacoby and Brendan Buckley  
Tree-Ring Laboratory  
Lamont-Doherty Geol. Obs.  
Palisades, New York 10964  
(914) 359 2900

**Introduction:**

We have definitively found evidence of 1906 earthquake disturbance in coast redwood trees at two locations in northern California and there is evidence of disturbance by the 1906 earthquake in a Douglas fir centrally located in our study area. We have also found evidence of movement by the 1906 and more than one previous event on an offset creek near the central part of our primary study area. Sections from stumps near the offset creek show disturbance in the ring sequences other than fire-related damage. We were better able to identify the fault trace in part of the field area because of some recent logging and obtained more samples from along the fault than on earlier collections. We have crossdated root portions from five different trees submerged at Mad River Slough near the Mendocino Triple Junction at the southern end of the Cascadia Subduction zone. Although it took a few years for all of the trees to completely die, the situation indicates that one event, probably a submergence, caused the death of all trees and root systems. Radiocarbon dates place the death of the trees in the same range as other submergence dates to the north in Washington produced by Atwater, Stuiver and Yamaguchi.

**San Andreas Fault (north of San Francisco)**

Previously we collected and processed sections and tree-core samples inland from the general area of the fault and from the fault zone itself in order to develop a regional chronology for crossdating disturbed trees and to date times of disturbance respectively. Due to lack of funding there was no progress made in calendar 1990. With the renewal support we were able to continue the research. Although we had made considerable progress with the earlier samples, it was necessary to obtain more for a control/dating chronology near the study area and for more fault-zone samples. Due to the recent logging in one area we were better able to discern the fault zone, sag ponds, in echelon declivities, and to get samples from trees at strategic locations where fault rupture was likely to have disturbed

the trees. At the offset creek we mapped the drainage displacement and collected several more sections from strategically placed stumps. The drainage was offset approximately three times the estimated displacement for this area due to the 1906 earthquake. Several stumps were at the edge of the offset or within a graben-like zone extending from the ends of the offset along the fault trace. These were sampled and are being processed. First appraisal reveals substantial disturbances in the tree rings but, partly for that reason, the dating will be difficult. These are the most promising specimens we have obtained thus far. We discovered some abandoned logs on a hillside a few miles away and these are very promising for adding to and extending the regional or control chronology.

To study analogs for and dating of known response of coastal redwoods to earthquakes we obtained core samples from Plantation near the study area, from along the San Andreas fault near Watsonville and from Grizzly Flats, a USGS trenching site also in the Watsonville region. There are clear effects of the 1906 event at the Plantation and the Watsonville sites. The only core from a tree of considerable age on the fault at Grizzly Flat shows a clear response to trauma by greatly decreased growth but we do not have sufficient samples from this site to date the event. These analogs help define the type of signal that occurs in the coast redwood tree-ring record in response to earthquakes.

### Cascadia Subduction Zone

Upon obtaining much better samples from the Mad River Slough locality through the cooperation of B. Atwater and G. Carver, we were able to definitively crossdate the root segments (The trees and stumps are decayed away.) of five trees. The tree deaths took place over a period of possibly as long as four growing seasons. Even within one root segment there can be more than a year's difference in last cells formed at different points around the circumference. This is because portions of partially drowned trees can survive different lengths of time. Trees, with no central nervous system, can sustain partial life and cambial-cell division can continue if there is any carbohydrate and growth hormone reaching the cell division site. Limited subsidence in an intertidal zone places a complex and variable stress on trees. The roots may be partially aerated during low tides and if they are near a freshwater channel the salt effects may be minimized and the trees may even survive the subsidence with limited damage. This phenomena of varying degrees of damage within closely-spaced trees was observed at Cook Inlet, Alaska. The few years for death to occur in the cambial layers of all the roots

dated at Mad River Slough lead us to infer that a single event could have caused the eventual death of all five trees. We are working on a long chronology from living Sitka spruce near Mad River Slough and finalizing the root chronology in an effort to absolutely date the outer rings of the roots. High-precision radiocarbon dates for wood from the Mad River root sections are in process. Previous radiocarbon dating places the roots within the age of our adjacent chronology. These results will be related to the ongoing work of Atwater and Yamaguchi in Washington.

### Acknowledgements

The investigator was guided to the Watsonville sites by D. Schwartz of the USGS in Menlo Park. C. Prentice, also from Menlo Park, has visited the field area near Gualala and suggested other sampling sites in the vicinity. The Mad River Slough study has benefitted from discussions with B. Atwater of the USGS in Washington and he has aided in arranging for high-precision radiocarbon processing. The investigator also visited Cook Inlet, Alaska and discussed the effects of subsidence on trees there with B. Atwater and D. Yamaguchi of Univ. of Colorado. G. Carver of Humboldt State Univ. has also been a major participant in the Mad River Slough study.

## Instrument Development and Quality Control

9930-01726

E. Gray Jensen  
Branch of Seismology  
U.S. Geological Survey  
345 Middlefield Road - Mail Stop 977  
Menlo Park, California 94025  
(415) 329-4729

### Investigations

This project supports other projects in the Office of Earthquakes, Volcanoes and Engineering by designing and developing new instrumentation and by evaluating and improving existing equipment in order to maintain high quality in the data acquired by the Office. Tasks undertaken during this period include development of a digital seismic telemetry field station, construction of new master clocks and writing software for Seismic Group Recorders (SGR) and the new Real Time Processor (RTP) of the CALNET, among other things.

### Results

A production prototype of digital seismic telemetry (DST) field station was built and field tested. The field station amplifies and filters three seismic channels and then digitizes them with a 16-bit analog-to-digital converter. The samples are transmitted serially at 9600 baud in real-time. The unit was tested using two transmission methods. The first used a special, commercially built radio transmitter and receiver capable of sending 9600 baud data. The other method tested used the FAX modem built into the field station transmitting via a microwave channel. Both methods were successful in sending noise free data. These tests demonstrated the soundness of the overall field station design and of data transmission by FAX modem. This now gives us the ability to deploy digital stations using our conventional microwave and VHF radio links for telemetry. Twenty production model field stations are now being constructed. Successful tests were also been performed on a sixteen station serial data receiver board which will funnel the data received at a central site to a PC.

Four of the new precision electronic clocks, Master Clock III, were built and put into service. Their operation in the field has been quite successful. A new version of the program which runs on a laptop computer and is used by field operators to program SGR's was written. The new version is much simpler to use and speeds up the SGR programming operation.

PC-AT software was written which reads seismic data from a Tustin A/D converter and time information from a parallel interface and sends the data to transputers in another PC over a high speed serial link. This is seismic data acquisition part of the new RTP system Rex Allen has been developing. Once this software was put into operation, problems were discovered in the transputer code. Unfortunately, Rex Allen retired at the end of September. Fred Fischer will be taking up the challenge of making the new RTP operational.



# Temporal Correlation Between Coda $Q^{-1}$ and b-Value in Northern California

Grant No. 14-08-0001-G1966

Anshu Jin and Keiiti Aki  
Department of Geological Sciences, USC  
Los Angeles, CA 90089-0740  
(213) 740-8255

## Abstract

From the analysis of local earthquake coda waves recorded by Wood-Anderson (1940-1947) and Benioff (after 1947) short-period vertical seismographs at station Mt. Hamilton, California, we found a large and systematic temporal variation in coda  $Q^{-1}$  in northern California during the 50-year period from 1940-1990.

Maximum likelihood estimates of b-value are determined for earthquakes with magnitude  $M \geq 3.0$ ,  $M \geq 3.5$ , and  $3.0 \leq M \leq 4.0$  and occurred in the area within 120 km around Mt. Hamilton (corresponding to the area where coda  $Q^{-1}$  is determined). Comparison of coda  $Q^{-1}$  and b-value led to a result that coda  $Q^{-1}$  correlates NEGATIVELY with b-value, determined from earthquakes with magnitude  $3.0 \leq M \leq 4.0$ , with the correlation coefficient of 0.76. The significance of correlation cannot be rejected at the confidence level of 0.966. There is no significant correlation between coda  $Q^{-1}$  and b-value determined using earthquakes  $M \geq 3.0$  and  $M \geq 3.5$ . These observations can be explained by the creep model proposed by Jin and Aki (1989) provided that the characteristic crack size of northern California corresponds to earthquake magnitude of 4.0 which is larger than that of southern California ( $\sim 3.0$ ). Further studies on earthquake scaling are needed to confirm the existence and scale length of such a characteristic size in northern California.

## Data.

About 650 earthquakes with magnitude 2.5-3.2 occurred during 1940-1990 within 60 km from MHC are selected for coda analysis. Their epicenters are shown in Fig. 1 by small solid circles. Solid triangles in Fig. 1 represent the seismic stations operating by U.C. Berkeley.

Wood-Anderson ( $T_0=1.0s$ ) seismograms (1940-1947) and Benioff ( $T_0=1.0s$ ,  $T_g=0.2s$ ) seismograms (after 1947) at Mt. Hamilton (MHC in Fig. 1) are used for coda analysis. A comparison between the results obtained using Wood-Anderson and Benioff seismograms for 20 earthquakes showed that the difference between  $\bar{\beta}_0$  values determined from two different seismograms is negligibly small compared to the magnitude of the variation in  $\bar{\beta}_0$ .

The larger circle in Fig. 1 indicates the area sampled by coda waves (as singly-scattered S waves) in this study. The b-value was also estimated from earthquakes within the larger circle.

## Method.

For a seismogram of a local earthquake recorded by a seismograph with relatively narrow frequency response (such as Wood-Anderson and Benioff short-period seismograph), the coda amplitude at lapse time  $t$ ,  $A(t)$  can be expressed as

$$A(t) = A_r \left(\frac{t}{t_r}\right)^{-\alpha} \exp[-\beta(t-t_r)]$$

where  $t_r$  is a reference time selected to be at least twice the arrival time of direct S wave and  $A_r$  is peak-to-peak amplitude at  $t_r$ .  $\alpha$  is the geometrical spreading factor and  $\beta$  is related to  $Q^{-1}$  by the relation of  $\beta = \pi f Q^{-1}$ .

For each seismogram, we select the portion of coda waves from twice the S-wave travel time to about 80s, which corresponds to the farthest scatterers located at about 120 km from the station assuming that coda waves are S to S back scattered waves. We then choose about 10 wave groups with duration  $T$  of 3-4s. distributed at equal interval over the selected portion of the seismogram. For each wave group, we measure the peak-to-peak amplitudes and compute the average within the duration  $T$  as  $A(t)$ , where  $t$  is the midpoint of the arrival time of the wave group measured from the earthquake origin time. The average frequency  $f = N/2T$ , where  $N$  is the number of extrema in the time interval  $T$ .

#### Correlation between $\bar{\beta}_0$ and b-value.

We calculated means of  $\alpha_0$  and  $\beta_0$  (designated as  $\bar{\alpha}_0$  and  $\bar{\beta}_0$ , respectively) over 11 consecutive earthquakes with 5 overlapped by neighboring points and estimated the standard error of the mean.

Figure 2 gives  $\bar{\alpha}_0$  and  $\bar{\beta}_0$  plotted against the midpoint of the occurrence times of the earthquakes used for their evaluation. The average predominant frequency and the time window are shown at the right top corner of Figure 2. The corresponding  $Q^{-1}$  are calculated by  $\beta = \pi f Q^{-1}$ .

A continuous catalog of earthquakes in northern California since 1910 is available at U.C. Berkeley. The detection was considered to be complete for  $M \geq 3.0$ , except the early year (1910-1940) and during intense aftershock sequences and swarms while a few small earthquakes were missed (Bolt and Miller, 1975).

We selected earthquakes located within 120 km from MHC, and executed aftershocks which occurred within 1 year from a main shock. The b-value was then calculated by the use of the Utsu-Aki formula:

$$b = \frac{\log_{10} e}{(\bar{M} - M_0)}$$

where  $\bar{M}$  is the average magnitude of a group of earthquakes with  $M \geq M_0$ . We estimated  $b$  for (a)  $M_0 = 3.0$ ; (2)  $M_0 = 3.5$ ; and (3)  $M_0 = 3.0$  and clipped the earthquakes with magnitude larger than 4.0. For case (1),  $\bar{M}$  is the average magnitude over 100 consecutive earthquakes with 50 overlapped by neighbors; for case (2),  $\bar{M}$  is that over 60 consecutive earthquakes with 30 overlapped by neighbors; and for case (3),  $\bar{M}$  is that over 80 consecutive earthquakes with 40 overlapped by neighbors. Figure 3 gives the b-value versus midtime for above three cases.

After finding the values of time series at equal intervals for both b-value and coda  $Q^{-1}$  using the 3-point Lagrangian interpolation, we calculated the temporal correlation coefficients between the coda  $Q^{-1}$  and b-value with no time lag. We found that  $\bar{\beta}_0$

correlates **negatively** with **b**-value, for case (3) with the correlation coefficient of 0.76. The significance of correlation cannot be rejected at the probability of 96.6%. There is no significant correlation between  $\bar{\beta}_0$  and **b** determined for  $M \geq 3.0$  nor  $M \geq 3.5$ .

As shown in Figure 4 cross-correlation function with time lag between **b** determined for  $3.0 \leq M \leq 4.0$  and  $\bar{\beta}_0$  demonstrates that the strongest correlation occurs at zero time lag. Figure 5 gives the relation between  $\bar{\beta}_0$  and **b** determined for  $3.0 \leq M \leq 4.0$ .

#### Creep Model.

Jin and Aki (1989) proposed the creep model as shown schematically in Figure 6. They assume that aseismic creep activities tend to increase the crack density and coda  $Q^{-1}$  in a seismic region. If the creep fracture occurs with a certain predominant crack size, the spatial stress concentration may enhance seismicity only for earthquakes with the size comparable to the crack size. If this characteristic magnitude  $M_c$  is in the lower part of the magnitude range for which the **b**-value is estimated, the enhanced seismicity at  $M_c$  will show the increase in **b**. On the other hand, if  $M_c$  is in the upper part of the magnitude range, it will decrease **b**. In the case of southern California, the critical magnitude,  $M_c$ , is about 3. In fact, the scale length corresponding to the so-called source  $f_{\max}$  of large earthquakes, the constant corner frequency for small earthquakes, and the minimum magnitude (Aki, 1987) suggest that the characteristic magnitude for southern California is about 3. The result here provides that the characteristic crack size of northern California may be  $M=4.0$ . Further studies on earthquake scaling law are needed to confirm the existence and scale length of such a characteristic size in northern California.

#### References.

- Aki, K., Magnitude-frequency relation for small earthquakes: A clue to the origin of  $f_{\max}$  of large earthquakes, J. Geophys. Res., 92, 1349-1353, 1987.
- Bolt, A. B., and R. D. Miller, Catalogue of earthquakes in northern California and adjoining areas, 1 Jan., 1910-31 Dec., 1972, Seismographic Stations, U.C. Berkeley, 1975.
- Jin, A., and K. Aki, Spatial and temporal correlation between coda  $Q^{-1}$  and seismicity and its physical mechanism, J. Geophys. Res., 94, 14041-14059, 1989.

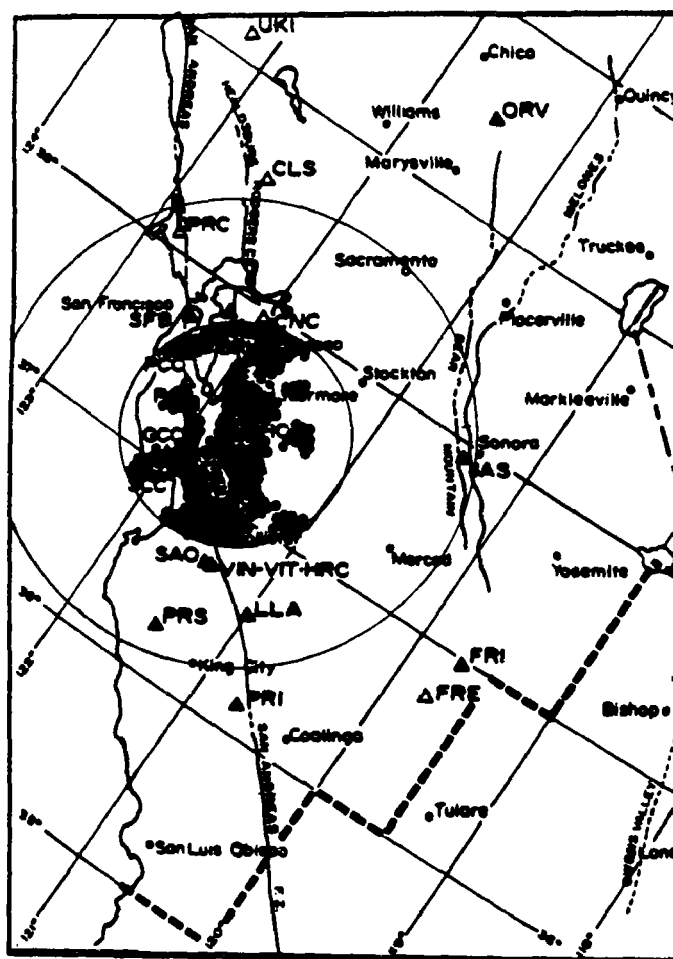


Figure 1

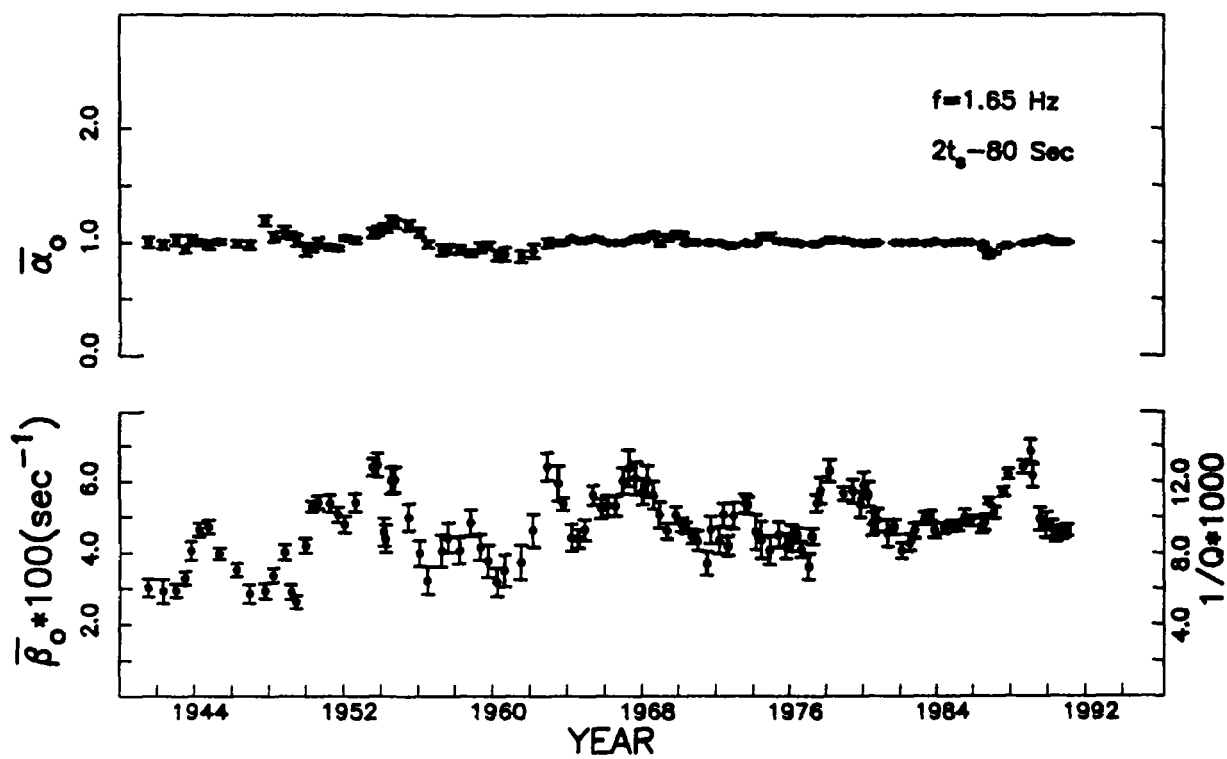


Figure 2

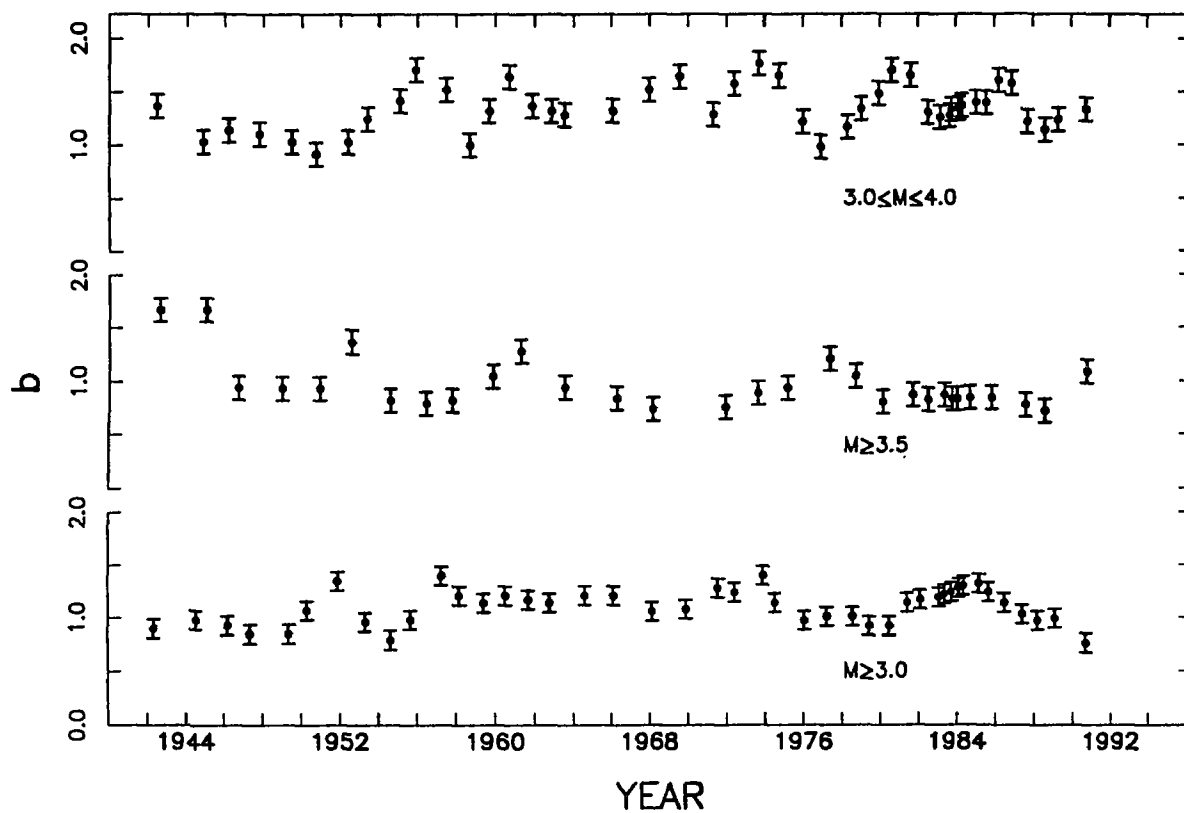


Figure 3

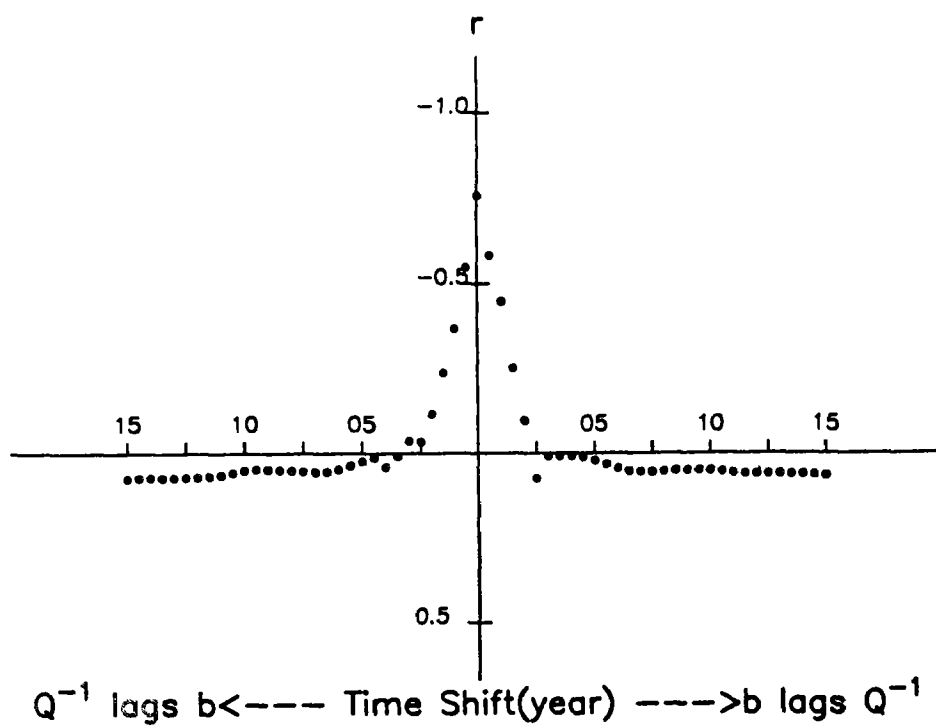


Figure 4

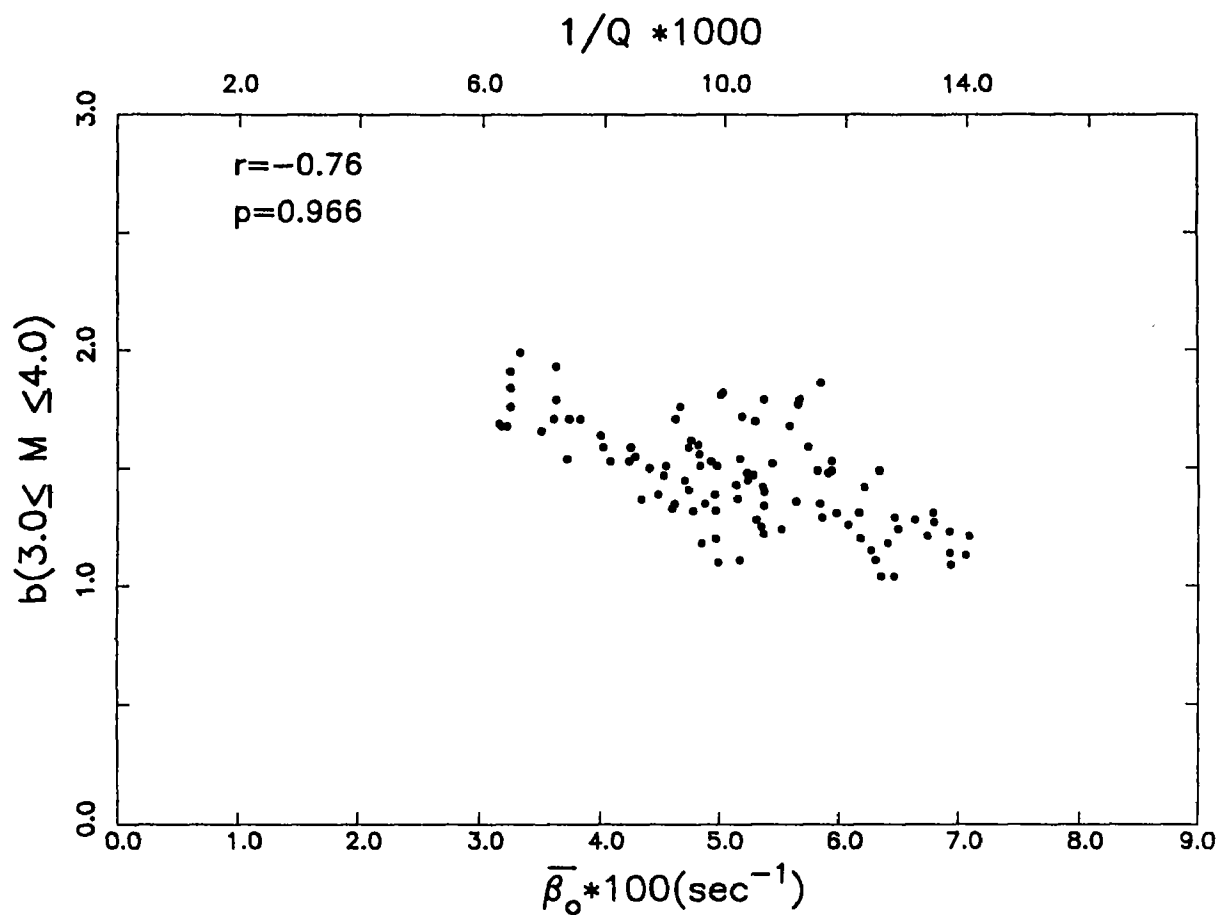


Figure 5

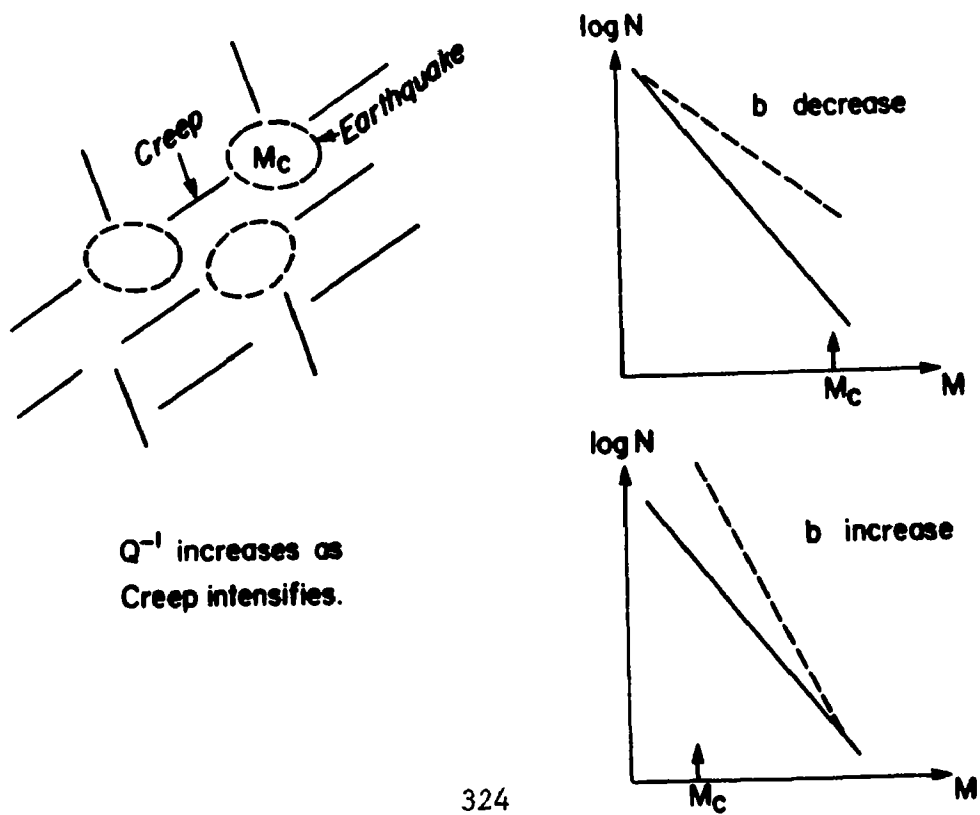


Figure 6

**Monitoring the Southern San Andreas Fault —  
A Monument Anchoring Experiment**

14-08-0001-G1786

Hadley O. Johnson, Frank K. Wyatt,  
and Duncan Carr Agnew  
Institute of Geophysics and Planetary Physics  
University of California, San Diego  
9500 Gillman Drive  
La Jolla, California 92093-0225  
(619) 534-2019

This grant supports the operation of a fiber-optic anchoring experiment on the Coachella segment of the San Andreas Fault—specifically, on the western flank of Durmid Hill, near the termination of the San Andreas Fault and its junction with the Brawley Seismic Zone. The experiment involves measuring the differential vertical motion of four points in the ground from depths of 1.65 m to 48 m. The goal of this project is to measure and understand the stability of the near-surface material in the region to determine if it is stable enough to support precise measurements of strain and tilt. Efforts at Piñon Flat Observatory (PFO) have shown that, in the period range of months to minutes, observatory-based instruments can resolve signals up to one thousand times smaller than geodetic surveying techniques can; and that, if such instruments are adequately anchored to depth, they can also accurately record the secular accumulation of deformation. The goal of this project is to determine how (if at all) such anchoring can be done in the soft sedimentary material of the Coachella Valley. This area, along the eastern shore of the Salton Sea has been identified as one of the more likely initiation points for a great earthquake during our lifetime.

Construction at the field site MEK<sup>1</sup> began in September, 1990, after preparation of the optical-fiber sensors in our lab, and after the hot summer weather of the Imperial/Coachella Valley. By using lengths of optical fiber for the interferometric path-length measurement, as opposed to tensioned wires or laser interferometry in evacuated pipes, it is possible to make many differential measurements in the same borehole rather easily, with high precision and low cost. The installation went fairly well considering the novelty to us of drilling in such gooey material (i.e., we were lucky), and data recording began on December 13. Tables 1 and 2 list the measurements being made, and specifies the sensitivity of the various channels.

We have already found several results from these measurements. The most important fact for us is that the sum of the three short-interval fiber measurements (SHAL, MIDL, and DEEP) generally track the single fiber measurement over the whole interval (LONG) quite well: this consistency shows that all the sensors are operating as planned. We can also see signals of some geophysical import on several of the fibers, most clearly on the longest one: vertical strain changes caused by air-pressure loading and the solid-earth tides. We have determined the response to these using the pressure record at the site and the nearest earth-tide strain records we have (at PFO, 65 km away), with results given in Table 3. Results from vertical anchoring at PFO are also included for comparison.

---

<sup>1</sup> The site was identified MEK after Merlin E. Kesel, on whose property it is located, and whose family has been extremely helpful in maintaining the site.

Table 1  
MEK Displacement/Fiber Sensors

Name	Fiber Depths (m)		Length (m)	Sensitivity <sup>†</sup> (per count)
	Shall*	Deep*		
MEK LVDT <sup>#</sup>	1.65	5.11	3.46	720 nE <sup>1</sup>
MEK SHAL	5.11	7.90	2.79	-24.4 nE <sup>2</sup>
MEK MIDL	7.90	22.90	15.00	-4.55 nE <sup>2</sup>
MEK DEEP	22.90	47.82	24.92	-2.74 nE <sup>2</sup>
MEK LONG	5.11	47.82	42.71	-1.60 nE <sup>2</sup>

\* – Fiber depth refers to depths below the nominal ground surface for shallow and deep arms of each Michelson interferometer.

† – Sensitivity given in strain.

# – Invar-rod measurement.

1 – For displacement, the sensitivity is: count = 208 nm

2 – For displacement, the sensitivity is: count = -68.2 nm

Table 2  
MEK Temperature and Pressure Sensors

Name	Depth (m)*		Sensitivity (per count)
	BVF	ABS	
MEK AIR	--	--	0.02 °C <sup>1</sup>
MEK INST	--	--	0.02 °C <sup>1</sup>
MEK 1M	1.02	2.67	0.02 °C <sup>1</sup>
MEK 3M	3.00	4.65	0.02 °C <sup>1</sup>
MEK 9M	8.99	10.64	0.244 m°C
MEK 20M	19.91	21.56	0.244 m°C
MEK BARO	--	--	8.27 Pa

\* – BVF: distance Below Vault Floor;

ABS: absolute depth from the ground surface.

1 – Complete equation is  $T = 0.02^{\circ}\text{C}/\text{count} + 20^{\circ}\text{C}$ .

Table 3  
Estimates of Ground Elastic Moduli

Where/What	$-\epsilon_z/\epsilon_A$	$\nu$	$-D_z/P$	$-P/\epsilon_z$	$E$
MEK	0.61	0.38	--	--	
APR @day	--	--	8.8 nm/Pa	4.9 GPa	1.6 GPa
APR @week	--	--	7.1 nm/Pa	6.0 GPa	2.0 GPa
Nominal Rock	0.333	0.25	--	--	15. GPa
PFO	0.10	0.09	--	--	2.3 GPa
APR @day	--	--	2.8 nm/Pa	8.6 GPa	7.5 GPa
APR @week	--	--	1.6 nm/Pa	15. GPa	13. GPa

APR – Air Pressure Response estimates at different periods.

$\epsilon_z$  – Obs. vertical strain;  $\epsilon_A$  – Obs. areal strain (but at PFO, not MEK);

$\nu$  – Estimated Poisson's ratio.  $D_z$  – Obs. vertical displacement;  $P$  – Obs. air pressure;

$E$  – Estimated Young's modulus from air pressure and from rainfall loading.

As the table shows, we estimate -6.0 GPa for the long-period ratio of air-pressure to strain over the 43-m long depth interval, which amounts to only 40% of the modulus seen for the granitic materials at our base site PFO.<sup>2</sup> The apparently exaggerated response of the ground at MEK to (estimated) areal earth-tides gives a Poisson's ratio for the "rock" at MEK of 0.38—quite high, leaning toward fluid-like behavior. We can combine these results to obtain Young's modulus, which we find to be one-seventh of that deduced for PFO. This result matches the relative weakness of the material at MEK. Once the air pressure signal is removed from the fiber signals, the residual strain from all four depth intervals is quite smooth.

All measurements remained stable—varying less than 250  $\mu\text{m}$ —throughout the spring of 1991, but began to show increasingly large displacements beginning in early August (though the scale of Figure 1 makes it hard to see, the SHAL sensor began to drift rapidly by day 1991:217). In searching for a possible source of these signals, we became aware that Mr. Kesel had been heavily drip-irrigating a row of palm trees about 10 meters north of our site.

<sup>2</sup> Air pressure loading of the ground depends on its permeability, and so is frequency dependent; all estimates give an upper bound on the ground's true modulus. At higher frequencies, yet another measurable load (though just barely) is provided by the trains on the nearby track, another indication of the sensitivity of measurement.



This had been done up until 1991:226 when the water was turned off because the “ground had become saturated.”<sup>3</sup> The water was turned on again on 1991:236, until, at our request, the irrigation was turned off a second time on day 1991:247. (Mr. Kesel has expressed his willingness to leave it off for the indefinite future.) Figure 1 shows the dramatic response of the ground at the site. Note that all the data shown are interval measurements; these show that the interval between 5 and 8 m lengthened by a total of ~4.5 mm in two episodes, correlated with, but lagging the application of water at the ground surface. The top interval also changed its length, but by a much smaller amount and in the opposite sense; the signal is also visible on the Middle interval (though only barely at the resolution of Figure 1). We suspect that the reason for this behavior is that the orientation and dip of the local strata are such as to conduct water from the palm orchard to a depth of 5–6 m at the location of our measurements.

Two aspects of this incidental signal deserve comment. One is that it is very large compared to the resolution of the techniques we are using (something interferometers handle particularly well), yet barely above the noise level of even the most precise geodetic techniques. This leads us to wonder how many other apparent tectonic signals have been caused by this kind of local motion. The second point is that the source of the signal is deep: a geodetic marker anchored to a few meters would usually be thought to be immune to this kind of problem, but this clearly would not have been the case here. Prolonged rainstorms should be expected to lead to large monument motions in this area.

---

<sup>3</sup> Saturating the ground there is not that hard to do, the clayey material in this section of the Coachella Valley is generally impervious to water; plants tend to grow only where the soil has been cultivated to accept moisture, such has been done around the base of the palm trees.

# Vertical Ground Motions: Durmid Hill Test Site

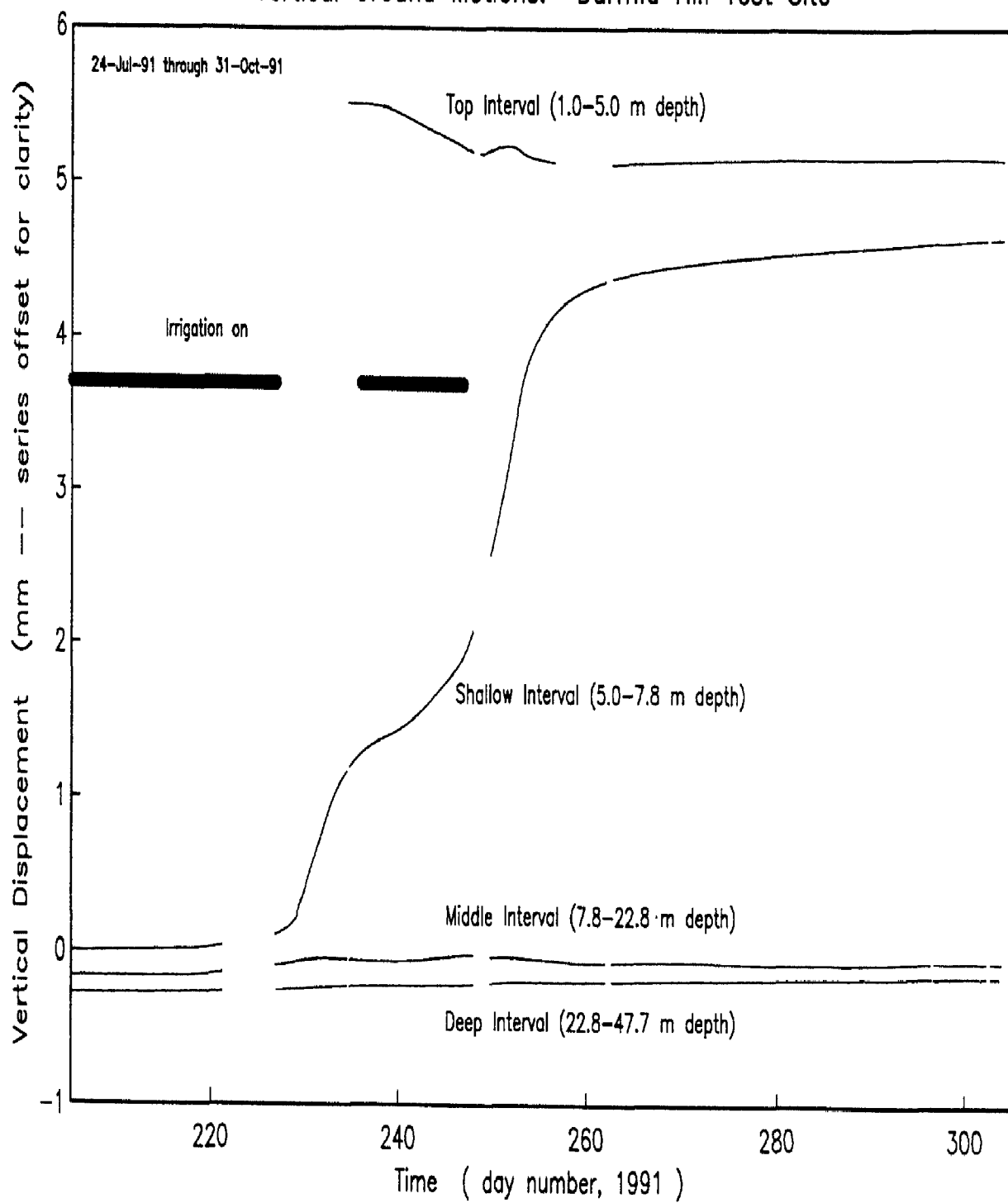


Figure 1

## CENOZOIC TECTONIC AND PALEO GEOGRAPHIC EVOLUTION OF THE PUGET LOWLAND SEISMIC ZONE

9450-50551

Samuel Y. Johnson  
Branch of Sedimentary Processes  
U.S. Geological Survey  
MS 939, Box 25046, DFC,  
Denver, Colorado 80225  
(303) 236-1545

### **Investigations**

This research is designed to describe and interpret the stratigraphy, sedimentology, petrology, and age of Cenozoic units within and bounding the Puget Lowland seismic zone (Figure 1), with the goal of reconstructing the Cenozoic paleogeography of the region. Questions posed include the following: What sedimentary basins formed, what was their geometry, what were the tectonic controls on their origins, and at what rates did they subside? What is the petrology of Cenozoic sediments and in what environments were they deposited? How deeply were sediments buried as determined by thermal maturity and diagenetic studies? Where, when and how were Cenozoic strata deformed?

When these data are collected and analyzed, other important questions can be posed. Are there offsets of mismatched sedimentary facies, petrofacies, or burial-history trends across the Puget Lowland seismic zone that indicate significant lateral offset or horizontal shortening? If so, what units or features can be used as piercing points or markers in constraining amounts, rates, and timing of offset? Is there evidence for large throughgoing fault systems that have displaced units and(or) influenced depositional patterns? Are offsets distributed across wide zones? Do identified structures coincide with known zones of recent seismicity? If not, should identified structures be considered zones of potential seismicity?

Project investigations began during FY91 and consisted largely of collecting field and borehole core data from Eocene sedimentary rocks. Surface outcrops of Eocene strata were examined in reconnaissance throughout the Puget Lowland seismic zone; detailed stratigraphic and sedimentologic studies were undertaken at Tiger Mountain, in the Morton anticline area, and in the Centralia coal mine (Figure 1). Four nearly complete borehole cores (WC-83-5, WC-83-6, WC-83-14, WC-83-17; Figure 1) belonging to the Weyerhaeuser Corporation were described in detail. Two other Weyerhaeuser cores (WK-110-OB and WK-42-OB) and core from the Standard Oil Company Alderwood #1 were also sampled. Cumulatively, stratigraphic sections totalling more than 2,000 m were measured and sampled.

Data collected during this initial field season are now being compiled and analyzed. Sedimentologic data are being plotted on vertical profiles that will be used to document and reconstruct depositional environments and systems. Petrologic data are needed to provide constraints on paleogeography and sediment dispersal patterns. To that end, thin sections of 63 samples have been prepared and will be analyzed petrographically, and 11 samples have been given to a colleague for analysis of heavy mineral content. The geochronologic framework needed to place these sedimentologic data in their temporal context will be provided by isotopic dates, tephra-correlation studies, and paleontologic investigations. Fifteen samples of volcanic tuffs and shallow intrusions have been submitted for mineral

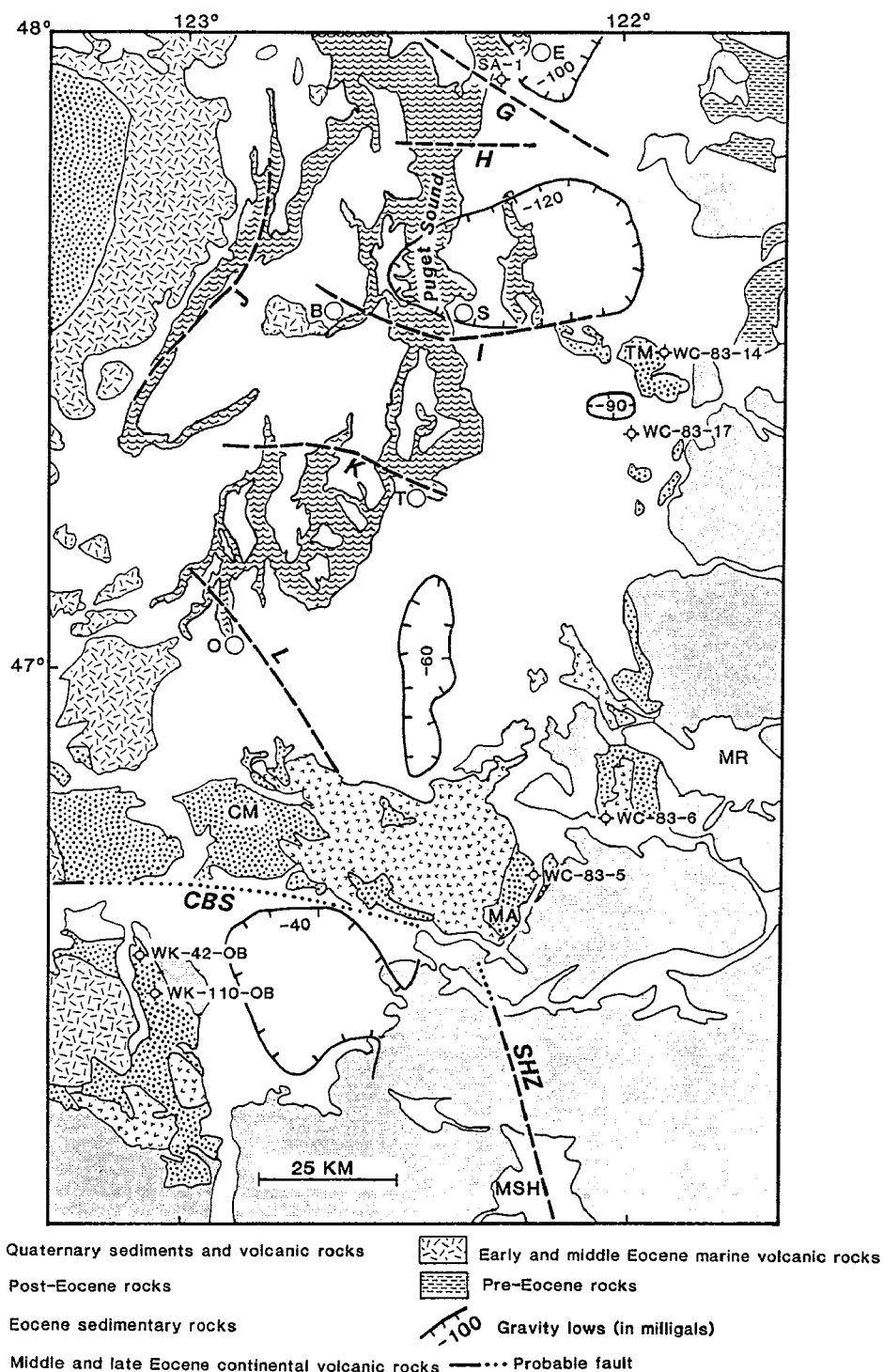


Figure 1. Schematic geologic map of the Puget Lowland seismic zone, showing locations of concentrated FY91 field work (TM, MA, CM) and borehole cores described and sampled (for example, WC-83-14). Probable faults include structures *G*, *H*, *I*, *J*, *K*, and *L* of Gower and Yount (1985), the Saint Helens seismic zone (*SHZ*) of Weaver and Smith (1983), and an inferred structure on the northern margin of the Chehalis sub-basin (*CBS*). Other abbreviations as follows: B, Bremerton; CM, Centralia Mine; MA, Morton anticline area; MR, Mount Rainier; MSH, Mount Saint Helens; O, Olympia; S, Seattle; T, Tacoma; TM, Tiger Mountain. Gravity data from Bonini and others (1974).

separations and will ultimately be dated using the Ar-Ar or fission-track method. Twenty four samples of volcanic tuffs have been submitted to Paul Hammond of Portland State University who is conducting a regional tephra-correlation study using XRF and INAA geochemical analyses provided by the USGS. Twenty seven samples were submitted to micropaleontologists for identification and biostratigraphic/paleoecologic analysis of foraminifera and ostracodes. Finally, the burial and thermal histories of these strata are being examined by vitrinite reflectance analysis (24 samples submitted) and organic geochemical analysis (six samples submitted). Data from these different analyses will be integrated to develop paleogeographic models that constrain tectonic evolution.

## **Results**

**Preliminary** results from the surface sections or cores described in detail are summarized below:

### *1. Tiger Mountain-Black diamond area: Surface outcrops and borehole core from WC-83-14 and WC-83-17 (Figure 1).*

Field work at Tiger Mountain focussed on the Middle Eocene Raging River Formation, the oldest (early Narizian) exposed Cenozoic sedimentary unit in the central and southern Puget Lowland. The unit may be as thick as 1000 m and consists (in ascending order) of four main facies: (1) massive coarse breccia of inferred alluvial-fan origin; (2) parallel- and cross-stratified conglomerate and conglomeratic sandstone of inferred braided fluvial origin; (3) bioturbated sandstones and mudstones of inferred shallow-marine origin; (4) massive and laminated mudstones of inferred deep-marine (bathyal, based on foraminifera) origin. The upper two facies and the contact with deltaic deposits at the base of the overlying Tiger Mountain area were penetrated in borehole WC-83-14, from which 470 m of continuous core were described. The unit therefore records a major, previously unrecognized early Tertiary transgressive event in the Puget Lowland. Additionally, 475 m of the Puget Group were described and sampled in detail from borehole WC-83-17. These strata are entirely nonmarine and record regression and basin-filling. Ongoing work will describe the petrology of these units and constrain their ages, refine sedimentologic interpretations, and demonstrate their paleogeographic and paleotectonic significance.

### *2. Morton anticline area and borehole core from WC-83-5 and WC-83-6 (Figure 1).*

Work in the Morton anticline area concentrated on measuring and describing exposures of the Puget Group that underlie volcanic rocks of the Northcraft Formation. Four stratigraphic sections were measured and sampled in detail: (1) 451 m of continuous core from borehole WC-83-5; (2) 264 m of continuous core from borehole WC-83-6; (3) ~ 100 m of section in the Snow Creek drainage; (4) ~ 400 m of section at Bergen Mountain. Collectively, the sections are characterized by thick, alternating intervals of nonmarine and less common marine strata. Ongoing work will test the hypothesis that the marine intervals represent regional transgressive events that can be broadly correlated. Analysis of DOE seismic data through the Morton area may assist in developing a regional sequence-stratigraphic framework.

The Morton area is located near the inferred northern termination of the right-lateral St. Helens seismic zone (SHZ; Figure 1) defined by Weaver and Smith (1983). This structure coincides with a major crustal boundary between Eocene basaltic basement to the west and pre-Tertiary continental basement to the east, and probably has been an important tectonic element throughout the Cenozoic. The zone apparently does not offset volcanic rocks of the late Middle Eocene Northcraft Formation (Figure 1), suggesting that offset

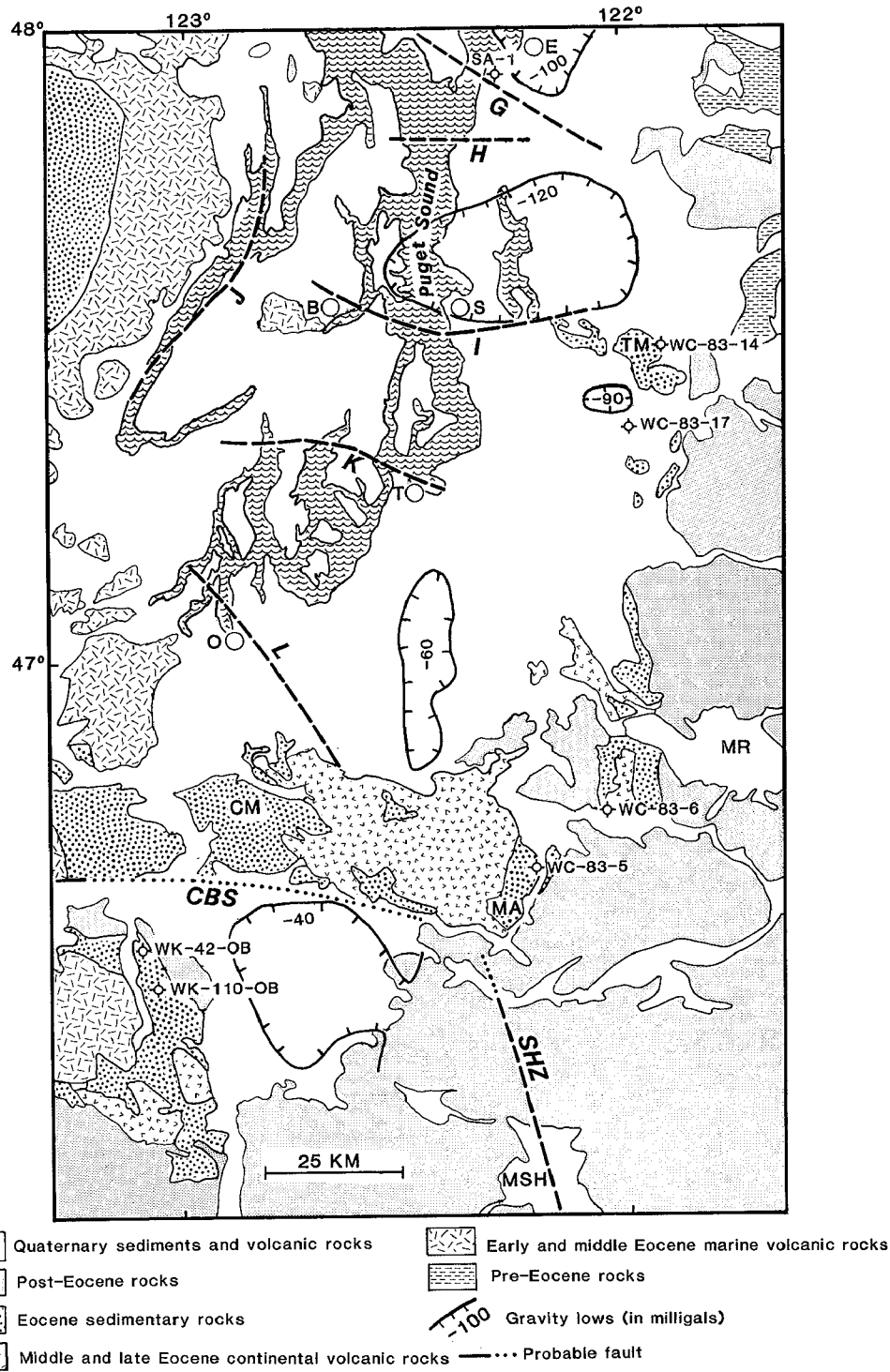
may have been transferred to adjacent fault zones. Hypotheses to be tested include the following: (1) The *SHZ* bends abruptly to the west into a compressional structure (a restraining bend) that defines the northern boundary of the Chehalis sub-basin. (2) Offset on the *SHZ* is transferred ~10 km to the east onto a structure that extends up the axis of the Tilton River valley north of Morton. Preliminary stratigraphic analysis suggests vertical offset of more than 1,000 m across this valley, and strata on both flanks of the valley are anomalously tightly folded and complexly deformed. (3) Displacement on the *SHZ* is transformed to the north into distributed shear in the Puget Lowland along with some zones (for example, 1 and 2 above) of more concentrated deformation.

### 3. *Centralia coal mine. (Figure 1)*

A detailed ~180 m thick section of the Skookumchuck Formation was measured that contains one thick (~60 m) marine interval overlain and underlain by nonmarine rocks, including thick coals. Ongoing work will test the hypotheses that these thick marine intervals and their associated surfaces of transgression can be used as regional time lines that can be recognized in outcrops, from well logs, and on seismic lines. Ongoing petrologic and geochronologic studies will further constrain the paleogeographic and paleotectonic significance of these strata.

## References

- Bonini, W.E., Hughes, D.W., and Danes, Z.F., 1974, Complete Bouguer gravity anomaly map of Washington: Washington Division of Geology and Earth Resources, Geologic Map GM-11.
- Gower, H.D., and Yount, J.C., 1985, Seismotectonic map of the Puget Sound region, Washington: U.S. Geological Survey Map I-1613.
- Weaver, C.S., and Smith, S.W., 1983, Regional tectonic and earthquake hazard implications of a crustal fault zone in southwestern Washington: *Journal of Geophysical Research*, v. 88, p. 10,371-10,383.



## **Next Generation Seismic Studies of the New Madrid Seismic Zone**

**#14-08-0001-G1534**

**Arch C. Johnston and Jer-Ming Chiu  
Memphis State University  
Center for Earthquake Research and Information  
Memphis, TN 38152  
901-678-2007**

**Robert B. Herrmann  
Department of Earth and Atmospheric Sciences  
Saint Louis University  
3507 Laclede  
St. Louis, MO 63103  
314-658-3131**

### **Investigations Undertaken**

Since mid-October 1989, the 40 three-component PANDA (Portable Array for Numerical Data Acquisition) stations have been deployed in the central New Madrid seismic zone (NMSZ) in 2- to 6-km interstation spacings. More than 500 earthquakes with magnitude ranging from -2.0 to 4.6 were recorded on-scale by PANDA during the 2 years of field operation. The onset of P and S arrivals can be unambiguously determined from the vertical component and two horizontal components, respectively, for accurate and reliable earthquake locations that are otherwise impossible to obtain from single-component regional seismic network data alone. The PANDA deployment will continue at least to the end of February 1992.

### **Results Obtained**

Three-component digital seismograms collected by PANDA are characterized by (1) very weak direct S arrivals on the vertical component, which can, however, be identified unambiguously from the two horizontal components, and (2) at least two prominent secondary arrivals between the direct P and S arrivals: one (Sp) dominant on the vertical component and the other (Ps) with smaller amplitude on the two horizontal components (Figure 1). Travel time differences between the Sp and S and between the P and Ps are the same from different earthquakes to the same station and are different between stations. Polarization analyses of three-component seismograms and travel time measurements confirm the interpretations that these two secondary arrivals are the P-to-S (Ps) and S-to-P (Sp) converted waves originating at the bottom of the sedimentary cover beneath each station. Therefore, travel time differences between the direct and the converted waves are used to calculate the depth to the bottom of the unconsolidated sediments beneath each station by assuming almost vertical raypaths for the direct and the converted waves. A three-dimensional representation of the geometry of the sedimentary basin in the upper Mississippi embayment is thus constructed by contouring the converting point beneath each PANDA station (Figure 2). The Tertiary boundary of the embayment was digitized and used to define the outer boundary of the sedimentary basin. In general, the geometry of the bottom of the sedimentary basin is very smooth except for the central portion where the contact between the sedimentary basin and the underlying Paleozoic sedimentary rock



is disturbed. This disturbed area coincides with the upward extension of the southwest-dipping fault zone ( $32^\circ \sim 52^\circ$  dip angle) and may represent deformation from recent tectonic activity underlying rift system.

The frequency content of the direct and the converted waves is different. In general, the direct S wave is characterized by lower frequency content on the horizontal component and the S-to-P converted wave is characterized by higher frequency content on the vertical component. Their ray paths are almost identical. Spectral ratios of the direct S and the S-converted P waves are calculated to study the relations between the attenuation features of P ( $Q_p$ ) and S ( $Q_s$ ) waves in the sedimentary basin. Preliminary results for PANDA stations with well-constrained spectral ratios give an estimation of  $Q_p$  ranging from 15 to 60 and  $Q_s$  ranging from 15 to 30 for the sedimentary basin in the upper Mississippi embayment (Figure 3).

Three-dimensional velocity inversions for P and S waves are calculated independently to investigate velocity structures in the upper crust. Preliminary inversion results suggest a P-wave low-velocity zone at a depth between 2.5 and 5 km which may be associated with clastic sediments filling the graben beneath the Paleozoic sedimentary rock layers. Earthquakes were relocated by using the new velocity model after inversion. Figure 4 shows two representative cross-sectional views of the central NMSZ, obtained from two data bases, one located by a regional network model (regional), and the other by a new velocity model obtained from velocity inversions. The linear fault zone features were significantly improved when the new velocity model was used.

Unlike the broad and almost vertical fault zone extending from near surface to lower crust by many previous studies in the NMSZ region, cross-sectional views of the new data clearly define a narrow inclined fault zone dipping toward the southwest with  $\sim 52^\circ$  dip in the southern portion and  $\sim 32^\circ$  dip in the northern portion of the central NMSZ (Figure 5). Seismicity extends from beneath the sedimentary basin ( $\sim 0.6$  km) to about 15 km depth with a concentration between 5 to 8 km. An apparent contortion of the seismic zone between the northern and southern portions of the central NMSZ occurs at the intersection with the southwest segment around Ridgely, Tennessee. In contrast to the central NMSZ, the northern end of the southwest segment, the southern end of the northeast segment, and the northwest segment of the NMSZ are characterized by an almost vertical fault zones (Figure 6) that intersect with the central zone around Ridgely, Tennessee, and around New Madrid, Missouri, respectively. Seismicity around these intersections is the highest in the region.

During the 2 years of PANDA operation, seismicity shows a seasonal pattern that can be correlated with the fluctuation of regional water level. Such correlations may suggest that seasonal variations of regional hydro-induced pressure in the upper crust from water level changes on the surface may play an important role in the generation of earthquakes in the central NMSZ.

## **Reports**

Bataille, K., and J.M. Chiu, Polarization analysis of high-frequency, three-component seismic data, *Bull. Seismol. Soc. Am.*, v. 81, no. 2, 622-643, 1991.

- Booth, D.C., H.J. Rowlands, and J.M. Chiu, Observations of shear-wave splitting in the New Madrid seismic zone, eastern USA, presented at the ESSA meeting, Oct. 1991.
- Chen, K.C., J.M. Chiu, Y.T. Yang, S.C. Chiu, A.C. Johnston, and the PANDA Group, Determination of  $Q_p - Q_s$  relations in the sedimentary basin in the upper Mississippi embayment using converted phases, presented at the ESSA meeting, Oct. 1991.
- Chen, K.C., J.M. Chiu, Y.T. Yang, S.C. Chiu, A.C. Johnston, and the PANDA Group, Three-dimensional geometry of the sedimentary basin and its tectonic implications in the upper Mississippi embayment: Results from the PANDA experiment, *EOS*, v. 71, no. 17, p. 264, presented at the Spring AGU meeting, 1991.
- Chiu, J.M., G. Steiner, R. Smalley, and A.C. Johnston, PANDA: A simple, portable seismic array for local- to regional-scale seismic experiments, *Bull. Seismol. Soc. Am.*, v. 81, no. 3, 1991.
- Chiu, J.M., G. Steiner, R. Smalley, A.C. Johnston, and the PANDA Group, The PANDA II - a PC-based seismic array, presented at the ESSA meeting, Oct. 1990.
- Chiu, J.M., A.C. Johnston, and the PANDA Group, The September 26, 1990, Md=4.8, Cape Girardeau Earthquake and its aftershocks, presented at the ESSA meeting, Oct. 1990.
- Chiu, J.M., K.C. Chen, Y.T. Yang, S.C. Chiu, A.C. Johnston, and the PANDA Group, A high-resolution PANDA experiment in the central New Madrid seismic zone, *EOS*, v. 71, no. 49, p. 1435, presented at the Fall AGU meeting, Dec. 1990.
- Chiu, J.M., K.C. Chen, Y.T. Yang, S.C. Chiu, A.C. Johnston, and the PANDA Group, A high-resolution PANDA experiment in the central New Madrid seismic zone, invited talk at the GSA meeting, Oct. 1990.
- Chiu, J.M., K.C. Chen, Y.T. Yang, S.C. Chiu, A.C. Johnston, and the PANDA Group, A high-resolution PANDA experiment in the central New Madrid seismic zone, presented at the ESSA meeting, Oct. 1990.
- Chiu, J.M., Y.T. Yang, K.C. Chen, Z.S. Liaw, S.C. Chiu, A.C. Johnston, PANDA Group, and R.B. Herrmann, 3-dimensional fault zone geometry and sedimentary basin configuration in the central New Madrid seismic zone determined from PANDA array data, presented at the ESSA meeting, Oct. 1991.
- Chiu, S.C., H. Hwang, J.M. Chiu, and A.C. Johnston, The Risco, Missouri earthquake, May 4, 1991, presented in the ESSA meeting, Oct. 1991.
- Herrmann, R.B., E.J. Haug, A.C. Johnston, and J.M. Chiu, Progress in implementing the cooperative New Madrid seismic network, presented at the ESSA meeting, Oct. 1991.
- Johnston, A.C., An overview of the New Madrid seismic zone, presented at the ESSA meeting, Oct. 1991.
- Wuenscher, M.E., R.B. Herrmann, and Z. Liu, Attenuation of body waves at the New Madrid seismic zone, presented in the ESSA meeting, Oct. 1991.
- Yang, Y.T., J.M. Chiu, Z.S. Liaw, K.C. Chen, S.C. Chiu, A.C. Johnston, and the PANDA Group, Fault zone geometry and crustal velocity structures in the central New Madrid seismic zone using the PANDA data, *EOS*, v. 71, no. 17, p. 264, presented at the Spring AGU meeting, May 1991.

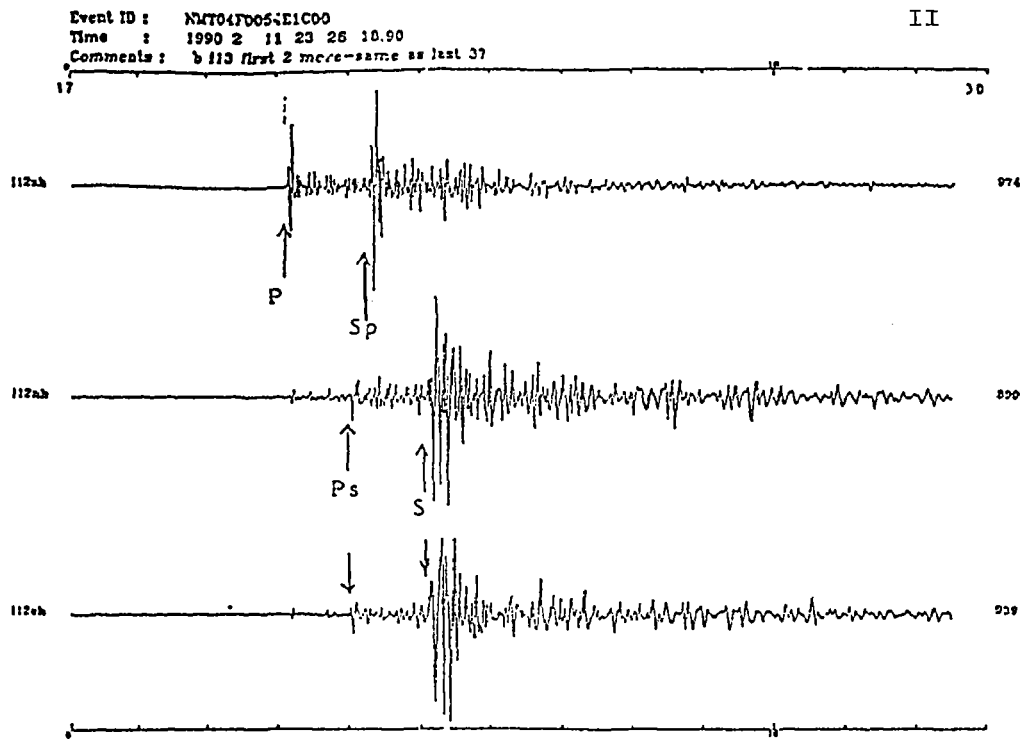


Figure 1. Typical three-component digital seismograms recorded by the PANDA station in the New Madrid seismic zone.

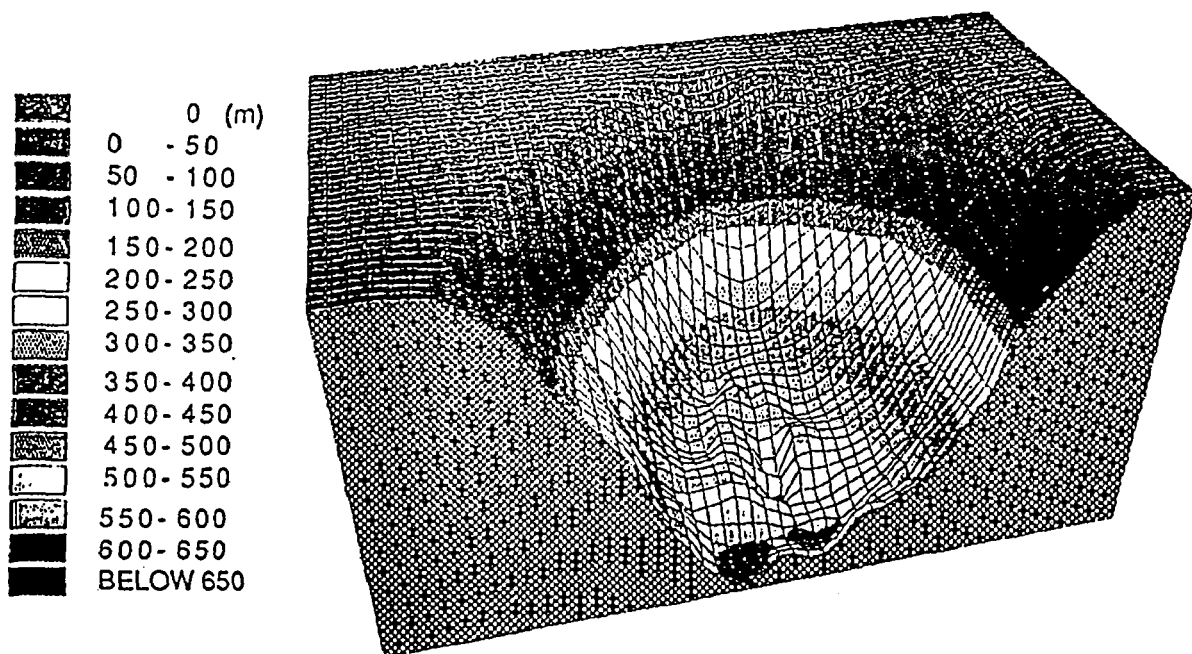


Figure 2. Three-dimensional representation of the geometry of the sedimentary basin in the upper Mississippi embayment determined from the delay time between the direct waves and the converted waves from the bottom of the sedimentary basin.

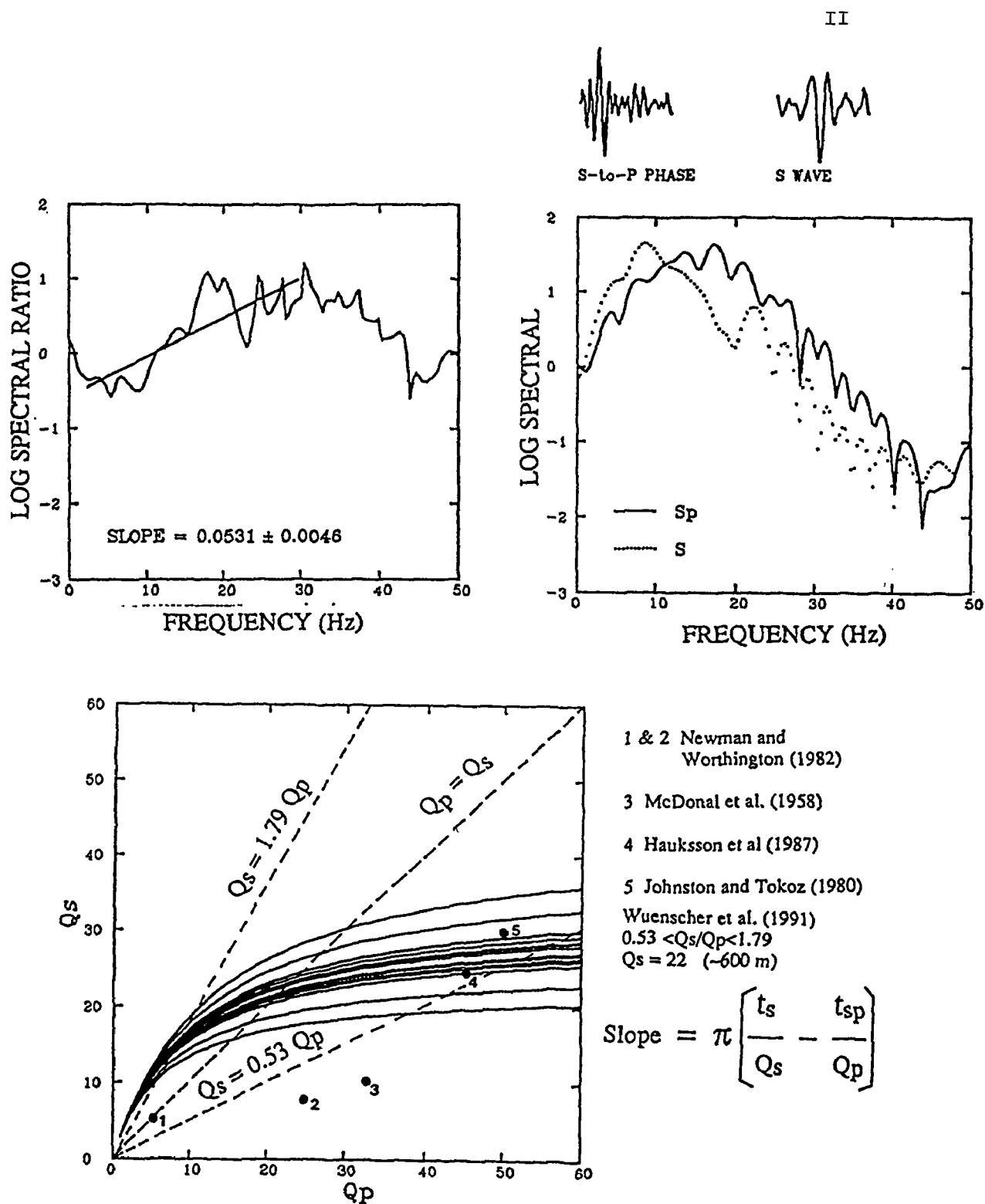


Figure 3. Amplitude spectra of direct S and the S-to-P (Sp) converted waves (upper right). Spectra ratio of the two waves is shown in the upper left. The  $Q_p$  and  $Q_s$  relations are determined from the slope of the spectra ratio as shown in the bottom.

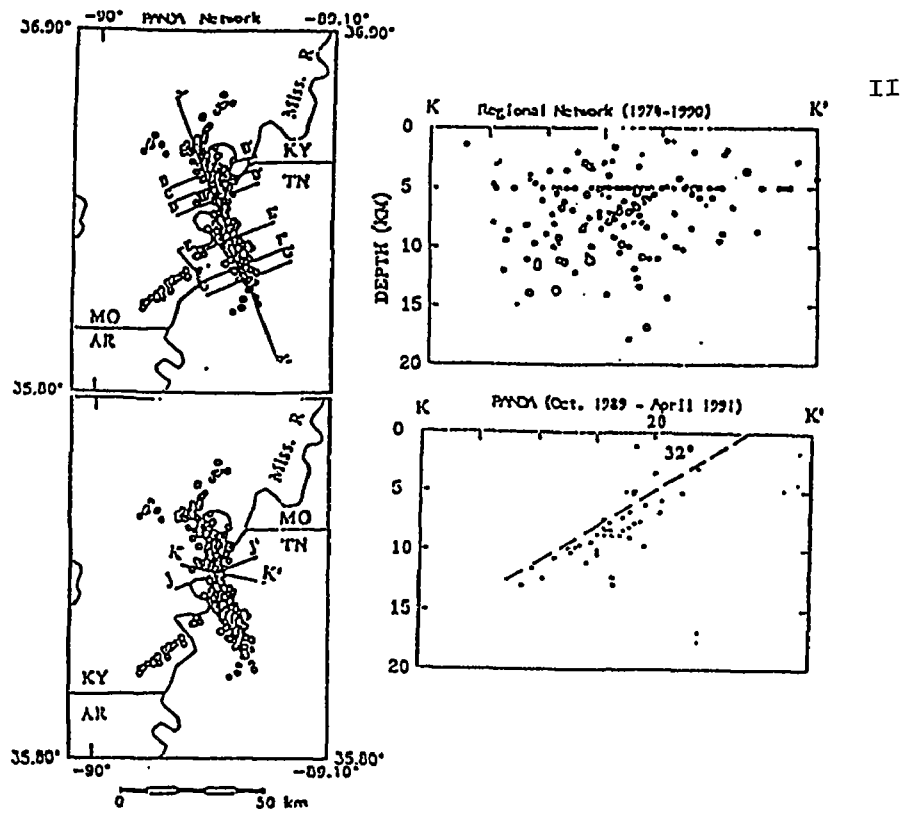


Figure 4. A comparison of a cross-sectional view of seismicity in the central New Madrid seismic zone (K-K') using regional network database (upper right) and PANDA data (lower right).

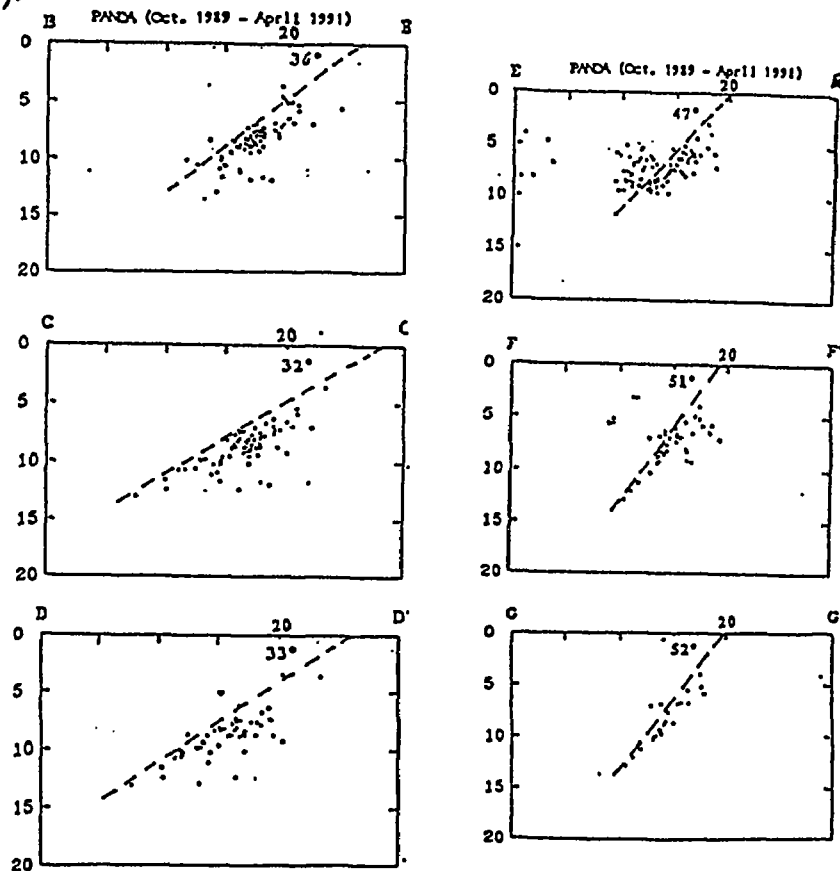


Figure 5. Three cross-sectional views of the northern (left) and southern portions of the central New Madrid seismic zone from 2 years PANDA data showing shallow angle southwest dipping seismic zone. The change of dipping angles from 32° to 52° occurred at the intersection of the southwestern segment with the central segment.

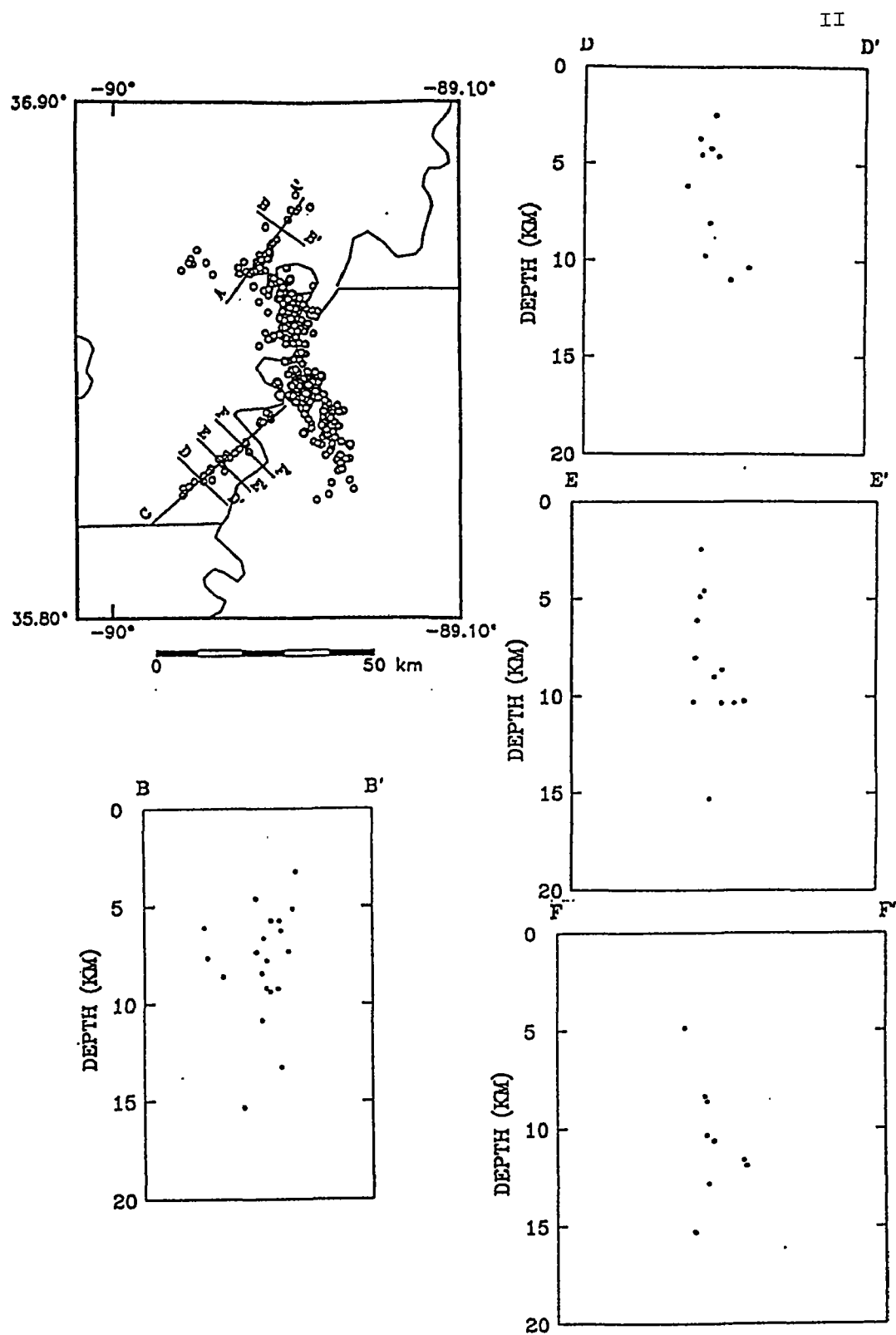


Figure 6. Cross-sectional views of the north (lower left) and southwest (right three) segments of the New Madrid seismic zone showing almost vertical dipping zones.

**Collaborative Research (Memphis State University and  
Saint Louis University): "The Cooperative New Madrid  
Seismic Network"**

**#14-08-0001-G1923**

**Arch C. Johnston and Jer-Ming Chiu  
Memphis State University  
Center for Earthquake Research and Information  
Memphis, TN 38152  
901-678-2007**

**Robert B. Herrmann  
Department of Earth and Atmospheric Sciences  
Saint Louis University  
3507 Laclede  
St. Louis, MO 63103  
314-658-3131**

**Investigations Undertaken**

As originally proposed, the cooperative New Madrid network would consist of 40 three-component, digital telemetered, seismic stations to replace the current regional networks which consist of some 50+ short-period, low-dynamic-range, vertical-component stations. Two data centers, one at CERI and the other at SLU, and five regional nodes will be established. Due to a reduced level of funding, some compromises had to be made to maintain something close to the current monitoring capability. While maintaining mostly digital stations, some of the data received at regional nodes would remain analog using conventional FM telemetry. These data will be digitized at the regional node sites. Greater dynamic range can still be achieved by employing gain-ranging techniques, using PANDA II type hardware. Figure 1 shows the locations of a data center located at CERI in Memphis, TN and a regional node at Marked Tree, Arkansas as well as a proposed regional node near Hayti, Mo. Concentric circles, at 40 and 100 km have been drawn to provide a rough estimation of the range of telemetry coverage possible with the digital and analog telemetry schemes. The range of the digital telemetry can be improved by increasing power and/or by providing towers at station sites which may require a power budget of 4-5 times greater than that used by current analog sites.

**Progress Summary:**

Progress has been made toward implementation of the cooperative New Madrid network in three principal areas.

**1) Installation and testing of the VSAT satellite telemetry system.**

Very small aperture terminal (VSAT) satellite telemetry equipment has been installed at CERI in Memphis, TN and at Marked Tree, AR. Preliminary testing of the VSAT located at CERI has been completed successfully. Currently, we have been successful in establishing two-way communications through the Scientific Atlanta VSAT system. The current setup uses two ports on the same PAD for testing the USNSN facilities. Both ports are presently attached to a VAX 11/785 (VMS), and will be left there for the duration of

the testing phase. Several sets of tests will be implemented soon to verify the integrity of the rollback system for handling data transmission problems. Once the rollback system has been verified, we will begin implementing the full set of USNSN protocols which will include downloading commands to remote field sites, making data requests to the USNSN, and checking out other features of the system.

After remaining problems with the VSAT telemetry system are worked out, the next step is to begin transmitting regional seismic data via satellite to receive at two regional data centers. A PC based field data acquisition system will be implemented and installed at the Marked Tree node later to accomplish the data transmitting test.

## 2) Installation and testing of PC based digital data acquisition systems.

Two digital data acquisition systems are being evaluated at CERI and at SLU. Both make use of 386/486 IBM compatible PC computers and A/D-multiplexer hardware developed by the USGS (Lee et al., 1989; Tottingham et al., 1990). The main differences between the two systems are the operating system software used. Currently installed at CERI is an 128-channel acquisition system based on two Compaq 386/25 CPUs running the MS-DOS operating system and the IASPEI software. The IASPEI software is used for both on-line digital data acquisition and off-line data processing. The two PCs are networked via LANTASTIC hardware/software. The principal drawback of the system is the inherently single task nature of the DOS operating system. This necessitates the use of two networked PCs, one for real time data acquisition, the second to read the collected data and perform off-line processing. It was also found that considerable care is necessary in the installation of the Lee's hardware to eliminate noise in the digital data caused by ground loops.

The second digital data acquisition system being evaluated is based on the same hardware configuration as the Lee's system, but makes use of the multi-tasking UNIX operating system. Applications software for this system has recently been developed at Saint Louis University by Eric Haug. Similar hardware and software will be setup at CERI to test and implement the application software.

## 3) Development of PANDA II gain-ranging, analog telemetry system.

A 5-step gain-ranging PANDA II system has been designed and is currently undergoing field testing at CERI. This system is an outgrowth of the current PANDA system (Chiu et al., 1991) with major improvements in dynamic range, telemetry topology and network geometry, and increased mobility of the network and central recording facilities. The gain-ranging front-end system was designed to achieve at least 126 dB of dynamic range. The PANDA II hardware overcomes the inherent limitations of any traditional telemetered system while maintaining the ability to use conventional, low-cost FM telemetry components. The PANDA II hardware can be considered as an alternative for portions of the new network.

## Reports

Haug, E.J., R.B. Herrmann, and J.M. Chiu, (1991), The cooperative New Madrid seismic network - Implementation of regional network nodes, *Seismol. Res. Lett.*, 62(1), 33, presented at the annual SSA meeting, March 1991.



Herrmann, R.B., E.J. Haug, A.C. Johnston, and J.M. Chiu, Progress in implementing the cooperative New Madrid seismic network, presented at the ESSA meeting, Oct. 1991.

### References

Chiu, J.M., G. Steiner, R. Smalley, and A.C. Johnston (1991). PANDA: A simple, portable seismic array for local- to regional-scale seismic experiment, *Bull. Seismol. Soc. Am.*, 81(3), 1000-1014.

Lee, W.H.K., D.M. Tottingham, and J.O. Ellis (1989). Design and implementation of a PC-based seismic data acquisition, processing, and analysis system, *IASPEI Software Library*, 1, 21-46.

Tottingham, D.M., J.O. Ellis, and W.H.K. Lee (1989). A low-cost 128-channel seismic data acquisition and recording system, *EOS*, 70(43), p. 1189.

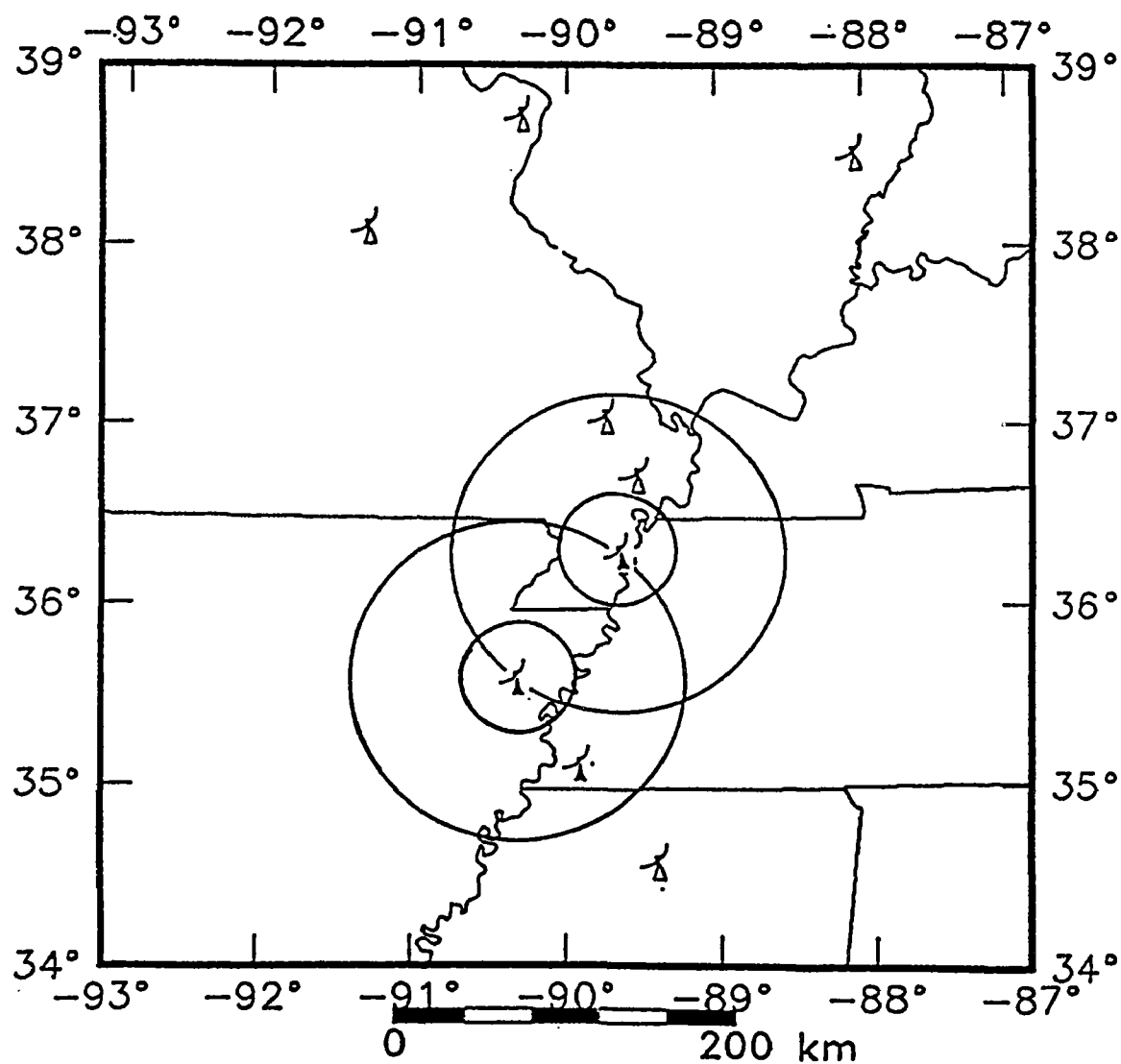


Figure 1. Distribution of regional VSAT nodes. Concentric circles are plotted at 40 and 100 kilometers around proposed CER nodes

## TILT, STRAIN, AND MAGNETIC FIELD MEASUREMENTS

9960-2114

M. J. S. Johnston, R. J. Mueller, G. D. Myren  
Branch of Tectonophysics  
U. S. Geological Survey  
Menlo Park, California 94025  
415/329-4812

### Investigations

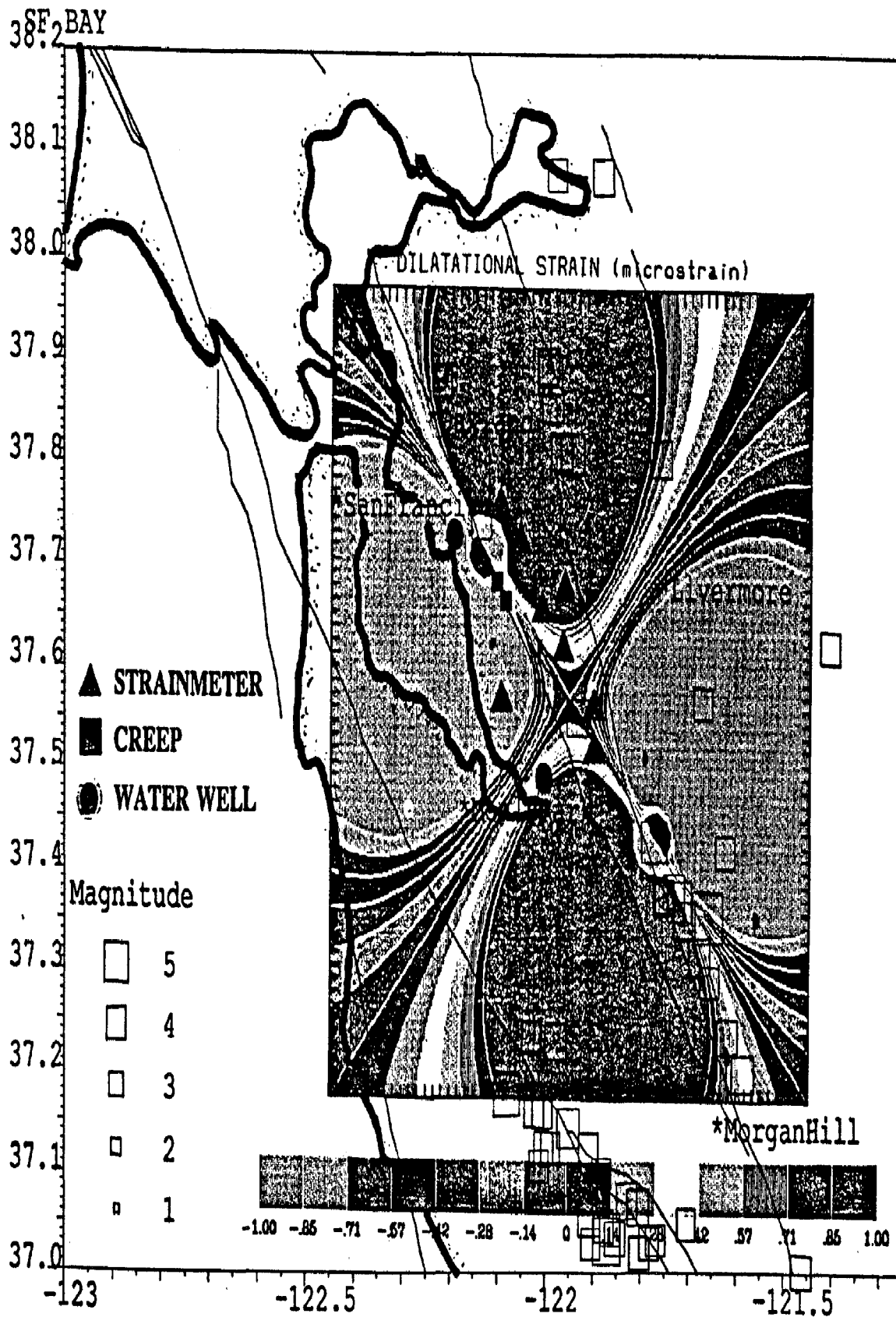
- [1] To investigate the mechanics of failure of crustal materials using data from both deep borehole tensor and dilational strainmeters and near surface strainmeters, tiltmeters, and arrays of absolute magnetometers.
- [2] To develop physical models of incipient failure of the earth's crust by analysis of real-time records from these instruments and other available data.

### Results

- [1] **A FOCUSED EARTHQUAKE PREDICTION EXPERIMENT ON THE HAYWARD FAULT: ARRAY PLANS AND EXPECTED STRAINS AND DISPLACEMENTS FOR RUPTURE OF THE SOUTHERN SEGMENT OF THE HAYWARD FAULT.**

The identification of reliable short- and intermediate-term precursors to damaging earthquakes remains an critical challenge to the earthquake hazard reduction program. To this end, a focused earthquake monitoring experiment has been planned for the southern segment of the Hayward fault. Instruments to be used in this experiment include, dilational strainmeters, tensor strainmeters, water well monitors, creepmeters, continuous GPS displacement monitors, seismic velocity and acceleration transducers. The strainmeters and seismometers will be installed in boreholes at about a 200 m depth. At this depth, measurement precision about 20 dB below that of surface instruments can be attained. Short-term strain changes less than one ppb can easily be identified. The borehole array of eight to ten sites, have been chosen along the segment of the Hayward fault between San Leandro and Milpitas with most sites at distances from 2 km to 7 km from the Hayward Fault. These sites are shown in Figure 1 together with a contour map showing the expected strain release for a worst case scenario of a magnitude 7 earthquake and seismicity during the past 20 years on this segment of the fault. Data will be transmitted using digital satellite and radio telemetry to Menlo Park, Ca. for analysis and display. Various other geophysical and geological data are also be collected during the borehole drilling program. Surface fault displacement will be monitored with creepmeters. An initial three creepmeters are installed within the City of Hayward. Continuous GPS displacement monitors are installed near near the north end of the array. The overall array design was influenced by the form and amplitude of strain and displacement fields calculated from simple dislocation models of various possible damaging earthquakes that might occur on either the southern segment of the Hayward fault, or on the Calaveras fault. Completion of this array is expected by the end of 1992.

# PROPOSED MONITORING SITES



\* Figure 1. Strain, water level, creep, and 3-component seismometer sites on the Southern Hayward fault. The contour plot shows expected strain resulting from a "worst case" scenario for rupture between San Leandro and Calaveras Reservoir as expected for a magnitude 7+ earthquake.

[2] **SLOW EARTHQUAKES WITHIN THE SAN ANDREAS FAULT SYSTEM**

Slow earthquakes (ie fault slip episodes without seismic radiation in the normal seismic frequency bands) are of three main types: 1)  $s_p$  - Slow earthquakes that precede, and evolve, into "normal" earthquakes, 2)  $s_f$  - Slow earthquakes that follow "normal" earthquakes, and 3)  $s_{NS}$  - Slow earthquakes with no associated seismicity. Evidence for these events has generally been indirect (eg enhanced tsunami generation, anomalous normal modes, earthquake code, etc) with a few exceptions. Quantification of these events is now possible with networks of high-resolution borehole strainmeters recently installed in western U.S., Japan, and Iceland. For the 16 earthquakes with  $M_L > 5.5$  that have occurred in California during the past eight years with recording borehole strainmeters less than 10 rupture lengths away, no indication of  $s_p$  events has yet been found.  $s_f$  followed the April 24, 1984  $M_L$  6.1 Morgan Hill earthquake and the October 18, 1989  $M_L$  7.1 Loma Prieta earthquake. More than 30  $s_{NS}$  events have occurred. These events are mostly associated with fault creep episodes or occur within the Long Valley volcanic caldera. For the San Andreas fault system therefore,  $s_p$  slow earthquakes appear to be rare (non-existent).  $s_f$  events appear to occur more frequently, particularly after large earthquakes, but the total moment release is minimal compared that released seismically. Moment release for  $s_{NS}$  events may be larger than that from  $s_f$  events but in no case have we seen indications of events on multiple instruments with moments exceeding  $10^{24}$  dyne-cm.

[3] **LOCAL DIFFERENTIAL MAGNETIC FIELDS AT PARKFIELD, CALIFORNIA: JULY, 1985 TO JULY, 1991.**

A differentially connected array of seven proton magnetometers has operated in the Parkfield region since 1985. Each magnetometer automatically measures total magnetic field intensity to an accuracy of either 0.25 nT or 0.125 nT every 10 minutes. The data are telemetered to Menlo Park, California for on-line processing and analysis to identify tectonomagnetic anomalies related to crustal deformational and/or earthquake processes. During this six year period only three unusual events with marginal amplitudes are observed; 1) from March 1987 to July 1987 a 0.7 nT magnetic field intensity decrease and subsequent increase back to normal is observed at magnetometer TFLM, 2) a 0.6 nT decrease is observed at magnetometer TFLM from the beginning of 1991 to the present, and 3) from about 1989 to the present a rate change of +0.5 nT/a is observed at magnetometer AGDM. The most significant systematic rate increase in seismic moment release in the Parkfield region occurred during the past year while two of the three magnetic events have occurred on two independent magnetometers. However, no seismic events with  $M_L > 3.7$  have occurred. While there are suggestions of changes during mid-1987 and mid-1991 in the 2-color laser geodimeter line that monitors horizontal ground displacement near TFLM, these changes are either marginal or complicated by meteorologic effects. Changes in long-term creep rate are unremarkable during this time period. An exception is a change in creep rate at a single creepmeter during mid-1991, which is complicated by meteorologic effects. A model of differential fault slip with little stress and strain redistribution until 1990, but perhaps increasing since then, would best describe these various data at this time.

[4] **EARTH STRAIN NOISE FROM DEEP BOREHOLES NEAR THE SAN ANDREAS FAULT SYSTEM FROM 0.01 SECONDS TO 100 MEGASECONDS**

Records from an array of borehole strainmeters along the San Andreas fault system are used to determine comparative ground noise over ten decades of frequency (100 to  $10^{-8}$  Hz) in a variety of locations. In particular, we search for differences in response between instruments in 1) fault locked and fault creeping

sites, 2) near-fault and far-fault sites, and 3) near-fault sites and sites in a volcanically active region. Also, we make an initial identification of strain noise attenuation with depth. The eight borehole instruments used are all installed at approximately 200 m depth. Contrary to some expectations, the general characteristics of power spectral density estimates obtained at all sites are similar. With the exception of about 10 dB microseismic noise peaks and 30 to 40 dB peaks at earth tidal frequencies, the spectra decrease from about -80 dB at a frequency of  $10^{-8}$  Hz (100 megaseconds) to about -220 dB at a frequency of 10 Hz (0.1 seconds) in roughly an  $f^{-2}$  dependence on frequency. Strain in deep boreholes can thus be measured as well in these different tectonic and volcanically active regions as in aseismic regions. Strain transients are observed infrequently on near-fault instruments, particularly where it is actively creeping, but these do not contribute significantly to noise power spectra determined from long record sections. Initial comparison with near-surface (2m) and intermediate-depth (30m) strain instruments indicates a 10 dB reduction in noise from 2m to 30m and a another 10 dB reduction in noise from 30m to 200m.

[5] **BOREHOLE STRAIN ARRAY IN CALIFORNIA**

A network of 15 borehole strainmeters along the San Andreas fault zone and in the Long Valley Caldera continue to be monitored and maintained. All instruments are installed at depths between 117-m and 324-m and all are between 1-km and 5-km from the the surface trace of the fault. High frequency dilatometer data in the frequency range 0.005 Hz to 100 Hz are recorded on 16-bit digital recorders with least count noise less than  $10^{-11}$ . Low frequency data from zero frequency to 0.002 Hz are transmitted through the GOES satellite to Menlo Park, CA, using a 16-bit digital telemetry system. At the USGS in Menlo Park the data are displayed in "almost real time" and are continuously monitored with detection algorithms for unusual behavior. Least-count noise is about  $5 \cdot 10^{-12}$  for the on-site digital recordings, and about  $2 \cdot 10^{-11}$  for the satellite telemetry channels. Earth strain tides, strain transients related to fault creep and numerous strain seismograms from local and teleseismic earthquakes with magnitudes between -1 and 6 have been recorded on these instruments. Static moments and total earthquake moments are determined from the co-seismic strains and total strain changes observed with the larger events.

[6] **CROWLEY LAKE AND SAN ANDREAS LAKE WATER LEVEL MONITORING**

Water level monitoring sites have been installed on Lake Crowley in the Long Valley/ Mammoth Lakes region and San Andreas lake on the San Andreas fault just south of San Francisco. These data provide differential water level measurements (tilt) with a measurement precision of less than 1 mm on baselines of 5 to 8 kilometers. Monthly averages of the data from San Andreas lake between 1979 and 1989 indicate a tilt rate of  $0.02 \pm 0.08$  microradians/yr (down S34°E).

[7] **DIFFERENTIAL MAGNETOMETER ARRAY IN CALIFORNIA**

We continue investigations of local magnetic fields and relationships to crustal strain and seismicity in the Parkfield region and in southern California. The network consists of 9 stations which are all sampled synchronously every 10 minutes and transmitted with 16-bit digital telemetry to Menlo Park, CA through the GOES satellite. Data are monitored daily with particular attention to the seven stations operating in the Parkfield region of central California and the three stations operating in the Long Valley caldera. At these latter sites a magnetic field anomaly first became obvious in late 1989 and in continuing to the present in concert with anomalous 2-color geodetic strain measurements and spasmodic swarms of minor earthquakes.

[8] **CONTINUOUS HIGH PRECISION BOREHOLE STRAIN MEASUREMENTS NEAR THE LOCKED AND CREEPING SECTIONS OF THE SAN ANDREAS FAULT**

Deep-borehole strainmeters have been operating since 1984 at sites near the northern and southern creeping/locked transition zones and in the "Big Bend" region of the San Andreas fault in northern and southern California, respectively. These instruments resolve strain changes to better than 1 part per billion (ppb) over periods of months to minutes. The last five years of strain data show long periods of uniform crustal strain, infrequent episodes of aseismic strain sometimes resulting from aseismic fault creep, and high frequency straingrams and strain field offsets generated by local earthquakes. Whereas simple views of the earthquake rupture process have suggested that: 1) substantial non-linear deformation occurs prior to rupture, 2) the scale of this deformation exceeds the eventual earthquake rupture dimensions, and 3) the properties of near-fault materials may vary with time and location, these high resolution borehole strain recordings indicate: 1) minimal short-term non-linear precursive strain occurs, 2) the size of fault patches that initiate failure are probably less than a few hundred meters in size while the eventual earthquake rupture dimensions can be several tens of kilometers, 3) no evidence of variations in near-field material properties, and 4) strain offsets from local earthquakes that are largely transmitted elastically despite complex geology and fault geometry. In the case of the recent October 18, 1989,  $M_L$  7.1 Loma Prieta earthquake, strain data from two instruments near San Juan Bautista, 5 km to 10 km southeast of the final southern extent of the rupture, indicate that any precursive failure in the hypocentral region (with a form similar to that during the earthquake) was at least a 1000 times smaller in the minutes to months before the earthquake. This, in turn, constrains the maximum amount of horizontal or vertical displacement in the hypocentral region to be at most, a few millimeters, if any occurred at all. As more borehole strainmeters are installed, these data will continue to place increasingly tighter constraints on physical processes that occur at the earthquake source.

[9] **ULTRA BROAD BAND DATA FROM AN ARRAY OF DEEP BOREHOLE STRAINMETERS ALONG THE SAN ANDREAS FAULT SYSTEM**

Records from an array of borehole strainmeters along the San Andreas fault system are used to determine comparative seismic response over nine decades of frequency (100 to  $10^{-7}$  Hz) for local earthquakes, teleseismic earthquakes and "slow" earthquakes. The dynamic range of the borehole instruments exceeds 140 dB. Comparison of the short-period portion of the earth-strain noise spectrum (20 to 500 seconds) with average spectra determined from pendulum seismometers suggest that the observed seismic noise is predominately dilational energy. Simultaneous strain and seismic velocity measurements of incident P- and S-wave amplitudes are used to estimate wavefield inhomogeneity, free surface reflection coefficients, and local P velocity. Estimates of these parameters for moderate magnitude ( $M_w \approx 6$ ) earthquakes agree well with those calculated from an anelastic half-space model with incident inhomogeneous waves. Total seismic moments determined from zero frequency strain steps for approximately 40 moderate magnitude earthquakes are approximately 20% greater than seismic moments determined from displacement spectra from instrument corrected seismic velocity data. This would indicate that only minimal aseismic moment release accompanies seismic moment release for these earthquakes.

## Reports

- Mueller, R. J., M. J. S. Johnston, and J. O. Langbein, 1991, Possible Tectonomagnetic Effect Observed from Mid-1989 to Mid-1990 in Long Valley Caldera, California. *Geophy. Res. Lett.* **18**, 601-604.
- Hill, D. P., M. J. S. Johnston, J. O. Langbein, C. E. Mortensen, A. M. Pitt, and S. Rojstaczer, 1991, Response Plans for Volcanic Hazards in the Long Valley and Mono Craters Area, California. U. S. Geological Survey Open-File Report 91-270
- Johnston, M. J. S., 1991, Recent Seismomagnetic and Volcanic Events: Implications for Physical Mechanisms, Abs for IUGG/IASPEI Meeting, August 11-24, Vienna, IASPEI Session SW11, p264.
- Johnston, M. J. S., and A. C. Fraser-Smith, 1991, On Physical Mechanisms Pertaining to the Loma Prieta Earthquake ULF Electromagnetic Emissions, Abs for IUGG/IASPEI Meeting, August 11-24, Vienna, IASPEI Session SW11, p262.
- Johnston, M. J. S., 1991, Earth Strain Noise from Deep Boreholes Near the San Andreas Fault System from 0.01 Seconds to 100 Megaseconds. *Trans. Am. Geophys. Un.*, **72**, 292.
- Linde, A. T., M. T. Gladwin, and M. J. S. Johnston, 1991 Tidal Strain Response Before the 1989 Loma Prieta Earthquake: An Unsuccessful Search For Variations in Mechanical Properties. *Geophy. Res. Lett.* , (in press).
- Johnston, M. J. S., 1991, Slow Earthquakes Within the San Andreas Fault System. *Trans. Am. Geophys. Un.*, **72**, 484.
- Johnston, M. J. S., G. D. Myren, A. T. Linde and M. T. Gladwin, 1991. High Precision Continuous Strain Measurements near the Locked and Creeping Sections of the San Andreas fault. Joint US/China Workshop on Focused Earthquake Prediction Experiments. San Juan Bautista, California, 16-19 September, 1991.
- Johnston, M. J. S., R. D. Borchardt, G. D. Myren, and G. Glassmoyer, 1992. Ultra Broad-band Data from an array of Deep Borehole Strainmeters along the San Andreas Fault System, Workshop on "Frontiers of Broad Band Seismology", Seismographic Station, U.C. Berkeley, January 9-10, 1992.

**Marine Seismic Investigations  
of the East Bay Faults**  
14-08-0001-G2123  
01 Aug 91-31 Jul 92

David L. Jones and Thomas V. McEvilly  
Seismographic Station  
Dept. of Geology and Geophysics  
University of California  
Berkeley, CA 94720

Phone: (510) 486-7347  
FAX: (510) 486-5686  
e-mail: tvmcceilly@lbl.gov

### **Project Description**

This UC/USGS cooperative project supported the acquisition of nearly one million traces of multichannel airgun seismic profiling data from the Sacramento river delta through Carquinez strait into San Pablo and San Francisco bays, and then out to sea nearly 100 km beyond the Golden Gate. The primary purpose of the survey, now known as BASIX (Bay Area Seismic Imaging Experiment), is an investigation of the crustal structure and fault geometries within the complex plate boundary in the Bay Area. The survey, conducted in September, 1991, employed the USGS research vessel S.P. Lee with a source array of 12 airguns, and a 120-channel buoyed, telemetered receiver array which was moved each day along the line. The USGS contribution to the project was the ship and crew, the airguns, navigation, and the DFSV recording system. The UC Berkeley contribution was the subcontract to the commercial geophysical contractor for the telemetry system, at a cost which exhausted the funds provided in the award. We have asked for a supplement and no-cost extension to the award for FY92 to allow processing and interpretation of the data acquired.

### **FY91 Accomplishments (01-30 September)**

Despite only two month's activity in FY91 under this award, much was accomplished, and the total funding was expended:

Survey execution The survey was conducted in September. Data reduction is very involved due to the non-coincident source and receiver lines (and the fact that the ship traversed each line segment in both directions, on different courses), and the current-induced shift of the buoyed receivers during a night's recording. Navigation by GPS and Del Norte must be recovered from the onboard computer disks and merged with the DFSV records. This merging of the full geometry and trace data will not be completed before year's end. We have extracted one night's trace data (spread 108) and a receiver gather of that night's shots is presented in Figures 1 and 2.

Complementary studies Land receiver arrays were deployed, supported by other resources, by UC Berkeley, USGS, and Stanford scientists, to complement the marine data and to extend survey coverage to wide angle. An example of land recording is illustrated in Figure 3 in a relatively short offset land-receiver gather for the same source array shown in Figure 2 for a marine receiver. A large number of land sites were occupied throughout the survey. High-resolution data also have been acquired.



AGU Poster session A special poster session has been arranged at the Fall AGU Meeting on the BASIX experiment. All aspects of the project will be featured.

### FY92 Schedule

The FY91 effort exhausted the available funding, as reduced in the actual award, with the data acquisition subcontract. No support remains with which to reduce, analyze and interpret the data - researchers participating in the experiment and data reduction until now have been supported by other projects. Assuming the supplement request is granted, we will be able to devote the necessary human resources to the study in FY92.

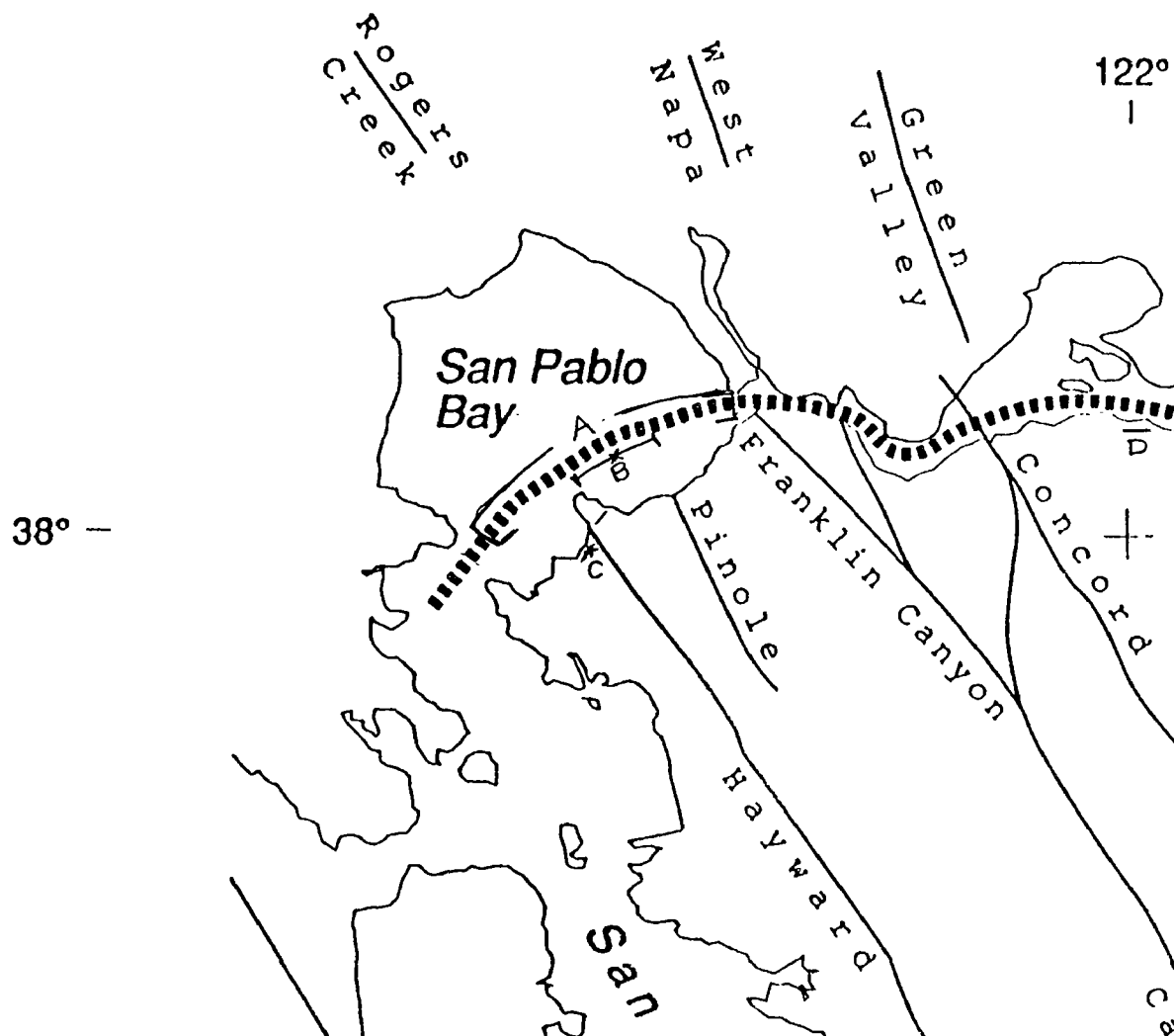


Figure 1. Map of early BASIX survey line, showing line 108 (track 'A', one night's shooting, some 700 shots) illustrated in Figures 2 and 3. Segment 'B' is the receiver spread for line 108. Figure 2 is a marine receiver gather from near the center of the spread. Figure 3 is a receiver gather from a land sensor array on Point Pinole (segment 'C'), near the western end of line 108. Segment 'D' is another land array deployed for that portion of the survey crossing the Antioch and Concord faults.

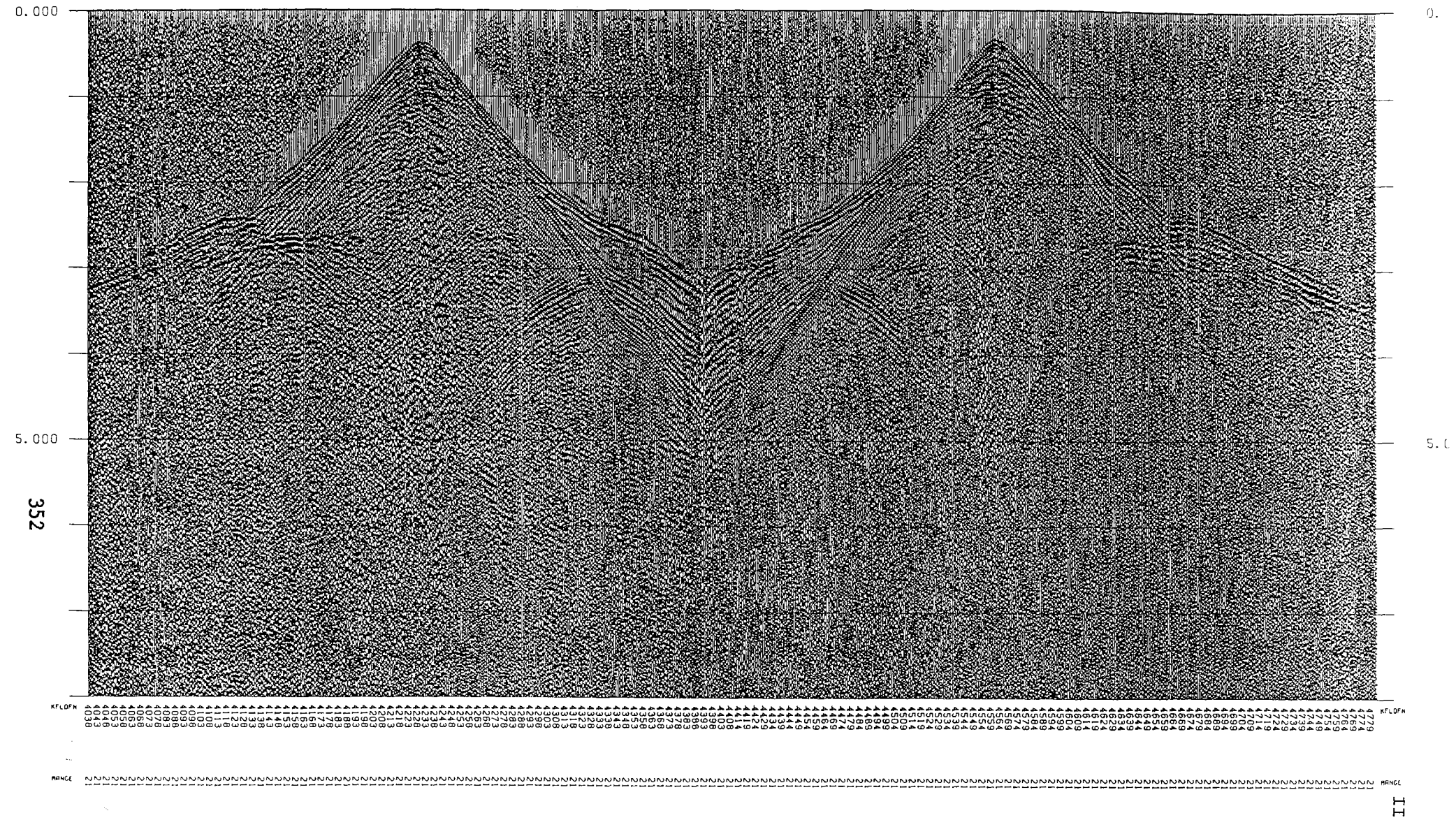
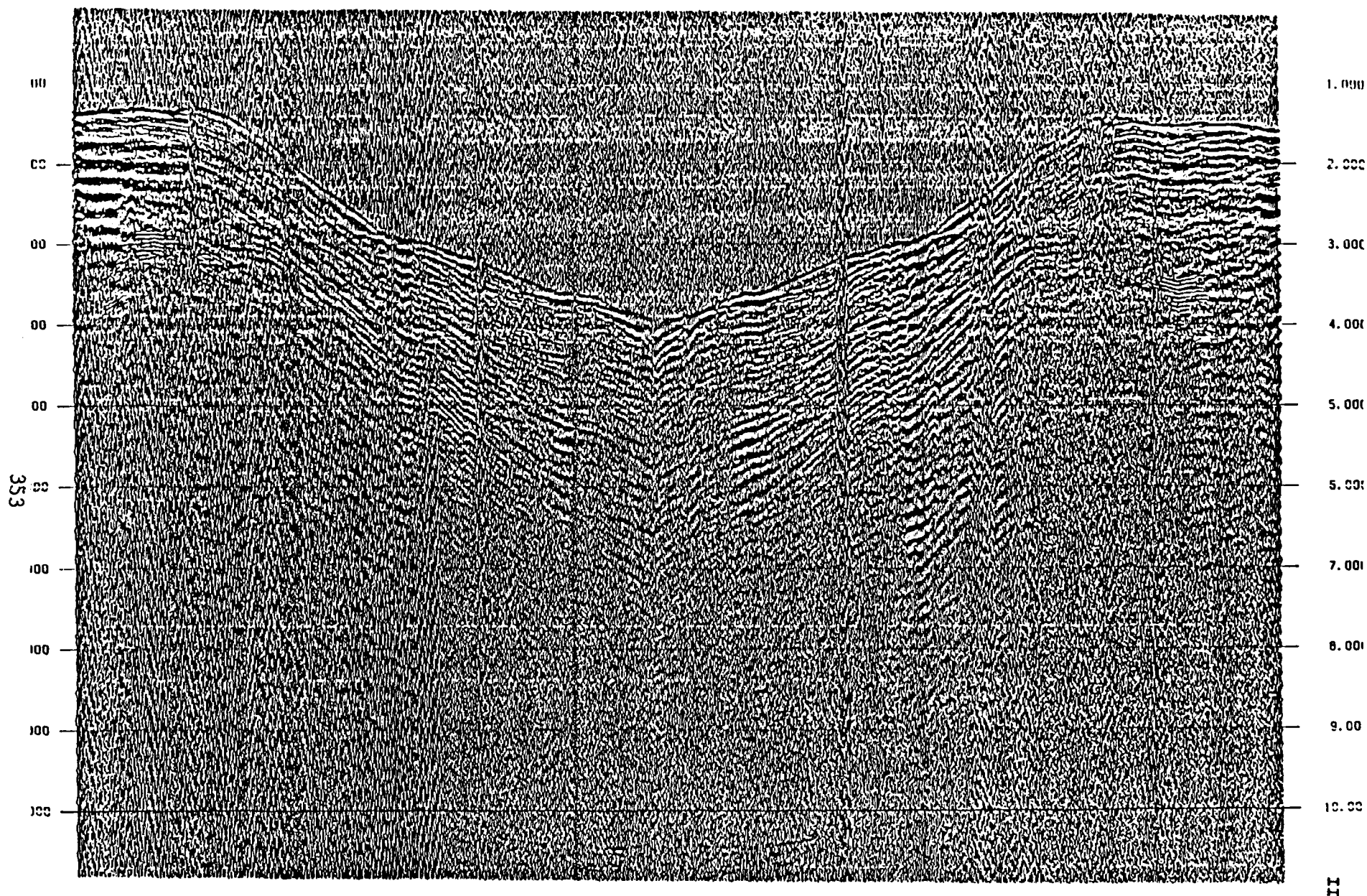


Figure 2. Receiver gather for a sensor near the center of spread 108. Eight seconds of data are shown.. Apparent symmetry of the gather reflects the 'two-way' shooting of the line segments each night. The receiver array was fixed and the ship in the course of each night's shooting ran upstream and downstream tracks.



**Figure 3.** Receiver gather for a land sensor from the Point Pinole (west) array which was deployed as the ship traversed the Hayward fault crossing in San Pablo Bay. This sensor was located on land near the west end of the marine receiver array, where the ship track turns south, on a course roughly equidistant from the receiver, explaining the near-constant offset at the ends of the symmetrical gather.

Tectonics of the Chabot-Mission faults.  
Award Number: 14-08-0001-G2136  
David L. Jones  
Department of Geology and Geophysics  
University of California  
Berkeley, CA 94720  
415-642-2514

Investigations undertaken in FY 1991.

This investigation of the Chabot-Mission fault system is aimed at increasing our understanding of an important seismogenic zone along which slip apparently is being transferred from the Calaveras fault to the Hayward fault. Despite active seismicity along this transfer zone, no surface rupture has been detected, and neither the Chabot nor the Mission faults are included in Alquist-Priolo zoning. Because the tectonic history of these faults is so poorly understood, we are currently unable to evaluate their potential for producing damaging earthquakes in the future, nor has the style of expectable fault movement (e.g., strike slip, dip-slip, or oblique slip) been clearly established.

The specific aims of this study are to: 1) determine the width of the zone of deformation that can be attributed to movement along the Chabot-Mission faults, and attempt to delineate the principal strand(s) along which the latest detectable movement has occurred; 2) establish the structural style of deformation across the entire width of the fault zone to provide long-term strain indicators necessary to establish the kinematic history of the faults; 3) search for stratigraphic and structural ties across the fault zone that will permit an assessment of the long-term history of displacement along the seismogenic zone; and 4) search for evidence that will establish the youngest episode of movement along these faults.

Preliminary investigations of the Chabot-Mission fault system commenced in August, 1991, with reconnaissance field studies in the Niles Canyon, Morrison Canyon, and Alum Rock Creek regions, in order to characterize the style of deformation within the fault zone and to collect samples for paleontologic examination. Based on these scattered and incomplete observations, the following tentative conclusions can be drawn:

1. The Mission fault system is a wide and complex fault zone that exhibits a significant component of west-vergent thrust displacement that locally places strata of Cretaceous age over Plio-Pleistocene deposits;
2. Several important contacts between stratigraphic units that previously were interpreted as depositional, are, in fact, significant faults, so the number of recognized fault strands within the fault zone has increased.

3. New stratigraphic units have been recognized, based on paleontologic criteria, that hitherto have not been identified anywhere in the Bay region. These new data will provide important constraints for analyzing the displacement history.

4. In contrast to thrust displacements observed within the Mission fault zone, the Chabot fault appears to exhibit an important component of dip-slip normal fault displacement. Thus, the relation of these two structures is not yet clear, nor has it been established where to change from compressional to extensional behavior takes place.

## Earthquakes and the Statistics of Crustal Heterogeneity

9930-03008

*Bruce R. Julian*

Branch of Seismology  
U.S. Geological Survey  
345 Middlefield Road - MS77  
Menlo Park, California 94025  
(415) 329-4797

### Investigations

Both the initiation and the stopping of earthquake ruptures are controlled by spatial heterogeneity of the mechanical properties and stress within the earth. Ruptures begin at points where the stress exceeds the strength of the rocks, and propagate until an extended region ("asperity") where the strength exceeds the pre-stress is able to stop rupture growth. The rupture termination process has the greater potential for earthquake prediction, because it controls earthquake size and because it involves a larger, and thus more easily studied, volume within the earth. Knowledge of the distribution of mechanical properties and the stress orientation and magnitude may enable one to anticipate conditions favoring extended rupture propagation. For instance, changes in the slope of the earthquake frequency-magnitude curve ("b-slope"), which have been suggested to be earthquake precursors and which often occur at the time of large earthquakes, are probably caused by an interaction between the stress field and the distribution of heterogeneities within the earth.

The purpose of this project is to develop techniques for determining the small-scale distributions of stress and mechanical properties in the earth. The distributions of elastic moduli and density are the easiest things to determine, using scattered seismic waves. Earthquake mechanisms can be used to infer stress orientation, but with a larger degree of non-uniqueness. Some important questions to be answered are:

- \*\* How strong are the heterogeneities as functions of length scale?
- \*\* How do the length scales vary with direction?
- \*\* What statistical correlations exist between heterogeneities of different parameters?
- \*\* How do the heterogeneities vary with depth and from region to region?

Scattered seismic waves provide the best data bearing on these questions. They can be used to determine the three-dimensional spatial power spectra and cross-spectra of heterogeneities in elastic moduli and density in regions from which scattering can be observed. The observations must, however, be made with seismometer

arrays to enable propagation direction to be determined. Three-component observations would also be helpful for identifying and separating different wave types and modes of propagation.

The stress within the crust is more difficult to study. Direct observations require deep boreholes and are much too expensive to be practical for mapping small-scale variations. Earthquake mechanisms, on the other hand, are easily studied and reflect the stress orientation and, less directly, its magnitude, but are often not uniquely determined by available data.

This investigation uses earthquake mechanisms and the scattering of seismic waves as tools for studying crustal heterogeneity.

## Results

### Volcanic and Geothermal Earthquake Mechanisms

Work under this project during calendar year 1991 has been devoted to seismological field experiments at geothermal areas in California and Iceland. This work, which is being carried out in collaboration with Dr. G. R. Foulger of the University of Durham, England, and is supported by a G. K. Gilbert Fellowship, is aimed at improving our understanding of "non-double-couple" (NDC) geothermal earthquakes. In the last several years, evidence has accumulated of the reality of these anomalous and poorly understood earthquakes, whose mechanisms can not be explained by shear faulting. It is likely that understanding the processes that cause NDC earthquakes will help in predicting volcanic activity and in prospecting for and exploiting geothermal energy.

A primary factor limiting our understanding of non-double-couple earthquakes has been a lack of high-quality recordings of them. The purpose of the field experiments was to obtain such data, using dense networks of three-component digitally recording instruments. The use of three-component sensors produces usable data from shear waves as well as compressional waves, and digital recording produces on-scale signals that make possible interpretation of amplitudes and waveforms, which contain far more information than do first motions alone.

The experiments were conducted at The Geysers geothermal area, California, during March and April, 1991, and at the Hengill geothermal area, Iceland, during July, August, and September. The Hengill area is the richest known source of non-double-couple earthquakes in the world. The Geysers is an area of exceptionally high seismicity, but so far no convincing evidence of NDC mechanisms has been found there.

At The Geysers, fifteen instruments were operated for 30 days in an area about 20 km in diameter. The Hengill network was larger and denser, with 30 instruments operating for 60 days in a 25-km region. Data from these instruments will be supplemented by data from permanent networks operating in the same areas: the UNOCAL Corporation's 28-station network at The Geysers, and the digital South Iceland seismic network at Hengill. The network geometries were designed on the basis of seismological considerations, and not ease of access. The location of the earthquake activity at both places was known in advance, and at

Hengill we optimized the network geometry by tracing rays through a three-dimensional crustal model of the area, obtained in a previous tomographic study. We believe this is the first time information of this type has been used in the design of a seismic experiment. At The Geysers, available information on crustal structure was less detailed, and legal constraints on access to land were severe, so the stations were deployed with the primary aim of supplementing the existing UNOCAL network.

The strategy followed, of recording continuous data instead of only computer-identified "events", greatly increased the data volume and meant that most stations had to be visited every three days. Because of the way the Hengill network was designed, half of the stations were accessible only on foot. Nonetheless, no significant data loss resulted from the strenuous nature of the field operations.

These experiments used Reftek brand recording instruments supplied by the equipment pools of the Incorporated Institutions for Research in Seismology (IRIS), and the British Natural Environment Research Council (NERC). The Hengill experiment is one of the largest yet performed using the relatively new IRIS/PASSCAL-type instruments, and one purpose of the Geysers experiment was to gain familiarity with them so as to ensure success in Iceland. Nevertheless, the rate of hardware and software failure was fairly high, and resulted in the loss of about 10% of the data in Iceland. A detailed report on the technical details of equipment performance has been written and provided to the managers of the equipment pools and other interested people.



**Proposal to Collaborate with the U.S. Geological Survey Deep  
Continental Studies Group on the North Deployment of the  
Pacific Northwest Refraction Experiment**

Agreement No. 14-08-0001-G2073

G. Randy Keller and Kate C. Miller  
Department of Geological Sciences  
The University of Texas at El Paso  
El Paso, Texas 79968-0555  
915/747-5501

The Pacific Northwest Refraction experiment was conducted in September of 1991. Final data tapes have not been prepared, but initial evaluations of the data collected were very encouraging. The University of Texas at El Paso (UTEP) focused its effort on the first deployment of this experiment which was located in the western portion of the State of Washington. UTEP students in fact surveyed the line and established the location for the seismic recording sites. UTEP was responsible for the participation of Canadian workers who brought over 200 seismograph systems to the experiment. In addition, UTEP personnel headed a 3-component recording effort which employed 28 PASSCAL (Program for Array Seismic Studies of the Continental Lithosphere) instruments. Finally, we provided 4 students to work directly with the U.S. Geological Survey and help deploy its instrumentation. After the main UTEP effort in Washington, 7 UTEP personnel continued to aid with the second deployment in the experiment. This deployment was primarily located in western Oregon.

Although it has not been possible to begin the seismic data analysis, the UTEP group has prepared a preliminary data base for the seismic measurements, constructed a series of gravity maps of the region, and thoroughly surveyed the previous literature on the region.

## **Paleoseismic Investigation of the Central and Southern Reelfoot Scarp, Tennessee**

Agreement No. 14-08-0001-G2116

Keith I. Kelson  
William Lettis & Associates  
1000 Broadway, Suite 612  
Oakland, CA 94607  
(510) 832-3716

Roy VanArsdale  
The University of Arkansas  
Department of Geology  
118 Ozark Hall  
Fayetteville, AR 72701  
(501) 575-3355

### **Objective of the Study**

- Assess the presence or absence of near-surface stratigraphic and/or structural evidence of pre-1811 large-magnitude earthquakes along the central and southern Reelfoot scarp, Lake County, Tennessee
- Refine existing geologically based estimate of the large-magnitude earthquake recurrence interval along the northwest-trending trend of seismicity within the New Madrid Seismic Zone, via near-surface excavations across the Reelfoot Scarp.
- Assess possible influences of surficial deformation associated with large-magnitude earthquakes in the Reelfoot Lake area based on middle and late Holocene meander patterns of the Mississippi River.

### **Progress to Date**

- Conducted field reconnaissance of central and southern Reelfoot Scarp and produced detailed topographic profiles of the scarp at four possible trench locations. The goal of these activities was to select and prioritize possible trench locations. The sites were prioritized based on: (1) likelihood of encountering colluvial material on the downthrown (eastern) side of the scarp; (2) scarp height and maximum slope angle; (3) vertical surface separation; (4) likelihood of encountering datable material; (5) groundwater conditions; and (6) permission to excavate from land owner and lessee.
- Obtained permission to excavate trenches and to drill hand-auger boreholes from land owners and lessees for three of four priority sites.
- Three hand-auger borings along the proposed top priority trench location (the Donaldson site) were completed in order to assess groundwater conditions and stratigraphy prior to incurring excavation costs. After excavation, five additional borings were completed within and west of the trench to provide additional stratigraphic information.

- On 8 October 1991, we excavated a 90-m-long trench across the scarp at the Donaldson site, located approximately 3 km northeast of the town of Tiptonville. The trench was 1.2 m wide and up to 3.5 m deep, and was shored using hydraulic shores per OSHA regulations. Groundwater conditions and caving side walls precluded excavating deeper than 3.5 m. Logging was conducted at a scale of 2 inches to 1 meter, between 8 October and 29 October 1991. The trench was backfilled and the area remediated on 29 and 30 October.
- Aerial photography at scales of 1:18,000 and 1:58,000 has been purchased for analysis of fluvial meander patterns in the vicinity of the Tiptonville dome. Through initial analysis of the small scale photography, we have identified several meander domains and subdomains that yield a first estimate of meander migration patterns. We have obtained soil survey maps for the entire study area and are currently compiling these maps to obtain relative age-estimates of the domains. We hope to better constrain these relative age-estimates through interaction with State of Tennessee personnel, university personnel, and private consultants also researching river pattern morphology.

### **Results to Date**

- Stratigraphy exposed in the trench included fine-grained sands and silty sands interpreted as natural levee deposits, probably from the Mississippi River, overlain by clays interpreted as overbank deposits. The stratigraphic sequence provided distinct, planar, continuous marker beds from which to assess the location and style of deformation associated with the scarp. These beds define a broad monoclinal fold having an amplitude greater than about 5 m, consisting of three smaller scale monoclines each having amplitudes of about 1 to 2 m. The eastern end of the monocline was not exposed because of the limited trench depth. Associated with each smaller scale monocline are numerous down-to-the-west normal faults having vertical separations of up to 8 cm. Because of the location of these faults within the monoclines and their decrease in amount of throw down-section, we interpret that they are probably a result of extension along the crest of the large-scale fold. Also, we interpret that if the Reelfoot fault extends to the surface, its trace lies to the east of the base of the scarp. At the Donaldson site, such an interpretation places the surface projection of the fault within or at the western margin of Reelfoot Lake.
- Colluvial deposits derived from the scarp thicken to the east away from the base of the scarp. These deposits consist of two units that either represent colluviation after the 1811-1812 earthquake episode, or colluviation after a penultimate event and after the 1811-1812 episode. We are testing the possibility of an event prior to 1811 through analysis of the amount and location of deformation of the marker beds relative to the amount and location of deformation of the present ground surface.
- Three areas exposed in the trench contain evidence of liquefaction, all of which are most likely a result of the 1811-1812 earthquakes. All three liquefaction features can be traced downward to sources in well-sorted fine-grained sand; none of the three features reaches the present ground surface.
- A deposit containing several pot sherds is inset into and provides a minimum age for the natural levee deposits exposed in the trench. Based on analysis by Tennessee Division of Archaeology personnel, the deposit containing the artifacts dates between 800 and 1000 A.D., and is most likely about 900 A.D.

- A second concentration of similar artifacts, believed to be of the same time period, lies at the top of a silty sand deposit that is located at one of the three areas containing abundant evidence of liquefaction. This lensoidal silty sand contains evidence of moderate soil development and is laterally discontinuous. It is possible that this deposit is a paleo-sand blow, although it may also be a discontinuous levee deposit. We have sampled this deposit, other unequivocal liquefaction deposits, and possible source beds for grain size analysis, in order to address the possibility that the silty sand is a paleoliquefaction deposit. If the deposit is a paleo-sand blow, the artifacts provide good temporal control on the causative earthquake. At this time, however, any evidence of a paleo-earthquake is equivocal.

### **Publications**

Kelson, K.I., VanArsdale, R., and Simpson, G.D., in preparation, Results of trenching investigations across the central Reelfoot Scarp, Lake County, Tennessee: Manuscript to be submitted to Seismological Research Letters, November, 1991.

## FAULT MECHANICS AND CHEMISTRY

9960-01485

C.-Y. King  
 Branch of Tectonophysics  
 U.S. Geological Survey  
 345 Middlefield Road, MS/977  
 Menlo Park, California 94025  
 (415) 329-4838

### Investigations

- [1] Water temperature and radon content were continuously monitored at two water wells in Parkfield, California.
- [2] Water level was continuously recorded at six other wells in central California.
- [3] Water temperature and electrical conductivity were periodically measured, and water samples were taken from most of these wells and two springs in San Jose for chemical analysis.
- [4] Implications of slip events generated on a laboratory fault are studied.

### Results

#### [1] **Earthquake Mechanism and Predictability Shown by a Laboratory Fault**

A long sequence of slip events generated in a laboratory fault model, which consists of a circilinear chain of eight spring-connected blocks that are elastically driven to slide on a frictional surface, shows the following characteristics: (1) Slip events of greatly different sizes can be generated by a fairly uniform fault. (2) Most of the strain energy is released by a few large events. (3) Large events do not recur at regular time intervals but are approximately time predictable. (4) Large events occur when strain is simultaneously built up to a critical level at most locations. They are preceded by foreshocks and triggered by the last "foreshock". (5) The positions of the blocks after large events are more irregular than the pre-event positions. (6) Smaller events tend to occur more frequently in the last half of a "seismic" cycle, however, their sizes do not increase accordingly. (7) Smaller events, although insignificant in releasing strain energy, serve to adjust the stress distribution along the fault to a condition of simultaneous strain buildup to a critical level for most blocks, in preparation for the occurrence of the next large event. (8) The recurrence relation resembles the Gutenberg-Richter relation, except for a falloff for the largest events due to finite capacity of the fault system to store energy. (9) Slip distributions are not self similar. (10) Stress drop increases with event size. (11) Stress drops for smaller events are

very small fractions of the corresponding absolute stresses. (12) Energy density along ruptured segments does not increase with event size. Larger events occur when longer segments are stressed to the critical level. (13) Rupture tends to propagate in the forward direction due to a built-in asymmetry of the model. (14) Average slip velocity increases with block displacement. (15) Duration of slip is short compared with the overall rupture time. (16) Rupture-propagation velocities scatter considerably, but tend to increase with event size and have an upper limit of P-wave velocity. (17) Rupture-initiation locations are usually not close to maximum-slip locations. (18) Very few aftershocks occur due to a lack of some time-dependent element in the model. These results imply: (1) Friction along seismogenic faults may not necessarily be very inhomogeneous. (2) Large earthquakes may be a stress-roughening process, whereas smaller earthquakes, a stress-smoothing process. (3) Earthquakes are a self-organized critical phenomenon, but not exactly fractal. (4) Short-term earthquake prediction is difficult; precursor-monitoring networks should cover an entire seismic gap, not just some perceived asperities, in order to detect the condition of simultaneous strain buildup to near-critical level. (5) Spatial extent of premonitory anomalies should increase with earthquake magnitude. (6) Hypocenters determined from telemetered data may not be rupture-initiation points as is commonly assumed. (7) Both the stress-roughening nature of large earthquakes and the presence of some time-dependent elements are needed for the generation of aftershocks.

## [2] Hydrogeochemical Measurements Along the Hayward Fault

Hydrogeochemical measurements have been made about once a month, and more frequently when needed, since 1976 at two springs in Alum Rock Park in eastern San Jose and since 1980 at two shallow wells in eastern Oakland along a 55-km segment of the Hayward fault. Temperature, electrical conductivity, and water level or flow rate are measured *in situ* with portable instruments. Water samples are taken at the same time for chemical and isotopic analyses in the laboratory.

The measured flow rate was not affected significantly by the seasonally-varying rainfalls, but it showed a long-term decrease of about 40 percent since 1987, when a five-year drought began in California. It also showed several temporary increases that lasted a few days to a few months with amplitudes of 2.4 to 8.6 times the standard deviation above the background rate. Five of these increases were each recorded a few days after an earthquake of magnitude 5.0 or larger as listed below:

<u>Date</u>	<u>Location</u>	<u>Magnitude</u>	<u>Distance (km)</u>
84-04-24	Morgan Hill	6.2	18
86-03-31	Mt. Lewis	5.7	15
88-06-13	Alum Rock	5.3	8
89-04-03	Alum Rock	5.0	5
89-10-17	Loma Prieta	7.1	40

Two of these increases are arguable because of small amplitude (1988 Alum Rock; only 2.4 standard deviations above background) or data gap (Loma Prieta). None of them appear to be caused by rainfalls or stress changes associated with the earthquakes, but they may be induced by strong seismic shaking. No significant flow increase was recorded after any smaller or more distant earthquakes, including the two magnitude 5 earthquakes that occurred near and prior to the Loma Prieta on the San Andreas fault. Two other flow increases were recorded in 1982, but they were not correlated with any significant earthquakes; these increases were possibly induced by unusually heavy rainfall.

The water in both wells showed seasonal temperature and chemical variations largely in response to rainfall. It also showed some clear chemical changes unrelated to rainfall in 1980 that lasted a few months; they were followed by some magnitude 4 earthquakes 50–80 km away. The chemical compositions at one of the wells and at the two springs also showed some longer term variations correlatable with the five listed earthquakes; these correlations suggest the possibility of a common tectonic origin. The last variation at this well occurred abruptly in 1989 shortly before a magnitude 5 earthquake 54 km away. However, no other hydrochemical changes were recorded at about the time of some 20 other earthquakes of magnitude 4.0 or larger in the study area.

## Reports

- King, C.Y., 1991, Multicycle slip distribution along a laboratory fault, *J. Geophys. Res.*, **96**, 14,377–14,381.
- King, C.Y., 1991, Multicycle slip distribution along a laboratory fault (abs.), *Eos, Trans. Am. Geophys. Union* Program and Abstracts Supplement for Spring 1991 Meeting, 275.
- King, C.Y., 1991, Earthquake source characteristics and predictability shown by a laboratory fault model (abs.), *Eos, Trans. Am. Geophys. Union*, 1991 Fall Meeting Program and Abstracts, 458.
- King, C.Y., Basler, D., Presser, T., Evans, W., White, D., 1991, Geochemical measurements along Hayward fault (abs.), submitted to *2nd Conference on Earthquake Hazards in the East San Francisco Bay Area*.

## Investigation of Seismic Wave Propagation for Determination of Crustal Structure

9950-01896

Kenneth W. King  
U.S. Geological Survey  
Branch of Geologic Risk Assessment  
Box 25046, MS 966  
Denver, CO 80225  
(303) 236-1591

### Investigations

1. Seismic refraction surveys at the U.S. Air Force Academy, Colorado Springs, Colo. (in collaboration with Earl Cassidy, USGS-WRD). During May, 1991, as part of a USGS study of ground-water contamination caused by leaking toxic materials in abandoned waste-disposal sites on the Academy grounds, twenty-five high-resolution refraction profiles were acquired to determine depth to bedrock, water table depth, and to reveal geologic structure overlying the bedrock. The profiles covered about 3000 m at three different locations on the Academy grounds.
2. Coachella Valley, Southern California (in collaboration with M.J. Rymer and R.V. Sharp, both at USGS): high-resolution seismic reflection (Mini-Sosie) studies of the southern San Andreas fault system. During April, 1991 about 19 km of reflection data were acquired in this region as part of a multidisciplinary effort to understand the regional Quaternary stratigraphy and deformation history and the location, kinematics, geometries, and rates of slip of active faults. The data were recorded with 1 s record length and 9.1 to 15.2 m shot-and-geophone intervals (sgi). These recording parameters focused on the 50 to 500 m depth range. The data were processed following the standard common depth point (CDP) technique into 12 stacked records (nominally 12-fold).
3. San Francisco Bay Area (in collaboration with M.J. Rymer, USGS): high-resolution seismic reflection (Mini-Sosie method and conventional 12-gauge shotgun source) studies of faults in Palo Alto, Los Altos, Stanford University Campus, and Mountain View, Calif. These faults, which are located in heavily populated areas, have been previously identified through geologic mapping and aerial photo interpretation. The goal of the seismic investigations is to determine the extent of these faults into unmapped areas where their existence is only inferred. These data should also provide information about Quaternary stratigraphy, deformation history, and possibly slip rates. During May, 1991 about 2.7 km of reflection data were acquired across four different faults. These data were recorded with 0.5 s record length and 1.5 to 3 m sgi to focus on the 20 to 100 m depth interval.
4. New Madrid Seismic Zone - Seismic reflection studies of the Bootheel Lineament (in collaboration with E.S. Schweig, Memphis State Univ., Memphis, TN). This study has several goals that were generally determined from interpretation of FY90 acquired seismic reflection data, they are: 1) to increase 3-D coverage of the main lineament, 2) extend seismic lines acquired in FY90 to the east and west to determine if flower structures are unique to the lineament zone, 3) to determine where possible piercing points exist, 4) to acquire new data over the best developed scarp on the lineament, and 5) to re-examine areas of incoherent reflection energy, identified on FY90 Mini-Sosie profiles, with higher resolution methods that will provide information on near-surface strata. During the summer of 1991 15.5 km of Mini-Sosie method and 2.1 km of 12-gauge shotgun source high-resolution seismic reflection data were acquired to accomplish these goals. Recording parameters of 1.5 to 2.4 m sgi for the shotgun data and 15 m sgi for the Mini-Sosie data emphasized target zones in the 10 to 500 m depth range.



5. New Madrid Seismic Zone - Seismic reflection studies of the Crittenden County fault (in collaboration with L.R. Kanter, Memphis State Univ., Memphis, TN). These data were acquired in order to extend information on this fault's geometry and location (obtained from FY90 reflection studies) further to the southwest, and to re-examine areas of incoherent reflection energy, identified on FY90 Mini-Sosie profiles, with higher resolution methods that will provide information on Holocene stratigraphy and possible faults. During the summer of 1991 about 8.0 km of Mini-Sosie method and 0.26 km of 12-gauge shotgun source high-resolution seismic reflection data were acquired. Recording parameters of 1.83 m sgi for the shotgun data and 15 m sgi for the Mini-Sosie data emphasized target zones in the 10 to 500 m depth range.
6. New Madrid Seismic Zone - (in collaboration with R.B. VanArsdale, Univ. of Arkansas, Fayetteville): Investigations for evidence of faulting beneath the margins of Crowley's Ridge at locations other than those documented by FY90 reflection studies and to determine the strikes of the faults imaged in 1990. During the summer of 1991 about 11.5 km of Mini-Sosie method and 1.6 km of 12-gauge shotgun source high-resolution seismic reflection data were acquired. Recording parameters of 2.44 m sgi for the shotgun data and 15 m sgi for the Mini-Sosie data emphasized target zones in the 10 to 500 m depth range. The shotgun source data should reveal if Quaternary strata are faulted in the regions overlying faulted Tertiary units.
7. New Madrid Seismic Zone: USGS program to acquire seismic reflection data on: 1) the Crittenden County fault, 2) features seen as surface lineations and/or structures (faults?) in vibroseis reflection profiles near Kennet, Lepanto, and Jonesboro, Arkansas, 3) the Cottonwood Grove fault near Ridgely, Tennessee, and 4) areas of incoherent reflection energy, identified on FY90 Mini-Sosie profiles, with higher resolution methods that will provide information on recent stratigraphy and possible faults. During the summer of 1991 about 23.0 km of Mini-Sosie method and 1.22 km of 12-gauge shotgun source high-resolution seismic reflection data were acquired. Recording parameters of 1.5 to 2.4 m sgi for the shotgun data and 15 m sgi for the Mini-Sosie data emphasized target zones in the 10 to 500 m depth range.
8. D.L. Carver and R.A. Williams completed a 12-gauge shotgun seismic source overhaul and upgrade. Analysis of seismic data acquired with this source showed that it produces a significant amount of undesirable acoustical noise. This noise often interferes with the arriving desirable signal. To reduce the noise longer custom-made steel barrels were designed and produced that place the seismic source discharge point further below the ground surface in order to attenuate the audible gun-blast sound. Also, in collaboration with a local firearms expert, several safety improvements were suggested for the barrels, receiver, and bolt.

## Results

1. The refraction data were interpreted and processed into depth sections that generally detail the upper 25 m of the ground surface. A bedrock surface and two-to-three overlying unconsolidated units were identified on most of the profiles. These data will be useful in tying together the information obtained from a series of boreholes drilled primarily on the perimeters of the landfills. An interpretation of the refraction study results were summarized in a letter and submitted (along with copies of the depth sections) to the USGS Water Resources Division - the agency in charge of the overall investigation.
2. Preliminary results and interpretation of the 12 CDP stacked sections indicate that zones of incoherent energy, narrowest at the surface but widening rapidly at relatively shallow depths, underlie the surface traces of these faults. The near-surface zone of incoherent energy on the San Andreas fault near Durmid Hill is nearly 1.5 km wide. Processing on all profiles is continuing.
3. These data are currently being processed into 8 stacked CDP profiles.
4. These data are currently being processed into 11 stacked CDP profiles.

5. These data are currently being processed into 5 stacked CDP profiles.
6. The data are currently being processed into 11 stacked CDP profiles.
7. The data are currently being processed into 19 stacked CDP profiles.
8. (Carver and Williams) The new barrels are thicker-walled to prevent splitting and blowouts. The shotgun receiver was also custom-built with thicker steel and reinforcements to improve reliability and safety. Field use of the re-designed source has improved productivity, primarily because the increased source durability reduced break-downs. The deeper discharge point also places the source in firmer ground and improves source coupling. The source was used in New Madrid seismic zone field work during August, 1991 and produced much less unwanted noise.

### Reports

- Kanter, L. R., E. S. Schweig, E. A. Luziatti, and K. M. Shedlock, 1991, Cenozoic deformation along the Crittenden County fault zone, northeastern Arkansas: Seis. Soc. Am. Eastern Section, 63rd Annual Meeting Program and Abstracts, Memphis.
- King, K. W., D. L. Carver, R. A. Williams, and D. M. Worley, 1991, Site response studies in west and south Seattle, Washington, in A.M. Rogers, W.J. Kockelman, G. Priest, and T.J. Walsh, eds., Assessing and Reducing Earthquake Hazards in the Pacific Northwest: U.S. Geological Survey Professional Paper, (in press).
- Nichols, T. C., R. A. Williams, K. W. King, and D. D. Eberl, 1991, Investigation of foundation problems related to heaving of soils and weathered bedrock in the Pierre Shale southwest of Denver, Colorado: U.S. Geological Survey Open File Report 91-281.
- Odum, J. K., K. M. Shedlock, J. A. Michael, D. M. Worley, and E. A. Luziatti, 1991, A seismic reflection survey of the northwestern boundary of the Reelfoot Rift near Marston, Missouri [abs.], EOS, Transactions, Am. Geophy. Union, v 72, no 44, p 429.
- Schweig, E. S., L. R. Kanter, F. Shen, Y. Li, R. B. VanArsdale, E. A. Luziatti, and K. M. Shedlock, 1991, The Bootheel Lineament: Results of trenching and shallow seismic reflection studies: Seis. Soc. Am. Eastern Section, 63rd Annual Meeting Program and Abstracts, Memphis.
- Sexton, J. L., H. Henson, P. Dial, D. Victory, and K. M. Shedlock, 1991, Mini-Sosie high-resolution seismic reflection surveys in the New Madrid seismic zone: Seis. Soc. Am. Eastern Section, 63rd Annual Meeting Program and Abstracts, Memphis.
- Shedlock, K. M., W. J. Stephenson, E. A. Luziatti, and M. J. Rymer, 1991, Near-surface structure of the San Andreas and associated faults in southern California [abs.], EOS, Transactions, Am. Geophy. Union, v 72, no 44, p 351.
- VanArsdale, R. B., E. Schweig, L. Kanter, R. Williams, and K. M. Shedlock, 1991, Preliminary study of the subsurface structure of Crowley's Ridge, northeast Arkansas: Seis. Soc. Am. Eastern Section, 63rd Annual Meeting Program and Abstracts, Memphis.
- VanArsdale, R. B., R. A. Williams, E. S. Schweig III, L. R. Kanter, K. M. Shedlock, K. W. King, G. Sherer, W. McMurtrey, and E. Luziatti, Shallow seismic reflection surveys in the New Madrid seismic zone - preliminary seismic reflection study of Crowley's Ridge, northeast Arkansas: Seism. Res. Lett. (in review).

## Central Aleutians Islands Seismic Network

Agreement No. 14-08-0001-A0259

Carl Kisslinger and Bruce Kindel  
Cooperative Institute for Research in Environmental Sciences  
Campus Box 216, University of Colorado  
Boulder, Colorado 80309

(303) 492-6089

### Brief Description of Instrumentation and Data Reduction Methods

The Adak seismic network consists of 13 high-gain, high-frequency, two-component seismic stations and one six-component station (ADK) located at the Adak Naval Base. Station ADK has been in operation since the mid-1960s; nine of the additional stations were installed in 1974, three in 1975, and one each in 1976 and 1977.

Data from the stations are FM-telemetered to receiving sites near the Naval Base, and are then transferred by cable to the Observatory on the Base. Data were originally recorded by Develocorder on 16 mm film; since 1980 the film recordings are back-up and the primary form of data recording has been on analog magnetic tape. The tapes are mailed to CIRES once a week.

At CIRES, the analog tapes are played back through an analog-to-digital (a-to-d) converter into a computer at four-times the speed at which they were recorded. This computer then digitizes the data, automatically detects events, demultiplexes each event, and writes them to disk. These events are edited to eliminate spurious triggers, and a tape containing only seismic events is created. All subsequent processing is done from this tape. Times of arrival and wave amplitudes are read from an interactive graphics display terminal. The earthquakes are located using a program originally developed for this project by E. R. Engdahl, which has been modified several times since.

### Termination of the Network

By decision of the U.S.G.S., the Central Aleutian Islands Seismic Network (CASN) is terminated. The clean up of the station sites and recording equipment will be completed in the spring or early summer of 1992, when weather permits field operations. Responsibility for station ADK, the observatory, and the vault has been returned to the U.S.G.S. Support of the operation of station ADK by CIRES stopped on November 1, 1991.

In view of the decision to close the network, no maintenance was performed during 1991. As of January 1991, so few stations remained in operation due to battery failures, that a decision was made to cease all recording.

### Current Observations

The catalog produced by the CASN extends from August, 1974 through September, 1990. A partial gap exists for May, 1986 through 1988 because of the work

load created by the number of aftershocks from the May 7, 1986 earthquake. Work in 1991 has concentrated on cleaning up as much of this backlog as possible with available resources.

Some of the older data (early 1980s) that were archived on to 9-track tapes have been lost because of the natural deterioration of these tapes with age. For this reason, all archived wave-form data have been transferred to 8mm (Exabyte) tapes, which supposedly have a longer shelf life and require significantly less storage space.

The location work for this report includes: (1) 482 earthquakes located for January through May, 1989; (2) 218 earthquakes located for October through December, 1989; (3) 77 earthquakes located for January and February, 1990; and, (4) 239 earthquakes located for June through September, 1990.

The total of events located for all time periods is 1016. Forty-two of the 1989 events and ten of the 1990 events, which were located with data from the Adak network, were also large enough to be located teleseismically (U.S.G.S. PDEs). The epicenters of the 1989 and 1990 events are shown in Figures 1 and 2, respectively.

Cross-sections for the 1989 and 1990 data and a catalog of all hypocenters determined for the time period reported are included in our Semi-Annual Data Report to the U.S.G.S. Recent research using these data is reported in the Technical Summary for U.S.G.S. Grant No. G1368.

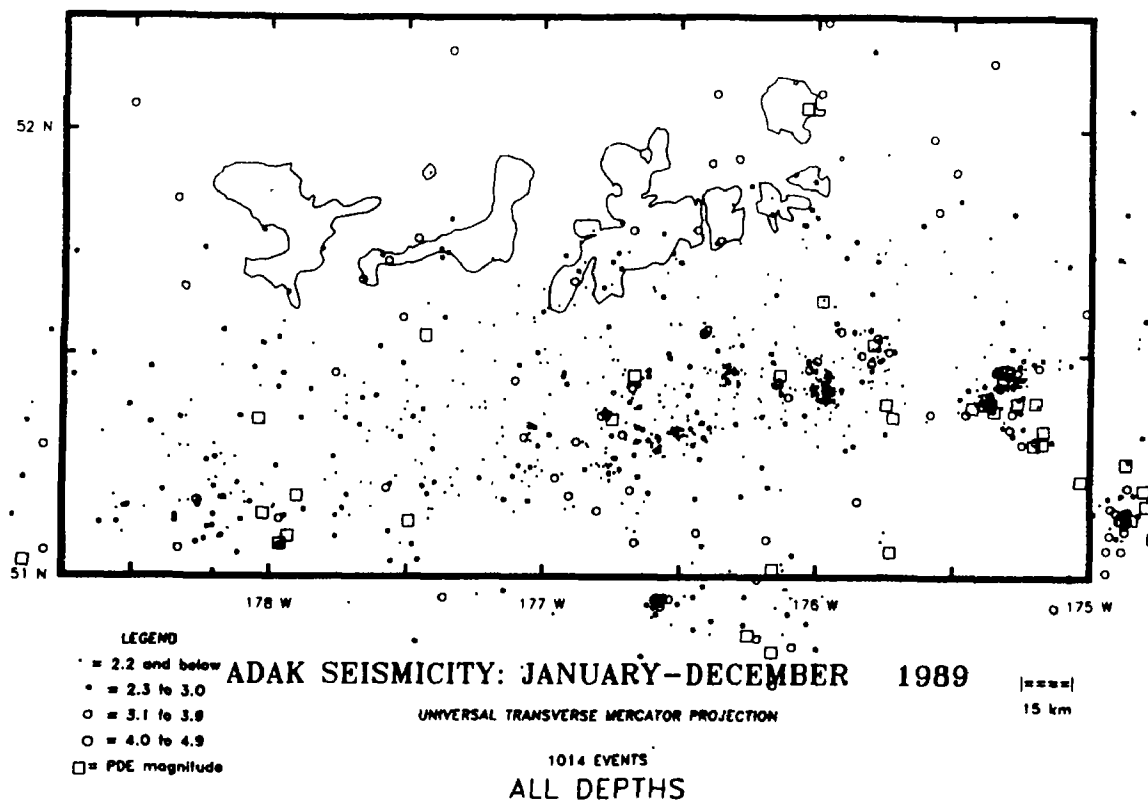


**Figure 1:** Map of seismicity located for January through December, 1989. Events located for this report include January through May, and October through December, 1989. All epicenters were determined from Adak network data. Events marked with squares are those for which a teleseismic body-wave magnitude has been determined by the U.S.G.S.; all other events are shown by symbols which indicate the duration magnitude determined from Adak network data. The islands mapped (from Tanaga on the west to Great Sitkin on the east) indicate the geographic extent of the Adak seismic network.

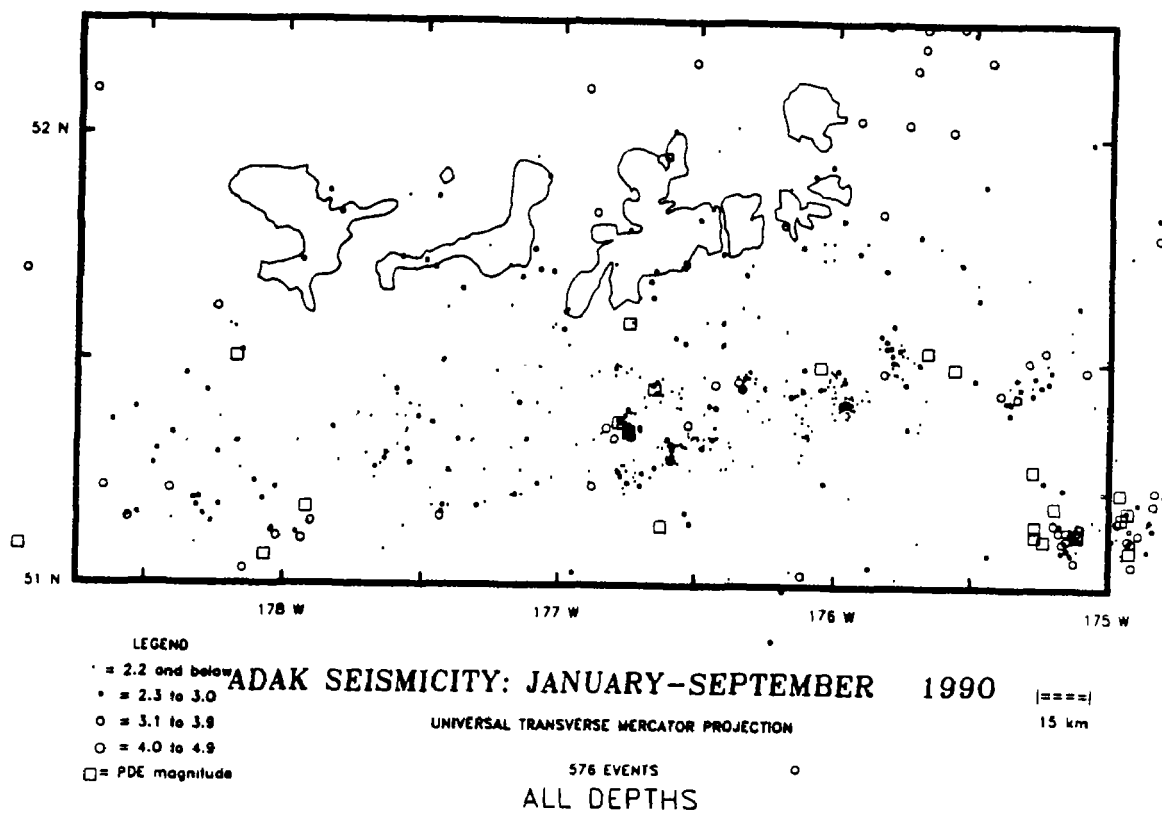


**Figure 2:** Map of seismicity located for January through September, 1990. Events located for this report include January and February, and June through September, 1990. Symbols as in Figure 1.

## Alaska Seismic Studies

9930-01162

John C. Lahr, Christopher D. Stephens,  
Robert A. Page, Kent A. Fogleman  
Branch of Seismology  
U. S. Geological Survey  
345 Middlefield Road, Mail Stop 977  
Menlo Park, California 94025  
(415) 329-4744

Investigations

1. Cooperated with the Geophysical Institute of the University of Alaska (UAGI) and the USGS National Earthquake Information Center (NEIC) in the operation of the Alaska Earthquake Information Center (AEIC) in Fairbanks. The AEIC is responsible for recording and analyzing Alaskan earthquake data and disseminating earthquake information and advisories to government agencies and to the public. As part of AEIC, continued lead role in collection and analysis of data from the high-gain short-period seismograph network extending across southern Alaska from the volcanic arc west of Cook Inlet to Yakutat Bay, and inland across the Chugach Mountains.

2. Cooperated with the Branch of Igneous and Geothermal Processes, UAGI, and the Alaska Division of Geological and Geophysical Surveys in operating the Alaska Volcano Observatory (AVO). Under this program, we have principal responsibility for monitoring the seismicity of Redoubt, Spurr, and Hayes, the three most northern Aleutian arc volcanoes.

3. Cooperated with the Branch of Engineering Seismology and Geology and the UAGI in operating 15 strong-motion accelerographs in southern Alaska, including 11 between Icy Bay and Cordova in the area of the Yakataga seismic gap. The instrument at Icy Bay was removed from an unsatisfactory location in July and will be reinstalled in 1992.

Results

1. Preliminary hypocenters have been determined by the AEIC for 3029 earthquakes that occurred in southern Alaska during the period January-June 1991 (Figures 1 and 2). Twelve of these events had magnitudes of 4.5  $m_b$  and larger. Focal mechanisms for about 300 of these events were determined using initial P-wave polarities.

The largest shock to occur beneath central and southern Alaska was a magnitude 6.1  $m_b$  shock on May 1 located 114 km deep within the Wadati-Benioff seismic zone (WBZ) and about 160 km NNW of Anchorage (62.5°N, 151.4°W). This shock was felt widely throughout southern Alaska and caused slight damage in the epicentral area (NEIC). No immediate aftershocks were detected, but this is not

unusual for intermediate-depth earthquakes. In contrast, eight well-recorded aftershocks were detected for a much shallower WBZ shock of magnitude 5.4  $m_b$  that occurred on April 26 and was located 38 km deep in the WBZ about 15 km WNW of Anchorage (61.3°N, 150.2°W). Accurate relative locations of the mainshock and its aftershocks are aligned along a NNE trend similar to the strike of one of the nodal planes of the mainshock focal mechanism (Figure 3), thus constraining this to be the probable fault plane. Relatively few WBZ shocks in southern Alaska have had aftershock sequences from which the orientation of the rupture surface can be constrained.

The most unusual earthquake occurrence was a 6.2  $m_b$  (6.5  $M_s$ ) shock on February 21 located at shallow depth near the edge of the continental shelf in the Bering Sea (58.43°N, 175.45°W; not shown in figures), an area devoid of historical seismicity. This event generated a small tsunami with maximum wave heights of 30 cm at Dutch Harbor and 22 cm at Adak (NEIC). A magnitude 5.0  $m_b$  foreshock preceded the mainshock by 40 min, and six aftershocks with magnitudes of 3.4–4.1  $m_b$  followed within 8 hours. From the focal mechanism of the mainshock and tectonic considerations this event is interpreted as having involved normal faulting with a large component of left-lateral strike-slip within a WNW-ESE-trending graben structure inboard of the continental margin (Mike Marlow, personal communication, 1991).

A magnitude 5.5  $m_b$  crustal shock on June 24 was located close to the Fairweather fault trace near Cross Sound (58.4°N, 137.1°W). The focal mechanism determined from initial P-wave polarities is compatible with dextral motion on a nearly vertical plane with a strike closely aligned with the local trend of the fault. One aftershock (4.7 ML, PMR) was detected. In January 30, a magnitude 4.0  $m_b$  shock was located a few km southeast of the June earthquake.

Other notable crustal shocks include: continuing aftershock activity in the northern Gulf of Alaska (near longitude 143° W and south of latitude 59°N) from a sequence of three large earthquakes in 1987–88 (Lahr and others, 1988); a magnitude 4.4  $m_b$  shock on February 19 beneath northern Cook Inlet (61.0°N, 150.9°W) in an area that has experienced an elevated level of activity for about the last 2½ yr; a magnitude 4.1  $m_b$  event in western Alaska (61.9°N, 160.1°W; not shown in figures) on January 26 and a magnitude 4.3 ML shock on June 28 (58.4°N, 155.8°W), both in areas characterized by low rates of seismicity; and a tightly clustered swarm of 17 events with magnitudes ranging from 0.9–3.2 that were located along the Lake Clark fault near 60.4°N, 153.7°W and occurred between January and April.

No unusual patterns of seismicity were observed in or around the Yakataga seismic gap.

2. The location program HYPOELLIPSE (Lahr, 1989) has been modified to compute travel times and emergence angles for events that are located at a higher elevation than the recording station.



This feature was required for use around volcanoes, due to their topographic relief and the very shallow depths of many of the volcanic events. The elevation ( $E_0$ ) of the "top" of the flat-layered velocity model is specified, and should correspond to the elevation in kilometers above sea level of the highest point in the region. Station elevations are also specified with respect to sea level, and a station may be located within any layer of the model. Earthquake depths are computed with respect to sea level, so negative depths, up to  $-E_0$  km, are allowed.

3. During July an active seismic experiment was conducted on Redoubt volcano. The permanent network, with seismic equipment at 8 sites, was augmented by 20 PASSCAL instruments which were installed between July 3 to 9 and removed on July 25 and 26. The PASSCAL instruments were arranged in three linear arrays, extending from the summit down the flanks of Redoubt to the north, southwest, and southeast. Four 1000-lb charges were detonated, three in glacial kettles near the end of the arrays, and one in a glacial crevasse a few hundred meters south of the dome.

Preliminary analysis of data from the shots has been used to develop a new velocity model for Redoubt. The new model was used to relocate seismic activity that accompanied the 1989-1990 Redoubt eruption (Figure 4).

4. Preliminary results from a more detailed analysis of seismic events from the energetic swarm that beginning about one day prior to the initial eruption of Redoubt volcano on December 14, 1989, have shown that for at least the first 16 hr nearly all of the events have strikingly similar waveforms. Moreover, although the dominant frequencies in the spectra of the events vary with station distance and azimuth, spectral peaks occur at the same frequencies for all of the stations. These observations suggest that the events may have been generated by repeated excitation of the same source. Initial modelling (Bernard Chouet, personal communication, 1991) has shown that the observed spectral characteristics can be explained by vibrations within a single fluid-filled crack having dimensions on the order of 250 m.

5. A new velocity model that includes station corrections has been derived for the area around Mt. Spurr using local earthquakes that were well-recorded by the recently upgraded network. Using this model the average RMS residual for a set of 1,399 earthquakes that occurred between 1980-1989 was reduced from 0.20 to 0.05 s, and concentrations of hypocenters appear to be more tightly grouped. Beneath the volcanic edifice, seismicity occurs between depths of 2 and 9 km below the summit, and at least five distinct centers of seismicity can be resolved: a main cluster about 4 km across that has been continually active since at least 1980, a second cluster offset 2 km to the north which primarily comprises earthquakes from an intense swarm that occurred in 1982 (Page and others, 1982), two less active zones centered about 7 and 15 km west of the main cluster, and a zone beneath Crater Peak 4 km south of the main cluster which was the locus of a swarm that occurred in

August 1991. A previously diffuse zone of seismicity centered about 15 km south of Mt. Spurr near the Chackachatna River now appears to contain at least three clusters that together form a zone with a distinct SW-NE trend subparallel to but offset by about 5 km to the northwest from the Lake Clark fault.

6. Absolute pressure transducers were installed at Anchorage, Sterling, and Homer, and a differential pressure transducer was installed at the Drift River (DFR) seismic station 12 km north of Redoubt volcano. These sensors will be used in conjunction with seismic data to monitor the Cook Inlet volcanoes for explosive eruptions.

### References

- Lahr, J. C., 1989, HYPOELLIPSE/Version 2, a computer program for determining local earthquake hypocentral parameters, magnitude, and first motion pattern, U. S. Geol. Surv. Open-File Report 89-116, 94 p.
- Lahr, J. C., R. A. Page, C. D. Stephens, and D. H. Christensen, 1988, Unusual earthquakes in the Gulf of Alaska and fragmentation of the Pacific Plate, Geophys. Res. Let., v. 15, p. 1483-1486.
- Page, R. A., J. A. Waller, and C. D. Stephens, 1982, Recent seismicity around Spurr, Redoubt, and Iliamna volcanoes, southern Alaska, Proc. 33rd Alaska Sci. Conf., 1982, Amer. Assoc. Adv. Sci, Arctic Div., p. 129.

### Reports

- Jolly, A. D., R. A. Page, C. D. Stephens, and J. C. Lahr, 1991, Seismicity in the vicinity of Mt. Spurr volcano, south-central Alaska, based on a revised velocity model [abs.], EOS, Trans. Amer. Geophys. Union, v. 72, n. 44, p. 567.

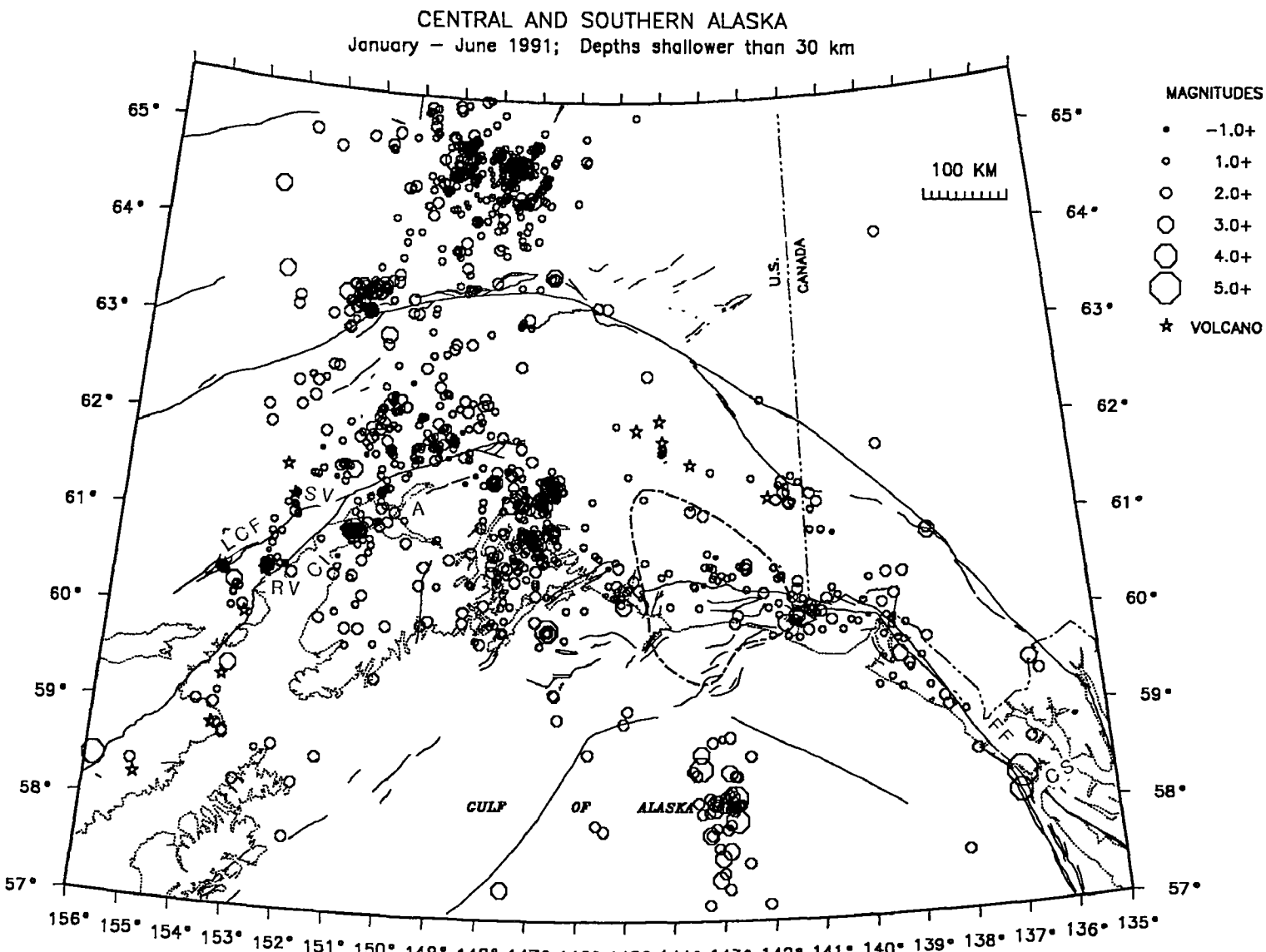


Figure 1. Epicenters of 1426 shallow earthquakes that occurred between January and June 1991. Magnitudes are determined from amplitudes of seismic signals; the magnitude threshold for completeness varies across the network. Contour with alternating long and short dashes outlines inferred extent of Yakataga seismic gap. Neogene and younger faults (George Plafker, personal communication, 1988) are shown as solid lines. A - Anchorage, CI - Cook Inlet, CS - Cross Sound, FF - Fairweather fault, LCF - Lake Clark fault, RV - Redoubt volcano, SV - Spurr volcano.

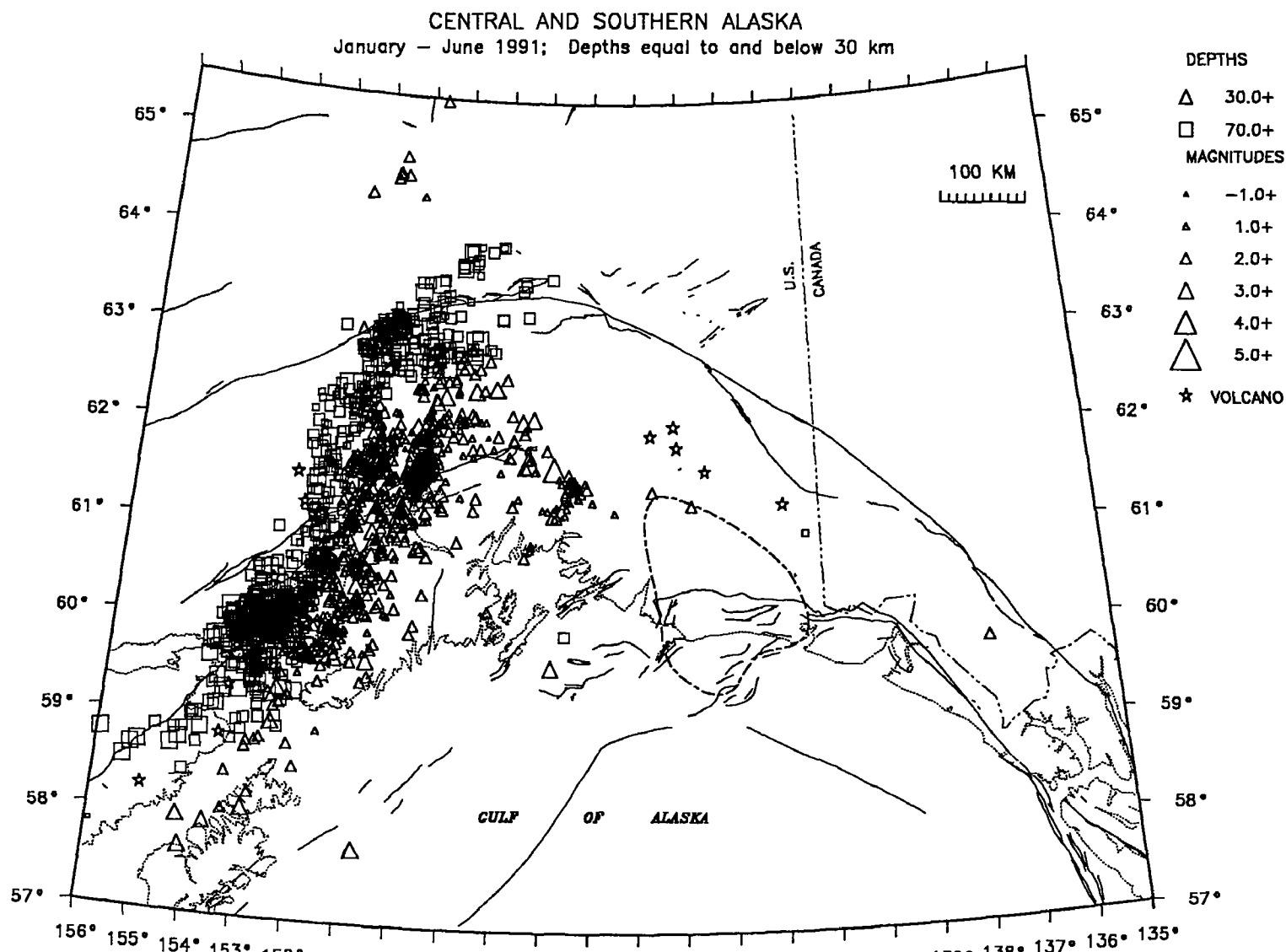


Figure 2. Epicenters of 1603 shocks deeper than 30 km that occurred between January and June 1991. Depths of earthquakes north of 64.5° N are suspect. See Figure 1 for details about magnitudes and identification of map features.

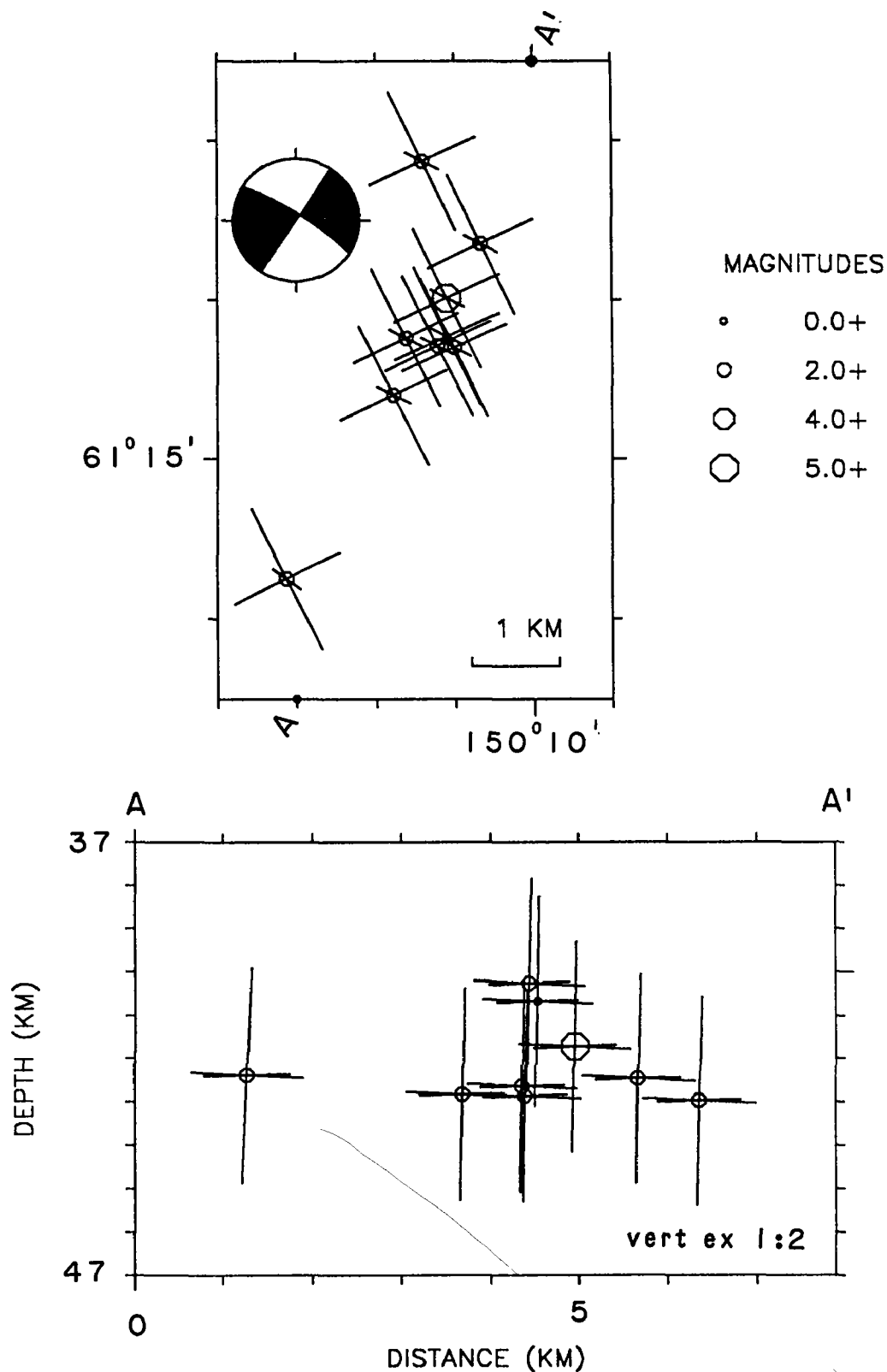


Figure 3. (upper) Relocated epicenters of the April 26 mainshock and six aftershocks determined using a homogeneous set of seismic phases. Axes of 68% confidence error ellipsoids are shown as bars. Focal mechanism of the mainshock determined from initial P-wave polarities is shown as equal area projection of lower hemisphere, compressional quadrants shaded. (lower) Hypocenters projected onto vertical plane oriented along line A-A' indicated above. Note 1:2 vertical exaggeration and that top of depth axis is at 37 km.

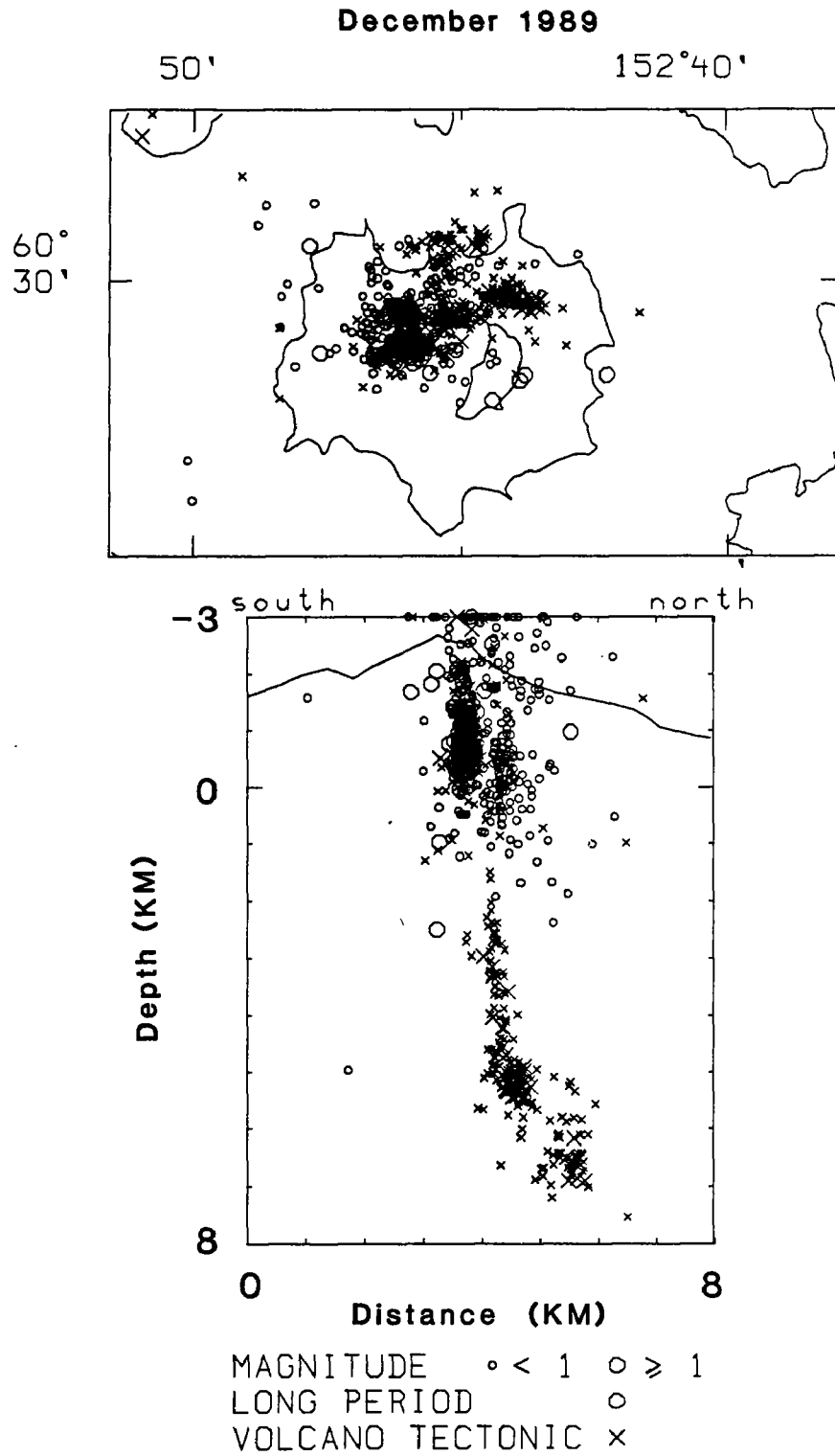


Figure 4. Map and north-south oriented cross section of volcanic activity recorded near Redoubt volcano during December 1989.

## **Coastal Tectonics Western United States**

9910-01623

Kenneth R. Lajoie  
Branch Engineering Seismology and Geology  
U. S. Geological Survey  
345 Middlefield Road MS 977  
Menlo Park, California 94025  
(415) 329-5747

### **Investigations**

The principal subject of investigation is the study of recent and coseismic deformation along the Pacific coast of the United States with. Particular focus is in the southern California area. Opportunistic investigations outside this subject and area are undertaken when necessary, or if data pertinent to the general field of coastal tectonics can be obtained at minimal cost and effort.

1. Mono Basin earthquake, October 23, 1990. With Malcolm Clark, David Hill, Alan Lindh, David Openheimer and James Yount.
2. Coastal tectonics central Chile. With Steve Ward (UC Santa Cruz) and Sergio Barrientos (U Chile).
3. Pleistocene deformation Los Angeles Basin, California. With Steve Ward (UC Santa Cruz) and Dan Ponti.
4. Pleistocene deformation Camarillo Hills Ventura County, California. With Dan Ponti and Chuck Powell.
5. Pasadena earthquake, June 27, 1991. With Dan Ponti.
6. Feasibility study of ESR dating technique. With Tracy Furutani.

### **Results**

1. A M5 earthquake struck Mono Basin east of Yosemite National Park on October 23, 1990 at 11:15 P.M. PDST. Seismic data (Openheimer) show that one foreshock preceded the mainshock by eight seconds, and at least 67 aftershocks occurred between October 24 and

December 22. Because the seismic network east of the Sierra Nevada is sparse, derived epicenters and focal depths are fair to poor. First-motion data from the foreshock, the mainshock and two aftershocks indicate the rupture occurred on either a plane striking  $332^\circ$  and dipping  $75^\circ$  southwest, or a plane striking  $55^\circ$  and dipping  $75^\circ$  southeast. The trends of both planes parallel the trends of regional faults (Figure 1), including the nearby Sierra Nevada range-front fault. The direction of extension for normal-oblique slip on either plane parallels the direction of estimated regional extension based on geologic data. However, neither seismic nor geologic data constrain the rupture to either possible plane. The rupture could have occurred on the range-front fault, or on a fault antithetic to it. The initial magnitude estimate of 5.7-6.0 from seismic stations west of the Sierra Nevada suggested possible ground rupture and serious damage from primary and secondary seismic effects. Field observations (Clark and Yount) revealed no surface rupture on faults in the epicentral region and only minor damage in Mono Basin and the surrounding area. The damage consisted mostly of minor landslides in road cuts and objects knocked from shelves. The sparse data indicate a maximum Modified Mercalli intensity of V to VI about 6 km south of the epicenter. The earthquake was felt in San Francisco, 290-km west of Mono Basin. This fact and the initial overestimation of the magnitude suggest that seismic attenuation through the root of the Sierra Nevada is lower than previously assumed.

2. Preliminary data from emergent marine terraces at a few localities in central Chile between latitudes  $28^\circ$  and  $38^\circ$  south yield regional uplift rates of 0.1 to 0.4 m/ka. Fluvial terraces along a few of the major rivers reveal no tilt perpendicular to the coastline over at least the last 1.2 my. Tilted marine terraces and uplift rates greater than 1.0 m/ka are rare and where present probably reflect local complications in the otherwise uniform subduction process. On the Arauco Peninsula ( $38^\circ$  south) three emergent Pleistocene strandlines are warped across a broad anticline (Kaizuka and others, 1973). Assuming an age of 120 ka for the lowest strandline yields an uplift rate of 1.9 m/ka at the axis of the fold; this rate is among the highest known Pleistocene uplift rates in the world. Mocha Island and Santa Maria Island, which lie north and south of the headland of the Arauco Peninsula, respectively, both have extensive sets of emergent Holocene strandlines. Correlating the highest strandlines on Mocha and Santa Maria with the break in the Holocene sea level curve yields uplift rates of 6.6 and 2.9 m/ka, respectively. On Mocha at least 31 beach ridges form up to eleven poorly defined terraces, but no ridge or terrace can be traced around the island. The highest terrace at 35 m correlates with the sea-level curve at 7.2 ka and -14 m. On Santa Maria up to 41 beach ridges also form eleven poorly defined terraces. The highest terrace at 12 m correlates with the sea-level curve at 5.1 ka and -5 m. The origin of the ridges and terraces on these two islands is uncertain. The terraces might reflect coseismic uplift and the ridges might reflect major storms. In any event, the rapid uplift of the islands probably reflects significant coseismic slip on steeply dipping secondary faults above the main megathrust. If



so, the coseismic slip on the megathrust during the great 1960 earthquake may have been uniform, not variable as previously modeled. Also, a small rupture on a steeply dipping secondary fault could produce greater uplift than a major rupture on the megathrust.

3. Data from space geodesy reveals about 8 mm/yr of north-south crustal shortening in the northern part of the Los Angeles basin between the San Gabriel Mountains and the Palos Verdes peninsula (Ward). Geomorphic data suggest that most of this movement occurs on the north dipping frontal fault system along the southern margin of the San Gabriels (Lajoie). But, some of the movement most likely occurs on the southeast dipping Palos Verdes fault. Slip on the Palos Verdes fault could be estimated by inverting the crustal deformation reflected in the numerous emergent Pleistocene marine terraces that notch the flanks of the Palos Verdes Peninsula (Ward). Published data from Woodring and others (1946) were revised to estimate the elevations of the shoreline angles of the terraces (Lajoie). The ages of terraces 5 and 7, the two most continuous terraces, are estimated to be 295-355 and 580-780 ka, respectively. These ages are derived by extrapolating an uplift rate of 0.21 m/ka based on amino-acid age estimates of three lower terraces (Ponti, Lajoie). If the uplift of the Peninsula results entirely from repeated thrust displacements on the Palos Verdes fault it is possible to estimate its geometry and slip rate. Preliminary computer modeling (Ward) indicates that earthquakes of magnitude 6.0 and 6.5 would recur every 150 and 900 years, respectively.
4. Recent excavations for residential development in the Camarillo Hills in Ventura County exposed a thick section of Pleistocene continental and marine sediments, which are warped into a tight anticline. The topography of the hills mimics the anticline, indicating young and possibly ongoing deformation. We (Ponti and Lajoie) visited the site to map the stratigraphy, collect sediment samples for paleomagnetic analysis and collect fossil shells for dating purposes. The fossil assemblage is similar to many other warm embayment assemblages in the Los Angeles basin believed to correlate with the 300-ka sea-level highstand (Powell). Our preliminary paleomagnetic data indicate normal polarity, but paleomagnetic data by others suggests that part of the section has reversed polarity. Amino-acid and ESR data should provide a more secure age for these highly deformed sediments.
5. A M6 earthquake struck the Pasadena area on June 27, 1991 at 7:45 A.M. PDST. We (Ponti and Lajoie) were in the Camarillo area at the time and proceeded to Pasadena to investigate possible primary and secondary effects. We found no surface rupture at several localities where the Sierra Madre fault is well exposed. Secondary effects included landslides on steep slopes and significant structural damage, mainly to brick buildings and chimnies.
6. While investigating various aspects of dating Quaternary marine shells by the ESR technique, a means of dating carbonatites was established. Also, ESR data from marine shells

at a primary test site near Santa Barbara yield a preliminary age of 122 ka. Previous amino-acid data yielded a suspect age of 40-60 ka. Natural radiation (gama) levels in the ground were estimated for several sites in central Chile by conducting ESR analyses of fossil marine shells from marine terraces whose ages have been reasonably estimated.

## **Reports**

Clark, M. C., Hill, D., Lajoie, K. R., Lindh, A. R., Openheimer, D. and Yount, J. C., 1991, Mono Basin Earthquake of October 23, 1990: USGS administrative report.

## Geodetic Strain Monitoring

9960-02156

*John Langbein*

Branch of Tectonophysics  
U.S. Geological Survey  
345 Middlefield Road MS/977  
Menlo Park, California 94025  
(415) 329-4853

### Investigations

Two-color geodimeters are used to survey, repeatedly, geodetic networks within selected regions of California that are tectonically active. This distance measuring instrument has a precision of 0.1 to 0.2 ppm of the baseline length. Currently, crustal deformation is being monitored within the south moat of the Long Valley caldera in eastern California, across the San Andreas fault at Parkfield, California, at three locations near Palmdale, California on a section of the San Andreas fault that is within its Big Bend region, and at two locations near Pinon Flat, California. Periodic comparisons with other other two-color geodimeters are conducted both at Parkfield and at Mammoth Lakes. These intercomparisons measurements serve as a calibration to monitor the relative stabilities of these instruments.

### Results

#### **1. Long Valley Caldera**

The line length changes measured using a two-color geodimeter still show high extension rates within the Long Valley Caldera. Figure 1 shows the line-length changes measured from mid 1983 to 27 monuments using our centrally located monument at CASA. The location of these baselines along with other baselines that are infrequently measured is shown in Figure 2. As discussed in previous Technical Summaries, the rates of extension decreased steadily from mid 1983 through mid 1989. However, in October 1989, the extension rates picked-up dramatically, most notably for KRAKA-TAU and KNOLLS. Several months after the noted increase in strain rate, the rate of earthquake swarm activity increased. This temporal relation between deformation and seismic activity is illustrated in Figure 3.

By modeling the geodetic data since 1983 using a combination of point sources to represent magma intrusion and rectangular dislocations to represent fault slip in the south moat, we have inferred that the most recent round of deformation is primarily a result of inflation directly beneath the central part of the resurgent dome of this caldera. In contrast, the deformation during 1983 to 1985 was a result of a combination of right lateral fault slip in the south moat and broad zone of inflation within the resurgent dome. The results from modeling suggest that the inflation sources have remained at 7 to 8 km depth for the past 8 years.

## 2. Parkfield

Frequent measurements of a 17 baseline networks are made for a geodetic network near Parkfield, California. Approximately one-half of these baselines straddle the San Andreas Fault along the segment that last ruptured in 1966. The data from these baselines are shown in Figures 4a and 4b.

In Figure 5, I have taken the liberty to compress the measured length changes into a 3 component model which facilitates the detection short-term anomalies. In this particular model, I have extracted parameters for slip of the San Andreas fault, areal dilatation, and tensor shear along the San Andreas. The modeled slip is for the 5 km long segment centered at CARR and it is assumed that the inferred slip is uniform from the surface down to 20 km. Of course, the measured line-length changes are most sensitive to the shallow component of slip. The inferred shear strain factors into the slip (or its deficit) that has not been adequately modeled by the slip on the CARR segment and adjacent segments NW and SE of CARR. Finally, the areal dilatation is a combination of both tectonic dilatation plus and changes in the stability of this particular instrument. The stability is periodically checked with a second, two-color instrument. These periodic measurements have shown that the apparent large fluctuations in areal dilatation as measured by the Parkfield instrument during most of 1989 and part of 1990 are most likely caused by drift of the Parkfield instrument. The bottom trace shows the difference in the apparent dilatation of the two instruments. If it is assumed that the second instrument has not drifted, then the correlation between the differential measurements in the last trace are correlated with the areal dilatation detected by the Parkfield instrument.

The high background shear strain rate of  $0.7\text{ppm/yr}$  is a result of the model assumptions of zero slip rate below 20 km and to the NW and to the SE of the CARR segment. Had we used more realistic rates for these patches on the fault plane, the value of secular shear would be reduced. Finally, a change in shear strain could be caused by a change in slip on these unmodeled segments or a regional change.

The apparent long-term variations, especially in shear, are purely an artifact of the model being a poor fit to the entire data set. In computing these parameters, the computer algorithm fits a time function of these three parameters to a 3 month long epoch. To extend the model in time by 2 months, a second set of parameters are estimated for the following 3 month interval having a 1 month overlap with the first epoch. The parameters from the 5 month long interval are combined using the results from the 1 month long overlap. This process was continued for the time span since mid 1986. Although the model from any 3 month epoch provides an adequate fit to its 3-month long data section, the predicted line-length changes from the model over the 5 year interval do not fit the observations.

## 3. Palmdale

We currently measure the line-length changes from 3 networks near Palmdale, California. The concept for these networks is to monitor variations in strain accumulation both spatially and temporally within a confined tectonic setting. The results from 2 of these networks are shown in Figure 6 and in the table. For the third network, known as the Buttes, we have only two measurements of line-lengths, one set that has made in March 1991 and the second was made 6 months later. Because of the short interval, we have not computed the strain rate for this network. However, data from the Buttes should be an important component in estimating the spatial distribution of strain since this network is located approximately 35 km north of the San Andreas Fault in the

Mojave desert.

The other two networks straddle the San Andreas fault, but are located approximately 50 km apart. The Pearblossom network consists of 12 radially distributed baselines that use a single monument as the central instrument station. In contrast, the Palmdale network consists mostly of a subset of baselines that were measured by the Geodolite. We currently use four stations, BURN, LEONA, MINT and RITTER RIDGE as central stations and measure distance using a two-color geodimeter to those monuments that are within 10 km of these central points. To make each of the four sub-networks with a radial distribution of baselines, we have installed a few extra monuments. Thus our Palmdale network consists of 30 baselines which can be measured with the two-color.

At Pearblossom, we now have measurements of line length change since 1980 for this radial network that spans the San Andreas fault. As discussed in previous reports, the strain accumulation has been simple shear across the San Andreas fault at a nearly steady  $0.233 \pm 0.004$  ppm/yr (tensor).

At Palmdale, we currently have seven measurements of this network since early 1989. The reduction of these line-length changes into strain accumulation is preliminary since the observations have not been thoroughly checked for survey errors and operator blunders. However, as the data in Figure 6 and the secular strain rates in the table indicate, the temporal character and the magnitude of strain accumulation for these two networks are similar. Note that in the figure and in the table, I have used coordinates that are parallel and normal to the local strike of the San Andreas fault, N65W.

Secular Strain Rates relative to N65W		
Network	Pearblossom	Palmdale
Fault Parallel	$-0.028 \pm 0.005$ ppm/yr	$+0.024 \pm 0.053$ ppm/yr
Fault Shear	$+0.233 \pm 0.004$ ppm/yr	$+0.171 \pm 0.042$ ppm/yr
Fault Normal	$-0.019 \pm 0.005$ ppm/yr	$+0.031 \pm 0.052$ ppm/yr
Dates	1980.82 - 1991.79	1989.09 - 1991.78

#### 4. Pinon Flat and Anza

We have also been monitoring the strain accumulation in two networks that are located in the area of the Pinon Flat Observatory which is operated by UC San Diego. The location of these two networks is shown in Figure 7. The Pinon network, which uses the central monument at GREEN, was initially surveyed in early 1986 and has been remeasured between 3 to 4 times each year. Since this network is fan shaped rather than the more conventional radial configuration, the effect the stability of individual monuments becomes a significant factor that adds noise to our inference of strain accumulation. The results of calculating strain accumulation at Pinon from the two-color geodimeter measurements are shown in Figure 8 and in the table below. Although the secular rates are on the order of 0.1 ppm/yr, the variation in strain between successive surveys is between 0.1 and 0.5 ppm. Most likely, the apparent high noise is due to the less than optimal configuration of this network.

The Anza network consists of two central stations, OPENVIEW and TABLE, and several other stations near the San Jacinto fault. Over the past 3 years, we have detected a significant,  $0.23 \pm 0.02$  ppm/yr, of fault shear which has been accumulating

steadily. Because these two sub-networks are nearly radial, the variations in strain about a secular rate is less than that observed at Pinon. We also detect that the rate of fault shear strain decreases by a factor of 2 from the Anza network to the Pinon network.

Secular Strain Rates relative to N45W		
Network	Pinon	Anza
Fault Parallel	$-0.107 \pm 0.015$ ppm/yr	$-0.110 \pm 0.035$ ppm/yr
Fault Shear	$+0.109 \pm 0.014$ ppm/yr	$+0.228 \pm 0.023$ ppm/yr
Fault Normal	$+0.170 \pm 0.023$ ppm/yr	$+0.070 \pm 0.023$ ppm/yr
Dates	1986.21 - 1991.73	1988.33 - 1991.79

## 5. Northern California

During the summer of 1991, we established two geodetic networks designed to measure strain accumulation due to subduction of the Gorda Plate near Crescent City, California. The first network is located approximately 20-km from the coast and consists of 11 baselines in the area known as the High Plateau. The second network is located 90-km further inland from the first near Fort Jones, California. This network consists of 8 baselines. We expect to remeasure these networks infrequently over the next 5 years. With two accurate measures of the strain rate provided by these networks, we can test the hypothesis of whether the Gorda Plate is locked beneath the North American Plate.

FIGURE 1. A plot of changes in line length for the baselines that use CASA as a common station. The line-length changes have been normalized to the nominal baselines length therefore transforming the displacements from units of mm to parts per million (ppm). The error bars represent plus or minus one standard deviation.

FIGURE 2. The location of the baselines that are measured using a two-color geodimeter are shown along with the location of the boundaries of the Long Valley caldera (solid line) and the resurgent dome (dashed line).

FIGURE 3. Plot showing the relation between inflation of the caldera and the seismicity within the caldera since mid 1983. The bottom plot shows the time and size of all earthquakes greater than M1.5 that occurred within the caldera. The upper panel shows the cumulative moment release of caldera quakes (and those under Mammoth Mountain, too) (scale on left), and the extension observed on the baseline CASA-KRAKATAU which nearly spans the resurgent dome (scale on right).

FIGURE 4a. Plot of the two-color geodimeter data for measurements of line-length changes since mid 1984 for those baselines that cross the San Andreas fault near Parkfield. The error bars represent one standard deviation of each observation. The data as plotted has had a linear trend removed and the computed secular rate is next to the plot of the residuals.

FIGURE 4b. Same as Figure 4a except that these baselines do not cross the San Andreas fault.

FIGURE 5. Results of computing fault slip, areal dilatation, and shear strain from frequent measurements of 15 out of the 18 baseline network at Parkfield. The utility of this analysis is to examine *short-term* variations in the deformation near Parkfield. Also plotted are the results of the variations in "length-scale" of the Parkfield instrument relative to the length-scale of the portable geodimeter. Notice that the large steps in dilatation in April 1989 and in May 1990 mimic the variations in length scale. During that interval, the Parkfield instrument clearly had instrumental problems. For further discussion of this plot, see the text.

FIGURE 6. The cumulative strain changes observed both at Pearblossom network and at Palmdale network using measurements from a two-color geodimeter. The coordinates have been rotated into a fault parallel (N65W) and fault normal system. The error bars represent the formal one-standard deviation level from propagating the individual standard errors of the measurements and normalized to the expected misfit of a model of spatially uniform strain accumulation.

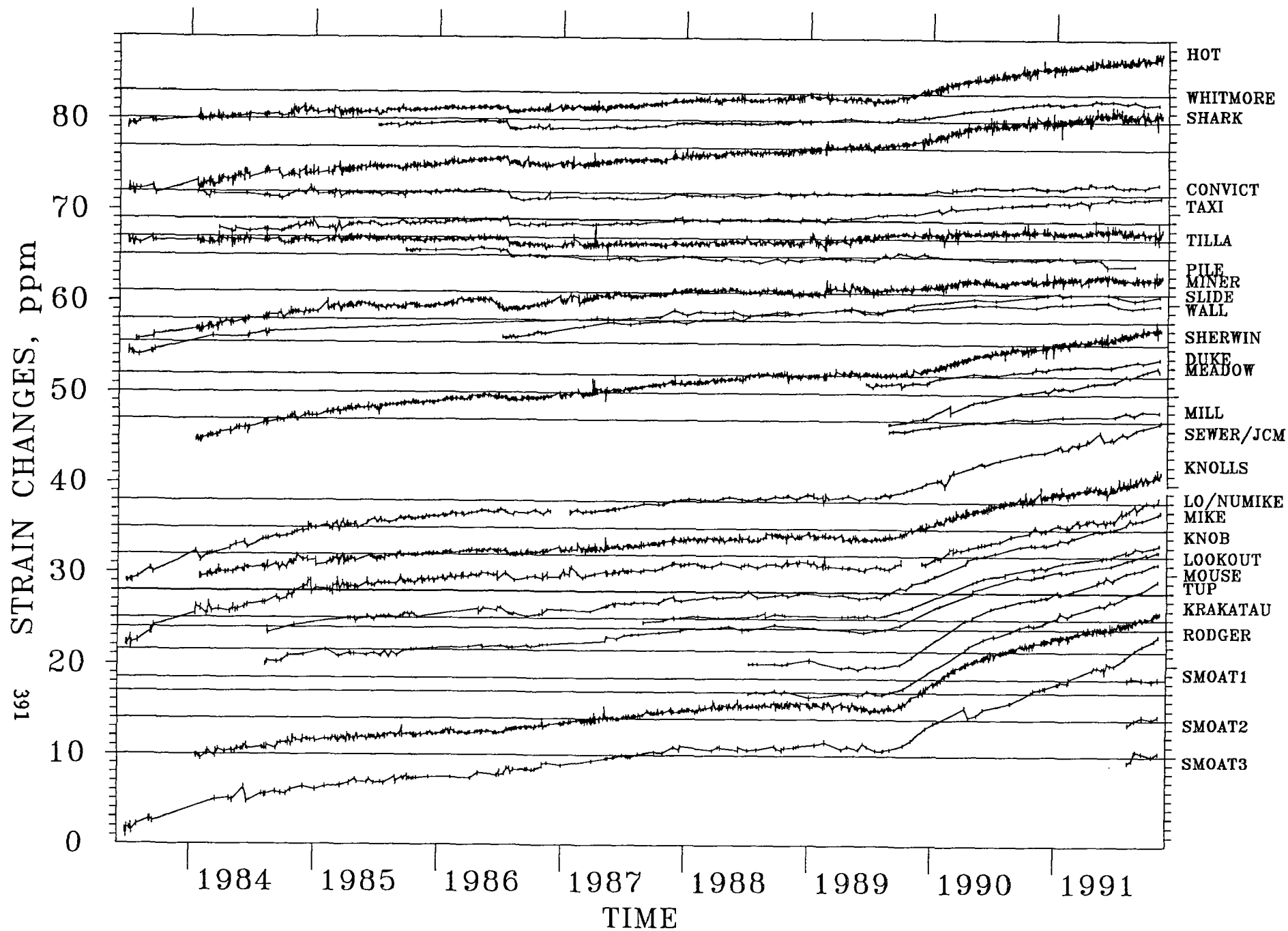
FIGURE 7.

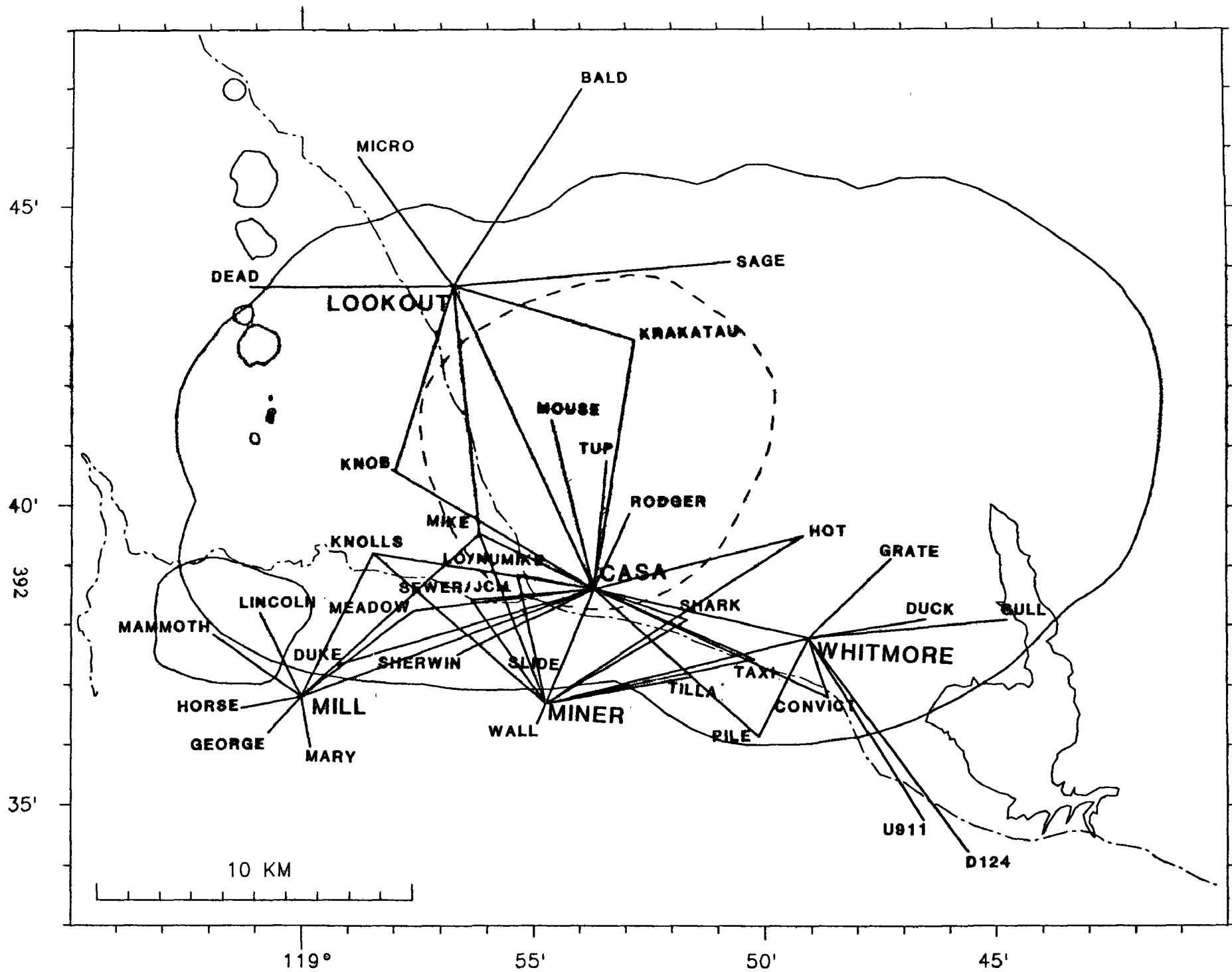
Map showing the locations of the baselines near Pinon Flat and Anza that are measured using a two-color geodimeter. Typically, the Pinon network which uses the central monument at GREEN is measured 3 to 4 times each year, but the other baselines of the Anza network are measured twice each year.

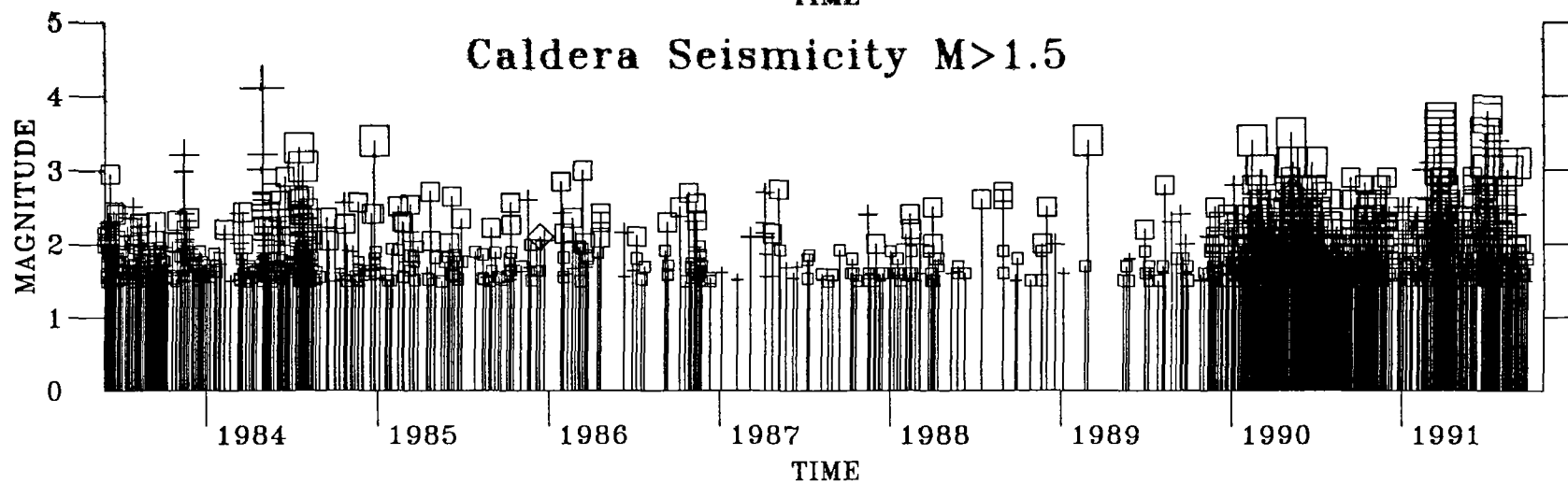
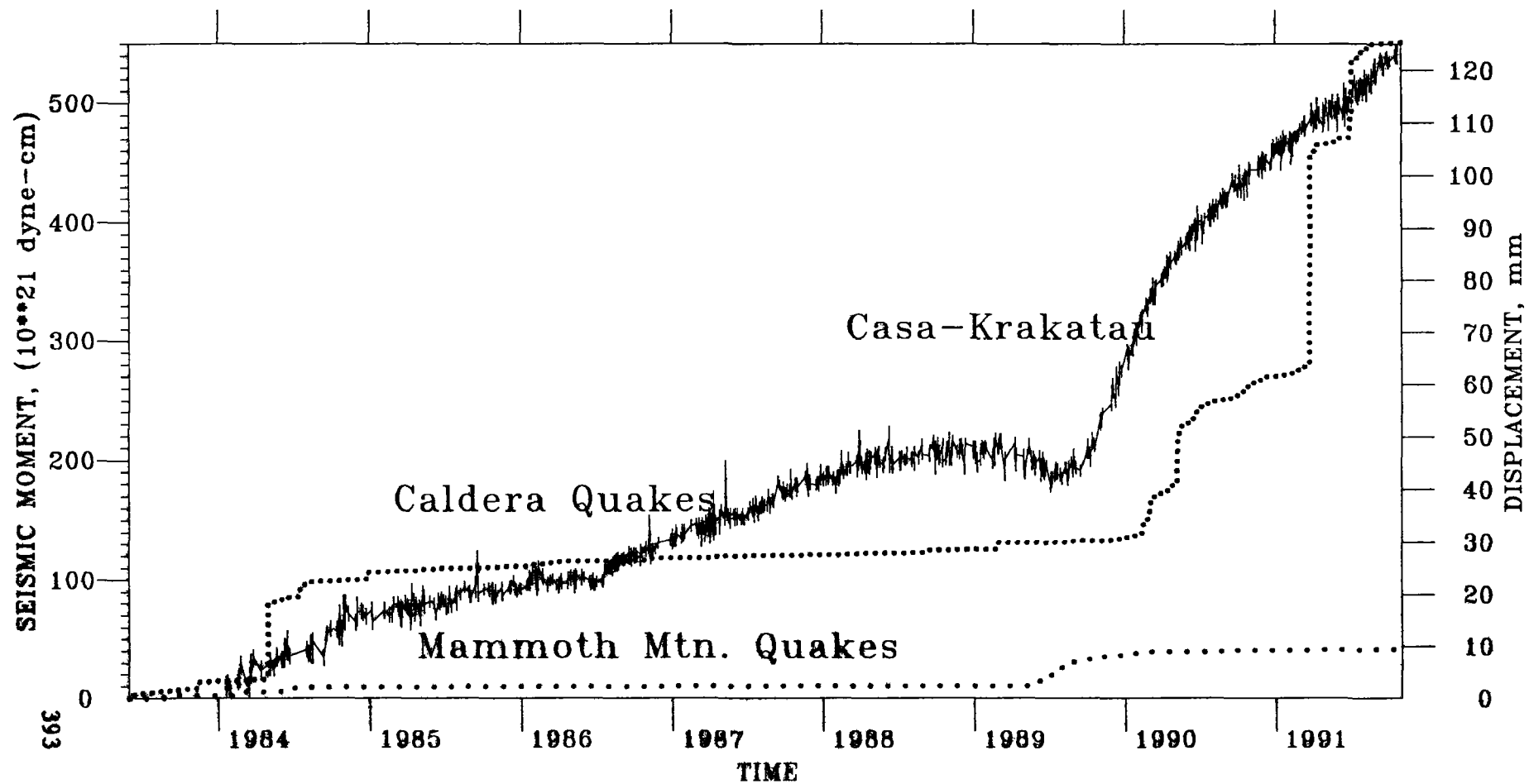
FIGURE 8. The cumulative strain changes observed both at Pinon network and at Anza network using measurements from a two-color geodimeter. The coordinates have been rotated into a fault parallel (N45W) and fault normal system. The error bars represent the formal one-standard deviation level from propagating the individual standard errors of the measurements and normalized to the expected misfit of a model of spatially uniform strain accumulation.



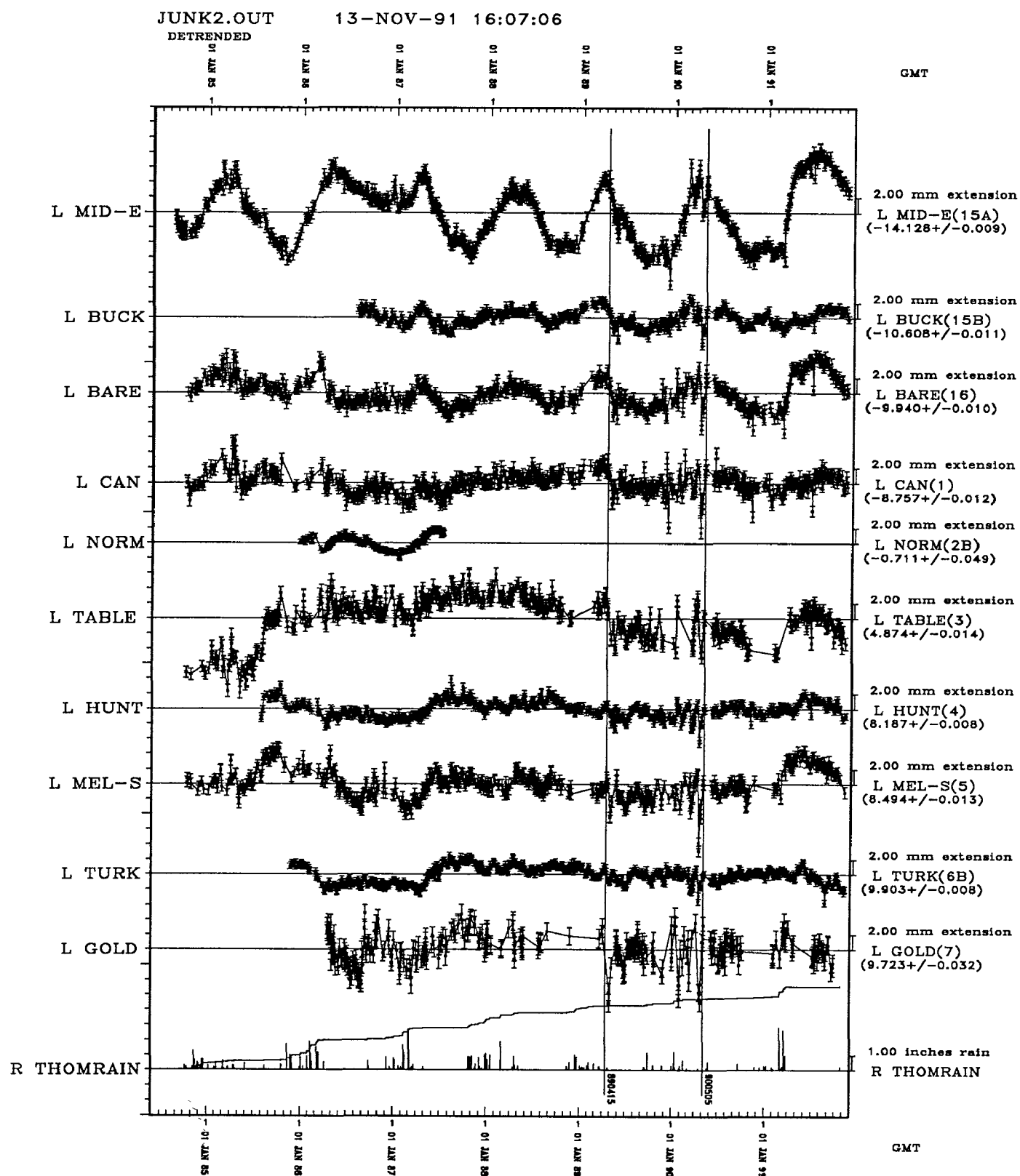
# OBSERVED STRAIN CHANGES from CASA



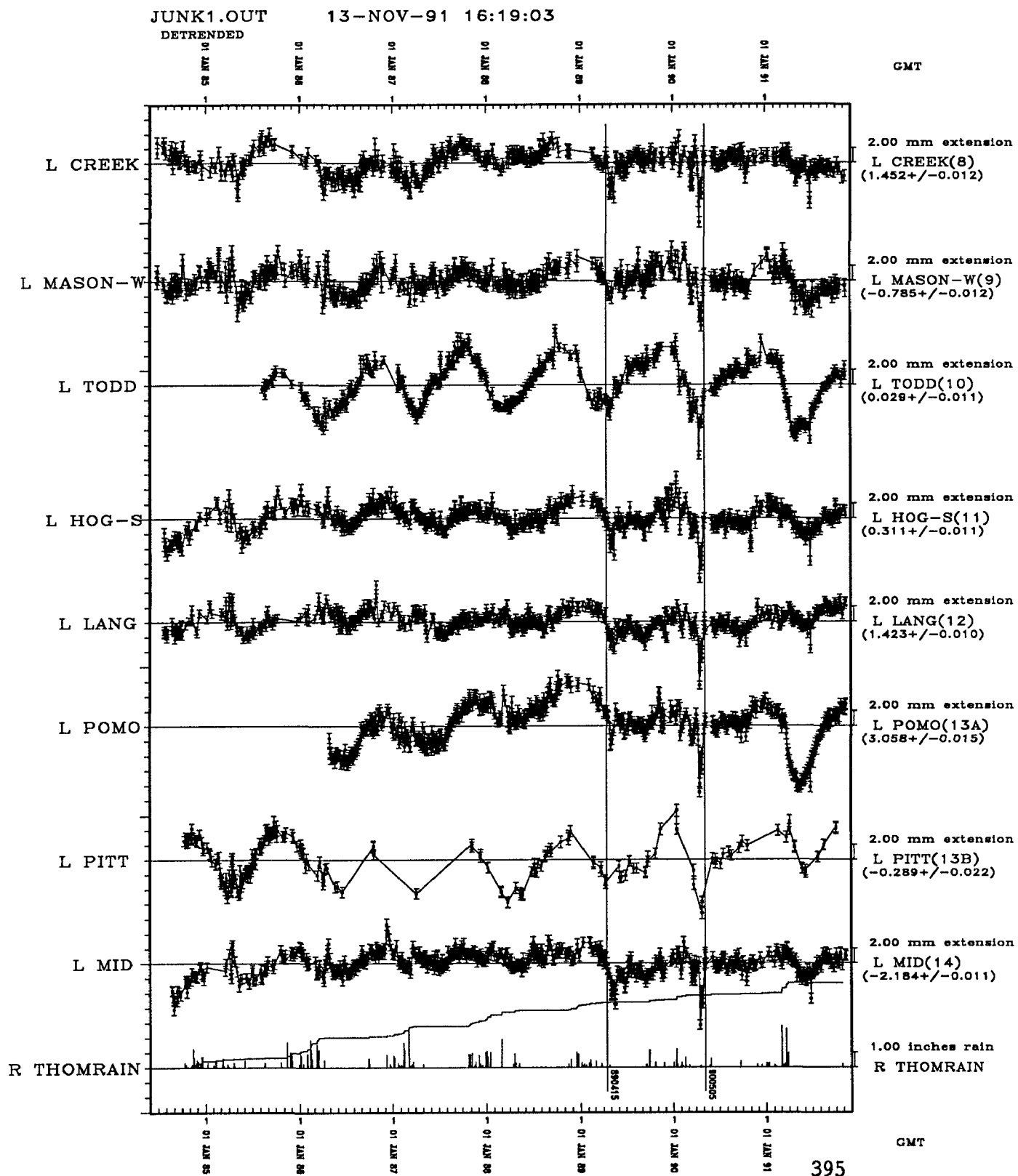




# Fault crossing Baselines



## Non-fault crossing baselines



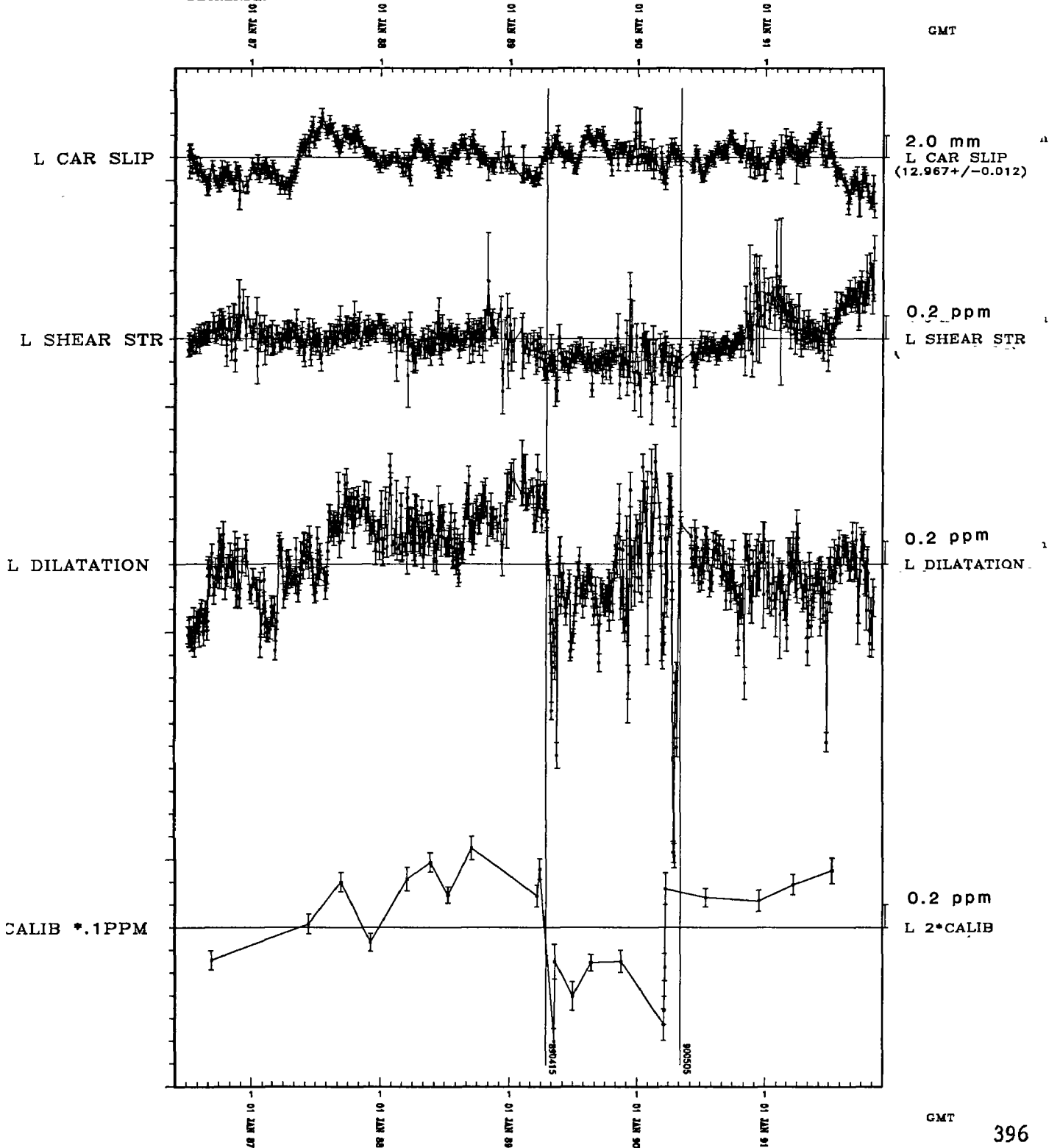
Non-fault crossing baselines

# Model of slip and strain from two-color data

JUNKX.OUT

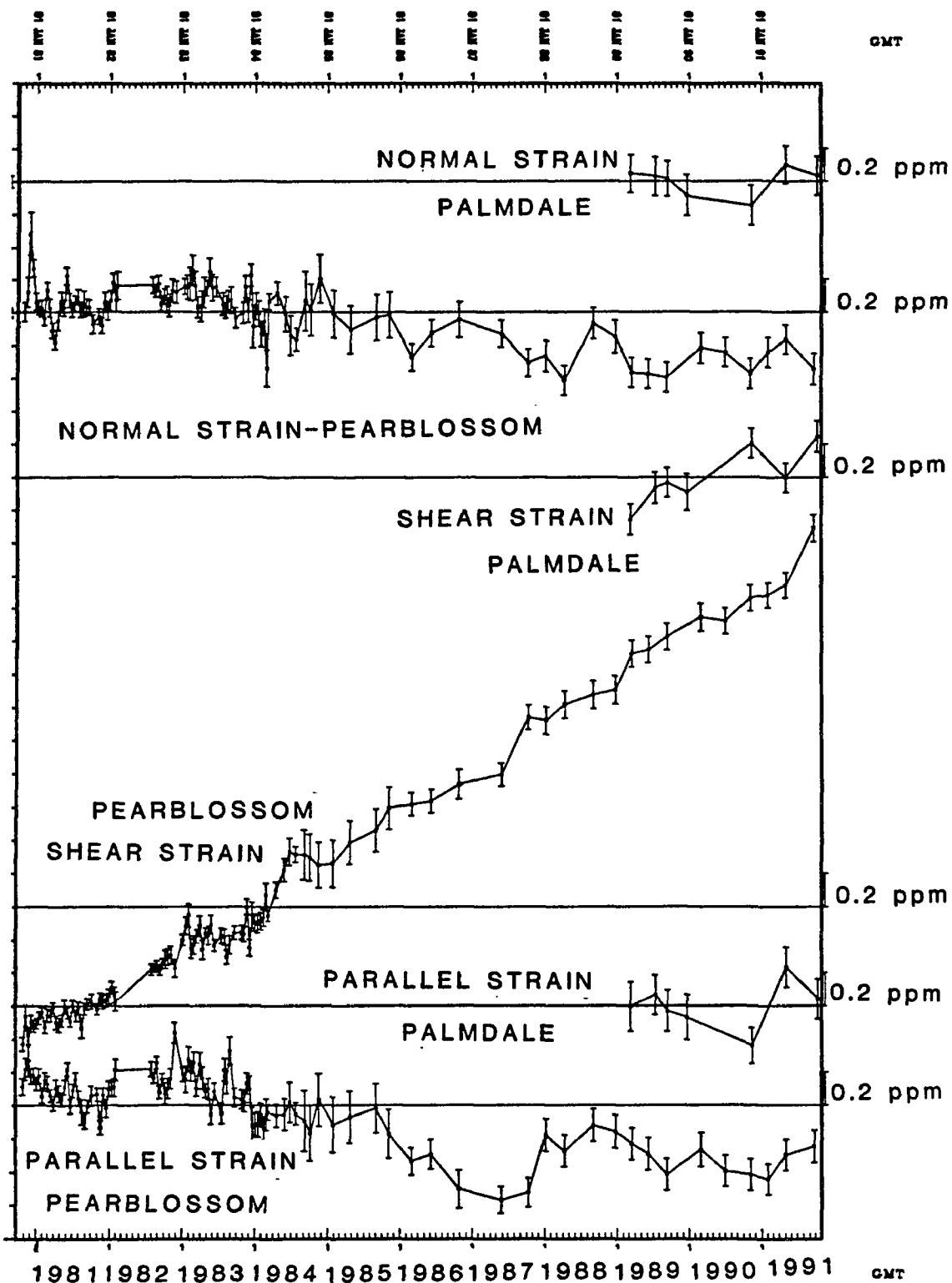
13-NOV-91 17:05:16

DETRENDED



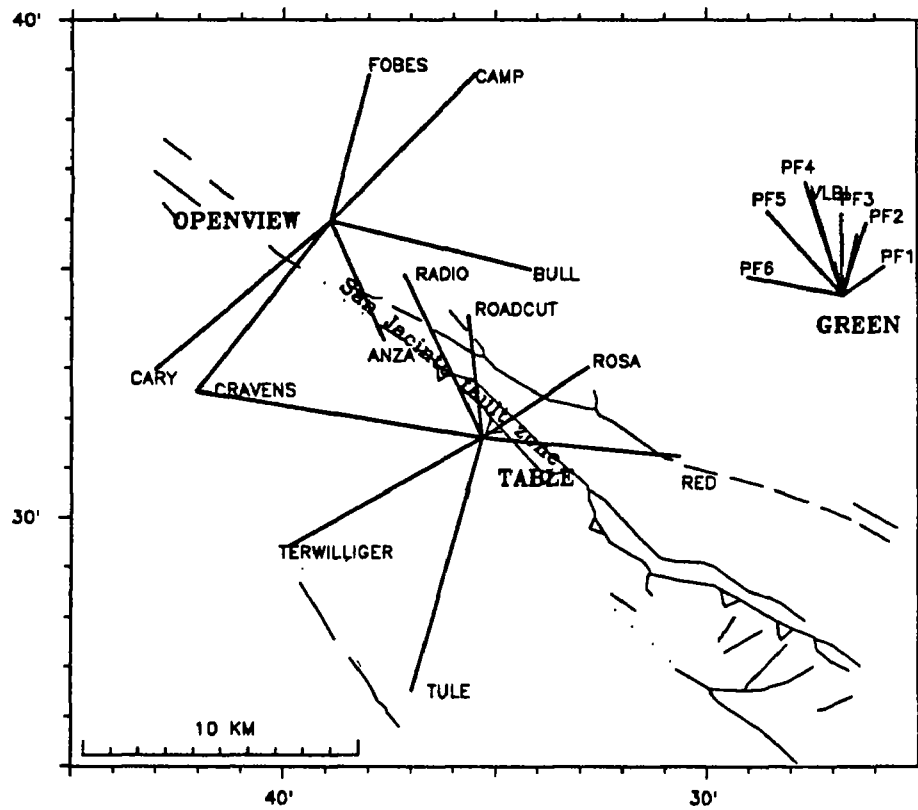
# Model of slip and strain from two-color data

## Strain changes from Pearblossom and Palmdale



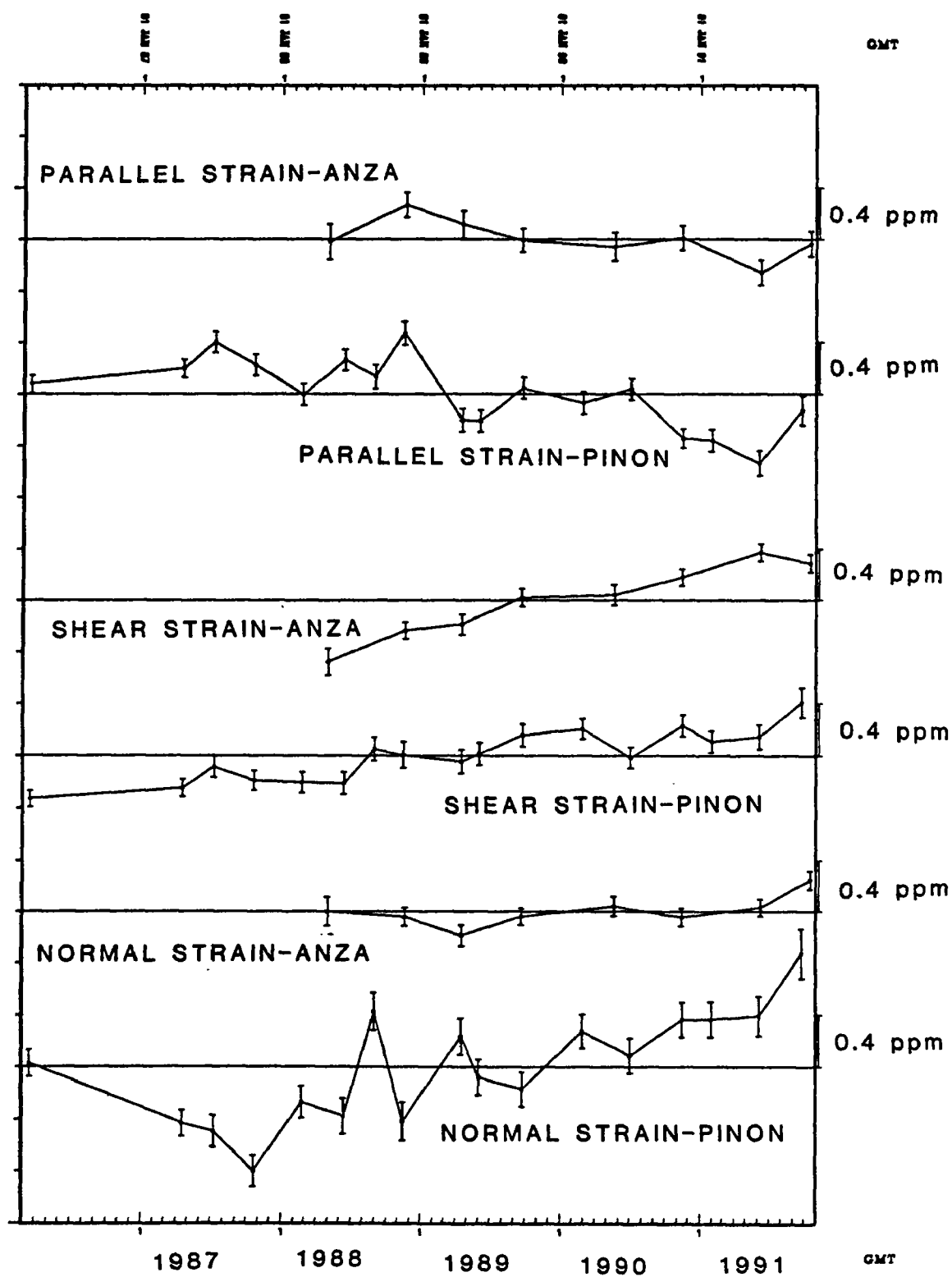
Strain changes from Pearblossom and Palmdale

## ANZA & PFO TWO-COLOR NETWORKS





## Strain change from Pinon and Anza networks



## Strain change from Pinon and Anza networks

## Parkfield Prediction Experiment

9960-04561

*John Langbein*

Branch of Tectonophysics  
U.S. Geological Survey  
345 Middlefield Road MS/977  
Menlo Park, California 94025  
(415) 329-4853

### Investigations

This project coordinates the different experiments at Parkfield run by both USGS and non-USGS investigators. Some of the experiments are focused on the prediction in the short-term of the next Parkfield earthquake. Other experiments will document pre-seismic, the co-seismic, and post-seismic events. Both data from seismicity and from deformation are examined for significant events. This project has been examining the formal rules used in either calling an "alert" or "status-level".

### Results

#### 1. Significant Signals

The table summarizes the events in the past 1.75 years that meet established criteria to be called either an "alert" or "x-level status". For purposes of semantics, low-level signals which meet the "C" and "D" levels are called "status-levels", and the larger signals which meet the "A" and "B" levels remain as "alerts".

The most notable event during the course of this experiment is the B-level alert in March 1991. As noted by the table, Parkfield had substantial rainfall during that month. Although the two, simultaneous creep events at XPK1 and XVA1 were in excess of 5 mm, there were no other signals detected on neighboring strain instruments or geodetic networks. We can only conclude that these events were a result of shallow slip with a depth of less than 0.1 km. The rain also triggered other creep events and surges on other Parkfield creepmeters. The apparent surge on X461 was in reality a flooded instrument.

#### 2. Rain and Creep

I have examined both the creepmeter and rainfall data from Parkfield and I have estimated the amount of rain necessary (but not sufficient) to trigger fault creep. Three observations are important; 1) Heavy rainfall does not always trigger creep. 2) Some creepmeters are more sensitive than others to the effects of rain. 3) The amount or intensity of rain is not linearly related to the ensuing creep. I can only give a lower bound on the amount of rain that is necessary to trigger a creep event. If significant creep of more than 1 mm over 7 days has been detected and if more than 20 mm of rain has occurred on any single day during the 7 day window, then the creep can be

considered to be triggered by rainfall. I propose that in the future when creep occurring under these circumstances that formally meets a status level, then we discount the level by one letter grade. For instance, last March's B-level alert from creep should be discounted to a C-level status because of the heavy rainfall.

The data that I used to establish the relation between rainfall amounts and creep are from two sources. The rainfall data are daily amounts of precipitation observed since 1961 at the Thomason Ranch located 2 km north of Parkfield. Because the data are recorded manually, there may be errors in recording the observations. Nonetheless, this set is the most complete record that we have for Parkfield. Our digitally recorded rain gauges were installed in 1985. Since most of the creepmeters were installed well before 1985, using the Thomason rainfall record maximizes the number of observed creep events. Although creep is recorded at 10 minute intervals, only the most recent two years of 10-minute data are accessible from the computer. However, we have data available from each instrument's installation date up to the present which have been decimated to a daily value to conserve disk space. Because the records of creep and rain were compared using daily values, the actual timing between the creep event and its possibly correlated rainfall is uncertain by plus or minus one day. So with this as a caveat, I used two schemes to relate creep and rain.

In the first scheme, I found all creep "events" which exceeded 1 mm in one day for all 11 creepmeters in the Parkfield region. I found 52 "events" excluding the effects of the 1966 earthquake recorded on the creepmeter CRR1. Of these events, 8 events coincide with either Coalinga or the Loma Prieta earthquakes, or in one case, excavation near the instrument XMM1 in 1986. Of significance are 9 "events" and possibly 3 others which had rain either in the week preceding the event or rain on the day of the event. For these 9 rainfall "induced" events, approximately 20 mm or more of rain fell during one day in the preceding week.

The second method found all creep events that exceeded 1 mm over a seven day period which qualifies the events at the D-level. This method found all the events from the first scheme plus many more. Of the 106 identified creep events, 9 were triggered by either the Loma Prieta or the Coalinga earthquakes, 1 was triggered by excavation near the creepmeter, and 33 followed rain falling within the previous 7-days. Shown Figure 1 are the values of the observed creep and the maximum amount of daily rainfall during the week previous to the creep events. Of the 33 rain related events, 11 of the events occurred on XPK1 and 6 occurred at XMM1. Although the amount of rainfall and triggered creep are not correlated, it appears that 2-cm of rain is necessary to trigger the larger creep events.

### 3. Review of criteria of status levels

We are investigating the use of a matched filter to identify signals from the network of instruments used to measure deformation. There are several advantages of the matched filter; 1) Quantifies the confidence that a signal differs from the background noise level of the instrument. 2) We can use the same technique on all instrument types. And, 3) the statistic are simple once the time-series from an instrument has been pre-whitened. To date, I have looked at the application of this technique for creepmeter, and to a lesser degree, the two-color network and the water well network.

The concept of a matched filter is described in text books on communication theory. Basically, the filter runs a cross-correlation between the data and a signal which is a specified function and then dnormalizes the result to the power density spectrum of the data noise. For the Parkfield data, I have been using functions that describe rate

changes from the background secular rate. Using this technique, I can obtain sensitivity curves for each instrument once its power density spectrum is estimated. Figure 2 shows the results for four creepmeters in the Parkfield network. For instance, for an averaging time of 3 hours, the XMM1 instrument can detect a 0.018 mm creep event. The signal to noise ratio,  $\rho = 1.0$  for this sized event with a corresponding 68% confidence. Should the event be twice 0.018 mm, the signal to noise ratio is doubled and the confidence level 95% that this event differs from the background rate. At 24 hour intervals, this instrument is less sensitive to cumulative slip, having only a 0.07 mm threshold for  $\rho = 1$ . The reduced sensitivity comes from the power density function having  $f^{-2}$  frequency dependence.

With the sensitivity as a function period determined for each creepmeter, I then used the matching filter technique to identify "events" from data from 12 creepmeters since January 1989 through mid 1991. Clearly, with the high sensitivity (0.05 mm) that is described in the previous paragraph and the large creep events (0.5 mm) identified in the table, the matched filter would find many events having  $\rho > 2$ . Figure 3 summarizes the statistics for creep. For a given averaging interval, I have counted all events that exceed a prescribed signal to noise ratio ( $\rho^2$ ). The first observation is that we identify orders of magnitude more "creep" signals having  $\rho^2 > 4$  than that predicted had the data been purely brownian noise. Secondly, if we only wanted to average one "D-level" event in each month, then we would we would adjust our threshold levels. For example, using  $\rho^2 = 2000$  for the 3 hour averaging interval would give us approximately of one "flagged" event each month from all of the 12 instruments. Using this value of signal to noise on the 0.018 mm sensitivity of XMM1 would correspond to a 0.8 mm creep event in 3 hours, which is within the range of 1.5 mm prescribed in the Parkfield Scenarios and Response plan.

Table. 1990 Parkfield alerts.

Date	Location	Description	Size	Level	Comments
900125	Middle Mtn	Earthquake	M 1.5	D	
900129	Car Hill	Shear Strain		D	ends 900215; NOT combined to C; possible instrument problems
900206	Joaquin Cyn	Water Level	-2 cm	D	
900330	Middle Mtn	Creep	0.6 mm	D	Two adjacent creepmeters
	Middle Ridge	Creep	0.3 mm		
	Middle Mtn	Water Level	-15 cm	D	combine with creep to C
900427	Middle Ridge	Creep	1.5 mm	D	
	XVA1	Creep	1.4 mm		30 min after XMD1
	Middle Mtn	Creep	0.2 mm		2 hours after XVA1
900512	Slack Canyon	Earthquake	M 2.6	D	
900606	Middle Ridge	Creep	0.7 mm		
	Middle Mtn	Creep	0.2 mm	D	
	Middle Mtn	Water Level	-12 cm	D	combine with creep to C
900729	Middle Mtn	Earthquake	M 1.6	D	
900802	Cholame	Earthquake	M 3.1	D	
900807	Middle Mtn	Water Level	-4 cm	D	
900828	Cholame	Earthquake	M 2.9	D	
900908	Turkey Flat	Water Level	3 cm	D	
900910	Mid Mtn (PKF area)	Earthquake	M 3.3	D	combine with water to C
900911	Slack Cyn (PKF area)	Earthquake	M 3.3	D	combine with water to extend C
900930	Mid Mtn	Earthquake	M 1.7	D	
901001	Mid Mtn	Earthquake	M 1.1	D	extends existing D
901001	Mid Mtn	Water Level	-12 cm	D	combine with seismicity to C
901006	Mid Mtn	Earthquake	M2.3	D	
901019	Middle Ridge	Creep	0.85 mm	D	
901023		Two-color	Dilatation	D	ended 901113
901114	Middle Mtn	Earthquake	M3.2	C	
901116	Middle Mtn	Earthquake	M2.2	D	combine with 901114 to extend C
901116	Middle Mtn	Earthquake	M1.3		combine with M2.2 to D
901128	Middle Mtn	Earthquake	M2.2	D	
901130	Middle Mtn	Earthquake	M2.8	C	
901130	Middle Mtn	Earthquake	M1.8	D	
901204	Middle Mtn	Earthquakes	M1.7, M1.5	C	
901211	XMM1, XMD1	Creep	1 mm	C	
901211	Middle Mtn	Water level	-13 cm	D	

Note. Right lateral creep, water level rises, and compressive strain are positive.

1990 Combined Alert Totals: 8 C alerts, 11 D alerts.

Table. 1991 Parkfield alerts.

Date	Location	Description	Size	Level	Comments
910109	Parkfield	Earthquake	M 3.1	D	
910121	Cholame Valley	Earthquake	M 2.9	D	
910201	Middle Ridge	Creep	1.3 mm	D	
910204	Cholame Valley	Earthquake	M 2.8	D	Combine to C
910205	Middle Mtn	Earthquake	M 2.1	D	
910210	Middle Mtn	Earthquake	M 2.0	D	
910307	SW Trace (Hearst)	Creep	-5.4 mm	D	rain related
910311	Middle Mtn	Earthquake	M 1.8	D	
910319	XPK1 and XVA1	Creep	5 mm in 16 hours	B	raining
910319	XMM1	Creep	Surge 3.3mm in 7 days	D	Rain in past week
910322	Middle Mtn	Earthquake	M 2.2	D	
910327	X461	Creep	1.9mm in 7 days	D	rain in past week
910330	X461	Creep	2.9mm	D	Surge over past 10 days
910331	XMM1	Creep	0.8 mm in 30 minutes	D	
910331	Middle Mountain	Water well	9 cm	D	Familiar combination, no C
910409	Middle Mountain	Earthquake	M 2.7	D	
910410	Middle Mountain	Earthquake	M 2.1	C	2 earthquakes M>1.5 in 72 Hrs
910412	Middle Mountain	Earthquake	M1.8 and M2	C	
910426	Middle Mountain	Earthquake	M 1.6	D	
910506	Middle Mountain	Earthquake	M 1.9	D	
910508	Middle Mountain	Earthquake	M 1.9	D	
910521	XMM1	Creep	0.7 mm in 30 min.	D	
910521	Middle Mountain	Water Well	4 cm	D	Familiar combination
910711	Middle Mountain	Earthquake	M 2.0	D	
910722	Middle Mountain	Earthquake	M 1.6	D	
910726	Middle Mountain	Water Well	-12 cm	D	
910806	Slack Canyon	Earthquake	M 2.7	D	
910903	Middle Mountain	Earthquake	M 2.2	D	
910925	Middle Mountain	Earthquake	M 2.2	D	
911018	Parkfield	Earthquake	M 2.6	D	South end of M. Mtn.
911020	XMD1 & XMM1	Creep	2 events of 0.6mm in 1 hr	C	
911020	Middle Mountain	Water well	6 cm drop	D	
911108	Slack Canyon	Earthquakes	M 2.8?	D	

Note. Right lateral creep, water level rises, and compressive strain are positive.

1991 Combined Alert Totals: 1 B alert, 3 C alert, 29 D alerts.

Total alerts since beginning experiment: 1 B alert, 30 C alerts, 85 D alerts.

Figure 1. Results of correlating rainfall triggered creep events and the amount of rainfall during a single day in the week before the creep event. See the text for more information.

Figure 2. The results of using a matched filter to estimate the amount of slip needed over a specified interval for the signal to noise ratio,  $\rho = 1$ .

Figure 3. The number of creep events which exceeded a specified ratio of signal to noise. Here, 3 different averaging intervals, 3 hours, 1 day, and 1 week, were used in a matched filter to identify creep events and to quantify their signal to noise ratio. The value plotted as symbols are the result of counting the events from the output of the matched filter from 12 Parkfield area creepmeter over a 2.5 year interval. The smoothed line is a least squares fit of signal to noise to the actual counts. The dashed lines which fall rapidly would be the predicted number of events had the data been drawn from brownian noise.

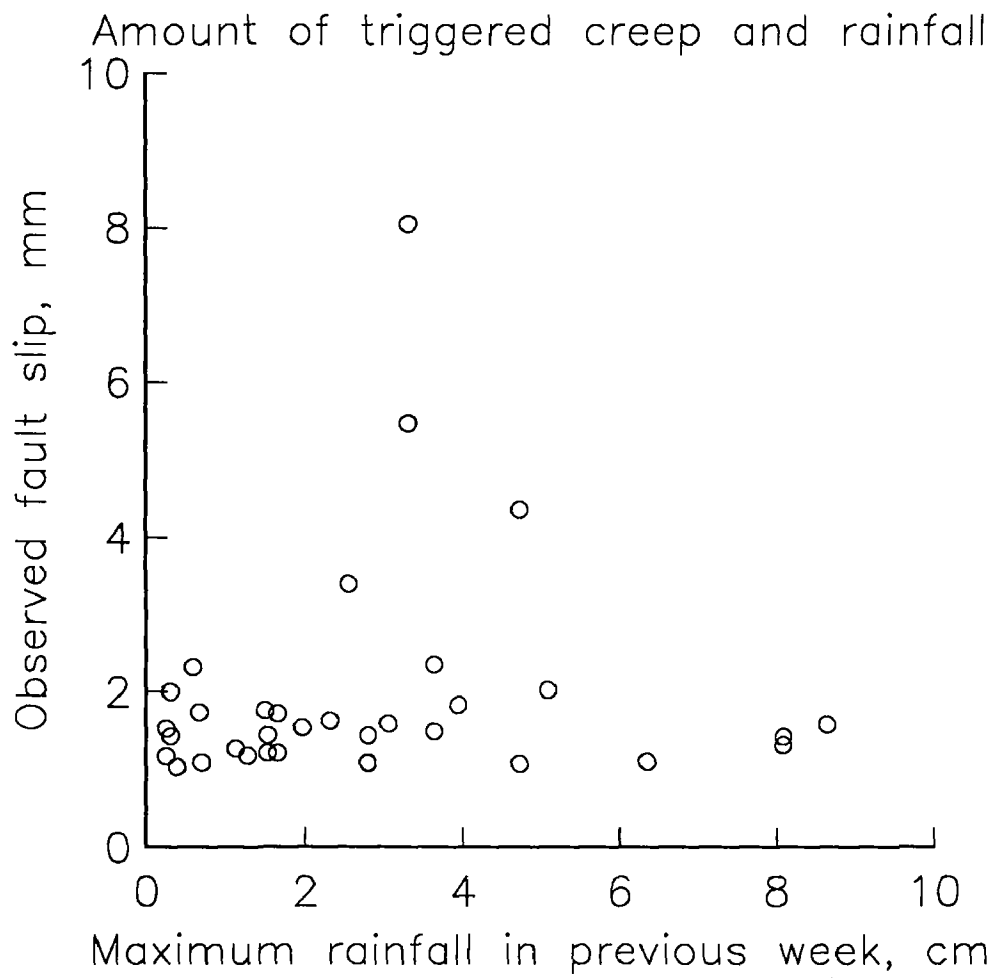


FIGURE 1



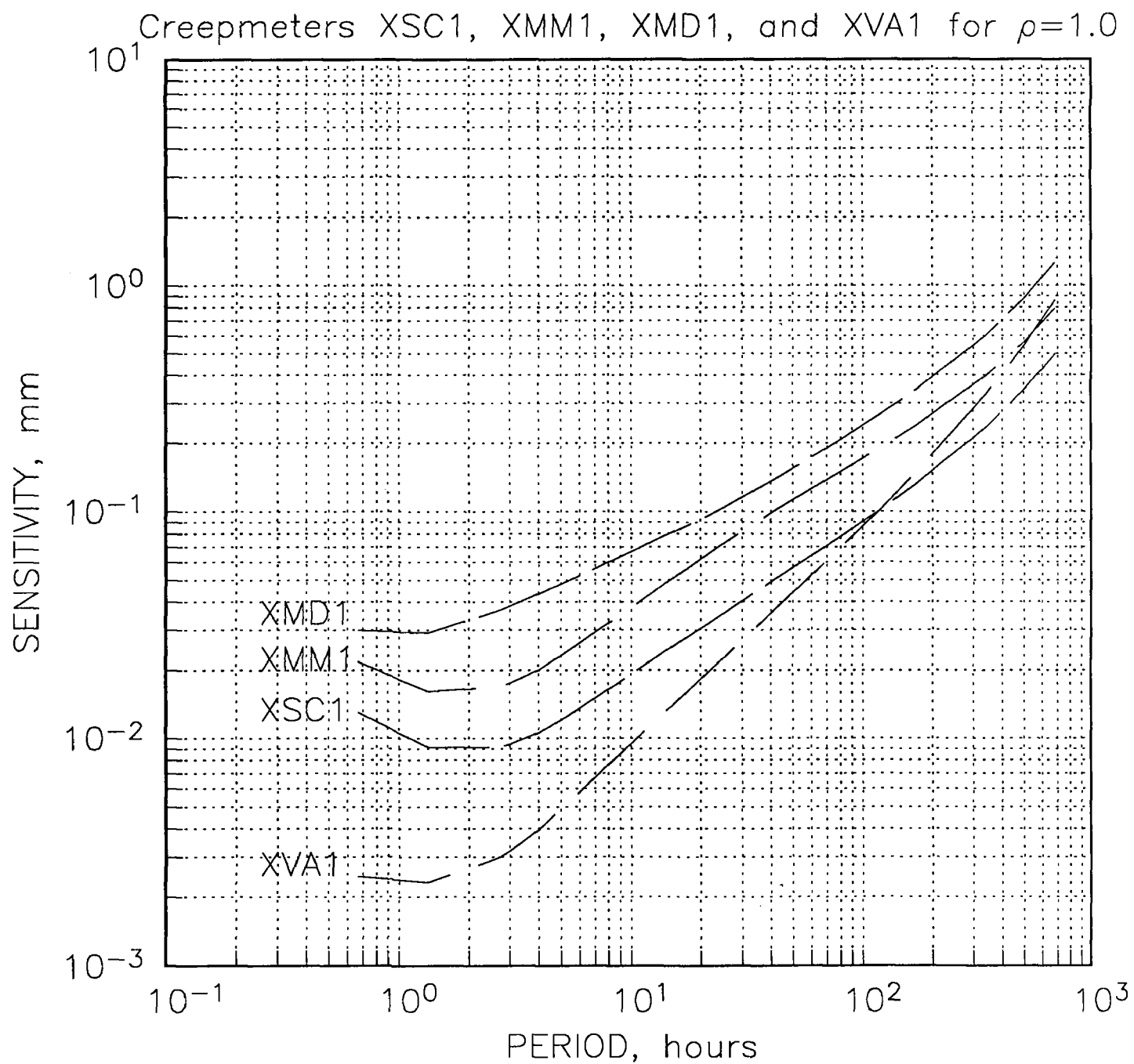


FIGURE 2

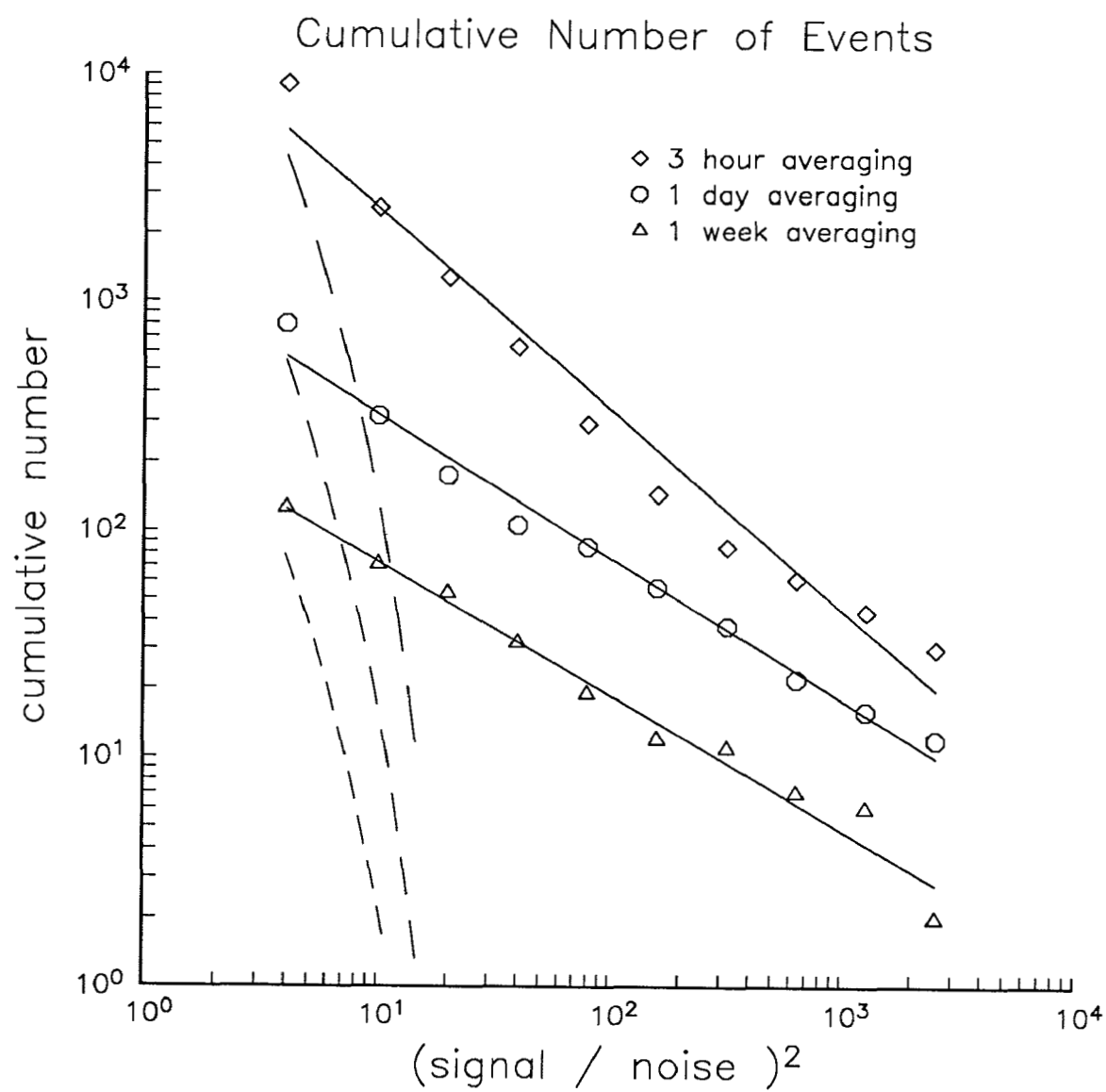


FIGURE 3

## **Broad Band Regional Wave Propagation and Lithospheric Structure in the New Madrid Region**

Grant No. 14-08-0001-G2137

Charles A. Langston  
Pennsylvania State University  
Department of Geosciences  
440 Deike Building  
University Park, PA 16802

(814) 865-0083

### **Investigations Undertaken**

An analysis of crustal structure under the IRIS station CCM (Cathedral Caves, Missouri) is in progress using teleseismic P wave and S wave receiver functions. The objective is to investigate crustal structure important to local and regional wave propagation for earthquakes in the New Madrid region. In particular, results of the structure study will be used to understand S wave propagation from the Cape Girardeau earthquake of 26 Sept. 1990 (Mb 4.7) and other small events near New Madrid. Detailed velocity structure is needed to understand aspects of P and S waveforms for use in source parameter inversion.

### **Results Obtained**

A suite of teleseisms were collected for the CCM station through the IRIS Data Management Center. Three-component P waveforms with high signal-to-noise ratios were then processed to obtain teleseismic receiver functions. Processing consisted of the standard technique of deconvolving the vertical component from the radial and tangential components.

Figure 1 shows the high-quality radial receiver functions obtained from this deconvolution process. The primary characteristic of these data is that secondary Ps conversions and other scattered coda waves are quite small for this station. Of note are two presumed Ps conversions arriving approximately 6 and 7 seconds after direct P. These two conversions must be caused by structure near the Moho on the basis of arrival time. Tangential motions are quite small (not shown), being approximately one tenth the maximum amplitude of the radial motions. The generally small amplitudes of secondary radial phases and tangential motions indicate that the lithosphere under CCM is quite transparent, seismically speaking, and has few large velocity contrast interfaces or major lateral heterogeneity.

Nevertheless, a detailed look at the radial receiver functions of Figure 1 shows that there are changes in relative amplitudes of the largest Ps conversions with source backazimuth. This may indicate the presence of interface dip on those

interfaces producing the conversions. This observation is subject to further study and analysis.

Figure 2 displays two earth models used for preliminary analysis of the radial data. The Ginzburg model is based on P wave refraction measurements and consists of a crust 41 km thick. Of note is a high velocity layer, the so-called "rift pillow" under the Reelfoot rift zone, just above the Moho. A synthetic radial seismogram was computed for an incident P plane wave under this plane layered structure and is shown in the top panel of Figure 3. The Moho and top of the high velocity layer produce two distinctive Ps conversions which are reminiscent of the data in Figure 1.

However, timing of these two phases indicate that the overall crustal thickness must be larger to match those seen in the data. The Ginzburg model was modified by simply lowering the Moho and thickening the high velocity layer above it. This model is shown by the dotted line in Figure 2 and the synthetic response is shown in the lower panel of Figure 3. The timing of the Ps arrivals now match those in the data. In addition, a distinctive backswing after the second Ps conversion in the data suggests the existence of a low velocity zone (LVZ) below the Moho. A LVZ is needed to produce a Ps conversion of opposite polarity compared to those produced at the Moho and top of the high velocity layer. The LVZ is included in the modified Ginzburg model shown in Figure 2 and produces the phase annotated by the arrow in Figure 3. This LVZ structure effect needs verification through collection of more high quality P wave data and inclusion of other kinds of data sets.

The principal result of this preliminary modeling is that the crust under CCM may be as much as 13 km thicker than previously suspected. This result will be the object of further study with the incorporation of other data sets, specifically teleseismic SV waves, and previously collected refraction data.

Figure 4 shows a good example of S data from a deep South American earthquake recorded at CCM. The Tangential component shows a very simple S pulse. However, the vertical and radial SV waveforms display large Sp conversions and reverberations within the lithosphere. The SV wave ray parameter is comparable to the P wave slowness in the upper mantle. When an S to P conversion occurs in the crust, the resulting P waves are trapped within the crust and upper mantle. Figure 4 shows a particularly prominent SpPmP phase arriving after direct S. Both Sp and SpPmP constrain the depth of the Moho and location of other major interfaces within the crust and upper mantle. These data will be included in a simultaneous inversion of P wave and S wave receiver functions to constrain structure under CCM.

## Reports Published

Langston, C.A. (1991). Crustal structure at Cathedral Caves, Missouri, inferred from teleseismic receiver functions (abstract), 63rd Annual Meeting Eastern Section, Seismological Society of America, Center for Earthquake Research and Information, Memphis State University, Memphis, TN 38152.

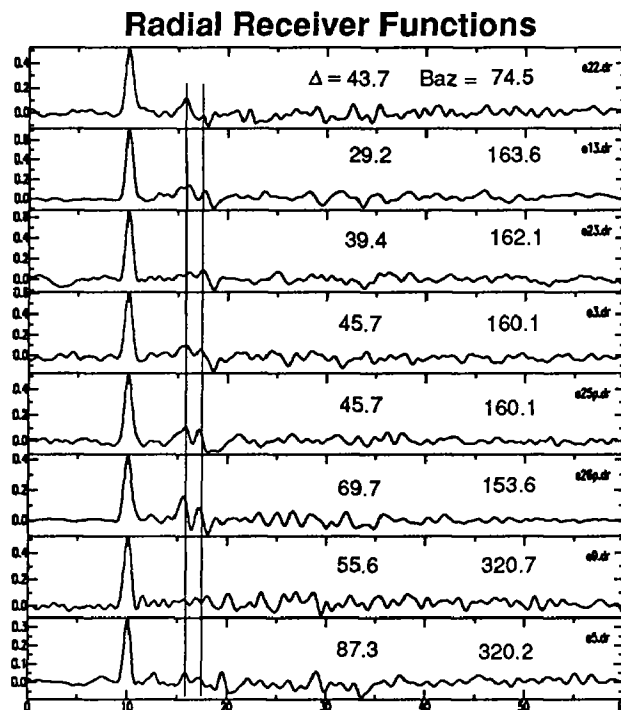


Figure 1 - Radial receiver functions arranged by distance and backazimuth. The vertical lines show the arrival times of two, distinct Ps conversions. Time is in seconds.

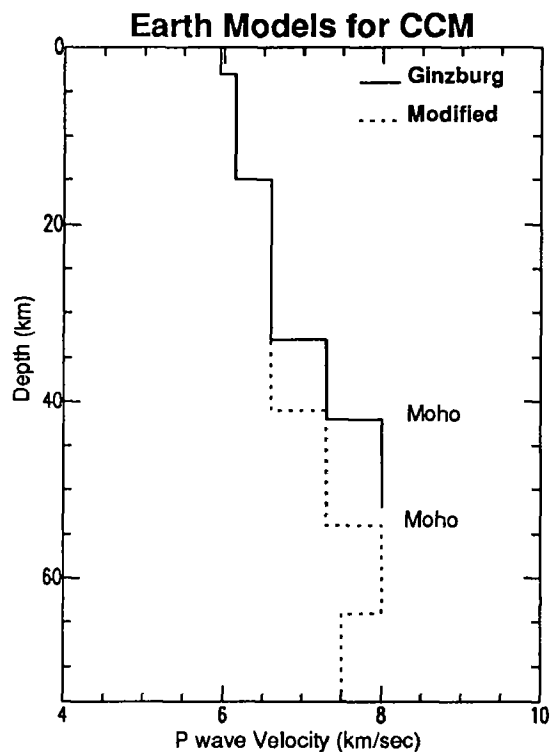


Figure 2 - Structure models for CCM station. The model shown by the solid line is based on P wave refraction measurements (Ginzburg et al, 1983, Deep structure of northern Mississippi embayment, AAPG Bull., 67, 2031 - 2046).

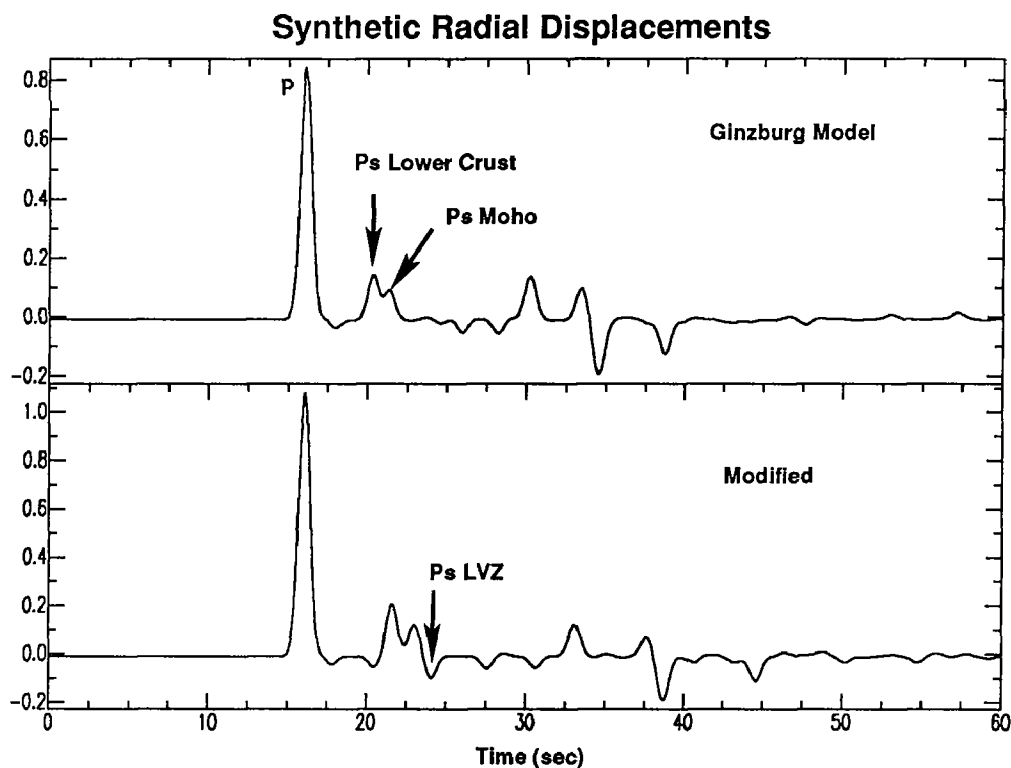


Figure 3 - Synthetic radial displacements for the earth models of Figure 2. Important Ps conversions are annotated by arrows.

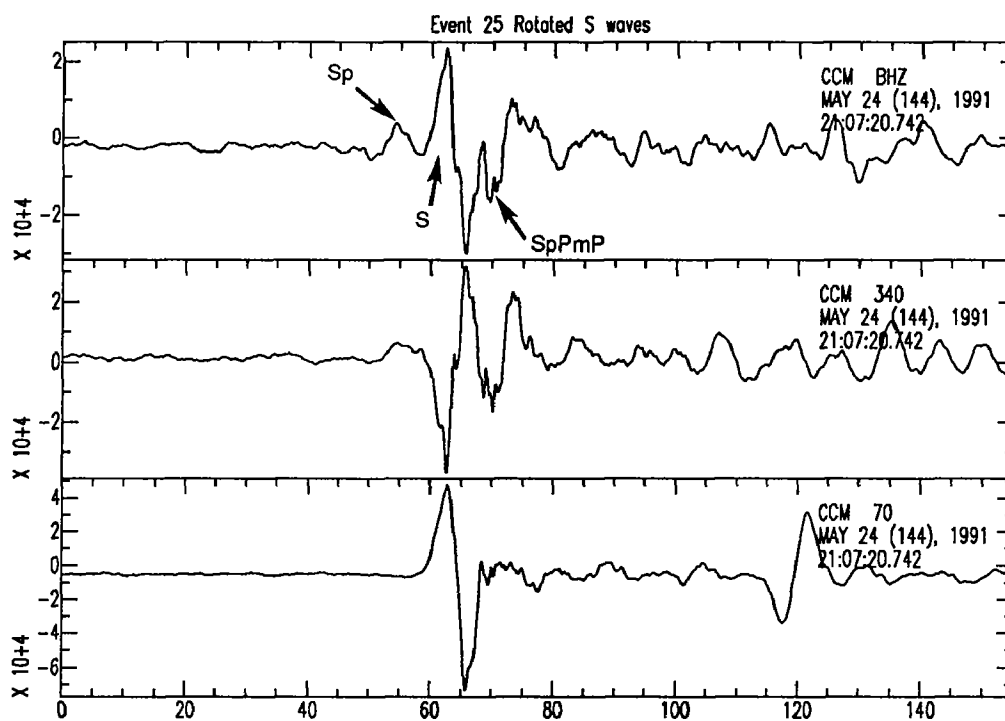


Figure 4 - S waves recorded at CCM from a deep South American Earthquake. From top to bottom are vertical, radial and tangential motions. Important SV-to-P conversions are annotated by arrows.

## Earthquake Hazard in the Santa Barbara Channel from Strain Rate Measurements Using the Global Positioning System

Contract 14-08-0001-G1956

Kristine Larson  
Colorado Center for Astrodynamics Research  
University of Colorado  
Boulder, CO 80309  
(303) 492-6583

Frank Webb  
Jet Propulsion Laboratory, MS 238-624  
Pasadena, CA 91109  
(818) 354-4670

### Investigation

The objective of our research is to measure strain rates across the Santa Barbara Channel. We repeated a GPS survey in this region which was first done in 1987. As part of our work, we installed reference marks at three sites

### Reference Mark Installation

Prior to the field experiment, reference marks were established at three sites SOLEDAD 1872 1934, Santa Rosa Island; CENTER 1874 1934, Santa Cruz Island; and LA CUMBRE, in Santa Barbara County. These marks were established and their positions surveyed with respect to the GPS mark using a Leitz SET2 Total Station with a 2" angular precision and 3 mm + 2 ppm distance precision. Azimuth measurements were made with a Brunton Compass assuming a magnetic declination of 14°. These observations were then adjusted to obtain the best estimate of the reference mark offsets from the main marks.

### GPS Survey

The 1991 Santa Barbara Channel GPS experiment was conducted June 3 through 6, 1991. We made observations at 7 sites, as described in our previous report. We used Trimble 4000SST receivers, which were loaned to us by JPL and UNAVCO. Additionally, data were collected by Bendix (under contract to Goddard Space Flight Center) at Vandenberg. The GPS satellites were tracked on 4 consecutive days, from 15:30 UTC to 23:00 UTC.

This summer we analyzed both the 1987 and 1991 campaigns using the GIPSY software developed by JPL. Precision of the baselines across the Santa Barbara Channel ranges from 2 to 8 millimeters. Interstation velocity estimates will be presented at the fall meeting of the American Geophysical Union in December 1990.

### Availability of Data

The GPS data from this experiment can be obtained in the RINEX format from Kristine Larson, (303) 492-6583.

## Microearthquake Data Analysis

2-9930-01173

W. H. K. Lee  
 U.S. Geological Survey  
 Branch of Seismology  
 345 Middlefield Road, Mail Stop 977  
 Menlo Park, California 94025  
 (415) 329-4781

### Investigations

The primary focus of this project is the development of state-of-the-art computation for analysis of data from microearthquake networks. For the past six months I have been involved in:

(1) Implementing Seismic Instrumentation for Topical Volcano Studies

In collaboration with Gray Jensen and Sam Rodriguez, I am designing and implementing seismic instrumentation for topical volcanic studies. Two portable arrays (one telemetered and one hardwired) are being implemented to meet the scientific objectives of volcano research. These two portable arrays are based in PC-technology, and are designed to have a dynamic range of about 90 db. The hardwired array will have 64 channels, and the digital telemetered array will have up to 48 channels. As of November, 1991, assembling of the hardwired array has almost been completed and is scheduled for field test early next year. A prototype of a digital telemetered station was completed and is now being field tested.

(2) Mathematical Introduction to Seismic Tomography

In collaboration with Victor Pereyra, a professional mathematician, I have completed a draft for a chapter in a "Seismic Tomography" book being edited by H. M. Iyer. We summarized the basic mathematics needed by seismologists to start doing seismic tomography research.

### Reports

Novelo-Casanova, D. A. and W. H. K. Lee (1991). Comparison of techniques that use the single scattering model to compute the quality factor  $Q$  from coda waves, *Pure Appl. Geophys.*, v. 135, p. 77-89.

Lee, W. H. K. (1991). Progress report on the IASPEI Software Library, (Abstract). IASPEI Program and Abstracts, IUGG XX General Assembly, p. 232.

Fujita, K., S. A. Estes, W. H. K. Lee, R. Hutt, A. G. Larionov, and B. M. Kozmin, (1991). Deployment of a PC-based digital recording system at Yakutsk, USSR, (Abstract), *EOS*, v. 72, p. 345.



## Northern and Central California Seismic Network Processing

9930-01160

Fredrick W. Lester  
Branch of Seismology  
U.S. Geological Survey  
345 Middlefield, MS 977  
Menlo Park, CA 94025  
(415) 329-4747

### *Investigations*

1. In 1966 a seismographic network (CALNET) was established by the USGS to monitor earthquakes in central California. In the following years the network was expanded to monitor earthquakes in most of northern and central California, particularly along the San Andreas Fault, from the Oregon border to Santa Maria. In its present configuration there are over 300 stations in the network, and more than 60 of those consist of more than one component. Also recorded are signals from more than 60 stations operated by other agencies or institutions, including the University of California, Berkeley, the University of Nevada, Reno, the California Institute of Technology, the California Department of Water Resources, and the Lawrence Livermore National Laboratory. The primary responsibility of this project is to monitor, process, analyze, and publish seismic data recorded from this network.
2. This project maintains a seismic data base of CALNET data for the years 1969 to the present on both computers and magnetic tapes for those office staff who are doing research using the network data.
3. Project staff often act as the primary spokesperson or authority when inquiries are received from the press, the public, or scientists from both inside and outside the Geological Survey regarding earthquakes that have been recorded by the network. Inquiries include simple questions about recent earthquakes in the region, such as the date and time of occurrence, the location, and the magnitude of the earthquake. Or they may be somewhat complex and require expert opinion or interpretation, such as the relationship of recent swarms of earthquakes to historical seismicity, and how each relates to the seismogenic potential of a region or fault.
4. As time permits research projects are undertaken by project personnel on some of the more interesting or unusual events or sequences of earthquakes that have occurred within the network, or related topics.

### *Results*

1. Figure 1 illustrates most of the 9148 earthquakes located in northern and central California and vicinity during the time period April through September 1991. Figure 2 shows the location of the seismographs used to locate earthquakes during that time period. That level of activity is relatively normal for a six month time period.

The most significant earthquakes during this time period occurred along or off the coast of California, mostly during July and August. The largest earthquake recorded in or around northern or central California since the Loma Prieta earthquake of October 1989 occurred on August 17. It was magnitude 6.8 and was located off the coast, west of Crescent City. It was part of a sequence of earthquakes that began on July 13 when a magnitude 6.7 earthquake was

recorded in the same region. A magnitude 6.0 earthquake also occurred as part of this sequence on August 17 and many smaller related events were recorded through September.

Another significant coastal earthquake occurred on September 17 in region northwest of San Simeon. It was magnitude 5.0 and was followed by smaller aftershocks over a period of several days. This was the largest earthquake in that region since a magnitude 5.4 earthquake on August 29, 1983.

Seismic data recorded by the network are being processed using the CUSP (Caltech USGS Seismic Processing) system. CUSP was designed by Carl Johnson in the early 1980's and has since undergone some revisions for the Menlo Park operation. On September 1, 1989 we began using revised CUSP software in a generic format. This new format makes CUSP more universally acceptable to groups that are using or plan to use it in the future because the commands are relatively non-specific to any particular group operation.

In late October 1990 we began using new software and hardware to process the earthquake data. At that time we converted from very old DEC PDP 11/44 computers and Tektronics 4014 terminals to the faster and more powerful DEC 3100 workstations. The new workstations now perform all of the functions of the older computers and terminals, and more, including automatic event detection and preliminary processing, and final manual processing. The new program used for final manual processing of the data is called TIMIT. This new program incorporates the old processing program QED, plus includes many new features which make processing much smoother, faster, and more efficient. TIMIT is still undergoing revision and upgrading to reduce bugs and problems and incorporate new software and hardware features.

This year we hope to begin publishing, on an annual or semi-annual basis, a catalog of earthquakes for northern and central California. The format is not yet established but it will probably be some type of listing of events accompanied by a text explaining the processing procedures and what is in the catalog, maps showing the epicenters and possibly cross sections and focal mechanisms, and a description of important earthquakes or earthquake sequences. The catalog will be approximately complete at the magnitude 1.5 in the central core of the network and something approaching M2.0 in the more remote portions of the net.

2. The current catalog is relatively complete and correct through June 1991. The data from July through September are somewhat incomplete and some errors still remain to be identified and corrected. Additional data from earthquake sequences that occurred in July and August along or off the northern California coast, from approximately Shelter Cove north, are currently being processed and will be included as they are finalized. Also, quarry blasts need to be identified for September.
3. More than 50 requests were received for seismic data which required computer searches of the data base. Most of the searches were for specific regions and time periods. Some were more complex requiring multiple searches and some interpretation. Data from these searches were most often distributed as printed listings, but but some were also sent as data files over electronic mail or files on magnetic tape.

Along with requests for computer data searches the project normally receives 10 to 25 telephone inquiries per week that request simple information about recent earthquakes, ongoing or past USGS research, or that request maps and publications and some interpretation of geologic information. During periods of higher than normal seismic activity the project may receive as many as 20 to 30 requests of this type per hour.

Recognition of earthquake risk and related hazards has increased dramatically since the Loma Prieta earthquake of October 1989. A consequence of this has been an increase in insurance

claims related to earthquakes that has resulted in an increase in insurance company requests for data searches for recent earthquake activity. Another consequence of that earthquake is the increasingly common request from homeowners or potential homeowners for information about all types of geologic hazards, particularly earthquake hazards, in the area around their homes or where they plan to purchase a home.

4. At the present time David Oppenheimer and Nan MacGregor-Scott are investigating earthquakes in the east San Francisco Bay region in the area approximately bounded by the Hayward fault, the Great Valley, Suisun Bay, and the Calaveras Reservoir. Under investigation is the seismic potential of the region as related to slip along several important faults, including the Calaveras-Sunol, the Franklin, the Antioch, the Greenville, and the Concord faults. Results of this investigation will be presented at the Conference on Earthquake Hazards in the Eastern San Francisco Bay Region. This conference is to be held on the campus of Hayward State University in March 1992.

### *Reports*

None

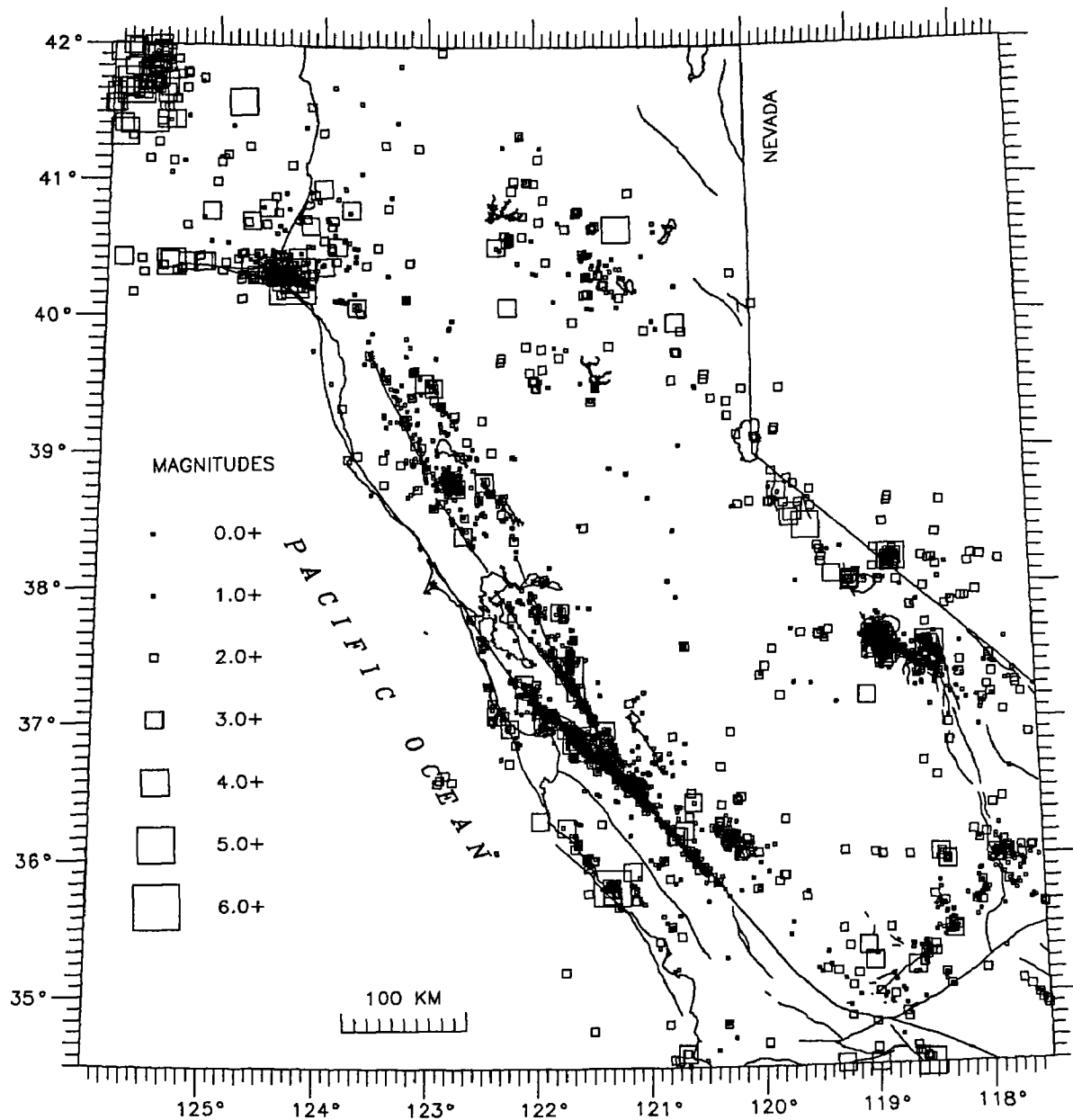


FIGURE 1. Seismicity for April - September 1991

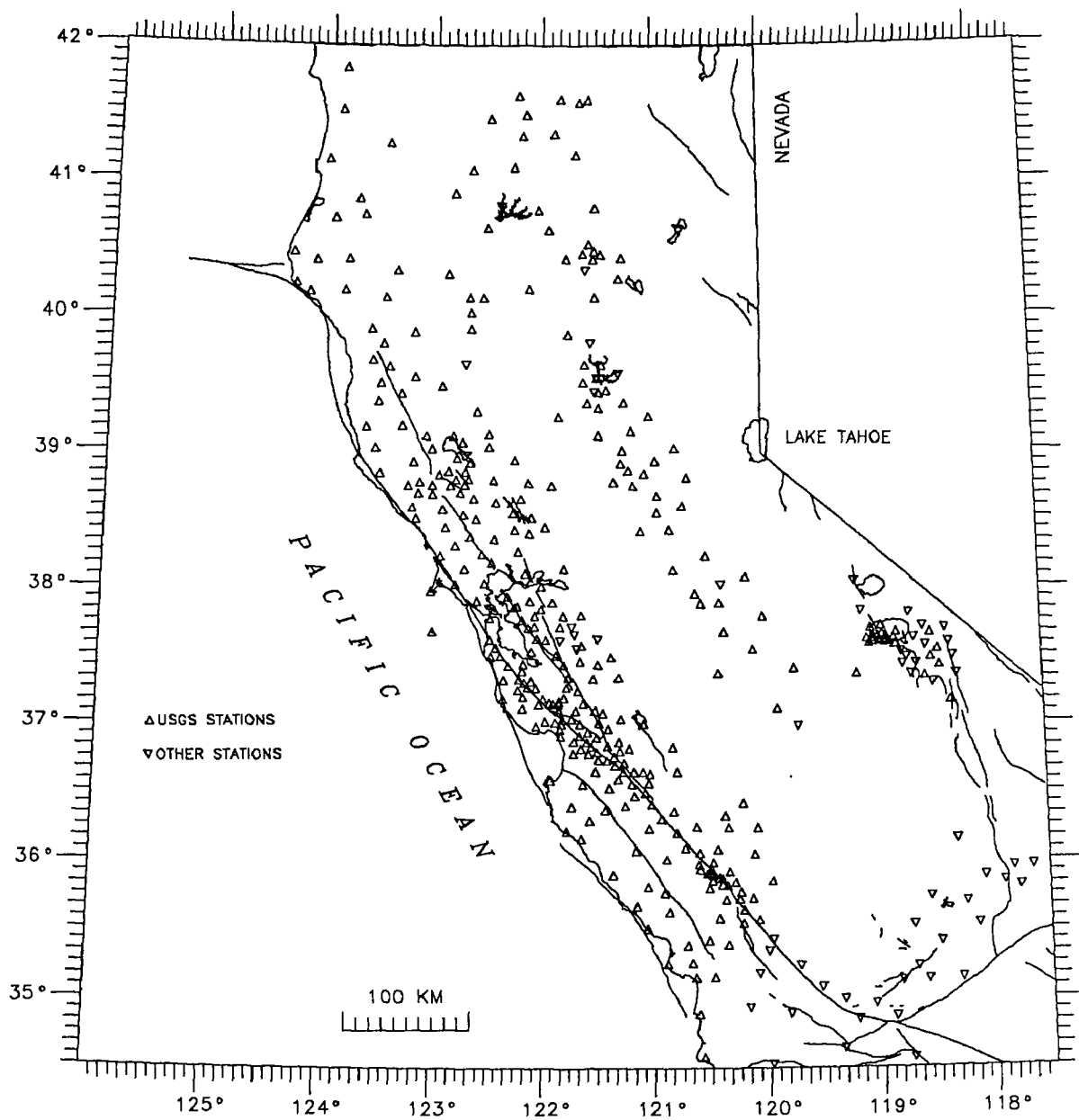


FIGURE 2. Seismographic stations April - September 1991

## **Paleoseismic Investigations Along the Northern Reach of the Calaveras Fault Zone, Alameda County, California**

Agreement No. 14-08-0001-G1987

William R. Lettis, Keith I. Kelson, and Gary D. Simpson  
William Lettis & Associates  
1000 Broadway, Suite 612  
Oakland, CA 94607

(510) 832-3716

### **Objective of the Study**

- Obtain detailed paleoseismic information at the Leyden Creek research site along the northern Calaveras fault zone, including Holocene slip rate(s), amounts of displacement per event, and timing of paleoseismic surface-rupture events.

### **Progress to Date**

- Obtained excavation permits from all land owners and lessees.
- Prepared detailed topographic map (Scale 1:465, contour interval = 0.5 m) of the Leyden Creek site using a TOPCON total station. Based on field observations, delineated surficial deposits and several fluvial terrace surfaces on this map.
- Drilled and logged 21 boreholes (13 via a truck-mounted, solid-stem auger; 8 via hand auger) to help delineate near-surface stratigraphic relations, to assist in siting exact trench localities, to help identify and delineate possible piercing lines, and to test stratigraphic and structural models developed during analysis of trench exposures.
- Excavated 3 east-west-oriented trenches across the major active trace of the Calaveras fault zone. The southern wall of each of these trenches was gridded and logged in detail at a scale of 2 inches to 1 meter. These trenches were excavated to expose stratigraphic and structural relations from which to assess paleoseismic characteristics of the fault.
- Excavated and logged 2 soil test-pits to assess the thickness of surficial deposits beneath selected fluvial terrace surfaces, and to provide rough age-estimates of the terrace surfaces.
- Four charcoal samples from critical stratigraphic horizons were submitted for radiocarbon analysis. Three of these will most likely require AMS dating techniques to obtain an age-estimate.
- Invited informal peer review of excavations and current working models. Attendees included scientists from the U.S. Geological Survey, California Division of Mines and Geology, California Division of Safety of Dams, Lawrence Berkeley Laboratory, East Bay Regional Park District, private industry consultants, and local universities.
- Excavations were backfilled and the area remediated in mid-October, 1991.

## **Results to Date**

- Several episodes of surface rupture have occurred at the Leyden Creek site within the middle to late Holocene. The number and relative timing of surface ruptures interpreted from trench exposures are based on the presence of numerous generations of fissure fills along the fault trace, several scarp-derived colluvial wedges (some of which have been subsequently faulted), and truncated fault strands. Trench exposures suggest at least four, and possibly as many as eight, prehistoric rupture episodes. Age-estimates obtained from radiocarbon analysis of charcoal samples will provide constraint on the timing of some of these episodes.
- Based on trench exposures, drillhole data, and field mapping, a buried bedrock margin of the Leyden Creek valley is oriented approximately normal to the fault trace. This paleo-margin, which is between 6 and 9 meters deep, is displaced approximately 70 meters in a right-lateral sense from the present bedrock valley margin on the opposite side of the fault. Radiocarbon samples from lowermost strata exposed in the trenches will provide a minimum age for this possible piercing line. We anticipate that these data will yield an approximation of the maximum slip rate on this reach of the Calaveras fault zone.
- A primary goal of this investigation was to test the hypothesis that a paleochannel present on the upstream (downthrown) side of the fault, and a narrow bedrock notch on the downstream (upthrown) side of the fault, could be used as a piercing line to obtain the amount of displacement along the fault. Trench exposures and borehole data indicate that two coarse-grained paleochannels are present on the upstream side of the fault. Near-surface data suggest that both of these paleochannels are oriented nearly perpendicular to the fault approximately 20 meters west of the fault scarp, but then both turn to the south and are oriented parallel to the base of the fault scarp. Thus, these paleochannels cannot be used as piercing lines and provide no clear information on the amount of displacement (and hence the slip rate) along the Calaveras fault.

## **Publications**

- Kelson, K.I., Lettis, W.R., and Simpson, G.D., 1991, Paleoseismic investigations along the northern Calaveras fault, Alameda County, California: Geological Society of America Abstracts with Programs, v. 23, no. 2, p. 41.
- Kelson, K.I., Lettis, W.R., and Simpson, G.D., in press, Progress report on paleoseismic investigations at Leyden Creek, northern Calaveras fault zone, Alameda County, CA: Abstract submitted to the 1992 Conference on Earthquake Hazards in the Eastern San Francisco Bay Area, Hayward, CA, March, 1992.
- Kelson, K.I., and Lettis, W.R., in press, Regional distribution of slip in the San Francisco Bay region: Abstract submitted to the 1992 Conference on Earthquake Hazards in the Eastern San Francisco Bay Area, Hayward, CA, March, 1992.
- Simpson, G.D., Lettis, W.R., and Kelson, K.I., in press, Initiation of research into the northern termination of the Calaveras fault, Contra Costa County, CA: Abstract submitted to the 1992 Conference on Earthquake Hazards in the Eastern San Francisco Bay Area, Hayward, CA, March, 1992.

## **Analysis of Quaternary Deformation, Calaveras-Concord Fault Stepover, Contra Costa County, California**

Contract # 14-08-0001-G2140

William R. Lettis, Keith I. Kelson, and Gary D. Simpson  
 William Lettis & Associates  
 1000 Broadway, Suite 612  
 Oakland, California 94607  
 (510) 832-3716

### **Research Objectives**

The northern Calaveras fault zone represents the most prominent, potentially hazardous fault within the San Francisco Bay region for which little information is known regarding location, slip rate, structural character, and earthquake potential. The objectives of this study are to better define the location of the northern Calaveras fault and to acquire specific data regarding its northern termination and structural relationship with the Concord fault. We are assessing the seismic hazard and structural character of the northern Calaveras fault zone via compilation of a tectonic map, aerial photograph interpretation, and creation of a detailed Quaternary strip map along the fault north of Sunol Valley. The detailed geologic and geomorphic map of the fault zone will lead to a better understanding of the nature of interaction between the Calaveras and Concord faults, the definition of segment boundaries, the lateral continuity of individual fault strands within the zone, and whether the rate of activity progressively decreases or abruptly dies out northward along the fault. Together with fault behavioral data developed during our ongoing paleoseismic studies near Leyden Creek, we hope to provide important input for estimating the time-dependent probabilities of large-magnitude earthquakes on the Calaveras fault.

As an extension of our work on the Calaveras fault, we are compiling published data on long-term (geologic) and short-term (historic) slip rates on faults in the San Francisco Bay region. We will use this compilation to compare regional deformation (geological and geodetic slip rates and creep rates) along different spatial transects and to assess whether current data are sufficient to account for all horizontal slip predicted by current plate motion models. We have resolved available slip rate data into vector components parallel and perpendicular to predicted present-day motion between the Pacific and North American plates (exclusive of Basin and Range extension), and have compared the cumulative slip within and between individual transects.

### **Progress to Date**

- Our research of the northern Calaveras fault is in its initial phase. We have compiled existing literature into a comprehensive fault map of the Calaveras fault north of Sunol Valley. This map covers parts of the Dublin, Diablo, Las Trampas Ridge, and Walnut Creek 7.5' quadrangles and incorporates our own mapping with the previous mapping of Herd (1978), Dibblee (1980), and CDMG (1982).
- We have obtained 1937 through 1940 aerial photography of the northern Calaveras fault zone and are presently compiling photo interpretation along the entire reach.



- We have selected 4 paths between the Farallon Islands and Stockton with which to compare cumulative slip rates and plate motion models, and have compiled published geologic and geodetic slip rates and creep rates. Slip rates have been resolved parallel and perpendicular to the predicted plate motion.
- Preliminary comparisons have been made across the four paths between the cumulative values of the published slip and creep rates and the values obtained from plate motion models.

### Publications

Simpson, Gary D.; Lettis, William R.; and Kelson, Keith I., 1991. Initiation of Research into the Northern Termination of the Calaveras Fault, Contra Costa County, California: 1992 Conference on Earthquake Hazards in the Eastern San Francisco Bay Area. Hayward, March, 1992.

Kelson, Keith I. and Lettis, William R., 1991. Regional distribution of slip in the San Francisco Bay region: 1992 Conference on Earthquake Hazards in the Eastern San Francisco Bay Area. Hayward, March, 1992.

Operation of Borehole Tiltmeters  
at Pinon Flat Observatory, California  
and Analysis of Secular and Tidal Tilt

14-08-0001-G1765

Judah Levine  
Joint Institute for Laboratory Astrophysics  
Campus Box 440  
University of Colorado  
Boulder, Colorado 80309  
(303) 492 - 7785

Objectives: To install borehole tiltmeters at Pinon Flat Observatory in Southern California; to compare the performance our instruments installed at three different depths; to analyze the data at secular and tidal periods; and to compare our results with those obtained from other instruments at the same site.

Results: We currently have three instruments installed at Pinon Flat Observatory and all three have been operating during this report period. We have continued to use finite element methods to estimate the relationship between the regional tilt vector and the tilts recorded by our instruments. Our work during this period has concentrated on estimating the sizes of two effects: the effects resulting from a borehole that is not perfectly vertical and the effect of a variation in the topography of the weathering layer boundary.

The placement of the cylindrical instrument capsule at the bottom of the borehole has been described in our previous reports. The weight of the capsule is supported by a hemispherical knob welded to the center of a plate at the bottom of the casing, but this knob does not constrain the horizontal position of the instrument. Three contact points are welded to the instrument capsule near the top and three near the bottom. These contact points are equally spaced around the circumference of the capsule. Two of the contact points are rounded pieces of metal and the third is a leaf spring. The spring presses the other two contact points against the sides of the borehole. This design minimizes the effect of tilt-strain coupling if the casing is vertical since the side of the casing serves as the reference for the instrument, but it is an-isotropic azimuthally. Strains that deform the borehole along the azimuth of the springs simply cause the springs to expand and are not transmitted to the capsule, while strains in the two other orientations are transmitted via the contact points without attenuation. The result is an an-isotropic strain-tilt coupling. Alternatively, this effect may be viewed as producing tilts along the axis of the spring from an isotropic strain field (See Fig. 1). This effect is essentially independent of frequency since the spring is very stiff so that its resonant frequency is much higher than any frequency we can observe.

An additional tilt-strain coupling results from the weathering layer if the boundary between that layer and the shallower material is not flat. The size of this effect can only be estimated since the short-wavelength topography of the weathering-layer boundary is not

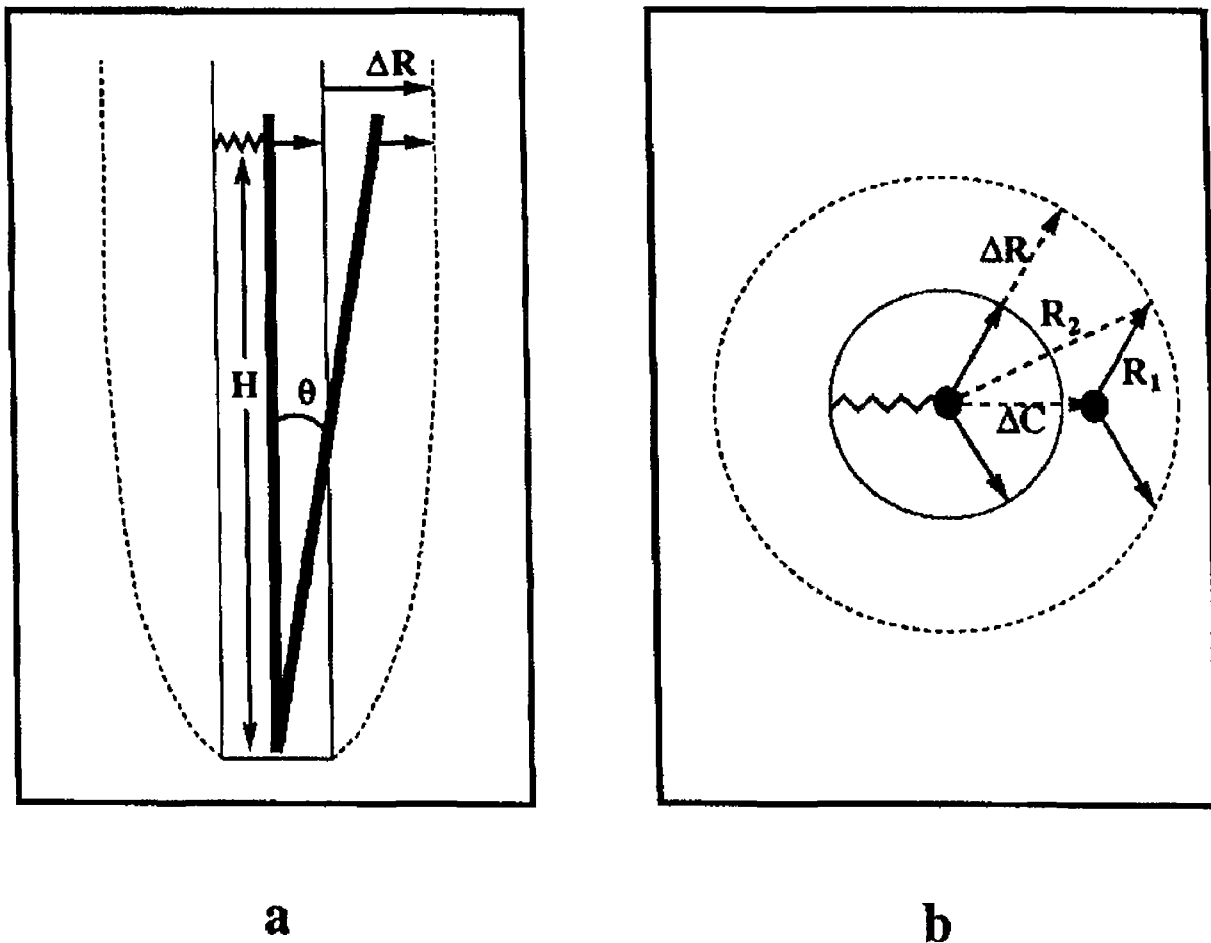


**Figure 1.** A side view (a) and a top view (b) of the tilt produced by a uniform expansion of the borehole. The capsule references the sides of the hole using two contact points shown as arrows and a spring.

known. The effect falls off with distance from the boundary, so that it is most important for BOB.

These models have important consequences for borehole tilt measurements. We are currently conducting several experiments to test these predictions. We are measuring the explicit angular dependence of the tilt signal by rotating the tiltmeters and we are also constructing several different mounting systems to verify the importance of the coupling between the casing and the instrument.

**Summary of Data Collected:** We acquire the data from our three instruments at PFO (2 channels/instrument) every 6 minutes. These same values are also transmitted to the PFO central recording trailer and are digitized and recorded there 12 times/hour.

## Slip History of San Andreas and Hayward faults

9910-04192

J. J. Lienkaemper  
Branch of Engineering Seismology and Geology  
U.S. Geological Survey  
345 Middlefield Road, MS 977  
Menlo Park, California 94025  
(415) 329-5642

### Investigations

Determine slip rates and earthquake recurrence times on San Andreas and Hayward faults. Compare rates of geologically determined surface slip to rates of historic creep and geodetically determined deep slip. Analyze effects of structural complexity and fault segmentation upon inferring recurrence from slip rate.

### Results

1. Creep Rates, Hayward Fault. Along most of the fault, offset features yield creep rates of 3.5-6.5 mm/yr over decades, but a 4-km-long segment in south Fremont has crept at 8.5-9.5 mm/yr [Lienkaemper *et al.*, 1991]. We theorize that the ~9 mm/yr creep rate in south Fremont represents the full long-term slip rate on the fault. Testing this theory, we trenched the Masonic site in Union City, 1989-90.
2. Quaternary Slip Rates, Masonic Site. We identified 6 buried fan units offset by the fault by: C) 0-20 m, E)  $40 \pm 6$  m, G)  $66 \pm 5$  m, I)  $88 \pm 5$  (?) m, K)  $131 \pm 6$  (?) m, and M)  $167 \pm 6$  (?) m. Radiocarbon dates constrain slip rate for 3 units: 1)  $8.5 \pm 1.4$  mm/yr on E (4.7 ka),  $8.0 \pm 0.6$  mm/yr (8.3 ka) on G, and  $\leq 9.2$  mm/yr (14.2 ka BP) on K. The rate of unit G, 8 mm/yr, is distinctly more reliable than the other two because the age of onset for the unit is especially well-constrained. More trenching and radiocarbon dating may modify the rate of unit E. We cannot yet distinguish any changes in slip rate during latest Quaternary and Holocene at this site at a 95% confidence level. These slip rates support our theory of a  $\geq 9$  mm/yr long-term slip rate for the Hayward fault based on the highest historical creep rates.
3. Mapping Holocene traces, Hayward fault. I completed the strip map of the Hayward fault at 1:24,000 for publication in 1992. For this, we flew 1:4000 scale low-sun-angle, color aerial photos along the main fault; and 1:8000 and 1:10,000 photos of the southern extension and its branches. Using these I recognized unmapped creeping traces and sites for the study of prehistoric large earthquakes on the Hayward fault.

### Reports

- Borchardt, G., J. J. Lienkaemper, and K. Budding, Holocene slip rate of the Hayward fault at Fremont, California (abstr.): 2nd Conf. Earthquake Hazards, Eastern San Francisco Bay Area, Hayward, March 1992.
- Lienkaemper, J. J., and G. Borchardt, Holocene slip rate of the Hayward fault at Union City (abstr.): 2nd Conf. Earthquake Hazards, Eastern San Francisco Bay Area, Hayward, March 1992.
- Lienkaemper, J. J., G. Borchardt, and M. Lisowski, Historic creep rate and potential for seismic slip along the Hayward fault, California: *Jour. Geophys. Res.*, 96, 18,261-18,283, 1991.
- Lienkaemper, J. J., and G. Borchardt, Hayward fault : Large earthquakes versus surface creep (abstr.): 2nd Conf. Earthquake Hazards, Eastern San Francisco Bay Area, Hayward, March 1992.

## Analysis of Borehole Strainmeter Data

Grant 14-08-0001-G2064

Alan T. Linde and I. Selwyn Sacks  
 Department of Terrestrial Magnetism  
 Carnegie Institution of Washington  
 5241 Broad Branch Rd. NW  
 Washington DC 20015  
 (202) 966 0863

### Overview

This grant did not commence until June of 1990, but since then we have been concentrating on completing a study of possible tidal amplitude changes associated with the Loma Prieta earthquake of 1989. This study is now complete and what follows is the basis of a paper to be published in *Geophysical Research Letters*. Please note that this study was in collaboration with M. Gladwin (University of Queensland) and M. Johnston (U. S. Geological Survey), both of whom are coauthors on the paper.

### Abstract

The Loma Prieta earthquake of 1989 provided an opportunity for a sensitive test of suggestions that earthquakes may be preceded by variations in Earth tidal strain amplitudes. Such variations have been proposed as providing an advantageous technique for detecting precursory changes in elastic parameters in a seismogenic zone. We have analyzed data from two borehole strainmeters continuously operating within 40 km of the epicenter and within about 10 km of the southern end of the rupture. A preliminary report on some of these data incorrectly concluded that significant tidal admittance variations occurred during the year preceding the earthquake. We are now unable to identify any precursory changes in M2 and O1 tidal amplitudes and estimate that any large scale changes in Young's modulus must have been less than about 2%. If these results apply generally, we would conclude that variations in elastic material properties prior to earthquakes do not occur throughout substantial volumes of the subsequent hypocentral region.

### Introduction

Nishimura (1950) first suggested that changes in Earth tidal response might be a useful method for monitoring crustal elastic properties and perhaps predicting earthquakes. A number of other studies have been made on time variations of tidal amplitudes in seismically active regions (e.g. Mikumo *et al.*, 1978; Kato, 1979; Mao *et*

*al.*, 1989) but none of these has provided strong evidence to support or refute the usefulness of the technique for earthquake prediction. Finite element analysis techniques have been used (Beaumont and Berger, 1974; Tanaka, 1976) to calculate tidal response anomalies as a function of changes in elastic properties of various shaped source regions.

The Loma Prieta earthquake ( $M_L$  7.1, October 18, 1989) is the largest California earthquake in recent years, and is the largest to occur relatively close to any of the continuous strain monitoring sites in California. Elsewhere we have reported on a lack of observed short term strain precursors to this earthquake (Johnston *et al.*, 1990). Johnston and Linde (1990), in preliminary analysis of data from one of these sites, have reported on a precursory tidal amplitude anomaly for this earthquake but that earlier analysis included then undetected artifacts in the data. We have now analyzed the data from both sites in order to determine if any significant changes in tidal amplitudes occurred during the several years preceding the earthquake.

Initial plans for borehole strain instrumentation in the San Juan Bautista area, just to the south of the Loma Prieta break, called for the installation of a modest network of 5 to 7 sites. Unfortunately, due to a variety of constraints, only 3 sites were installed; 2 were in operation during the period studied here. These instruments are a tensor (three component) strainmeter (Gladwin *et al.*, 1986) and a Sacks-Evertson strainmeter (dilatometer) (Sacks *et al.*, 1971). The instrument sites and their relation to the earthquake fault are shown in Figure 1. The tensor instrument (SJT) is 38 km from the epicenter and the dilatometer (SRL) is a little closer (33 km).

The data from the instruments are collected in Menlo Park via satellite digital telemetry (Silverman *et al.*, 1989). SJT is sampled every 18 minutes, SRL every 10 minutes. Both instruments have more than adequate sensitivity and frequency response to ensure that the Earth tides can be detected and recorded with good precision.

## Analysis

We have concentrated our analysis of the strain data on the approximately two years preceding the earthquake. Our conclusions apply to earlier data also but for a variety of technical reasons (post installation effects, various instrument modifications and less reliable telemetry) the earlier data exhibit greater variability. For the period shown in the plots, SJT has been operating without modification and the data stream has been consistently reliable and undisturbed by site visits. A number of problems have complicated the record from SRL; we have removed from the data artifacts introduced by various site visits, although (see below) we have reason to believe that, after mid March 1989, the data from SRL may have been subjected to a slowly decreasing effective gain; during 1990 a steady decrease in gain became apparent.

The tidal analyses have been carried out using two independent procedures; a linear least square inversion (Gladwin *et al.*, 1985) and the BAYTAP(G) routine based on Bayesian statistics (Ishiguro *et al.*, 1984). Excellent agreement was obtained for the calculated tidal amplitudes. We have performed a variety of tests with both real and synthetic data to ensure that the results are reliable and robust. Time variations of the

M2 and O1 tidal amplitudes from the two sites are shown in Figure 2. We have used 60 day windows for the analysis, with sequential windows sliding forward by 30 days. The time tag associated with each analysis is taken as the midpoint of the window. From the SRL site we get estimates of the dilatational strain. The SJT instrument gives three components of strain; as plotted these are defined by:

$$\begin{aligned} e_a &= e_{xx} + e_{yy} \\ \gamma_1 &= e_{xx} - e_{yy} \\ \gamma_2 &= 2 * e_{xy} \end{aligned}$$

with  $x$  axis east and  $y$  axis north. Note that all of the traces are characterized by long term constancy of both the M2 and O1 amplitudes. Formal error bars (1 standard deviation) are given for all points and in some cases, particularly for the larger amplitude signals, the error bars are obscured by the point symbol. In general, as one would expect, the errors are larger for the smaller amplitude signals, which are all shown at their absolute levels. Confidence in the reliability of our measurements is also enhanced from the fact that the amplitude ratios of M2 to O1 for all components are in good agreement with the theoretically calculated ratios. For all the tidal amplitude signals, there are no variations which can be considered significant in the 2 years preceding the earthquake. The standard deviations of these values are about 1% for the M2  $e_a$  and  $\nabla$  amplitudes, about 2% for the corresponding O1 amplitudes and somewhat larger for the lower amplitude tidal components. We estimate the threshold for detecting departures from constant values as being at about the 2% level.

In 1987, the SRL instrument apparently developed a downhole leak in the cable or at the cablehead. This required a modification in the electronics which has allowed stable operation of the instrument, as evidenced by the constancy of the tidal admittance during 1988. Unfortunately, in March 1989 (marked by \* on the plot) this modification was partially undone, with the result that the effective gain of the instrument began gradually and continuously to decrease. (The instantaneous gain change caused by this has been removed from the data.) During the remainder of 1989 the loss of gain is too small for us to quantify, but after about the start of 1990 there was a clear steady decrease in the effective gain which we were able to verify. This instrument measures dilatational strain and since variations in atmospheric pressure produce corresponding changes in dilatational strain in the near surface rock, we can check for changes in instrumental gain by calculating the pressure admittance versus time. Figure 3 shows the pressure admittance and M2 (Figure 3a) and O1 (3b) tidal amplitudes for SRL following the March 1989 modification; a faulty pressure transducer was also replaced at that time. While we do not expect the admittance and tidal amplitude values to track precisely, it is clear that starting at about the beginning of 1990 both the admittance values and the tidal amplitudes show similar and consistent decreases. This apparent loss of gain of the instrument is to be expected under the post March 1989 operating conditions. We have used the pressure admittance values to provide a gain correction for the tidal amplitudes and those corrected values are shown in Figure 2 with dashed lines and open circles. This correction results in rather constant values for the tidal amplitudes

until about mid 1990 when there may have been a real decrease in the pressure admittance and thus the correction produces larger tidal amplitudes. The need for correcting these post 1990 tidal values somewhat decreases the weight we can give to these values from SRL, but it appears that there were no significant changes in the post-seismic M2 and O1 tidal amplitudes at SRL, consistent with the lack of any change at SJT. (Remember also that these reservations do not apply to the pre- and co-seismic SRL data.)

We do not detect any coseismic change in the strain tidal amplitudes (at the 2% level) and the tidal amplitudes following the earthquake are at the same levels as before it. Thus any changes in elastic parameters introduced as a result of rock fracturing during the earthquake are also quite small or localized to a small volume. If we had reported a precursory effect without noticing any coseismic change we may have questioned the validity of the result, although for this type of phenomenon the absence of the latter does not necessarily exclude the possibility of recording the former.

## Discussion

The finite element modeling papers (Beaumont and Berger, 1974; Tanaka 1976) were written at a time when dilatancy was thought to be a wide scale precursory phenomenon. The modeling estimates by Beaumont and Berger of variations up to 60% in strain tides were based on large dilatant zones in which the seismic compressional wave velocity was reduced by 15%. Such large effects are no longer considered likely but we can use our results to place upper constraints on precursory strain induced variations in elastic properties of the seismogenic zone for the Loma Prieta earthquake. The modeling in Beaumont and Berger indicates that our sites are favorably located for detection of any significant variations in elastic properties in the site region. If such changes occurred before the Loma Prieta earthquake, our monitoring sites would surely have been within about 30 km of such a zone and could have been as close as 10 km or 15 km. Beaumont and Berger's work shows the latter situation would provide near maximum sensitivity for detection and, even for a more remote source, our sites would be well placed to experience the resultant tidal amplitude changes. If such changes did take place, then changes in Young's modulus over any large (kms) spatial extent had to have been less than about 2%. The corresponding change in  $V_p$  would be less than about 1%, a limit lower than that which has been set from travel time residuals for local earthquakes (Steppe *et al*, 1977) or for teleseismic events (Robinson and Iyer, 1976). The alternative possibility, which we cannot exclude, is that significant moduli changes occurred in a small preparation zone. This may remain an important issue in the mechanics of rupture, but is essentially academic in terms of precursor detection since we do not know the location of initiation of a future earthquake and, in many cases, cannot physically locate instruments very close to such a location even if we did know where it would be.

We conclude that there were no identifiable (greater than 2%) precursory changes in the solid earth tidal amplitudes for the Loma Prieta earthquake in the area about 35 km to the south of the epicenter. This result places a significant constraint on such



precursory effects and also corrects an earlier report of a positive result for this effect. That preliminary work by Johnston and Linde (1990) was in error, principally because not all the effects of electronic modifications to the SRL instrument were recognized and removed from the data at that time. The results obtained here are consistent with a report by Gladwin *et al* (1991) in which they noted the constancy of the Earth tidal amplitudes before the Loma Prieta earthquake. To the extent that our observations from these sites can be generalized, it now appears less likely that variations in Earth tidal amplitudes can serve as earthquake precursors.

### *Acknowledgements*

Doug Myren has provided valuable help in the operation of the SRL station, and we appreciate very much the work of Kate Breckenridge in maintaining the data acquisition files. Duncan Agnew first noted the possibility that a site visit may have been overlooked in the preliminary work. We thank Y. Tamura for supplying a copy of the BAYTAP(G) analysis program and for discussions on its use.

### **References**

- Beaumont, B., and J. Berger, Earthquake prediction: modification of the Earth tide tilts and strains by dilatancy, *Royal Astron. Soc. Geophys. Jour.* 39, 111–121, 1974.
- Gladwin, M. T., R. L. Gwyther, and R. Hart, Tidal calibration of borehole vector strain instruments, *Trans. Am. Geophys. Un.*, 66, 1057, 1985.
- Gladwin, M. T., R. L. Gwyther, R. Hart, M. F. Francis and M. J. S. Johnston, Borehole tensor strain measurements in California, *Jour. Geophys. Res.*, 92, 7981–7988, 1986.
- Gladwin, M. T., R. L. Gwyther, J. W. Higbie and R. Hart, A medium term precursor to the Loma Prieta earthquake? *Geophys. Res. Lett.*, 18, 1377–1380, 1991.
- Ishiguro, M., T. Sato, Y. Tamura, and M. Ooe, Tidal data analysis – an introduction to Baytap, *Proc. Institute of Statistical Mathematics*, 32, 71–85, 1984.
- Johnston, M. J. S., A. T. Linde, and M. T. Gladwin, Near field high resolution strain measurements prior to the October 18, 1989, Loma Prieta,  $M_S$  7.1 earthquake, *Geophys. Res. Lett.*, 17, 1777–1780, 1990.
- Johnston, M. J. S., and A. T. Linde, Possible change in Earth tidal response before the October 18, 1989, Loma Prieta  $M_L$  7.1 earthquake, *Trans. Am. Geophys. Un.*, 71, 1461, 1990.
- Kato, M., Observations of crustal movements by newly-designed horizontal pendulum and water-tube tiltmeters with electromagnetic transducers (2), *Bull. Disas. Prev. Res. Inst. Kyoto Univ.*, 29, 83–97, 1979.
- Mao, W. J., C. Ebblin, and M. Zadro, Evidence for variations of mechanical properties in the Friuli seismic area, *Tectonophysics*, 170, 231–242, 1989.

- Mikumo, T., M. Kato, H. Doi, Y. Wada, T. Tanaka, R. Shichi, and A. Yamamoto, Possibility of temporal variations in Earth tidal strain amplitudes associated with major earthquakes, *Earthquake Precursors: Proceedings of the US-Japan Seminar on Theoretical and Experimental Investigations of Earthquake Precursors*, eds. C. Kisslinger and Z. Suzuki, 123-136, Center for Academic Publications Japan, Tokyo, 1978.
- Nishimura, E., On Earth tides, *Trans. Am. Geophys. Un.*, *31*, 357-376, 1950.
- Robinson, R., and H. M. Iyer, Temporal and spatial variations of travel-time residuals in central California for Novaya Zemlya events, *Bull. Seis. Soc. Am.*, *66*, 1733-1747, 1976.
- Sacks, I. S., S. Suyehiro, D. W. Evertson, and Y. Yamagishi, Sacks-Evertson strainmeter, its installation in Japan and some preliminary results concerning strain steps, *Pap. Meteorol. Geophys.*, *22*, 195-207, 1971.
- Silverman, S., C. Mortensen, and M. J. S. Johnston, A satellite-based digital data system for low-frequency geophysical data, *Bull. Seis. Soc. Am.*, *79*, 189-198, 1989.
- Steppe, J. A., W. H. Bakun, and C. G. Bufe, Temporal stability of P-velocity anisotropy before earthquakes in central California, *Bull. Seis. Soc. Am.*, *67*, 1075-1090, 1977.
- Tanaka, T., Effect of dilatancy on ocean load tides, *Pure Appl. Geophys.*, *114*, 415-423, 1976.

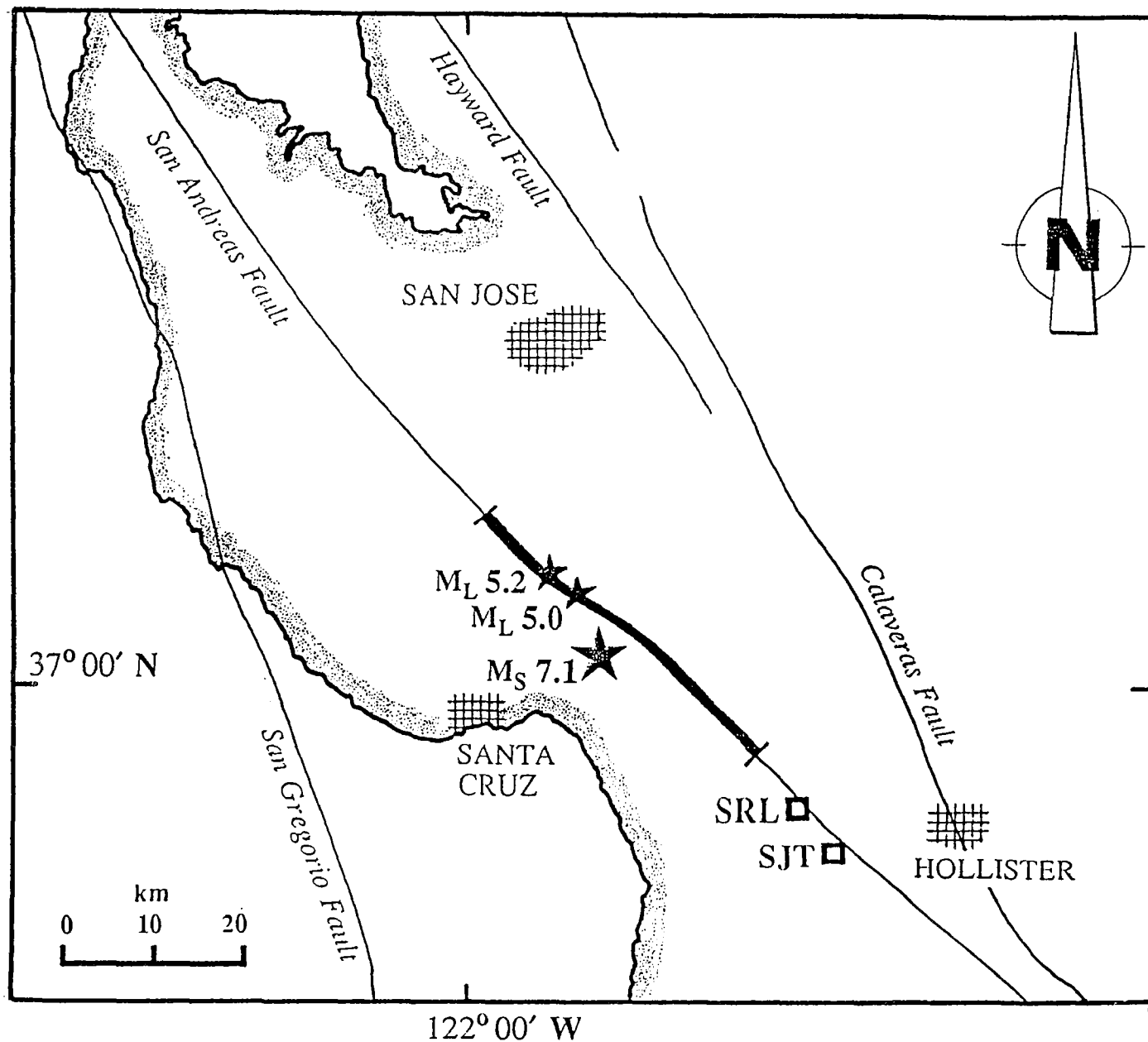


Figure 1. Map showing the two borehole strainmeter sites SRL and SJT in relation to the fault break of the Loma Prieta earthquake. The two smaller earthquakes marked are the Lake Ellsman events of 1988 and 1989.

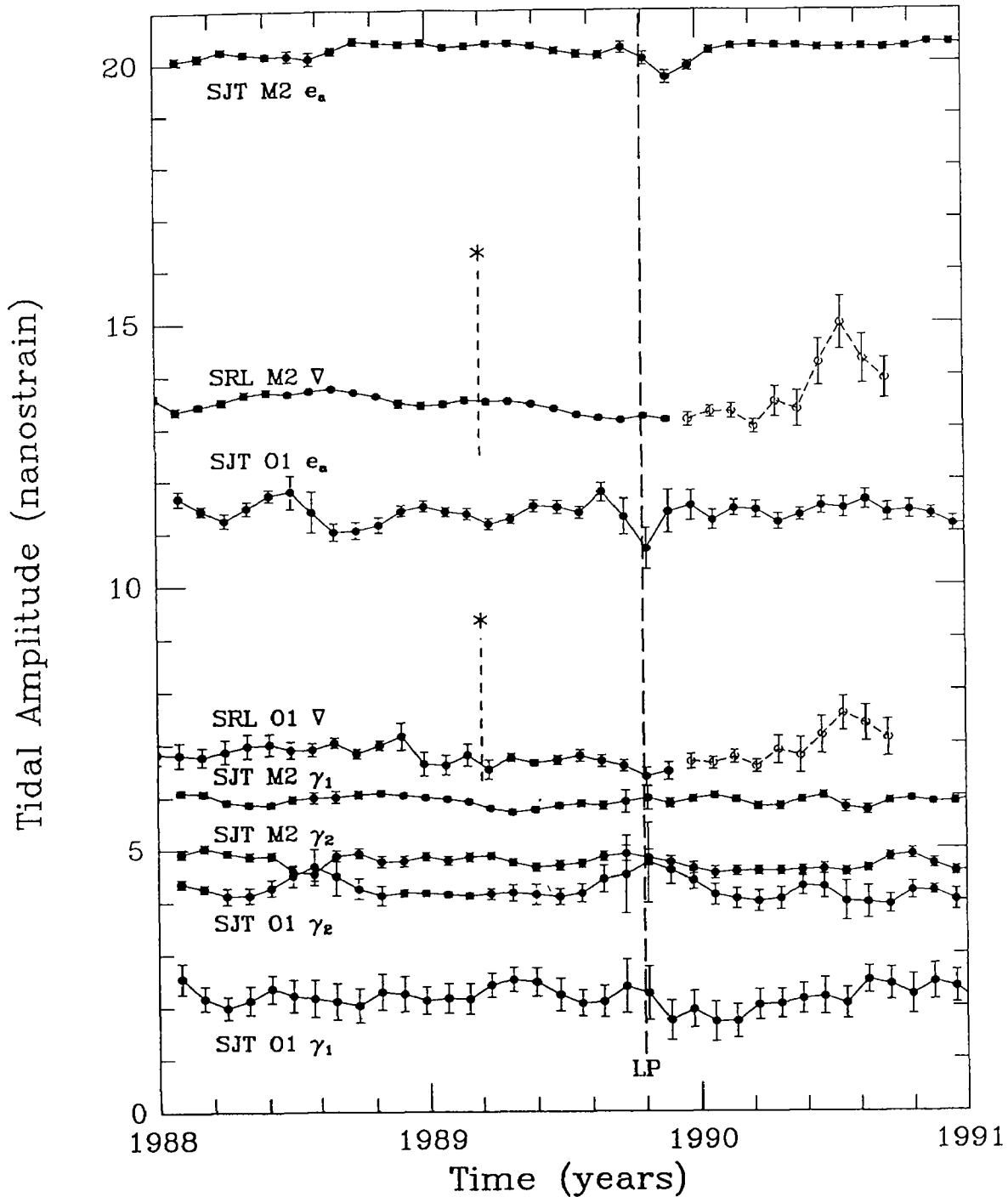


Figure 2. Earth tidal strain amplitudes, for tidal components M2 and O1, as a function of time at the sites SRL and SJT shown in Figure 1. Error bars are for one standard deviation. The long vertical dashed line marked LP indicates the time of the Loma Prieta earthquake. The shorter dashed lines, marked \*, show the time of an electronic change at SRL (see text). From 1990, SRL data have been gain corrected (using atmospheric pressure response) and are shown dashed with open circles (also see text). We find no significant variations in these amplitudes preceding the earthquake. Note also that the earthquake has not produced any significant coseismic or postseismic effect on tidal amplitudes. The larger values near the end of the SRL traces apparently result from an overcorrection.

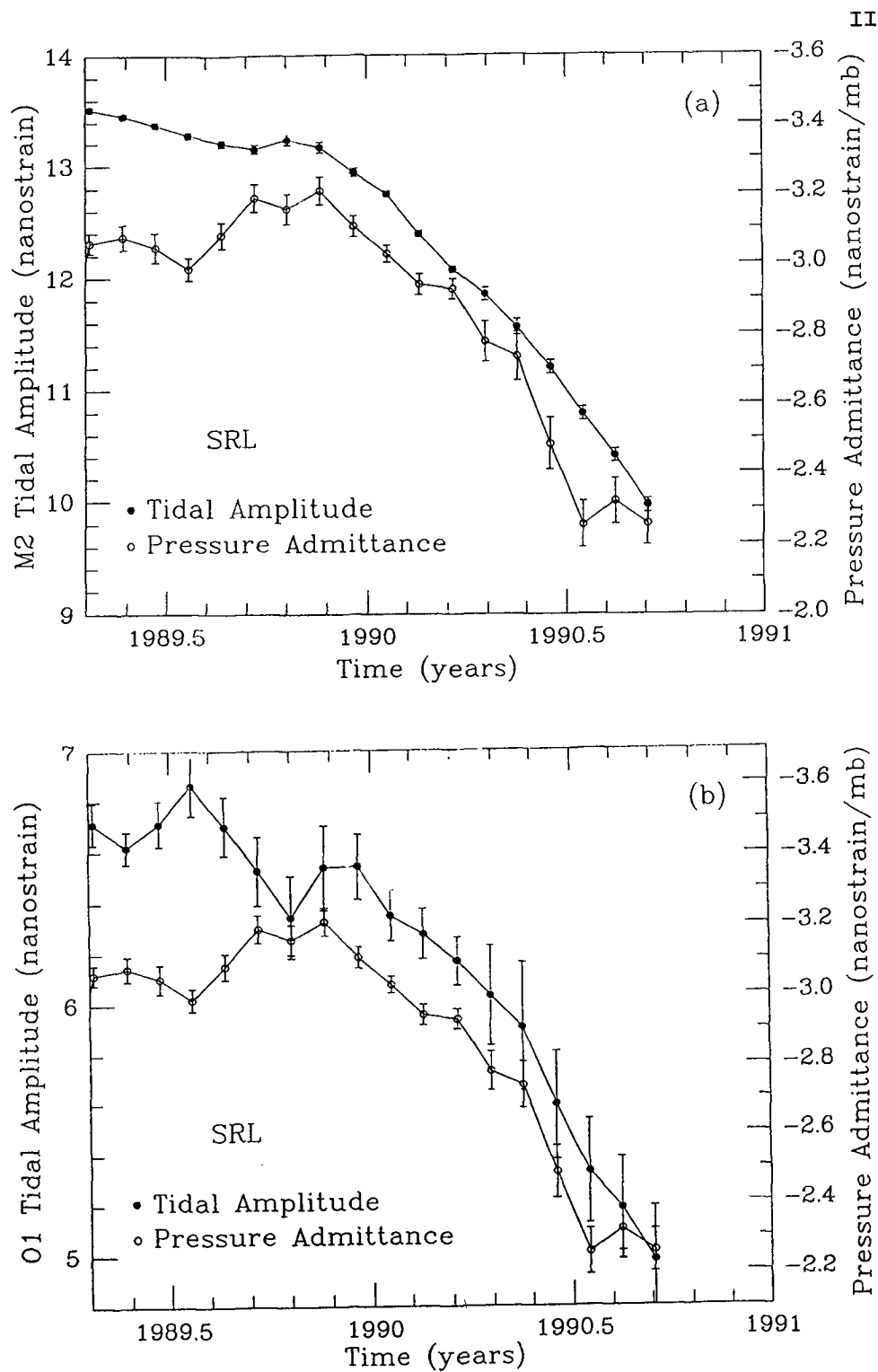


Figure 3. Pressure admittance and tidal amplitudes at SRL following the March 1989 electronic modification. M2 amplitudes are shown in (a) and O1 in (b). Pressure admittance is negative since an increase in atmospheric pressure produces contraction (negative strain) in the near surface rock. While the admittance undergoes real changes with time, it is clear that both tidal amplitudes and the admittances systematically decrease during 1990. This is attributed to a slowly decreasing effective gain of the instrument during that period.

## Installation of Borehole Strainmeters – Bay Area

Grant 14-08-0001-G2125

Alan T. Linde and I. Selwyn Sacks  
Department of Terrestrial Magnetism  
Carnegie Institution of Washington  
5241 Broad Branch Rd. NW  
Washington DC 20015  
(202) 966 0863

### Objective

This project, recently funded, is for construction and installation of Sacks-Evertson borehole strainmeters in the Bay Area and is a collaborative program with the U.S. Geological Survey, M. Johnston being the principal cooperating scientist.

### Progress to Date

It is very early in this program so that we do not expect to begin installation until well into 1992. Site selection has been made by M. Johnston and the initial drilling phase is under way. The holes currently being drilled are exploratory holes to determine if potential sites are suitable for borehole monitoring of strain.

We are currently reevaluating all details of the instrument design and construction with a view to improving instrument reliability. Instrument cable specifications have been modified to provide a more robust cable and more stringent testing conditions have been determined. Modifications to the instrument design include use of a thicker wall bellows (increasing from 0.001 inch to 0.0015 inch) which will reduce the possibility of imperfections in the bellows resulting in a leak; this is at the expense of some loss of gain but the instrument will still have sensitivity better than  $10^{-11}$ .

We expect that instrument construction will begin soon and that the installation will commence next spring when the holes will also be available.

## **Determination of Slip Rate and Paleoseismicity of the Rose Canyon Fault Zone, San Diego, California**

14-08-0001-G1982

Scott C. Lindvall  
Lindvall Richter Benuska Associates  
825 Colorado Boulevard, Suite 114  
Los Angeles, CA 90041  
(213) 254-5257

Thomas K. Rockwell  
Department of Geological Sciences  
San Diego State University  
San Diego, CA 92182  
(619) 594-4441

### **OBJECTIVES:**

This study expands on our previous work (Lindvall et al., 1990; Rockwell and Lindvall, 1990) in which we identified the principal strand of the Rose Canyon fault zone and documented evidence for recurrent Holocene surface-rupturing earthquakes at a trench site located on a Holocene terrace of Rose Creek. The purpose of this study was to continue investigating the Rose Canyon fault at this site, using 3-D trenching to determine: 1) a Holocene slip rate and 2) the timing of past earthquakes and the amount of slip produced in these events, if possible.

### **INVESTIGATION:**

We reoccupied our 1989 trench site with the intent of exposing the fault zone in three dimensions and resolving slip based on displaced fluvial features. This site, which is covered by artificial fill and an asphalt parking lot surface, was originally identified in early air photos that predate the development of the site in 1960.

Initially, we excavated two fault-parallel trenches to further establish the site's stratigraphy and identify any linear fluvial features or sedimentary structures that could be used as piercing points for defining horizontal and vertical offset. We found only one such feature, a distinct gravel-filled channel oriented normal to the fault. The channel was the only coarse, gravelly channelized deposit that was found in over 65 m of linear trench amidst the relatively fine-grained, weakly stratified, silty to clayey sand deposits of probable floodplain origin. We then had the artificial fill removed to a depth of 2 - 2.5 m to the top of the natural deposits over a large area (12 x 8 m) in order to facilitate tracing the distinct gravel channel into and across the multiple strands of the fault. From the floor of this large rectangular excavation, a series of parallel and orthogonal connecting trenches were excavated by hand to expose the channel into and across the different strands of the fault, leaving the channel preserved in blocks of native sediment.

After all of the trench faces were logged, they were surveyed with a Wild Total Station to accurately locate each exposure in 3-D space. Several charcoal samples were collected and are being prepared to submit for age dating.

## RESULTS:

We were successful in determining a Holocene slip rate of 1.1 mm/yr based on an offset buried channel. The channel was found offset across multiple strands of the fault, but grading operations at the site in 1960 cut out the stratigraphic unit containing the channel west of the westernmost strand exposed in our trenches (Figure 1). The minimum displacement recorded by the channel is 8.7 m of dextral slip with less than 1 m of west-side-up vertical slip.

Using a minimum of 8.7 m of brittle slip and a maximum age of the channel at 8,155  $\pm$  234/-202 years B.P., we obtain a minimum early Holocene to present slip rate of 1.07  $\pm$  0.03 mm/yr. The age of the channel is presently constrained by AMS dates of detrital charcoal collected during the previous study in 1989. Two samples from unit C3, which underlies and predates the channel, yielded radiocarbon ages of about 7.4 ka and 7.9 ka. Combining these two dates and dendrochronologically correcting them yields a weighted, 2-sigma (95% confidence) date of 8155  $\pm$  234/-202 years B.P.

Dates from charcoal samples collected during this investigation will better constrain the age of the channel and hence, refine this minimum Holocene slip rate for Rose Canyon fault.

## REPORTS:

Lindvall, S.C. and Rockwell, T.K., 1991, Minimum Holocene slip rate for the Rose Canyon fault zone in San Diego, California, *Eos Transactions, American Geophysical Union*, v. 72, no. 44, p. 351.

Rockwell, T.K., Lindvall, S.C., Haraden, C.C., Hirabayashi, C.K., and Baker, E.D., 1991, Minimum Holocene slip rate for the Rose Canyon fault in San Diego, California, in Abbott, P.L. and Elliot, W.J., eds., *Environmental Perils, San Diego Region*, published for the Geological Society of America Annual Meeting by San Diego Association of Geologists, p. 37-46.

## REFERENCES:

Lindvall, S.C., Rockwell, T.K., and Lindvall, C.E., 1990, The seismic hazard of San Diego revised: New evidence for magnitude 6+ Holocene earthquakes on the Rose Canyon fault zone: *Proceedings of the Fourth U.S. National Conference on Earthquake Engineering*, Palm Springs, California, May 1990, v. 1, p. 679-688.

Rockwell, T.K. and Lindvall, S.C., 1990, Holocene activity of the Rose Canyon fault in San Diego, California, based on trench exposures and tectonic geomorphology: *Geological Society of America Abstracts with Programs*, v. 18, no. 1, p. 177.



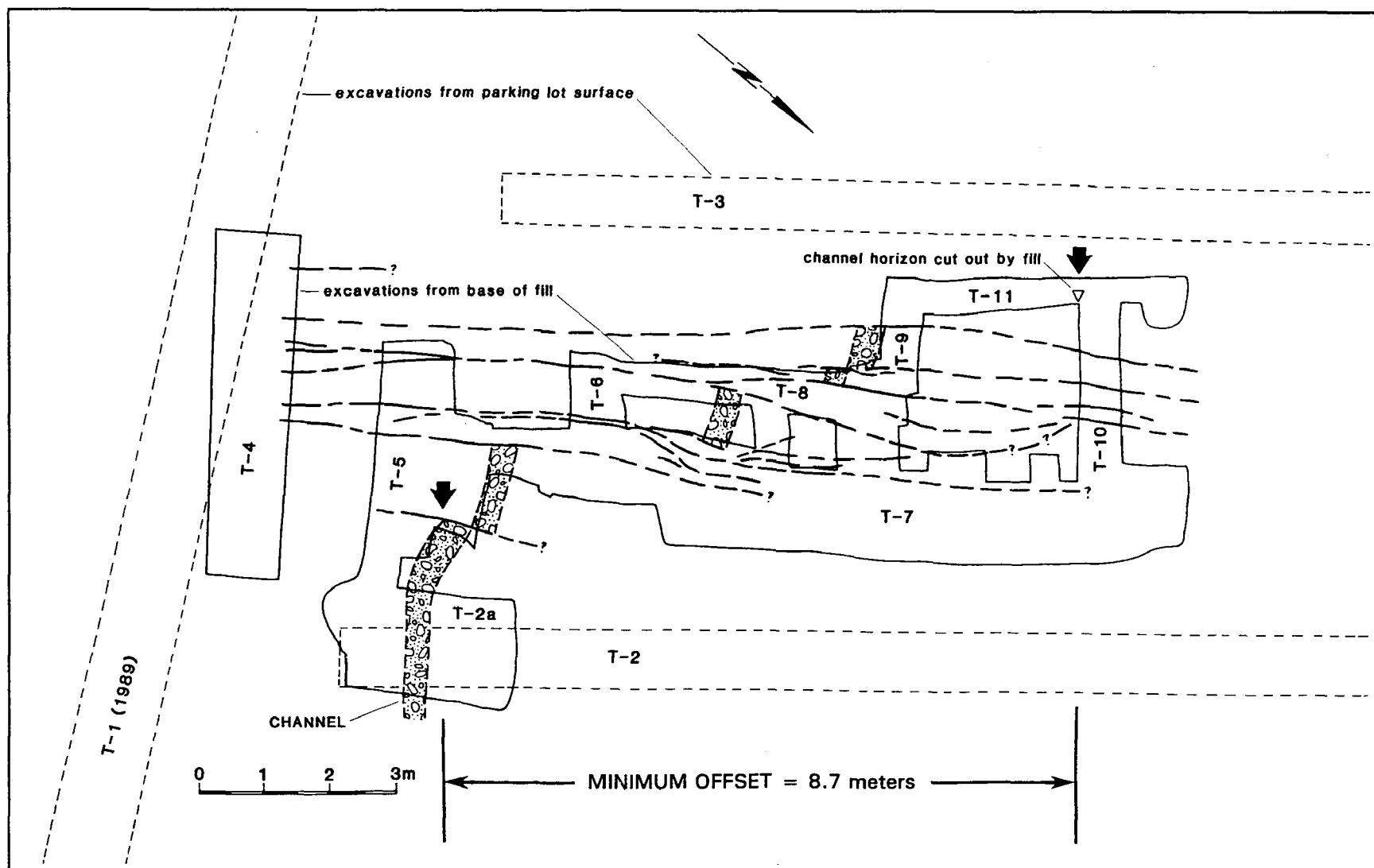


Figure 1. Map view of trenches, faults, and the offset channel at the Beach Cities Operating Center site. Trenches 1-3 (dashed lines) were excavated from the parking lot surface, whereas trenches 4-11 (solid lines) were hand dug from the floor of the large excavation (not shown) that removed the artificial fill.

## CRUSTAL STRAIN

9960-01187

M. Lisowski, J.C. Savage, W.H. Prescott, N.E. King, J.L. Svarc, M.H. Murray  
 Branch of Tectonophysics  
 U.S. Geological Survey  
 345 Middlefield Road, MS/977  
 Menlo Park, California 94025  
 (415) 329-4855

### Investigations

The principal subject of investigation was the analysis of deformation in a number of tectonically active areas in the United States.

Geodolite surveys during the reporting period include measurement of the Coastal San Luis (CA), Loma Monitor (CA), Hanford (WA), and Mt. St. Helens (WA) networks. Global Positioning System (GPS) surveys in California include the southern California and Parkfield Monitor networks, Parkfield network, Parkfield quadrilateral, Mammoth-Mono Chain network, Mt. Lassen-Mendocino network, and five profiles in the San Francisco Bay Area. GPS surveys outside of California include the Roseberg (OR), Juan de Fuca (WA), Katmai (AK), and Shumagin (AK) networks. Some Geodolite stations in the Coastal San Luis, Hanford, and Mt. St. Helens networks were occupied with GPS. Additional intermediate GPS sites tie the Hanford, Mt St. Helens, and Columbia River networks. The May, 1991, Juan de Fuca GPS survey was a cooperative effort with the Canadian Geological Survey, SCRIPPS, and JPL. We occupied five onshore sites to support the first epoch measurement of the position of two sea-floor acoustic transponders. GPS surveys near Mt. St. Helens and Mt. Lassen were joint efforts with the Cascade Volcano observatory. The personnel and equipment of the Crustal Strain project and Modeling and Monitoring Crustal Deformation project were pooled for the Mammoth-Mono Chain GPS survey. A list of field surveys during this reporting period is given in Table 1.

We purchased six Ashtech dual-frequency GPS receivers during FY 91 (in addition to the four acquired in FY 90). These receivers track the C/A coded  $L_1$  carrier and codeless  $L_2$  carrier phase signals. The receivers are compact, self-contained, and have low power requirements (12 Watts). The receivers can operate on battery power unattended for up to seven days. Initial problems with intermittent memory loss and inability to track when placed near communication facilities have been resolved. The quality of the  $L_2$  data is not as good as the  $L_1$ . A receiver firmware upgrade, expected soon, will improve the quality of the  $L_2$  data. We have upgraded our computers and are streamlining our data reduction procedures to cope with the increased amount of data that can be collected. The project's five TI-4100 receivers, as currently configured, do not allow simultaneous sampling with the global tracking sites. A signal degradation technique known as Selective Availability (SA), which became active in July of 1991, results in phase deviations between receivers that do not sample the wave front at the same instant. We are experimenting with a laptop-computer

based data sampling and recording system. This system allows simultaneous sampling and cures persistent problems with the TI-4100's data recording and the display units. Although the TI-4100 are bulky, power hungry, difficult to operate, and can only track four satellites at a time, they do provide  $L_1$  and  $L_2$  P-code pseudorange and carrier phase signals. This combination simplifies repairing cycles slips and provides the optimum data for resolving integer cycle ambiguities in the carrier phase data.

Measurements between two stations of a planned four-station continuously recording GPS network to monitor the Hayward fault began on September 9, 1991. The sites are located in San Leandro and Hayward. Sites are being evaluated for future installation of two Trimble dual-frequency receivers.

Table 1. Field Surveys 01 May 1991 to 30 September 1991

Project	Region/ Program	Survey Dates	Field Days	Geod- olite Lines	GPS Station Days	Local Ties	GPS Sta- tions	Local Sta- tions
S. California GPS Monitor	SCAL	91/05/04--08	5		21	3	21	3
Coastal San Luis Geodolite	SCAL	91/05/14--05/15	2	18				
Coastal San Luis GPS	SCAL	91/5/16	1		6	1	6	1
Juan de Fuca	PACNW	91/05/28--06/02	10		41	29	12	5
Napa GPS recovery	CORE	91/06/10--06/11	2		11		9	
Loma Geodolite Monitor	CORE	91/6/20	1	3				
Loma GPS Monitor	CORE	91/6/25	1		4		4	
Parkfield GPS Monitor	CORE	91/5/26	1		5		5	
Katmai GPS Array	VOLHAZ	91/06/21--07/02	10		47	1	10	1
Shumagin GPS Array	CORE	91/07/03--07/08	6		27		9	
Mammoth+Mono Chain GPS	VOLHAZ	91/07/11--07/16	6		41		35	
Hanford Geodolite	PACNW	91/07/22--07/24	3	31				
St Helens Geodolite	PACNW	91/07/26--07/29	4	26				
St Helens and Hanford GPS	PACNW	91/07/30--08/01	3		17		16	
Roseberg GPS	PACNW	91/08/02--08/04	2		10	4	9	4
Mt Lassen-Mendo GPS	PACNW	91/08/04--08/06	3		15	5	10	4
Loma GPS Profile + Monitor	BAFEP	91/08/26--08/29	4		20	2	15	2
SBay GPS Profile	BAFEP	91/09/03--09/06	4		22	1	17	1
CBay GPS Profile	BAFEP	91/09/09--09/12	4		20		16	
GG GPS Profile	BAFEP	91/9/16	1		6		6	
NBay GPS Profile	BAFEP	91/09/17--09/20	4		25		18	
Totals			77	78	338	46	218	21

## Results

### 1. *Deformation of the Hanford, Washington, Network 1972–1991*

The Hanford trilateration network is located near Richland in south central Washington on a Federal reservation (the Hanford site) used in part to store radioactive wastes. The network lies in the back-arc region of the Cascadia subduction zone, 450 km east of the deformation front and 150 km east of the Cascade volcanoes. The strain accumulation there deduced from the trilateration measurements is shown in Figure 1. The circled points lie more than two standard deviations from the mean of all of the data. The measurements are adequately represented by the linear fits shown in the figure, and the slopes of those linear fits suggest that the strain accumulation rate is no more than one or two nanostrain/year.

### 2. *Strain Accumulation of the Loma Prieta Geodolite Monitor Network Prior to the Loma Prieta Earthquake*

Geodetic measurements of distance from a monument on Loma Prieta, 11 km northeast of the epicenter of the Loma Prieta earthquake ( $M_s = 7.1$ ; October 17, 1989), to three stations 31 to 43 km distant provide an unusually complete record of deformation in the epicentral area. The Geodolite measurements were discussed by *Lisowski et al.*, [*Geophys. Res. Lett.*, **17**, 1211–1214, 1990], but at the time of that publication only preliminary reductions of the GPS data were available. The GPS data as finally reduced are shown in Figure 2 along with the previously reported Geodolite measurements. The offset between the two data sets is of no significance as the GPS measurements are not referred to the same station marks as the Geodolite measurements. However, the trends in the two data sets should be identical. Linear fits to both data sets are shown for the 1987.7–1989.9 interval (the interval over which GPS data are available). The slopes of those linear fits are shown in the figure. The two slopes do not differ at the two-standard-deviation significance level. We had earlier attached marginal significance to the change in slope in the Geodolite measurements to Allison starting in 1988.5 at the time of the first foreshock. The GPS data do not support that interpretation. Thus, the possibility of a geodetically detected precursor to the Loma Prieta earthquake is more dubious in light of the GPS observations.

### 3. *The Uncertainty in Earthquake Conditional Probabilities*

The Working Group on California Earthquake Probabilities (WGCEP) questioned the relevance of uncertainty intervals assigned to earthquake conditional probabilities on the basis that the uncertainty in the probability estimate seemed to be greater the smaller the breadth of the recurrence-interval distribution. That paradox depends upon a faulty measure of uncertainty in the conditional probability; with a proper measure of uncertainty no paradox exists. Also, the assertion that the WGCEP probability assessment in 1988 correctly forecast the 1989 Loma Prieta earthquake is challenged by showing that the posterior probability assessed after the occurrence of the earthquake based on the 1988 WGCEP distribution as the prior probability reverts to a nearly informationless distribution.

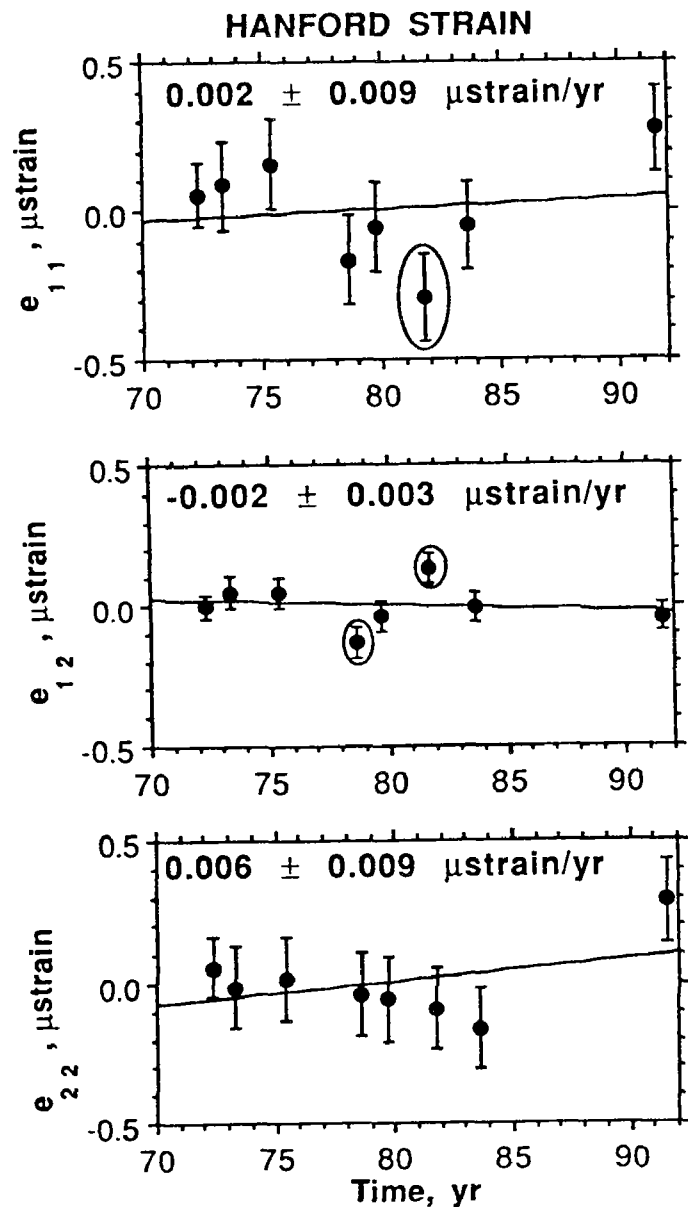


Figure 1. Tensor strain accumulation in the Hanford, Washington, Geodolite network referred to a coordinate system with the 1 axis directed east and the 2 axis north.

Error bars denote one standard deviation on either side of plotted point.

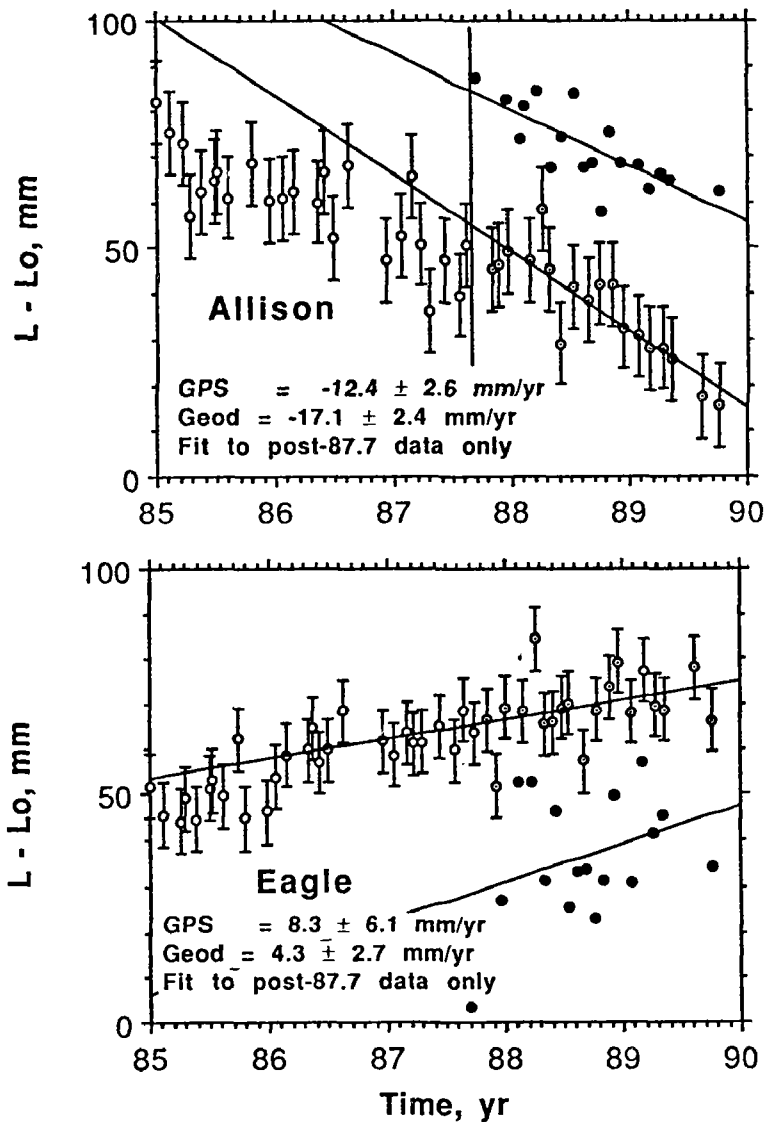


Figure 2. Distance from Loma Prieta to Allison (upper) and Eagle (lower) as measured by Geodolite (open circle with error bars) and GPS (solid circle).

### 1. Hayward Fault Permanent GPS Array

On September 9, 1991, the Crustal Strain project began daily GPS observations of a baseline across the Hayward fault. We will use this data to monitor the Hayward fault, serve as a fiducial site, study the signal and noise spectra, and determine the effects of various processing strategies. Two codeless dual-frequency Ashtech receivers collect data 24 hours a day, at 30 second intervals. The baseline is 8.1 km long and strikes nearly north-south. We use the Bernese version 3.2 software to process daily seven-hour sessions in semi-automated mode. Currently, the main technical barrier to automation is the noise in the  $L_2$  phase data. Figure 3 shows the  $L_3$  solution for seven-hour sessions. The rms errors for the  $L_3$  solution are 2.7 mm in length, 2.7 mm in the north and east components, and 9.6 mm in the vertical component. We have found that very short sessions of only two or three hours yield poor results; the difference in the  $L_3$  solution between two-hour and seven-hour sessions may be 1–2 cm for the north component and 5–10 cm for the east component. The  $L_1$  and  $L_2$  solutions are not satisfactory, since the ionospheric delay apparently does not cancel even between stations separated by only 8 km. The rms errors for the  $L_1$  and  $L_2$  solutions are 14.0 and 22.4 mm in length, 13.9 and 23.5 mm in the north, 5.2 and 12.9 mm in the east, and 15.7 and 23.0 mm in the vertical. For each component, the  $L_1$ ,  $L_2$ , and  $L_3$  solutions differ systematically by up to several cm and the  $L_1$  and  $L_2$  solutions are highly correlated.

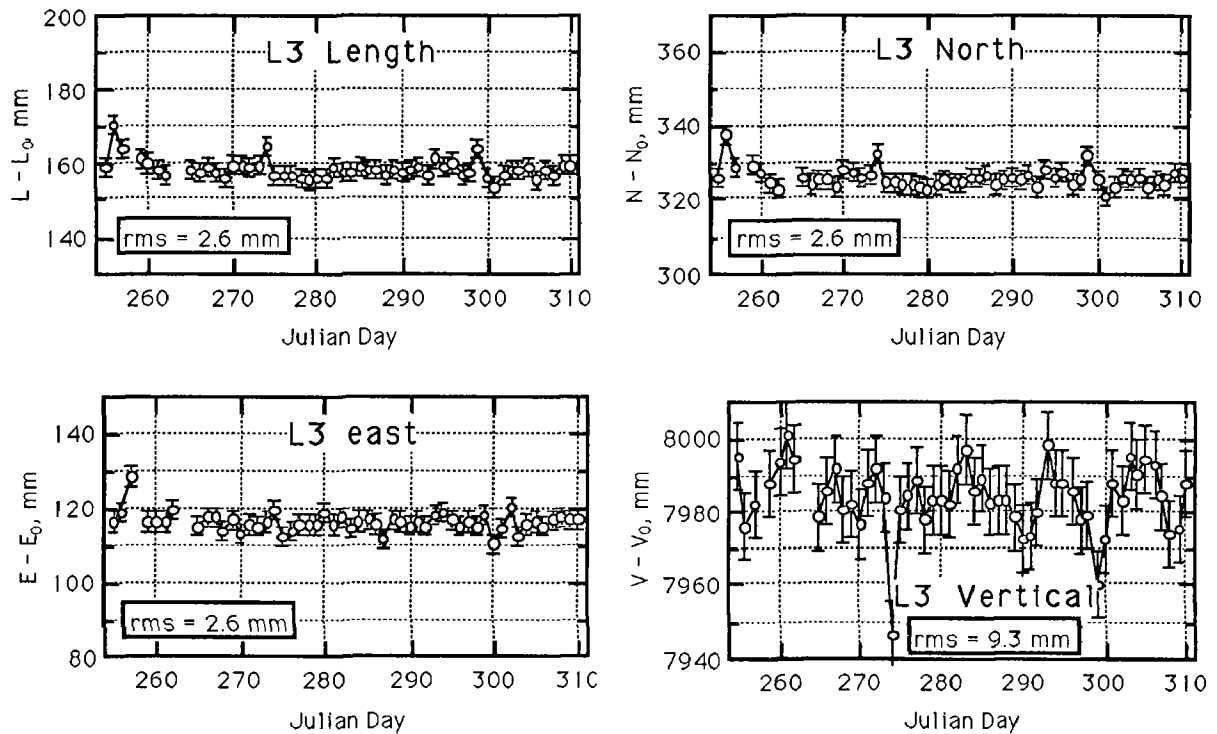


Figure 3. Length and vector components as a function of time for the 8.1 km baseline between the continuously recording GPS receivers near the Hayward fault. Error bars are  $\pm 1$  sd as derived by the rms scatter about the mean.

## 5. *Preliminary Comparison of Repeatability of GPS Observations in the Loma Monitor Network*

We have begun a comparison of relative locations estimated from GPS observations processed with the Bernese 3.2 and GAMIT 8.2.6 software packages. Nine GPS observations collected using TI-4100 receivers over a one-year period beginning in September 1987 of the north-south oriented 43-km Loma Prieta to Allison baseline and the east-west oriented 32-km Loma Prieta to Eagle baseline were used in the comparison. Additional observations from North American CIGNET fiducial sites, typically spanning 3 to 5 days, were included to improve orbit estimation. Equivalent estimation techniques were used to model the atmosphere and satellite orbits. Ionosphere-free bias-fixed results using both Bernese and GAMIT are shown in Figure 4.

In general, the Bernese and GAMIT estimates are in good agreement. The north component for each baseline differ by less than 1 mm on the Loma Prieta–Eagle baseline and less than 5 mm on Loma Prieta–Allison. The weighted root-mean-square (wrms) scatter of the north-component estimates about a linear trend 4 mm for both baselines. The estimates in the vertical, typically the most poorly resolved component from GPS observations, show centimeter-level agreement and several centimeter-level scatter. The most significant difference between the Bernese and GAMIT estimates is in the east component of both baselines. Although they generally differ by less than 10 mm, four estimates differ by up to 25 mm. The wrms scatter of the GAMIT estimates is better than that of the Bernese, with the Loma Prieta–Eagle baseline scatter improving from 15 to 4 mm (equivalent to the north component estimates) and the Loma Prieta–Allison scatter improving from 12 to 8 mm. We believe that most of these differences are due to the improved ambiguity resolution techniques used by GAMIT, which fixed all biases on these short baselines.

## 6. *Farallon Islands Geodolite Network.*

North of the San Francisco peninsula, it is difficult to obtain geodetic measurements across the San Andreas fault because the fault lies offshore or right on the coast. The Farallon Islands, 45 km west of San Francisco, provide a platform for such measurements. Since late 1978, the Crustal Strain project has measured a five-line, 50-km trilateration network between the Farallons and the coast. Each baseline has been measured 7 to 12 times with Geodolite. Since 1986, the network has also been observed annually with GPS. There is a systematic difference of a centimeter or more between Geodolite and GPS measurements. This bias is not observed at other networks measured with both Geodolite and GPS, and is unexplained at this time. For the 12 years of Geodolite observations, the principal strain rates are  $0.134 \pm 0.017 \mu\text{strain/yr}$  oriented  $\text{N}84^\circ\text{W} \pm 3^\circ$  and  $-0.100 \pm 0.018 \mu\text{strain/yr}$  oriented  $\text{N}06^\circ\text{E} \pm 3^\circ$ . This implies a maximum engineering shear strain rate of  $0.234 \pm 0.019 \mu\text{strain/yr}$ , oriented  $\text{N}39^\circ\text{W} \pm 3^\circ$ , consistent with the local strike of the San Andreas fault ( $\text{N}40^\circ\text{W}$ ). Total fault-parallel displacement across the network is  $10 \pm 1 \text{ mm/yr}$ . For the simplest dislocation model of constant fault slip below some locking depth, the observed surface deformation requires  $23.0 \pm 2.5 \text{ mm/yr}$  of strike slip below 15 km on the San Andreas fault. However, there is no unique solution, and there are other fault geometries for which a satisfactory solution may be found.

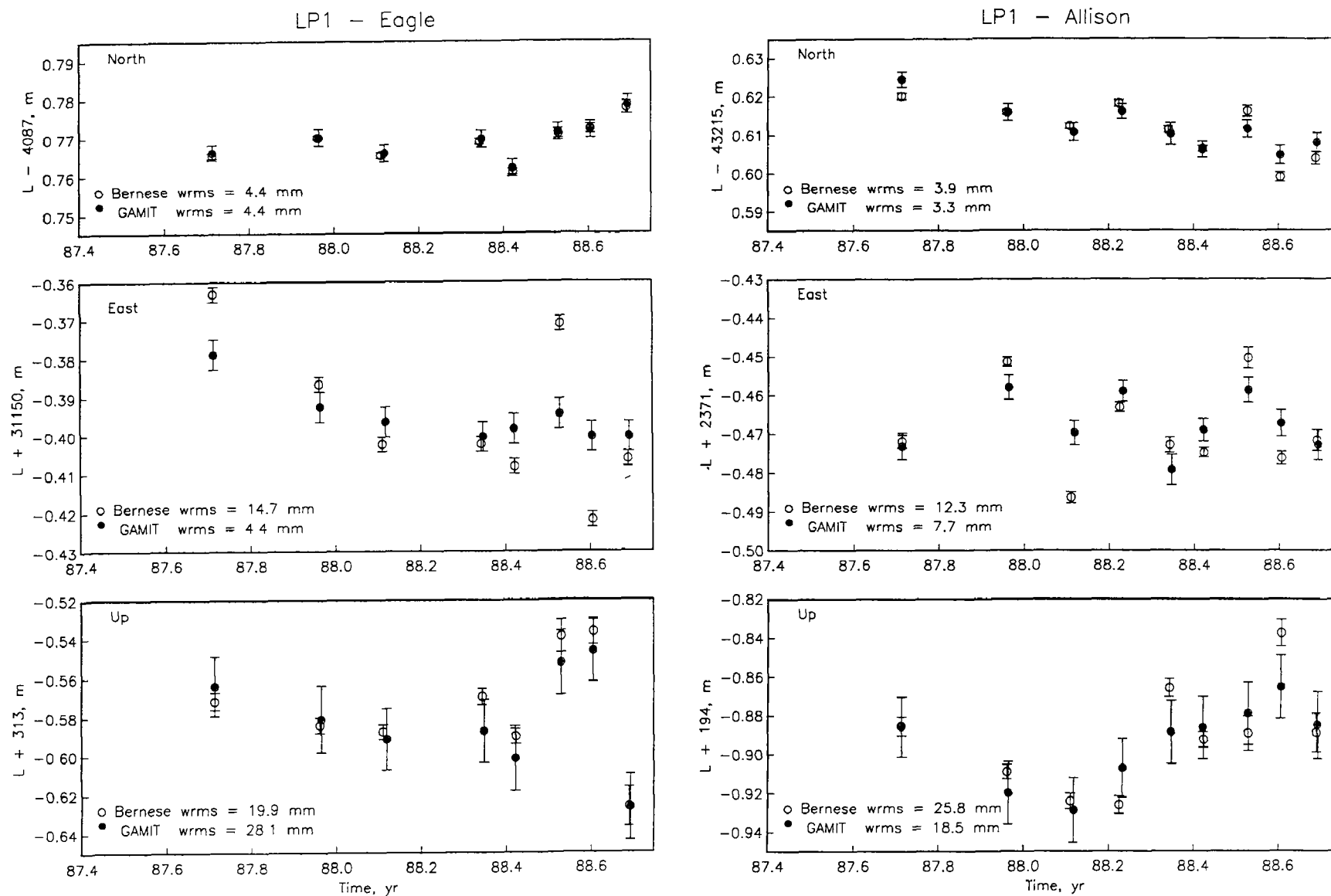


Figure 4. North, east, and up vector components of GPS bias-fixed estimates of the Loma Prieta to Allison and Loma Prieta to Eagle baselines. The open circles were estimated using the Bernese software and the solid circles were estimated using GAMIT. The error bars (1 standard error) are estimated by each software. The weighted root-mean-square (wrms) scatters are with respect to a weighted linear fit to the data.



## 7. Surface Deformation After the Loma Prieta, California, Earthquake

Repeated measurements of a 13-station GPS profile extending 100 km across the strike of the San Andreas fault near the rupture zone of 1989  $M_s$  7.1 Loma Prieta earthquake show significant post-seismic deformation. We measured the relative positions between the geodetic stations 2, 6, 14, 49, 91, 153, 335, and 476 days after the earthquake with TI-4100 receivers. All data was reduced with Bernese 3.2 software and relative positions are from orbit-improved, fixed-ambiguity solutions. The relative positions appear to change linearly with time. We use the average station velocities relative to a station 20 km east of the fault to describe the post-seismic deformation. The dislocation model includes 83 mm/yr of shallow (4 to 11 km depth) and 15 mm/yr of deep (below 11 km) right-lateral slip on the San Andreas fault and 15 mm/yr of right-lateral slip on the Calaveras fault to approximate the parallel component of the post-seismic velocities. The fault-perpendicular velocity is best explained by the horizontal collapse at a rate of 110 mm/yr of the rupture zone in the depth interval 3 to 7 km.

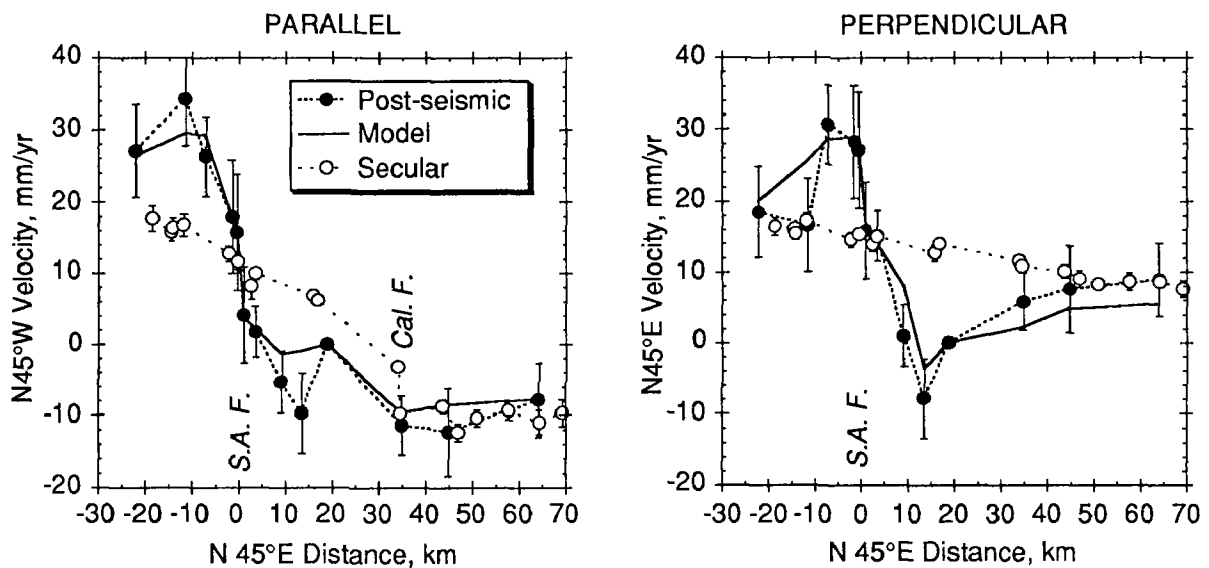


Figure 5. The fault-parallel and fault-perpendicular relative velocity components as a function of distance from the San Andreas fault for the 1.3 year post-seismic interval (solid circles), a preliminary uniform slip dislocation model (solid line), and the 20-year pre-seismic average measured across a trilateration network (open circles). Displacements are relative to the station located 20 km east of the fault.

## 8. Deformation of the Mt. St. Helens, Washington, Network 1982–1991

The Mt. St. Helens network extends for 120 km along the Cascade Volcanic Arc from the Columbia River to just beyond the Cowlitz River. Trilateration surveys in 1982 and 1991 show a low rate of strain accumulation across the network. Principal strain rates (extension reckoned positive) are  $0.050 \pm 0.020 \mu\text{strain/yr}$  oriented  $N6^\circ E \pm 15^\circ$  and  $0.019 \pm 0.021 \mu\text{strain/yr}$  oriented  $N96^\circ E \pm 15^\circ$ . The rate of straining, however, does not appear to be uniform within the network. Within 20 km of Mt. St. Helens we find a near

uniaxial north-south extension at a rate of  $0.148 \pm 0.043 \mu\text{strain/yr}$ . Strain accumulation rates in parts of the network farther from the volcano are less than  $0.030 \mu\text{strain/yr}$  and are not significant at one standard deviation.

### Reports

- King, N.E., and D.C. Agnew, How large is the retrograde annual wobble?, *Geophys. Res Lett.*, **18**, 1735–1738, 1991.
- Lienkaemper, J.J., G. Borchardt, M. Lisowski, Historic creep rate and potential for seismic slip along the Hayward fault, California, *J. Geophys. Res.*, **96**, 18261–18283, 1991.
- Lisowski, M., Recent plate motions and crustal deformation, *Rev. of Geophy.*, 162–171, 1991.
- Savage, J.C., and M. Lisowski, Strain accumulation along the Denali fault at the Nenana River and Delta River crossings, Alaska, *J. Geophys. Res.*, **96**, 14481–14492, 1991.
- Savage, J.C., M. Lisowski, and W.H. Prescott, Strain accumulation in western Washington, *J. Geophys. Res.*, **96**, 14493–14507, 1991.
- Savage, J.C., Criticism of some forecasts of the National Earthquake Prediction Evaluation Council, *Bull. Seismol. Soc. Am.*, **81**, 862–881, 1991.

# CRUSTAL VELOCITY STRUCTURE AND GROUND RESPONSE IN THE PUGET SOUND/WILLAMETTE LOWLAND REGION

9930-03791

James Luetgert, Walter D. Mooney  
Branch of Seismology  
U.S. Geological Survey  
345 Middlefield Road, MS977  
Menlo Park, California 94025  
(415) 329-4763

## Investigations

Despite the importance of the Pacific Northwest as a natural laboratory of active tectonic processes, and of seismic and volcanic hazards, only a limited amount of deep seismic profiling has been conducted in this region. Our present knowledge of the structural framework of the Pacific Northwest is largely based upon projections of surface geology to depth, inferences from gravity, aeromagnetic and magnetotelluric data, limited seismic reflection data and observed patterns of seismicity. We began to address this deficiency in September, 1991, with a major active seismic field program that was initiated by the USGS Earthquake Hazards Reduction and Deep Continental Studies Programs.

Several key objectives are being targeted in this work:

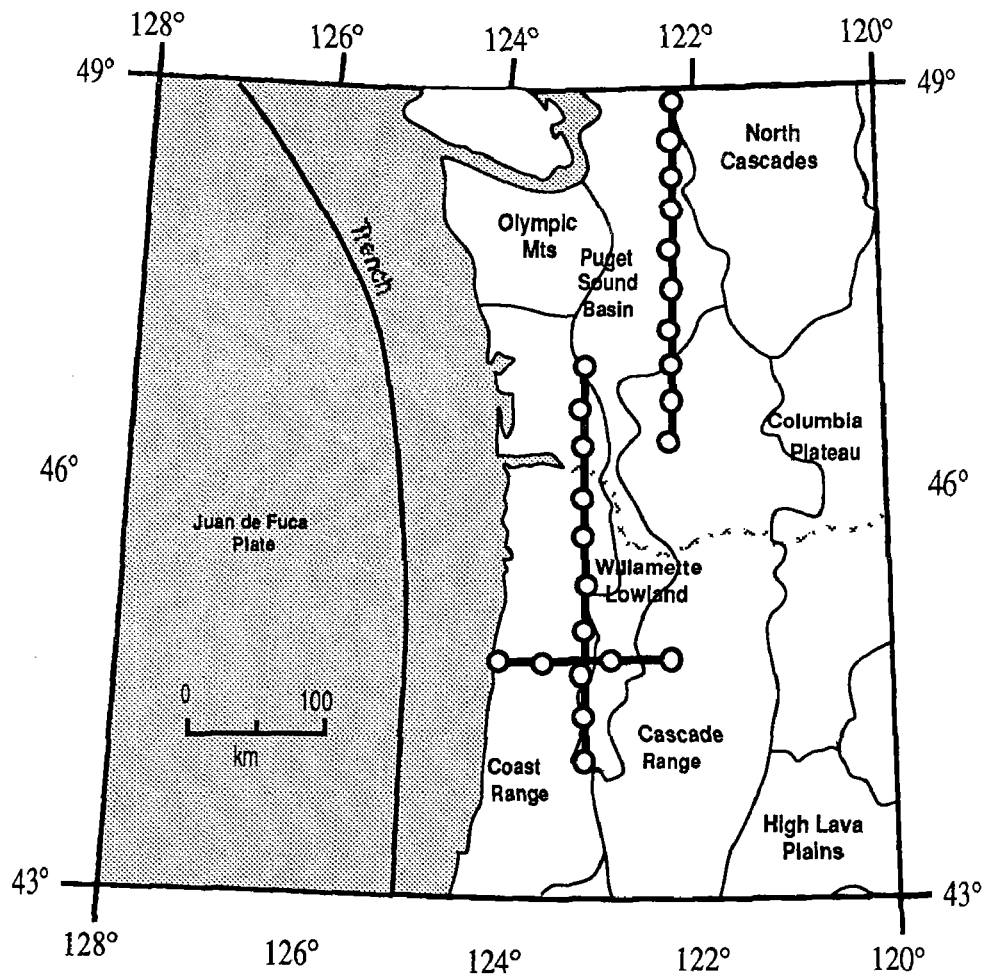
- Determination of the relationships between seismicity and structure - What is the relationship between forearc seismicity and crustal and upper mantle structure? Is there a north-south change in crustal structure that correlates with seismicity patterns? Are the apparent lineaments in seismicity observed in southern Washington related to velocity/structural boundaries? Are there structural boundaries/offsets which have not yet revealed themselves in the seismicity?
- Definition of the tectonic regime of the Pacific Northwest - What is the structure of the sedimentary basins of the Puget Sound Basin and Willamette Lowlands and how have these basins evolved as accretion has continued to the west? Are the mid- and upper-crustal rocks in the Puget Basin cut by subsurface (seismogenic?) fault offsets as inferred from gravity and aeromagnetic data? What is the nature and structure of terrane boundaries? Do accreted terranes extend to depth?
- Definition of the geometry of the subduction zone interface. - What is the deep crustal structure of the Willamette Lowland and Puget Sound Basin? What is the along-strike geometry of the continental and oceanic Mohos?

In addition to fundamental seismic velocity and structural information about the forearc region, this study provides numerous controlled explosions which are being used to calibrate the existing earthquake net, and will provide hundreds of measurements of local ground response and apparent attenuation within the Puget Sound and Willamette Valley region.

A high resolution seismic refraction/wide-angle reflection profile was collected in two end-to-end 250 km segments extending from the US-Canada border to the southern end of the Willamette Lowlands in central Oregon. These two segments were located (1) on the east flank of the Puget Sound Basin of Washington and (2) on the west flank of the

Willamette Lowland of Oregon. Recording instruments were sited at ~700 m intervals along the profile and shotpoints were located at 25-30 km intervals. A third, east-west, segment was located across the central Oregon Coast Ranges and up to the foothills of the Cascades Range. A total of 24 large bore-hole shots, ranging in size from 900 to 1800 kg, were fired, and recording was accomplished with a large complement of seismographs, including: 200 Seismic Group Recorders (SGRs), 185 PRS-1s, 18 PRS-4s, 30 6-channel REFTEKS, 120 FM-Cassette recorders, and two 96-channel seismic reflection spreads. These profiles provide more than 700 km of deep seismic data, and define the crustal and upper mantle structure in unprecedented detail.

The principal goal in FY91 was the collection, collation and distribution of the data. In FY92, the data will be analyzed and interpreted using existing forward modeling and inversion techniques. These data will provide velocity and structural control for the crust and upper mantle in the fore-arc region and will provide constraints on the interpretation of gravity, aeromagnetic, magnetotelluric, seismic reflection, and seismicity data. The resultant structural framework is essential to the accurate evaluation of mechanisms for crustal earthquakes and will substantially improve our ability to locate and evaluate earthquakes recorded by the existing earthquake net.



Location of the three profile segments recorded in 1991.

## **Results**

The field program was successfully completed in September, 1991 with participation of numerous institutions including University of Texas at El Paso, Oregon State University, University of Wyoming, University of British Columbia, Geological Survey of Canada, University of Victoria. In spite of generally noisy recording conditions due to the high population density in this area, first arrival energy was seen to distances exceeding 280 km.

The data is presently being played back and collated for analysis. From examination of preliminary data playbacks, it is clear that both the Puget Basin and the Willamette Lowlands show thick sedimentary sections of variable thickness along the profiles. Local first arrival time delays help delineate sub-basins. In general for the north-south segment at the eastern margin of the Puget Basin, clearly identifiable arrivals are limited to first-breaks with little PmP energy and, as yet, no identified Pn arrivals. The northern half of the north-south segment at the western margin of the Willamette Lowlands appears to be similar to the Puget Basin segment. Its southern half, in contrast, exhibits strong wide-angle reflections, likely from the mid-to-lower crust.

**Reports** The following papers were published (or in press) by the P.I.'s in FY90/91:  
(Abstracts excluded)

1. (A) Luetgert, J.H., Mooney, W.D., E. Criley, G.R. Keller, J. Gridley, K. Miller, A. Tréhu, J. Nabelek, S.B. Smithson, C. Humphreys, N.I. Christensen, R. Clowes, and I. Asudeh, 1991. Crustal Architecture of the Pacific NW: The 1991 Seismic Field Experiment, EOS, 72:44:323.
2. (A) Mooney, W.D., J. Luetgert, E. Criley, G.R. Keller, J. Gridley, K. Miller, A. Tréhu, J. Nabelek, S.B. Smithson, C. Humphreys, N.I. Christensen, R. Clowes, and I. Asudeh, 1991. The 1991 Pacific Northwest Seismic Field Experiment, EOS, 72:44:326.
- 3.(P) Hughes, S. and Luetgert, J.H., 1991, Crustal structure of the New England Appalachians and the Adirondack Mountains, *Jour. Geophys. Res.* 96, B10, 16,471-16,494.
- 4.(P) Hughes, S. and Luetgert, J.H., 1991, Crustal structure of the Southeastern Grenville Province, Northern New York State and Eastern Ontario, *Jour. Geophys. Res.* (in press)
- 5.(P) Hennet, C., Luetgert, J.H., and Phinney, R.A., 1991, The crustal structure in central Maine from coherency processed refraction data, *Jour. Geophys. Res.*, 96, 12,023-12,037.
- 6.(P) Zelt, B.C., Ellis, R.M., Clowes, R.M., Kanasewich, E.R., Asudeh, I., Luetgert, J.H., Hajnal, Z., Ikami, A., Spence, G.D., and Hyndman, R.D., 1991, Crust and Upper Mantle Structure of the Intermontane Belt, Canadian Cordillera, *Can. Jour. Earth Sci.* (in press)
- 7.(P) Ocola, L.C., Luetgert, J.H., Aldrich, L.T., Meyer, R.P., and Helsley, C.E., 1991, Velocity structure of the coastal region of Southern Peru from seismic refraction/wide-angle reflection data, *B.S.S.A.* (in press)

8. (P) Mooney, W.D. and Meissner, R., 1991, Multi-genetic origin of crustal reflectivity: a review of seismic reflection profiling of the continental lower crust and Moho, in: *The Continental Lower Crust*, D. Fountain, R. Kay, and R. Arculus, editors, Elsevier, Amsterdam (74 MS pg., 15 Figs., in press).
9. (P) Durrheim, R. A. and Mooney, W. D., 1991, Archean and Proterozoic crustal evolution: evidence from crustal seismology, *Geology*, 19, 606-609.
10. (P) Catchings, R.C. and Mooney, W.D., 1991, Basin and Range crustal and uppermost mantle structure, Northwest to central Nevada, *Jour. Geophys. Res.*, 96, 6247-6267.
11. (P) Hamilton, R.M. and Mooney, W.D., 1990, Seismic-wave attenuation associated with crustal faults in the New Madrid Seismic Zone, *Science*, 248, 351-354.
12. (P) Kenya Rift International Seismic Project (KRISP) Working Group (Forty co-authors, including W. D. Mooney and J.H. Luetgert), 1991, The structure of the Kenya Rift Valley from a recent lithospheric explosion seismic experiment (KRISP 90), *Nature* (submitted 5/91).
13. (P) Fuis, G.S. and Mooney, W.D., 1990, Lithospheric structure and tectonics from seismic refraction and other data, in: R.E. Wallace, editor, *The San Andreas Fault System*, California, U.S. Geological Survey Prof. Paper 1515, 207-236.
14. (P) Stanley, W.D., Mooney, W.D., and Fuis, 1990, Deep crustal structure of the Cascade Range and surrounding regions from seismic refraction and magnetotelluric data, *Jour. Geophys. Res.*, 95, 19,419-19,438.
15. (P) Fuis, G.S., Ambos, E.L., Mooney, W.D., Christensen, N.I., and Geist, E., 1991, Crustal structure of accreted terranes in the Chugach Mountains and Cooper River Basin, southern Alaska from seismic refraction results, *Jour. Geophys. Res.*,
16. (P) Meissner, R. and Mooney, W.D., 1991, Speculations on continental crustal evolution, EOS, Am. Geophys. Union, (8 Ms. Pgs., 3 Fig.), in press (short contribution like a *Geology* article).
17. (P) Mooney, W.D., and Meissner, R., 1991, Continental crustal evolution: Geophysical Observations, EOS, Am. Geophys. Union, (13 Ms. Pgs., 4 Fig.), in press (companion paper to above; also like a *Geology* article).
18. (P) Benz, H.M., Smith, R.B., and Mooney, W.D., 1990, Crustal structure of the western Basin-Range Province, Nevada, from seismic refraction data: results from the 1986 IRIS-PASSCAL investigation, *Jour. Geophys. Res.*, 95, 21,823-21,842.
19. (P) Holbrook, W.S., Mooney, W.D., and Christensen, N.I., 1991, Seismic velocity structure of the lower continental crust, in *The Continental Lower Crust*, D. Fountain, R. Kay, and R. Arculus, editors, Elsevier, Amsterdam (50 MS pg., 13 Figs., in press).

## TEMPORAL AND SPATIAL BEHAVIOR OF LATE QUATERNARY FAULTING, WESTERN UNITED STATES

9950-04540

Michael N. Machette  
Branch of Geologic Risk Assessment  
U.S. Geological Survey, Box 25046, MS 966  
Denver, Colorado 80225  
(303) 236-1243

### PURPOSE OF PROJECT

To define regional variations in the time-space distribution of late Quaternary paleoseismic activity as a guide to understanding the accumulation and release of strain on extensional faults in the Western United States. This project serves as an umbrella for diverse but interrelated paleoseismic studies in the interior of the Western United States. We will study selected historic faults to interpret the paleoseismic and neotectonic history in regions of active faulting, especially those in the Central Nevada Seismic Belt. Our research will apply paleoseismologic studies to important problems at three different scales by: (1) refining methodologies for dating fault movements that are applicable to a wide variety of tectonic problems and areas, (2) examining the long-term behavior and interaction of faults in a broad region (ca. 20,000 km<sup>2</sup>) that are exposed to the same regional stress field, and (3) studying the time-space distribution of strain release in the upper crust on a regional (province-wide) scale.

### INVESTIGATIONS

1. Kathy Haller and Michael Machette are compiling a database of Quaternary faults in a neotectonic transect across the Basin and Range Province from the Wasatch fault zone to the eastern front of the Sierra Nevadas. The limits of the transect are 39° and 41° N. and 111° and 120° W. This east-west transect allows us to build upon the Wasatch fault zone study (Machette and others) and the 1°x2° quadrangle fault mapping in Utah by BGRA personnel (Anderson, Barnhard, and Bucknam). Thus, our main concern for completing a systematic fault study now lies with parts of Nevada; previous mapping in Nevada by Barnhard (Elko 1°x2°), Wallace (Winnemucca 1°x2°), and Bell (Reno 1°x2°) can be used with the addition of specific age data for faults. This past summer, Haller (assisted by Jim Goddard, Utah State University, Logan) completed field reconnaissance of late Quaternary faults in the eastern half of the Millett 1°x2° quadrangle last summer and she has been analyzing FY 90 data for the Ely 1°x2° quadrangle. This leaves the Lovelock and western half of the Millett 1°x2° quadrangles as our main mapping objectives for the next 2 years (FY 92-93).

These fault data are being compiled using the USGS's PG-2 analytical plotter and aerial photographs (for digitization at a scale of 1:24,000 using ARCINFO and for publication at 1:250,000 scale). Most of the mapped faults have been compiled at 1:24,000 scale; digitization awaits installation of a multiuser ARCINFO license, implementation of *Ala Carte* (Macintosh-based front end for ARCINFO), and acquisition of new Ethernet communications software (*Pathworks*); all of which should be in place by late 1991. We will be cooperating with personnel of the Nevada Bureau of Mines (John Bell and colleagues), and the University of Nevada's Center for Neotectonics (Steven Wesnousky and colleagues) in this compilation.

2. In late September, Machette and Haller excavated six exploratory trenches south of Winnemucca, Nev. Four sites on the 1915 Pleasant Valley rupture were selected and trenched in order to investigate the timing of prehistoric faulting; two additional sites on nearby pre-1915 fault scarps were trenched. Kelvin Berryman of the New Zealand Geological Survey will be cooperating in this aspect of our study.

3. Although not funded by NEHRP, Crone and Machette completed a manuscript that describes the results of their 1991 Gilbert Fellowship field studies of the 1988 earthquakes at Tennant Creek, Australia. The manuscript has been submitted for publication as a USGS Bulletin and contains lithologic/structural logs of the four trenches, detailed site maps, plots of scarp profiles, and preliminary results of TL and ESR dating. In addition, they prepared two abstracts for the GSA meeting in San Diego in October 1991.

4. Machette spent about half of the reporting period as chairman of a USGS Review Panel for the Jordanelle Dam near Heber, Utah. The Panel was convened by Rob Wesson (OEVE Chief) at the request of the Utah Congressional Delegation and given the charge to assess the adequacy of the Bureau of Reclamation's investigations of geotechnical problems at the Jordanelle site.

## RESULTS

1. Fault scarps in the eastern half of the Millett 1°x2° quadrangle appear to be generally younger than those in the Ely 1°x2° quadrangle to the east on the basis of initial aerial-photo reconnaissance and scarp morphology data collected this summer and previously by Pearthree and others (1990; USGS Contract Report 14-0001-08-G1360). The distribution of scarps is denser in the Millett quadrangle than to the east, and several faults cut deposits related to the most recent pluvial episode (latest Pleistocene, ca. 12-15 ka). Some of the longer range-front faults, such as the Toyaibe, appear to be segmented, on the basis of their ages of most recent movement. In addition, frontal faults of the Cortez, Eastgate, Simpson Park, Toyaibe, and Shoshone Ranges and piedmont faults in Crescent Valley appear to have been active in the Holocene. Thus, the abundance of scarps, their often fresh appearance, and their crosscutting relations with young lake deposits indicate much more late Quaternary fault activity in the Millett and Winnemucca 1°x2° quadrangles than in eastern Nevada (Elko and Ely 1°x2° quadrangles) and western Utah. This relation becomes even more pronounced westward in the Central Nevada Seismic Belt (Fairview Peak, Dixie Valley, and Pleasant Valley faults). The region of minimum paleoseismic activity in the Nevada part of the transect appears to be the north-south corridor between Eureka and Ely, which lies near the medial and highest part of the Basin and Range Province. However, even this region has relatively abundant late Quaternary fault scarps compared to the western part of Utah, with the Fish Springs fault being the notable exception. We are beginning to see evidence that the position of the Central Nevada Seismic Belt and the surrounding area of relatively high paleoseismic activity (in relation to the province as a whole) reflects the loci of modern, active extension that is concentrated along the western margin of the province, which contains the topographically lowest valleys in the northwestern part of the Basin and Range. On the other hand, the frequency of surface-rupturing earthquakes (M 7+) on the Wasatch fault zone (about 400 years vs tens of thousands of years for adjacent faults) could represent a trailing-edge effect as the Basin and Range Province (as a whole) moves westward from the Colorado Plateaus and Rocky Mountains Provinces; the Wasatch fault zone is bounds the lowest basins of the northeastern part of the Basin and Range Province. Further development of the relation between topography and recency and abundance of faulting requires completion of our mapping of Quaternary faults in western Nevada and analysis of scarp data to delineate spatial and temporal patterns and timing of Quaternary faulting.

2. The four trenches across the surface rupture of the 1915 Pleasant Valley earthquake, south of Winnemucca, Nev., reveal evidence of several prehistoric faulting events. Two trenches each were placed across the Tobin and Pearce scarps (the medial sections of the 1915 rupture), but no suitable trenching sites were found on the China Mountain or Sou Hills scarps (the distal sections of the 1915 rupture). The Mazama ash (ca. 6,600 yr B.P.) outcrops along Sheep Creek near the north end of the Tobin scarp. The ash is within terrace alluvium that appears to have been faulted by only one event—the 1915 earthquake. Thus, the minimum recurrence interval for a "Pleasant Valley like" earthquake is at least 6,600 years, and may be substantially more (several tens of thousands of years?). The scarp we excavated about 50 m south of Sheep Creek is >7 m high on pre-late(?) Pleistocene alluvium and colluvium, indicating a history of multiple faulting events. The second site, which is just south of Jim Creek (about 2.5 km



northwest of the Sheep Creek site), exposes pre-late(?) Pleistocene alluvium with a thick, well-developed Bt horizon that probably is faulted by only one or two prehistoric events (total scarp height of about 1 m). This site is near the northern end of the Tobin scarp and may not record all of the events that occurred at the Sheep Creek site to the south.

The third and fourth trench sites are on the Pearce scarp, which is a right-stepping extension of the Tobin scarp to the south. Both trenches along the Pearce scarp cross large (8-13 m high) scarps that clearly resulted from multiple prehistoric faulting events. The tectonic stratigraphy in these trenches is dominated by loess (derived from Quaternary lake deposits) and debris flows that postdate the underlying platform of middle(?) Pleistocene alluvium; as such, these trenches present special challenges to map and decipher previous faulting events. However, small pockets of Mazama ash are preserved in a wide graben exposed in a trench near Siard Canyon, and we are hopeful that other datable horizons will be found. No trenches were excavated along the China Mountain and Sou Hills scarps because evidence of prior faulting is sparse, recorded on bedrock or steep hillslopes, or restricted to small (1-m-high) scarps on pre-late(?) Pleistocene alluvium.

Two additional trenches were excavated along fault scarps that were not ruptured in 1915. The southern trench crosses a 9-m-high scarp that is a basinward splay of the Tobin scarp, and the northern trench crosses a 4-m-high scarp of the frontal fault of the Sonoma Range near Elbow Canyon in Grass Valley, about 12 km south of Winnemucca. Both of these trenches show evidence of multiple faulting events, which should be datable using TL and C<sup>14</sup> analysis. The history of faulting along the Sonoma Range is particularly interesting in that it may indicate if the Central Nevada Seismic Belt has reoriented itself into a northeast-trending zone (China Mountain/Tobin/Pearce/Sou Hills) from a former a north-trending zone that included Grass Valley.

We hope that careful mapping and TL dating will help us decipher the timing of prehistoric faulting events along the Pleasant Valley scarps and nearby scarps. The results of this study will be compared to recent work by Bell and dePolo on the 1934 Cedar Mountain faults, prior work by Bell on the 1954 Dixie Valley fault, and to work planned by Wesnousky on the 1954 Fairview Peak fault. Within the next few years we should be able to assemble a realistic paleoseismic chronology for the Central Nevada Seismic Belt and will be able to assess whether its recent history of spatial and temporal clustering is characteristic for the Quaternary and whether this seismic zone may be a reasonable analog for other major extensional fault zones in the Western United States, such as the Wasatch fault zone in Utah.

3. Preliminary results from our Gilbert Fellowship research on the Marryat Creek and Tennant Creek sites (Crone and others, 1991, in press; Machette and others, 1991) show that these historic intraplate earthquakes reactivated ancient faults. However, there was no clear evidence of fault-scarp derived colluvium in the Quaternary deposits in any of the six trenches, and there is no compelling geomorphic evidence of prehistorical faults scarps at any of the sites. The oldest age estimates that John Prescott (University of Adelaide, Australia) has obtained for us on eolian sand at Tennant Creek is  $61 \pm 5$  ka. These relations indicate that the historical earthquakes were associated with faults that had ruptured in the past, but that the recurrence interval for surface-rupturing earthquakes on these faults is probably measured in time increments of tens of thousands of years and possibly hundreds of thousands of years or more (millions of years?). These investigations of historical intraplate faulting and our brief observations of a trench across the 1968 Meckering (WA) fault scarp suggest that Australian intraplate faults have long repeat times; with this in mind, the concept of recurrence intervals may not be appropriate for earthquakes that occur in the 'stable' interiors of continents. Perhaps hazard assessments in Australia and other continental interiors should be based models where moderate- to large-magnitude earthquakes can occur at any time on suitably oriented faults, rather than only on faults having demonstrable Quaternary movement.

4. The USGS Review Panel prepared an Open-File Report (91-398) which summarized their investigations into geotechnical aspects of the Jordanelle damsite near Heber, Utah. The Review Panel concluded that they found no safety concerns relating to geologic or seismologic issues that remain to be resolved.

The near-complete exposure of the foundation rock, an effort which is unprecedented for a damsite such as Jordanelle, has provided an excellent base for the U.S. Bureau of Reclamation's comprehensive and detailed mapping of the foundation exposures and allowed them to integrate extensive subsurface drill-hole data with surface geology. The Panel reviewed the U.S. Bureau of Reclamation's investigations at the Jordanelle damsite with reference to purported hazards from active faulting, leaky and crumbly foundation rock, landsliding, embankment failure due to ground shaking from earthquakes, and induced seismicity—each of which are important considerations in the design and construction of a critical facility. The Panel was satisfied that the U.S. Bureau of Reclamation had fully demonstrated that these issues do not constitute a *bona fide* threat to the dam.

## REPORTS

- Crone, A.J., Machette, M.N., Bowman, J.R., and Prescott, J.R., 1991, Surface faulting and earthquake recurrence in 'stable' continental interiors—Examples from Australia and North America: Geological Society of America Abstracts with Programs, v. 23, p. A431.
- Crone, A.J., Machette, M.N., Bowman, J.R., Geologic investigations of the 1988 Tennant Creek, Australia, earthquakes—Implications for paleoseismicity in stable continental regions: U.S. Geological Survey Bulletin, 112 ms. p., 2 plates, in press.
- Machette, M.N., Crone, A.J., Bowman, J.R., and Prescott, J.R., 1991, Surface ruptures and deformation associated with the 1988 Tennant Creek and 1986 Marryat Creek, Australia, intraplate earthquakes: Geological Society of America Abstracts with Programs, v. 23, p. A224.
- Machette, M.N., Personius, S.F., and Nelson, A.R., The Wasatch fault zone, USA, *in* Bucknam, R.C., ed., Atlas of Active Faults Worldwide: Cambridge University Press, 58 ms. p., in press.
- U.S. Geological Survey Staff, 1991, Review of geotechnical aspects of the Jordanelle damsite, Heber, Utah: U.S. Geological Survey Open-File Report 91-398, 43 p.

## **The Downhole Seismology Project at Parkfield**

USGS, #14-08-0001-G1968  
P.E. Malin and M.G. Alvarez  
Duke University, Durham, NC

### **Introduction.**

In the past year and a half the MEQ data reduction and our analysis part of the Parkfield Downhole Seismology Project has been performed at Duke University, in Durham, NC. Data are continuing to be distributed to UCB and the USGS on a weekly basis, using both a new computer transfer via FTP and Email, as well as the traditional mailing of tapes. In 1991, we have published or have participated in the publishing of the following paper based on data from the project:

1991 Malin, P.E., and M.G. Alvarez. Stress Diffusion along the San Andreas Fault at Parkfield, Manuscript submitted to Science in 4/91.

### **Current Investigations.**

Our most recent work has concentrated on the regional distribution of microearthquake moment release near Parkfield. By separating microearthquakes by region, we have observed a location-dependent increase in the rate of cumulative moment (and, by implication, fault slip) near and on the San Andreas fault at Parkfield, CA. The subset of events outside of the Parkfield segment of the San Andreas fault show increased rates of cumulative moment beginning in April 1990. The subset at Parkfield shows the same increase some 4 to 8 months later. Prior to this change and back as far as June 1987, the average cumulative moment rate was nearly constant, except for the occurrence of an  $M=4$  event in May 1989. Since this event, the cumulative moment rates have increased non-linearly with time. We suggest the data give evidence of a southward diffusing stress front, propagating at a speed of 45 to 90 km/yr.

The region of the Parkfield microearthquake study is shown in Figure 1, along with the epicenters of all the events and the sites of the borehole seismographs used to detect and locate them. Figure 2 shows these events in cross section. Figure 3 shows the cumulative moment of Parkfield events from June 1987 to several months after May 1989, when the  $M=4$  event took place. This earthquake occurred midway between the 2 southernmost recording sites and at a depth of more than 8 km, a somewhat uncommon location for events of any size. The moments of individual events were calculated by integrating the S-wave displacement and velocity spectra over frequency and assuming that the resulting values fit a frequency-squared model of the earthquake source (5). Summing these moments as a function of time yields the curve in Figure 3, which also shows the least-squares trend line and resulting residuals. (For reasons of scale, the moment of the  $M=4$  event has been omitted from the figure.)

The trend line and residual moments suggested to us that Parkfield microearthquake activity was being driven by some steady process in which the fault would slip rapidly forward in one period, as evidenced by increased activity, only to lag behind in the next period. It thus seemed possible to anticipate periods of overall increased and decreased seismicity, albeit without reference to any particular

location, event size, or precise timing. The  $M=4$  event occurred in a period when microearthquake activity was lagging behind the average. However this event was not anticipated on the basis of the prior cumulative moment data, as no events of this magnitude took place in the earlier lulls in cumulative moment. A significant departure from this trend began after the first quarter of 1990, and differed by region, as illustrated in Figure 4.

The change in seismic activity can be separated by region, as indicated by the boxes shown in Figures 1 and 2. Boxes 3 and 4 divide the seismicity taking place on the San Andreas fault into northern and southern segments, Box 3 and 4 contain the Parkfield segment, Box 2 containing the segment to the north. Box 1 contains all events surrounding but not on the Parkfield segment. We propose that the cumulative moment data give evidence of a stress diffusion process taking place somewhere below the seismically active region north of Parkfield. Our proposal stems from the observation that the 1990 change in cumulative moment took place first in the north and then some 4 to 8 months later in the south. Since the distance between the centers of the boxes used to separate the regions is about 30 km, the propagation speed of the implied disturbance is on the order of 45 to 90 km/year. Theoretical analysis of stress relaxation below the seismogenic zone indicates that when propagation speeds are reduced to less than 100 to 200 km/year by "barriers" or "asperities" (inhomogeneities in crustal strength), the result is elastic loading of these features (12). The rate of loading would be proportional to the seismicity and the trend of the cumulative moment.

Figure 1. Map showing locations of the Parkfield borehole seismographs (triangles), the epicenters of 2,187 microearthquakes, and the regions discussed in the text and other figures. The westward fanning of events in Box 2 is due in part to the poor station coverage and faster velocities in this region.

Figure 2. Hypocenters of events in Boxes 2, 3 and 4 projected onto vertical planes through the zone of highest seismicity in each box. These planes probably correspond to the San Andreas fault. The seismicity in Box 3 shows clustering which is not seen in Box 2. The dashed lines indicate the approximate outlines of the aseismic patches where moderate earthquakes might take place in the future (1). The recording stations are shown as solid triangles.

Figure 3. The cumulative moment, trend for all four boxes. This figure illustrates the southward migration of moment release described in text (interpreted as a diffusion front). The  $M=4$  event that occurred in 5.89 is removed from the moment contribution and shown by the vertical dotted line.

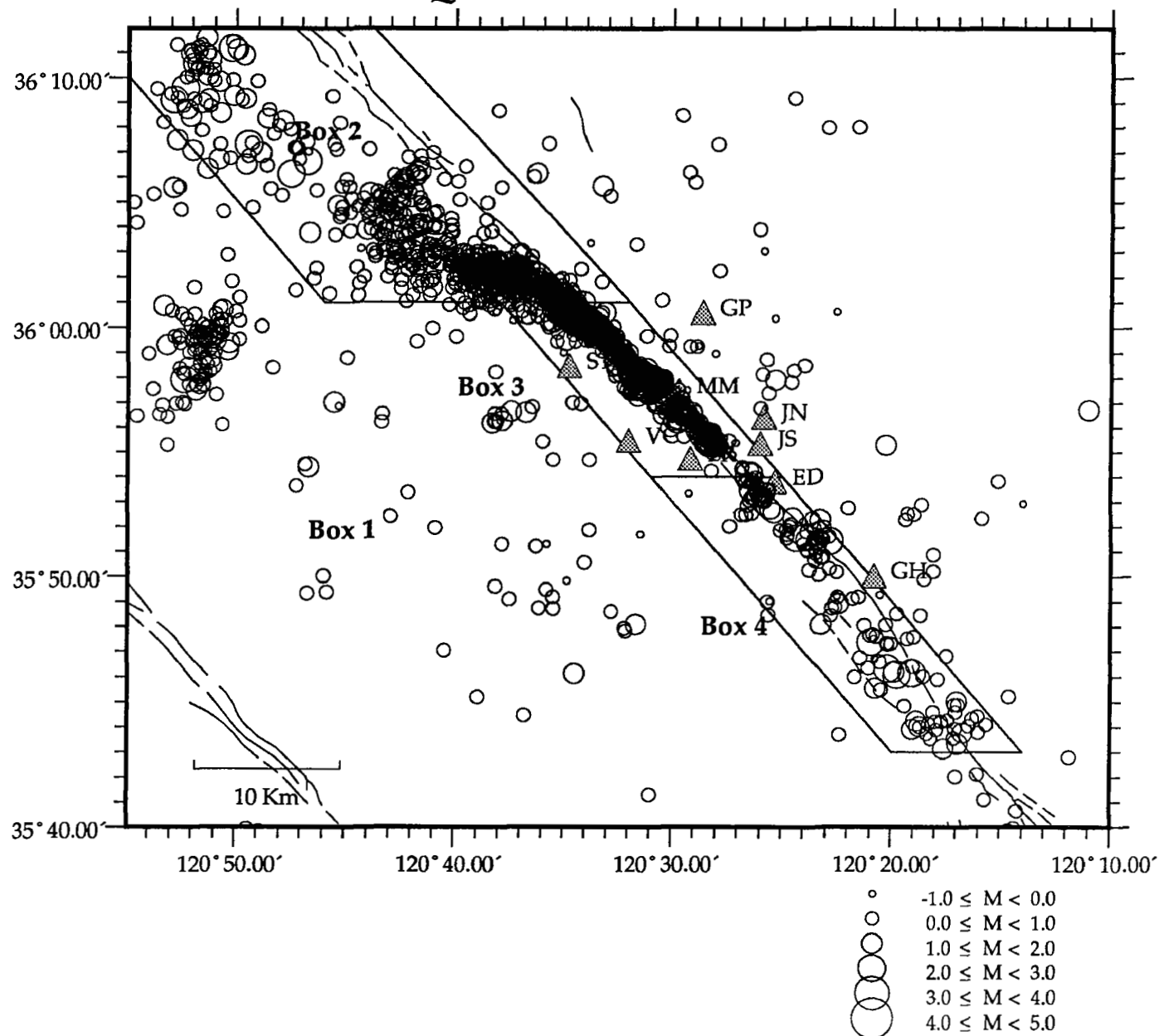
Figure 4. Seismicity along the trend of the SAF through time. The magnitude of the events are represented by the varying size of circles and by contours. Arrows point out the proposed diffusion front described in text

#### References and Notes

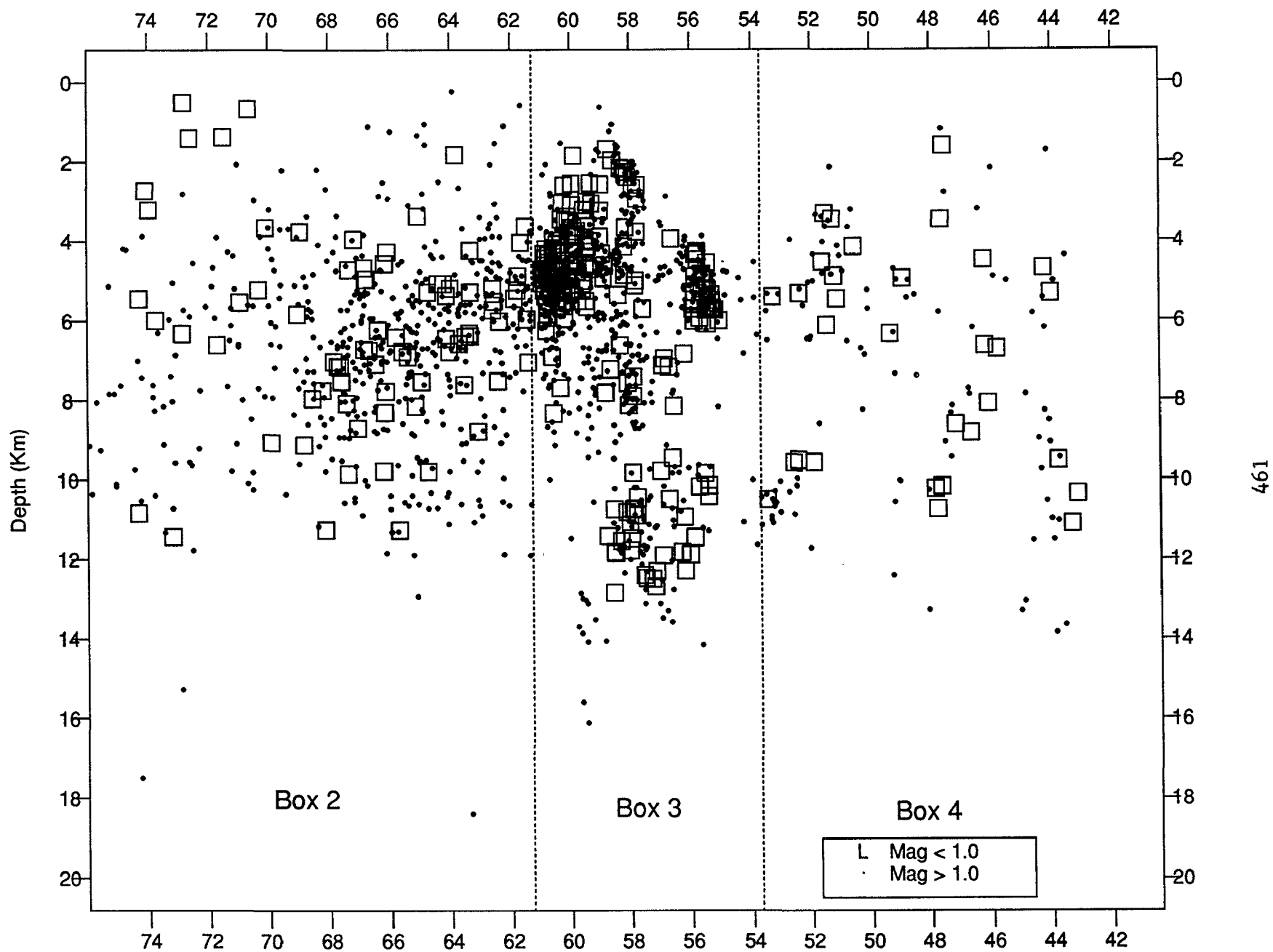
1. W. H. Bakun and T. V. McEvilly, *Science* **205**, 1375 (1979).
2. W.H. Bakun and T.V. McEvilly, *J. Geophys. Res.* **89**, 3051 (1984).
3. W. H. Bakun and A. G. Lindh, *Science* **229**, 619 (1985).
4. P. E. Malin et al., *ibid* **244**, 557. (1989)

5. D. J. Andrews, in *Earthquake Source Mechanics*, American Geophysical Union Monograph 37, K. Aki and P. Richards, Eds., American Geophysical Union, Washington, D. C., (1986).
6. J. D. Sims, *USGS Misc Field Studies Map MF-2115* (1990).
7. W. R. Dickinson, *Bull. Geo. Soc. Am.* **77**, 707 (1966).
8. A. G. Lindh and D. M. Boore, *Bull. Seismol. Soc. Am.* **71**, 95 (1981).
9. B. Voight, *Science* **243**, 200 (1989).
10. F. K. Lehner, V. C. Li, J. R. Rice, *JGR* **86**, 6155 (1981).
11. J. E. Dennis and D. J. Woods, *SIAM* **87**, 116 (1987)
12. N. Toksoz et al., *Pure Appl. Geophy.* **117**, 1258 (1979).
13. C. H. Scholz, *Nature* **267**, 121 (1977).
14. We thank numerous colleagues at the University of California at Berkeley and the United States Geological Survey, with whom we have shared the effort of keeping the Parkfield downhole seismology project alive, and without whose efforts none of the results discussed here would have been possible.

# Parkfield EQS dated 12 31 1988 to 05 01 1991

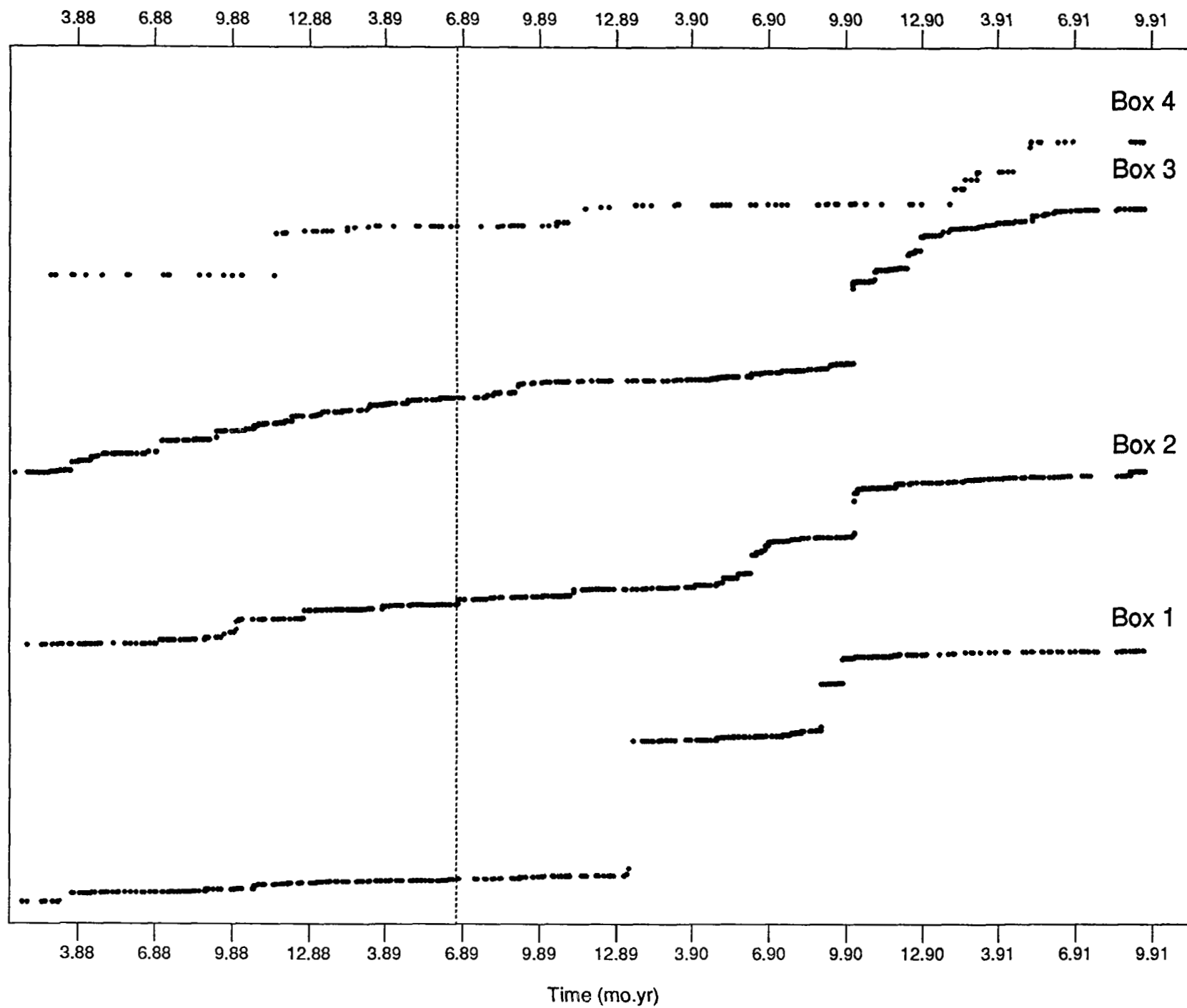


II



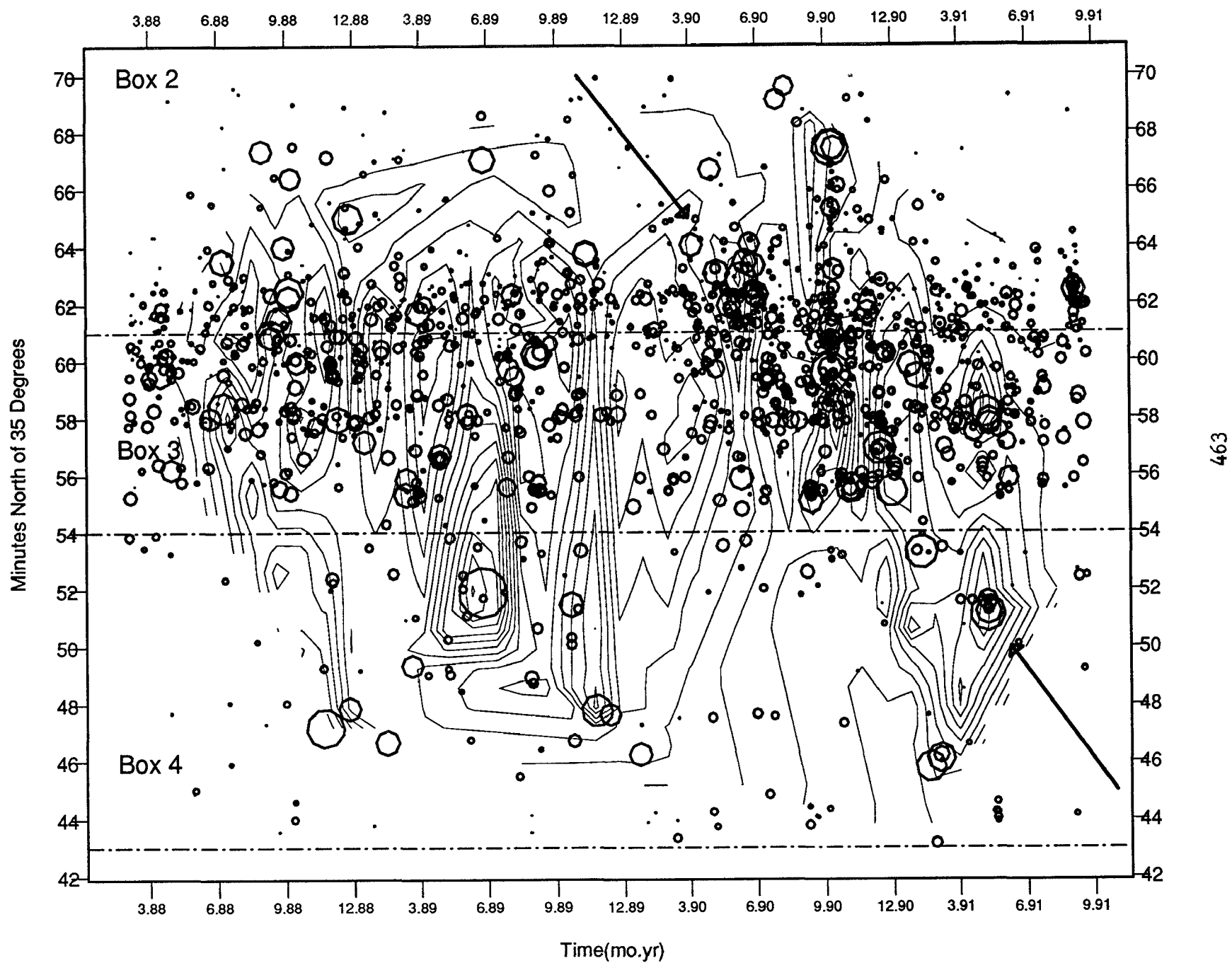
II

Relative Cumulative Moment (dyne-cm)





II



Leveling survey of the Imperial  
Valley Mekometer network

14-08-0001-G1961

Ronald G. Mason  
Geology Department  
Imperial College  
London SW7 2BP, England  
011-44-71-589-5111

### Investigation

This project involves leveling the main block of the existing high precision edm network to first order accuracy and extending it, and the measurements, to provide better coverage of the Imperial fault and Brawley seismic zone north of their junction (Figure 1). This is the first time any part of the network has been leveled. The results will produce no immediate scientific return, but will provide a basis for monitoring future movements in three dimensions.

### Results

The fieldwork, started during the last week of January, was completed by the end of April. 172 stations in the main block, and 48 in the extension, were leveled using trigonometric techniques. Connections were also made to 17 NGS benchmarks, five of which have been occupied repeatedly by GPS during the past few years. In all, this involved about 400 km of leveling line. Analysis of the results indicates a mean standard error of 1.77 mm, which compares with a standard error of about 0.9 mm in the most recent (1987) edm survey. Note that until they are tied in horizontally to the previously existing network, the new stations can be used only for monitoring vertical movements.

It was not part of the 1991 program to make horizontal measurements. However, because of an impending kinematic GPS survey of a substantial part of the main block by Yehuda Bock, Scripps Institution of Oceanography, whose purpose was to evaluate kinematic GPS as an alternative to classical techniques for surveying spatially dense small-aperture networks, we remeasured the lengths of all lines crossing the Imperial fault, where the greatest changes since 1987 were to be expected.

Details of the GPS survey have been given elsewhere (Bock, Y. and J. Genrich, 1991). In brief, 67 main block stations and five NGS benchmarks were occupied during four days in early May (Figure 1). The results, which have not yet been fully evaluated, will allow comparison of the 1991 vertical GPS measurements with the results of our near simultaneous leveling survey, and the 1991 horizontal GPS measurements with the results of our 1987 edm survey and our 1991 survey of fault-crossing lines.

Bock, Y. and J.F. Genrich (1991), High temporal and spatial resolution of crustal deformation with GPS, U.S. Geol. Survey Open File Rept. 91-352, pp 232-242.

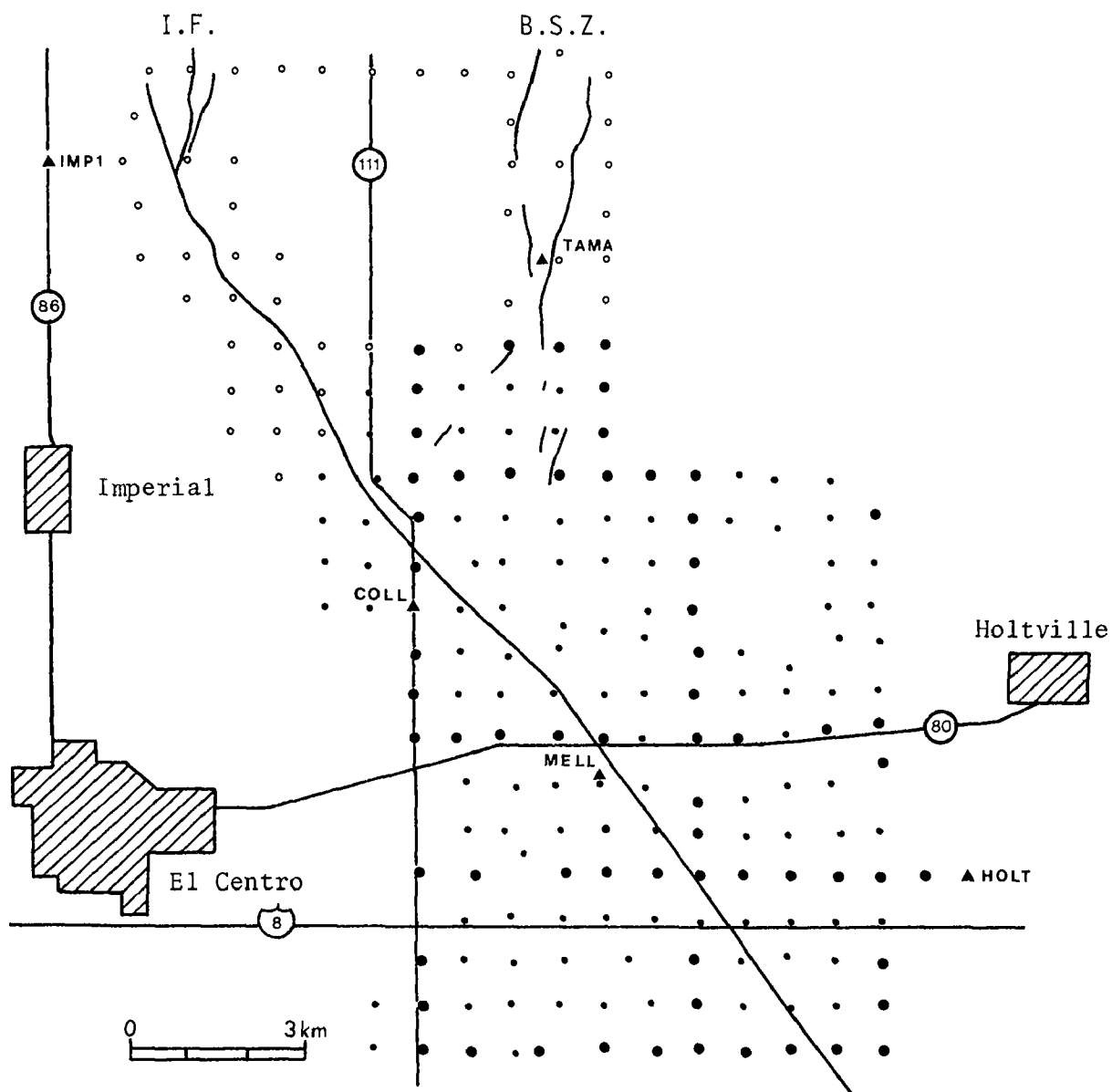


Figure 1. Stations leveled in 1991. Newly built stations, for which horizontal coordinates are not yet available, are indicated by open circles. Large solid circles indicate stations used also in the kinematic GPS survey.

## BAY AREA SEISMIC IMAGING EXPERIMENT (BASIX)

9460-30071, 9930-04323

J. McCarthy, T. Brocher and the BASIX Working Group<sup>1</sup>  
 Branches of Pacific Marine Geology and Seismology  
 U. S. Geological Survey  
 345 Middlefield Road, MS/999  
 Menlo Park, California 94025  
 (415) 354-3140; (415) 329-4737

### Investigations

The principal subject of investigation was the imaging of the structure of the crust in the San Francisco Bay Area using an integrated suite of seismic reflection and refraction profiling methods.

In September, 1991, nearly 80 km of deep-penetration multichannel seismic reflection profiles were acquired in the Sacramento Delta and San Francisco Bay from near Antioch (Rio Vista) to the Golden Gate and beyond to the offshore extension of the San Andreas fault (Figure 1). These profiles were acquired using a 5858 cu. in. airgun array towed from the S.P. Lee recorded using 60 to 120 moored hydrophones whose signals were telemetered for recording on the S.P. Lee. The receivers were spaced at 50 to 100 m intervals and the S.P. Lee fired its airgun array at 50 m intervals to obtain the 100- to 400 fold reflection profile. The data were recorded to 16 s to insure the imaging of the entire crust down to the Moho.

More than 60 temporary seismic recorders were positioned both on and offshore to record seismic signals generated by the airgun array at wide-angles (Figure 1). The USGS deployed 23 five-day recorders along the seismic reflection lines to record seismic reflections and refractions to offsets as large as 250 km. Investigators from Stanford University deployed 36 PASSCAL Reftek recorders, mainly in a fan geometry, to look for offsets in arrival times of reflections from the upper mantle at the major strike slip faults in the Bay Area. Investigators from the Branch of Atlantic Marine Geology and Woods Hole Oceanographic Institution deployed an array of 5 ocean-bottom seismometers in two locations to provide more accurate velocity and reflection control on the crustal structure beneath the San Francisco Bay and the outer continental shelf offshore the Peninsula. In addition, the permanent CALNET array recorded the S.P. Lee airgun shots; these data have been dubbed and selected stations will be examined to complete the wide-angle coverage.

A third component of seismic reflection profiling conducted by BASIX consists of high-resolution seismic imaging of the shallow sedimentary sequence within the San Pablo and San Francisco Bays. Two surveys were conducted in the fall of 1991, totalling more than 80 km, using the David Johnson, to provide detailed information for the delineation of fault traces and structure within the bays.. Both analog and digital high-resolution profiles were recorded, using both Uniboom and airgun sources.

<sup>1</sup>The BASIX Working Group includes: R. Anima, J. Childs, P. Hart, and M. Marlow of the Branch of Pacific Marine Geology; R. Clymer, D. Jones, E. Karageorgi, T. McEvilly, and Pat Williams of UC Berkeley; M. Moses and A. Michael of the Branch of Seismology; U. ten Brink of the Branch of Atlantic Marine Geology; S. Holbrook of Woods Hole Oceanographic Institution; S. Klemperer and G. Thompson of Stanford University; and K. Furlong of Pennsylvania State University.

## BASIX Seismic Reflection Lines and Wide-angle Recordings

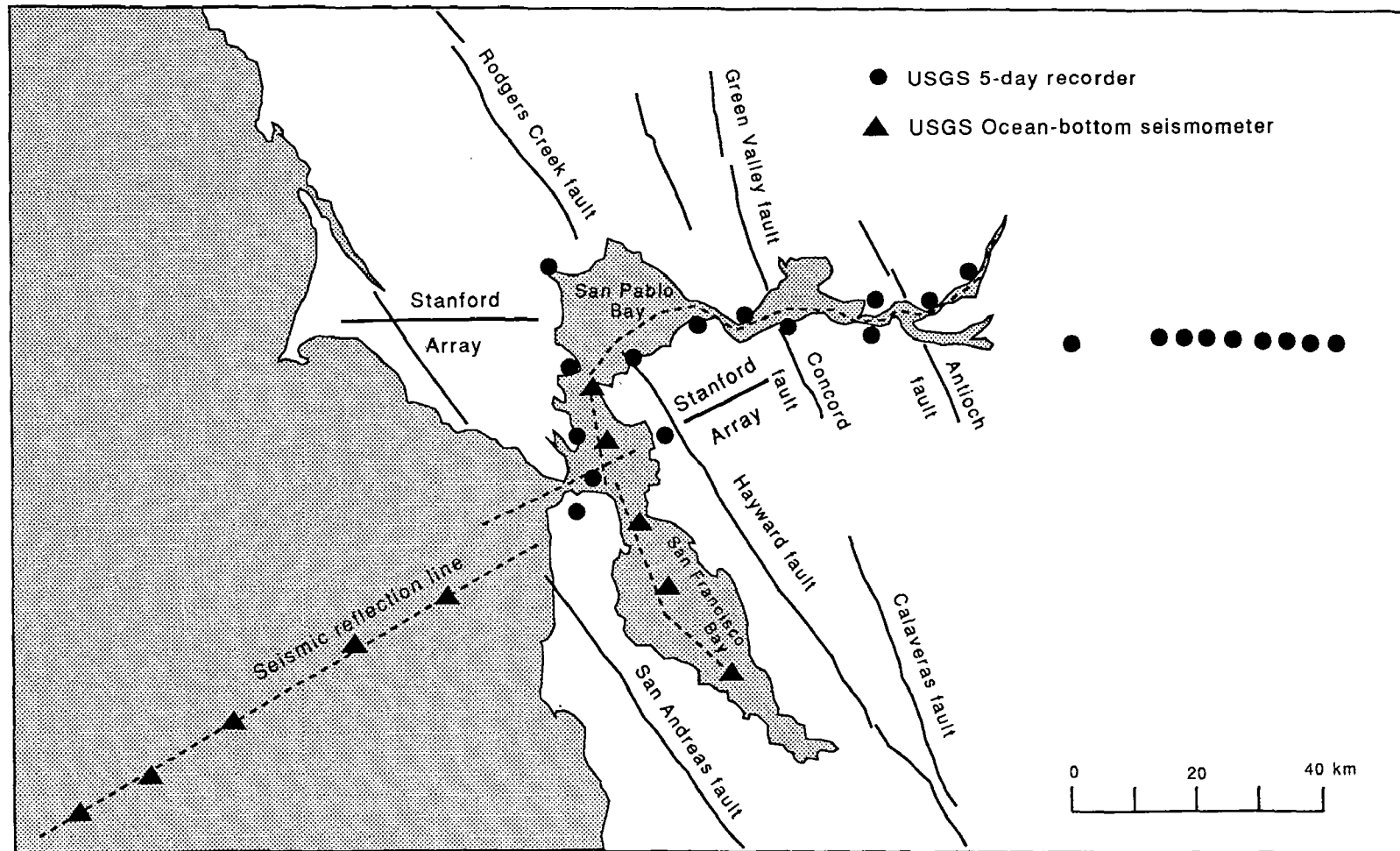


Figure 1. Index map showing location of seismic reflection lines and wide-angle recorders. CALNET stations, which also recorded the airgun signals, are not shown in this figure.

## **Results**

### **1. Deep-penetration Multichannel Seismic Reflection Profiling in San Francisco Bay**

The vast amount of multichannel seismic reflection data recorded by the S.P. Lee are in the process of being demultiplexed and edited at the DISCO Seismic Reflection Processing Center in Menlo Park. The data, recorded as common shot gathers, are being sorted to common receiver gathers to facilitate the editing and processing of the data. About 30% of the data have been played out, we expect to complete the processing of these data in FY92. Preliminary analysis of these data indicate the presence of several reflections in the upper 6 s of the crust (see example in Figure 2), which we expect to help us delineate the subsurface geometry of the major faults in the Bay Area.

### **2. Wide-angle Seismic Reflection and Refraction Profiling**

Data from ten OBS wide-angle stations recorded by the USGS have been reduced and plotted. Five of these stations recorded along the offshore California margin. The data recorded are of high-quality (see Figure 3) and will be used to constrain the velocity and crustal structure of the continental margin. The remaining OBS profiles were acquired in San Francisco Bay. These profiles show mid- to lower-crustal reflections which will be important for the evaluation of the along-strike continuity of crustal reflectors.

Data recorded by the USGS five-day recorders are in the initial stage of playback. Preliminary plots of selected portions of these data indicate that signals generated by the airgun array are observed to ranges in excess of 140 km, and these data should allow resolution of the crustal structure and velocities in the vicinity of the East Bay faults (Figure 4). Due to the high-density of five-day stations along the Bay, we also plan to construct a low-fold seismic reflection profile along the multichannel reflection data to determine whether recording the airgun signals onshore produces a higher-quality reflection image of the middle to lower crust.

Wide-angle data recorded by Stanford University using PASSCAL Reftek recorders are also in the initial stage of analysis. Preliminary plots show that the quality of these data is similar to that recorded by the five-day recorders, and should provide important constraints on the existence of major structural changes across the main seismogenic faults in the Bay Area.

Wide-angle data recorded by the CALNET array is in the process of being dubbed and analyzed. We plan to invert the first arrivals on these data using tomography to obtain a 3-dimensional seismic velocity model of the crust in the Bay Area. Data from selected CALNET stations will also be used to supplement the recordings made by the USGS OBSs and five-day recorders as well as those obtained by the PASSCAL Refteks deployed by investigators from Stanford University.

### **3. High-Resolution Seismic Reflection Profiling**

These data were acquired to determine the Neogene stratigraphy and deformation patterns in the San Francisco and San Pablo Bays. The analog data are in the process of being analyzed for the AGU Meeting in December, but reveal a number of important, if currently poorly understood, structures in the Neogene record. The tilting and geometry of observed reflections in San Pablo

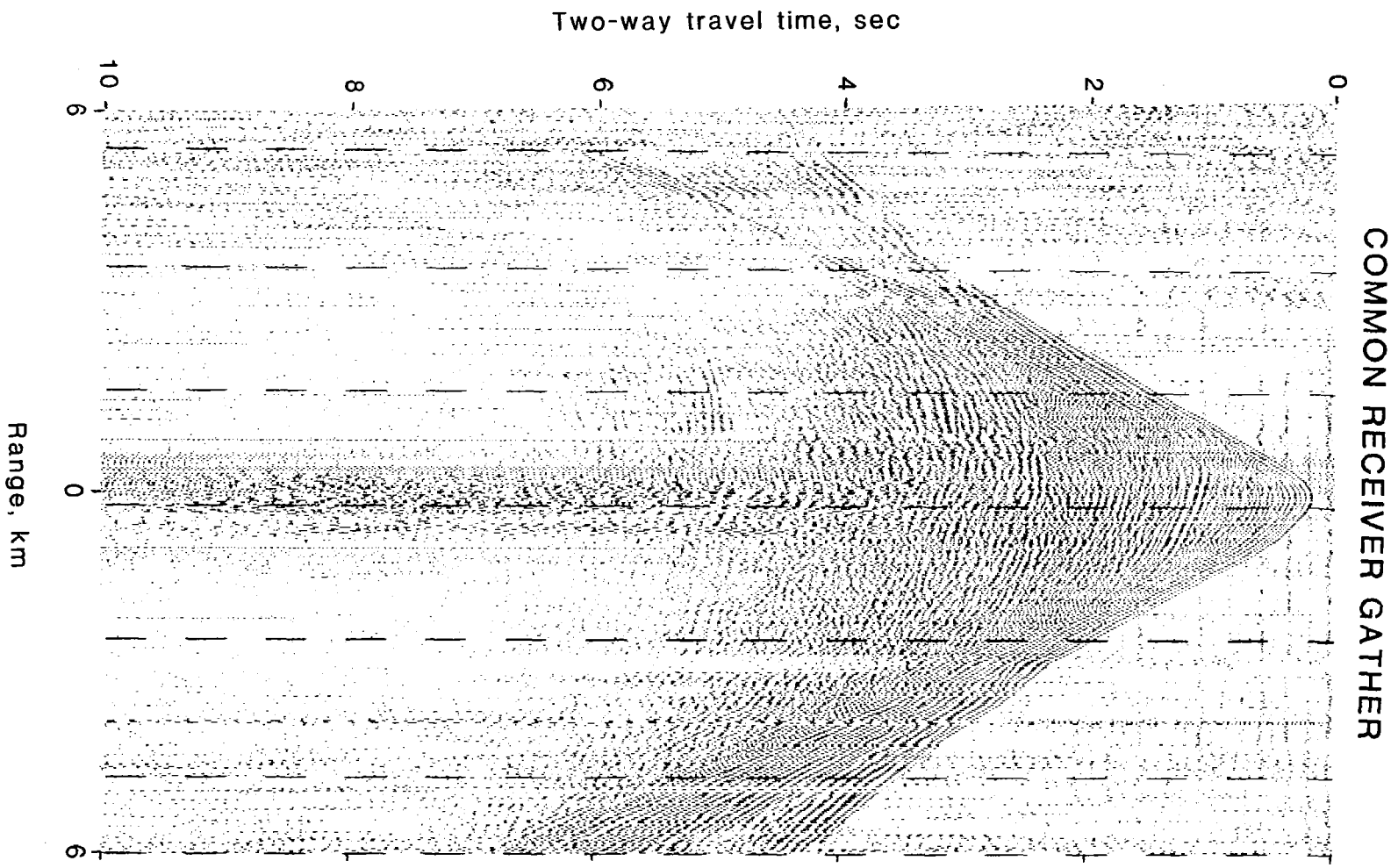


Figure 2. Example of seismic reflection gather acquired using tethered hydrophones recorded on the S.P. Lee.

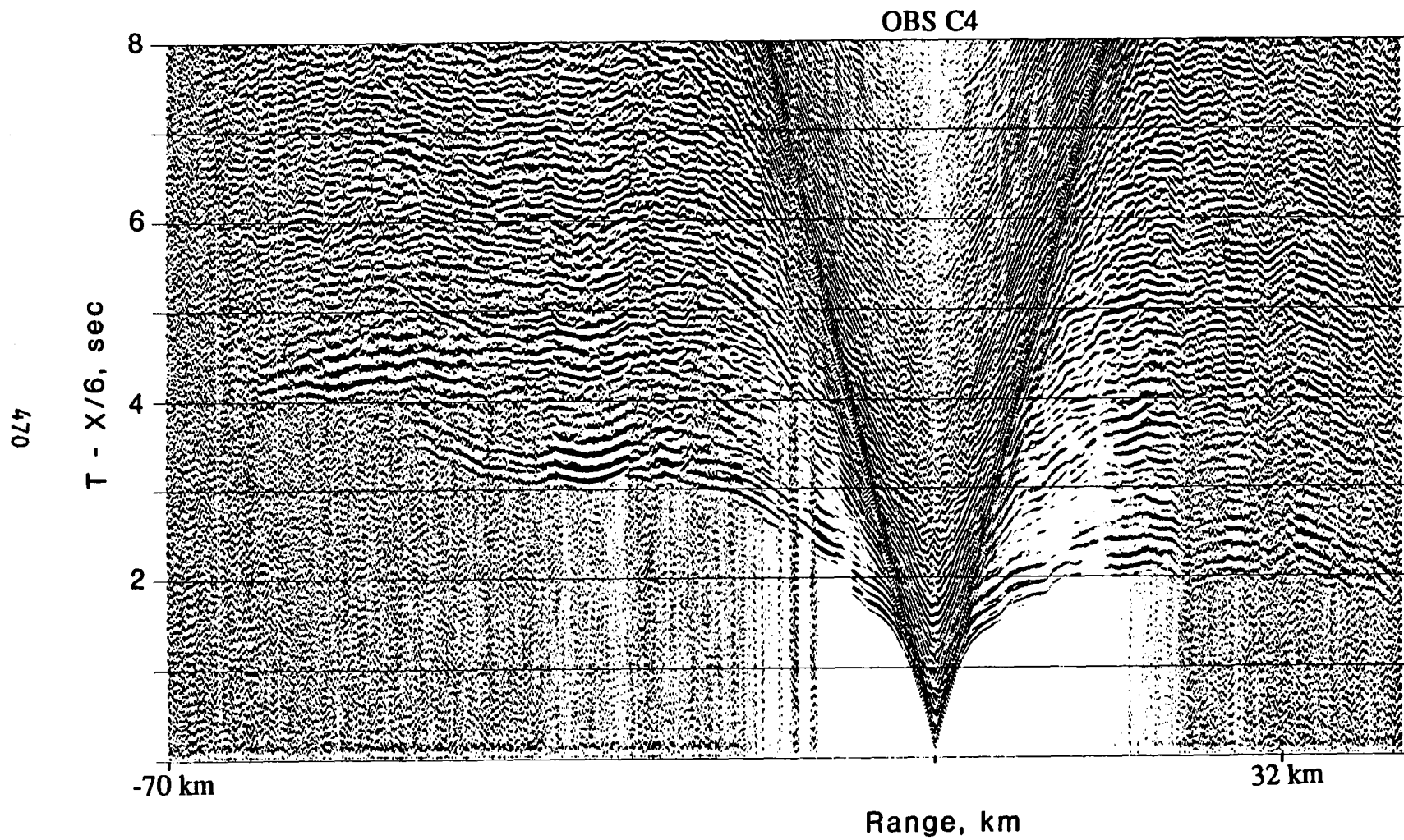


Figure 3. Example of an ocean-bottom seismometer recording from the offshore seismic reflection profile of the California continental margin.



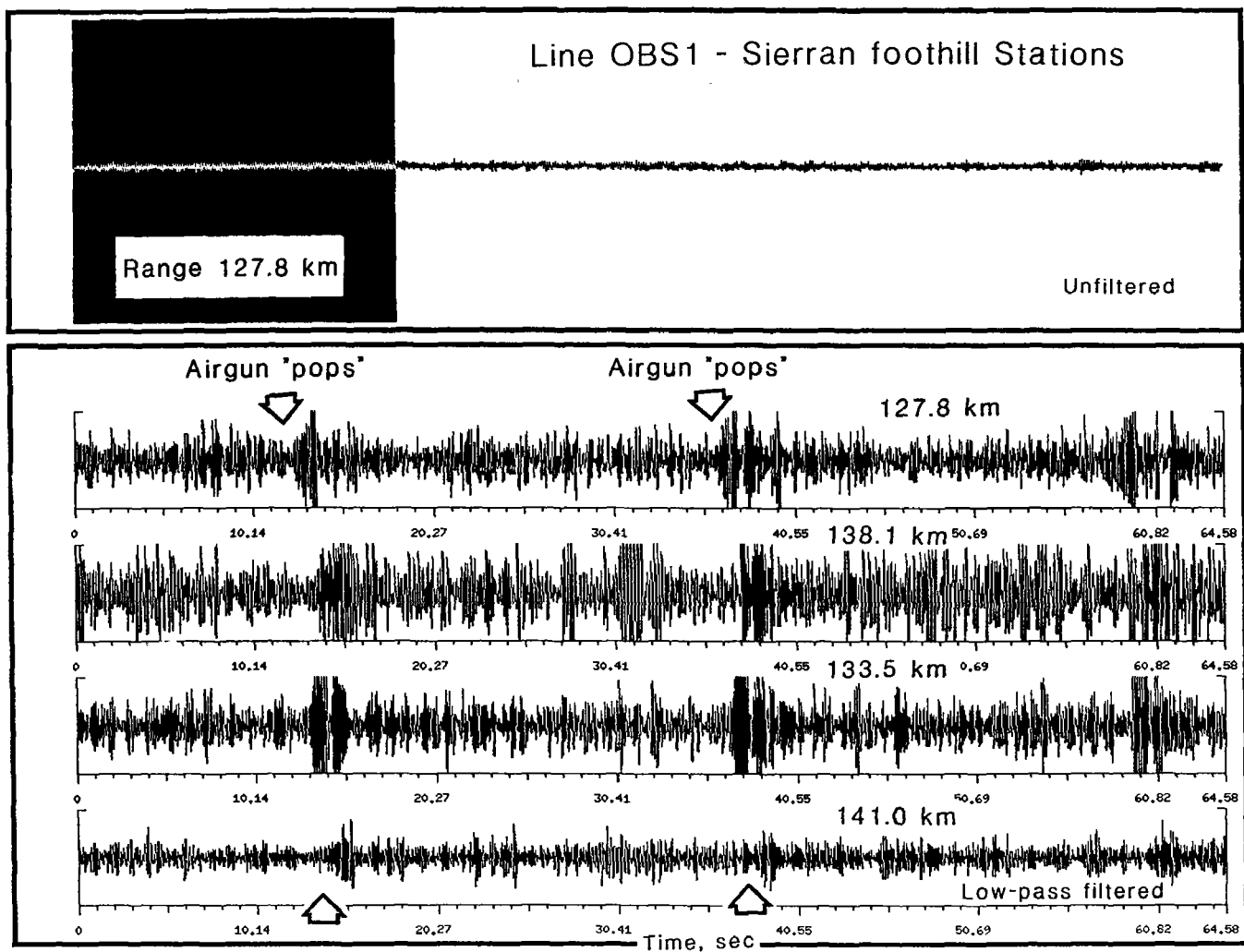


Figure 4. Example of data recorded by 4 different USGS five-day recorders in the western Sierran foothills (near Copperopolis) from airgun shots in San Francisco Bay along the OBS deployment. There is a dramatic improvement in signal levels after simple low-pass filtering.

Bay correlate with interpretations of the prominent gravity anomaly over this bay. Basin-filling sediments thicken westward while clear evidence of faulting and disruption can be observed on the eastern side of the bay in the vicinity of the Rodgers Creek fault. Faulting along the Hayward fault is observed, although the offsets are subtle and will require much more analysis before the observed deformation can be fully understood. Observed scour and fill near Pittsburg can be related to the last glacial lowstand, and provide the basic framework to understand the original shape of the bay and recent stratigraphy. The digitally recorded high-resolution data are being processed, mainly to suppress multiple reflections.

## **Reports**

- Anima, R., and P. Williams, High resolution marine-profiling in BASIX: Complex structures of major East Bay faults, EOS Trans. AGU, 72, 446, 1991.
- Brocher, T.M., S.L. Klemperer, U.S. ten Brink, and W.S. Holbrook, Wide-angle seismic profiling of San Francisco Bay Area faults: Preliminary results from BASIX, EOS Trans. AGU, 72, 446, 1991.
- Furlong, K.P., J. McCarthy, T. McEvilly, Geometry and kinematics of the Pacific-North American plate boundary in the San Francisco Bay Area: A testable model for BASIX, EOS Trans. AGU, 72, 445-6, 1991.
- Hart, P.E., and R. Clymer, Geometry of San Francisco Bay Area faults: Preliminary results from BASIX, EOS Trans. AGU, 72, 446, 1991.
- Holbrook, W. S., and U. S. ten Brink, Preliminary cruise report - San Francisco Bay and Margin Seismic Experiment, Ocean Bottom Seismometer Operation, Sept. 1991. 17 pages, 11 figures, Sept. 1991.
- Jones, D.L., A.J.H. Lomax, and T.V. McEvilly, BASIX Motivation: Tectonics of a transpressive plate boundary - A new paradigm for the Central California Coast Ranges, EOS, Trans. AGU, 72, 446, 1991.
- Klemperer, S.L., and BASIX Working Group, Bay Area Seismic Imaging eXperiment: Fan-profiling to Image the maximum depth of penetration of the San Andreas, Hayward, and Calaveras faults, EOS, Trans. AGU, 72, 446, 1991.

**ACTIVE MARGIN TECTONICS, PACIFIC NORTHWEST REGION****9910-04492**

P. A. McCrory

Branch of Engineering Seismology and Geology  
U. S. Geological Survey  
345 Middlefield Road, MS 977  
Menlo Park, California 94025  
(415) 329-5677 or (FTS) 459-5677

**Investigations undertaken**

FY91 research focused on the record of late Cenozoic tectonism preserved along the northwestern Pacific margin. Current work involves detailed study of sedimentary sequences in coastal southern Washington selected to obtain as complete a time record as possible and to document regional variation in the amount of vertical tectonic movement. FY89 field investigations identified several sites along coastal Washington with geomorphic and stratigraphic evidence of youthful folding, faulting, uplift or subsidence. Strata at these sites are being measured and sampled in detail for tephra, microfossil, depositional facies, and geohistory-backstrip analyses.

Geologic field investigations during this reporting period included stratigraphic measurement, description, and sampling of the North Pratt Cliffs, Cape Elizabeth, and Whale Creek-Raft River sections of the Quinault Formation.

Construction of a geologic cross-section of the tilted and faulted Pleistocene deposits exposed in the sea cliffs in the Raft River area to quantify the amount of tectonic shortening.

Field reconnaissance in the Raft River area for evidence of recent tsunami-subsidence occurrence. Submission of fossil wood material for  $^{14}\text{C}$  age dating of a possible tsunami-subsidence deposit.

Collection of peat and fossil shell material from an upper Pleistocene deposit in the Kalaloch area for Ur-series and ESR age dating.

Lab investigations during this reporting period included microscope analysis of microfossil material from sedimentary rock samples collected in FY89 and processed in FY90 and FY 91.

Results obtained

1. The three sedimentary sequences measured and described during FY91 display evidence of syndepositional deformation such as slumping, liquifaction, sand venting which may be related to seismic shaking. Contacts between the Quinault Formation and the underlying accretionary prism rocks (Hoh Formation) suggest active diapirism during deposition of the Quinault Formation. There is some evidence that diapirism continued into the late Quaternary.
2. Documented offsets of an upper Pleistocene deposit at several sites along the coast. Some offsets clearly reflect tectonic activity, others may be caused by landsliding.
3. Rock samples collected in FY89 have been reprocessed to concentrate microfossils for analyses of age and uplift data.
4. Continued analyses of sedimentary rock samples collected in southern Washington in FY89 for age and uplift data.

Reports published

None this reporting period.

# SEISMIC WAVE MONITORING AT PARKFIELD, CALIFORNIA

14-08-0001-G1703

T.V. McEvilly, R. Clymer, T. Daley, B. Foxall, E. Karageorgi, A. Michelini  
Seismographic Station, University of California, Berkeley, CA 94720  
and  
Earth Science Div, Lawrence Berkeley Lab, Berkeley, CA 94720

## INTRODUCTION

Three programs of seismic wave analysis continue: Earthquake recording with the high-resolution seismic network (HRSN), begun in December, 1986; controlled-source monitoring with HRSN begun in June, 1987; and controlled-source experiments with the Varian well vertical array (VWVA), begun in November, 1987.

The HRSN (Figure 1) consists of ten, 3-component, borehole seismometers surrounding the 1966 Parkfield epicenter. Data-acquisition features digital telemetry with 125-Hz bandwidth and 16-bit resolution, and can operate in external-trigger (*i.e.*, controlled-source) or event-trigger (earthquake) modes. Network characteristics are shown in Table 1.

The VWVA extends to 968m depth at a site 2 km from the San Andreas fault (Figure 1), close to the nucleation zone of the expected magnitude 6 Parkfield earthquake. Early vertical seismic profile (VSP) results indicating local anisotropy were shown in Daley and McEvilly, 1990. Data have been recorded on a Sercel 338 96-channel reflection system.

## INVESTIGATIONS

1) *Earthquakes.* Local microearthquakes of magnitude about -0.5 to about +2 are routinely recorded on scale. A 3-D velocity model and a high-precision relative hypocenter location procedure for clustered events with similar waveforms have been developed, and are now being used for high-resolution analysis of local earthquakes. Clustered events are being studied for evidence of temporal changes in fault zone processes and properties, including anisotropy, in cooperation with R. Aster of U.C. San Diego. Relocated events are being used to study failure processes, fault zone structure, and material properties within the Parkfield nucleation zone.

2) *Controlled-source monitoring with HRSN.* From June, 1987 through August 1991, the HRSN has been illuminated 36 times with S-waves of three polarizations at eight source positions throughout the study zone, using a shear-wave Vibroseis source, in an on-going monitoring program. The resulting data contain a temporal record of wave propagation characteristics throughout the nucleation zone. Albeit complexly encoded, the wave fields recorded contain the evidence for any nucleation-induced changes in velocities, attenuation or anisotropy. Data reduction is accomplished at the University of California's Lawrence Berkeley Laboratory (LBL), at LBL's Center for Computational Seismology (CCS). A paper summarizing this study is presently in press.

3) *Controlled-source monitoring with VWVA.* Analysis of local anisotropy and velocity structure using short-offset VSP's and 3-D generally anisotropic models is an ongoing topic of research at CCS in collaboration with several European scientists, and VWVA VSP data sets are prominently featured in this effort.

## DATA COLLECTED

- Full-time, event-triggered recording of earthquakes has continued in the past year. Event data are archived as IEEE-format binary files on magnetic tape with simple headers.
- Five vibrator data sets have been collected and the data reduced in FY91. Data after routine processing (edit, stack, correlation, gather by source site) are archived in SEG Y format on magnetic tape.

## RESULTS

### 1) *Earthquake studies:*

- A final 3-D velocity model has been established, and a paper on the modeling process and results has been published.
- A graduate student working with Parkfield earthquake data and 3-D modeling has completed his studies.
- Local Parkfield events have been picked and relocated with the 3-D model through December, 1990.
- In a major effort, we have defined, gathered, and archived clusters of events with similar waveforms through 1989. About 500 events were relocated through the 3-D model for analysis. The result is 70-80 clusters defined within our network (Fig 1), with 2-18 events/cluster. About two-thirds of the total events are clustered. Many clusters span the three years of data collection.
- We have completed the automated picking of relative P and S arrival times within clusters (using B. Foxall's cross-correlation, cross-coherence procedure), and high-precision relative relocation of cluster events. Many of the relocated clusters span only 100-200m (Fig 2).
- Procedures have been developed to efficiently add post-1989 data to the clusters.
- In the work with R. Aster, we are studying S-wave polarization variations within the clusters, and the implications for anisotropy.

The archived clusters will be the basis for further studies: of rupture processes on small patches of the fault using either theoretical or empirical Green's functions (Foxall).

2) *Controlled-source studies - HRSN.* The final working data sets for analysis are "time gathers": one source into one receiver gathered across calendar time, producing 720 files, each containing, at present, 35 similar traces. The time gathers are then examined for variations in waveform parameters.

Most displays to date show only seasonal variations in various properties (travel time, amplitude, spectral properties). Seasonal variations are due to very near-surface moisture changes under the vibrator (Clymer and McEvilly, 1981). The magnitude of the variation varies considerably from site to site. This is illustrated for two paths in Figure 4 for spectral amplitude. The path from vibrator position (VP) 2 to MMN shows an overall trace amplitude change - the shear-wave vibrator couples to the ground better in the dry summer - but little change in the shape of the spectrum, or (not shown) in the travel time. Path 4-MMN data, on the other hand, show a significant change in the shape of the amplitude spectrum, with higher frequencies being increased relative to low frequencies in the dry months when the vibrator couples better, and in travel time (not shown).

A paper on the controlled-source work has gone through final revisions and is in press.

Figure 5 illustrates a travel-time anomaly that appears on paths that pass through the vicinity of VP 2, south-west of the 1966 epicenter. The figure shows grey-scale displays of relative travel-time change (correlation lag) across time gathers in a moving window. Several paths show relative advances in travel time of 30-60 msec for a band of late phases (the dark zones at late times), beginning in mid-1988. This effect is particularly well developed on most paths from source site 2, although it is seen from other source sites as well. Path 6-FRO, on a north-west azimuth, does not show the effect. Energy on this path may preferentially refract through the intact granites lying south-west of the SAF, and thus not sample the area of VP2. Data from the path from VP2 to SMN, to the north-west, similarly do not show the effect. Figure 6 shows windowed travel-time changes of individual prominent late phases from various source sites into VCA. All the arrivals examined show a significant advance, with the exception of those from sites to the north-west.

Figure 6 summarizes the paths examined to date. The wide solid and narrow dashed lines indicate paths that respectively show and do not show the anomaly. There is an indication of a zone of anomalous velocity south-west of Middle Mountain.

## References

- Clymer, R.W., and McEvelly, T.V., 1981. Travel time monitoring with VIBROSEIS, *Bull. Seism. Soc. Amer.*, **71**, 1902-1927.
- Daley, T.M., and T.V. McEvelly (1990). Shear Wave Anisotropy in the Parkfield Varian Well VSP, *Bull. Seis. Soc. Am.*, **80**, 857-869.

## Published Papers, Reports, Abstracts

- Clymer, R.W., E.D. Karageorgi, A. Michelini, and T.V. McEvelly, 1991. Anomalies in Controlled-Source Waveform Parameters at Parkfield, *Seis. Res. Letts*, **62**, 46. -abstract
- Daley, T.M., and T.V. McEvelly, 1991. Update of shear-wave anisotropy measurements at the Parkfield Varian well, *Seis. Res. Letts*, **62**, 46. -abstract
- Karageorgi, E., R. Clymer and T.V. McEvelly, 1991. Shear-wave monitoring at Parkfield with Vibroseis, *Seis. Res. Letts*, **62**, 46. -abstract
- Karageorgi, E., R. Clymer and T.V. McEvelly, 1992. Seismological studies at Parkfield: II. Search for temporal variations in shear wave propagation using Vibroseis, *Bull. Seism. Soc. Am.*, in press.
- Michelini, A. (1991). Fault zone structure determined through the analysis of earthquake arrival times, PhD. Thesis, Univ Calif, Berkeley.
- Michelini, A., and T.V. McEvelly (1991). Seismological studies at Parkfield: Simultaneous inversion for velocity structure and hypocenters using cubic B-splines parameterization, *Bull. Seis. Soc. Am.*, **81**, 524-552.

Table 2. Parkfield HRSN Instrumental Description

STATIONS(Since 13 Jan 1988)

<u>Station</u> <u>Name</u>	<u>Lat.</u> <sup>1</sup> <u>(N)</u>	<u>Long.</u> <sup>1</sup> <u>(W)</u>	<u>Surface</u> <u>Elev.(m)</u> <sup>2</sup>	<u>Sensor</u> <u>Elev.(m)</u> <sup>2</sup>	<u>Z</u>	<u>Polarities</u> <sup>3</sup>		<u>Sensor</u>
						<u>H1</u>	<u>H2</u>	
EAD	35.89522	120.42262	503	258	D	170°	260°	L22 <sup>5</sup>
FRO	35.91095	120.48688	549	265	D	338°	248°	L22
GHI	35.83225	120.34728	427	364	U	out	?	L22
JCN	35.93897	120.43112	567	343	D	0° <sup>4</sup>	270°	L22
JCS	35.92117	120.43400	488	333	U	300°	210°	HS1 <sup>6</sup>
MMN	35.95650	120.49600	735	514	D	175°	265°	L22
RMN (GP)	36.00087	120.47772	1198	1125	D	310° <sup>4</sup>	40° <sup>4</sup>	L22
SMN	35.97297	120.57988	732	450	D	120°	210°	L22
VAR	35.92608	120.44705	509	-63	U	15	285	1023 <sup>7</sup>
VCA	35.92162	120.53392	789	589	D	200°	290°	L22

<sup>1</sup> Sites located with GPS; datum = NAD84. (Conversion to NAD27: +0.00004° latitude, -0.00101° longitude.)

<sup>2</sup> Height above mean sea level. (Conversion to height above ellipsoid: -34m.)

<sup>3</sup> Direction of ground motion (east from true north) producing positive digital counts as recorded on SEG-Y tape in field and as archived at Berkeley

<sup>4</sup> These channel polarities are reversed on archive tapes generated by UCSB/Duke

<sup>5</sup> Mark Products, 2 Hz, 5.5 K $\Omega$ , 0.7 damping, 0.60 v/cm/s

<sup>6</sup> Geospace, 4.5 Hz, 1250 $\Omega$  coils, 0.49 v/cm/s open circuit; 0.6 damping with 2500 $\Omega$  shunt resistance; vertical - 1660 $\Omega$  (8 phones, 2 parallel stacks of 4 in series), 1.30 v/cm/s; horizontals - 830 $\Omega$  (single phones), 0.33 v/cm/s

<sup>7</sup> Litton, 4.5 Hz, 670 $\Omega$ , 0.7 damping, 0.39 v/cm/s

#### SIGNAL CONDITIONING & TELEMETRY

Digitizers: RefTek 24, 3-component, DC coupled, 80 dB gain, 125 Hz 12-pole Butterworth anti-alias filters, 16-bit conversion, 500 samples per second per channel, asynchronous sampling clocks among sites.

Telemetry: Digital, RefTek radios, 216-220 MHz, 38.4 Kbaud, RefTek44 multiplexer (Interface to recorder).

#### RECORDING SYSTEM

WESCOMP II: LSI-11-based VSP recording system, 32 channels, SEG-Y output tape, for event and Vibroseis recording.

HRSN Specs

3/10/91



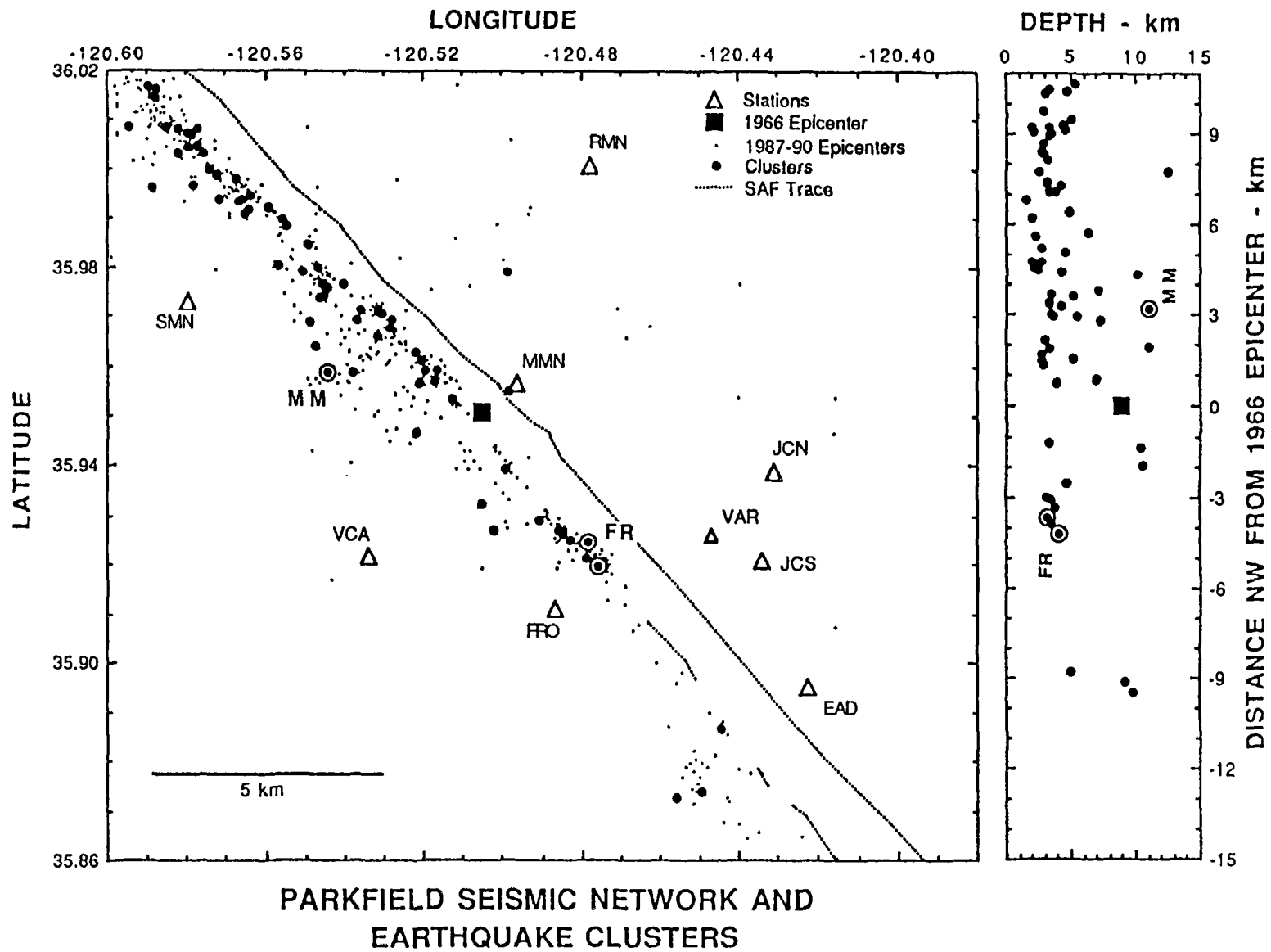


Figure 1. Parkfield location, showing the High-Resolution Seismic Network (HRSN), and 6/87-12/90 seismicity as relocated through the UCB 3-D velocity model, with identified clusters.

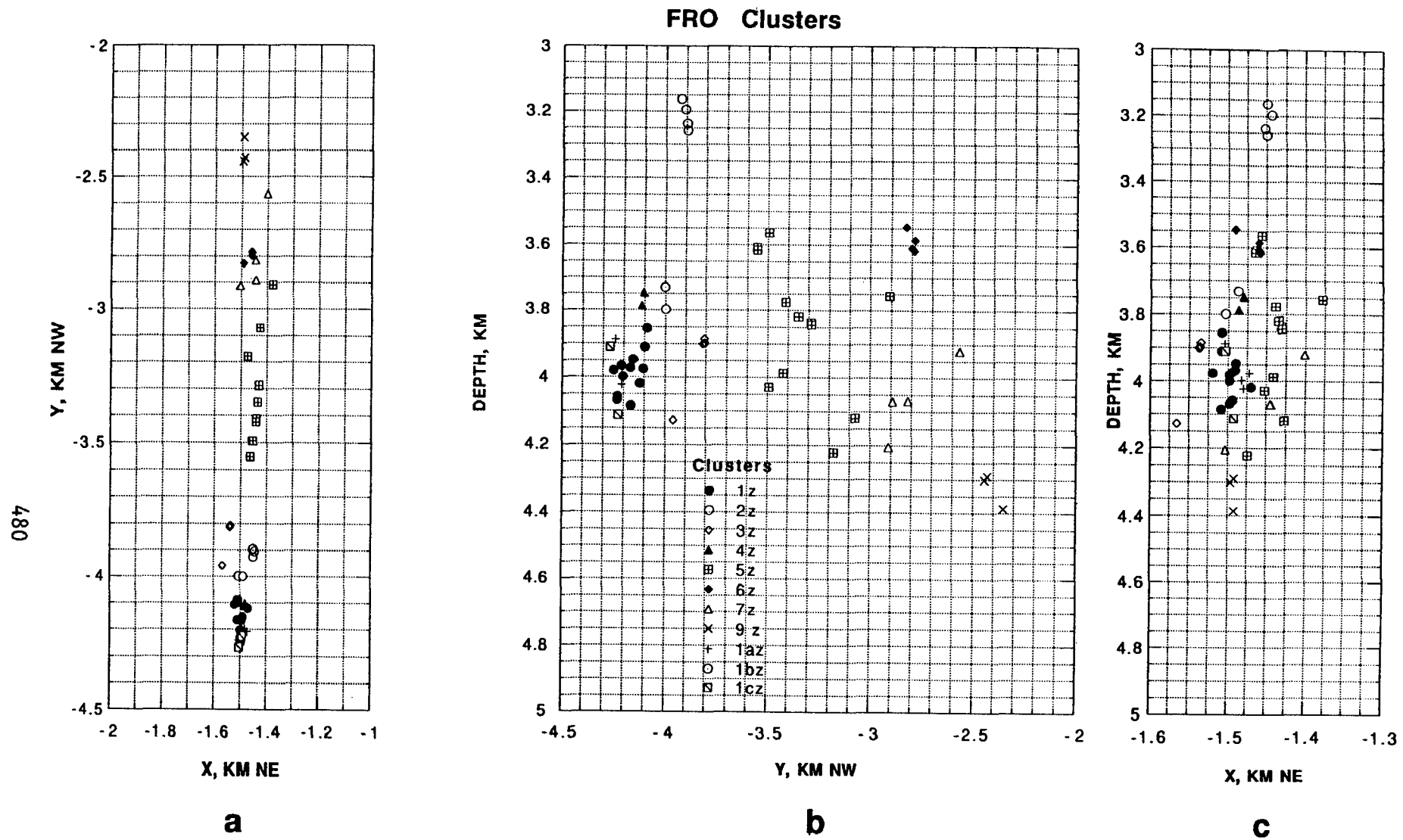


Figure 2. Microearthquake clusters in the vicinity of HRSN station FRO. a) map view, with X- and Y-axes perpendicular and parallel to the local strike of the San Andreas fault (SAF), and center of coordinates at the epicenter of the 1966 Parkfield earthquake. b) and c) are cross-sections parallel and perpendicular to the SAF. Note the changes in scale.

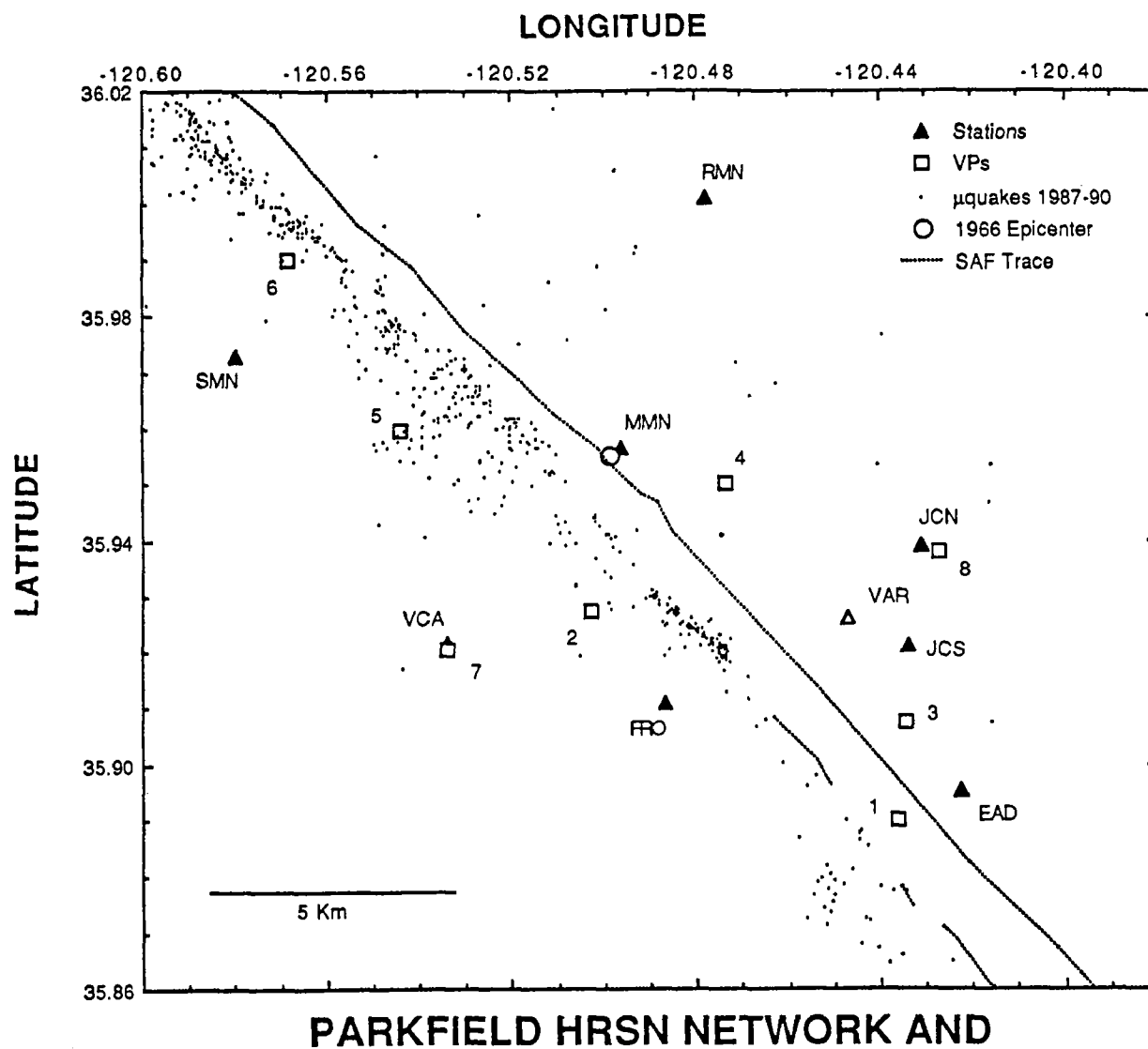


Figure 3. Location map, showing the vibrator monitoring sites and the HRSN.

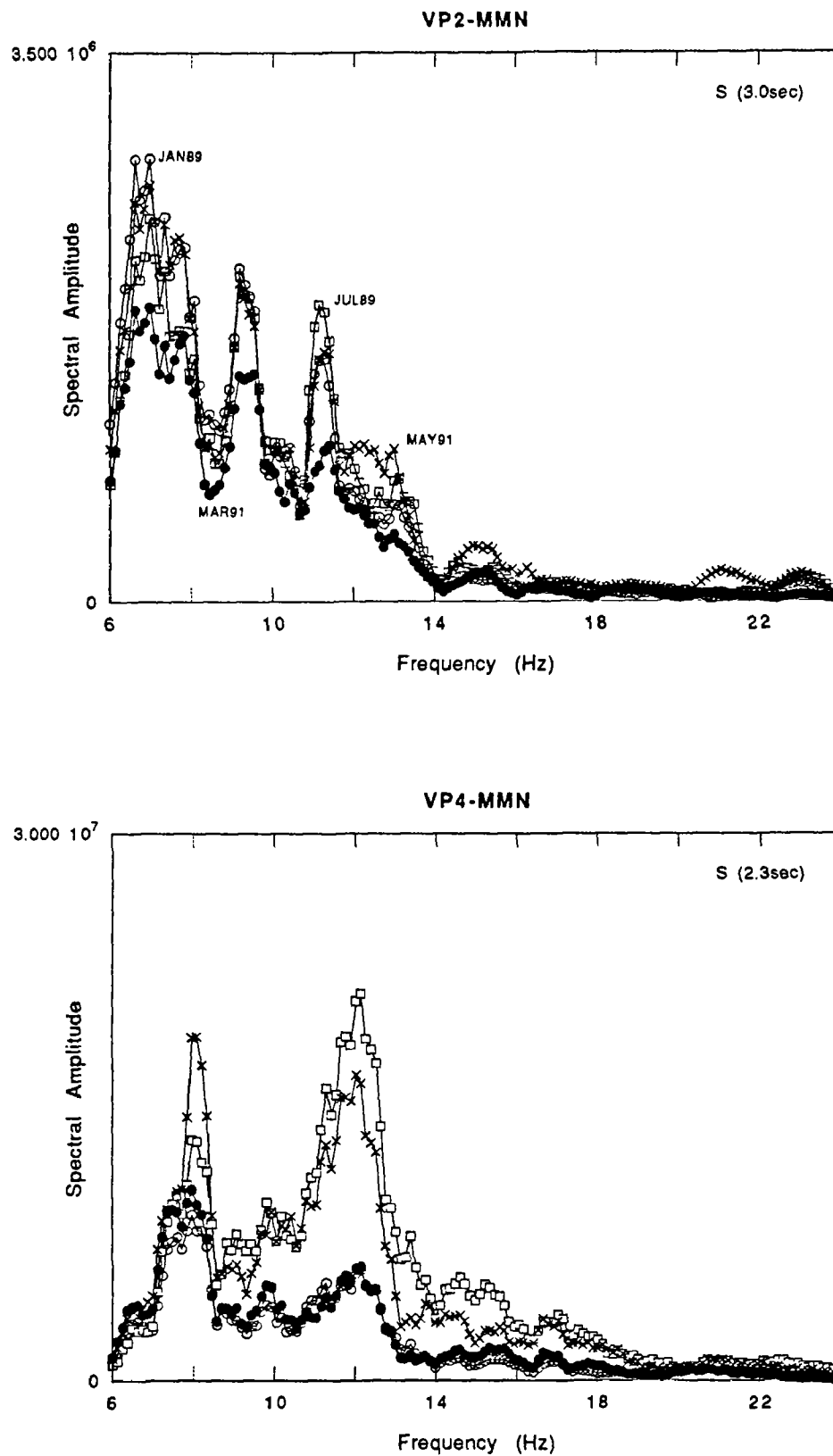


Figure 4. Amplitude spectra, showing seasonal variations in frequency content of the direct S arrival on two paths.

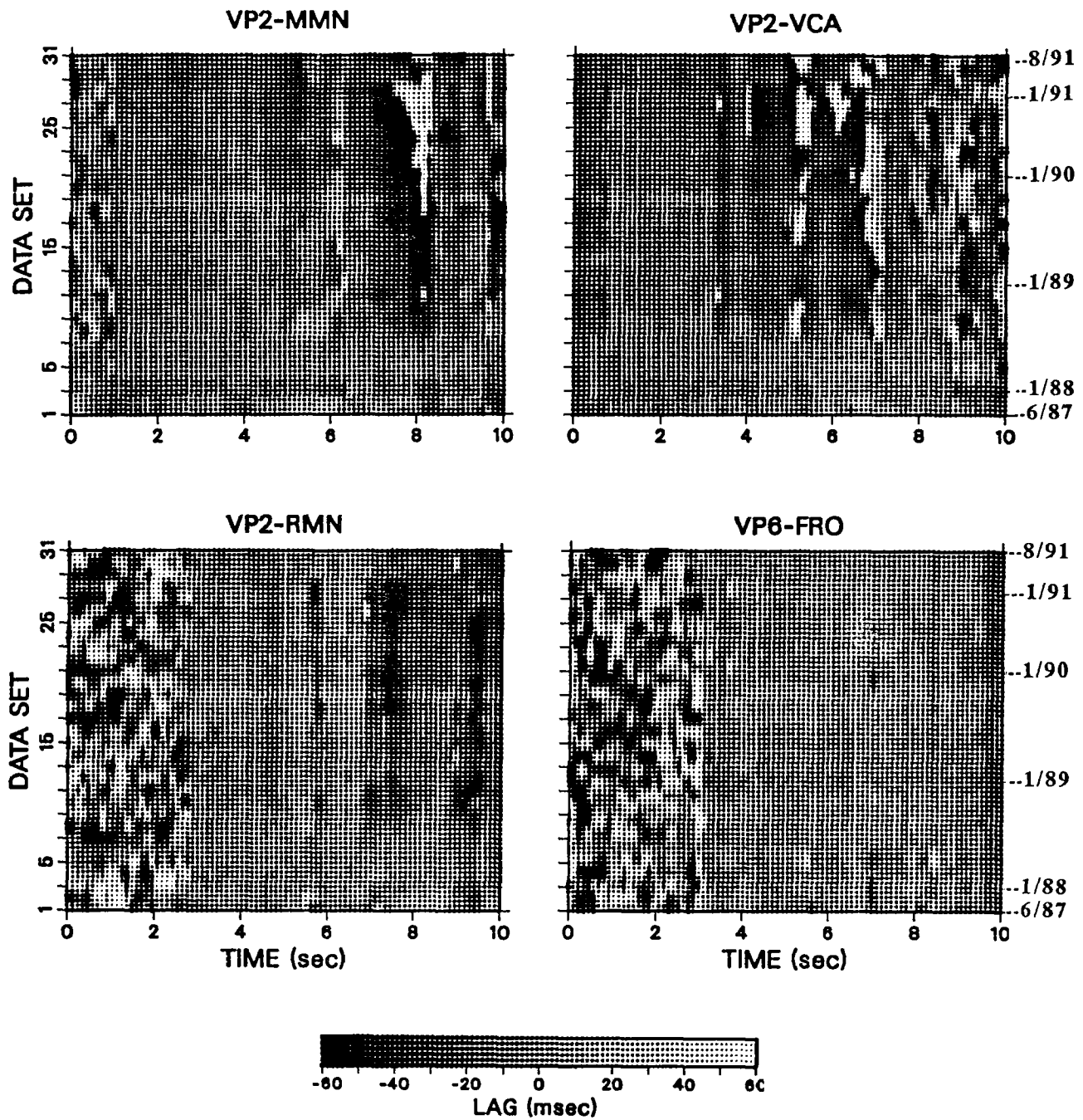


Figure 5. Travel-time change relative to data set 6 (April '88) by cross-correlation in a moving time window. Three of these show the late 30-60msec advance (dark zones) beginning in mid-1988, as discussed in the text.

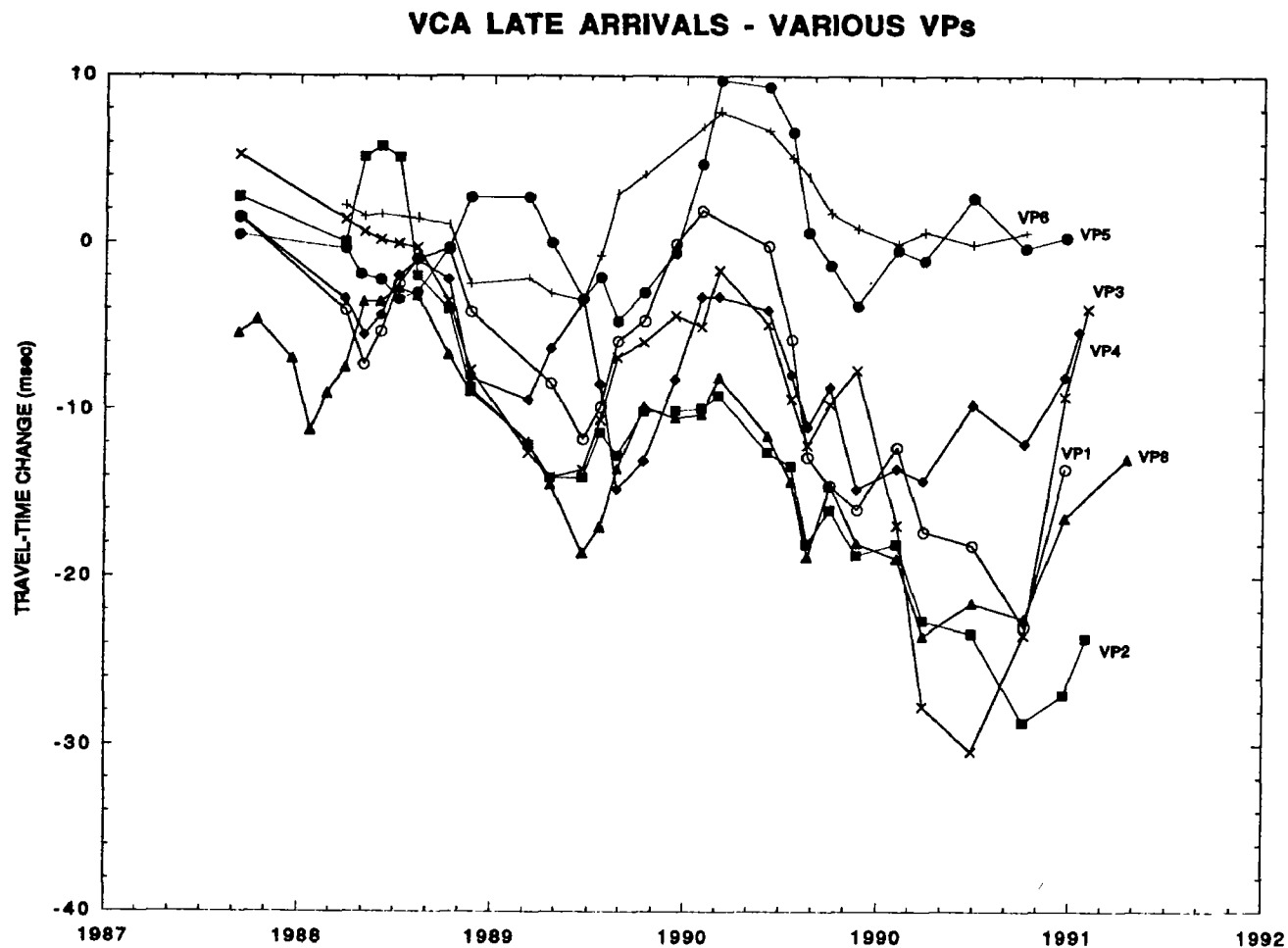


Figure 6. Relative travel-time variations measured on paths into VCA from several source sites, calculated by a cross-correlation, cross-spectral technique in fixed time windows centered on prominent late phases .

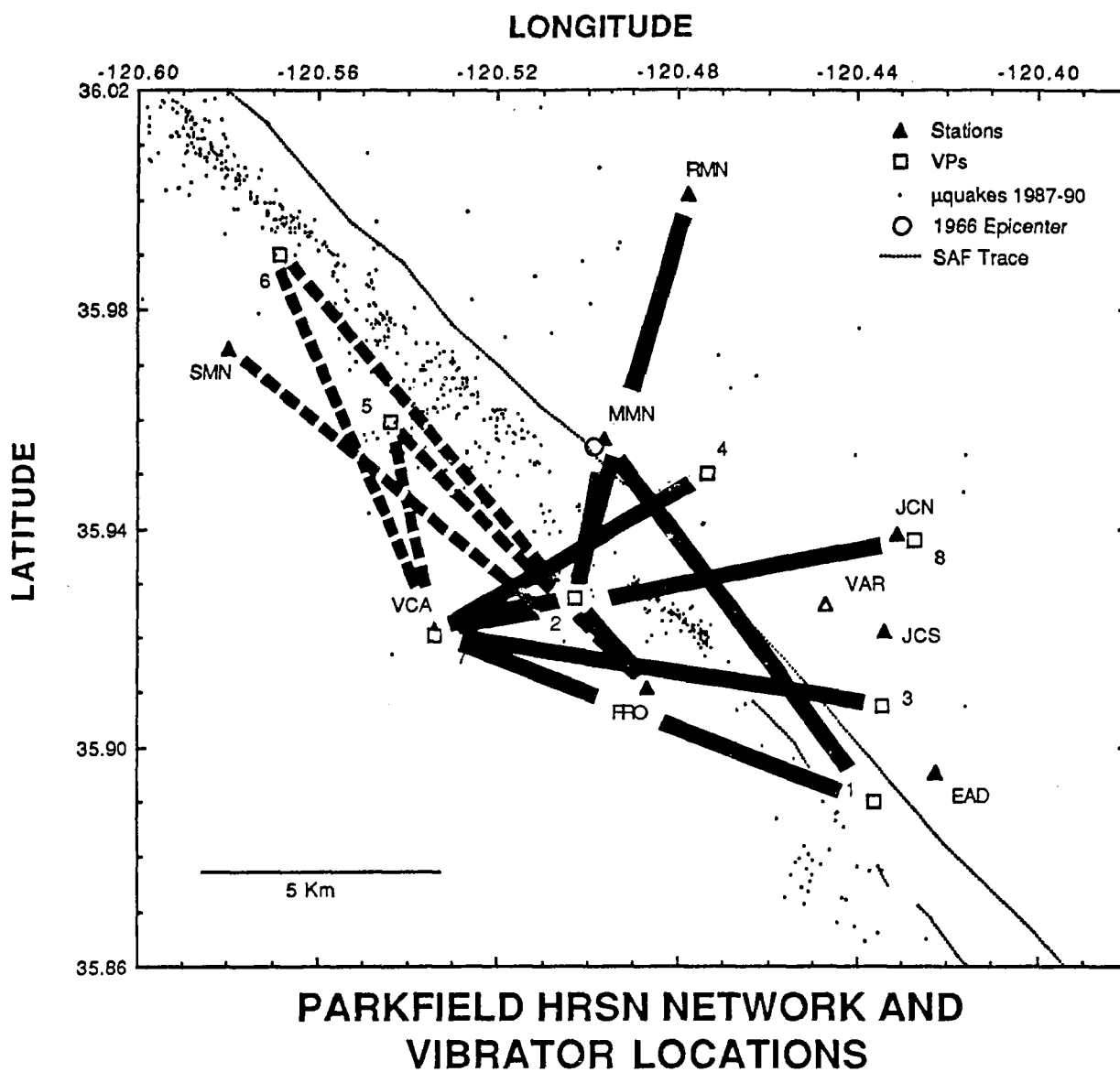


Figure 7. Base map showing source-receiver pairs that have been examined for late-phase travel-time anomalies. Wide solid and narrow dashed lines indicate time gathers with and without anomalies.

## Bay Area Digital Seismic Network

14-08-0001-G2122

01Sept91-30Sep92

Thomas V. McEvilly and Barbara Romanowicz  
Seismographic Station  
Dept. of Geology and Geophysics  
University of California  
Berkeley, CA 94720

Phone: (510) 486-7347  
FAX: (510) 486-5686  
e-mail: tvmceville@lbl.gov

### Project Description

This UC/USGS cooperative project is the installation of a new digital seismographic network in the San Francisco East Bay region along the full length of the Hayward fault (Ellsworth on the southern half - UC the north). The purpose is to achieve a substantial improvement in the resolution with which we can monitor seismicity to very small magnitudes and fault-zone processes on the Hayward fault. Ultimately some 24 stations are planned with wide dynamic range and frequency bandwidth (>20 bits, 250 Hz), with on-scale recording to 0.5 g. Current funding will allow installation of perhaps 12-16 initial stations.

### FY91 Accomplishments (01-30 September)

Despite only one month's activity in FY91 under this award, a substantial startup effort was mounted:

Borehole sensor installations. Existing geophones from UC/LBL stock were provided to Malcolm Johnston in order to insure that his pilot exploratory holes for the borehole strainmeter project, which are immediately cemented upon completion, would be equipped with downhole sensors for the digital network. Other 'off-the-shelf' borehole seismometers were supplied from USGS. (Drilling costs for installing network seismometers were deleted from the UC award, so holes of opportunity are being used wherever possible. A borehole sonde was developed for deployment of multi-component sensors downhole to 1000 ft depth. Experience at other sites (Parkfield, the Geysers, Long Valley) and the known Bay Area noise levels render surface sites there only marginally effective as high-resolution, high-frequency stations.) Boreholes of opportunity have also been found in Alameda (Kyle Rollins project), at the east approach to the Bay Bridge (courtesy of CALTRANS) and on the Berkeley/LBL grounds (three holes exist). Figure 1 summarizes the installation progress as of mid-November. So far, most hole depths are around 500 ft. We would prefer emplacement depths of 800-1000 ft.

Sensor selection. Tests were initiated on appropriate sensors for the network. The high-frequency operation planned for the network calls for better noise characteristics above 15Hz than are available in conventional 2 or 4.5 Hz velocity geophones. We are testing low-noise accelerometers, and one such comparison is presented in Figure 2. Presently we are leaning to a 4-component (three accelerometers and a redundant vertical velocity sensor) instrument package.



Data acquisition system. Specifications were developed for the network data acquisition systems and a request for bids was issued. The system will sample at up to 1000 sps and telemeter continuously a data substream, using Pacific Bell's new digital network. On-site backup will exist and central site event triggering will be a possible mode of operation. At mid-November a vendor has not yet been selected.

Schedule. Sensors and data acquisition equipment will be ordered in December. Station sites will continue to be sought and instrumented throughout the year. Telephone lines will be arranged for definite sites.. Central site software and hardware will be purchased/developed early in 1992. In the late spring the prototype remote sites will be activated and the telemetry system tested under real operation.

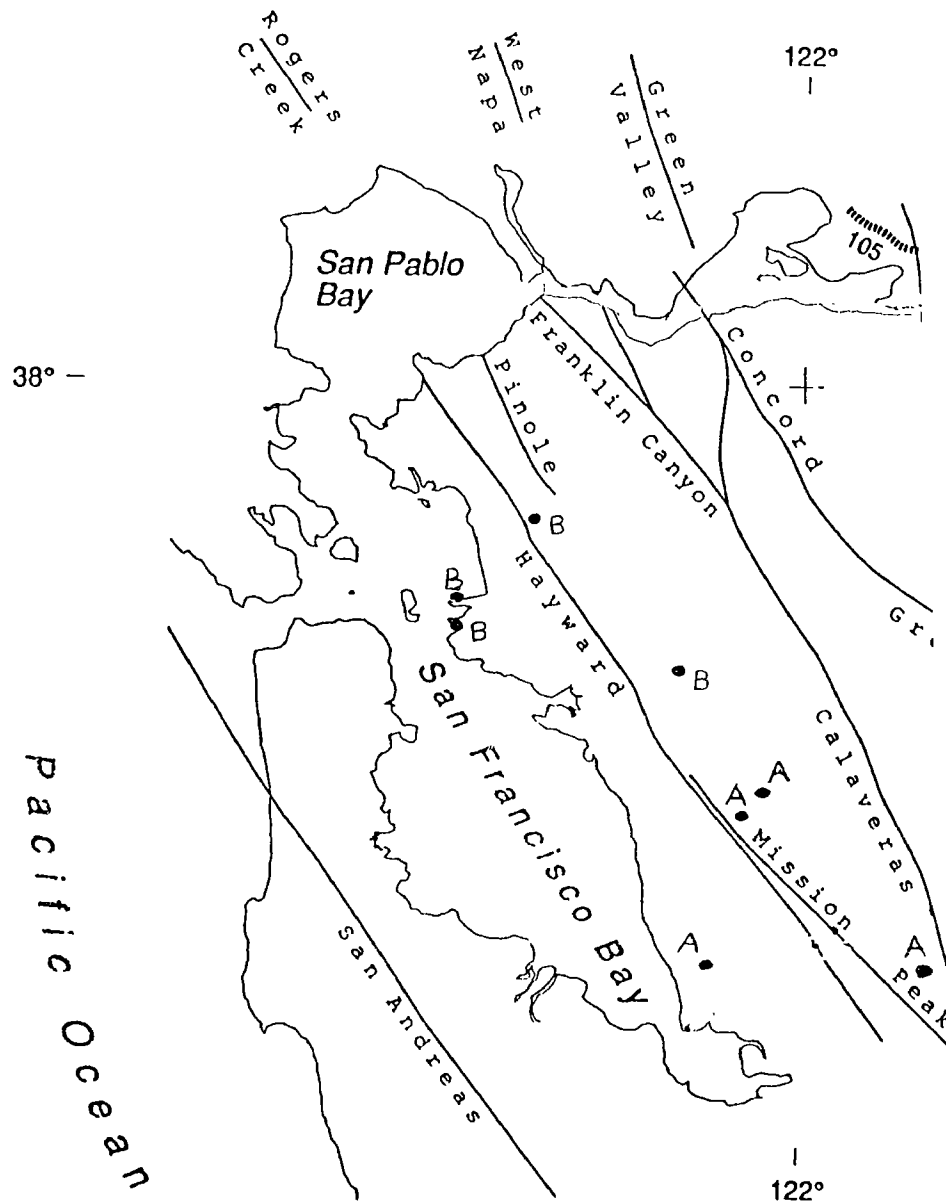


Figure 1. East Bay network station sites with (A) borehole sensors installed, as of mid November, 1991. (B) sites are presently available or planned borehole sites to be used when available.

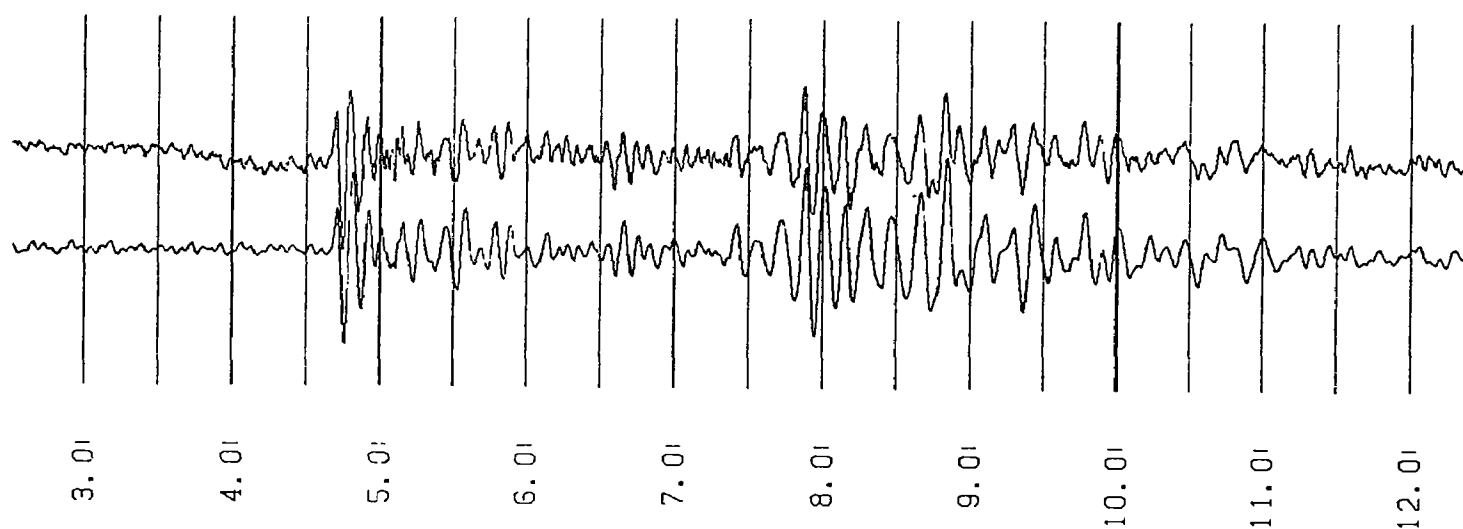


Figure 2. Preliminary sensor comparison between conventional 4.5 Hz velocity geophone (lower trace) and wide-band (0.1- 600 Hz) accelerometer, integrated to velocity (both sampled at 1000 sps with 250 Hz anti-alias filter), for the recording of a  $m=1.2$  event about 25 km from the sensors, which were installed in a common sonde at the bottom of a 550-ft borehole on the fault at the stadium on the UC Berkeley campus. 60 Hz noise and the presence of tube waves degraded this comparison somewhat, and the experiment will be repeated more carefully. Initial results suggest that the 0.5g full-scale accelerometer will serve well as the detector for the small microearthquakes, particularly at frequencies above 10 Hz.

## **Parkfield Earthquake Prediction Experiment: Earthquake Seismology**

9930-02098

Andrew J. Michael  
Branch of Seismology  
U.S. Geological Survey  
345 Middlefield Road, MS/977  
Menlo Park, California 94025  
(415)329-4777

### **Investigations:**

The principal subject of investigation is an attempt to understand the structure and behavior of the seismogenic zone at Parkfield, California in order to better understand the physical processes that control the earthquake generation cycle in that area. In addition we have been attempting to apply these ideas to other areas to determine if we have uncovered processes that are generally applicable or if they are specific to the Parkfield area. To accomplish this we have maintained a detailed catalog of Parkfield hypocenters and focal mechanisms and determined a three-dimensional velocity model of the Parkfield region. This velocity modeling work is in collaboration with Donna Eberhart-Phillips.

In order to test the ideas we have developed at Parkfield we have also been determining a three-dimensional velocity model for the Loma Prieta, California area. To provide greater control of the model and hypocentral locations with respect to surface features a series of six calibration shots were recorded on the CALNET array and a distributed deployment of portable receivers in May of 1991.

In September of 1991 I participated in Jill McCarthy's marine seismic reflection experiment that aimed to determine fault structures under the San Francisco Bay and associated waterways. My involvement with the experiment was to coordinate the recording of the airgun blasts on the CALNET array. This data will be analyzed during fiscal year 1992.

Other research includes further studies of the stress state surrounding in the Loma Prieta and Whittier Narrows regions in order to better understand the coseismic effect of the mainshocks.

### **Results**

The most important result to come out of this project is the discovery of relations among fault behavior and the material properties of the rocks that contact the fault at seismogenic depths. Regions of high moment release appear to correlate with high seismic velocities whereas rupture initiation or termination may be associated with lower seismic velocities. These relations point toward a physical understanding of why faults are divided into segments that can fail independently, an understanding that could improve our ability to predict earthquakes and strong ground motion.

The use of three-dimensional velocity models to understand the processes that result in fault segmentation could be very important because other work at Parkfield,

CA has shown that surface fault geometry is not simply related to the fault geometry at seismogenic depths. The offset in Cholame Valley is one of the largest on the San Andreas Fault and has often been cited as the feature that terminates the rupture of the Parkfield earthquakes. However, the use of the three-dimensional velocity model to relocate both background seismicity and the 1966 aftershocks has shown that this offset does not exist at seismogenic depths. Thus the offset in the fault may be limited to the upper 1 to 3 kilometers. The one unusual feature observed in the Cholame Valley seismicity is the existence of some normal faulting mechanisms. However, they are not distributed throughout the valley as might be expected but instead lie in the same plane of hypocenters as strike-slip mechanisms that define a planar San Andreas fault.

Preliminary results from the Loma Prieta calibration shots have been used to calculate station corrections for the CALNET stations with respect to the three-dimensional velocity model. However the relationships between the shallow Loma Prieta aftershocks and the surface faults is still enigmatic.

The efforts to unravel the very heterogeneous stress state left by the Loma Prieta earthquake are still ongoing. Currently we are testing a variety of methods to compare the aftershock focal mechanisms to the stresses imposed by the mainshock in order to find a method that is sufficiently robust with respect to errors both in the mainshock rupture pattern and the aftershock hypocenters and focal mechanisms. Some of the stress inversion techniques being used at Loma Prieta were developed and tested on the Whittier Narrows aftershocks sequence. There we were able to show that the stress state during the aftershocks had a significant component of spatial heterogeneity but were unable to relate this to the mainshock rupture. However, tests using simulated data suggested that the errors in the data were large enough to mask the effects of the mainshock's dislocation. At Loma Prieta the errors are comparable, but the mainshock is larger and the simulations suggest that we should be able to define its effects.

### **Reports:**

- Michael, A. J. , 1990, Energy constraints on kinematic models of oblique faulting: Loma Prieta versus Parkfield-Coalinga, abstract, EOS, 71, 1646.
- Aviles, C.A. and Michael, A. J., 1990, Complications at the southern end of the 1966 Parkfield rupture zone, abstract, EOS, 71, 1473.
- Michael, A. J., 1991, Spatial variations in stress within the 1987 Whittier Narrows, California, aftershock sequence: new techniques and results, J. Geophys. Res., 96, 6303-6320.
- Michael, A. J., and Eberhart-Phillips, D. M., 1991, Relationships between Fault Behavior, Subsurface Geology, and Three-Dimensional Velocity Models, Science, 253, 651-654.
- Eberhart-Phillips, D. M., Michael, A. J., and W. D. Stanley, 1991, Overpressure in the Parkfield Preparation Zone?, abstract, Seismology Research Letters, 62, 46.

# INDEX 1

## INDEX ALPHABETIZED BY PRINCIPAL INVESTIGATOR

		Page	Goal
Abers, G. A.	Lamont-Doherty Geological Observatory	1	I
Abers, G. A.	Lamont-Doherty Geological Observatory	121	II
Agnew, D. C.	California, University of, San Diego	126	II
Algermissen, S. T.	U.S. Geological Survey	755	III
Allen, G.	U.S. Geological Survey	131	II
Anderson, R. E.	U.S. Geological Survey	133	II
Andrews, D. J.	U.S. Geological Survey	763	III
Arabasz, W. J.	Utah, University of	135	II
Arabasz, W. J.	Utah, University of	765	III
Atwater, B. F.	U.S. Geological Survey	137	II
Aydin, A.	Stanford University	6	I
Beavan, J.	Lamont-Doherty Geological Observatory	139	II
Beavan, J.	Lamont-Doherty Geological Observatory	145	II
Bernknopf, R. L.	U.S. Geological Survey	766	III
Biegel, R. L.	Lamont-Doherty Geological Observatory	8	I
Bierman, P.	Washington, University of	151	II
Bilham, R.	Colorado, University of	153	II
Bilham, R.	Colorado, University of	157	II
Bird, P.	California, University, Los Angeles	159	II
Boatwright, J.	U.S. Geological Survey	9	I
Bock, Y.	California, University of, San Diego	166	II
Bolton, P. A.	Battelle Seattle Research Center	917	IV
Bonilla, M. G.	U.S. Geological Survey	172	II
Boore, D. M.	U.S. Geological Survey	768	III
Borchardt, G.	Soil Tectonics, Berkeley, California	174	II
Borchardt, R. D.	U.S. Geological Survey	177	II
Borchardt, R. D.	U.S. Geological Survey	769	III
Borchardt, R. D.	U.S. Geological Survey	771	III
Borchardt, R. D.	U.S. Geological Survey	773	III
Boyd, T. M.	Colorado School of Mines	11	I
Brady, A. G.	U.S. Geological Survey	774	III
Brady, A. G.	U.S. Geological Survey	776	III
Breckenridge, K. S.	U.S. Geological Survey	777	III
Brown, R. D.	U.S. Geological Survey	186	II
Bucknam, R. C.	U.S. Geological Survey	188	II
Bundock, H.	U.S. Geological Survey	787	III
Butler, H. M.	U.S. Geological Survey	191	II
Campbell, R. H.	U.S. Geological Survey	919	IV
Carver, G.	Humboldt State University	192	II
Catchings, R. D.	U.S. Geological Survey	195	II
Celebi, M.	U.S. Geological Survey	199	II
Celebi, M.	U.S. Geological Survey	789	III
Chang, T. S.	Memphis State University	790	III
Chang, T. S.	Memphis State University	796	III
Choy, G. L.	U.S. Geological Survey	923	IV
Clarke, S. H.	U.S. Geological Survey	205	II
Clark, M. M.	U.S. Geological Survey	202	II

Clayton, R. W.	California Institute of Technology	213	II
Combellick, R. A.	Alaska Geological Survey	219	II
Crone, A. J.	U.S. Geological Survey	221	II
Crosson, R. S.	Washington, University of	16	I
Crosson, R. S.	Washington, University of	231	II
Davis, T. L.	Davis and Namson Consultants	234	II
Day, S.	San Diego State University	926	IV
Dewey, J. W.	U.S. Geological Survey	236	II
Dieterich, J.	U.S. Geological Survey	802	III
Dmowska, R.	Harvard University	18	I
Doser, D. I.	Texas, University of, El Paso	22	I
Durkin, M. E.	Michael E. Durkin and Associates	931	IV
Dusseau, R. A.	Wayne State University	934	IV
Ellsworth, W. L.	U.S. Geological Survey	240	II
Engdahl, E. R.	U.S. Geological Survey	245	II
Espinosa, A. F.	U.S. Geological Survey	248	II
Etheredge, E.	U.S. Geological Survey	805	III
Evans, B.	Massachusetts Institute of Technology	25	I
Evans, J. R.	U.S. Geological Survey	250	II
Fischer, F.	U. S. Geological Survey	254	II
Fletcher, J. B.	U.S. Geological Survey	28	I
Fletcher, J. B.	U.S. Geological Survey	255	II
Frankel, A.	U.S. Geological Survey	808	III
Galehouse, J. S.	San Francisco State University	256	II
Gibbs, J. F.	U.S. Geological Survey	810	III
Gilbert, L.	Lamont-Doherty Geological Observatory	269	II
Gladwin, M. T.	Queensland, University of	273	II
Goldhaber, M.	U.S. Geological Survey	811	III
Goter, S. K.	U.S. Geological Survey	940	IV
Graves, R. W.	Woodward-Clyde Consultant	819	III
Guccione, M. J.	Arkansas, University of	276	II
Habermann, R. E.	Colorado, University of	279	II
Hall, N. T.	Geomatrix Consultants	288	II
Hall, N. T.	Geomatrix Consultants	290	II
Hall, W.	U.S. Geological Survey	32	I
Hamburger, M. W.	Indiana University	34	I
Harp, E. L.	U.S. Geological Survey	824	III
Harty, K. M.	Utah Geological Survey	825	III
Hartzell, S. H.	U.S. Geological Survey	830	III
Hauksson, E.	California Institute of Technology	39	I
Helmberger, D. V.	California Institute of Technology	43	I
Herrmann, R. B.	Saint Louis University	294	II
Herrmann, R. B.	Saint Louis University	296	II
Herrmann, R. B.	Saint Louis University	841	III
Herrmann, R. B.	Saint Louis University	942	IV
Hickman, S. H.	U.S. Geological Survey	46	I
Hill, D. P.	U. S. Geological Survey	299	II
Holcomb, G.	U.S. Geological Survey	303	II
Holmes, W. T.	Rutherford and Chekene	948	IV
Hunt, R. N.	U.S. Geological Survey	304	II

Hutt, C. R.	U.S. Geological Survey	843	III
Irwin, W. P.	U.S. Geological Survey	306	II
Jachens, R. C.	U.S. Geological Survey	308	II
Jackson, M. D.	U.S. Geological Survey	48	I
Jacoby, G.	Lamont-Doherty Geological Observatory	315	II
Jacoby, G.	Lamont-Doherty Geological Observatory	951	IV
Jensen, E. G.	U.S. Geological Survey	318	II
Jin, A.	Southern California , University of	319	II
Johnson, H. O.	California, University of, San Diego	325	II
Johnson, S. Y	U.S. Geological Survey	329	II
Johnston, A. C.	Memphis State University	334	II
Johnston, A. C.	Memphis State University	341	II
Johnston, M. J. S.	U.S. Geological Survey	344	II
Jones, D. L.	California, University of, Berkeley	350	II
Jones, D. L.	California, University of, Berkeley	354	II
Julian, B. R.	U.S. Geological Survey	356	II
Kanamori, H.	California Institute of Technology	52	I
Kanamori, H.	California Institute of Technology	55	I
Keller, G. R.	Texas, University of, El Paso	359	II
Kelson, K. I.	William Lettis & Associates	360	II
King, C.-Y.	U.S. Geological Survey	363	II
King, K. W.	U.S. Geological Survey	366	II
Kisslinger, C.	Colorado, University of	58	I
Kisslinger, C.	Colorado, University of	369	II
Kulm, L. D.	Oregon State University	954	IV
Lahr, J. C.	U.S. Geological Survey	373	II
Lajoie, K. R.	U.S. Geological Survey	381	II
Langbein, J.	U.S. Geological Survey	385	II
Langbein, J.	U.S. Geological Survey	400	II
Langston, C. A.	Pennsylvania State University	409	II
Larson, K.	Colorado, University of	413	II
Lee, W. H. K.	U.S. Geological Survey	414	II
Lester, F. W.	U.S. Geological Survey	415	II
Lettis, W. R.	William Lettis and Associates	420	II
Lettis, W. R.	William Lettis and Associates	422	II
Levine, J.	Colorado, University of	424	II
Lienkaemper, J. J.	U.S. Geological Survey	426	II
Linde, A. T.	Carnegie Institute of Washington	427	II
Linde, A. T.	Carnegie Institute of Washington	436	II
Lindvall, S. C.	Lindvall Richter Benuska Associates	437	II
Lisowski, M.	U.S. Geological Survey	440	II
Liu, H. -P.	U.S. Geological Survey	845	III
Lockner, D.	U.S. Geological Survey	847	III
Luetgert, J.	U.S. Geological Survey	449	II
Machette, M. N.	U.S. Geological Survey	453	II
Madin, I. P.	Oregon Dept. of Geology and Mineral Res.	854	III
Malin, P. E.	Duke University	457	II
Marks, C.	Seattle, City of, Washington	964	IV
Mason R. G.	Imperial College	464	II
May, P. J.	Washington, University of	966	IV

McCarthy, J.	U.S. Geological Survey	466	II
McCrary, P. A.	U.S. Geological Survey	473	II
McEvilly, T. V.	California, University of, Berkeley	76	I
McEvilly, T. V.	California, University of, Berkeley	475	II
McEvilly, T. V.	California, University of, Berkeley	486	II
McGarr, A.	U.S. Geological Survey	855	III
Michael, A. J.	U. S. Geological Survey	489	II
Minster, J. B.	California, University of, San Diego	491	II
Mooney, W. D.	U.S. Geological Survey	493	II
Mori, J.	U.S. Geological Survey	498	II
Mortensen, C. E.	U.S. Geological Survey	505	II
Morton, D. M.	California, University of, Riverside	507	II
Moses, T. H.	U.S. Geological Survey	85	I
Mueller, C. S.	U.S. Geological Survey	858	III
Mueller, C. S.	U.S. Geological Survey	967	IV
Munson, P. J.	Indiana University	510	II
Nelson, A. R.	U.S. Geological Survey	512	II
Nicholson, C.	California, University of, Santa Barbara	86	I
Nishenko, S. P.	U.S. Geological Survey	968	IV
Noller, J. S.	William Lettis and Associates	519	II
Obermeier, S. F.	U.S. Geological Survey	521	II
Okol, E. A.	Northwestern University	89	I
Olshansky, R. B.	Illinois, University of Urbana-Champaign	862	III
Oppenheimer, D. H.	U.S. Geological Survey	525	II
O'Rourke, T. D.	Cornell University	866	III
Palmer, S. P.	Washington Dept. of Natural Resources	873	III
Park, R. B.	U.S. Geological Survey	528	II
Park, S. K.	California, University of, Riverside	529	II
Person, W. J.	U.S. Geological Survey	877	III
Peppin, W. A.	Nevada, University of, Reno	92	I
Peppin, W. A.	Nevada, University of, Reno	538	II
Peterson, J.	U.S. Geological Survey	881	III
Plafker, G.	U.S. Geological Survey	542	II
Ponti, D. J.	U.S. Geological Survey	549	II
Potter, C. J.	U.S. Geological Survey	554	II
Prentice, C.	U.S. Geological Survey	560	II
Qamar, A. I.	Washington, University of	973	IV
Reasenber, P. A.	U.S. Geological Survey	563	II
Reilinger, R. E.	Massachusetts Institute of Technology	570	II
Repetski, J. E.	U.S. Geological Survey	573	II
Rockwell, T.	San Diego State University	578	II
Roeloffs, E.	U.S. Geological Survey	579	II
Rymer, M. J.	U.S. Geological Survey	975	IV
Safak, E.	U.S. Geological Survey	882	III
Saikia, C. K.	Woodward-Clyde Consultants	884	III
Salyards, S. L.	New Mexico State Univerity	587	II
Sarna-Wojcicki, A.	U.S. Geological Survey	590	II
Sass, J. H.	U.S. Geological Survey	892	III
Sato, M.	U.S. Geological Survey	593	II



Scholz, C. H.	Lamont-Doherty Geological Observatory	95	I
Schultz, A.	U.S. Geological Survey	599	II
Schwartz, D. P.	U.S. Geological Survey	977	IV
Schwartz, S. Y.	California, University of, Santa Cruz	604	II
Segall, P.	U.S. Geological Survey	607	II
Sharp, R. V.	U.S. Geological Survey	611	II
Shaw, H. R.	U.S. Geological Survey	614	III
Shaw, J. H.	Princeton University	619	II
Shearer, P. M.	California, University of, San Diego	97	I
Sieh, K.	California Institute of Technology	623	II
Silverman, S.	U.S. Geological Survey	628	II
Simpson, R. W.	U.S. Geological Survey	903	III
Sims, J. D.	U.S. Geological Survey	630	II
Sipkin, S. A.	U.S. Geological Survey	633	II
Smith, R. B.	Utah, University of	99	I
Smith, R. B.	Utah, University of	637	II
Snively, P. D.	U.S. Geological Survey	643	II
Sowers, J.	William Lettis & Associates	905	III
Spudich, P.	U.S. Geological Survey	907	III
Spudich, P.	U.S. Geological Survey	910	III
Spudich, P.	U.S. Geological Survey	912	III
Stark, T. D.	Illinois, University of	979	IV
Stein, R. S.	U.S. Geological Survey	648	II
Stewart, S. W.	U.S. Geological Survey	652	II
Stokoe, K. H.	Texas, University of, Austin	985	IV
Stover, C. W.	U.S. Geological Survey	989	IV
Stuart, W. D.	U.S. Geological Survey	104	I
Swanson, D. A.	U.S. Geological Survey	655	II
Swanson, M. T.	Southern Maine, University of	660	II
Sykes, L. R.	Lamont-Doherty Geological Observatory	662	II
Sylvester, A. G.	California, University of, Santa Barbara	665	II
Sylvester, A. G.	California, University of, Santa Barbara	669	II
Taggart, J. N.	U.S. Geological Survey	991	IV
Talwani, P.	South Carolina, University of	106	I
Tarr, A. L.	U.S. Geological Survey	992	IV
Taylor, C. E.	Dames & Moore, Inc.	914	III
Teng, T.	Southern California, University of	673	II
Tinsley, J. C.	U.S. Geological Survey	681	II
Tinsley, J. C.	U.S. Geological Survey	995	IV
Trehu, A.	Oregon State University	685	II
Tullis, T. E.	Brown University	686	II
Tuttle, M.	Lamont-Doherty Geological Observatory	998	IV
Tyler, M. B.	William Spangle and Associates, Inc.	1000	IV
Unruh, J. R.	California, University of, Davis	112	I
Valentine, D. W.	California, University of, Santa Barbara	694	II
VanArsdale, R. B.	Arkansas, University of	695	II
Vaughn, J. D.	Missouri Department of Natural Res.	698	II
Vernon, F.	California, University of, San Diego	115	I
Vernon, F.	California, University of, San Diego	703	II
Vidale, J. E.	U.S. Geological Survey	705	II
Weaver, C. S.	U.S. Geological Survey	712	II

Wells, R. E.	U.S. Geological Survey	716	II
Wentworth, C. M.	U.S. Geological Survey	718	II
Williams, P. L.	California, University of, Berkeley	721	II
Wyatt, F.	California, University of, San Diego	723	II
Wyss, M.	Colorado, University of	728	II
Yamaguchi, D. K.	Colorado, University of	1004	IV
Yamaguchi, D. K.	Colorado, University of	1006	IV
Yeats, R. S.	Oregon State University	741	II
Yeats, R. S.	Oregon State University	744	II
Yeats, R. S.	Oregon State University	748	II
Verkes, R. F.	U.S. Geological Survey	916	III
Zoback, M. L.	U.S. Geological Survey	749	II

# INDEX 2

## INDEX ALPHABETIZED BY INSTITUTION

		Page
Alaska Geological Survey	Combellick, R. A.	219
Arkansas, University of	Guccione, M. J	276
Arkansas, University of	VanArsdale, R. B.	695
Battelle Seattle Research Center	Bolton, P. A.	917
Brown University	Tullis, T. E.	686
California Institute of Technology	Clayton, R. W.	213
California Institute of Technology	Hauksson, E.	39
California Institute of Technology	Helmberger, D. V.	43
California Institute of Technology	Kanamori, H.	52
California Institute of Technology	Kanamori, H.	55
California Institute of Technology	Sieh, K.	623
California, University of, Berkeley	Jones, D. L.	350
California, University of, Berkeley	Jones, D. L.	354
California, University of, Berkeley	McEvelly, T. V.	76
California, University of, Berkeley	McEvelly, T. V.	475
California, University of, Berkeley	McEvelly, T. V.	486
California, University of, Berkeley	Williams, P. L.	721
California, University of, Davis	Unruh, J. R.	112
California, University of, Los Angeles	Bird, P.	159
California, University of, San Diego	Agnew, D. C.	126
California, University of, San Diego	Bock, Y.	166
California, University of, San Diego	Johnson, H. O.	325
California, University of, San Diego	Minster, J. B.	491
California, University of, San Diego	Shearer, P. M.	97
California, University of, San Diego	Vernon, F.	115
California, University of, San Diego	Vernon, F.	703
California, University of, San Diego	Wyatt, F.	723
California, University of, Santa Barbara	Nicholson, C.	86
California, University of, Santa Barbara	Valentine, D. W.	694
California, University of, Santa Barbara	Sylvester, A. G.	665
California, University of, Santa Barbara	Sylvester, A. G.	669
California, University of, Santa Cruz	Schwartz, S. Y.	604
California, University of, Riverside	Morton, D. M.	507
California, University of, Riverside	Park, S. K.	529
Carnegie Institute of Washington	Linde, A. T.	427
Carnegie Institute of Washington	Linde, A. T.	436
Colorado School of Mines	Boyd, T. M.	11

Colorado, University of	Bilham, R.	153
Colorado, University of	Bilham, R.	157
Colorado, University of	Habermann, R. E.	279
Colorado, University of	Kisslinger, C.	58
Colorado, University of	Kisslinger, C.	369
Colorado, University of	Larson, K.	413
Colorado, University of	Levine, J.	424
Colorado, University of	Wyss, M.	728
Colorado, University of	Yamaguchi, D. K.	1004
Colorado, University of	Yamaguchi, D. K.	1006
Cornell University	O'Rourke, T. D.	866
Dames & Moore	Taylor, C. E.	914
Davis and Namson Consultants	Davis, T. L.	234
Duke University	Malin, P. E.	457
Michael E. Durkin and Associates	Durkin, M. E.	931
Geomatrix Consultants	Hall, N. T.	288
Geomatrix Consultants	Hall, N. T.	290
Harvard University	Dmowska, R.	18
Humboldt State University	Carver, G.	192
Illinois, University of	Stark, T. D.	979
Illinois, University of, Urbana-Champaign	Olshansky, R. B.	862
Imperial College	Mason, R. G.	464
Indiana University	Hamburger, M. W.	34
Indiana University	Munson, P. J.	510
Lamont-Doherty Geological Observatory	Abers, G. A.	1
Lamont-Doherty Geological Observatory	Abers, G. A.	121
Lamont-Doherty Geological Observatory	Beavan, J.	139
Lamont-Doherty Geological Observatory	Beavan, J.	145
Lamont-Doherty Geological Observatory	Biegel, R. L.	8
Lamont-Doherty Geological Observatory	Gilbert, L.	269
Lamont-Doherty Geological Observatory	Jacoby, G.	315
Lamont-Doherty Geological Observatory	Jacoby, G.	951
Lamont-Doherty Geological Observatory	Scholz, C. H.	95
Lamont-Doherty Geological Observatory	Sykes, L. R.	662
Lamont-Doherty Geological Observatory	Tuttle, M.	998
William Lettis & Associates	Kelson, K. I.	360
William Lettis & Associates	Lettis, W. R.	420
William Lettis & Associates	Lettis, W. R.	422
William Lettis & Associates	Noller, J. S.	519
William Lettis & Associates	Sowers, J.	905

Lindvall Richter Benuska Associates	Lindvall, S. C.	437
Massachusetts Institute of Technology	Evans, B.	25
Massachusetts Institute of Technology	Reilinger, R. E.	570
Memphis State University	Chang, T. S.	790
Memphis State University	Chang, T. S.	796
Memphis State University	Johnston, A. C.	334
Memphis State University	Johnston, A. C.	341
Missouri Department of Natural Res.	Vaughn, J. D.	698
Nevada, University of, Reno	Peppin, W. A.	92
Nevada, University of, Reno	Peppin, W. A.	538
New Mexico State University	Salyards, S. L.	587
Northwestern University	Okal, E. A.	89
Oregon Dept. of Geology and Mineral Resource	Madin, I. P.	854
Oregon State University	Kulm, L. D.	954
Oregon State University	Trehu, A.	685
Oregon State University	Yeats, R. S.	741
Oregon State University	Yeats, R. S.	744
Oregon State University	Yeats, R. S.	748
Pennsylvania State University	Langston, C. A.	409
Princeton University	Shaw, J. H.	619
Queensland, University of	Gladwin, M. T.	273
Rutherford and Chekene	Holmes, W. T.	948
Saint Louis, University of	Herrmann, R. B.	294
Saint Louis, University of	Herrmann, R. B.	296
Saint Louis, University of	Herrmann, R. B.	841
Saint Louis, University of	Herrmann, R. B.	942
San Diego State University	Day, S.	926
San Diego State University	Rockwell, T.	578
San Francisco State University	Galehouse, J. S.	256
Seattle, City of, Washington	Marks, C.	964
Soil Tectonics, Berkeley, California	Borchardt, G.	174
Southern California, University of	Jin, A.	319
Southern California, University of	Teng, T.	673
Southern Maine, University of	Swanson, M. T.	660
South Carolina, University of	Talwani, K. H.	106

William Spangle and Associates, Inc.	Tyler, M. B.	1000
Stanford University	Aydin, A.	6
Texas, University of, Austin	Stokoe, K. H.	985
Texas, University of, El Paso	Doser, D. I.	22
Texas, University of, El Paso	Keller, G. R.	359
U.S. Geological Survey	Algermissen, S. T.	755
U.S. Geological Survey	Allen, G.	131
U.S. Geological Survey	Anderson, R. E.	133
U.S. Geological Survey	Andrews, D. J.	763
U.S. Geological Survey	Atwater, B. F.	137
U.S. Geological Survey	Bernknopf, R. L.	766
U.S. Geological Survey	Boatwright, J.	9
U.S. Geological Survey	Bonilla, M. G.	172
U.S. Geological Survey	Boore, D. M.	768
U.S. Geological Survey	Borcherdt, R. D.	177
U.S. Geological Survey	Borcherdt, R. D.	769
U.S. Geological Survey	Borcherdt, R. D.	771
U.S. Geological Survey	Borcherdt, R. D.	773
U.S. Geological Survey	Brady, A. G.	774
U.S. Geological Survey	Brady, A. G.	776
U.S. Geological Survey	Breckenridge, K. S.	777
U.S. Geological Survey	Brown, R. D.	186
U.S. Geological Survey	Bucknam, R. C.	188
U.S. Geological Survey	Bundock, H.	787
U.S. Geological Survey	Butler, H. M.	191
U.S. Geological Survey	Catchings, R. D.	195
U.S. Geological Survey	Campbell, R. H.	919
U.S. Geological Survey	Celebi, M.	199
U.S. Geological Survey	Celebi, M.	789
U.S. Geological Survey	Choy, G. L.	923
U.S. Geological Survey	Clarke, S. H.	205
U.S. Geological Survey	Clark, M. M.	202
U.S. Geological Survey	Crone, A. J.	221
U.S. Geological Survey	Dewey, J. W.	236
U.S. Geological Survey	Dieterich, J. H.	802
U.S. Geological Survey	Ellsworth, W. L.	240
U.S. Geological Survey	Engdahl, E. R.	245
U.S. Geological Survey	Espinosa, A. F.	248
U.S. Geological Survey	Etheredge, E.	805
U.S. Geological Survey	Evans, J. R.	250
U.S. Geological Survey	Fischer, F.	254
U.S. Geological Survey	Fletcher, J. B.	28
U.S. Geological Survey	Fletcher, J. B.	255
U.S. Geological Survey	Frankel, A.	808
U.S. Geological Survey	Goldhaber, M.	811
U.S. Geological Survey	Gibbs, J. F.	810
U.S. Geological Survey	Goter, S. K.	940
U.S. Geological Survey	Hall, W.	32
U.S. Geological Survey	Harp, E. L.	824
U.S. Geological Survey	Hartzell, S. H.	830
U.S. Geological Survey	Hickman, S. H.	46

U.S. Geological Survey	Hill, D. P.	299
U.S. Geological Survey	Holcomb, G.	303
U.S. Geological Survey	Hunt, R. N.	304
U.S. Geological Survey	Hutt, C. R.	843
U.S. Geological Survey	Irwin, W. P.	306
U.S. Geological Survey	Jachens, R. C.	308
U.S. Geological Survey	Jackson, M. D.	48
U.S. Geological Survey	Jensen, E. G.	318
U.S. Geological Survey	Johnson, S. Y.	329
U.S. Geological Survey	Johnston, M.J.S.	344
U.S. Geological Survey	Julian, B. R.	356
U.S. Geological Survey	King, C. -Y.	363
U.S. Geological Survey	King, K. W.	366
U.S. Geological Survey	Lahr, J. C.	373
U.S. Geological Survey	Lajoie, K. R.	381
U.S. Geological Survey	Langbein, J.	385
U.S. Geological Survey	Langbein, J.	400
U.S. Geological Survey	Lee, W. H. K.	414
U.S. Geological Survey	Lester, F. W.	415
U.S. Geological Survey	Lienkaemper, J. J.	426
U.S. Geological Survey	Lisowski, M.	440
U.S. Geological Survey	Liu, H. -P.	845
U.S. Geological Survey	Lockner, D.	847
U.S. Geological Survey	Luetgert, J.	449
U.S. Geological Survey	Machette, M. N.	453
U.S. Geological Survey	McCarthy, J.	466
U.S. Geological Survey	McCrorry, P. A.	473
U.S. Geological Survey	McGarr, A.	855
U.S. Geological Survey	Michael, A. J.	489
U.S. Geological Survey	Mooney, W. D.	493
U.S. Geological Survey	Mori, J.	498
U.S. Geological Survey	Mortensen, C. E.	505
U.S. Geological Survey	Moses, T. H.	85
U.S. Geological Survey	Mueller, C. S.	858
U.S. Geological Survey	Mueller, C. S.	967
U.S. Geological Survey	Nelson, A. R.	512
U.S. Geological Survey	Nishenko, S. P.	968
U.S. Geological Survey	Obermeier, S. F.	521
U.S. Geological Survey	Oppenheimer, D. H.	525
U.S. Geological Survey	Park, R. B.	528
U.S. Geological Survey	Person, W. J.	877
U.S. Geological Survey	Peterson, J.	881
U.S. Geological Survey	Plafker, G.	542
U.S. Geological Survey	Ponti, D. J.	549
U.S. Geological Survey	Potter, C. J.	554
U.S. Geological Survey	Prentice, C.	560
U.S. Geological Survey	Reasenber, P. A.	563
U.S. Geological Survey	Repetski, J. E.	573
U.S. Geological Survey	Roeloffs, E.	579
U.S. Geological Survey	Rymer, M. J.	975
U.S. Geological Survey	Safak, E.	882
U.S. Geological Survey	Sarna-Wojcicki, A.	590
U.S. Geological Survey	Sass, J. H.	892
U.S. Geological Survey	Sato, M.	593
U.S. Geological Survey	Schultz, A.	599

U.S. Geological Survey	Schwartz, D. P.	977
U.S. Geological Survey	Segall, P.	607
U.S. Geological Survey	Sharp, R. V.	611
U.S. Geological Survey	Shaw, H. R.	614
U.S. Geological Survey	Silverman, S.	628
U.S. Geological Survey	Simpson, R. W.	903
U.S. Geological Survey	Sims, J. D.	630
U.S. Geological Survey	Sipkin, S. A.	633
U.S. Geological Survey	Snively, P. D.	643
U.S. Geological Survey	Spudich, P.	907
U.S. Geological Survey	Spudich, P.	910
U.S. Geological Survey	Spudich, P.	912
U.S. Geological Survey	Stein, R. S.	648
U.S. Geological Survey	Stewart, S. W.	652
U.S. Geological Survey	Stover, C. W.	989
U.S. Geological Survey	Stuart, W. D.	104
U.S. Geological Survey	Swanson, D. A.	655
U.S. Geological Survey	Taggart, J. N.	991
U.S. Geological Survey	Tarr, A. L.	992
U.S. Geological Survey	Tinsley, J. C.	681
U.S. Geological Survey	Tinsley, J. C.	995
U.S. Geological Survey	Vidale, J. E.	705
U.S. Geological Survey	Weaver, C. S.	712
U.S. Geological Survey	Wells, R. E.	716
U.S. Geological Survey	Wentworth, C. M.	718
U.S. Geological Survey	Yerkes, R. F.	916
U.S. Geological Survey	Zoback, M.L.	749
Utah Geological Survey	Harty, K. M.	825
Utah, University of	Arabasz, W. J.	135
Utah, University of	Arabasz, W. J.	765
Utah, University of	Smith, R. B.	99
Utah, University of	Smith, R. B.	637
Washington Dept. of Natural Resources	Palmer, S. P.	873
Washington, University of	Bierman, P.	151
Washington, University of	Crosson, R. S.	16
Washington, University of	Crosson, R. S.	231
Washington, University of	May, P. J.	966
Washington, University of	Qamar, A. I.	973
Washington, University of	Swanson, D. A.	655
Wayne State University	Dusseau, R. L.	934
Woodward-Clyde Consultants	Graves, R. W.	819
Woodward-Clyde Consultants	Saikia, C. K.	884